ACL Injury Mechanisms and the Kinetic Chain Linkage: The effect of proximal joint stiffness on ACL injury risk.

by

Jordan Cannon

A thesis
presented to the University of Waterloo
in fulfillment of the
thesis requirement for the degree of
Master of Science
in
Kinesiology

Waterloo, Ontario, Canada, 2016

Author's Declaration

I hereby declare that I am the sole author of this thesis. This is a true copy of the thesis, including any required final revisions, as accepted by my examiners.

I understand that my thesis may be made electronically available to the public.

Jordan Cannon

Abstract

Recent literature has suggested that core and gluteal neuromuscular deficits are involved in the mechanism of non-contact ACL injury. Several research groups have identified dynamic valgus of the lower extremity to be an injurious posture that is predictive of future non-contact ACL injury risk. Aberrant kinematics of segments proximally in the kinetic chain, namely the trunk and hip, have also been observed to drive dynamic valgus during dynamic activities. Comprehensive investigation of the neuromuscular deficits postulated as the mechanism of injurious mechanics are lacking in the literature. Given that certain motions can be created by infinite muscle activation combinations, and that muscle activation contributes both force and controlling stiffness, this work aims to characterise any such deficits by examining the ability to modulate proximal joint stiffness to dynamically control distal segments of the kinetic chain. Three-dimensional lumbar spine stiffness and hip stiffness were quantified in participants deemed as 'high valgus' and 'low valgus' based on their frontal plane knee displacement during each task. The risk of non-contact ACL damage is highest among active females, justifying their choice to study. Eighteen female participants completed drop vertical jump (DVJ), stop jump (SJ), single leg drop (SLD) and single leg crossover drop (SLCD) tasks in order to measure medial knee displacement and associated proximal joint stiffness values. It was hypothesized that those with high valgus would not generate sufficient joint rotational stiffness at the lumbar spine, hip, or both, and thus aberrant kinematics and the injurious dynamic valgus motion would result. Those who were able to develop sufficient stiffness at the lumbar spine and hip had greater control over the kinetic chain and in doing so reduced dynamic valgus and likely their risk of future ACL injury. However, variance within subjects was found, specifically the same person would show a valgus landing on one trial, but not on another. This necessitated a change in

analysis to one considering the landings as case studies, and groupings of landings by whether valgus occurred or not, rather than by subjects. This was an unexpected, and therefore exciting part of the thesis journey. The results here provide insight into the motor control component of avoiding dynamic valgus and is the first work to confirm, and specifically characterize, a neuromuscular deficit at the core or hip. That deficit appears to be an inability to generate sufficient joint rotational stiffness in order to control the linkage. Given this insight, appropriate interventions and training programs may be designed to reduce one's risk of ACL injury.

Keywords: stiffness, stability, ACL, kinetic chain, injury risk, dynamic valgus

Acknowledgements

This thesis would not have been possible if not for the help, guidance, and support of many individuals. While there are too many to mention here, please allow me to briefly thank particular individuals that have been essential figures throughout my graduate degree.

Firstly, I would like to thank my supervisor, mentor, friend, and professional role model, Dr. Stuart McGill. As a man, a supervisor, and as a scientist, I hold him in the utmost regard. Dr. McGill has undoubtedly changed my life, from the very first moment I first sat in his classroom as an undergraduate student and got excited about biomechanics, research and science. He has encouraged me to think beyond the norm, and taught me to be a scientist – in the truest sense of the word. His passion, dedication and brilliance are truly inspiring, and are characteristics that I will strive to replicate throughout my career. I have a tremendous amount of respect and admiration for the work he has done throughout his glittering career, and I hope to have some fraction of the impact that he has had in both the research and clinical worlds. I owe Dr. McGill a huge debt of gratitude for all that he has done for me, particularly the level of confidence and trust that he has shown in my abilities, and his encouragement in my pursuits as a scientist. Simply put, he is an outstanding role model, and I consider myself extremely fortunate to have had the opportunity to work with him for the past 4 and a half years. I don't think I could have asked for a better supervisor, nor do I think I could have learnt so much from anyone else. Thanks Stu.

I would like to thank my committee members Dr. Stephen Brown, Dr. Steven Fischer and Dr. Stephen Prentice. A special thank you to Dr. Brown is necessary, he provided great insight and perspective on my work, and many of his own works greatly influenced this thesis. He was always available, and happy, to provide advice when needed, and his expertise was extremely

valuable. I thank Dr. Stephen Prentice for his contributions to my proposal and helpful comments that guided my thesis work. I would also like to thank Dr. Steven Fischer for agreeing to join my thesis committee late on, and the helpful comments and questions he contributed to strengthen this work.

I would also like to thank Dr. Andrew Laing and Dr. Jim Frank, both of whom I have sought advice from on several occasions regarding work, life and my future. I very much appreciate the time they spent with me to listen, and the thoughtful advice they provided. I would also like to express my sincerest gratitude to Denise Hay for all that she does for the graduate students in Kinesiology, we would all be lost without her.

There are many peers, colleagues and friends that I have met throughout my master's degree that have each, in their own way, helped shape this work and the scientist I am today. My classmates with whom many late nights were spent processing data and writing lab reports have become some of my closest friends, Ben Cornish, Benoit Lafleur, Maureen Riddell, Rachel Whittaker, I am glad we went through the process together. Special thanks to Dr. Christian Balkovec, Ben Lee, Natalie Sidorkewicz and Jordan Andersen, for welcoming me into the lab and allowing me to help with data collections and gain experience early on. The mathematician Jeff Barrett, thank you. Your help with mathematics and coding often saved me hours of frustration, while your unique perspective on my work was always appreciated. I very much enjoyed our numerous scientific discussions, and I always came away better from them. Countless coffee's and laughs made the late nights and long months bearable.

A separate paragraph to thank Dr. Edward Cambridge is necessary. The mentoring, friendship, and sage advice you have provided throughout my master's degree has been invaluable. Your clinical wisdom in combination with your vast understanding of biomechanics

has been instrumental in my own development. Many of our debates led to a deeper understanding of concepts, while many laughs have enabled me to get through this thesis. I eagerly await the great work you will produce, and discoveries you will make, as your career progresses, and I look forward to continued collaboration.

I would also like to thank Lori and Scott Courtemanche, not just for raising such a wonderful woman in Ali, but for opening your home to me and welcoming me into your family. Your generosity and support, especially over the last few months, are truly appreciated.

Everything I have achieved, and ever will achieve, can be attributed to my parents, Michael and Patricia Cannon. The sacrifices you have made for me and Michela have been too large, you always put us ahead of yourselves and I only hope I can repay you by taking advantage of the opportunities you have afforded me, and make you proud. If it weren't for your unwavering love, support and encouragement I would not be the man I am today, nor would I have been able to complete this thesis. Dad, you are my hero. You're the best man I know, and while I may never attain it, I will spend my life trying to emulate your generosity, selflessness and courage. Mum, you are the best support anyone could ask for. Knowing that you are always in my corner with timely, and straightforward, advice gives me the confidence to pursue new challenges knowing that you will always have my back. I would also like to sincerely thank my sister, Michela, for always being there for me. I am very fortunate to have a sister that is one of my closest friends, you do not realize just how much I value your opinion and appreciate the time you take to listen and provide guidance. You have an incredible ability to provide words of kindness and encouragement when they are most needed.

Finally, words cannot express how much I appreciate my best friend and love of my life, Ali Courtemanche. If it weren't for your continued love and support throughout this journey, I would never have been able to finish this work. Your understanding and encouragement knows no limits, as for too long this work has consumed me while a work-life balance has been completely lost. Your love knows no bounds, and I consider myself extremely fortunate to have such a kind and caring partner to spend my life with. Much has changed over the last 8 years, but having you as a constant in my life has always kept me positive, looking forward, and excited for our future together. I cannot wait to start our new adventure together, and see what else the future holds for us.

Table of Contents

List of Figures

List of Tables

Thesis Organization

The document presented here is broken up into six main chapters, each with multiple subsections. The chapters are: Introduction, Literature Review, Hypotheses, Methods, Results and Discussion. The introduction briefly describes the issue that is ACL injury and presents a general rationale for why this study is needed given previous works' contributions, and shortcomings, in characterising the mechanism and developing a prevention strategy. While conventionally a statement of hypotheses would be included in the introduction, in this document they can be found following the literature review. The intentional placement of the hypotheses are located as such since their rationale and origins stem from the literature review where a basic logic is laid out, and from which the hypotheses are generated. Similarly, the rationale for this study as a whole and the methodology to be utilised are motivated from the many works of research considered in the literature review. The methods section is broken up into data collection procedures and data processing - including the biomechanical models utilized. The results section presents the data and describes differences between groups by task. The discussion begins by revisiting the hypotheses and determining their veracity. The discussion aims to provide explanations for the results and what they mean when considered together as a collective story. Contributions and conclusions outlines the importance of this work, its meaning, and future directions. Appendices can be found at the end of the document that contain any supplementary material referred to throughout the document and any relevant data.

1.0 Introduction

1.1 The Issue

Dynamic valgus of the lower extremities has been identified as a risk factor for a multitude of acute and chronic lower limb injuries, and in particular, knee injuries. High external abduction moments experienced about the knee have been well documented as placing an individual at high risk for numerous knee injuries, including non-contact anterior cruciate ligament (ACL) tear and/or patellofemoral pain (PFP) and joint dysfunction.

Up to 250,000 ACL ruptures occur each year in the USA, of which, approximately 70% are non-contact injuries. Adolescent and collegiate female athletes suffer ACL injuries with a 4-6 fold greater rate than that of their male counterparts, and alone incur an estimated healthcare cost of $650 million annually (Blackburn, Norcross, & Padua, 2011; Hewett, Torg, & Boden, 2009; Hewett et al., 2005; Hewett, Myer, & Ford, 2004; Jamison, Pan, & Chaudhari, 2012; Myer, Ford, Paterno, Nick, & Hewett, 2008). Additionally, 12 – 20 years following traumatic ACL injury 50-100% of women will present with knee osteoarthritis (Hewett et al., 2009; Myer et al., 2008).

It has been reported that one in four knee injuries treated at sports medicine clinics are patellofemoral pain, accounting for over 5% of all presentations seen by sports medicine practitioners (Barton, Lack, Malliaras, & Morrissey, 2012; Collado & Fredericson, 2010; Nakagawa, Moriya, Maciel, & Serrão, 2012). PFP is said to occur in 9-15% of active populations, while up to 37% of military recruits experience symptoms during basic training (Barton et al., 2012; Collado & Fredericson, 2010; Powers, 2012). Taunton and colleagues (Taunton et al., 2002) reported that per annum up to 2.5 million runners are diagnosed with PFP, and that it remains the most common overuse running injury (as it has been over the last 20

years); citing abnormal lower extremity mechanics as one of the main, and modifiable, risk factors.

1.2 Rationale

The substantial economic burden, as well as future pain and overall health in individuals, associated with ACL injuries are rationale for investigation into injury mechanisms and appropriately directed interventions. Understanding injury etiology is necessary for designing and implementing appropriate preventative strategies. Previously, imbalances and asymmetries in strength and endurance between the quadriceps and hamstrings, and thigh and leg musculature have been proposed mechanisms. Knee joint angles, Q-angle and other local factors have also been historically cited as risk factors. However, interventions surrounding these mechanisms have proven largely ineffective in reducing one's risk of, or preventing, injury. More recently, neuromuscular deficits, impaired trunk proprioception, weak hip musculature and other proximal factors in the kinetic chain have been postulated as the cause of lower extremity dynamic valgus and thus increased injury risk. Thus, isolating the knee when investigating injury mechanisms and directing interventions as such are focusing on the site where injury presents, as opposed to where it originates. Ultimately, aberrant muscle activity, injurious kinematics and resulting kinetics are the product of motor control influences.

When muscles contract they create both force and stiffness. Stiffness is a major physical entity that the body uses to control motion. Further, any machine that has an articulating linkage must first establish proximal rooting and proximal stability to enable distal movement. The articulated system characterizing humans falls under the same law. This work aims to quantify the role of joint rotational stiffness of the spine and hip, and their influence on kinematics and specifically valgus presentation associated with acute ACL injury. Core stability - the

production, transfer and control of forces and motion to distal segments of the kinetic chain - is the foundation of optimal human movement (Zazulak, Hewett, Reeves, Goldberg, & Cholewicki, 2007b). Stiffness proximal to the hips allows for both the initiation of, and resistance to, motion in the lower limbs (McGill & Karpowicz, 2009). Thus, the dynamic stability of the knee is dependent on the control of all contributing segments to the movement, starting proximally at the trunk and radiating distally through the hips.

2.0 Literature Review

2.1 Anatomy of the ACL

The ACL attaches distally at the anterior intercondylar area of the tibia (just posterior to medial meniscus attachment site) and extends superiorly, posteriorly and laterally to attach to the posterior aspect of the medial side of the lateral femoral condyle (Figure 1). During extended knee postures the ACL is elongated significantly greater than with knee flexion (Utturkar et al., 2013). Additionally, peak ACL strain is observed at maximum knee extension during walking and landing as measured in vivo with sophisticated modeling techniques (Taylor et al., 2011, 2013). ACL injury has been documented to occur most frequently at less than 30^{o} knee flexion immediately prior to landing impact (Boden, Torg, Knowles, & Hewett, 2009; Hewett et al., 2009; Taylor et al., 2011). Applying a valgus moment (aka KAM) alone increases peak ACL strain by 34%, while in combination with internal rotation puts ACL strain in the optimal range for ACL rupture (Shin, Chaudhari, & Andriacchi, 2011). Thus, a valgus moment in combination with knee extension (in the absence of internal rotation) are able to cause sufficient elongation and tensile strain leading to ACL failure in vivo.

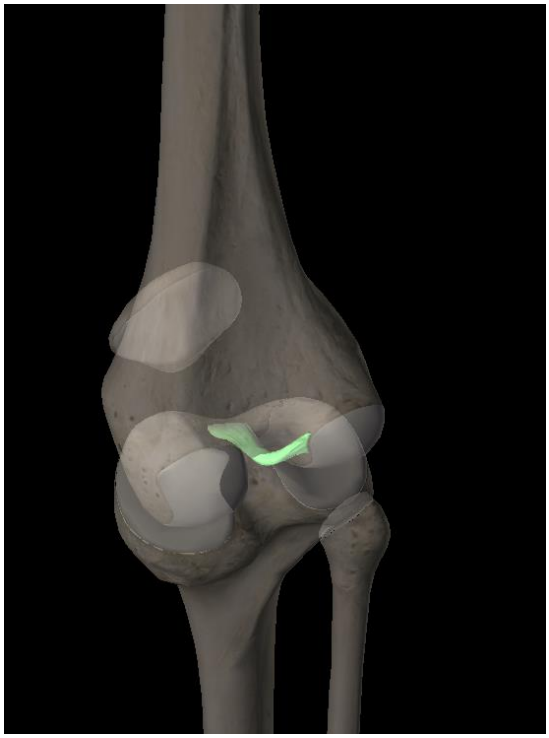

Figure 1: A visual representation of the attachments points and orientation of the anterior cruciate ligament (ACL). Essential Anatomy 3D.

2.2 Knee Abduction Moment

Currently a variable in predicting ACL injury risk is the external knee abduction moment (KAM) during a drop vertical jump (DVJ), for which a threshold has been developed to predict those 'at risk' and those 'not at risk'. The DVJ involves dropping from a box 31cm in height, with each foot landing on a separate force plate and then immediately performing a maximum vertical jump. It is during the contact phase of landing and the counter movement (deceleration of the body's COM) in which the KAM is calculated bilaterally. While dynamic knee valgus is used as an observable clinical indicator of ACL injury risk, it has been claimed that the quantifiable KAM threshold is able to aid in successful prediction of future non-contact ACL injury. A KAM of greater than 25.25 Nm places an individual 'at risk' for future non-contact ACL injury, while a KAM below this threshold places an individual in the 'not at risk' group. Work by Myer, Hewett and colleagues have demonstrated that a KAM of 25.25 Nm is the most

sensitive and specific threshold for dichotomising those who suffered non-contact ACL injury vs those who did not (Myer, Ford, Khoury, Succop, & Hewett, 2011; Myer et al., 2015; Myer, Ford, Brent, & Hewett, 2007; Myer, Ford, Khoury, Succop, & Hewett, 2010b).

2.3 Kinematics

Given that the biggest predictor of ACL injury risk is the frontal plane kinematics and kinetics at the knee (dynamic valgus and KAM), the contribution of frontal plane kinematics proximally in the kinetic chain as they pertain to the KAM will be the focus of this discussion.

2.3.1 Dynamic Valgus

Dynamic valgus of the lower extremity is characterised by hip adduction (femur relative to the pelvis) and knee abduction (tibia relative to the femur) - this is the classic posture cited as straining the ACL when it appears that the knee has collapsed medially. However, it has also been demonstrated that excessive valgus can occur while the tibia remains vertical and thus not contributing to dynamic valgus presentation (Powers, 2003). Upon landing, with the foot planted in neutral (i.e. no ankle eversion or foot pronation), the valgus posture is driven by segments superior to the knee joint. If one considers the initial contact (IC) phase upon landing, it is unlikely that the distal ankle causes valgus motion at the knee, but rather is a consequence of it. For ankle eversion to cause dynamic valgus, the aberrant movement would have to be initiated at the ankle and thus be the first instance of buckling in the kinetic chain. If the ankle were the site of buckling it would be expected that eversion sprains would accompany non-contact ACL injuries, given the mass of the upper body, thigh and leg segments superior to the ankle. Rather, during a DVJ as the valgus motion occurs, the feet are already planted on the ground and thus the terminal segment is closed and buckling occurs at the knee with resultant ankle eversion in

response to the knee (proximal tibia) moving medially (Powers, 2010a). This notion provides a rationale for the mechanism being a top-down, proximal-to-distal process.

Dynamic valgus often occurs during athletic movements such as landing and cutting, and is considered an injurious posture due to the concomitant KAM created by the vertical ground reaction force (vGRF) passing laterally to the knee joint centre (Figure 2B). However, other proximal factors in the kinetic chain can also create large KAM and the presentation of dynamic valgus at the knee (in the absence of tibial abduction). Primarily, the proximal factors in the frontal plane include lateral trunk lean, hip adduction and the combination of them to create 'pelvic drop' (Figure 2B). Pelvic drop is a term often used in the literature as it relates to its contribution to dynamic valgus and/or large KAM created by the seeming lateral drop of the pelvis. Since the pelvis itself is immovable, the appearance of pelvic drop can be created by lateral bend of the lumbar spine, ipsilateral hip adduction, and contralateral hip abduction. In combination with hip adduction, internal rotation has also been cited as contributing to dynamic valgus.

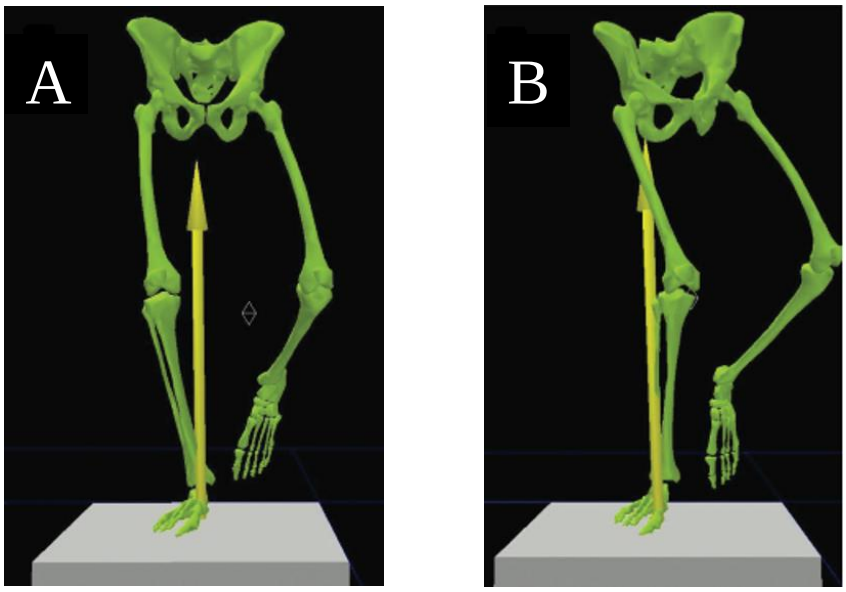

Figure 2: Two single leg drop landings from a frontal plane view. A) Optimal land with the knee over the ankle and control of the trunk and hip. The GRF passes medially to the knee and thus not an ACL injury mechanism. B) Aberrant kinematics displayed, including a lateral trunk lean and hip adduction creating 'pelvic drop' with resulting dynamic valgus causing the lateral GRF to pass laterally to the knee joint. Figure adapted from Powers, 2010.

2.3.2 Trunk Kinematics

In a video analysis of non-contact ACL injures it was observed that up to 16^{o} greater ipsilateral trunk lean (to the vertical) accompanied dynamic valgus during the IC phase of the injurious movement in injured athletes compared to uninjured athletes (Hewett et al., 2009). A lateral trunk lean serves to shift the COM of the body and allow for the vGRF to pass laterally to the knee joint centre, initiate medial knee collapse and thus experience a higher KAM (Hewett & Myer, 2011b; Souza & Powers, 2009a). Upon single leg landing or squatting, leaning of the trunk in the direction of the stance limb (in an attempt to maintain one's centre of mass within its base of support) can manifest in a valgus position of the lower limb (Powers, 2010). These trunk motions may also be a compensatory strategy in response to poor pelvic control by the hip musculature (Powers, 2010a).

If control of trunk accelerations during dynamic activities such as landing and cutting cannot be achieved, the mechanics of distal joints and segments must account for the concomitant external moments experienced. A lateral trunk lean towards a limb creates an external abduction moment at the ipsilateral hip, this external moment is balanced with an internal hip adduction moment of equal magnitude (Hewett & Myer, 2011a; Hewett et al., 2009). The internal hip adduction moment generated is required to maintain upright balance, yet contributes to the injurious valgus posture. Thus, a lateral trunk lean combined with hip adduction moment and large KAM exemplify how a biomechanical kinetic chain linkage exists in which the actions at one joint are propagated throughout the chain to cause, or increase one's risk of, ACL injury.

Additionally, in the sagittal plane there is a trade-off between the hips and knees upon bilateral landing. Landing with an anterior lean of the trunk decreases the knee-extensor moment whilst increasing the hip-extensor moment; conversely landing with an erect trunk increases the knee-extensor moment while reducing the hip-extensor moment. (Powers, 2003 and Powers, 2010). Thus, landing with an erect trunk can strain the ACL via quadriceps induced anterior tibial shear (Powers, 2010a). Video analysis of ACL injured athletes examining trunk kinematics found that a more erect trunk also accompanied greater knee extension in those who injured compared to uninjured athletes (Hewett et al., 2009). Increased knee extension would serve to increase the strain and forces on the ACL, and in doing so increase the likelihood of ACL injury (Kulas, Hortobágyi, & Devita, 2012). It has been noted that anterior-posterior trunk lean serves to modulate the strain and forces experienced by the ACL via its kinetic chain linkage with the hip and knee (Kulas et al., 2012). Landing with a more erect trunk (i.e. posterior trunk lean) increases hip and knee extension as well as increasing the quadriceps-to-hamstring activation and

the vGRF (Blackburn & Padua, 2009; Kulas et al., 2012). Conversely, an anterior trunk lean would serve to impart the opposite mechanics (an overall less erect kinetic chain) and in doing so decreases ACL strain and the forces imparted on it (Blackburn et al., 2011; Kulas et al., 2012).

However, contrasting evidence surrounding sagittal plane trunk lean has emerged in which the authors suggest an increased hip flexion angle accompanied with increased knee extension, increases one's risk of ACL injury - as determined by video analysis (Boden et al., 2009), Interestingly, these are the same authors who suggested a more erect trunk accompanied knee extension and ACL injury in the aforementioned video analysis (Boden et al., 2009; Hewett et al., 2009). Nevertheless, one cannot have a posterior trunk lean, a flexed hip and an extended knee. Powers (2010) reported that the ability of the gluteus medius to produce torque decreases with increased hip flexion, due to a reduced moment arm and suboptimal force-length characteristics Given that the gluteus medius plays a major role in abducting the hip, and in doing so avoiding dynamic valgus, gives merit to these conflicting results. It is suggested here that an optimal amount of anterior-posterior trunk lean would serve to be the most prophylactic regarding ACL injury – whereby a posterior trunk lean (erect trunk) initiates injurious mechanics as previously mentioned but anterior collapse diminishes the ability of the abductors to counteract dynamic valgus. Thus, optimal control of the trunk in the sagittal plane via core stiffness is necessary in order to allow hip musculature to appropriately stiffen in order to prevent hip adduction.

2.3.3 Hip Kinematics

Recently, a growing body of literature suggests that many traumatic knee injuries are not due to aberrant knee kinematics, but rather aberrant hip kinematics. Hip adduction and internal rotation have been shown to influence lower extremity alignment, placing the knee in vulnerable

postures (such as valgus of the lower extremity) and inducing excessively high loads on various structures of the joint (Powers, 2010a; Souza & Powers, 2009a). Of particular interest for this work, is the role of hip adduction and internal rotation as the primary contributor to medial knee displacement in creating a valgus posture (Powers, 2010a; Reiman, Bolgla, & Lorenz, 2009; Souza & Powers, 2009b). During hip adduction, the distal femur serves to move the knee joint medially, allowing dynamic valgus of the lower extremity and thus large KAM are created as the vGRF passes laterally to the knee joint centre. Hip adduction may be a compensatory response in order to maintain upright stance during a lateral trunk lean. However, hip adduction has also been observed in the absence of a lateral trunk lean during both unilateral and bilateral landings (Powers, 2010a). In this case, it would appear that the problem may not originate in the trunk, but rather at the hip.

In addition to causing dynamic malalignments, hip adduction alters the moment arm length of muscles surrounding the hip that are critical for pelvic stability. Work by Henderson and colleagues found that the gluteus medius moment arm was reduced by up to 25% during 30^{o} of hip adduction, while the gluteus minimus moment arm decreased by 30%, compared to a neutral position (Henderson, Marulanda, Cheong, Temple, & Letson, 2011). Reductions in moment arm lengths of the hip musculature during a movement, and the inability to use the hip abductors optimally, diminishes the ability to produce countering moments necessary to counteract dynamic valgus.

2.4 Neuromuscular Patterns

Considering the evidence regarding the influence of trunk and hip kinematics on their ability to modulate kinetic chain mechanics, it has been postulated that neuromuscular factors are the primary mechanism of ACL injury. It has been noted that neuromuscular deficits at the trunk

during dynamic movements (such as landing and cutting) can result in compensation strategies that increase moments at the knee (Hewett et al, 2005). While it has been suggested that frontal and sagittal plane motion of the trunk and pelvis may be employed to accommodate core and hip musculature weakness (Powers, 2010).

A prospective study by Zazulak and colleagues (2007) predicted ACL injury in females with a sensitivity of 89% (91% for all knee ligamentous injuries) considering neuromuscular factors related to core stability. The single best predictor (OR 3.48) of ACL injury was maximum lateral displacement of the trunk in response to a quick release mechanism, however, active proprioceptive repositioning as well as displacement in both directions in the sagittal plane also contributed to the predictive model (Zazulak, Hewett, Reeves, Goldberg, & Cholewicki, 2007a). Furthermore, purposeful core muscular engagement (compared to no engagement) has been shown to decrease frontal plane hip displacement as well as increase knee flexion angle – thus reducing ACL injury risk (Shirey et al., 2012). The ability of the core musculature to appropriately activate in order to control trunk accelerations and maintain stability are key components in the prevention of ACL injury.

Concurrent with the abnormal kinematic findings at the hip of those who suffer knee injuries, is aberrant muscle activity directionally opposite to the kinematics. Several longitudinal studies have noted weaknesses in hip extension, external rotation and abduction in those who suffer knee injuries compared to controls (Barton at al, 2013 and Collado & Fredericson, 2010). Weaknesses in hip external rotation and abduction correspond to the abnormal injurious kinematics of increased hip internal rotation and hip adduction displayed during dynamic activities (Lee, Souza, & Powers, 2012; Powers, 2010a). Powers (2010) noted that females who relied predominantly on the hip musculature to absorb impact forces during landing had lower

knee valgus angles, a 53% reduction in the average KAM and an overall reduced absorption of energy at the knee. The main function of the gluteus medius is to stabilize the femur and pelvis in the frontal plane, therefore it plays a critical role in preventing hip adduction (Powers, 2010a). The gluteus medius has received much attention in the literature as it relates to knee injury in general; reporting that aberrant activation patterns (time of onset, offset, duration and peak magnitude), and impaired muscle function (weakness and inhibition) may be the cause of dynamic valgus and the associated large strains of the ACL (Barton et al., 2012; Ford et al., 2006; Hewett, Ford, & Hoogenboom, 2010).

While it is widely accepted that neuromuscular deficits proximally in the kinetic chain are the mechanism of ACL injury, specific investigation of the mechanism are scarce. In 2005, Hewett and his group suggested that neuromuscular deficits were the cause of ACL injury but they have failed to follow up with investigations into the specific characteristics of the deficit. Electromyogram properties such as activation level, magnitude and onset/offset times have been investigated in some muscles that are implicated in the mechanism of injury, however, a comprehensive examination of the motor control component is lacking. Additionally, many of the muscles evaluated with EMG are inappropriate choices (such as quadriceps and hamstrings) given the evidence of proximal mechanisms as opposed to local factors, or are not considered in a complete evaluation of those ‘at risk’ vs those ‘not at risk’ beyond gender comparisons (Hewett, Myer, & Ford, 2006; Hewett, Zazulak, Myer, & Ford, 2005). Given that the specific mechanism still eludes researchers, conclusions on EMG studies often resort to generally vague suggestions, postulations and hypotheses opposed to definitive conclusions.

Given the capability of neuromuscular control of the trunk to predict ACL injury, and the recruitment of core musculature to prevent the associated aberrant kinematics - implementation

of (core) neuromuscular training programs are a logical step in the attempt to prevent ACL injury. However, to date many of these programs have focused on the knee as opposed to targeting proximal areas, and in doing so fail to consider the kinetic chain as a whole and ignore the importance of the brain-behavior relationship. Additionally, many of the unsuccessful core neuromuscular training programs are poorly designed and include inappropriate exercise selection (i.e. abdominal crunches, diagonal/cross crunches, deadlifts, biceps curls, bench press, machine weights etc.) (Chappell & Limpisvasti, 2008; Cochrane et al., 2010; Jamison, McNeilan, et al., 2012). The elucidation of the specific mechanisms that drive the injurious mechanics remain unclear, hence the prevalence of poorly designed intervention programs.

Strength, plyometrics and balance are suggested to be key components of a comprehensive program aimed at reducing ACL injury risk. However, studies reporting positive outcomes widely vary in which components were included and which weren't – suggesting that some key component is unknown. While programs may incorporate all three of these components, the additive benefits or potentially countering effects remain obscured. Originally, strength programs were aimed at reducing muscle weakness and thus, in theory, allowing greater force generation to resist harmful moments. Plyometric programs were seen as directly training the movement patterns akin to dangerous dynamic activities such as jumping, landing and cutting. While balance was aimed at maintaining the control of the knee joint and superior segments. Resistance training alone has not been shown to reduce ACL injuries, plus several studies have determined that hip strength has no relationship to injurious kinematics and kinetics at the knee (Herman et al., 2008; Powers, 2010a). One can train movement patterns and attempt to engrain optimal motor patterns, but this may be limited to the task being trained. For example, you may improve an athlete's performance on a DVJ but not reduce ACL injury risk during

sport-specific movements. Therefore, in a dynamic situation with various extrinsic variables to consider, a trained movement pattern alone may not be sufficient to prevent injurious mechanics. A rationale exists for not only training the movement (which itself can be unpredictable in a sport setting), but also the ability to appropriately respond to perturbations and changes in a dynamic environment in order to enhance injury resilience.

It has been demonstrated by several research groups that decreased KAM, valgus angle, peak vGRF, hip adduction moment and hip flexion moment are observed immediately following feedback and technique coaching, indicating that landing biomechanics were independent of muscle strength (Herman et al., 2009; Laughlin et al., 2011; Mizner, Kawaguchi, & Chmielewski, 2008). It has also been noted that maximal muscular effort of the hip abductors is unnecessary during dynamic activities such as landing, and that the activation level of the muscle – opposed to strength – may be more insightful (Struminger, Lewek, Goto, Hibberd, & Blackburn, 2013). These results would suggest that more complex mechanisms are involved in the stabilization of proximal joints and their ability to avoid injurious kinematics and kinetics of the lower limbs that lead to ACL injury.

It is interesting to consider that increased muscle activation beyond that necessary for dynamic joint stability could actually have a negative effect on the stability of the joint (Brown and McGill, 2005). Thus, the non-linear relationship of muscle force and stiffness as well as activation patterns suggests that optimal stability of a joint during dynamic activity will be achieved only when multiple muscles activate appropriately to balance moments about the joint (Brown and McGill, 2005).

2.5 Stiffness and Stability for Joint Integrity

Core stability – the ability to dynamically control the trunk over the pelvis in order to allow optimal production, transfer and control of forces and motion to distal segments of the kinetic chain - is the foundation of optimal human movement (Kibler, Press, & Sciascia, 2006; Zazulak et al., 2007a). The notion of 'proximal stability for distal mobility' is essential in integrating segments of the kinetic chain during athletically demanding movements (Kibler et al., 2006; McGill, 2009). Stiffness and stability proximal to the hips allows for both the initiation of, and resistance to, motion in the lower limbs (McGill, 2009). Thus, the dynamic stability of the knee is dependent on the control of all contributing segments to the movement, starting proximally with the trunk and radiating distally through the hips.

The role of core musculature to provide stiffness and stability to the spine is well documented (Bergmark, 1989; Brown, Howarth, McGill, Marshall, & Murphy, 2005; Brown & McGill, 2005, 2009; Cholewicki & McGill, 1996; McGill, 2007; Potvin & Brown, 2005; Reeves, Narendra, & Cholewicki, 2011). The osteoligamentous spine has been measured to tolerate compressive loads as little as 90 N before buckling (Crisco & Panjabi, 1991), yet in the presence of active muscular contributions values as high as 18,000 N can be safely tolerated (Cholewicki, McGill, & Norman, 1991). The stability of a joint is dependent on the active, passive and control system's ability to contribute stiffness to the joint. The control system includes the CNS, which acts to modulate joint stiffness via surrounding muscular contributions (active system) (Panjabi, 1992). Muscle stiffness, and thus its contribution to joint stability, is a function of neural drive originating from the CNS in response to proprioceptive feedback and the instantaneous task demand constraints (McGill, 2007). In the absence of sufficient stiffness joint integrity is compromised, whereby instability can occur and structures may be unable to resist perturbations

and excessive motion, ultimately resulting in injury. Joint stiffness also acts to arrest micromovements to reduce chronic joint pain and prevent the degradation of joint structures. Providing joint stiffness via active musculature minimises energy leaks and optimises performance by providing a rigid base from which to transmit forces through the linkage and allow efficient transfer of energy.

The aforementioned evidence suggests that a comprehensive examination of the relationships between active stiffness at proximal joints (i.e. the lumbar spine and hips) and ACL injury mechanisms are warranted, yet they are lacking in the literature. Jamison et al (2013) assessed core muscle activation during cutting, however they only considered three muscles (L5 extensors, internal and external obliques), while implying stiffness via co-contraction indices. They concluded that increased co-contraction of the L5 extensors, and thus lumbar spine stiffness, was associated with an increased KAM and ACL injury risk. However, inferring the complex modulations of spine stiffness with the use of co-contraction indices and limited muscles lacks biological fidelity, which may have led to ill-informed conclusions. Additionally, an erect trunk posture has been observed in those who injure, and are at risk to injure, the ACL. Thus, the high muscle activation magnitudes of the L5 extensors accompanied with an erect posture may have also been causing unbalanced three dimensional stiffness and in doing so negatively affecting lumbar spine stability.

Ford et al (2010) calculated joint stiffness values of the ankle, knee and hip during a DVJ in order to evaluate differences between gender and maturation level, as opposed to those directly quantified as at risk. Joint stiffness was calculated via the moment-angle relationship and thus provided only an external joint stiffness measurement void of direct neurological contribution by the way of active musculature. Interestingly, hip stiffness values were markedly

less in females compared to males, while male values increased with (one year) maturation and female values did not. Contrary to the authors' hypothesis, knee joint stiffness did increase with maturation in females. While this method provides a very general measure of joint stiffness, it further supports the notion that exploration of active proximal joint stiffness should be considered when investigating ACL injury mechanisms (Ford, Myer, & Hewett, 2010).

2.6 Summary

Given the evidence presented above, a biologically robust method of investigating proximal joint stiffness at the lumbar spine and hips in their ability to avoid dynamic valgus is warranted. It is well established that known aberrant kinematic patterns and injurious kinetics are likely the result of neuromuscular deficits originating proximally in the kinetic chain, yet specific characterization of such a deficit is incomplete. Aberrant kinematics play an important role in the manifestation of large KAM, thus, observation of the whole linkage (as opposed to joints and segments in isolation) and associated muscle activation patterns are essential in order to characterise where the deficit originates and how it propagates throughout the chain in a given individual. Muscle activation patterns integration with safe or aberrant kinematics have never been documented before for the musculature of the torso during a DVJ, yet such an analysis is critical in the formation of evidence based prevention strategies. Lumbar spine kinematics are of particular interest given the postulation here that the mechanism of injury is a proximal-to-distal process, and that lumbar spine motion influence trunk position, pelvic drop, hip kinematics and dynamic valgus presentation.

3.0 Hypotheses

Given the current state of knowledge, the next questions that will propel understanding of the mechanism of ACL injury risk were systematically considered. Then the following hypotheses were generated to enable probing of possible mechanism(s).

3.1 Statement of Hypotheses

1) Differences between groups will be observed in three-dimensional lumbar spine angles.
2) Three-dimensional lumbar spine joint rotational stiffness will be greater in the 'not at risk' group.
3) Differences between groups will be observed in three-dimensional hip angles.
4) Frontal and transverse plane hip joint rotational stiffness will be greater in the 'not at risk' group.
5) Gluteus medius' contribution to joint rotational stiffness will account for the largest differences between groups in the frontal plane.
6) Gluteus maximus superior's contribution to joint rotational stiffness will account for the largest differences between groups in the transverse plane.

Greater than 10% difference between groups in variables will be considered biologically significant.

3.2 Overview and Commentary on Hypothesis Generation

The KAM threshold was used to dichotomise the participants into 'at risk' or 'not at risk' for non-contact ACL injury. It was hypothesised that these groups will differ in their three-dimensional lumbar spine and hip joint rotational stiffness values. Since this is novel work and the variability within each group is unknown, no standards or precedence's exist for biological

significance – therefore the proposed difference of 10% is arbitrary. Determining what is 'sufficient' lumbar spine stiffness is dependent on the task demands, here it is considered to be developing enough three dimensional stiffness in order to control gross trunk motion and avoid known aberrant kinematics of the trunk. Sufficient frontal and transverse plane hip stiffness will be defined as such when it is able to prevent hip adduction and internal rotation respectively, thus reducing dynamic valgus presentation during the tasks. Given the role of the gluteus medius as a frontal plane stabilizer for the pelvis it was hypothesised that the contribution of gluteus medius to frontal plane hip stiffness will be the most distinguishable difference between those at risk and those not at risk. Deficient gluteus medius activity has been implicated as a primary cause in ACL injury, and during the unilateral tasks performed in this study will be particularly important in maintaining frontal plane control of the lower limb and pelvis. Additionally, it was hypothesized that gluteus maximus superior's contribution to JRS will play a large role given its ability to stiffen in the transverse plane and its role in stabilizing the pelvis.

Note: These were the original hypotheses generated from a review of the literature. However, the novel methods employed in this work to document muscle activation, force and stiffness revealed that the same individual could differ in the mechanics of their landings. Some experienced valgus and others did not, while the KAM did not necessarily capture these differences. This changed the analysis to group landings based on whether valgus occurred or not – this is explained later as the results emerge.

4.0 Methods

4.1 Study Design

In a cross-sectional study design eighteen participants (n = 18, age: 20.7 ± 1.3 years, height: 1.64 ± 0.05 m, mass: 65.2 ± 11.0 kg) came to the Spine Biomechanics Laboratory at the University of Waterloo for a single session in which electromyography (EMG), kinematics and kinetic data were collected during a series of tasks aimed at investigating the mechanism of ACL injury.

Participants completed a 'screening' task in the form of a Drop Vertical Jump (DVJ) for which a knee abduction moment (KAM) was initially used post-collection in order to classify individuals into one of two groups as they relate to ACL injury risk, given a threshold value developed by Hewett, Myer and colleagues. Additionally, participants completed variations of the DVJ in the form of single leg landing tasks, as well as a stop jump task. The purpose of these tasks is to provide more athletically demanding challenges than the standard DVJ in order to more clearly distinguish differences in motor control and neuromuscular strategies, if any, between the two groups. Although the outcome variable is dichotomised into 'at risk' or 'not at risk', it is recognised by the researcher that sub-groups based on severity of risk and/or adopted strategies may emerge. Dependent variables will include three-dimensional lumbar spine and hip joint rotational stiffness and associated linkage kinematics. Three good trials of every task will be collected in order to acquire representative data for each participant.

4.2 Data Collection

4.2.1 Participants

Female participants were recruited from the university population, including varsity and recreational athletes from a variety of sports (soccer, basketball, volleyball, rugby, martial arts). Recruiting university athletes from these sports (in particular soccer, volleyball and basketball) is ideal since they are a subset of the population at particularly high risk for ACL injury. If an athlete is at risk of ACL injury due to lower extremity mechanics, it is possible that they have incurred a previous ACL injury (thus excluded from this study) at some point in their career. As such, some of the eligible athletes may not be at risk due to their landing mechanics – and never have been – so have never injured and would not be excluded from this study. In an attempt to ensure that females who display at risk landing behaviours are included in this study, university aged recreational athletes were also recruited.

Each participants' specific anthropometric data were measured, including trochanter width, pelvic depth and chest depth which are necessary for biomechanical modeling processes.

4.2.2 Tasks

Each task was described and demonstrated by a research assistant as well as allowing the participant practice trials before collected trials began. No details on recommended technique were provided unless the task called for it. Three trials of every task were performed in order to obtain clean data and to ensure that collected data accurately represented the natural movement of the individual for the given task constraints. If one of the research assistants observed that the task was not sufficiently performed as necessary by the participant, or that the live data was obviously aberrant (i.e. EMG silence, non-physiological peak in EMG or force plate artifact)

then additional trials were recorded in order to ensure that three ‘good’ trials were collected for every task. Note, the trials deemed necessary to re-collect were not be immediately discarded but rather will be analyzed post-collection for determination of data analysis inclusion. The order of tasks were randomised for every participant in order to mitigate any effects of movement bias or fatigue.

A one second buffer of collected data was employed before commencement and following completion of a given task, to ensure that necessary data points were available for low-pass recursive filtering techniques of both kinematic and EMG data. Padding the data with one second of additional frames is sufficient for kinematic data (Howarth & Callaghan, 2009) and allowed for stabilization of filtered EMG data points before analysis and interpretation.

Three trials of the following tasks were performed:

- Drop Vertical Jump (DVJ) (Figure 3)
- Stop Jump (Figure 4)
- Single Leg Drop (Figure 5)
- Single Leg Crossover Drop (Figure 6)

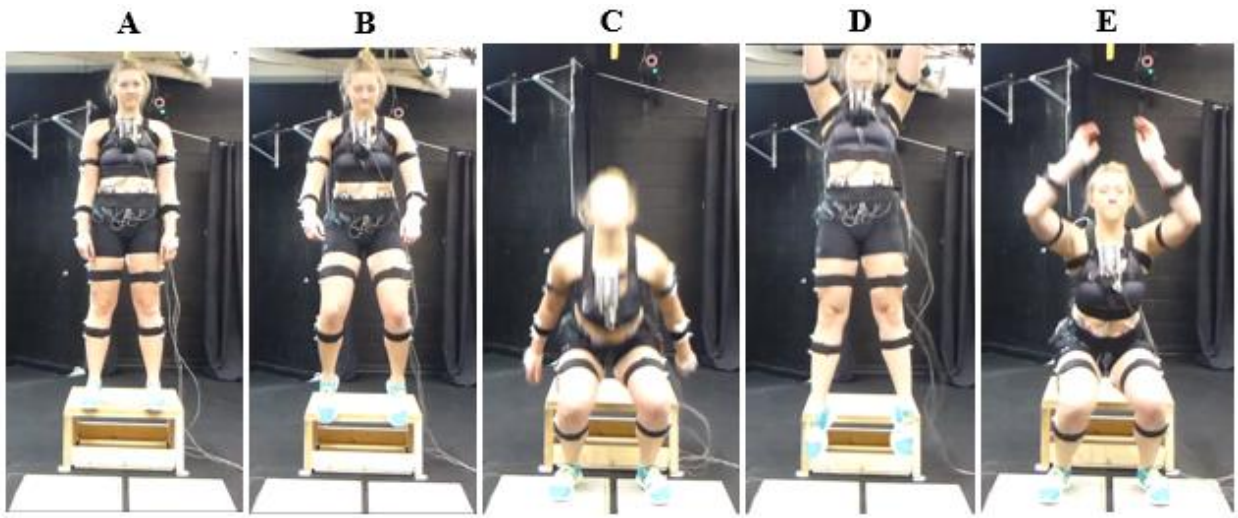

Figure 3: The stages of a standard DVJ from a 31 cm box onto two adjacent force plates. The participant begins feet shoulder width apart with the toes at the edge of the box (A). The participant initiates movement by 'dropping' both feet simultaneously off of the box (B) to each land on a force plate (C) before performing a maximal vertical jump (D) and landing back on the force plates (E).

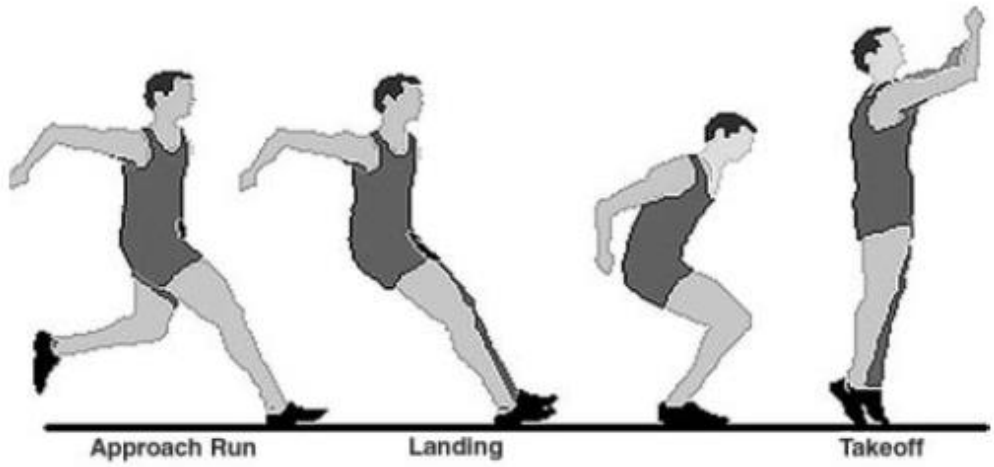

Figure 4: Stop jump task. The participant completes the approach run as fast as they can (comfortably), followed by a two-footed landing with each foot on a force plate to decelerate before initiating a countermovement jump vertically straight up and landing back on the force plates. Figure from Chappell et al 2007.

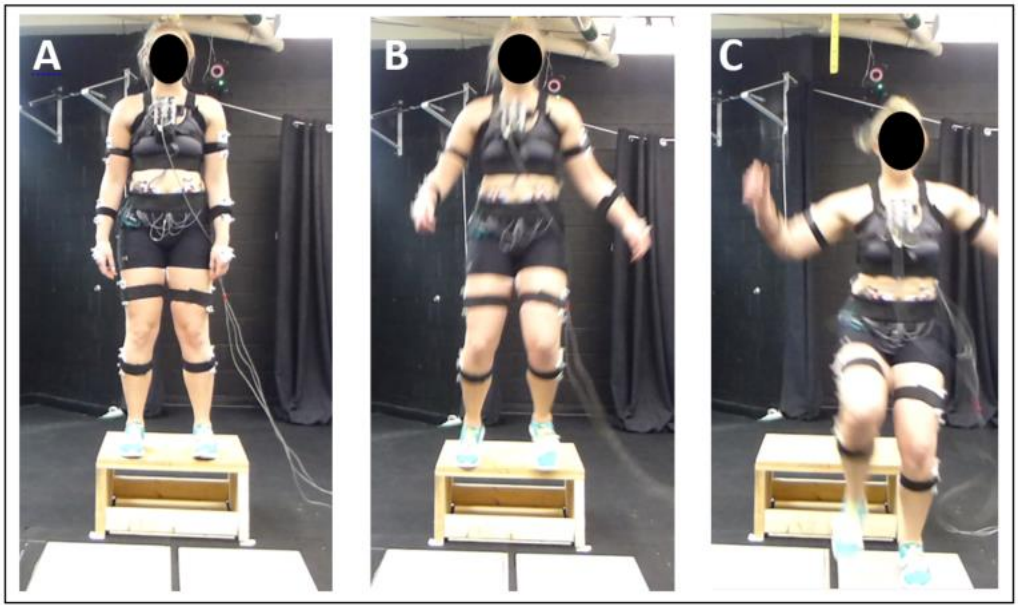

Figure 5: Single Leg Drop. The participant begins feet shoulder width apart with the toes at the edge of the box (A). The participant initiates movement by' dropping' both feet simultaneously off of the box (B). The participant lands with one foot, onto the ipsilateral force plate with the purpose of sticking the landing (C).

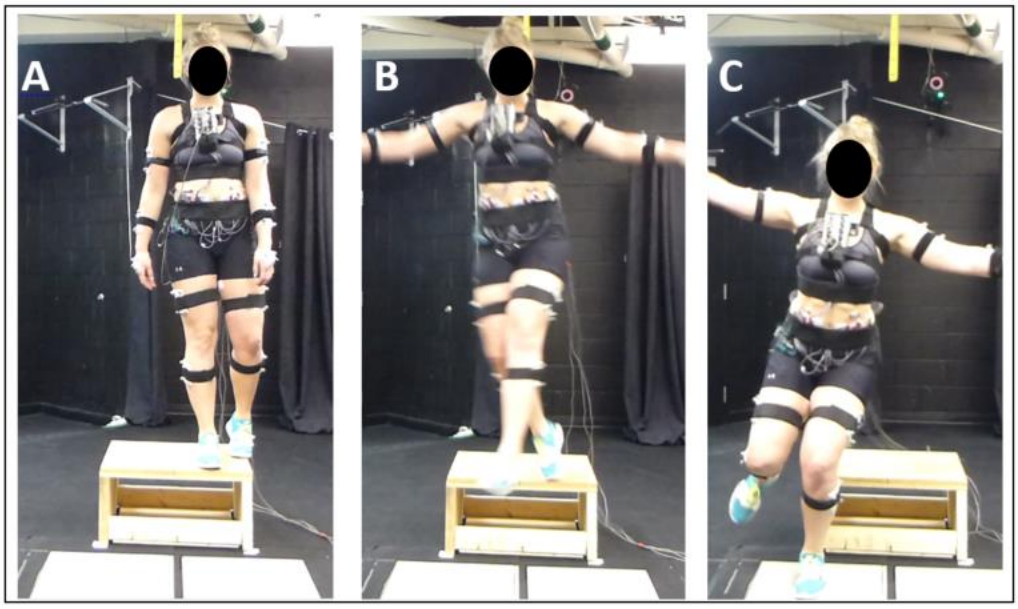

Figure 6: Single Leg Crossover Drop. For a left-footed land: The participant begins with the right foot on the left side of the box with the toes at the edge (A). The participant initiates movement by 'dropping' off of the box not stepping off (B). The participant lands with their left foot on the right force plate with the intention of sticking the landing (C).

4.2.3 Kinematics

In order to document body segment movement reflective markers were adhered to the skin with hypoallergenic tape, following standard operating procedures for the Spine Biomechanics lab, over the following landmarks bilaterally: 1st metatarsal head, 5th metatarsal head, posterior and inferior base of calcaneus, medial and lateral malleoli, medial and lateral femoral condyles, greater trochanters, lateral iliac crests, acromia, sternum and over C7. Rigid bodies were adhered to the skin with hypoallergenic tape over the following segments: feet (heel to lateral aspect), legs (halfway between lateral malleoli and lateral femoral condyle), thighs (midway between lateral femoral condyle and greater trochanter), sacrum and T12 (Figure 7). Each rigid body contained a minimum of 4 reflective markers adhered with tape arranged non-collinearly in order to track three dimensional kinematics. The VICON Nexus™ (Los Angeles, CA, USA) motion capture system was used to track the three-dimensional coordinates of the reflective markers during the various trials at a sample rate of 60 Hz.

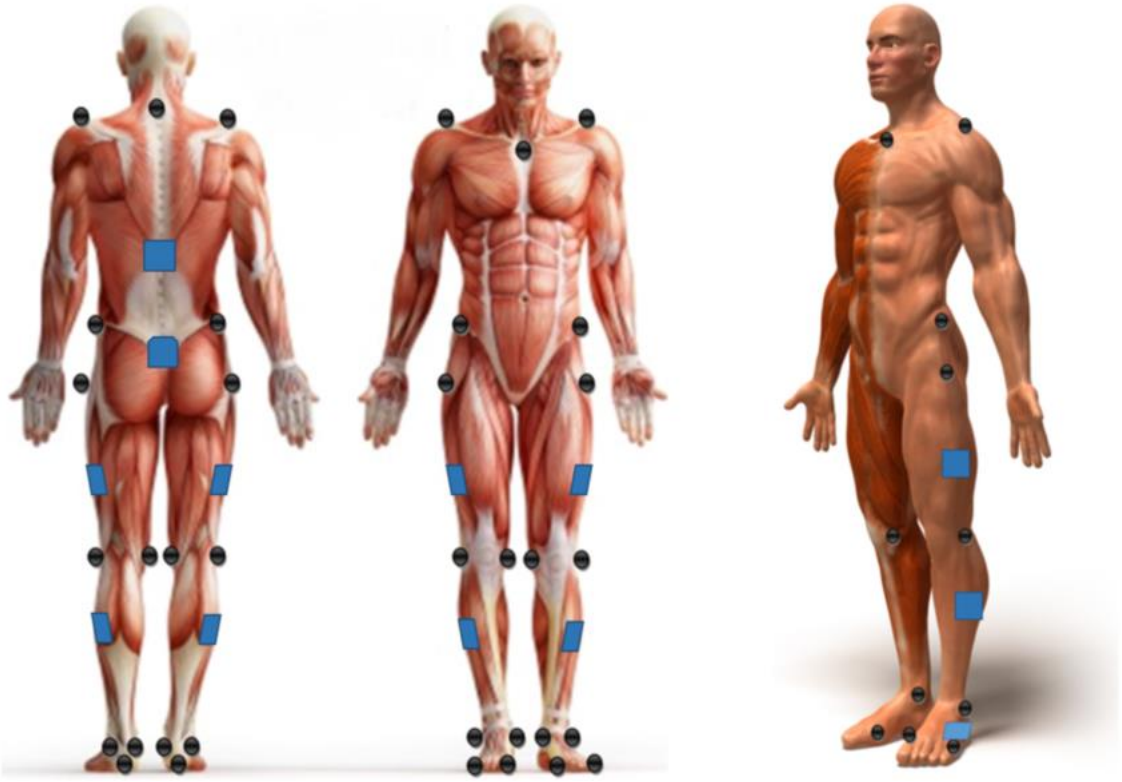

Figure 7: Motion capture individual marker and cluster placement.

4.2.4 Force Plates

Ground reaction forces (F_x, F_y, F_z) and moments (M_x, M_y, M_z) were collected using two force plates (AMTI, Watertown, Mass, USA) oriented adjacent to one another, using the VICON Nexus^{TM} (Los Angeles, CA, USA) software, sampled at a rate of 2160 Hz.

4.2.5 EMG

Twenty-four channels of EMG were collected bilaterally over the following muscles: rectus abdominis, external oblique, internal oblique, latissimus dorsi, upper (thoracic) erector spinae, lower (lumbar) erector spinae, tensor facsia latae, gluteus medius, gluteus maximus, rectus femoris, biceps femoris and adductor longus (Figure 8). Electrodes were placed in relation

to known anatomical landmarks (guided by SENIAM) while adjusting for individual morphological differences.

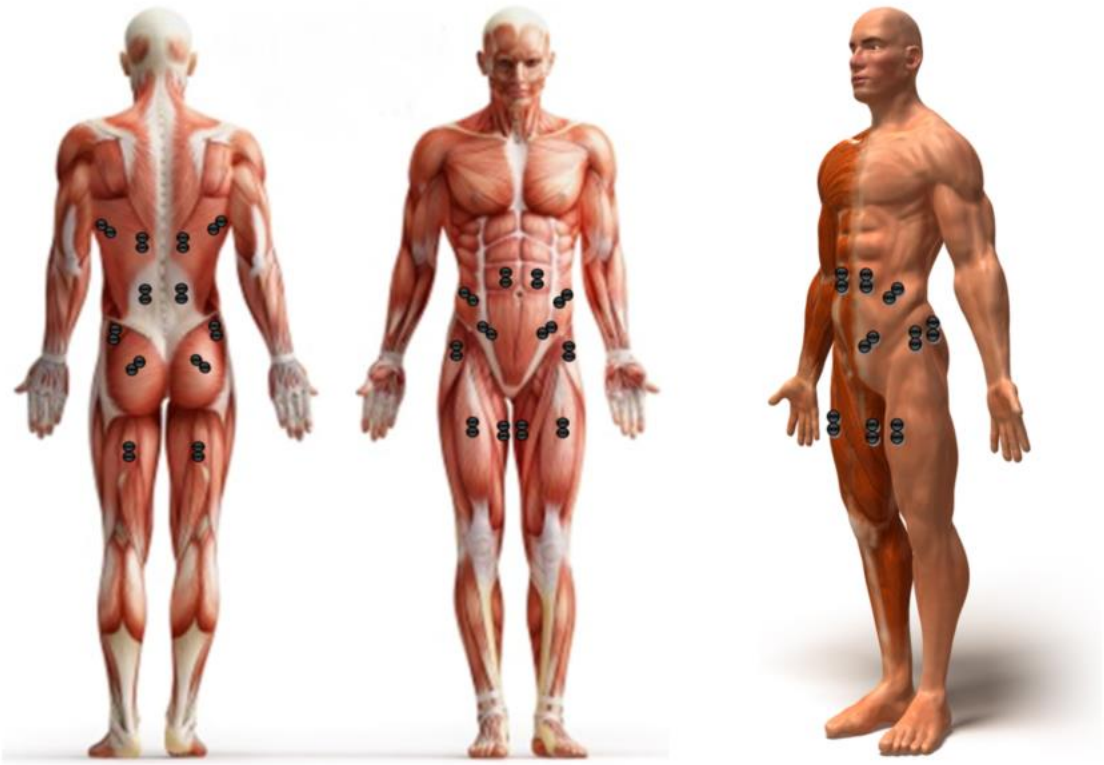

Figure 8: EMG electrode muscle placement.

Prior to electrode placement the skin was shaved, abraded with Nuprep™ abrasive skin prepping gel and then wiped with ethanol to cleanse the skin, in order to minimise skin impedance and obtain clean electromyogram signals. Ag-AgCl surface electrode pairs were positioned with an inter-electrode distance of approximately 2.5 cm and oriented in series, parallel to the direction of the muscle fibers to capture maximal common signal between the two electrodes.

Each participant performed a maximal voluntary isometric contraction (MVC) of each muscle for normalization. These normalization techniques aim to achieve maximum isometric

activation in ways that minimize the risk of injury and muscle avulsion (McGill, 1991). For the abdominal muscles (rectus abdominis, external oblique's and internal oblique's), participants adopted a sit up posture with the torso at approximately 45^{o} to the horizontal with the knees and hips flexed at 90^{o}. Manually braced by a research assistant, the participant was instructed to produce a maximal isometric flexion moment followed sequentially by a right and left lateral bend moment and a right and left axial twist moment. Latissimus dorsi MVC was performed with the participants standing and arm abducted to 90^{o} and the elbow flexed to 90^{o}, with the participants' arm braced by a research assistant the participant attempted to drive their arm down, and externally rotate with maximal effort. For the erector spinae musculature and gluteus maximus (it was found that higher values were obtained for the gluteus maximus using this MVC) a resisted maximal extension in the Biering-Sorensen position was performed for normalization, aided by scapular centration and a gluteal squeeze with hip extension. Gluteus medius and tensor facsia latae MVC trials were performed concurrently, with the participant in a side lying position attempting hip abduction (i.e. a lateral straight leg raise) against manual resistance. MVC for the rectus femoris involved the participant sitting on a therapy bed with their legs hanging over the edge and performing resisted knee extension and hip flexion moments. For the biceps femoris the participant lay prone on a therapy bed, flexed their knee to 90^{o} and with the research assistant bracing the leg the participant performed maximal isometric knee flexion. Adductor longus MVC's was performed with the subject supine, knees flexed to 45^{o} and resistance provided on the medial side of the knees as the participant attempted hip adduction.

The EMG signals were amplified (Bortec Biomedical, Calgary, Canada; Bandwidth = 10 – 1000 Hz, CMRR = 115 dB at 60 Hz, Input Impedance = 10 Giga Ω) and analog-to-digital

converted with a 16-bit converter at a sample rate of 2160Hz using the VICON Nexus™ (Los Angeles, CA, USA) system software.

4.3 Data Processing

Processing of kinematic, kinetic and EMG data will be described in detail in the following divisions of the *Data Processing* section.

4.3.1 Kinematics

Kinematic data for each task were examined on a frame-to-frame basis for marker orientation, trajectory veracity and examination of any missing data points. Given that three markers are necessary for tracking three-dimensional movement, additional fourth (and fifth) markers created built-in redundancy. In the event that a marker was missing data for greater than 200ms in duration, it was not used in the three-dimensional tracking of the rigid body for that duration of time. Missing data points less than 200 ms in duration were interpolated using a cubic spline in VICON Nexus™ (Los Angeles, CA, USA) as per recommendations by Howarth and Callaghan (2010).

Visual 3D software (C-Motion, Rockville, MD) was used to calculate hip functional joint centres and functional knee joint centres as per methods described by Schwartz & Rozumalski (2005) and Begon, Monnet, & Lacouture (2007). This method of determining joint centres is preferred over palpation techniques since it is more objective and inter/intra-rater reliability is not of concern. Briefly, the functional joint centre is calculated considering the motion of the proximal and distal segments (relative to the joint of interest) by computing the axis of rotation for every segment orientation observed. The most likely joint centre is determined via the

intersection of all computed axes of rotation (Schwartz & Rozumalski, 2005). For the hip, the participant was required to perform clockwise and counter-clockwise circumduction for 10 cycles in each direction. The functional knee joint centre required that the participant perform 10 cycles of full knee flexion and extension.

Three-dimensional joint kinematics were calculated in Visual 3D for the spine, hips and knees using rigid body segment clusters and known anatomical landmarks to form orthopaedic angles from Euler rotation sequences of the following order: (i) flexion/extension (sagittal plane), (ii) abduction/adduction (frontal plane), and (iii) axial rotation of the spine, internal/external rotation of hip and knee (transverse plane). The relative orientation of the trunk will be expressed with respect to the immovable pelvis, hip joint angles defined as the orientation of the thigh relative to the pelvis, and knee joint angles will be defined as the orientation of the shank with respect to the thigh.

Kinematic data were low pass second order Butterworth filtered (dual pass) with a cut-off frequency of 6 Hz (effectively creating a fourth order zero lag filter). Given that the high end frequency range of human movement is 6-10 Hz, using a cut-off frequency of 6 Hz is more than adequate to capture the movements being analyzed, and is more ideal for signal-to-noise purposes of human movement.

4.3.2 Kinetics

Visual 3D software (C-Motion, Rockville, MD) was used to employ a bottom-up inverse dynamics approach to calculate instantaneous reaction forces and internal joint moments during phases of a given task in which the foot (or feet) were in contact with the force plate(s). Kinetic data were low pass second order Butterworth filtered (dual pass) with a cut-off frequency of 12 Hz (effectively creating a fourth order zero lag filter).

4.3.3 Knee Abduction Moment

This work used 9 Hz and 50 Hz cut-offs for kinematic and kinetic data respectively, only to calculate the KAM during the standard DVJ so as to classify participants as at risk or not at risk. These were used since the original work in which the peak KAM threshold was developed using these frequency cut-offs (Hewett, Myer, et al., 2005; Roewer, Ford, Myer, & Hewett, 2014). Specifically, the peak KAM during the DVJ was calculated from initial contact (IC), defined as such when > 10 N is recorded on the force plate, until toe-off (TO).

4.3.4 Hip-Ankle Plane for Medial Knee Displacement

A body-fixed hip-ankle plane was created using Visual 3D software (Version 5, C-Motion, Rockville, MD) in order to calculate frontal plane knee displacement throughout the duration of each task (Figure 9). The functional joint centre of the hip, ankle joint centre (midpoint between the medial and lateral malleoli markers, and centre of the foot (midpoint between the first and fifth metatarsals) comprised the hip-ankle plane. Frontal plane knee displacement was calculated as the perpendicular distance between the functional knee joint centre and the hip-ankle plane. Medial knee displacement represents a valgus posture of the lower extremity, created by hip adduction and knee abduction.

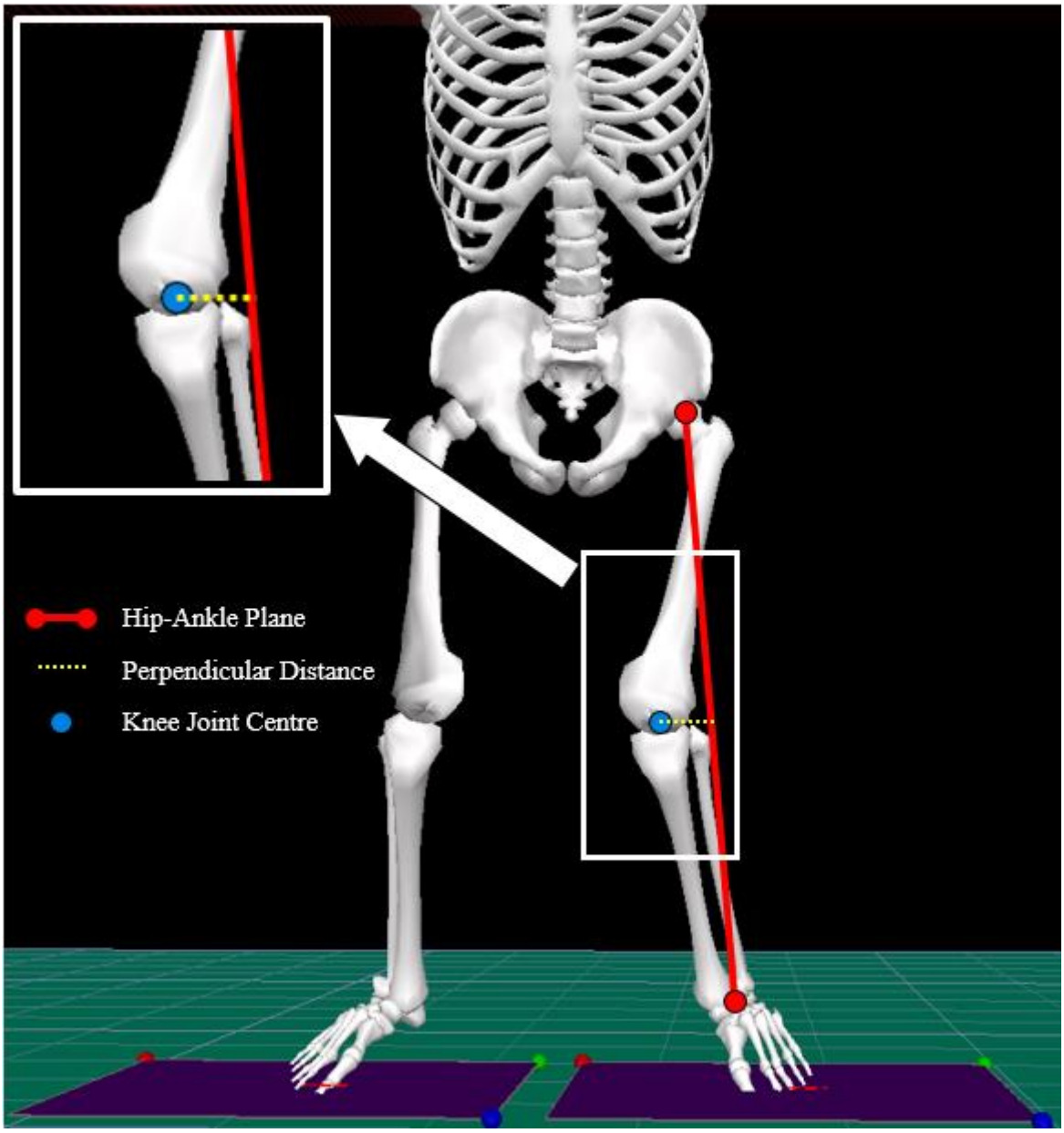

Figure 9: Visual representation of the body-fixed hip-ankle plane created as a measure of dynamic valgus. The perpendicular distance from the functional knee joint centre to the plane allowed for quantification of medial knee displacement.

The peak medial knee displacement of all trials of a given task were recorded before calculating the median value. An exclusion range of ± 20 % around the median was defined, and provided the thresholds to determine high or low valgus status for the given knee (Figure 10). On

the single leg landing tasks (SLD and SLCD) only the knee of the landing limb was of interest, thus two groups were defined as ‘High Valgus’ and ‘Low Valgus’ for these tasks. Since the DVJ and SJ are double limb tasks, each knee’s valgus status was independently defined, this would serve to split the groups into ‘High Valgus’ and ‘Low Valgus’ for the analysis of ipsilateral hip and knee variables. However, for the analysis of lumbar spine variables the trials were split into three groups: ‘Bilateral Valgus’, ‘Unilateral Valgus’, or ‘No Valgus’. ‘Bilateral Valgus’ comprised trials were both knees had been classified as high valgus, ‘Unilateral Valgus’ was when either one of the left or right knee was defined as high valgus, and finally ‘No Valgus’ was when neither the left or right were defined as high valgus.

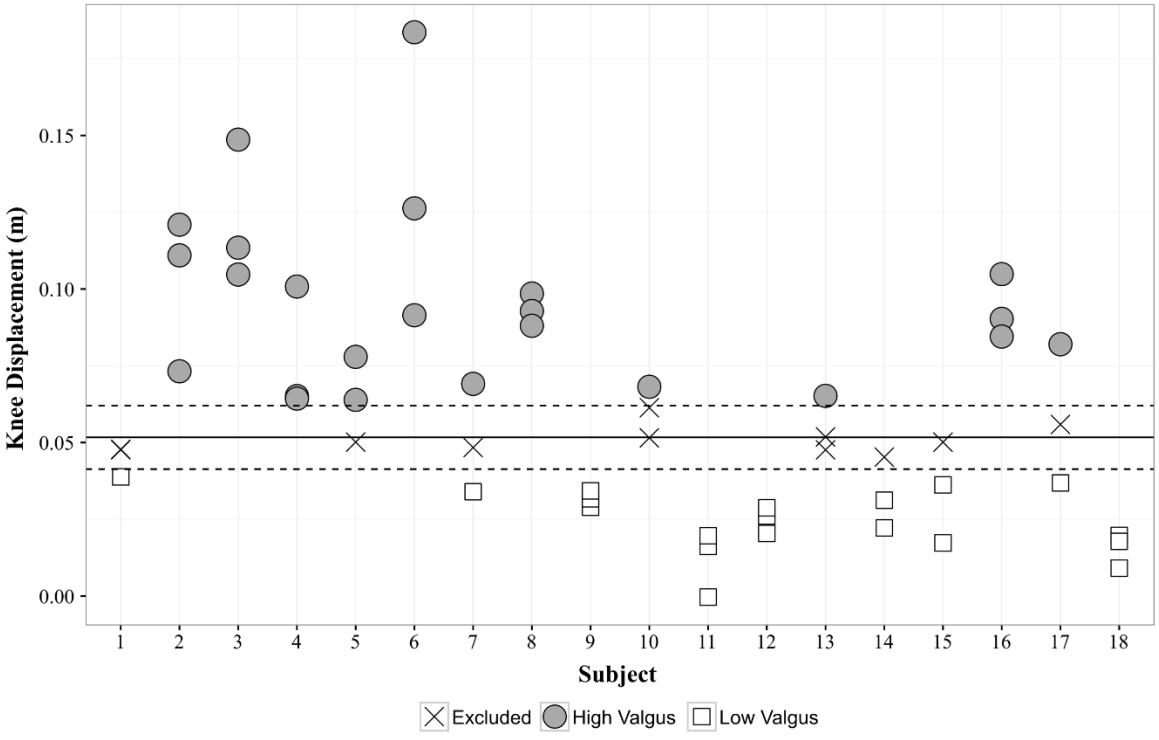

Figure 10: An example of how the peak medial knee displacement of a given knee for all trials of a task where used to dichotomize participants. Median value (solid line). Upper and lower limits of exclusion range (dashed lines). Note: the dichotomization of trials for each knee are presented in the results section at the beginning of the given task’s sub-section.

4.3.5 Electromyography

EMG data was digitally band pass filtered between 30 and 500 Hz. These cut-off values were used given the majority of the frequency content of surface electrodes is between 10 and 500 Hz, and recommendations to use a high pass filter of 30 Hz in order to eliminate ECG contamination (Drake & Callaghan, 2006).

The low and high pass filter used in the band pass were second order zero phase lag (dual pass) Butterworth filters. Steps in digitally processing the raw EMG included: removing the DC bias, full wave rectification and linear envelope (LE) using a low-pass Butterworth filter with a cut-off frequency of 2.5 Hz (after Brereton & McGill, 1998) before normalising the filtered LE signal to the maximum muscle activation elicited during the MVC for the given muscle. EMG data was then down sampled in order to be time synchronised with kinematic data sampled at 60 Hz.

4.3.6 RVC and Common Gain Factor

A reference voluntary contraction (RVC) was collected for the lumbar spine, and each hip, in order to account for discrepancies in model prediction of the joint moment and maintain mathematical validity. The procedure used in this work for calculating the common gain factor, often described as 'balancing the moments', aims to minimize the total sum of squared differences between the joint moment calculated using the linked-segment model (M_{LSM}) and that of the anatomically detailed EMG driven model (M_{EMG}) using a least squares difference approach (Equation 1). Specifically, a common gain factor (G) was calculated for each joint of interest of a given subject, to be applied to estimates of muscle force and stiffness. Applying a common gain to each muscle about a joint allows their relative contribution to the joint moment and joint rotational stiffness to be maintained given their myoelectric profiles. In this way the

model was adjusted (linearly) to fit to each participant, in order to account for between-subject differences in factors that influence the EMG-to-force transformations, such as muscle morphology (Cholewicki, McGill, & Norman, 1995).

$$\sum_{f=1}^{Frames} (M_{LSM} - G \cdot M_{EMG})^2 = min$$

The RVC for the lumbar spine involved the participant standing upright holding a 20 lbs plate directly in front of their body (the mass was decreased if necessary) in both hands with full elbow extension and shoulders flexed to approximately 90º. This creates a large moment about L4/L5 in the sagittal plane and requires substantial EMG activity. The resultant moment (Euclidean Norm of all three axes) was used in balancing the moments to account for the other planes. For the hips, a similar RVC was used but now the participants were in a semi-squat position before pushing the weight out in front of them. Similarly, this challenged predominantly the flexion/extension moment at the hip and thus the moment in this axis was used in balancing the moments.

4.3.7 Lumbar Spine Joint Rotational Stiffness

Lumbar spine joint rotational stiffness was quantified using a three-dimensional anatomically detailed lumbar spine model (See Figure 11) (including 98 laminae of muscle and a passive lumped parameter stiffness element) that is sensitive to individual movement and motor control strategies (Cholewicki & McGill, 1996). Briefly, normalised EMG data and lumbar spine generalised coordinates are input to the model. A distribution-moment model (DM model) is utilised to process the EMG and output muscle force and stiffness profiles with consideration of length and velocity (after Cholewicki & McGill, 1996; Ma & Zahalak, 1991). The stability analysis calculates the potential energy of the system utilizing the elastic energy of linear and

torsional springs (Figure 12). The resulting 18 degree-of-freedom (DoF) lumbar spine model produces an 18x18 symmetric square Hessian matrix of the second order partial derivatives of the potential energy function with respect to general displacements along each DoF (Cashaback & Potvin, 2012; Howarth, 2006). The potential energy function is a summation of the contributions from the muscle fascicles (linear springs), passive tissues (torsional springs), and that from any externally applied loads. Each diagonal element of the Hessian matrix represents the joint rotational stiffness about a particular axis of a joint in the lumbar spine, of interest in this work were the three axes about L4/L5 since this is where the most anatomical detail is contained in the model. For the purposes of this work the analysis stops here so as that the continuous measure of joint rotational stiffness can be examined with respect to medial knee displacement. However, the Hessian can be further processed to compute a stability index that represents the stability of the lumbar spine. Two main methods exist in which this can be done, either by taking the determinant of the Hessian matrix, or, by diagonalizing the Hessian to compute the eigenvalues and eigenvectors. Either method results in a determination that the lumbar spine has potential to experience unstable behaviour or not.

It is assumed that passive elastic energy storage from passive joint tissues can be neglected since the spine will not approach end range. However, muscle passive and active stiffness is accounted for in the DM approach. The DM approach will allow for analysis of individual muscle's stiffness values and their contribution to global joint stiffness. Summation of all muscle stiffness values (of those muscles surrounding the lumbar spine) provide an active musculature contribution to joint stiffness. However, it should be noted that the summed muscle stiffness's from the DM model are void of the generalised coordinates used in the JRS calculations and thus these values do not consider the geometric stiffness contributions.

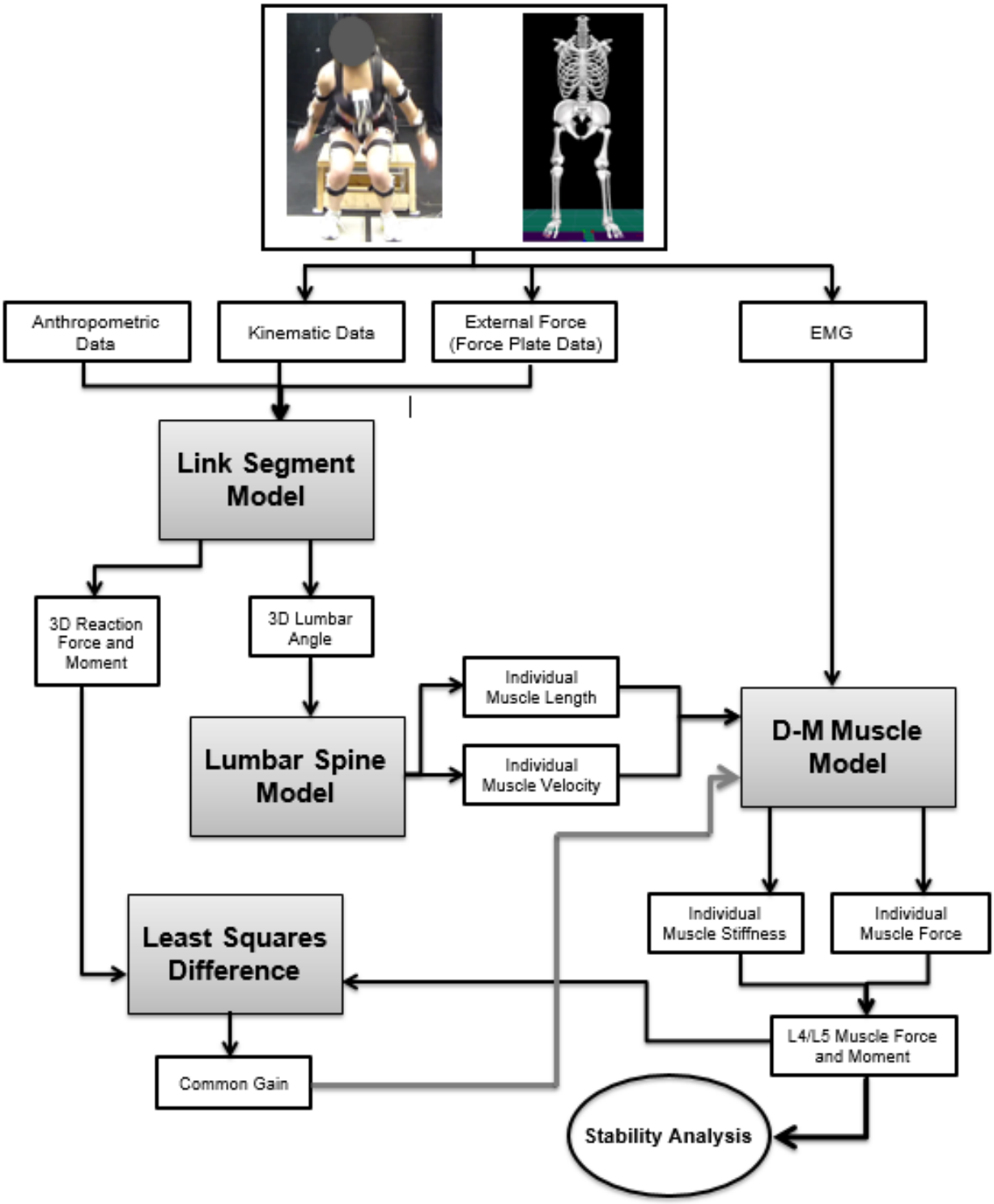

Figure 11: An overview of the lumbar spine model processes are presented to demonstrate the inputs, processing and outputs of each subcomponent as well as the interactions between them to comprise the complete model.

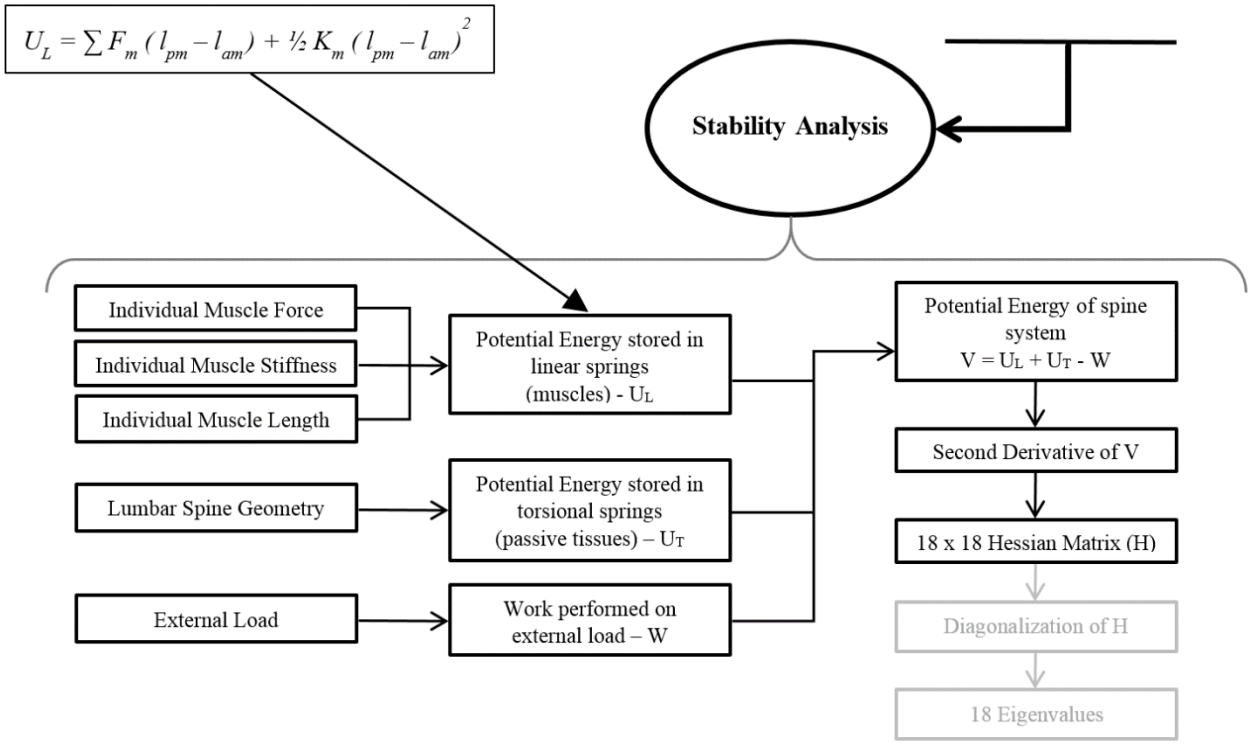

Figure 12: An overview of the Stability Analysis run following the Lumbar Spine Model. Note: for this work the values of interest were the JRS values of L4/L5 contained in the Hessian Matrix (H). Thus, the diagonalization of H to obtain stability was not necessary.

Work by Ikeda (2011) using the same Lumbar Spine Model and procedures as described above investigated each muscle's stability contribution along each DOF at L4/L5. In the simulation work Ikeda set the lumbar spine to neutral and turned all muscles on to 50% MVC, except the muscle of interest which would be turned off completely. This knockout approach allowed for evaluation of a single muscle's contribution to stability in the given DOF. The change in eigenvalues were then assessed, and if it was a > 10 % decrease the muscle of interest was deemed to be a significant stiffener/stabilizer in that DOF.

Using the results from Ikeda (2011), this work summed muscles' stiffness (from the DM) whose contribution were deemed biologically significant in a given plane of stiffness. This resulted in five planes: flexion/extension, right lateral bend, left lateral bend, right axial twist and left axial twist. The muscles contained in these planes can be found below. Note, when right and left planes exist the same muscle fascicles were included in each side but for the ipsilateral side of interest (i.e. right lateral bend included right external oblique, and left lateral bend included left external oblique). Muscles were able to be included in multiple planes since their ability to stiffen in a given DOF was of interest.

Flexion Extension Plane:

- Pars Lumborum
- Longissimus Thoracis
- Multifidus
- External Oblique

Lateral Bend Plane:

- External Oblique
- Internal Oblique
- Iliocostalis
- Latissimus Dorsi
- Pars Lumborum
- Psoas

Axial Twist Plane:

- External Oblique
- Internal Oblique
- Iliocostalis

In addition to examining the summed muscle stiffness values by planes as described above, muscle stiffness's were also summed based on quadrants. Each quadrant included muscles given their anatomical location with respect to the lumbar spine. Thus, quadrants consisted of right anterior, left anterior, right posterior and left posterior.

Posterior Quadrant:

- Iliocostalis
- Longissimus Thoracis
- Multifidus
- Quadratus Lumborum
- Latissimus Dorsi

Anterior Quadrant:

- Rectus Abdominis
- Internal Oblique
- External Oblique

Initial lumbar spine JRS and muscle stiffness data contained non-physiological noise, likely artifact from the calculation of instantaneous muscle velocity within the DM model. The data were low pass second order Butterworth filtered (dual pass) at a cut-off frequency of 12 Hz. This filtering process mirrored that of the kinetic data, and allowed for removal of noise while maintaining the shape and magnitude of the pre-filtered data (Appendix C).

4.3.8 Hip Joint Rotational Stiffness

In order to calculate hip stiffness about three axes, joint rotational stiffness (JRS) equations developed by Potvin & Brown (2005) will be used utilizing anatomical data from the Twente Lower Limb Model reported by Klein Horsman et al. (2007). An overview of the modelling processes can be seen in Figure 13; they are similar to that used at the lumbar spine with notable differences in the calculation of muscle force and stiffness, as well as the computation of JRS.

Use of the JRS equation requires input of:

1. Origin and insertion coordinates of muscles relative to the hip joint centre
2. Muscle force
3. Muscle stiffness

Potvin & Brown (2005) note that the JRS calculations assume one degree of freedom for one joint, however the equations may be modified appropriately to calculate 3D stiffness and stability values, as well as to consider multiple joints. The stability of a single degree of freedom system is equivalent to its rotational stiffness (Brown & Potvin, 2007a; Potvin & Brown, 2005). This approach does not include a passive component beyond that of muscle. Given that extreme joint angles towards end range are unlikely in the tasks being performed, it is assumed that passive contributions to stiffness are minimal and are thus excluded from this analysis. Active stiffness values are most sensitive to changes in muscle length and moment arm values, thus accuracy in muscle geometry is paramount in obtaining biologically meaningful results (Potvin & Brown, 2005).

The JRS equation:

$$JRS_x = F\left[\frac{A_Y B_Y + A_Z B_Z - r_x^2}{l} + \frac{q r_x^2}{L}\right]$$

Where,

JRS_x = the rotational stiffness contribution of a muscle about the x-axis of the hip joint

F = force of a particular muscle "m" considering muscle activation, stress, PCSA as well as force-length (active and passive) and force-velocity correction factors

l = 3D length of the muscle vector that crosses the hip joint

L = full 3D length of the muscle

r = 3D muscle moment arm

A_X, A_Y, A_Z = origin coordinates with respect to hip joint centre at (0,0,0) m

B_X, B_Y, B_Z = insertion (or initial node) coordinates with respect to hip joint centre at (0,0,0) m

q = muscle stiffness coefficient (proportionality constant) relating muscle force and length to stiffness

A full list of the necessary equations to derive JRS can be found in Appendix A.

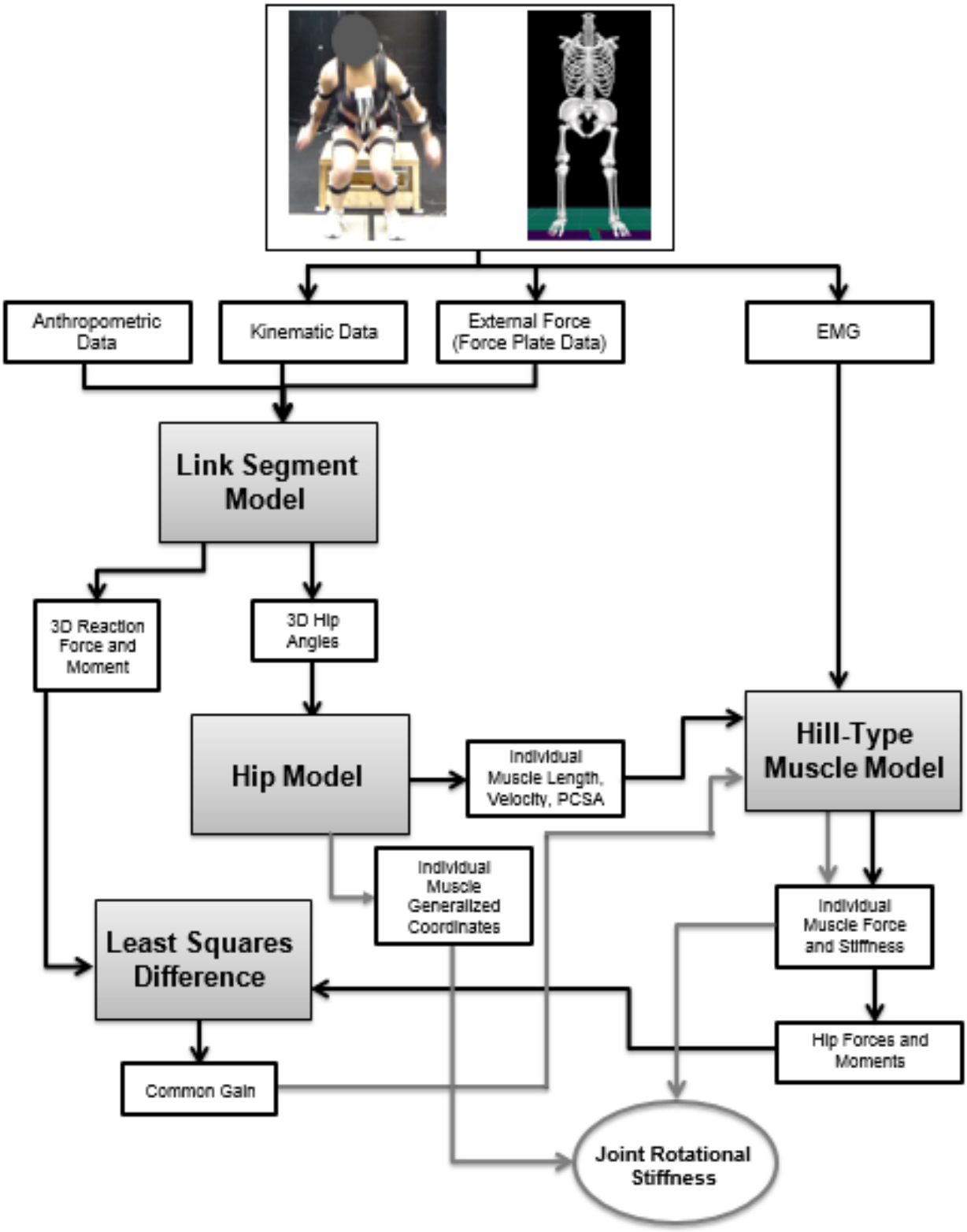

Figure 13: An overview of the procedures in collecting and processing data to allow for calculation of hip joint rotational stiffness.

1) Origin and Insertion Coordinates

Origin and insertion coordinates of all relevant hip musculature (65 muscle fascicles per hip), including abductors (Table 1) and adductors (Table 2), contributing to hip JRS will be taken from the work of Klein-Horsman and colleagues who described, in detail, muscle attachment coordinates with respect to the hip joint centre in their 'Twente Lower Limb Model' (Klein Horsman et al, 2007). The right hip joint centre was set to the origin of the local coordinate system (LCS) of the pelvis as per ISB recommendations (Figure 14), and thus all muscle origin and insertion coordinates are represented in this LCS (Wu et al., 2002). Muscle attachment sites represented in the LCS of the right hip are able to be applied to a LCS of the left hip in which the polarity of the z-axis values change. Muscles are split into anatomically and functionally relevant 'muscle parts' (i.e. fiber groupings) and within each 'part' a number of elements are used to model the muscle most accurately. The muscle geometry, joint kinematics and muscle contraction parameters described in the work by Klein Horsman and colleagues were developed with the purpose of implementation into biomechanical models. The data set has been adopted by many research groups including the OpenSim London Lower Limb Model developed by Modenese et al (2011) due to its mechanical suitability for biomechanical modeling.

Table 1: Origin and insertion coordinates of hip abductor muscles. Adapted from Horsman et al. (2007).

Muscle (part)	Elem. #	Origin					Insert.				
		X(cm)	Y(cm)	Z(cm)	Segm.	e(cm)	X(cm)	Y(cm)	Z(cm)	Segm	e(cm)
Glut. max. (sup.)	1	-7.91	7.77	-1.57	Pelvis	0.32	-4.04	5.70	7.47	Femur	0.28
	2	-8.98	5.51	-3.46	Pelvis		-4.31	2.63	7.74	Femur	
	3	-9.64	2.73	-5.01	Pelvis		-4.73	-0.44	7.99	Femur	
	4	-9.13	8.91	-2.68	Pelvis		-2.40	5.45	7.74	Femur	
	5	-10.33	6.77	-4.69	Pelvis		-2.60	2.37	8.02	Femur	
	6	-10.94	3.94	-6.19	Pelvis		-3.09	-0.69	8.26	Femur	
Glut. max. (inf.)	1	-10.74	-0.83	-7.52	Pelvis	0.25	-5.61	-7.16	4.07	Femur	0.37
	2	-9.87	-1.49	-7.31	Pelvis		-5.07	-8.47	3.75	Femur	
	3	-9.05	-2.56	-7.35	Pelvis		-3.66	-10.78	3.38	Femur	
	4	-10.25	-0.16	-6.86	Pelvis		-5.61	-7.16	4.07	Femur	
	5	-9.38	-0.82	-6.65	Pelvis		-5.07	-8.47	3.75	Femur	
	6	-8.65	-2.00	-6.80	Pelvis		-3.66	-10.78	3.38	Femur	
Glut. med. (ant.)	1	0.40	9.48	4.46	Pelvis	0.19	-3.03	-0.25	5.90	Femur	0.19
	2	1.43	9.03	4.56	Pelvis		-2.25	-0.44	6.19	Femur	
	3	2.49	8.19	4.26	Pelvis		-1.53	-0.54	6.42	Femur	
	4	0.93	9.95	5.22	Pelvis		-3.36	-1.09	6.20	Femur	
	5	1.80	9.36	5.09	Pelvis		-2.68	-1.50	6.56	Femur	
	6	2.81	8.47	4.72	Pelvis		-1.96	-1.60	6.79	Femur	
Glut. med. (post.)	1	-3.88	11.87	2.51	Pelvis	0.39	-3.85	0.88	4.50	Femur	0.04
	2	-6.02	10.15	-0.41	Pelvis		-4.01	0.86	3.97	Femur	
	3	-6.82	7.21	-2.31	Pelvis		-4.24	0.76	3.62	Femur	
	4	-4.81	13.46	2.07	Pelvis		-3.85	0.88	4.50	Femur	
	5	-7.34	12.41	-1.03	Pelvis		-4.51	0.39	4.66	Femur	
	6	-8.41	9.93	-3.06	Pelvis		-4.76	0.26	4.34	Femur	
Glut. min. (ant.)	1	-0.08	7.89	3.31	Pelvis	0.42	-1.50	-2.27	6.16	Femur	0.65
Glut. min. (mid.)	1	-2.26	7.55	1.73	Pelvis		-1.50	-2.27	6.16	Femur	
Glut. min. (post.)	1	-4.03	6.51	0.07	Pelvis		-1.50	-2.27	6.16	Femur	
Tensor fasc. latae.	1	2.83	7.99	4.76	Pelvis	0.32	4.68	-38.51	5.40	Tibia	0.40
	2	2.37	9.01	5.13	Pelvis		4.68	-38.51	5.40	Tibia	

Table 2: Origin and insertion coordinates of hip adductor muscles. Adapted from Horsman et al. (2007).

Muscle (part)	Elem. #	Origin					Insert.				
		X(cm)	Y(cm)	Z(cm)	Segm.	e(cm)	X(cm)	Y(cm)	Z(cm)	Segm	e(cm)
Add. brev. (prox.)	1	4.62	-1.30	-6.92	Pelvis	0.06	-1.85	-8.34	1.81	Femur	0.08
	2	5.07	-1.32	-7.12	Pelvis		-1.32	-9.52	1.92	Femur	
Add. brev. (mid.)	3	4.57	-1.82	-7.61	Pelvis		-0.96	-10.75	1.99	Femur	
	4	4.93	-1.84	-7.78	Pelvis		-0.68	-12.02	2.01	Femur	
Add. brev. (dist.)	5	3.86	-2.57	-8.34	Pelvis		-0.39	-13.28	1.97	Femur	
	6	4.09	-2.58	-8.45	Pelvis		0.02	-14.52	1.87	Femur	
Add. long.	1	5.25	-0.92	-6.64	Pelvis	0.03	1.54	-17.44	1.68	Femur	0.07
	2	5.44	-1.16	-6.89	Pelvis		1.84	-18.64	1.52	Femur	
	3	5.57	-1.37	-7.19	Pelvis		2.16	-19.86	1.44	Femur	
	4	5.63	-1.56	-7.51	Pelvis		2.49	-21.09	1.39	Femur	
	5	5.61	-1.73	-7.85	Pelvis		2.80	-22.31	1.29	Femur	
	6	5.50	-1.88	-8.20	Pelvis		3.07	-23.52	1.10	Femur	
Add. magn. (dist.)	1	-2.10	-7.10	-4.85	Pelvis	0.35	5.66	-36.31	-2.54	Tibia	0.38
	2	-1.51	-6.71	-5.57	Pelvis		5.66	-36.31	-2.54	Tibia	
	3	0.21	-5.78	-7.03	Pelvis		5.66	-36.31	-2.54	Tibia	
Add. magn. (mid.)	1	-2.79	-6.90	-4.94	Pelvis	0.10	1.82	-19.92	1.43	Femur	0.11
	2	-2.50	-6.68	-4.53	Pelvis		1.82	-19.92	1.43	Femur	
	3	-2.12	-6.60	-5.53	Pelvis		2.65	-23.01	0.99	Femur	
	4	-1.87	-6.42	-5.18	Pelvis		2.65	-23.01	0.99	Femur	
	5	-1.25	-6.21	-6.24	Pelvis		3.41	-26.12	0.90	Femur	
	6	-1.06	-6.07	-5.98	Pelvis		3.41	-26.12	0.90	Femur	
Add. magn.(prox.)	1	1.86	-4.50	-7.74	Pelvis	0.12	0.03	-10.75	1.54	Femur	0.19
	2	0.39	-5.33	-6.76	Pelvis		0.55	-12.77	1.52	Femur	
	3	1.13	-4.92	-7.25	Pelvis		1.07	-14.80	1.50	Femur	
	4	1.86	-4.50	-7.74	Pelvis		1.58	-16.82	1.48	Femur	

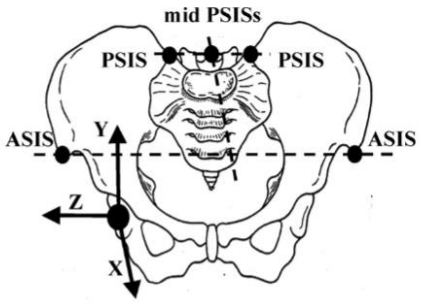

Figure 14: Local coordinate system of the pelvis in which all muscle origin and insertion coordinates are defined (Horsman et al., 2007; Wu et al., 2002).

2) Muscle Force

Instantaneous muscle force (for each muscle) were calculated using a Hill-type muscle model. Normalised EMG corrected for length, velocity and passive tissue were calculated via the following equations used by McGill & Norman (1986) which can be found in Appendix B:

$$\mathbf{F_m = G\left[\left(\frac{EMG}{EMG_{max}}\right)(P_0)(\Omega)(\delta) + F_{PEC}\right]}$$

Where,

F_m = Muscle force (N)

G = Error term or gain

$\frac{EMG}{EMG_{max}}$ = Normalised EMG amplitude

P_0 = Maximum isometric force (N)

Ω = Coefficient for force-velocity correction

δ = Coefficient for force-length correction

F_{PEC} = Force due to the passive elastic component

Muscle characteristics (PCSA, L_o, pennation angle) required in the hip muscle force calculations were taken from the same data set by Klein Horsman and colleagues from which muscle coordinates were taken (Table 3) (Klein Horsman et al., 2007). Note that all muscle element lines of interest at the hip joint are modelled as straight ('S') or multiple straight elements using via points ('VP') and thus none of the elements being used are modelled to curve around body contours. Rather, a given muscle (or muscle compartment) is broken into multiple straight elements which are able to collectively represent the mechanical nature of the muscle.

Table 3: Hip muscle characteristics from the Twente Lower Limb Model by Klein Horsman et al (2007).

Muscle	Origo	Ins.	# Elem.	S, BC or VP	PCSA (cm^2)	L_{opt} (cm)	L_{ten} (cm)	Mass (g)	Pen. ang. (°)
Add. brev. (prox.)	Surf.	Line (3)	6	S	3.8	9.5	0	38.3	0
Add. brev. (mid)				S	3.5	10.4	0	38.3	0
Add. brev. (dist)				S	3.2	11.2	0	38.3	0
Add. long.	Line (3)	Line (3)	6	S	15.1	10.6	0	168.5	0
Add. magn. (dist.)	Point	Line (2)	3	S	26.5	10.8	4.2	302.0	0
Add. magn. (mid.)	Surf.	Line (3)	6	S	22.1	10.4	0	243.0	0
Add. magn. (prox.)	Line (1)	Line (1)	4	S	5.0	10.7	0	56.0	0
Bic. fem. CL	Point	Point	1	S	27.2	8.5	13.0	245.0	30
Bic. fem. CB	Line (3)	Point	3	S	11.8	9.1	3.1	114.0	0
Ext. dig. long.	Line (2)	Point	3	VP	5.4	6.0	30.1	34.1	8
Ext. hal. long.	Line (2)	Point	3	VP	6.1	6.0	17.8	38.3	14
Flex. dig. long.	Surf.	Point	3	VP	6.6	3.8	16.6	26.7	28
Flex. hal. long.	Surf.	Point	3	VP	31.1	2.6	23.4	83.7	30
Gastrocn. (lat.)	Point	Point	1	BC	24.0	5.7	23.4	144.0	25
Gastrocn. (med.)	Point	Point	1	BC	43.8	6.0	21.2	278.0	11
Gemellus (inf.)	Point	Point	1	S	4.1	3.4	0	15.0	0
Gemellus (sup.)	Point	Point	1	S	4.1	3.4	0	15.0	0
Glut. max. (sup.)	Surf.	Surf.	6	S	49.7	12.0	0	629.0	0
Glut. max. (inf.)	Surf.	Line (2)	6	S	22.5	15.1	0	360.0	0
Glut. med. (ant.)	Surf.	Surf.	6	S	37.9	3.8	0	152.5	0
Glut. med. (post.)	Surf.	Surf.	6	S	60.8	4.5	3.0	287.0	16
Glut. min. (lat.)	Surf.	Point	3	S	10.0	2.8	7.3	29.1	0
Glut. min. (mid.)				S	8.1	3.4	7.3	29.1	0
Glut. min. (med.)				S	7.4	3.7	7.3	29.1	0
Gracilis	Line (1)	Point	2	VP	4.9	18.1	14.0	92.9	0
Iliacus (lat.)	Surf.	Point	3	BC	6.6	10.3	11.3	71.5	26
Iliacus (mid.)	Surf.	Point	3	BC	13.0	5.2	11.3	71.5	0
Iliacus (med.)	Surf.	Point	3	BC	7.6	8.9	15.5	71.5	0
Obt. ext. (inf.)	Line (1)	Point	2	S	5.5	6.9	3.5	40.0	0
Obt. ext. (sup.)	Surf.	Point	3	VP	24.6	2.8	3.0	72.0	0
Obturator int.	Surf.	Point	3	VP	25.4	2.1	8.2	55.0	0
Pectineus	Line (1)	Line (1)	4	S	6.8	11.5	0	82.4	0
Peroneus brev.	Surf.	Point	3	VP	19.0	2.7	6.4	53.9	23
Peroneus long.	Surf.	Point	3	VP	23.9	3.4	15.9	86.0	16
Peroneus tert.	Line (2).	Point	3	VP	6.2	4.3	10.0	28.0	19
Piriformis	Point	Point	1	S	8.1	3.9	1.6	33.0	0
Plantaris	Point	Point	1	S	2.4	4.8	35.0	12.0	0
Popliteus	Point	Line (1)	2	VP	10.7	2.4	1.0	27.0	0
Psoas minor	Point	Point	1	S	1.1	5.9	15.2	7.0	0
Psoas major	Surf.	Point	3	BC	19.5	9.9	11.3	204.0	13
Quadratus fem.	Line (1)	Line (1)	4	S	14.6	3.4	0	52.0	0
Rectus fem.	Point	Line (1)	2	S	28.9	7.8	9.6	239.0	22
Sartorius (prox.)	Point	Point	1	VP	5.9	34.7	7.9	217.0	0
Sartorius (dist.)	Point	Point	1	VP	5.9	34.7	7.9	217.0	0
Semimembr.	Point	Point	1	S	17.1	8.1	15.7	146.0	25
Semitend.	Point	Point	1	VP	14.7	14.2	23.7	220.0	0
Soleus (med.)	Line (2)	Point	3	S	94.3	2.4	8.5	238.5	64
Soleus (lat.)	Line (2)	Point	3	S	85.9	2.6	8.5	238.5	59
Tensor fasc. l.	Line (1)	Point	2	S	8.8	9.5	0	88.0	0
Tibialis ant.	Surf.	Point	3	VP	26.6	4.6	23.5	129.0	10
Tibialis post. (med.)	Surf.	Point	3	VP	21.6	2.4	11.0	55.9	25
Tibialis post. (lat.)	Surf.	Point	3	VP	21.6	2.4	11.0	55.9	43
Vastus interm.	Surf.	Line (1)	6	S	38.1	7.7	12.6	309.0	12
Vastus lat. (inf.)	Surf.	Line (2)	6	S	10.7	4.2	9.6	48.0	0
Vastus lat. (sup.)				S	59.0	9.1	9.6	568.0	0
Vastus med. (inf.)				S	9.8	7.6	9.6	78.0	0
Vastus med. (mid.)				S	23.2	7.6	9.6	186.0	0
Vastus med. (sup.)				S	26.9	8.3	9.6	236.0	0

A muscle line can be straight (S), curving around a bony contour (BC) or consist of via points (VP).

Muscles of the hip were analysed for their contribution to JRS in three planes. While most of the muscles will be directly measured with surface EMG, others will be driven neurally from only one pair of surface electrodes over a given muscle site (See Table 4). Differences in hip musculature's mechanistic capability will be preserved, however some muscles are able to be grouped in terms of their activation amplitude given equivalent neural drive (Heller et al., 2005). The method of implying deep musculature activation amplitude considering surface musculature has been suggested to be sufficiently valid in providing biological insight for biomechanical analyses (Brown & Potvin, 2007b; Heller et al., 2005; McGill, Juker, & Kropf, 1996). Work by Heller and colleagues (2005) derived a simplified model of hip musculature (from a more complex and complete model) that maintained physiological loading analogous to the more complex model during gait. In doing so, they pooled individual muscle's activity to be represented as a single muscle equivalent model. Although Heller grouped some muscles whose EMG signal this work will directly measure, the premise of their simplified model supports the rationale to drive deeper musculature (or grouped musculature) activation amplitude off of one common surface electrode site. It has previously been suggested that muscles, or the compartments of a muscle, only differ in neural drive if they each possess an individually specific nerve innervation (Segal, 1992). While the adductor muscles considered in this work are all innervated by the superior gluteal nerve (originating from L5, S1) and the abductor musculature from the obturator nerve (originating from L2, L3, L4), the author recognises that differences in motor unit recruitment between muscles and muscle compartments may exist during dynamic multi-planar tasks. Since muscles will be evaluated for their contribution to JRS, it will be assumed that the muscles (and muscle compartments) grouped together will receive equivalent neural drive during a given task, thus any error will be systematic in nature.

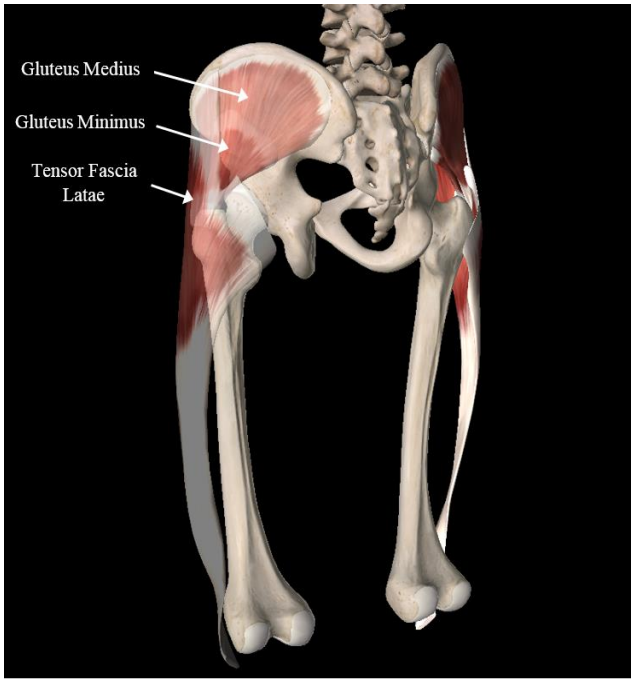

Figure 15: Visual representation of the abductors location and attachment sites, that will be used in calculation of frontal plane hip JRS. Essential Anatomy

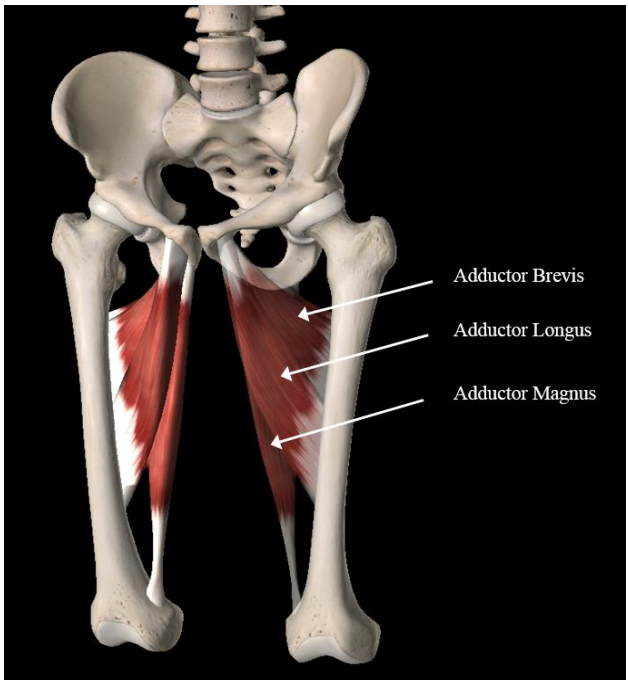

Figure 16: Visual representation of the adductors location and attachment sites, that will be used in calculation of frontal plane hip JRS. Essential Anatomy

Table 4: Hip musculature being measured directly via surface EMG electrodes, and the musculature not being directly measured but whose activation profiles will be inferred from a select muscle's surface EMG electrodes.

	Muscle
Directly measured	Gluteus Maximus
	Gluteus Medius
	Tensor Fascia Latae
	Adductor Longus

	Muscle	**Electrode Site**
Indirectly measured	Gluteus Minimus	Gluteus Medius
	Adductor Magnus	Adductor Longus
	Adductor Brevis	Adductor Longus

Despite not having an attachment on the proximal femur, the tensor fascia latae (TFL) wraps around the greater trochanter and inserts on the iliotibial (IT) band (See Figure 15). These structures can exert forces and act to minimise moments in the frontal plane of the hip, thus TFL as an abductor of the hip will be considered in its ability to contribute to joint stiffness.

3) Muscle Stiffness

Muscle stiffness will be calculated via the method introduced by Bergmark (1989)

$$k = \frac{qF}{L}$$

Where,

k = muscle stiffness

F = muscle force

L = total muscle length from origin to insertion

q = muscle stiffness coefficient relating muscle force and length

The value assigned to the *q* coefficient has substantial effects on the determination of a muscle's stiffness and thus its contribution to joint stiffness and stability. Brown & Potvin (2007) evaluated a range of *q* values (1 – 20) and the resultant muscle stiffness increased linearly with an increasing value of *q*. The *q* value has been reported in the literature to range from 0.5 to 50, with a mean of approximately 10. The selection of an appropriate *q* value depends on the muscles of interest, method of stiffness calculation and the non-linear relationship between force and stiffness. Given that a biologically accurate determination of the *q* value still eludes us, the large range of reported values is unsurprising. Limitations using the proportionality constant of *q* and Bergmark's equation for muscle stiffness include falsely assuming the relationship between muscle force, length and stiffness are linear (Brown & McGill, 2005; Cholewicki & McGill, 1995). Thus, uncertainty in the determination of an optimal *q* value for a given muscle exists, and many of the reported values and work in this area involve the muscles surrounding the spine. Despite the limitations, for the purpose of this work the *q* value will be set to 10 for all muscles of the hip. Given the cross-sectional design and comparison of two groups, this assumption should not have a large influence on the results. Any potential error introduced by the *q* value will be systematic and present to an equal magnitude in both groups.

The gluteus maximus will undoubtedly provide stiffening of the hip joint in the frontal plane, however its direction of stiffening potential is complex. The superior and inferior fibers of the gluteus maximus are distinguished as such with relation to the hip joint centre. When in anatomical position, the superior fibers act to abduct the hip and the inferior fibers to adduct the hip. However, with movement, fiber orientation and muscle line of action may change and could influence its action in the frontal plane. The point at which superior or inferior fibers may flip to produce the opposite action on the hip is not well defined. Given this information, gluteus

maximus' contribution to hip JRS in the frontal plane will make the assumption that the superior fibres always act to abduct the hip, while the inferior fibres act to adduct the hip.

Initial hip muscle force and stiffness data contained non-physiological noise, likely artifact from the calculation of instantaneous muscle velocity. The data were low pass second order Butterworth filtered (dual pass) at a cut-off frequency of 12 Hz. This filtering process mirrored that of the kinetic data, and allowed for removal of noise while maintaining the shape and magnitude of the pre-filtered data.

4.4 Statistical Analysis

Independent Variable:

- Medial knee displacement relative to hip-ankle plane

Dependent Variables:

- Lumbar Spine Stiffness
- Hip Joint Rotational Stiffness
- Lumbar Spine kinematics
- Hip Kinematics

A series of one-way ANOVA's were conducted with the independent variable being medial knee displacement. The primary dependent variables of this study were lumbar spine and hip JRS, and their kinematics were also of interest. In the event that significant differences were found when comparing lumbar spine variables for three groups, post-hoc comparisons were performed using pairwise t-tests with a Bonferroni adjustment. Statistical significance was set at the $p < 0.05$ level.

Special Note: As the thesis progressed it was clear that larger variability could occur within subjects than between subjects. Valgus behavior could occur in any person and we wanted to understand why. This biological fact required a shift in the statistical approach in order to probe the mechanism of valgus – which was the original motivation of this thesis. Thus, the valgus status of each independent trial of every subject was determined based on the threshold, trials within a subject were not collapsed and thus statistics were run on the number of trials in each group, not the number of subjects. This was an attempt to quantify medial knee displacement and proximal joint stiffness independently in every trial, and account for movement variability within a participant.

5.0 Results

Reported below for each task are joint angles and joint rotational stiffness values of the lumbar spine and hips for each valgus group. Specific summed muscle stiffness's about the spine and select muscle's contributions to hip JRS are included where relevant to the demands of the task or are of particular interest. Lumbar spine variables for the double leg landing tasks (DVJ and SJ) include three groups (bilateral, unilateral and no valgus) after analyzing each knee separately for valgus status. Hip variables include only two groups since only the valgus status of the ipsilateral side is of interest. Differences between groups are discussed in terms of statistical significance, however the author encourages the reader to consider the biological significance of such results and question what may be meaningful differences between groups, both for such cases in which statistical significance is met, and for those instances when it is not. Variables of interest reported in paragraphs include the mean and standard deviation of the group for the point of interest, whether as figures display the mean line and the standard error of the group. All figures (no indication of statistical significance) for every variable measured during each task can be found in Appendix C at the end of this document.

5.1 KAM vs Medial Knee Displacement

Upon initial analysis of participants' risk status using the KAM, several interesting discoveries were made. Initially it appeared that lumbar spine and hip joint angles were remarkably similar between groups, despite expected differences given the literature. Further, the KAM value was not necessarily capturing those individuals experiencing valgus collapse, and who would certainly be straining their ACL and determined at risk, clinically speaking. Nor was the KAM necessarily classifying some participants as low risk when they avoided such injurious

kinematics. Additional investigation with the measurement of medial knee displacement found this to be the case. Figure 17 shows a participant who was deemed ‘not at risk’ using their KAM of 21.47 Nm, yet in this particular trial the subject’s left knee experienced a peak medial displacement of 5 cm (the second highest peak medial knee displacement for the left knee of all participants’ trials of the DVJ). Additionally, this participant had the second highest body mass (80 kg) of the collected participants, thus a low body mass could not account for the lower moment being experienced. Normalizing knee joint moments to body mass (kg), height (m) or a mass x height (kg · m) did not further distinguish those experiencing dynamic valgus. Thus, it was concluded that separating participants based on dynamic valgus was more appropriate than the KAM given the deleterious effects of the posture, its ability to encapsulate aberrant kinematics and its strong association with ACL injury prediction.

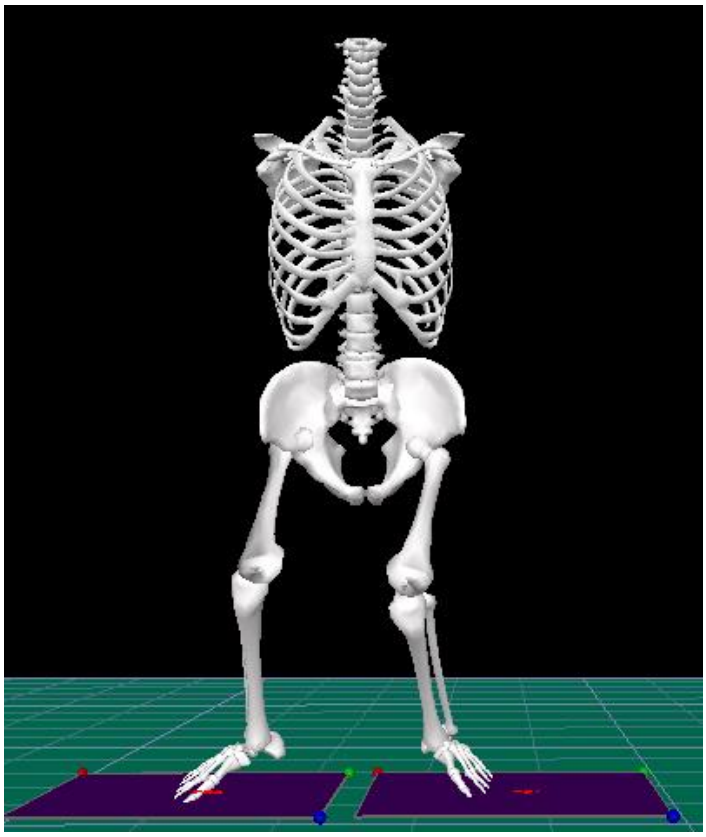

Figure 17: A participant deemed 'not at risk' on the left side using the KAM threshold, yet experienced large medial knee displacement and injurious dynamic valgus presentation.

5.2 DVJ

The left and right knee were deemed as high valgus, low valgus, or excluded as per the procedures described in section 4.3.4 of the Methods. The results of these procedures for the left knee and right knee are presented in Figure 18 and Figure 19 respectively. Time-normalized data is presented for the DVJ from the instant of initial contact (IC) to toe-off (TO).

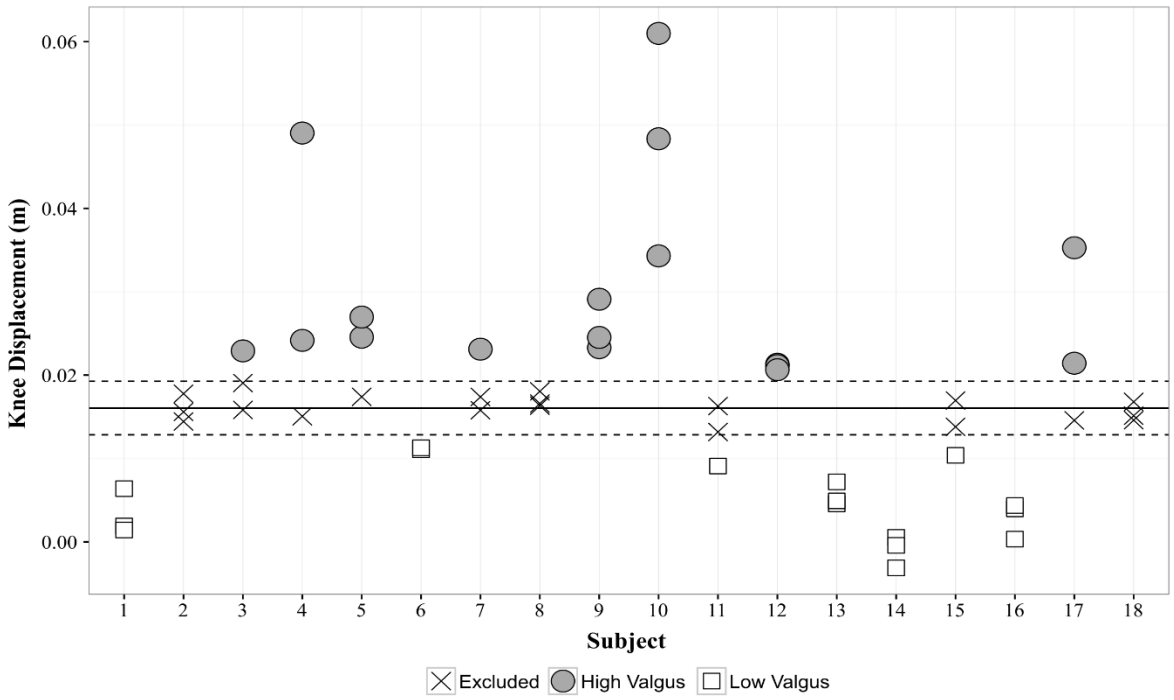

Figure 18: Left knee peak medial displacement for all trials. The solid line denotes the median value, while the dashed lines are the median value ± 20% to define thresholds for low and high valgus status. Trials within the dashed lines are excluded from analysis

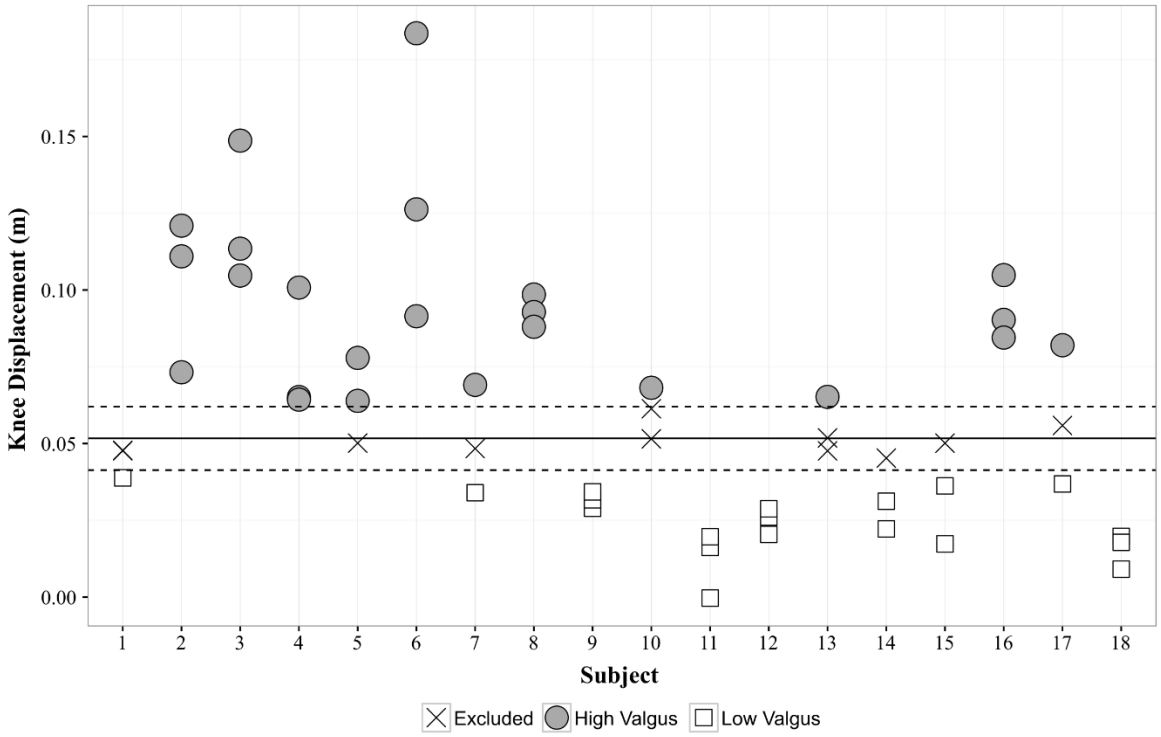

Figure 19: Right knee peak medial displacement for all trials. The solid line denotes the median value, while the dashed lines are the median value ± 20% to define thresholds for low and high valgus status. Trials within the dashed lines are excluded from analysis.

The bilateral valgus group displayed a statistically significant greater peak lumbar spine flexion angle of 37.4 ± 9.3º (F (2,42) = 6.9) than that of the unilateral valgus (25.9 ± 8.2º, p = 0.003) and no valgus (27.9 ± 7.4 º, p = 0.038) groups (Figure 20). The no valgus group elicited higher peak lumbar JRS than the bilateral and unilateral valgus groups in all three planes. However, statistical significance was obtained only in the sagittal plane lumbar JRS between the no valgus (818.4 ± 181 Nm/rad) compared to the bilateral valgus group (566.1 ± 56.3 Nm/rad) (F (2,42) = 3.433, p = 0.048) (Figure 21). The unilateral valgus peak of 760.4 ± 279 Nm/rad was not significantly different from the bilateral (p = 0.104) or the no valgus groups (p = 1.000).

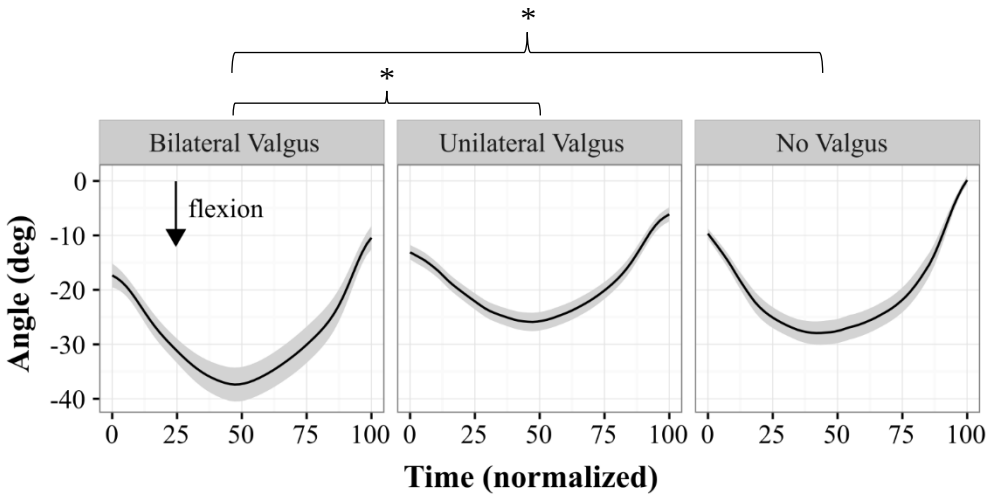

Figure 20: Lumbar Spine Angle – Sagittal Plane

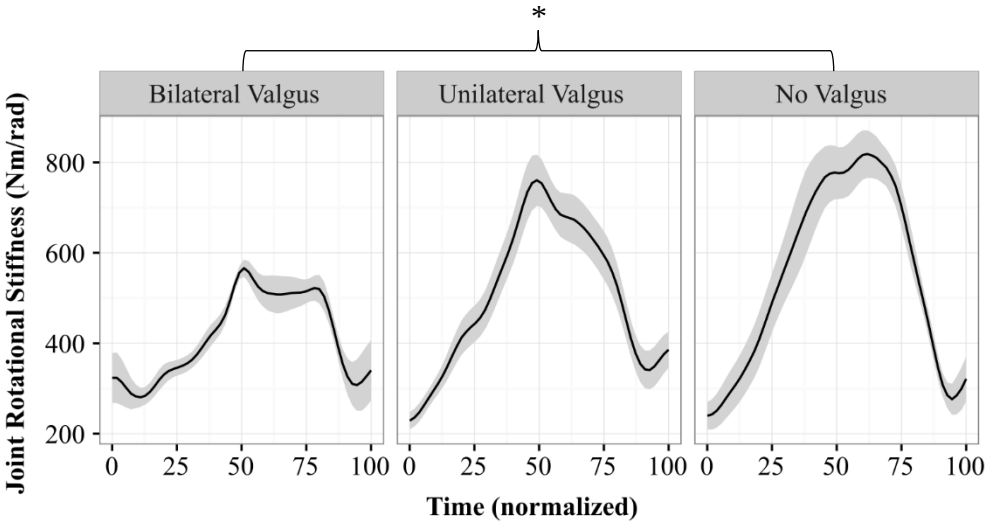

Figure 21: Lumbar Spine Sagittal Plane JRS.

No statistical differences were found in left hip angles between high valgus and low valgus groups, in either peak flexion (85.9 ± 7.7^{o} vs 83.5 ± 13.6^{o}, F (1,27) = 0.338, p = 0.56), minimum abduction (2.3 ± 7.7^{o} vs 4.9 ± 6.7^{o}, F (1,27) = 0.885, p = 0.56) (Figure 22), or peak external rotation (7.6 ± 3.7^{o} vs 8.7 ± 11.0^{o}, F (1,27) = 0.1523, p = 0.69) (Figure 23).

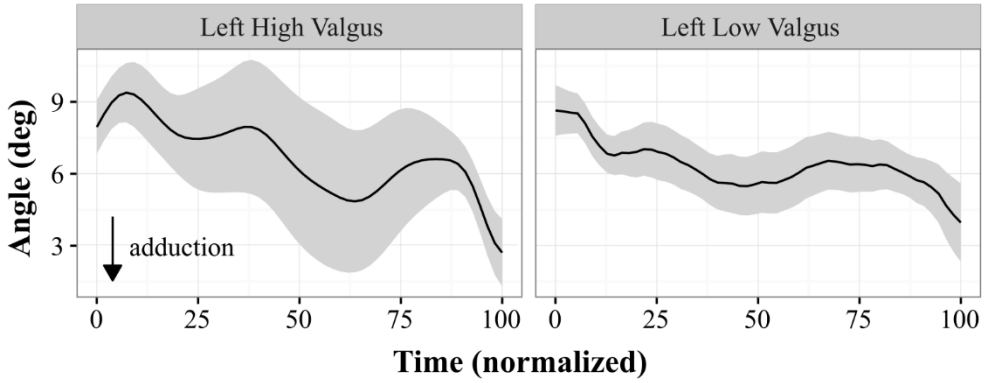

Figure 22: Left Hip Angle – Frontal Plane. Large standard error in the high valgus group suggest there was more variability in frontal plane angles.

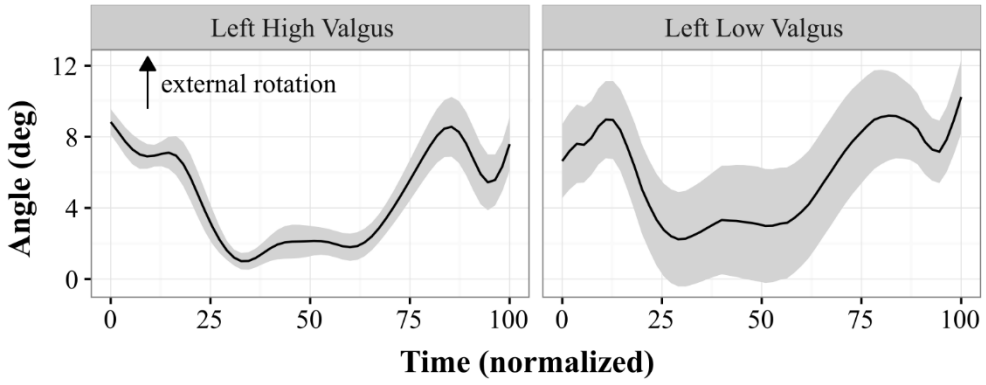

Figure 23: Left Hip Angle – Transverse Plane

Interestingly, while no significant differences in left hip adduction were observed between groups, the low valgus group displayed greater peak frontal plane JRS (5134.4 ± 2742 Nm/rad) than the high valgus (3504.2 ± 1987 Nm/rad) group (F (1,27) = 4.091, p = 0.051). With the abductors frontal plane JRS in the low valgus group (4780.0 ± 2702 Nm/rad) significantly

greater (F (1,27) = 4.4858, p = 0.042) than the high valgus abductors JRS (3095.5 ± 1966 Nm/rad) (Figure 24).

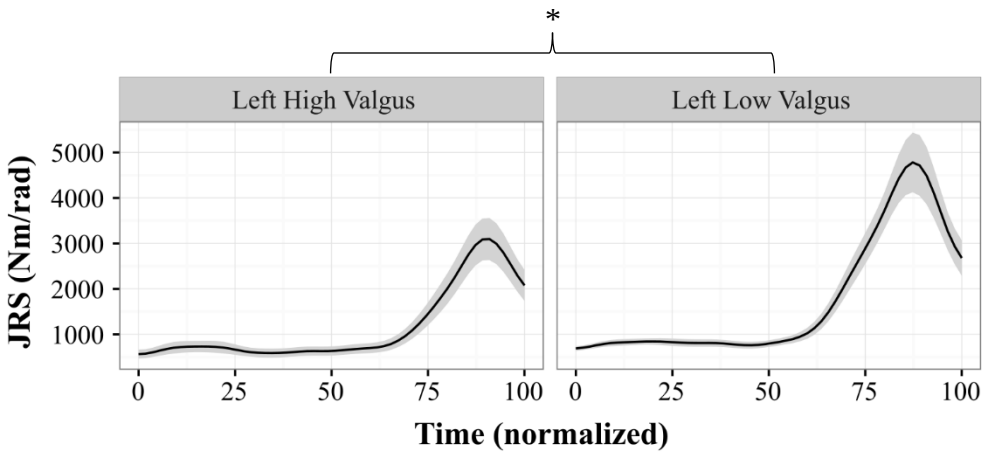

Figure 24: Left Hip Abductors JRS in the frontal plane. Low valgus group's peak JRS significantly greater than that of the high valgus group.

The low valgus group's JRS contribution from the left gluteus maximus superior was generally greater than the high valgus group in both the frontal plane (625.6 Nm/rad vs 484.9 Nm/rad) and the transverse plane (853.3 Nm/rad vs 735.9 Nm/rad) however these differences were not significant (p = 0.665). In the transverse plane the TFL's JRS was statistically different between groups (F (1,29) = 5.328, p = 0.028), with the low valgus group's peak of 27.4 ± 14.4 Nm/rad greater than the high valgus group's peak of 17.9 ± 6.8 Nm/rad. However, while the TFL's JRS was statistically different between groups, its overall contribution to the transverse plane's total JRS was approximately 1% for both groups. Thus, its biological significance and any substantial biomechanical contribution must be questioned.

Peak flexion of the right hip was significantly greater (F (1,34) = 5.703, p = 0.023) in the low valgus groups (89.1 ± 10.1^{o}) compared to the high valgus group (79.2 ± 13.5^{o}) (Figure 25). The low valgus group displayed greater peak right hip abduction of 16.6 ± 4.2^{o}, than that of the high valgus groups peak of 5.1 ± 6.9^{o} (F (1,34) = 16.27, p = 0.001) (Figure 26).

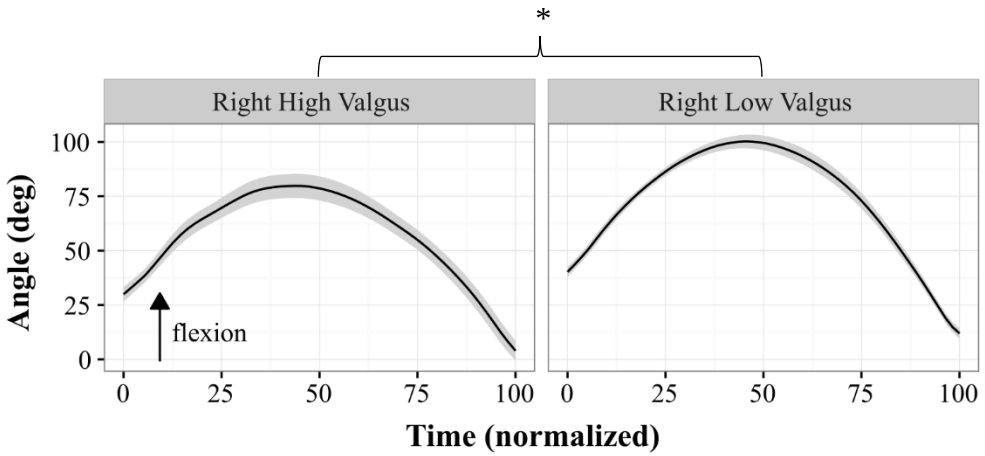

Figure 25: Right Hip Angle – Sagittal Plane

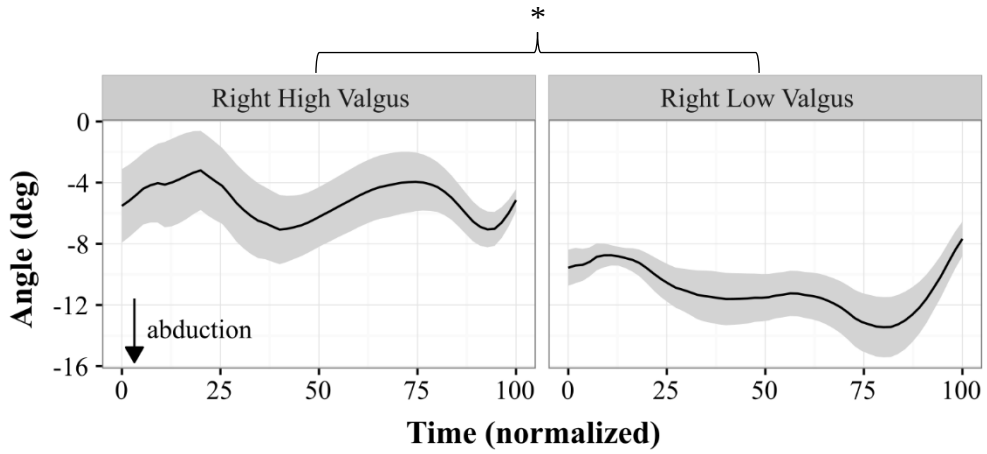

Figure 26: Right Hip Angle – Frontal Plane

While peak right frontal plane hip JRS showed a >20% difference between groups, statistical significance was not reached (F (1,34) = 1.155, p = 0.29) (Figure 27). Additionally, gluteus maximus superior's JRS was greater in the frontal plane in the low valgus (F (1,34) = 2.613, p = 0.116) group by >50 %, however these were not found to be significantly different (Figure 28).

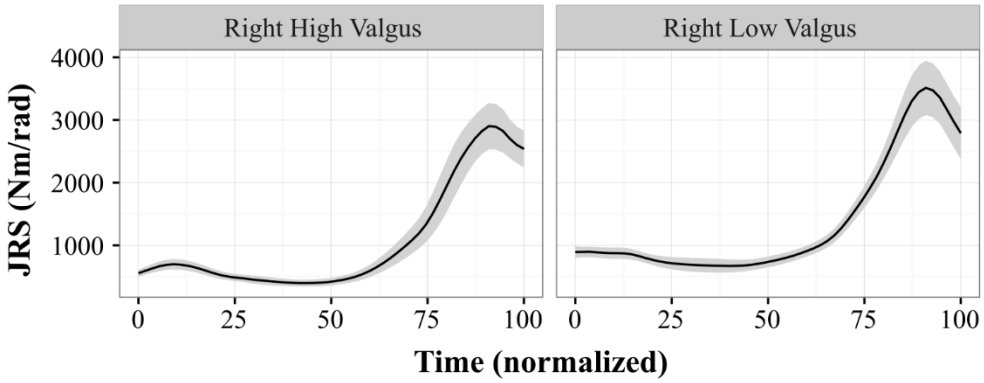

Figure 27: Right Hip JRS – Frontal Plane

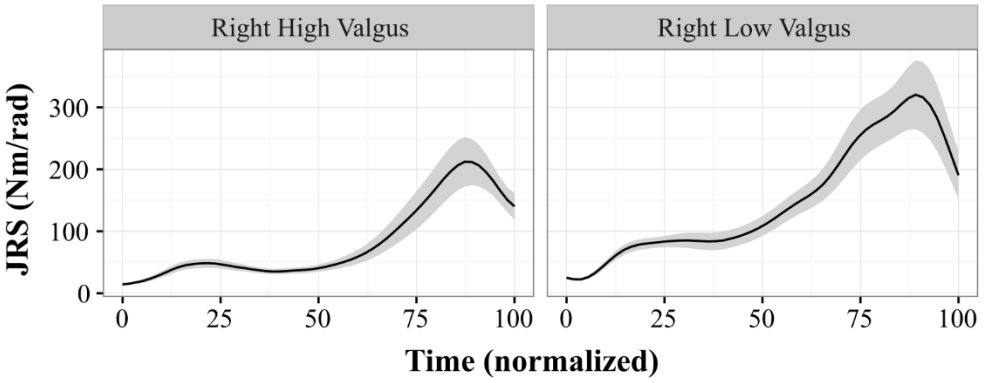

Figure 28: Right Gluteus Maximus Superior JRS – Frontal Plane

5.3 Stop Jump

The left and right knee were deemed as high valgus, low valgus, or excluded as per the procedures described in section 4.3.4 of the Methods. The results of these procedures for the left knee and right knee are presented in Figure 29 and Figure 30 respectively. Time-normalized data is presented for the SJ from the instant of initial contact (IC) to toe-off (TO).

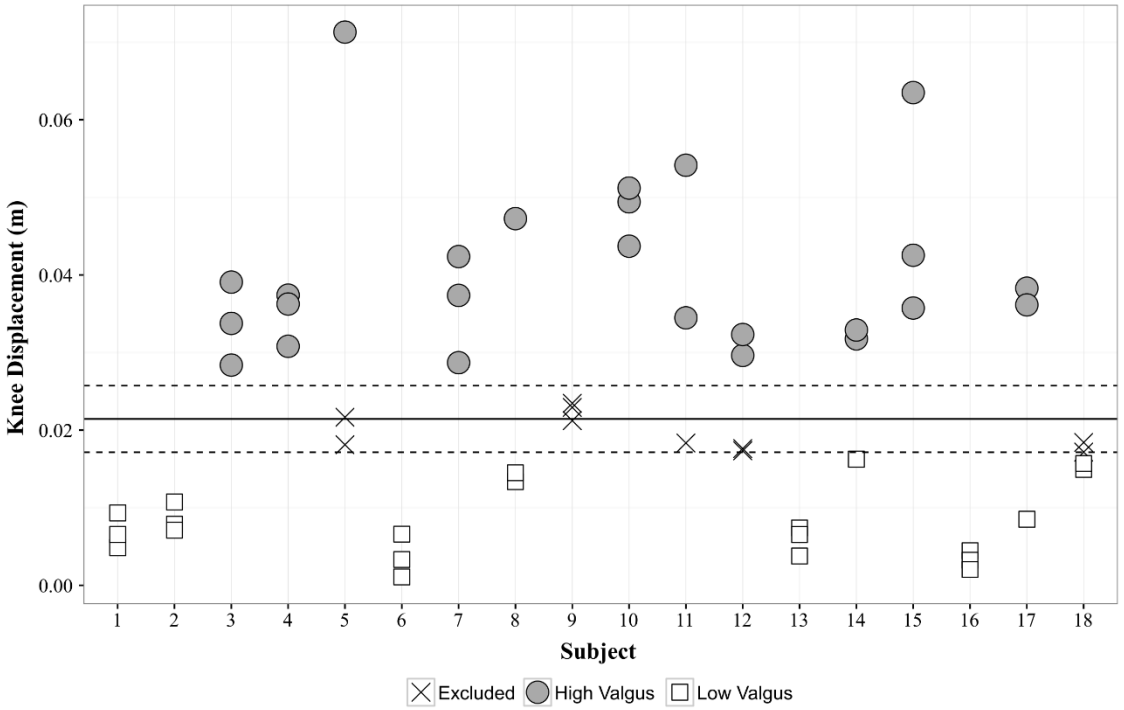

Figure 29: Left knee peak medial displacement for all trials. The solid line denotes the median value, while the dashed lines are the median value ± 20% to define thresholds for low and high valgus status. Trials within the dashed lines are excluded from analysis.

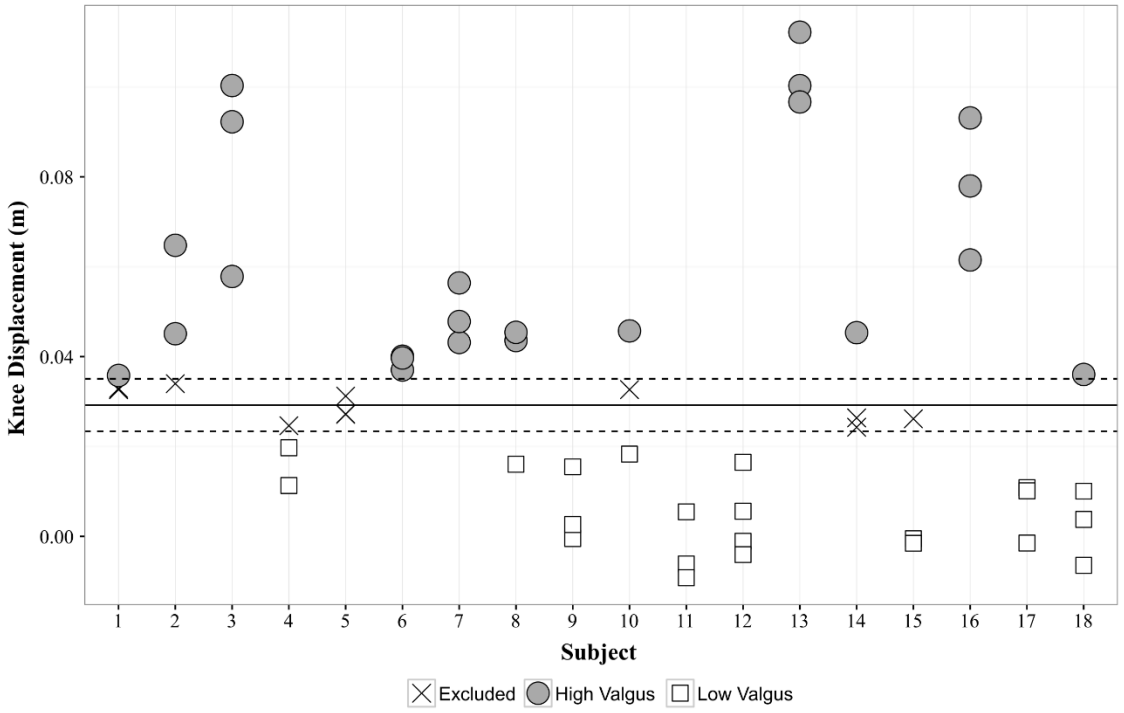

Figure 30: Right knee peak medial displacement for all trials. The solid line denotes the median value, while the dashed lines are the median value ± 20% to define thresholds for low and high valgus status. Trials within the dashed lines are excluded from analysis.

Sagittal plane lumbar spine angle was found to be significantly greater in the bilateral group (31.4 ± 8.2 ^{o}) than the no valgus group (24.5 ± 2.8^{o}) (F (2,44) = 3.332, p = 0.044), however neither were significantly different from the unilateral valgus group (28.6 ± 6.6^{o}) (Figure 31). Despite the SJ task being a double-leg task significant differences (F (2,44) = 7.132, p = 0.002) were observed in the peak right lateral bend angle between the bilateral (4.3 ± 3.4^{o}) and unilateral (1.4 ± 2.8^{o}) valgus groups (F (2,44) = 7.132, p = 0.011) as well as the bilateral and no valgus groups (p = 0.005). Additionally, the bilateral valgus group displayed a greater range of lateral bend motion of almost 6^{o} versus the no valgus groups range of 2^{o} (Figure 32).

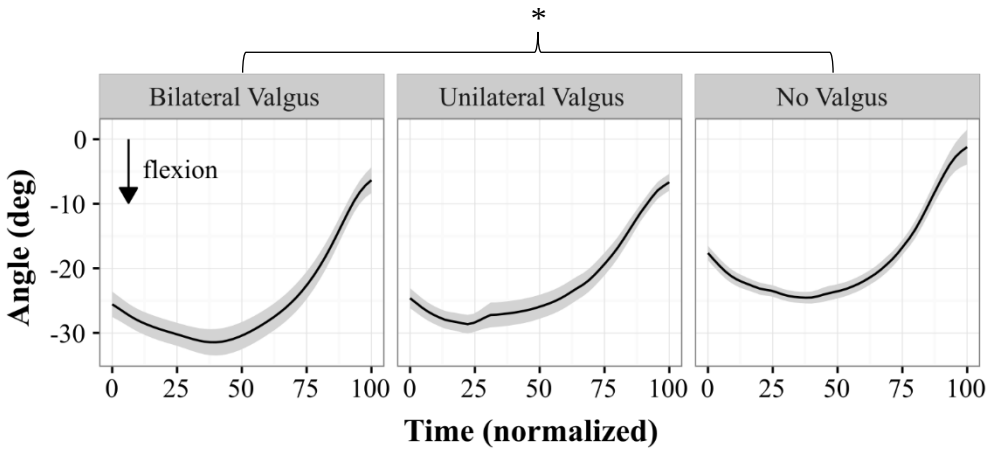

Figure 31: Lumbar Spine Angle – Sagittal Plane

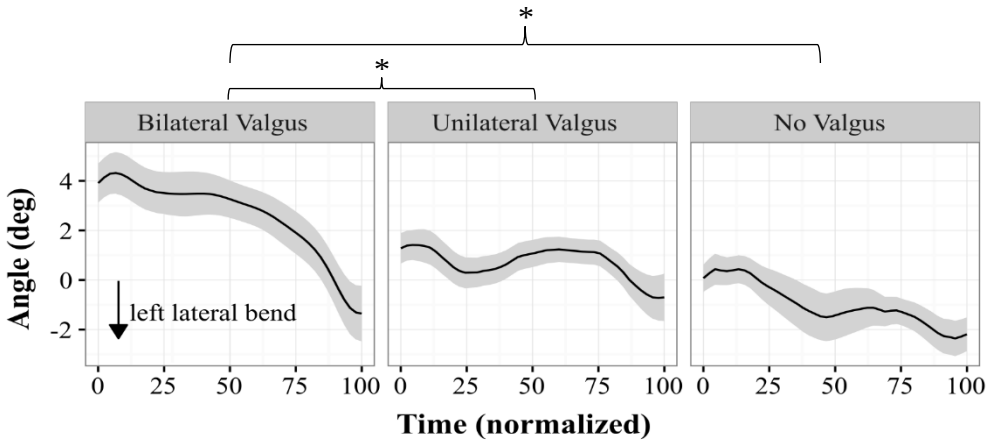

Figure 32: Lumbar Spine Angle – Frontal Plane

No differences were found in the sagittal, frontal or transverse planes of lumbar JRS between the three groups. A representation of the groups lumbar JRS can be seen in the Euclidean Norm JRS (Figure 33) where no differences were observed ($F(2,44) = 0.115$, $p = 0.892$).

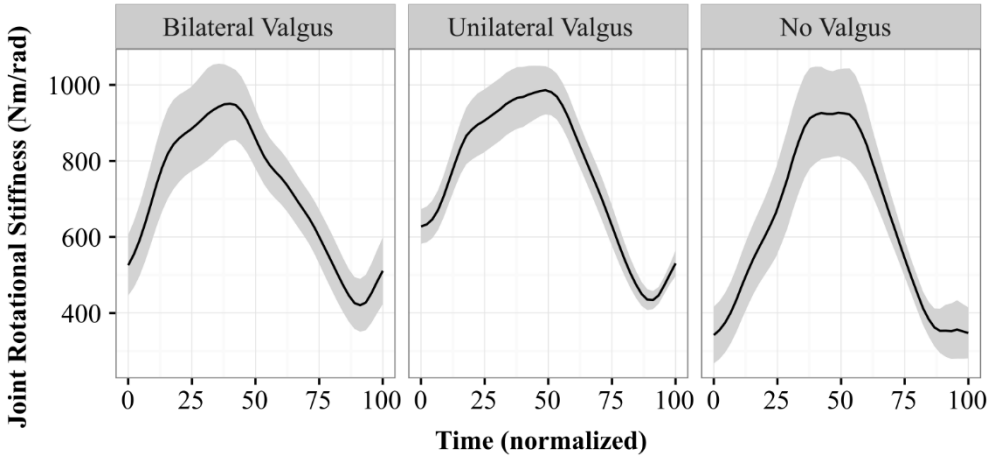

Figure 33: Lumbar Spine JRS – Euclidean Norm. This figure displays the same relationship between groups that was observed in all three axes of JRS.

The low valgus group displayed significantly greater abduction ($F(1,40) = 26.482$, $p < 0.0001$) and external rotation ($F(1,40) = 18.064$, $p < 0.0001$) than the high valgus group (Figure 34 and Figure 35).

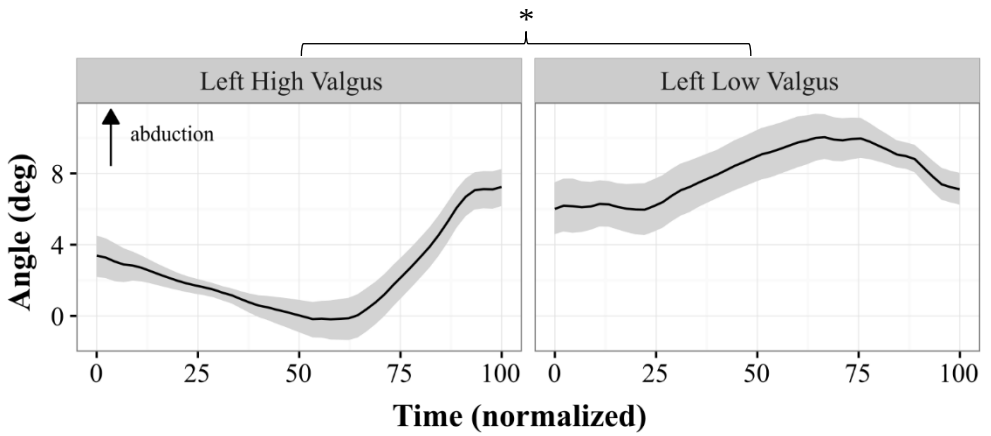

Figure 34: Left Hip Angle – Frontal Plane. The high valgus group tend toward less abduction throughout the trial while the low valgus group tends towards greater abduction.

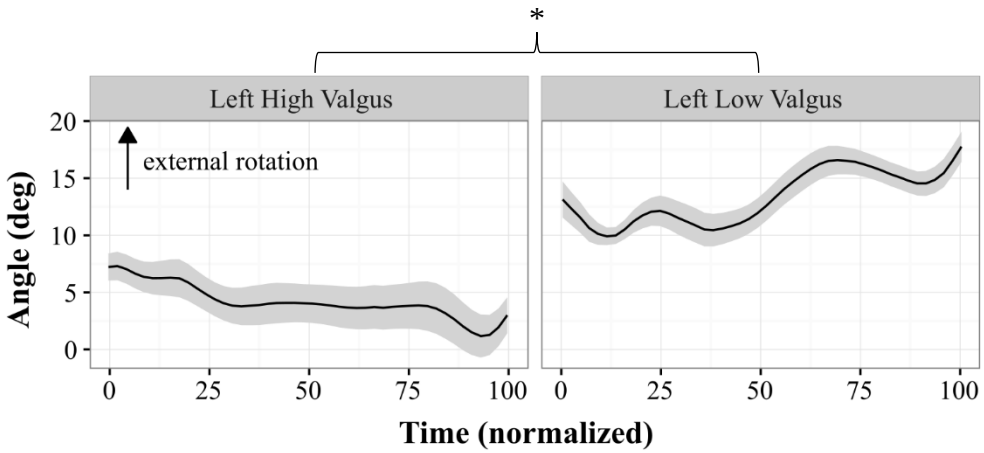

Figure 35: Left Hip Angle – Transverse Plane. The high valgus group tend toward less external rotation throughout the trial while the low valgus group tends towards greater external rotation.

Peak left hip JRS in the frontal plane (1895.2 ± 1518 Nm/rad) (Figure 36) and transverse plane (3237.4 ± 2210 Nm/rad) (Figure 37) of the low valgus group were > 20% higher than that of the high valgus group, however statistical significance was not reached (p = 0.09 and p = 0.211) for either. However, gluteus maximus superior's JRS was significantly greater in the low valgus group than the high valgus group in the frontal plane (F (1,42) = 7.737, p = 0.008) (Figure 38) and the transverse plane (F (1,42) = 5.061, p = 0.029) (Figure 39).

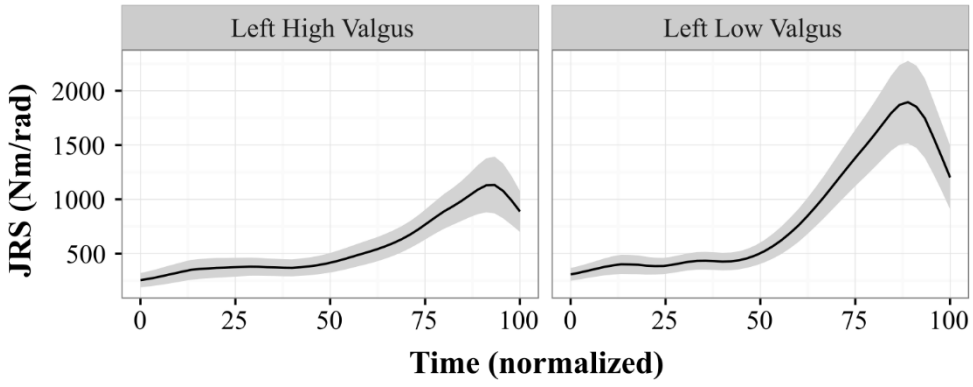

Figure 36: Left Hip Frontal Plane JRS.

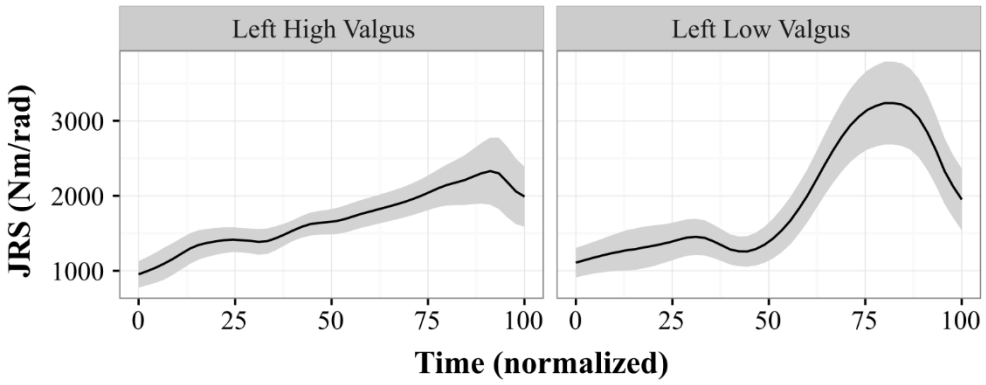

Figure 37: Left Hip Transverse Plane JRS.

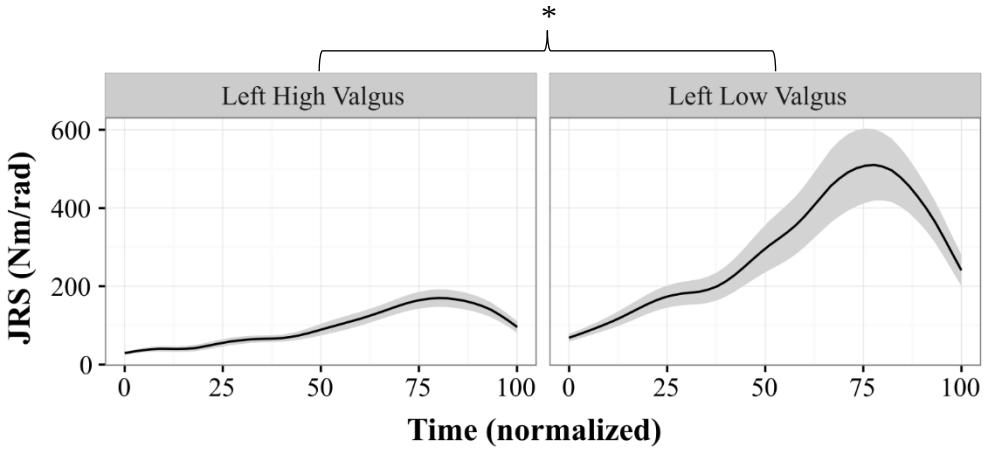

Figure 38: Left Gluteus Maximus Superior Frontal Plane JRS.

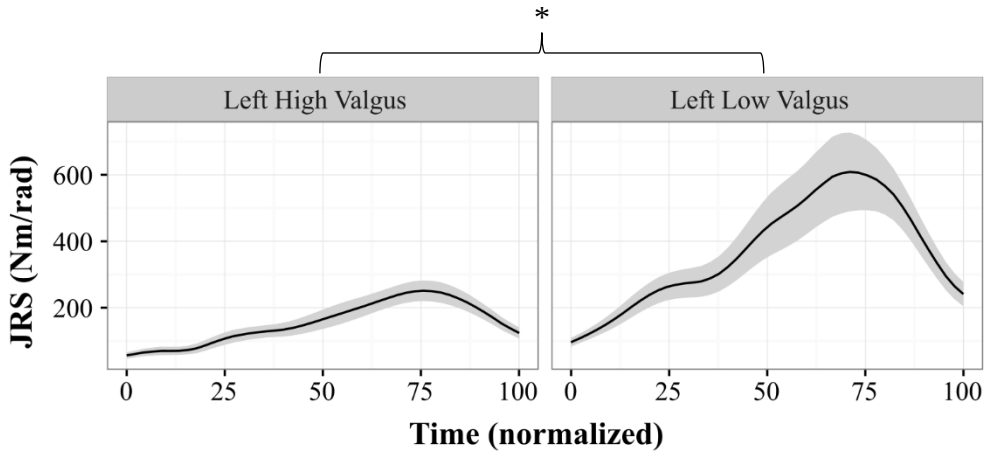

Figure 39: Left Gluteus Maximus Superior Transverse Plane JRS.

Peak right hip abduction was significantly greater in the low valgus group (2.4 ± 4.4°) than the high valgus group (6.0 ± 4.4°) (F (1,29) = 4.394, p = 0.047) (Figure 40). Transverse angles of the right hip were not significantly different between groups, however the low valgus group displayed greater external rotation than the high valgus group throughout the duration (F (1,29) = 0.053, p = 0.820) (Figure 41).

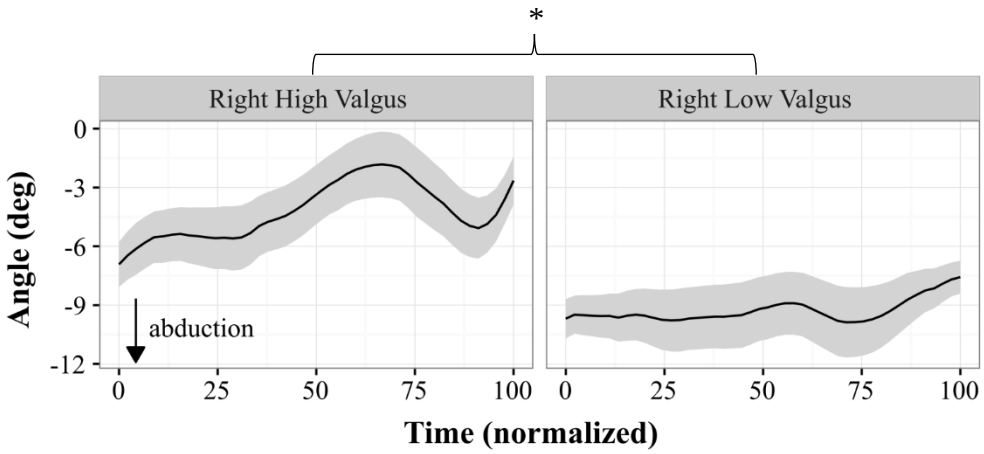

Figure 40: Right Hip Angle – Frontal Plane.

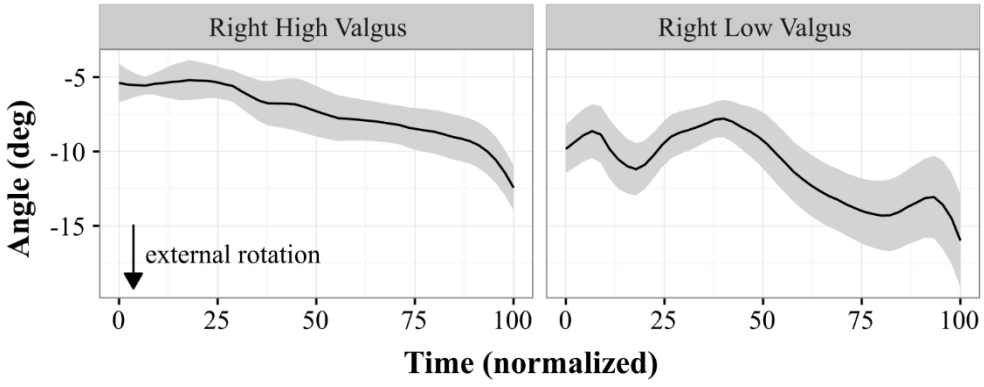

Figure 41: Right Hip Angle – Transverse Plane.

Despite the frontal plane angle of the right hip achieving significance, while the transverse plane angle did not, the opposite was true for the corresponding planes of JRS. Right hip frontal plane JRS (Figure 42) was greater in low valgus (3728.5 ± 2376.9 Nm/rad) than high valgus (2413.2 ± 1235 Nm/rad) but statistical significance was not achieved ($F(1,29) = 3.808$, $p = 0.061$). Conversely the right hip transverse plane JRS was significantly greater in low valgus (1312.6 ± 876 Nm/rad) than high valgus (706.7 ± 318.5 Nm/rad) ($F(1,29) = 6.8234$, $p = 0.014$) (Figure 43).

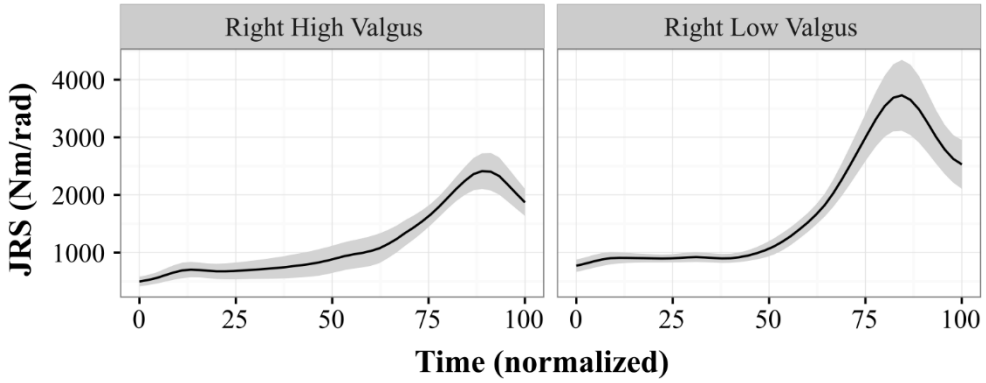

Figure 42: Right Hip Frontal Plane JRS.

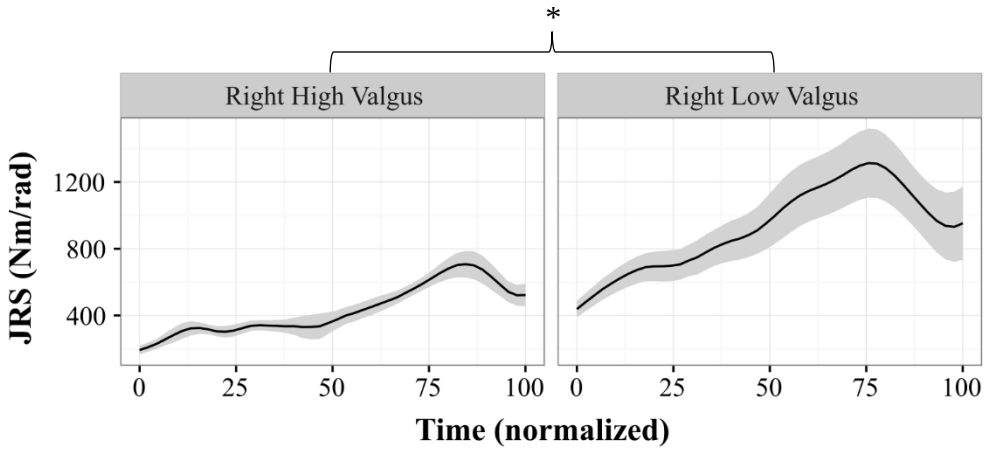

Figure 43: Right Hip Transverse Plane JRS.

Similarly to the left hip's JRS in the frontal plane, it was the gluteus maximus superior of the right hip that showed the largest differences (F (1,29) = 4.866 p = 0.035) between low and high valgus groups (Figure 44) opposed to the summed abductors JRS (Low: 3394.6 ± 2300 Nm/rad, High: 2257.4 ± 1266 Nm/rad, F (1,29) = 2.9587, p = 0.096) or gluteus medius' JRS (Low: 1595.3 ± 1037 Nm/rad, High: 1298.5 ± 634 Nm/rad, F (1,29) = 2.9587, p = 0.096). In the transverse plane the JRS of gluteus maximus superior was again significantly greater in the low valgus group (F (1,29) = 7.938, p = 0.008) (Figure 45) as was the TFL (F (1,29) = 6.331, p = 0.017).

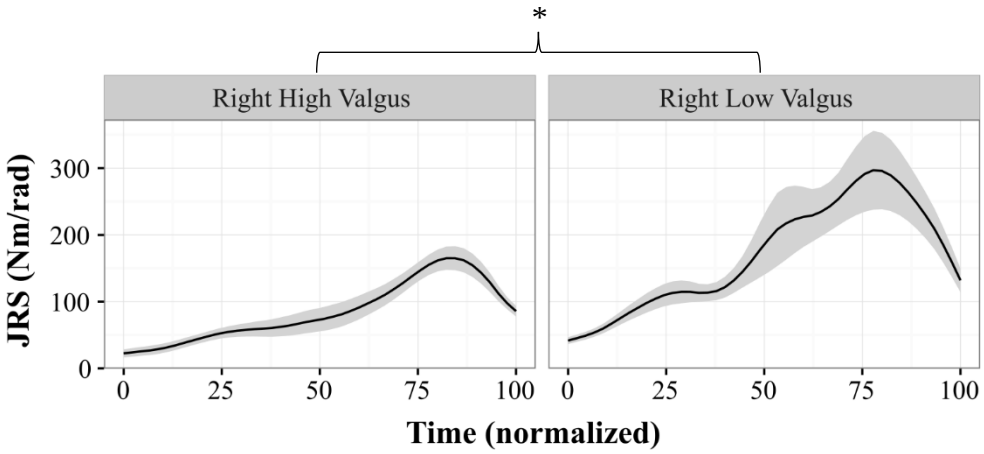

Figure 44: Right Gluteus Maximus Superior Frontal Plane JRS.

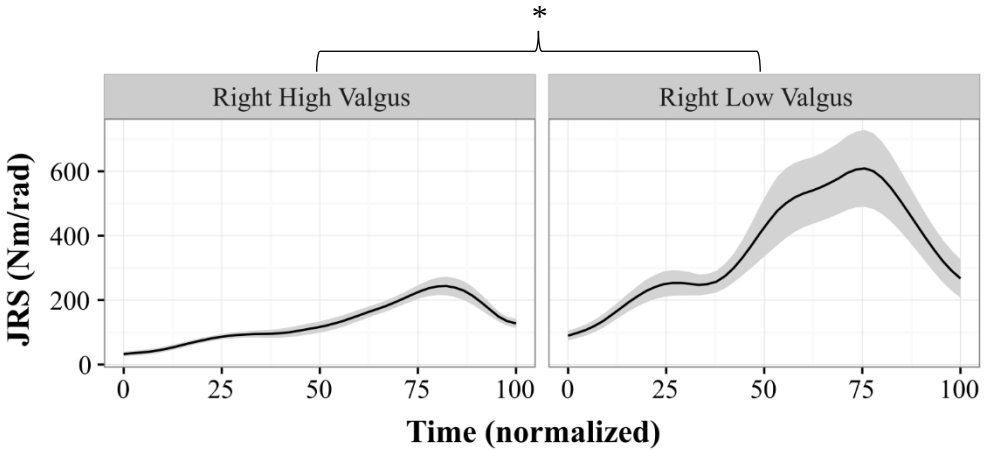

Figure 45: Right Gluteus Maximus Superior Transverse Plane JRS.

5.4 Single Leg Drop

The Single Leg Drop (SLD) task was done for each limb, thus each limb was independently defined as high valgus or low valgus. All hip variables reported are for the ipsilateral side of interest only. Given that hip angles are measured considering the femur's orientation with respect to the pelvis, on single leg support more exaggerated lateral trunk lean (void of lumbar lateral bend) was observed in some subjects. This could present as hip abduction in frontal plane hip angle, however, the action of the femur adducting in the hip joint in this posture would cause dynamic valgus, thus frontal plane knee angle is of interest in the single leg landings due to this phenomenon. Again, due to the nature of single leg landing and the increased frontal plane challenge, the previously defined 'planes' and 'quadrants' of summed muscle stiffness become of interest to infer possible areas of deficit.

5.4.1 Left SLD

The left knee's valgus status was determined as per the procedures described in section 4.3.4 of the Methods. The results of these procedures for the left knee are presented in Figure 46. Time-normalized data is presented for the SLD from the point at which the participant has left the box at the top of the drop until they land and regain their COM in upright single leg stance.

Lumbar spine flexion (Figure 47) peaked at 20.7 ± 12.0^{o} in the high valgus group and at 14.2 ± 12.0^{o} in the low valgus group ($F(1,37) = 2.843$, $p = 0.100$). Peak right lateral bend was significantly greater in high valgus (9.8 ± 4.5^{o}) than low valgus (5.2 ± 1.8^{o}) ($F(1,37) = 18.423$, $p = 0.0001$) (Figure 48). No significant differences in lumbar axial twist angle despite low valgus displaying greater peak right axial twist (Figure 49).

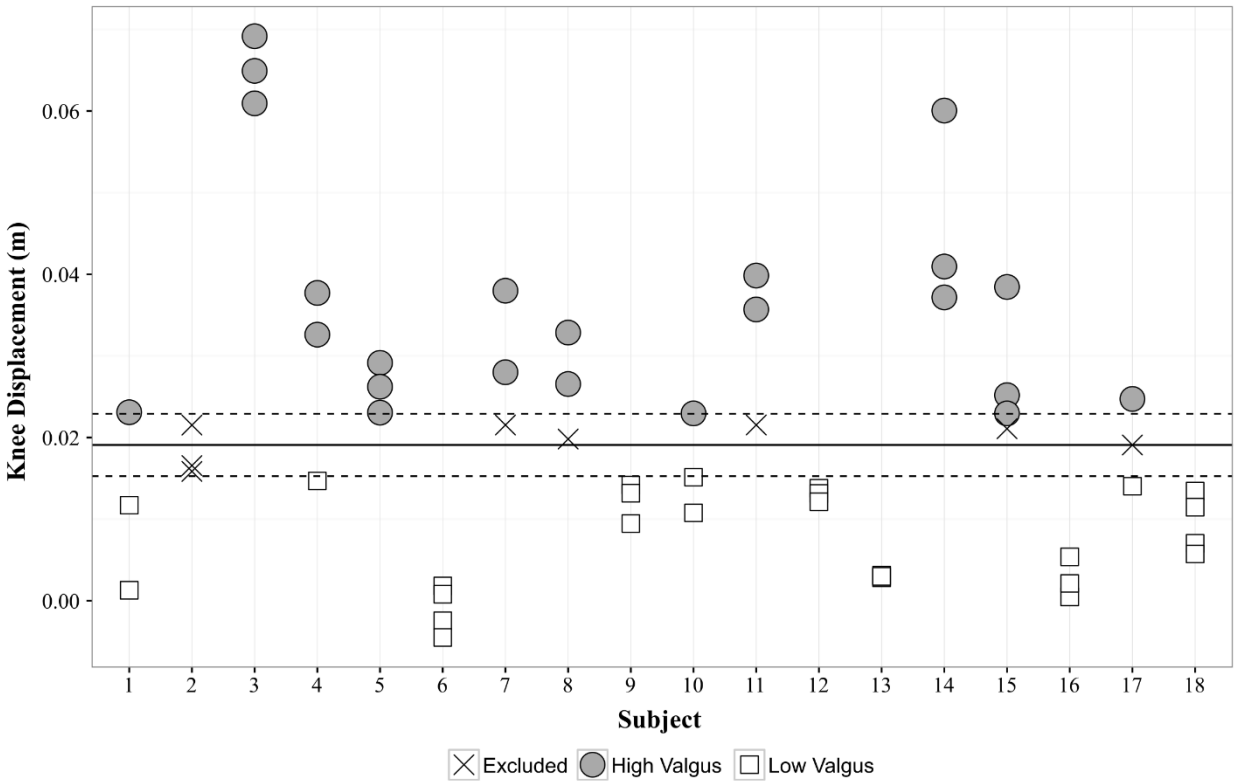

Figure 46: Left knee peak medial displacement for all trials. The solid line denotes the median value, while the dashed lines are the median value ± 20% to define thresholds for low and high valgus status. Trials within the dashed lines are excluded from analysis.

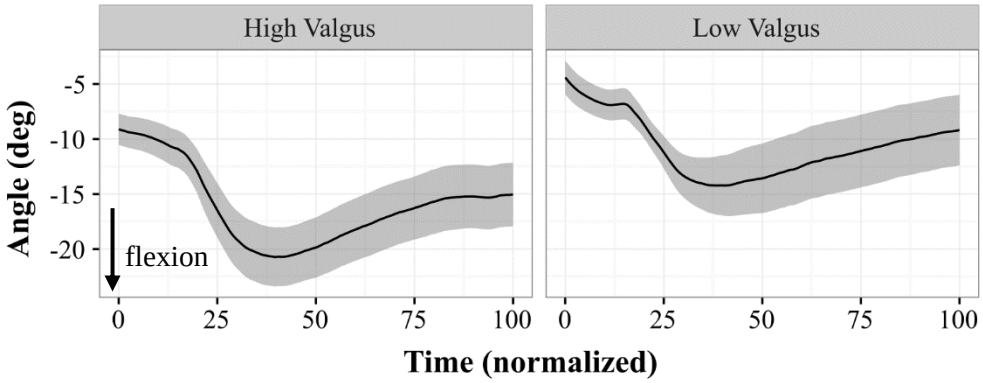

Figure 47: Lumbar Spine Angle – Sagittal Plane

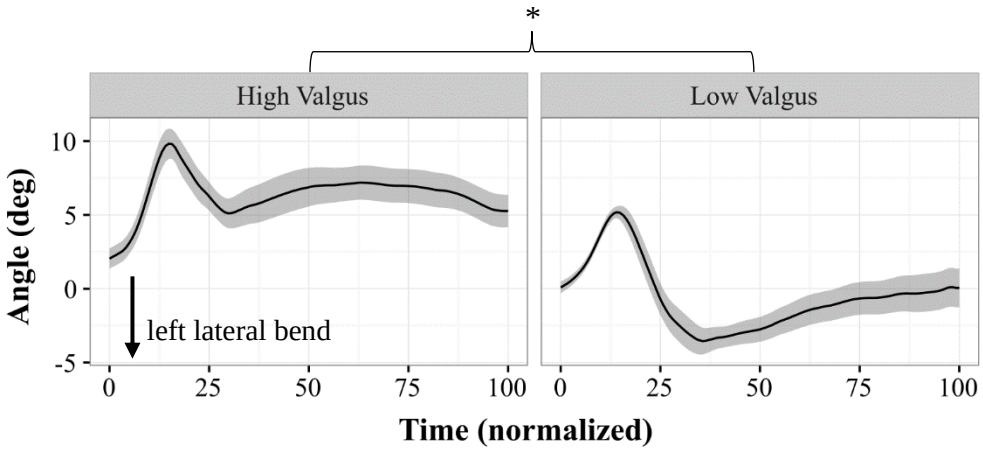

Figure 48: Lumbar Spine Angle – Frontal Plane

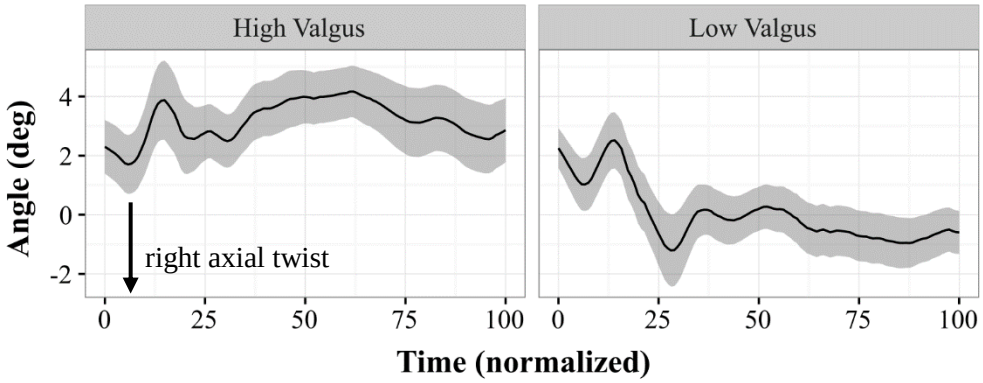

Figure 49: Lumbar Spine Angle – Transverse Plane

Left hip angles in all three planes were significantly different between groups. The low valgus group displayed significantly greater (F (1,37) = 7.933, p = 0.008) peak hip flexion (43.0 ± 7.9º) compared to the high valgus group (35.6 ± 8.3º) (Figure 50). In the frontal plane (Figure 51) the high valgus group presented with peak a hip adduction of 4.9 ± 4.2º, while the low valgus group's minimum abduction was 0.1 ± 6.0º and thus never dropped into adduction (F (1,37) = 9.103, p = 0.005). While in the transverse plane the low valgus group had a peak external rotation of 11.9 ± 6.7º, compared to the 4.8 ± 6.8º peak of the high valgus group (F (1,37) = 10.754, p = 0.002) (Figure 52).

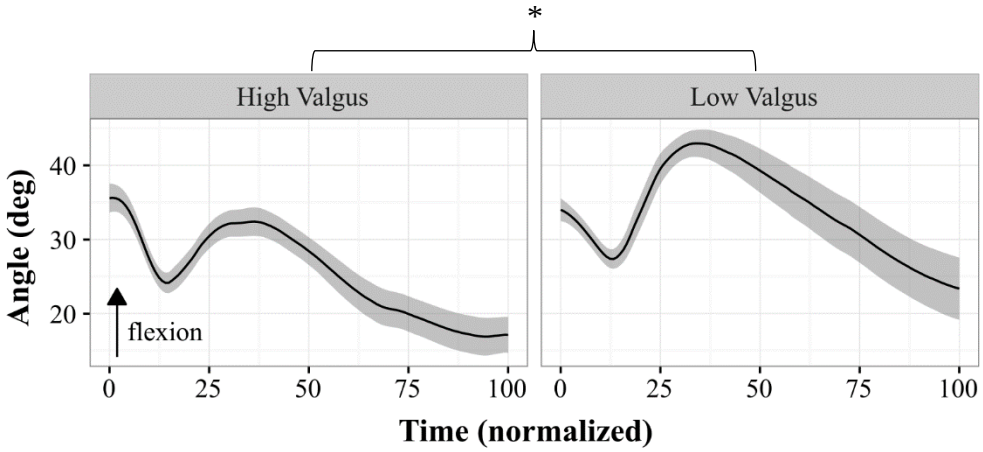

Figure 50: Left Hip Angle – Sagittal Plane

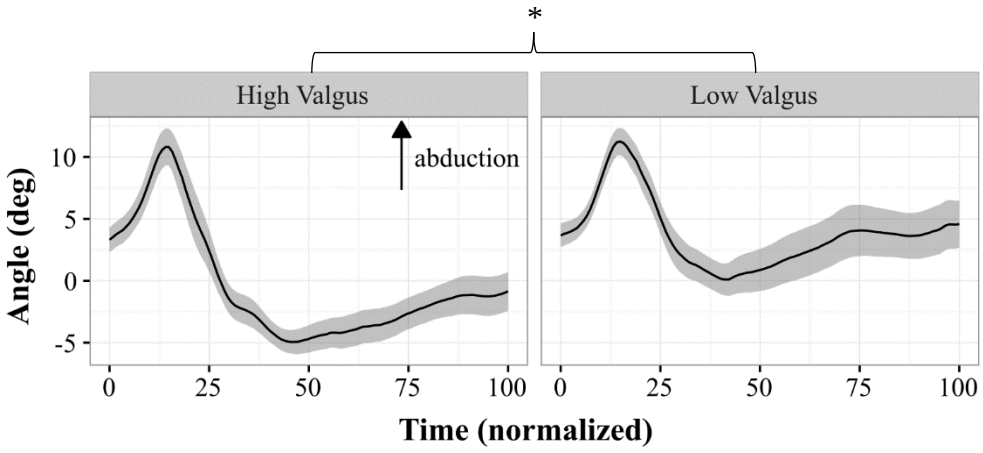

Figure 51: Left Hip Angle – Frontal Plane

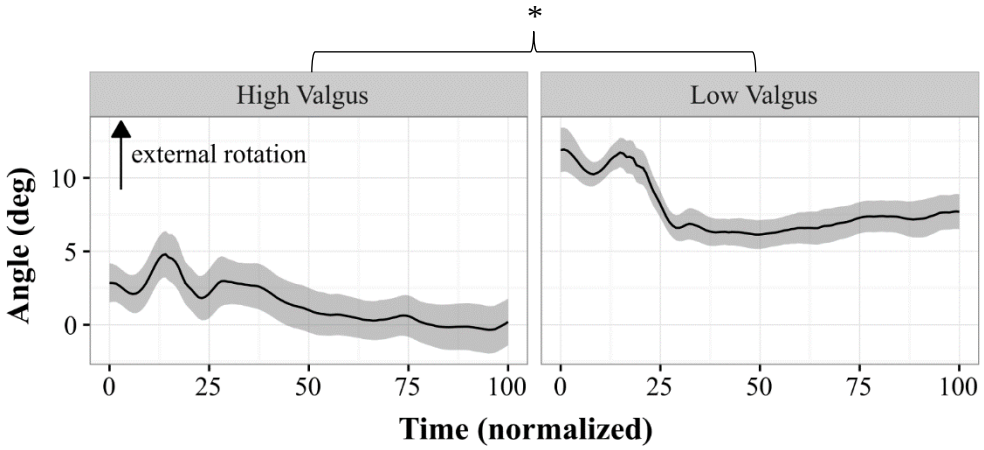

Figure 52: Left Hip Angle – Transverse Plane

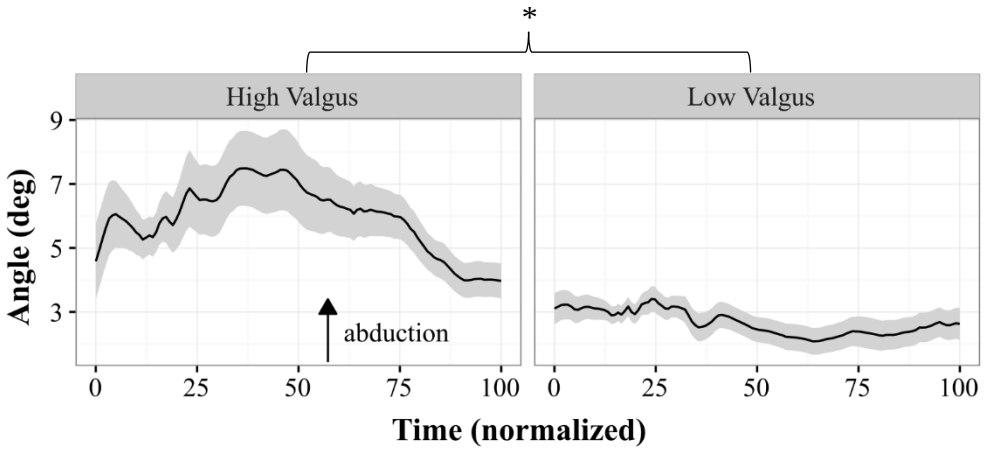

Figure 53: Left Knee Angle – Frontal Plane.

Peak knee abduction angle was significantly greater ($F(1,45) = 4.843$, $p = 0.032$) in the high valgus group (7.4 ± 6.6^{o}) compared to the low valgus group (4.5 ± 1.3^{o}) (Figure 53).

Lumbar JRS in all axes followed similar trends in shape with the low valgus group having statistically significant greater peak JRS in the transverse plane and the Euclidean Norm of the JRS, but not reaching significance in the sagittal and frontal plane. In the sagittal plane the low valgus group generated 478.6 ± 212 Nm/rad while the high valgus group managed 373.2 ±

135.6 Nm/rad (F (1,45) = 3.874, p = 0.05). Frontal plane lumbar JRS in low valgus was 306.6 ± 123.2 Nm/rad, compared to the 243.1 ± 87.8 Nm/rad in high valgus (F (1,45) = 3.948, p = 0.05). The low valgus group elicited 146.8 ± 72.7 Nm/rad of transverse plane JRS in comparison to the high valgus group's 109.9 ± 35.0 Nm/rad (F (1,45) = 4.547, p = 0.038) (Figure 54). Meanwhile the Euclidean Norm JRS (Figure 55) was significantly greater (F (1,45) = 4.243, p = 0.045) in low valgus (586.5 ± 245.8 Nm/rad) than high valgus (458.4 ± 160.0 Nm/rad).

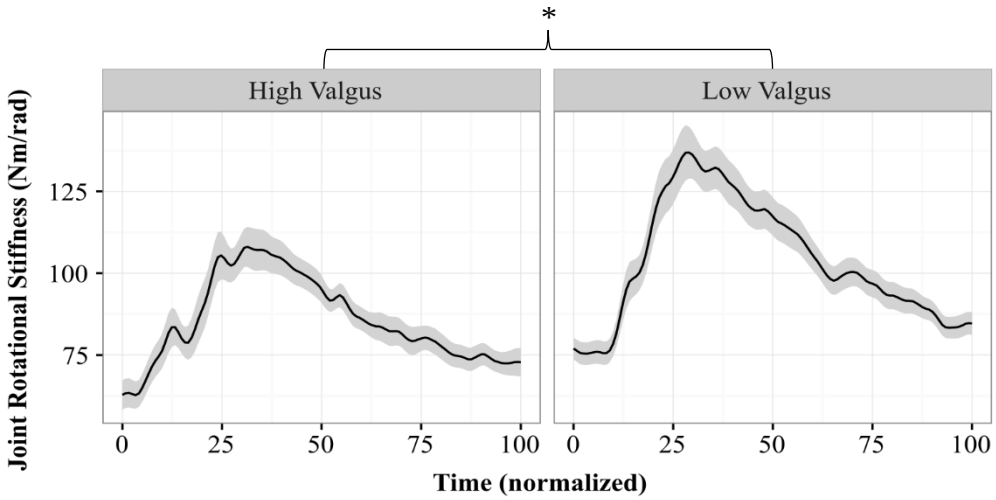

Figure 54: Lumbar Spine Transverse Plane JRS.

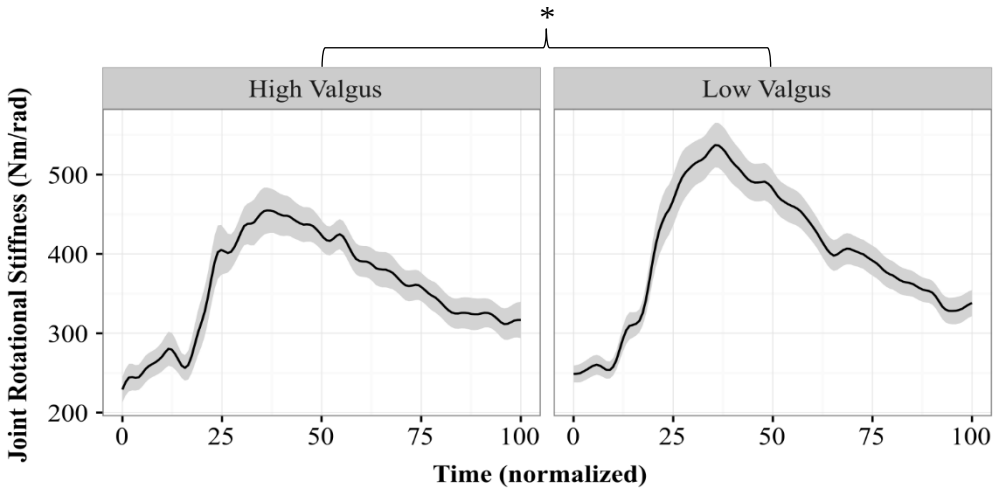

Figure 55: The Euclidean Norm of Lumbar Spine JRS.

Planes of summed muscle stiffness showed a consistent trend of low valgus having larger peak stiffness values. In both LB_R and LB_L planes low valgus peak stiffness were > 20% than high valgus, however LB_R did not achieve significance (F (1,45) = 3.890, p = 0.055) while LB_L differences were deemed significant between groups (F (1,45) = 8.157, p = 0.006) (Figure 56). Similarly, in the axial twist planes for both directions, low valgus had magnitudes of peak stiffness >20% than high valgus. However, AT_R (Figure 57) was deemed statistically significant (F (1,45) = 4.890, p = 0.032) while AT_L was not ((F (1,45) = 2.634, p = 0.108).

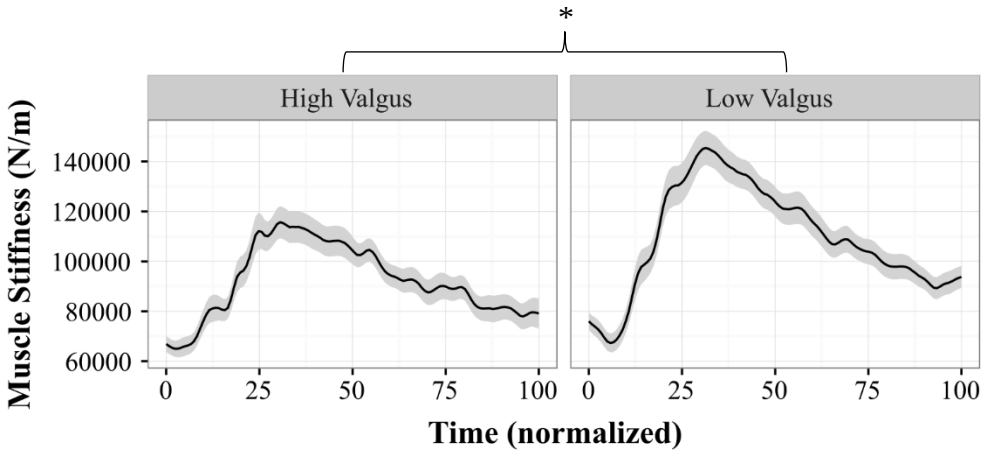

Figure 56: Summed muscle stiffness of the LB_L plane.

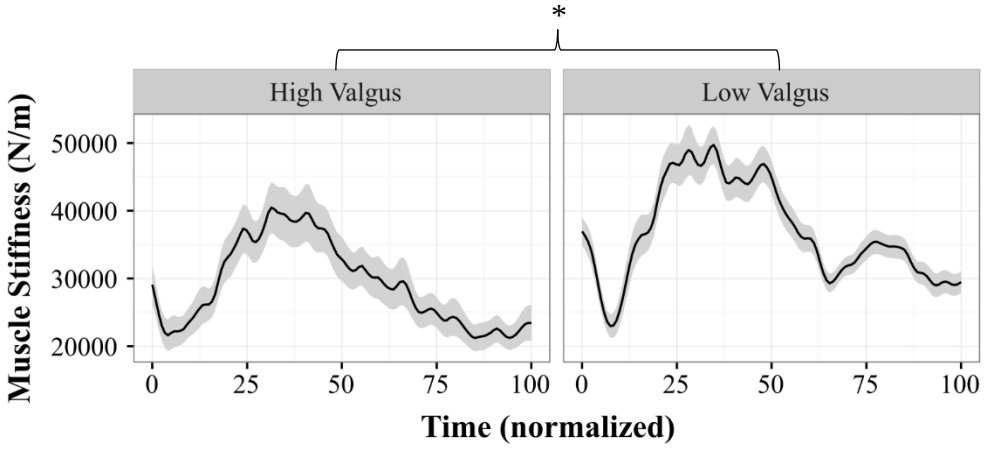

Figure 57: Summed muscle stiffness of the AT_R plane.

Quadrants' summed muscle stiffness were > 20 % larger in the low valgus group for the right anterior (F (1,45) = 3.949, p = 0.05) (Figure 58) and left anterior quadrants (F (1,45) = 3.362, p = 0.07) yet neither achieved significance. Conversely, the left posterior quadrants' difference was significantly larger in the low valgus group (F (1,45) = 4.539, p = 0.039) compared to the high valgus group (Figure 59). The right posterior quadrants were < 20% different between groups and were non-significant (F (1,45) = 1.333, p = 0.25).

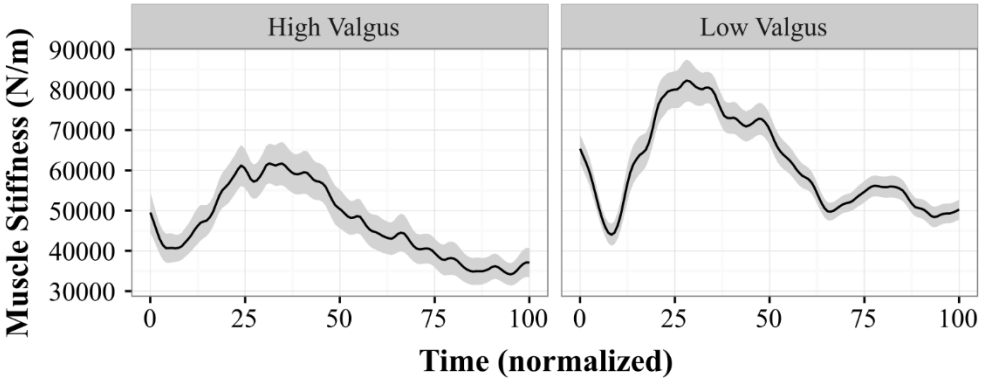

Figure 58: Right anterior quadrant summed muscle stiffness.

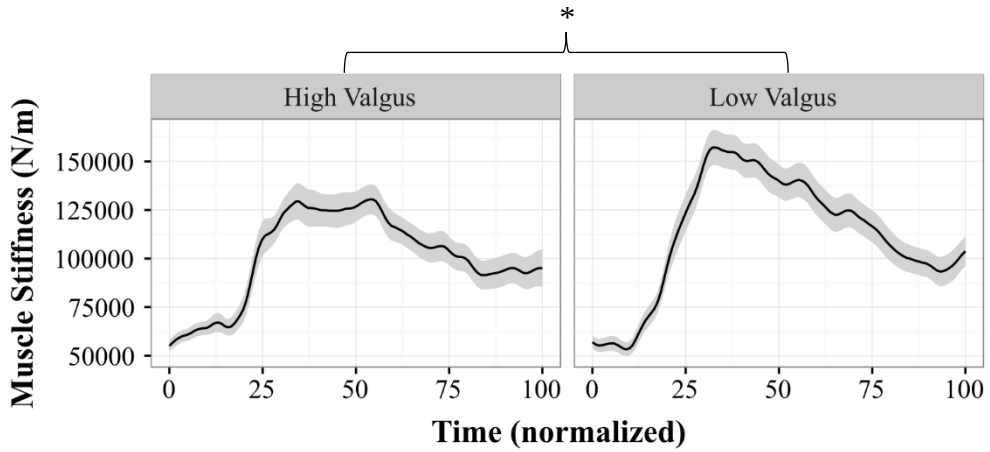

Figure 59: Left posterior quadrant summed muscle stiffness.

Frontal plane JRS at the left hip saw the low valgus group (3125.7 ± 1498 Nm/rad) have significantly greater peak values than the high valgus group (1853.0 ± 1060 Nm/rad) ($F(1,28) = 6.936$, $p = 0.013$) (Figure 60). Specifically, the summed abductors ($F(1,28) = 7.156$, $p = 0.012$), gluteus medius ($F(1,28) = 5.432$, $p = 0.027$) (Figure 61), and gluteus maximus superior's ($F(1,28) = 11.142$, $p = 0.002$) (Figure 62) frontal plane JRS was significantly greater in the low valgus group.

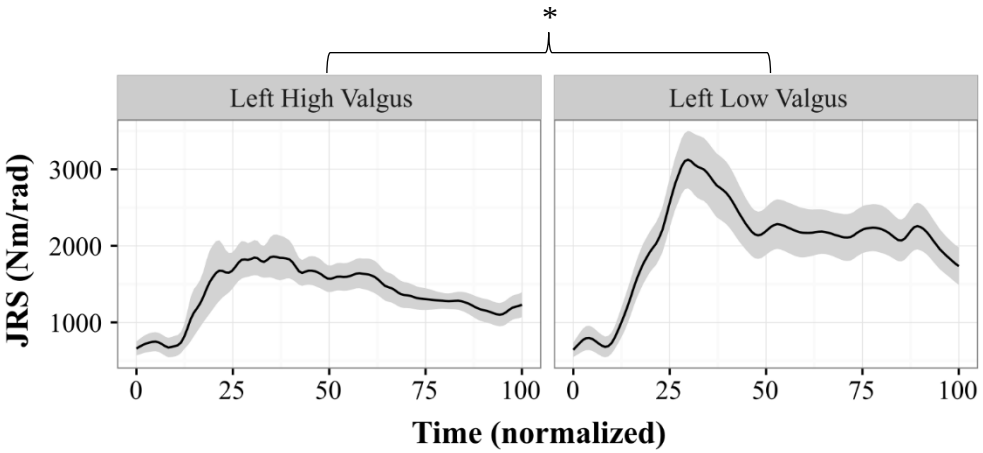

Figure 60: Left Hip Frontal Plane JRS.

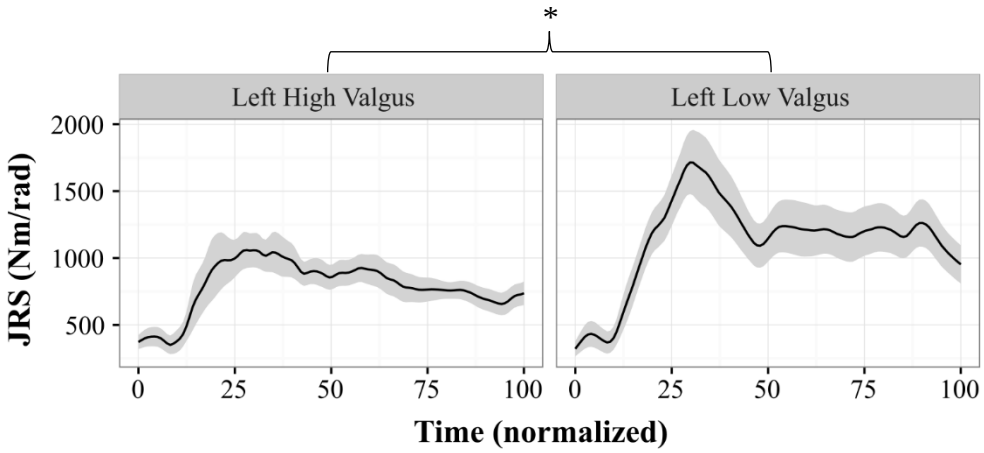

Figure 61: Left Gluteus Medius JRS contribution in the Frontal Plane.

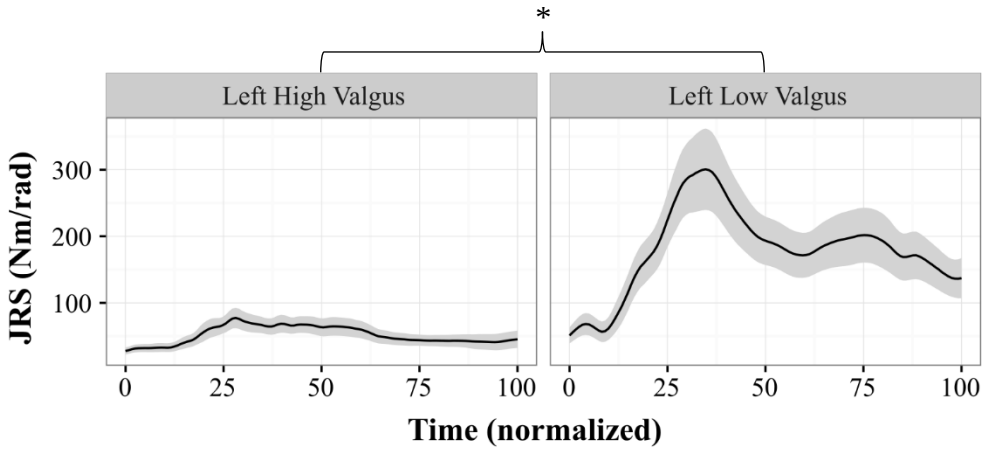

Figure 62: Left Gluteus Maximus Superior JRS contribution in the Frontal plane.

The transverse plane for left hip JRS shows similar results to that of the frontal plane. Total transverse plane JRS was significantly greater in the low valgus group ($F(1,28) = 9.853$, $p = 0.004$) with a peak of 1290.7 ± 745 Nm/rad compared to the high valgus groups peak of 541.9 ± 329.7 Nm/rad (Figure 63). The gluteus maximus superior's contribution to transverse plane JRS (Figure 64) was significantly higher in low valgus (367.4 ± 273.4 Nm/rad) than high valgus (95.7 ± 90.3 Nm/rad) ($F(1,28) = 10.09$, $p = 0.004$).

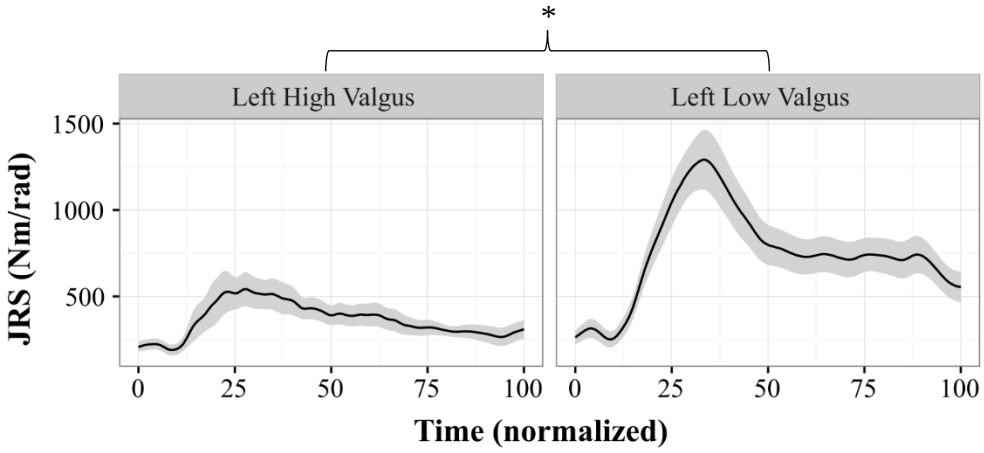

Figure 63: Left Hip Transverse Plane JRS.

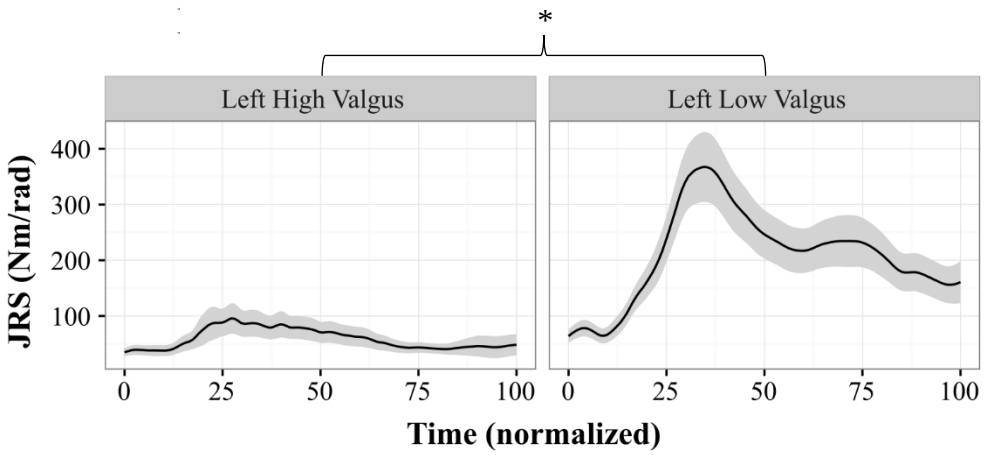

Figure 64: Left Gluteus Maximus Superior JRS contribution in the Transverse Plane.

5.4.2 Right SLD

The right knee's valgus status was determined as per the procedures described in section 4.3.4 of the Methods. The results of these procedures for the left knee are presented in Figure 65. Time-normalized data is presented for the SLD from the point at which the participant has left the box (at the top of the drop) until they land and regain their COM in upright single leg stance.

The high valgus group displayed significantly greater ($F(1,49) = 5.889$, $p = 0.019$) peak lumbar spine flexion (24.8 ± 10.7^{o}) than the low valgus group (18.0 ± 9.3^{o}) (Figure 66). In the frontal plane the high valgus group experienced greater lateral bend to the right (4.2 ± 7.4^{o} vs 1.1 ± 5.1^{o}) however this was not statistically significant ($F(1,49) = 3.285$, $p = 0.076$) (Figure 67). Axial twist of the lumbar spine was very similar in both groups and thus no significant differences existed between them (Figure 68).

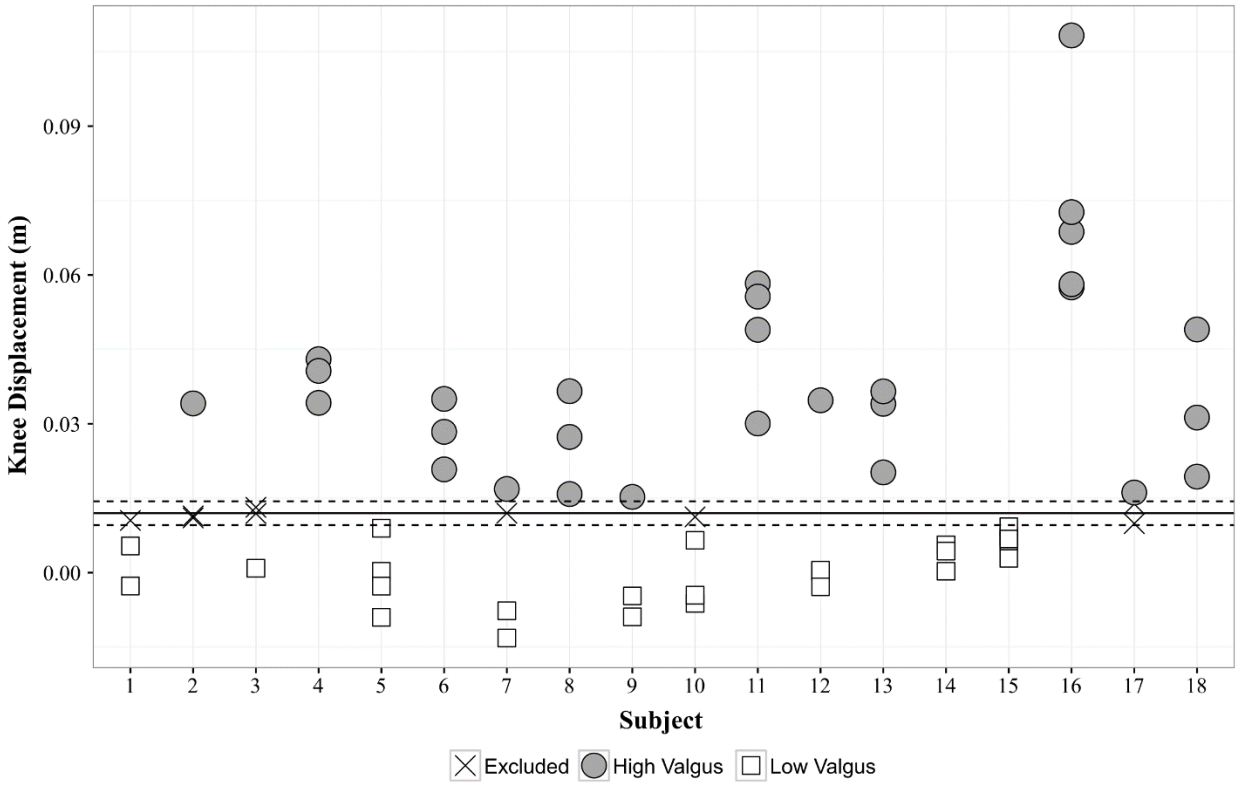

Figure 65: Right knee peak medial displacement for all trials. The solid line denotes the median value, while the dashed lines are the median value ± 20% to define thresholds for low and high valgus status. Trials within the dashed lines are excluded from analysis.

Right hip flexion (Figure 69) was slightly greater in the high valgus group (60.0 ± 12.3^{o}) than low valgus (55.1 ± 11.2^{o}) (F (1,49) = 2.231, p = 0.142). Peak hip abduction was significantly greater (F (1,49) = 10.142, p = 0.003) in the high valgus group (8.6 ± 4.6^{o}) than low valgus (2.8 ± 5.2^{o}) (Figure 70). Right knee peak abduction angle (Figure 71) was significantly greater (F (1,49) = 7.235, p = 0.009) in high valgus (5.4 ± 8.4^{o}) compared to low valgus (-0.26 ± 6.5^{o}), meaning that the mean peak never actually went into abduction, but got close to neutral.

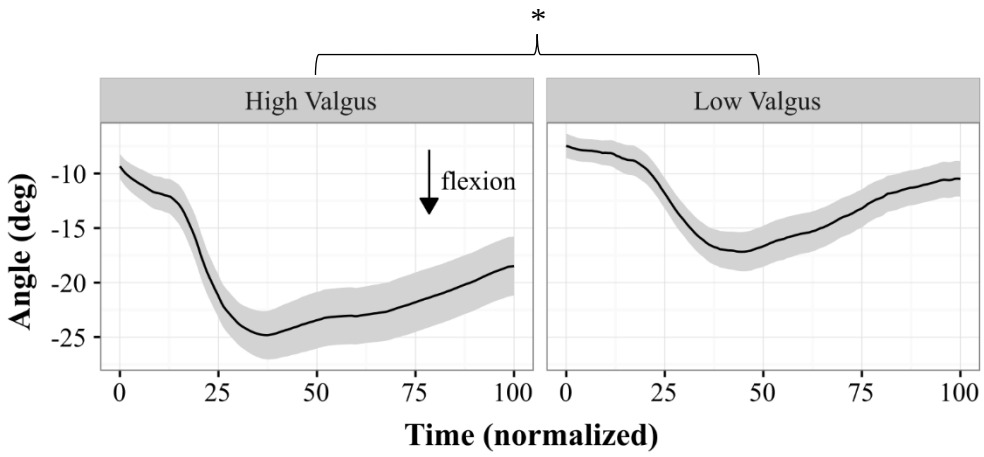

Figure 66: Lumbar Spine Angle – Sagittal Plane.

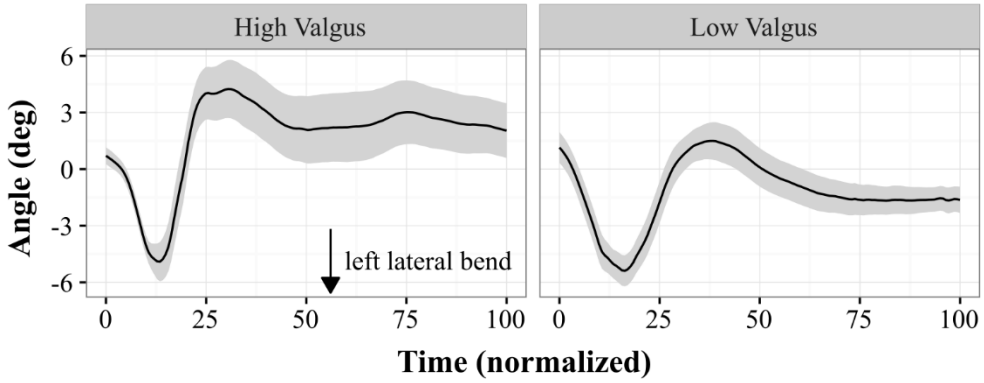

Figure 67: Lumbar Spine Angle – Frontal Plane.

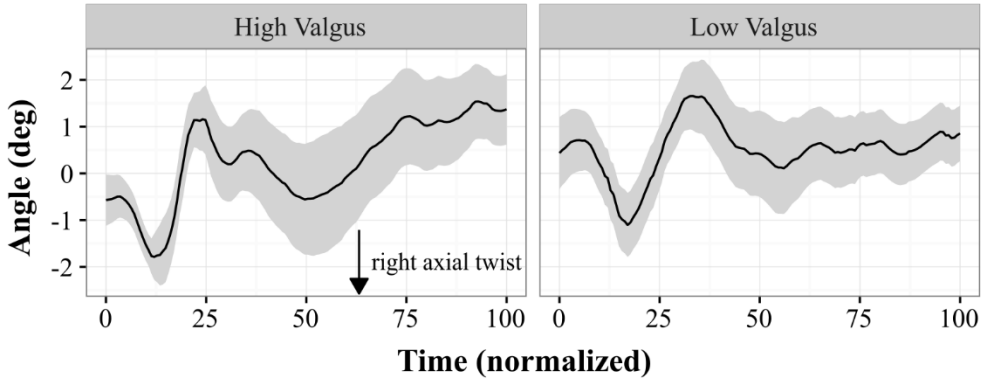

Figure 68: Lumbar Spine Angle – Transverse Plane.

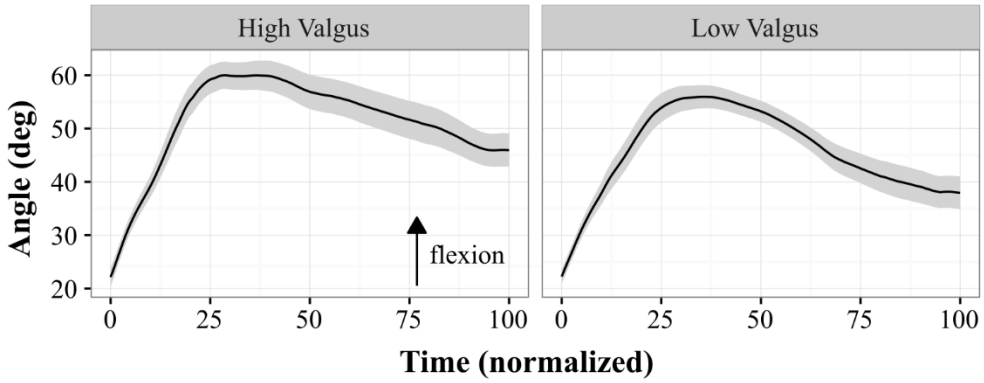

Figure 69: Right Hip Angle – Sagittal Plane.

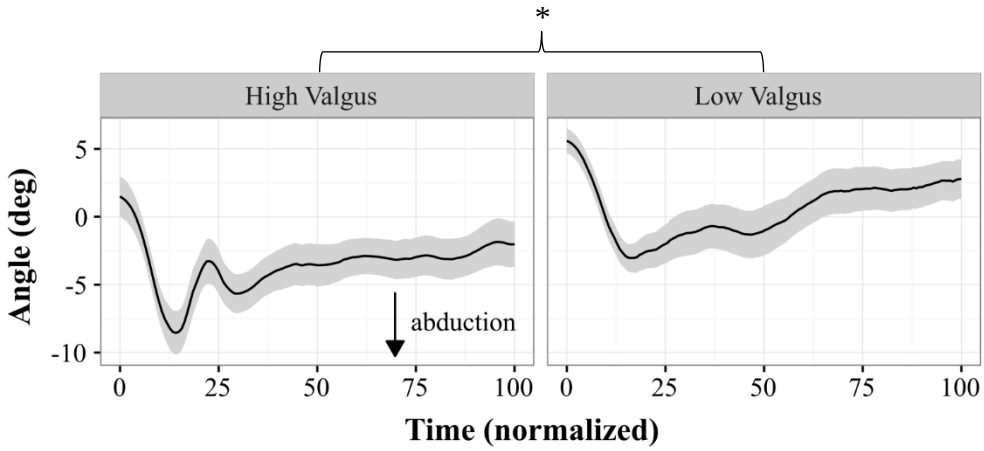

Figure 70: Right Hip Angle – Frontal Plane.

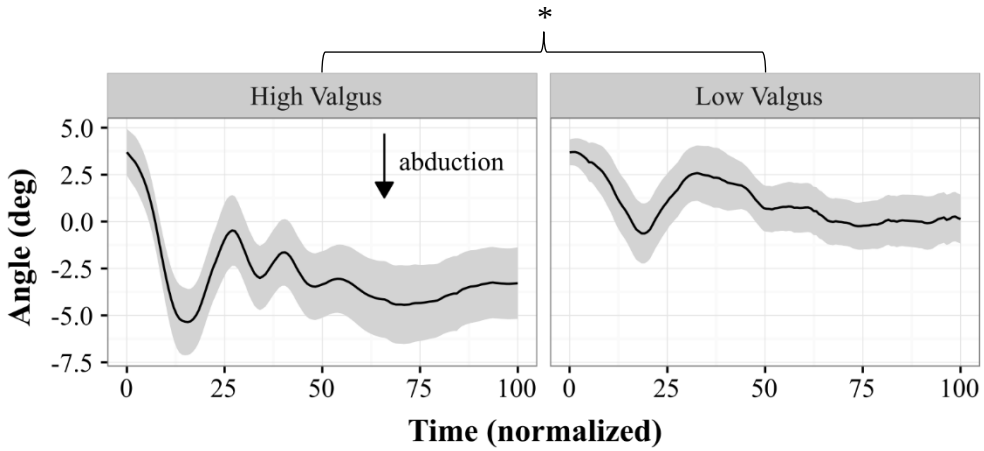

Figure 71: Right Knee Angle – Frontal Plane.

Lumbar JRS was generally higher in all three planes, however only the transverse plane resulted in statistical significance ($F(1,49) = 5.5302$, $p = 0.023$) with the low valgus group peak of 136.5 ± 53.8 Nm/rad and high valgus peak of 107.5 ± 26.8 Nm/rad (Figure 72). The Euclidean Norm JRS is a representative example of the trends observed in the sagittal and frontal plane (Figure 73).

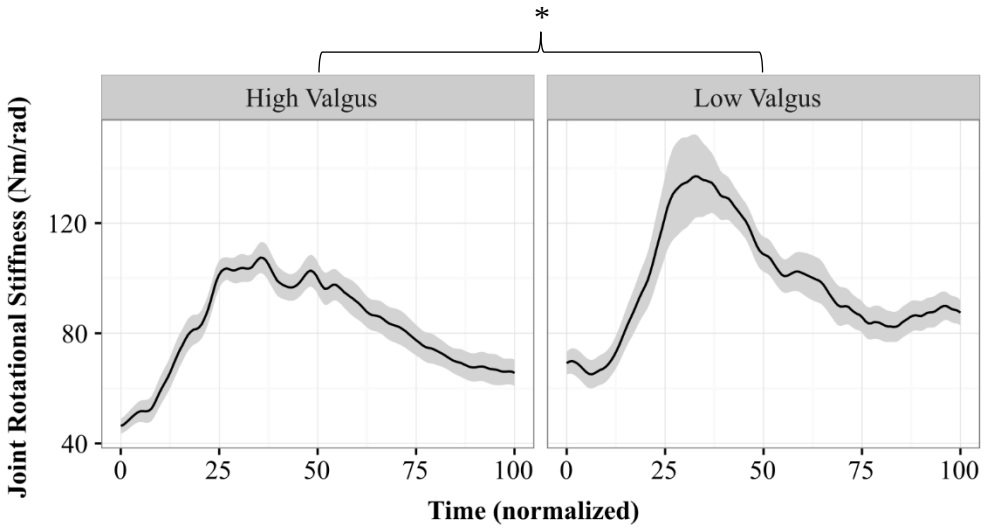

Figure 72: Lumbar Spine Transverse Plane JRS.

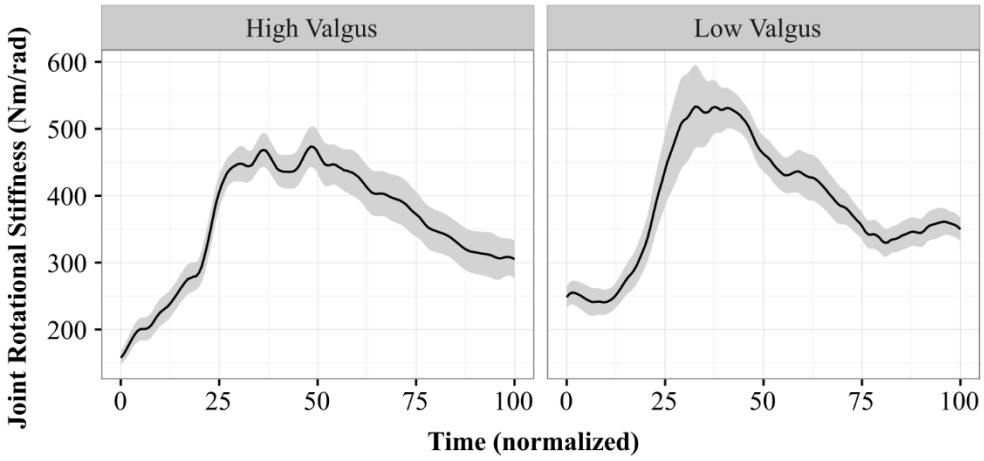

Figure 73: Lumbar Spine Euclidean Norm JRS. A representative example of the relative differences between groups as that seen in the sagittal and frontal plane JRS.

In the summed muscle stiffness variables several showed the low valgus group to be > 20% stiffer than the high valgus group. Significance was reached in the LB_R plane ($F(1,49) = 4.065$, $p = 0.049$, Figure 74), AT_R plane ($F(1,49) = 8.815$, $p = 0.004$, Figure 75) as well as the right anterior quadrant ($F(1,49) = 8.238$, $p = 0.006$, Figure 76) and left anterior quadrant ($F(1,49) = 4.491$, $p = 0.039$, Figure 77). While the FE plane and posterior quadrants showed no differences between groups.

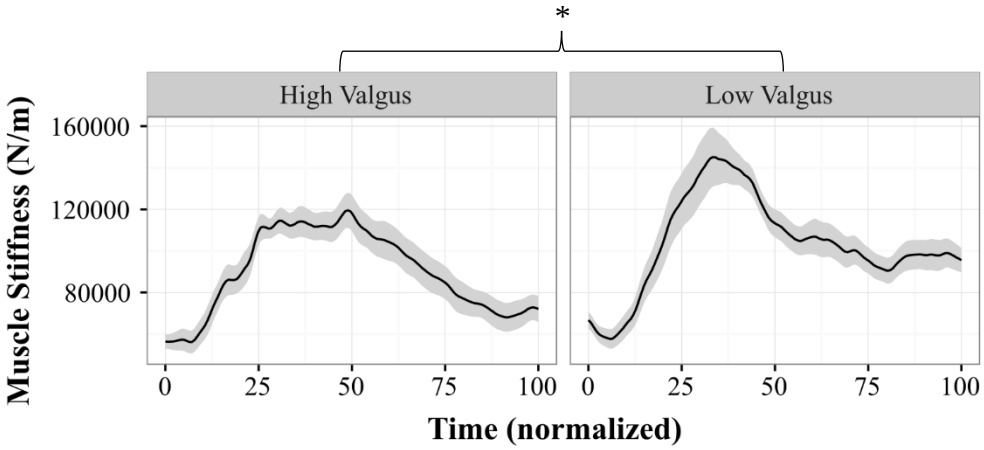

Figure 74: Summed muscle stiffness of the LB_R plane.

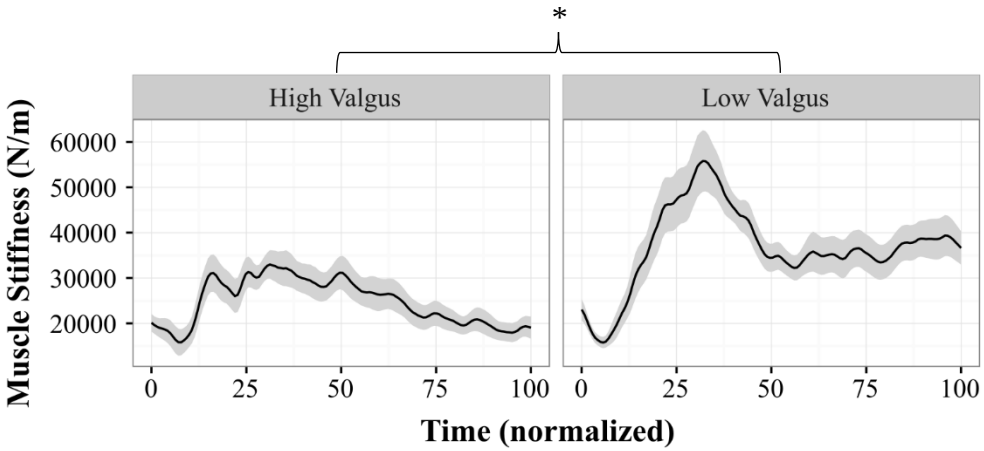

Figure 75: Summed muscle stiffness of the AT_R plane.

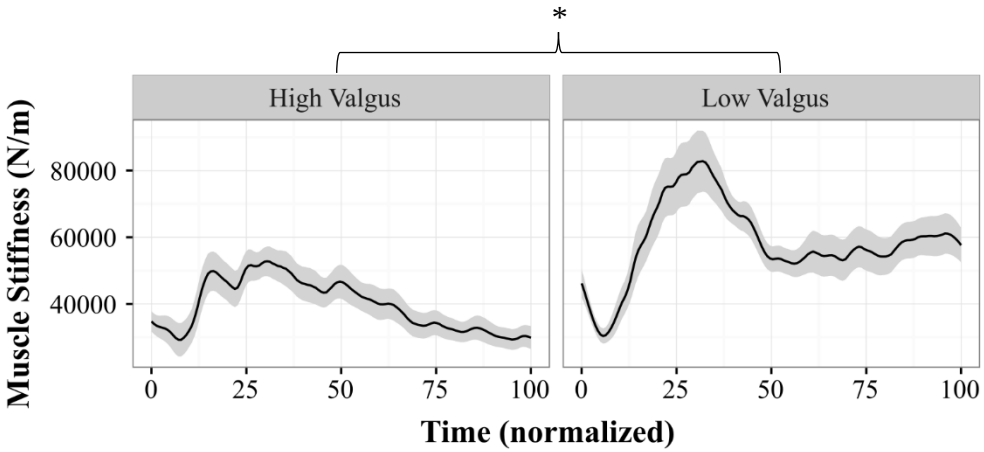

Figure 76: Right anterior quadrant summed muscle stiffness.

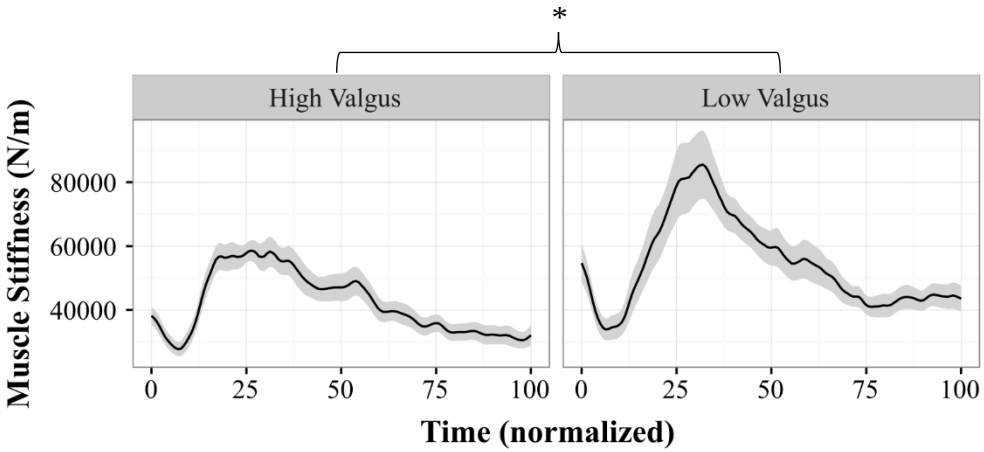

Figure 77: Left anterior quadrant summed muscle stiffness.

No statistically significant differences were found in the right hip peak frontal plane JRS (Figure 78) between low valgus (26478.0 ± 2173.2 Nm/rad) and high valgus (1875.1 ± 728.0 Nm/rad) groups ($F(1,49) = 1.963$, $p = 0.17$). Muscle contributions from the abductors, gluteus medius and gluteus maximus superior, to frontal plane hip JRS were similarly greater in the low valgus group but not statistically different. In the transverse plane the low valgus group's peak JRS of 908.1 ± 702.7 Nm/rad was not significantly greater than the high valgus group's 667.8 ± 248.2 Nm/rad ($F(1,49) = 1.731$, $p = 0.20$) (Figure 79). Right gluteus medius' contribution to transverse plane hip JRS was significantly greater ($F(1,49) = 4.617$, $p = 0.037$) in low valgus (416.3 ± 267.4 Nm/rad) than high valgus (264.6 ± 115.8 Nm/rad) (Figure 80).

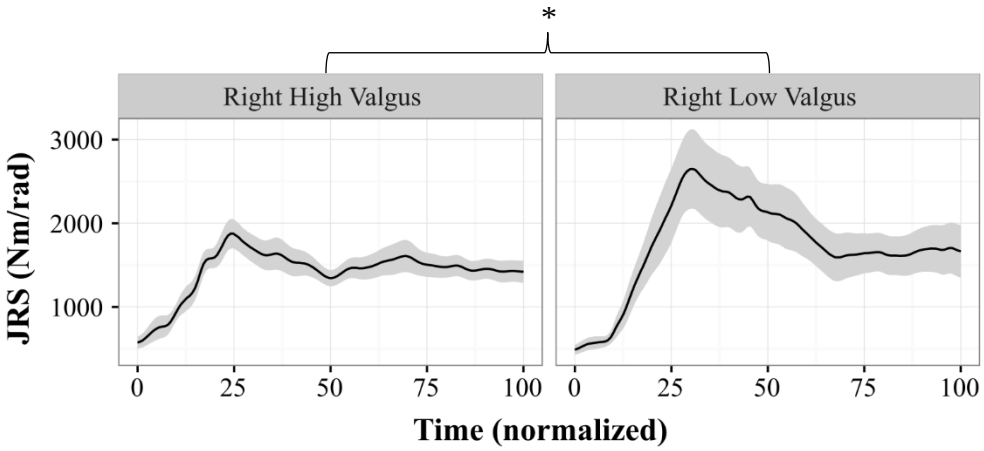

Figure 78: Right Hip Frontal Plane JRS.

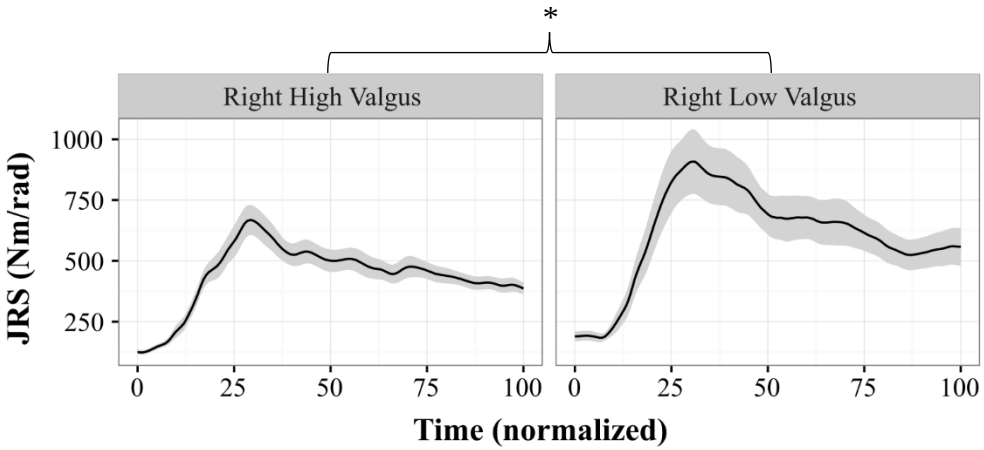

Figure 79: Right Hip Transverse Plane JRS.

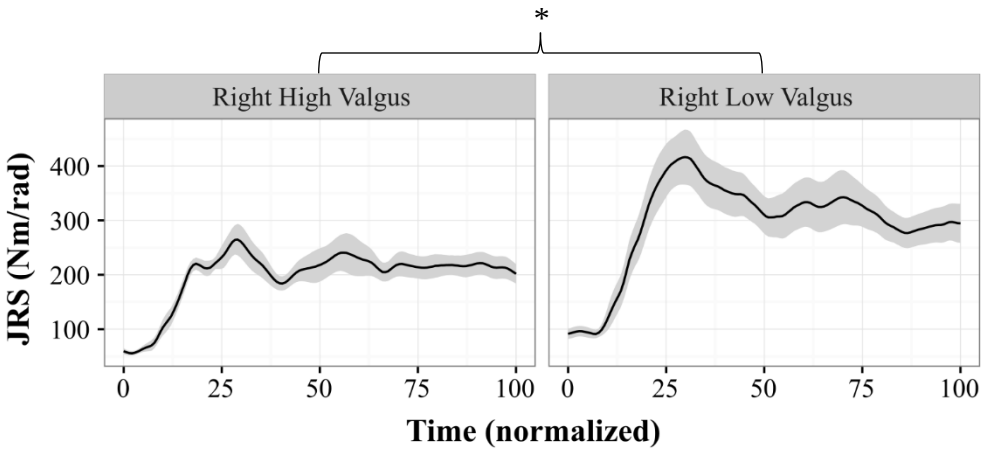

Figure 80: Right Gluteus Medius Transverse Plane JRS.

5.5 Single Leg Crossover Drop

The Single Leg Crossover Drop (SLCD) task was done for each limb, thus each limb was independently defined as high valgus or low valgus. All hip variables reported are for the ipsilateral side of interest only. Given that hip angles are measured considering the femur's orientation with respect to the pelvis, on single leg support more exaggerated lateral trunk lean (void of lumbar lateral bend) was observed in some subjects. This could present as hip abduction in frontal plane hip angle, however, the action of the femur adducting in the hip joint in this posture would cause dynamic valgus, thus frontal plane knee angle is of interest in the single leg landings due to this phenomenon. Again, due to the nature of single leg landing and the increased frontal plane challenge, the previously defined 'planes' and 'quadrants' of summed muscle stiffness become of interest to infer possible areas of deficit.

5.5.1 Left SLCD

The left knee's valgus status was determined as per the procedures described in section 4.3.4 of the Methods. The results of these procedures for the left knee are presented in Figure 81. Time-normalized data is presented for the SLCD from the point at which the participant has left the box (at the top of the drop) until they land and regain their COM in upright single leg stance.

Differences between low and high valgus groups in lumbar spine angles were unremarkable in all three planes, as were sagittal and transverse plane hip angles. However, peak left hip adduction was significantly greater ($F(1,47) = 13.620$, $p = 0.0005$) in the high valgus group (7.9 ± 5.8^{o}) in comparison with the low valgus group (1.5 ± 6.4^{o}) (Figure 82).

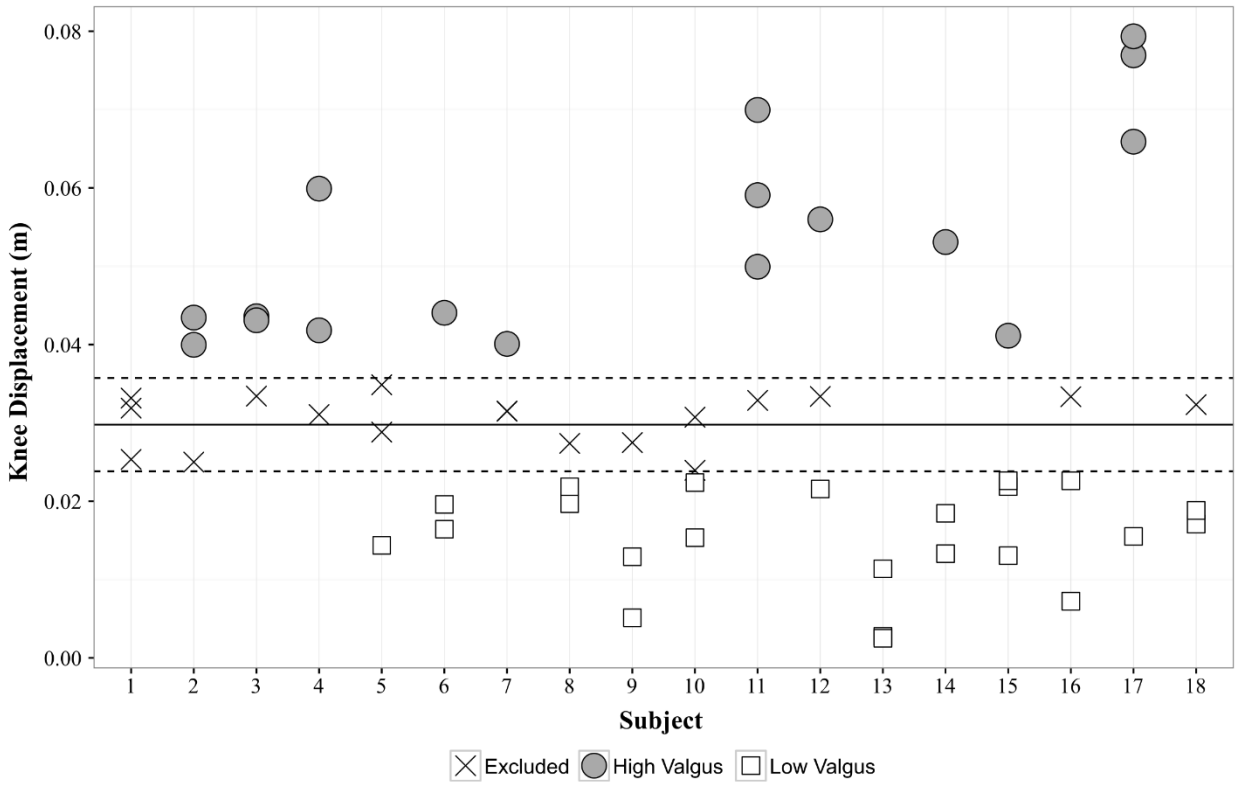

Figure 81: Left knee peak medial displacement for all trials. The solid line denotes the median value, while the dashed lines are the median value ± 20% to define thresholds for low and high valgus status. Trials within the dashed lines are excluded from analysis.

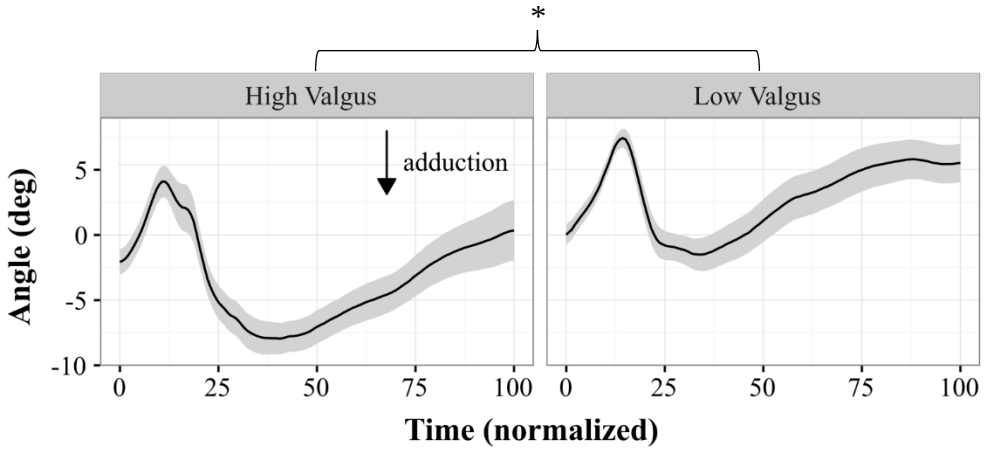

Figure 82: Left Hip Angle – Frontal Plane.

The low valgus group (154.2 ± 69.5 Nm/rad) had significantly more (F (1,47) = 4.389, p = 0.042) lumbar spine transverse plane JRS than the high valgus group (118.0 ± 47.8 Nm/rad) (Figure 83). Meanwhile differences in sagittal and frontal plane, as well as the Euclidean Norm JRS were non-significant differences between groups. The LB_R plane (F (1,47) = 4.207, p = 0.046), AT_R plane (F (1,47) = 4.925, p = 0.031) and right anterior quadrant (F (1,47) = 6.915, p = 0.011) summed muscle stiffness were significantly greater in the low valgus group opposed to the high valgus group by > 20 % (Figure 84).

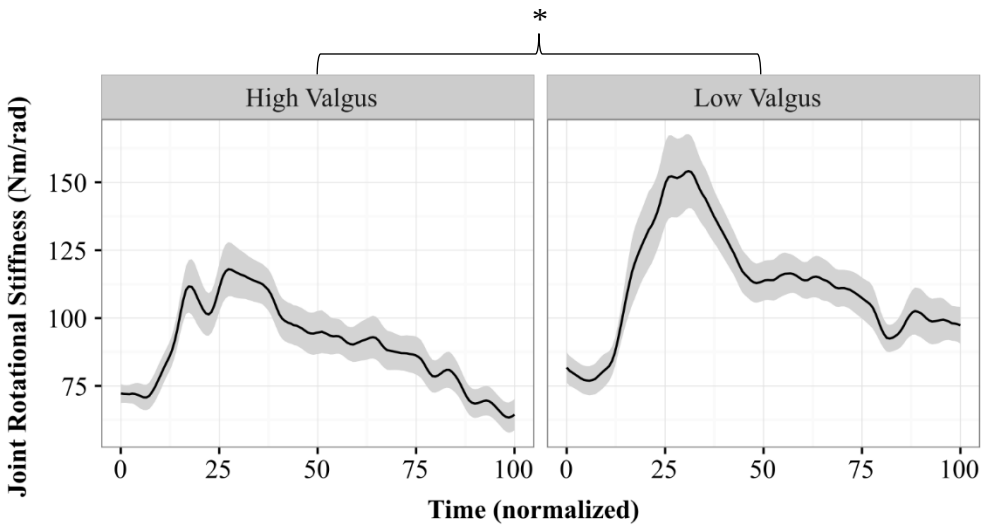

Figure 83: Lumbar Spine JRS – Transverse Plane.

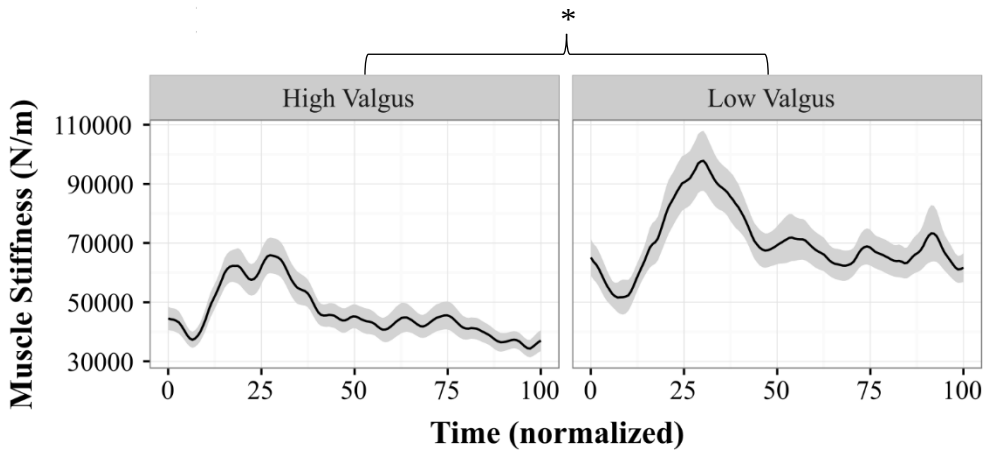

Figure 84: Right anterior quadrant summed muscle stiffness. Curves and relative magnitudes between groups are representative of LB_R and AT_R planes of summed muscle stiffness which were also significantly greater in the low valgus group.

The left hip sagittal plane JRS were significantly greater ($F(1,47) = 6.312$, $p = 0.017$), in the low valgus group (1702.3 ± 1271.9 Nm/rad) than high valgus group (769.4 ± 640.8 Nm/rad) (Figure 85). Also significantly greater in the low valgus group were peak hip frontal plane JRS ($F(1,47) = 10.802$, $p = 0.003$), abductors JRS ($F(1,47) = 9.905$, $p = 0.004$) and gluteus medius' JRS ($F(1,47) = 9.530$, $p = 0.005$) in the frontal plane (Figure 86). Gluteus medius' JRS contribution in the transverse plane was significantly greater in low valgus ($F(1,47) = 6.496$, $p = 0.018$).

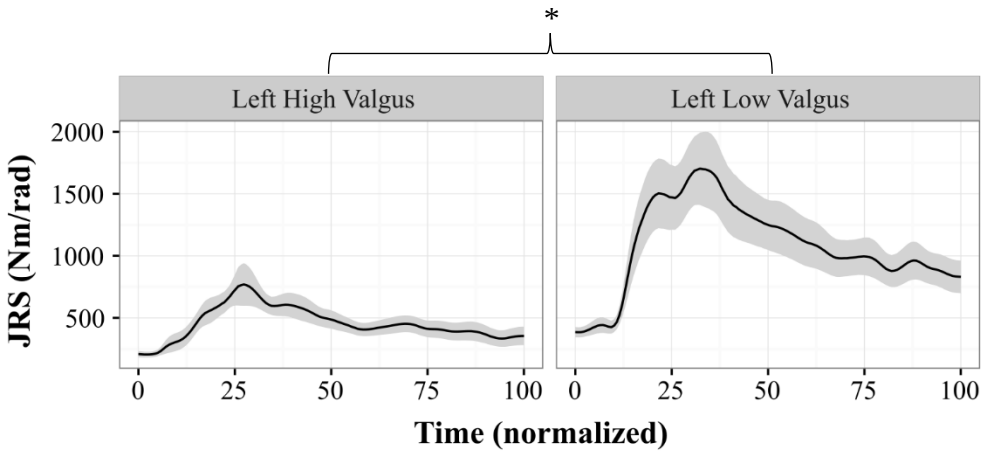

Figure 85: Left Hip Sagittal Plane JRS.

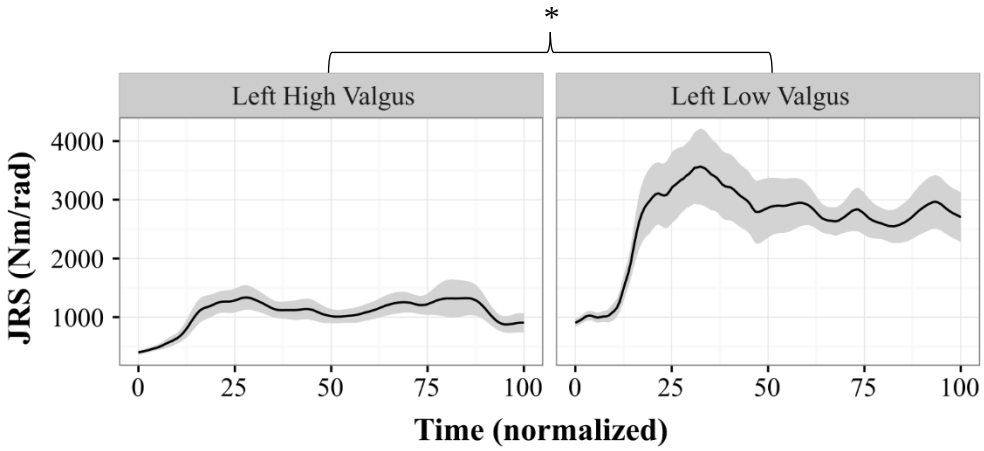

Figure 86: Left Hip Frontal Plane JRS. This figure is representative of abductors and gluteus medius' JRS trends and relative differences between groups which were also significantly greater in the low valgus group.

5.5.2 Right SLCD

The right knee's valgus status was determined as per the procedures described in section 4.3.4 of the Methods. The results of these procedures for the left knee are presented in Figure 87. Time-normalized data is presented for the SLD from the point at which the participant has left the box (at the top of the drop) until they land and regain their COM in upright single leg stance.

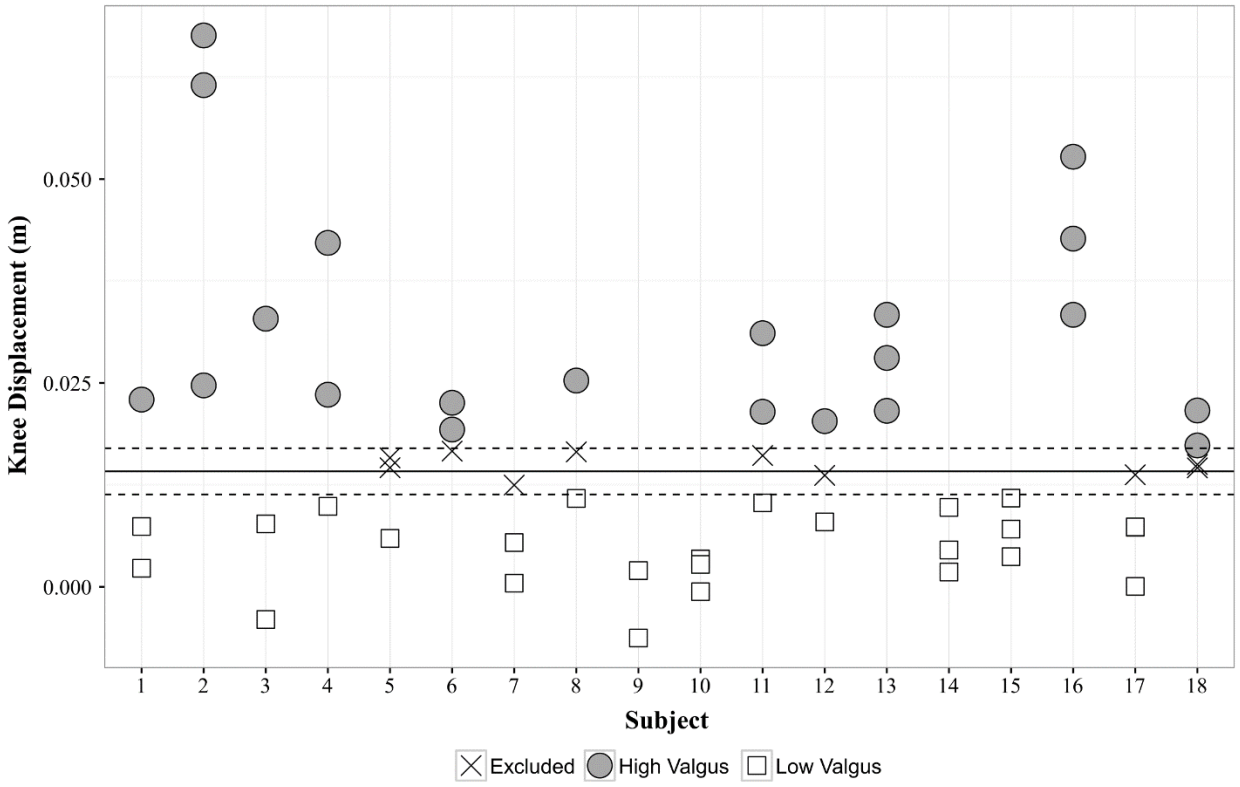

Figure 87: Right knee peak medial displacement for all trials. The solid line denotes the median value, while the dashed lines are the median value ± 20% to define thresholds for low and high valgus status. Trials within the dashed lines are excluded from analysis.

Peak lumbar spine flexion was significantly greater ($F(1,45) = 9.098$, $p = 0.049$) in the high valgus group (23.3 ± 11.6^{o}) than low valgus (16.9 ± 10.3^{o}) (Figure 88). The high valgus group also displayed greater right lateral bend following initial contact with a peak of 5.8 ± 4.6^{o}, versus the low valgus group's peak of 2.3 ± 3.7^{o} ($F(1,45) = 8.438$, $p = 0.006$). The high valgus also displayed 3.4^{o} greater peak hip abduction at IC than the low valgus group (Figure 89).

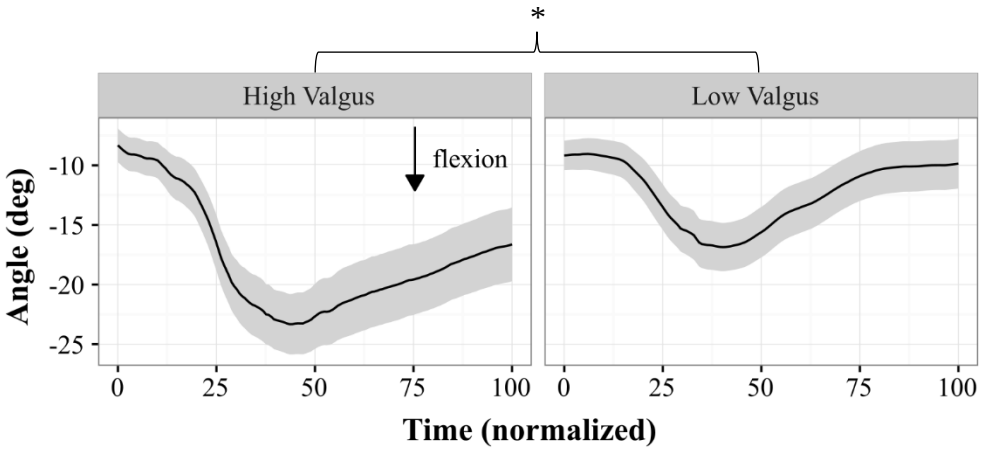

Figure 88: Lumbar Spine Angle – Sagittal Plane.

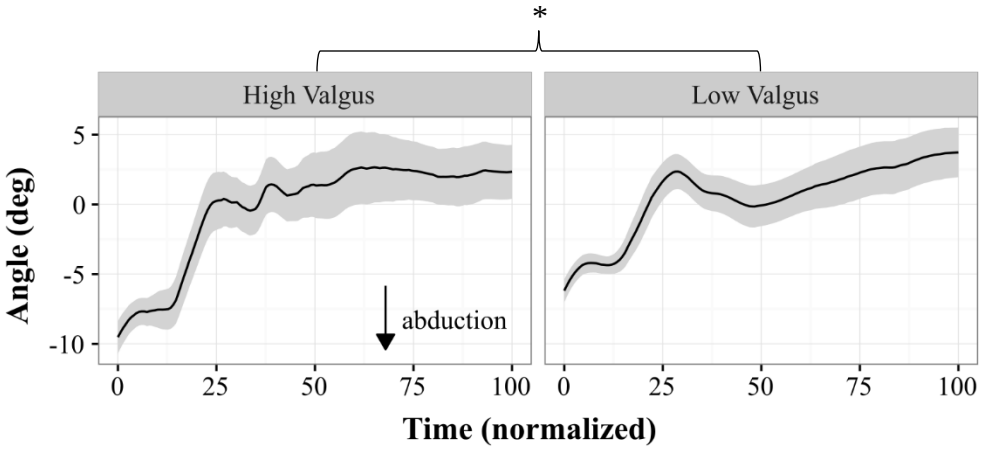

Figure 89: Right Hip Angle – Frontal Plane.

The low valgus group had greater peak lumbar JRS in all planes, however significance was only achieved in the transverse plane (F (1,45) = 5.010, p = 0.03) with the low valgus group having 30 Nm/rad greater JRS (Figure 90). In particular, the right (F (1,45) = 9.0035, p = 0.004) and left (F (1,45) = 5.717, p = 0.021) anterior quadrants also had significantly greater peak stiffness (Figure 91).

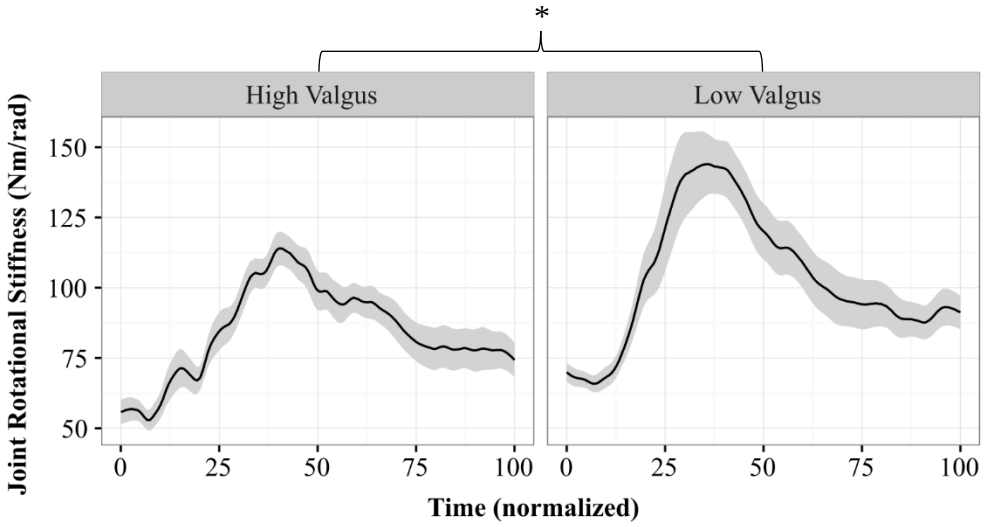

Figure 90: Lumbar Spine JRS – Transverse Plane.

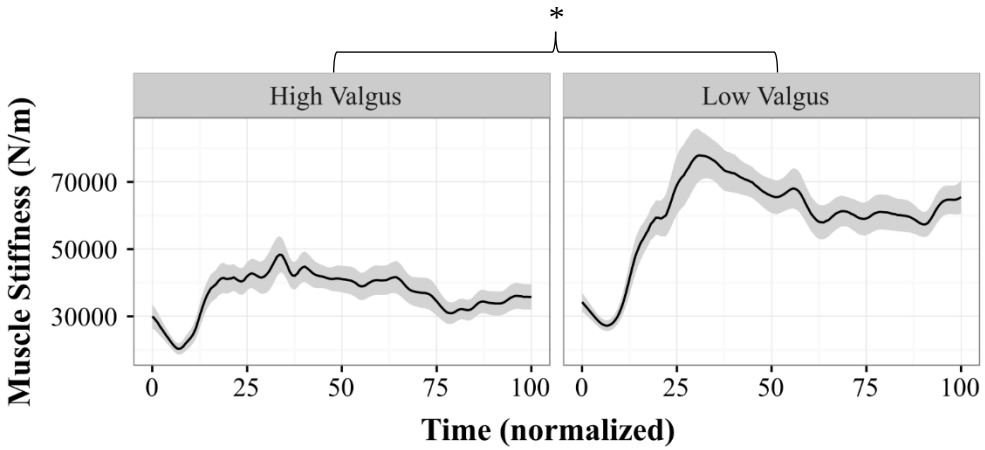

Figure 91: Right anterior quadrant summed muscle stiffness. This figure is also representative of the left anterior quadrant.

The right hip JRS were not significantly different in any plane between valgus groups despite > 20% difference in magnitude in the frontal (Figure 92) and transverse planes. The only variable that achieved statistical significance at the right hip was gluteus medius' contribution to transverse plane JRS (Figure 93), where the low valgus peak of 335.8 ± 215.6 Nm/rad was significantly greater than that of the high group's peak of 217.5 ± 52.3 Nm/rad ($F(1,45) = 4.327$, $p = 0.044$).

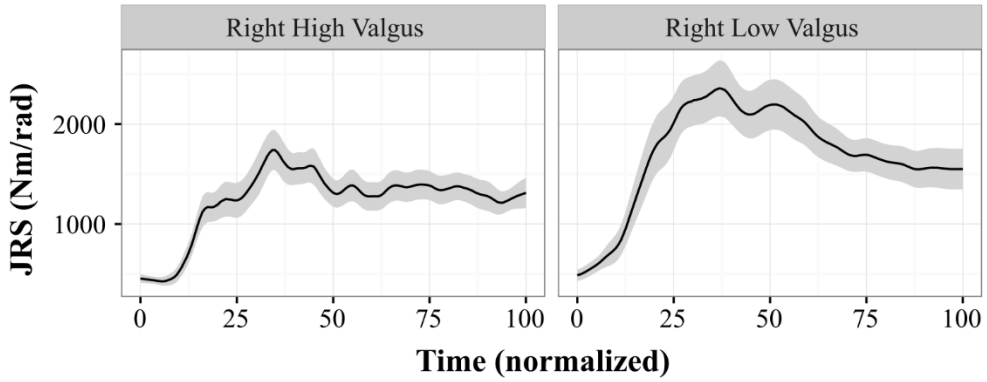

Figure 92: Right Hip Frontal Plane JRS.

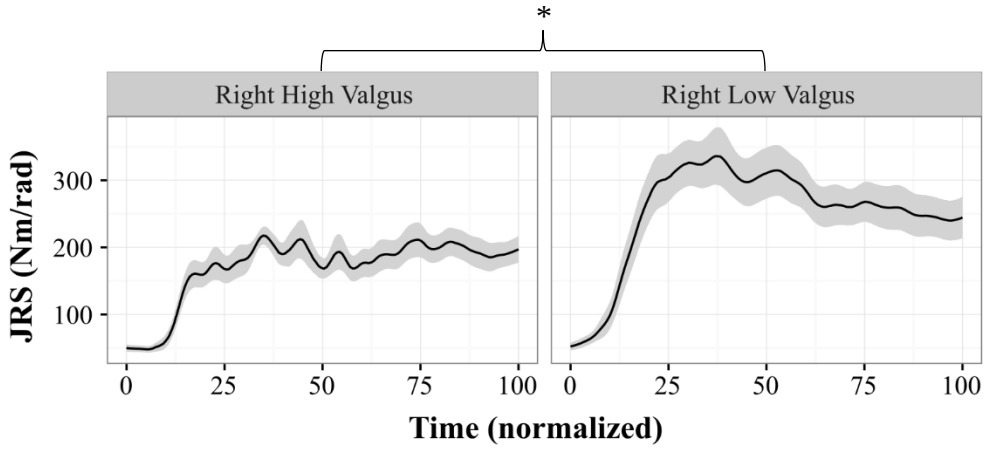

Figure 93: Right Gluteus Medius' Transverse Plane JRS.

5.6 Summary of Findings

In general trials in which large dynamic valgus (high valgus) were avoided, the participants displayed greater lumbar spine JRS and greater hip JRS. Meanwhile, they also exhibited more control of the linkage and avoided known injurious kinematics. A synergy emerged between gluteus medius and gluteus maximus superior in the low valgus group, in which both were substantial contributors to frontal and transverse plane hip JRS. However, in the case where either muscle was not appropriately stiffening, the other seemed to be able to assume the responsibility and ensure sufficient stiffness about the hip was achieved. A summary of findings comparing the magnitudes of high valgus to low valgus groups across tasks can be found in Table 5.

Table 5: Summary of findings for High Valgus compared to Low Valgus.

<table>
<tr><th></th><th>Kinematic Description</th><th>Lumbar Spine JRS</th><th>Hip JRS</th></tr>
<tr><td>DVJ</td><td>▪ Greater lumbar spine flexion
▪ Less hip flexion
▪ Greater hip adduction
▪ Greater hip internal rotation</td><td>o Less sagittal plane JRS
o Less Euclidean Norm JRS</td><td rowspan="4">• Less frontal plane JRS
• Less transverse plane JRS
• Less gluteus medius JRS contributions in frontal plane
• Less gluteus medius JRS contributions in transverse plane
• Less gluteus maximus superior JRS contributions in frontal plane
• Less gluteus maximus superior JRS contributions in transverse plane</td></tr>
<tr><td>Stop Jump</td><td>▪ No difference in lumbar spine
▪ Greater hip adduction
▪ Greater hip internal rotation</td><td>o No difference in JRS</td></tr>
<tr><td>Left Single Leg Landings</td><td>▪ Slightly greater lumbar spine flexion
▪ Greater hip adduction
▪ Ipsilateral pelvis drop
▪ Contralateral leg medial movement</td><td rowspan="2">o Less frontal plane JRS
o Less transverse plane JRS
o Less Euclidean Norm JRS</td></tr>
<tr><td>Right Single Leg Landings</td><td>▪ Lateral Trunk Lean to Right
▪ Greater action of right hip adduction, as distal femur moves medially
▪ Greater right knee abduction angle</td></tr>
</table>

6.0 Discussion

In the discussion section to follow the hypotheses are revisited and confirmed or rejected based on the evidence reported in the Results section. The results of each task are interpreted with consideration of all dependent variables. An interesting discrepancy between left and right landings is brought forth. The lumbar spine and hip JRS are discussed in context of any relevant literature to the topic of the thesis, before mechanisms and motor strategies are considered. The limitations of the work are discussed, and finally contributions and conclusions drawn from this work are laid out.

6.1 Hypotheses Revisited

The original statement of hypotheses in section 3.1 outlined that differences in dependent variables would be observed with respect to 'at risk' or 'not at risk' groups, as defined by the 25.25 Nm KAM threshold. As the project evolved the independent variable was changed from the KAM to peak medial knee displacement, in order to dichotomize participants and best answer the research question. A rationale for this is provided in the Results section 5.1 and is discussed below in section 7.2. Given this modification the hypotheses changed from referencing risk status to 'High Valgus' or 'Low Valgus' based on the procedures previously described. However, the main intent of the hypotheses were unaltered in their proposition that dependent variable measures would differ between groups.

Hypothesis 1:

Differences between groups will be observed in three-dimensional lumbar spine angles.

Generally, the high valgus group displayed greater lumbar spine flexion across all tasks. On the single leg landing tasks, the high valgus group also displayed more motion in lateral bend.

Hypothesis confirmed.

Hypothesis 2:

Three-dimensional lumbar spine joint rotational stiffness will be greater in the low valgus group.

Across all tasks lumbar spine JRS was greater in the low valgus group, particularly in the frontal plane and transverse plane for single leg landings. Planes and quadrants summed muscle stiffness indicate that greatest differences were in the frontal and transverse planes.

Hypothesis confirmed.

Hypothesis 3:

Differences between groups will be observed in three-dimensional hip angles.

The low valgus group consistently displayed greater hip abduction and external rotation than the high valgus group. The high valgus group weren't always necessarily adducted and internally rotated at the hip, but rather less abducted and less externally rotated. The differences in angles allowed the low valgus group to safely avoid dynamic valgus.

Hypothesis confirmed.

Hypothesis 4:

Frontal and transverse plane hip joint rotational stiffness will be greater in the low valgus group.

The low valgus group consistently elicited greater hip JRS in the frontal and transverse plane. Most notable differences between groups were in the frontal and transverse planes.

Hypothesis confirmed.

Hypothesis 5 and 6:

5) Gluteus medius' contribution to joint rotational stiffness will account for the largest differences between groups in the frontal plane.
6) Gluteus maximus superior's contribution to joint rotational stiffness will account for the largest differences between groups in the transverse plane.

On the DVJ the largest differences on the left side were gluteus medius, while on the right more gluteus maximus' role in the frontal plane. The stop jump task exposed extremely high differences in gluteus maximus contribution in particular, on both sides. Single leg landing tasks on the right highlighted largest differences in gluteus medius' contribution to the transverse plane JRS. On the left SLD gluteus medius in the frontal plane was the largest difference, while on the SLCD the largest difference was also gluteus medius, but in the transverse plane.

Hypotheses confirmed with caveat. *

***** Despite the largest differences were not always most prevalent for a particular muscle in a particular plane, the emergence that either the gluteus maximus superior or gluteus medius accounted for the largest differences emphasizes the importance of the gluteal complex in three-dimensional JRS.

6.2 KAM vs Medial Knee Displacement

It was noted that certain subjects landed 'harder' than others and incurred higher KAM magnitudes than those that landed 'softer'. However, this did not necessarily encapsulate the quality of their kinematics and the individual's ability to control the linkage. The high KAM in

this case often occurred prior to the counter movement and peak dynamic valgus presentation. In order to actually injure the ACL - aberrant kinematics leading to the injurious dynamic valgus posture, concomitant with a high load - would be necessary to strain the ACL to a point of failure. However, in controlled tasks such as those performed in this work, where there are no extrinsic variables to consider (as there may be in a sport setting), the inability to avoid valgus is indicative of deficits that may be inherent in the individual and would likely be present in more demanding movements. In such movements, higher loads are likely to be experienced given the demands of the sporting situation, it is then that aberrant control of the linkage in conjunction with the high loads of an explosive task would create an ideal situation for ACL failure. It is also worth noting the cumulative effect of dynamic valgus altering the stress-strain relationship with each successive lengthening. Ligamentous creep due to repetitive strain compromises its ability to withstand load, appropriately stiffen local musculature, and check shearing movement of the femur on the tibia (Baratta et al., 2001; McGill, 2007; Soma, 2015)

Work by Bates et al (2013) analyzed drop vertical jumps and recorded kinematics and kinetics of the knee at initial contact, and at the instance of peak vGRF. At initial contact compared to instance of peak vGRF, both limbs demonstrated more hip abduction (mean 4.4^{o} vs. 3.8^{o}) and less knee abduction (mean 1.9^{o} vs. 4.3^{o}), while the left KAM was greater (4.6 vs 3.7 Nm) and right KAM was lower (-1.4 vs 0.2), note the magnitude of moment is higher for right KAM but was actually an adduction moment (Bates et al, 2013). This demonstrates that at initial contact a higher KAM moment may be experienced in the absence of valgus, and not at the instance of peak vGRF. In an analysis of single leg landings that compared ‘soft’ and ‘hard’ landing techniques, it was found that at peak ACL force sagittal plane hip and knee kinematics differed significantly, while hip and knee moments did not (Laughlin et al 2011). While this

analysis was in the sagittal plane, it further supports the possibility that reported injurious kinematics may be observed in the absence of concomitant changes in knee moments.

Given that dynamic valgus is the injurious posture that is most recognized as inferring an individual's risk for future non-contact ACL injury, it was used to dichotomize participants instead of the KAM as initially proposed. The likelihood of dynamic valgus inducing harmful ACL forces and strains has been documented previously in the literature at a variety of sagittal and transverse plane knee joint angles (Fukuda et al., 2003; Kanamori et al., 2000; Lloyd & Buchanan, 2001; Markolf et al., 1995). Thus, evaluation of dynamic valgus as a measure of ACL injury risk is well established in the literature, with previous works having used hip adduction and knee abduction in combination to evaluate dynamic valgus, while other works have directly measured knee excursion in order to encapsulate both hip and knee frontal plane angles in one measure (Ford et al., 2006; Laughlin et al., 2011; Myer, Ford, & Hewett, 2011; Myer, Ford, Khoury, Succop, & Hewett, 2010a; Owens et al., 2009; Pollard, Sigward, & Powers, 2010; Sigward, Ota, & Powers, 2008; Sigward, Pollard, Havens, & Powers, 2012; Utturkar et al., 2013). Given the known biological implications of dynamic valgus on ACL loading and injury risk, splitting trials by at least a 40% difference in medial knee displacement suggests that differences found between these groups in proximal joint stiffness would be both biomechanically relevant, and hold biological significance.

While dynamic valgus presentation is used to infer injury risk, as was done in this study, no participants actually injured their ACL. Thus, deeming one's "injury risk" must be considered in context. This was not a prospective longitudinal study design in which future injury was recorded and directly linked back to dependent variables. However, magnitude of valgus presentation and KAM has been shown to be predictive of future non-contact ACL injury. This

may be due to the tendency for acute trauma when valgus presents in combination with large forces and moments creating an applied load greater than that of the tissue tolerance. Or, the repetitive sub-failure trauma from continual dynamic valgus reducing the failure tolerance until a point of failure is reached. In either case, the predisposition to present with dynamic valgus during athletic maneuvers puts one at risk of future non-contact ACL injury.

Given the disparity between the use of KAM (as originally proposed in this work) and peak medial knee displacement (as actually used in this work) in characterization of injury risk, as well as the variance of individuals within and across tasks – implications for screening must be considered. The use of a single KAM in 25.25 Nm as used by several research groups may not be sensitive enough to an individual's kinematics that put them at particular risk for injury. Additionally, taking the mean of the peak KAM across 3 trials may obscure the risk of injury in any given instant, as well as mask differences in other variables between trials that display large differences in KAM. Thus, a story may exist in the variance of an individual that is lost when one takes a mean of several trials. Meanwhile, collecting three trials of a task is standard practice in research with human participants in order to ensure clean, and representative, data is obtained. However, given individuals' variance within tasks and the story that may exist in this variance, one must consider how many trials may be necessary to observe the true variance and the associated injury risk. Additionally, the possibility of injury exists in any acute instance as previously described, thus multiple trials may be necessary to capture the injurious case if it does present. Conversely, collecting additional trials may allow for a learning effect to occur and the variance within an individual to decrease.

6.3 DVJ

The DVJ presented a sagittal plane challenge at the lumbar spine, and those who experienced bilateral valgus collapse also displayed lumbar flexion collapse (Figure 20), these participants generated substantially less lumbar spine sagittal plane JRS in comparison to the no valgus group who elicited higher lumbar JRS and less flexion (Figure 21). At the hips, high valgus trials generally displayed less hip flexion (Figure 25), abduction (Figure 26), while eliciting greater JRS from the gluteus medius (Figure 24) and gluteus maximus superior (Figure 28) in the frontal and transverse planes. The slightly greater hip flexion, with less lumbar spine flexion suggests the low valgus group avoided landing erect but did not collapse at the lumbar spine, thus tuning the anterior trunk lean appropriately to control the COM. In the frontal and transverse plane, the left hip saw a max of approximately 9^{o} abduction and 10^{o} external rotation in both groups, while on the right hip the low valgus group displayed 13^{o} abduction and 12^{o} external rotation and the high valgus group 7^{o} of abduction and 17^{o} external rotation. Other works have reported maximal frontal plane hip angles in the range of 2.1^{o} to 8.7^{o} abduction and 1.2^{o} to 18.5^{o} external rotation in high school and collegiate female athletes (Bates et al, 2013, Chappell and Limpisvasti, 2008, Myer et al 2006, Pollard et al, 2006, Souza and Powers, 2009). Several of these works included pre and post values with respect to training intervention programs aimed at reducing ACL injury risk, in which those identified as potentially at risk did not necessarily have more hip adduction and internal rotation, but less abduction and external rotation than their not at risk counterparts (Bates et al, 2013, Chappell and Limpisvasti, 2008).

6.4 Stop Jump

While the DVJ exposed differences largely in the lumbar spine JRS, the more demanding stop jump did not. The high valgus group displayed larger lumbar flexion than that of the no valgus (Figure 31) however, there were no differences of note in lumbar JRS in the statistical or biological sense. It was expected that this challenging task would have further exposed deficits in lumbar JRS, but rather it seemed the demands of the tasks required that a certain level of stiffness be achieved in order to appropriately transfer horizontal momentum upon landing, to vertical momentum in jumping. Insufficient lumbar JRS upon landing onto the force plates may have actually caused an individual to succumb to the horizontal momentum and lose whole body stability, resulting in falling anteriorly. Thus, it is suggested that the stop jump forced individuals to sufficiently stiffen about the lumbar spine in order to meet the moment demands placed on it and avoid buckling. The stop jump did however expose deficits in the hips, where the low valgus group displayed greater hip abduction (Figures 34, 40) and external rotation (Figures 35, 41). Additionally, the low valgus group, generated substantially larger frontal and transverse plane JRS, with contributions from gluteus maximus superior of particular distinction between the groups (Figures 38, 39, 44, 45). Maximal hip kinematic angles corresponded well with Chappell and Limpisvasti (2008) who reported angles for female collegiate athletes during the stop jump, in which maximum abduction was 8.3^{o} and maximum external rotation 20.0^{o}. In this work the low valgus maximum abduction angle were 8^{o} and 7^{o}, for the left and right hip respectively, while the high valgus group saw a maximum of 10^{o} on both sides. The maximum external rotation angles in the high group were 7.5^{o} and 12.5^{o} compared to the low valgus maximums of 17.5^{o} and 16.0^{o}, for the left and right hip respectively.

6.5 SLD and SLCD Left

Similar patterns were observed on left leg landing tasks, that were quite different strategies compared to that seen of right leg landings. On both SLD and SLCD a distinguishing variable between the groups was greater left hip adduction in the high valgus group, where the low valgus group stayed much closer to neutral following initial contact (Figures 51, 82). On the SLD right lateral bend accompanied the hip adduction in the high valgus group. Accompanying greater hip adduction in the high valgus group was substantially less JRS from the gluteus medius (Figures 61, 86) and gluteus maximus superior (Figures 62,64) in the frontal and transverse plane. Additionally, lumbar JRS in the low valgus group was greater in the transverse plane for both SLD and SLCD (Figures 54, 83) as were summed muscle stiffness's in anterior quadrants, lateral bend and axial twist planes (Figures 56-59, 84). Thus, those with low valgus had greater three-dimensional proximal joint stiffness.

6.6 SLD and SLCD Right

As noted above, single leg landings on the right side showed those in the high valgus group display a different kinematic pattern from that of left lands, but aberrant nonetheless. Of particular interest on the right SLD and SLCD are the high valgus group's increased right lateral bend (Figure 67) and hip abduction at initial contact (Figures 70, 89). These variables served to create a lateral trunk lean to the right, and right knee abduction angles (Figure 71). Once again, the low valgus groups displayed greater lumbar JRS particularly in the transverse plane (Figures 72, 90), and anterior quadrants (Figures 76, 91). Generally greater hip JRS was also observed in the low valgus group with gluteus medius' JRS in the transverse plane particularly distinguishable between groups (Figures 80, 93).

Work by Ford et al (2006) evaluated the kinematics of medial and lateral single leg drop landings of female collegiate basketball players (similar tasks to that of the SLCD and SLD in this work). They reported maximum adduction and abduction angles of 1.9^{o} and 17.0^{o} for the lateral land and 7.3^{o} and 7.6^{o} for the medial lands. While this work reported maximum abduction angles of 4^{o} - 10^{o} (both limbs and both groups) in the SLCD, while the SLD had maximum values of 3^{o} – 13^{o}.

6.7 Single Leg Lands Left vs. Right

Given the reported results and the inclination that left and right high valgus landing strategies were both aberrant (since they caused high medial knee displacement) yet very different from one another, visual inspection of single leg landing tasks (in Visual 3D) of multiple trials and subjects confirmed a fairly consistent pattern. As described above, on left landings the hip adducted and thus the ipsilateral side of the pelvis dropped, while the non-support right limb was often moved medially as the participant attempted to maintain the vGRF through the lumbar spine in order to maintain balance (COM within the BOS). This pattern quite obviously creates dynamic valgus, and would be expected to do so considering the left hip adduction (Figure 94-A). Conversely, on the right landings the high valgus group not only didn't display hip adduction, but actually displayed greater hip abduction in combination with right lateral bend of the lumbar spine. In other words, a right lateral trunk lean. In this instance, the right lateral trunk lean was so great that the femur relative to the pelvis is reported as hip abduction, yet the proximal action of the femur was to push its distal end (and thus the knee) medially. The proof of this is in the frontal plane right knee angle in which an abduction angle is present - yet as explained in the literature review of this thesis work – pure knee abduction with the foot planted is often an illusion since the tibia remains vertical, and the culprit is actually hip

adduction (Figure 94-B). Interestingly, in this instance the non-support limb is moved laterally to act as a counter-weight and help maintain balance. Trials that were deemed low valgus on either leg typically landed more neutral at the spine and hip with more knee flexion, they generally 'stuck the landing' with apparent ease and maintained the vGRF medially to their knee joint centre for the duration of the land (Figure 94-C). Figure 94 displays representative examples of each case, however, 91-B has exaggerated right lateral trunk lean - it is intentionally used as it makes the pattern clearer to see for the reader. Whether a high valgus trial was on a left or right leg land, both displayed poorer control of the kinematic chain relative to a low valgus trial – the distinguishable differences between these being less lumbar and hip JRS.

Of interest was the fact that every participant reported being right leg dominant. Unfortunately, this meant that the differing landing strategies between left and right were unable to be attributed to leg dominance or a related factor, since no left sided dominant participants were collected. On the DVJ task in particular the median value for the right peak medial knee displacement (approx. 5cm) was greater than that of the left knee (approx. 1.7 cm), while on the stop jump the right knee was only 1 cm greater than the left knee at 3cm. On the single leg landing tasks however, the right peak medial knee displacement was less than that of the left knee by 1-1.5 cm. Thus, evaluating the control of dominant and non-dominant limbs for both double and single leg landing tasks warrant future investigation, in which it is assured that left sided dominant participants are also recruited.

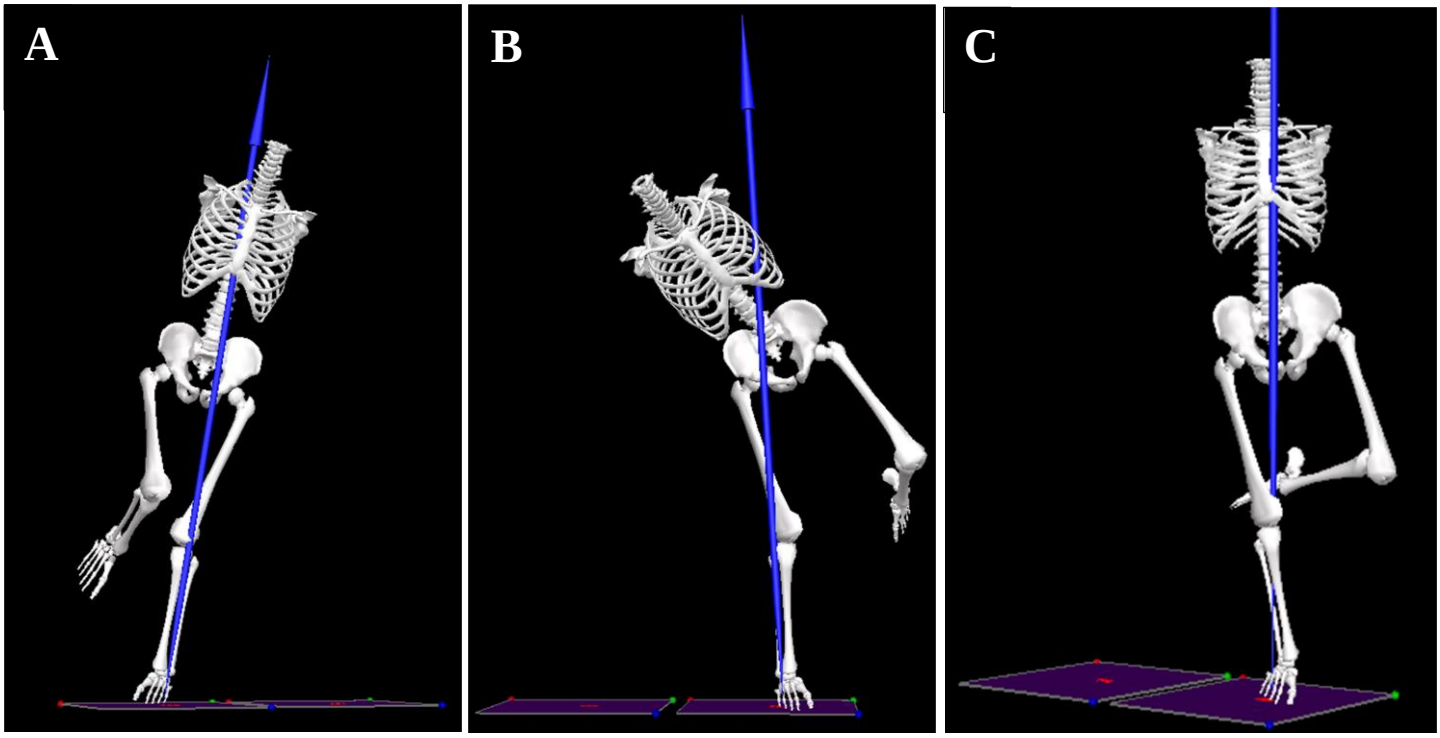

Figure 94: A) Typical pattern observed of high valgus on a left leg land. B) Typical pattern observed of high valgus on a right leg land. C) Typical pattern observed in a low valgus trial. Note: A and B are trials from a representative participant, who displayed high medial knee displacement on both landings, while C is another participant who was classified as low valgus.

Considering the aforementioned patterns of single leg landing, and the substantial interpretation it took to understand the kinematics of the whole linkage, one might suggest that a measure of lateral trunk displacement relative to the vertical, and/or, a measure of pelvic drop may be more appropriate to capture these phenomena. While these measures have certainly been reported before, the way in which they are produced is often excluded or do not include the influence of the lumbar spine (Chappell, 2008; Powers, 2010)(Powers, 2010b)(Powers, 2010b)(Powers, 2010b)(Powers, 2010b). Either could be created with lumbar spine lateral bend, hid adduction/abduction, or, some combination of lumbar spine and hip frontal plane kinematics. Reporting lumbar spine and hip kinematics separately, and then considering their combined results, allows for a one-to-one comparison with the controllers of such kinematics – the JRS.

6.8 Lumbar JRS

Zazulak and colleagues (2007) found that lateral trunk displacement and active trunk repositioning in response to a quick release mechanism predicted future non-contact ACL injury in females with 89% sensitivity (91% sensitivity for all knee ligament injuries). Furthermore, purposeful core muscular engagement has been shown to decrease frontal plane hip displacement as well as increase knee flexion angle – thus reducing ACL injury risk (Shirey et al., 2012). It has previously been demonstrated that trunk position significantly alters the kinematics, kinetics, muscle activity and energetics of the lower limbs during lunging, running and hopping (Farrokhi et al 2008; Teng and Powers, 2014). These support the notion that core stiffness is necessary in order to control the trunk and assist the hip musculature (via stabilization of the pelvis). The results from this work suggest that increased lumbar spine JRS (aka core stiffness) is a key component in maintaining the integrity of the kinematic chain during dynamic activities. Proximal stiffness is required to provide a rigid base from which energy and forces can be directed through, and propagated to the lower limbs. A compliant spine would allow the mass of the trunk and thus the body's COM to be uncontrolled, placing much higher demands on the lower limb musculature that now must adjust to whatever posture necessary, in order to maintain whole body stability.

The only previous attempt to investigate EMG of the trunk musculature in relation to ACL injury during a dynamic task, examined L5 extensors, external oblique and internal oblique during cutting (Jamison et al 2013). Jamison and colleagues' work determined a positive association between co-contraction of the L5 extensors and peak KAM, but a negative association with L5 co-contraction and trunk position. This led the authors to conclude that a stiffened spine and trunk may not be protective of the knee as increased KAM's were observed,

despite the finding that decreased sagittal plane trunk motion was associated with higher co-contraction. Several considerations regarding their analysis and interpretation of their findings need addressing. Firstly, they examined EMG activation, quantified co-contraction and inferred stiffness from it. While a stiff lumbar spine is often achieved by tuned co-contraction of the surrounding musculature, EMG alone cannot provide enough insight into the three-dimensional stiffness. It is worth noting that increased EMG activation and increased muscle force, may actually impose de-stabilizing forces at the spine (Brown and McGill, 2005). The highly non-linear relationship between EMG activation, force and stiffness demonstrates that early in activation large increases in stiffness occur. However, as activation continues to increase, the stiffness plateau's, while force continues to rise (Brown and McGill, 2005). At high levels of force, the muscle's stabilizing ability may be compromised and actually act to induce de-stabilizing forces (Brown and McGill, 2005). Additionally, their analysis did not consider the geometry or mechanistic function of the muscles and its role in combination with EMG activation to modulate stiffness. Secondly, the authors noted that EMG co-contraction was evaluated before initial contact with the force plates where the cut would occur, and that both speed and cut angle were significant co-variates for peak KAM upon initial contact. These factors likely influenced the KAM greater than the co-contraction of L5. Thus, their conclusions that a stiff lumbar spine may actually have a negative impact in the protection of the ACL are erroneous, given that their measures are unable to adequately quantify lumbar spine stiffness.

The results of this thesis are contrary to that of Jamison and colleagues (2013). In every task low valgus trials demonstrated greater lumbar spine JRS. Evaluation of summed muscle stiffness's demonstrated that less muscle stiffness in the anterior quadrants, as well as the lateral bend and axial twist planes were inherent in the high valgus group. The stiffness generated by

muscle planes or quadrants should not be thought of necessarily in its mechanical action in the direction of which it acts to create a moment, but rather in their ability to transmit stiffness through the fascia and tissue surrounding the spine. Given Jamison's limitations in capturing lumbar spine stiffness and their concession that more sophisticated models may be necessary, it is believed that the results in this thesis hold more biological fidelity and more accurately capture the role of lumbar spine stiffness. The lumbar spine model and stiffness analysis utilized in this work is the most sophisticated analysis in existence.

Other attempts to link core stability to lower extremity injuries used the biering-sorenson, side bridge and v-sit endurance tests to evaluate posterior, lateral and anterior musculature of the core, while also reporting maximum isometric hip strength values. After monitoring injury status of 140 (male and female) intercollegiate track and basketball athletes for the duration of one season, they concluded that proximal stability plays a large role in injury prevention. Of particular significance were the hip abduction and external rotation isometric strength values (Leetun et al 2004). In a clinical commentary surrounding the influence of abnormal hip mechanics on knee injury, it was reiterated that control of the trunk was of critical importance in preventing knee injury (Powers, 2010). However, it was suggested that the trunk/core musculature, beyond stabilizing the spine, would not be expected to control aberrant trunk kinematics associated with poor pelvic control, but rather the onus was on that of the hip musculature (Powers, 2010). Despite this impression, the author acknowledges that trunk proprioception deficits have been linked to knee injury and thus training programs involving the core musculature should be developed that consider dynamic pelvis stability (Powers, 2010).

The results of this work are contrary to this notion given the large differences in lumbar JRS observed between high and low valgus groups. The lumbar spine could certainly be in a

neutral position and stiff, while the trunk position is modified purely by the hips. However, the stabilization of the lumbar spine is necessary to prevent lumbar-driven pelvis motion. Additionally, if excessive lumbar spine motion is allowed to occur unrestrained from active muscle stiffness, the body's COM displacement is likely to become exaggerated, creating larger demands on the hip musculature to maintain the trunk's position. It is also recognized that core stiffness is necessary to optimally maintain the position and motion of the trunk over the pelvis and control the transfer of forces and motion through the linkage inferior to it (Kibler et al, 2006).

6.9 Hip JRS

Possible weaknesses or inhibitions in the hip musculature are consistently suggested to be the causal factor of dynamic valgus presentation (Hewett et al, 2005; Powers, 2010; Zazulak et al, 2005). It has also been demonstrated that increased use of the hip musculature serves to reduce loads experienced at the knee, however these have focused primarily on sagittal plane measures, or in females with patellofemoral pain (Stearns & Powers, 2014; Lee et al 2012). To date, muscles of the gluteal complex have been evaluated only for their activation amplitude, onset/offset timing, duration of activity and their link to aberrant hip kinematics. In an investigation aimed at comparing hip kinematics and muscle activation in PFP patients (compared to healthy controls) during various tasks, it was found that the PFP patients demonstrated greater hip internal rotation but greater gluteus maximus activation in running and a step-down task (Souza and Powers, 2009). While this is contrary to hypotheses that greater gluteus activation would serve to prevent aberrant kinematics, the authors suggested that the increased activation may have been an attempt to recruit a weak muscle in order to stabilize the hip joint (Souza and Powers, 2009). Similar to the work of Jamison et al (2013) as discussed

above, the authors did not consider the potential destabilizing effects of muscle force, while their sample was unique in that they had chronic PFP and thus potentially altered neuromuscular strategies. Additionally, in the drop vertical jump task the PFP group had greater hip adduction than the control group and less gluteus maximus activation, but differences were minimal and considered insignificant. Zazulak et al (2005) reported that females displaying valgus had decreased peak and mean gluteus maximus and gluteus medius activation in comparison to males who did not display valgus prior to, and during, the contact phase of drop landings. In a systematic review of gluteal muscle activity in PFP patients and the associated kinematics, it was found that impaired gluteal activation in the temporal domain led to increased hip adduction and internal rotation (Barton et al, 2012). While JRS has never been quantified at the hip, the reporting of known injurious kinematics concomitant with decreased EMG activation of the gluteal musculature suggests that lower JRS would be expected in those with high valgus.

Considering the results that gluteus medius and gluteus maximus superior played large, but alternating, roles in providing JRS in the frontal and transverse planes suggests synergistic behaviour. Posture mitigates the mechanical function of muscle, therefore high activation in a disadvantaged posture may actually lead to destabilizing forces. The ability of JRS to capture both the combined effect of geometric orientation and neural drive provides unique insight into the role of these muscles during dynamic tasks. Powers (2010) has previously noted the reduced torque producing ability of gluteus medius with increased hip flexion due to a decrease in its moment arm. Gluteus maximus superior acts to abduct the hip in anatomical position, and its moment arm is maintained throughout deep hip flexion and continues to produce hip abduction (Klein Horsman et al, 2007). Klein Horsman noted that external rotation is dominated by gluteus maximus while posterior gluteus medius assists in external rotation, as does the anterior

compartment until deep hip flexion. It was also reported in his work that hip abduction is primarily achieved by gluteus medius over a wide ROM, while gluteus maximus superior fibres assist in hip abduction (Klein Horsman et al, 2007). The described mechanical functions of these muscles substantiate their role in JRS production in those who avoided dynamic valgus. Additionally, the frontal and transverse plane moment arms of each of the gluteus maximus superior and gluteus medius provide a mechanical advantage that makes them very suitable stiffeners in combination with muscle activation. Their seemingly alternating contributions to JRS in some of the tasks evaluated in this work lead one to speculate that if either muscle is hindered in its JRS capacity that the CNS is able to appropriately coordinate neural drive accordingly to ensure the necessary JRS is produced via the unhindered muscle, or, most mechanical advantageous muscle. If this were the case, a neuromuscular deficit in the gluteal complex (as proposed in the high valgus group) would serve to impede JRS production and allow for the propagation of injurious mechanics.

The work presented in this thesis demonstrates that even with relatively small differences in hip angles, large differences in hip JRS (particularly in the frontal and transverse planes) were significant between high and low valgus groups. Additionally, gluteus medius and gluteus maximus superior were particularly distinguishable between groups, as the low valgus group demonstrated substantially larger JRS contributions from these muscles compared to the high valgus group. These findings are consistent with the literature's description of impaired gluteal function causing valgus, but this work demonstrates that looking beyond just EMG may be more insightful into neuromuscular deficits in the gluteal complex.

6.10 Mechanisms and Motor Strategies

Several works have linked a "stiffening strategy" to increased ACL injury risk, this is an unfortunate phrase given this theses definition of stiffness. The stiffening strategy has been characterized as less trunk, hip and knee flexion upon landing, thus the participant lands with triple extension of the joints and is a sagittal plane measure. This serves to increase moments at the knee, and requires more energy absorption at the knees by the quadriceps which may actually act to increase anterior tibial shear (Powers 2010). This type of landing strategy corresponds with what one might consider a "hard" landing due to the rigidity in the linkage and therefore be considered "stiff". Work by Lyle et al (2014) had male and female soccer players perform single leg landings and calculated an "average leg stiffness" as a global measure of multi-joint coordination. Their results showed that females displayed greater leg stiffness, and concluded that it was a compensatory strategy that may contribute to increased ACL injury risk. However, while they had participants perform single-leg drop vertical jumps, their COM measure was only done in the superior-inferior direction, thus negating the frontal plane challenge of the task. The leg stiffness calculation was done so by dividing the peak vGRF with COM displacement. In this case greater COM displacement would be considered protective, since it would reveal that participants landed with greater hip and knee flexion thus absorbing the energy using the hip musculature and in turn reducing loads at the knee. A measure of "joint stiffness" by Ford et al (2010) investigated the moment-angle relationship at the ankle, knee and hip during DVJ's in order to evaluate differences between gender and maturation level. Interestingly, hip stiffness values were markedly less in females compared to males, and did not increase over the time span of one year (Ford et al., 2010). While this method provides a very general the measure of external joint stiffness, void of direct neurological contribution by the way of active musculature,

it warrants the exploration of active hip joint stiffness when investigating ACL injury mechanisms.

The aforementioned investigations have provided conflicting evidence regarding "stiffness" and its link to ACL injury mechanisms. However, both methods of calculating stiffness were very different to that performed in this work, as neither considered the role of active musculature or the stabilizing contributions of muscle stiffness. No previous works, that the author is aware of, have investigated joint rotational stiffness at either the lumbar spine or hip as it relates to ACL injury mechanisms. Nor, have any works investigated the role of the core and hip musculature to the extent of this work.

The influence of multiple joint angles along the kinematic chain, and the resulting posture of the whole linkage further strengthens the case that looking at a single joint in isolation during such dynamic activities is ill advised. Each task analyzed in this thesis provided insight into differences between high and low valgus trials, while aberrant kinematics could vary from task to task, insufficient JRS at the lumbar spine and hips was a constant theme. Given that the stop jump seemingly required that participants meet the moment demands of the task with sufficient stiffness, the notion that the neuromuscular deficit is modifiable is supported. Evidence exists that the deficit is not in strength, but rather in appropriate coordination and recruitment of musculature about a joint (Herman et al., 2008; Powers, 2010a). The JRS analyses here would be further evidence that this is the case, and that the motor control influences on the mechanics are of critical importance. Other tasks that are able to require the participant to generate sufficient stiffness may provide insight for future training interventions. Particularly, a drop lateral jump may require the contralateral hip musculature to activate and appropriately stiffen in order to generate power in the push off. Differences in the position of the non-involved limb in single leg

landing also suggests that tasks which manipulate its position could be insightful, a single leg squat while modifying the projection of the non-involved limb (anteriorly, posteriorly, and laterally) may force a participant to actively reposition their COM using differing motor strategies, while the very nature of a single leg squat presents a substantial challenge in the frontal plane.

The results of this thesis indicate that aberrant kinematics at the trunk, hips and knees leading to injurious postures are the result of insufficient proximal joint stiffness at the lumbar spine and hip. Modulation of muscle stiffness about a joint and its global joint rotational stiffness act as the controller of the kinematic chain. Muscle stiffness is a function of neural drive originating from the CNS in response to proprioceptive feedback and the instantaneous task demand constraints, and acts to stabilize joints by resisting movements that would act to compromise joint integrity (McGill, 2007). Core and hip musculature must act synergistically to support one another in pelvic stabilization, and control of the trunk and the lower limb linkage. During single leg dynamic activities such as the SLD and SLCD analyzed in this thesis, it appears adequate stiffness at the lumbar spine and hip act to assist one another, where the loss of one creates demands so high at the other that aberrant kinematics ensue in an attempt to maintain whole body stability. Thus, stiffness is required throughout the linkage for local joint integrity as well as kinematic chain integrity.

If one considers a hierarchy of control, particularly on single leg landing tasks, it is reasonable to suggest that the CNS would prioritize control of the trunk to maintain whole body stability, over control of the knee. Brown et al (2003) examined sudden unloading of the hands under various conditions and knowledge of timing, they observed instances in which anticipatory action of postural (leg) muscles actually led to decreases in spinal stability. This supports the

notion that the CNS may place greater importance on maintaining whole body stability over that of a single joint, even if it must do so by reducing the stiffness and concomitantly increasing injury risk at said joint. However, stiffness is the variable that the CNS modulates, through which it controls the kinematics of the linkage. Thereby, proximal stiffness and control of the trunk are a necessary precursor to control segments within the linkage and avoid injurious postures, motions and resulting loads.

The notion of 'sufficient' or 'appropriate' stiffness is mentioned several times throughout this work, it is in reference to an unknown optimal value that is necessary to maintain the integrity of the linkage and avoid injurious kinematics. It is important to note that increased stiffness is not always prophylactic, as extremely high magnitudes may act to impose rigidity within a system and prevent motion that may be necessary to dissipate forces and transfer energy in a manner that reduces injury risk. However, in this work increased stiffness was deemed to be appropriate and sufficient, as it was a pre-condition to prevent high medial knee displacement and known injurious kinematics. Additionally, in the single leg landing tasks increased stiffness was observed in those with low valgus who adopted strategies that involved steering the projected vectors from the force plate through joint centres. This makes the stiffness strategy even more impressive, since once the force vectors have been directed through joint centres, less stiffness would be required from surrounding musculature to ensure joint stability, yet greater stiffness is continually observed suggesting that a safety margin of additional stiffness is employed. The gluteal musculature also provides stiffness for control and stabilization of the pelvis and trunk, while also directly resisting hip adduction and internal rotation. Therefore, training studies that focus on gluteal musculature activation only with the purposes of preventing

aberrant hip kinematics, may be overlooking their larger capabilities in maintaining the integrity of the linkage.

6.11 Limitations

This work was not without its limitations and assumptions. Firstly, eighteen university aged female recreational or university level athletes comprised the sample. Given that participants had to be free of previous low back and lower extremity injury, the decision was made to include recreational athletes. Recruiting only university level female athletes may have resulted in failing to capture anyone who displayed extreme valgus or the aberrant kinematics associated with ACL injury risk. If high level athletes have not yet suffered an ACL (or knee) injury, it is likely they are not at particular risk, while the athletes who have already injured were excluded. Secondly, given the inconsistencies of the KAM to capture those displaying dynamic valgus, it was presumed that dichotomizing participants on their peak medial knee displacement relative to the median value for the group would adequately expose differences in dependent variables. Since the KAM threshold was initially developed using a model that encapsulated dynamic valgus (as one of the only modifiable risk factors), and the well established use of dynamic valgus measures to infer ACL injury risk, the researchers were confident in its use. Furthermore, including an exclusion zone of 20% in either direction around the median peak medial knee displacement was an attempt to capture differences that exist between varying levels of dynamic valgus.

Several models were used in the calculations of JRS at both the lumbar spine and hips. At each joint data sets with high anatomical detail were used, the lumbar spine comprising 98 muscle fascicles and each hip 65 muscle fascicles. In addition to high anatomical detail the use

of EMG-driven muscle force and stiffness estimates enhance the biological fidelity of the work. Muscle behaviour were modelled as close to physiological observed phenomenon as possible in order to truly represent a muscles mechanistic characteristics. At each of the hips and lumbar spine a subject-joint specific common gain was used to correct for errors between inverse dynamics and EMG driven model estimates of joint moments. This gain was calculated from a controlled RVC and applied to all muscles during dynamic activities. Using an RVC for the gain calculation allows for stability in the measure and a consistent demand at each muscle during an isometric challenge, opposed to the demand placed on muscles during instantaneous changes during the dynamic tasks. Moreover, a common gain allows relative differences in muscle activation to be maintained, since they are all gained linearly by the same factor. By the same principal, error associated with using the gain factor is systematic in nature between joints and tasks within a participant.

Twenty-four channels of electromyography during dynamic tasks presents challenges in tracking all 24 muscles in real time for veracity, and to locate missing or non-physiological data. Thus, the EMG of each muscle during each task analyzed was visually inspected in the data processing stage and any trials with unrealistic activation amplitudes were discarded. Despite the challenges and time cost of including this many muscles, it undoubtedly provides great insight into the motor strategies being utilized, and is a necessity in understanding the proposed neuromuscular deficits associated with ACL injury.

Movement variability within, and between, subjects is inherent in any unconstrained movement task. Each trial of every task was analyzed independently for its valgus status and dependent variables of interest. In this way the variability within and between subjects was maintained, and, allowed to be analyzed independently in context of what happened in that given

trial. Movement in general, but particularly aberrant or injurious movement of the spine-hip-knee linkage can be complex to analyze in relation to one another. This analysis did not seek to understand interaction effects or confounding variables. Rather, the research question aimed to explore if high and low valgus presentation differed in proximal joint stiffness, thus, a comparison of each dependent variable between valgus status formed the rationale for analysis. Future work should aim to investigate how these complex mechanisms interact and act to support, or negate one another.

6.12 Contributions and Conclusions

The purpose of this work was to investigate the role of proximal joint stiffness in avoiding dynamic valgus. Joint rotational stiffness provides a unique method for which to encapsulate the global effect of musculature around a joint of interest, by incorporating the effect of active muscle stiffness and their geometric orientation given segment kinematics. This approach facilitated analysis beyond muscle activation in isolation, and in doing so advances understanding of the links inherent to cause and effect. This unique work appears to be the first of its kind related to ACL injury risk. While many research groups have postulated proximal neuromuscular deficits, it remained simply postulated. The results here provide insight into the motor control component of avoiding dynamic valgus, and is the first work to confirm and specifically characterize a neuromuscular deficit at the core or hip. That deficit appears to be an inability to generate sufficient joint rotational stiffness in order to control the linkage. This stiffness is the result of coordinated activation and stiffness of both core and hip muscles. This advance will provide a springboard for future work that will aim to develop training interventions for increasing an individual's proximal joint stiffness and thus avoiding dynamic valgus during controlled, and uncontrolled tasks. It is interesting to consider that EMG is often

the input to biomechanical modeling, while it is the output of the motor control system. In order to increase one's proximal joint stiffness and reduce ACL injury risk, inherent motor programs in an individual must be altered. Current thinking suggests that plastic changes in the motor cortex are necessary to re-write engrams that allow for enhancement of performance and injury resilience.

References

Baratta, R. V., Solomonow, M., Chu, D., LeBlanc, R., D'Ambrosia, R., D'Ambrosia, P., … Zhu, M.-P. (2001). 49th Annual Meeting of the Orthopaedic Research Society Poster # 0721. In *Journal of Biomedical Materials Research* (Vol. 21, pp. 2001–2001).

Barton, C. J., Lack, S., Malliaras, P., & Morrissey, D. (2012). Gluteal muscle activity and patellofemoral pain syndrome: a systematic review. *British Journal of Sports Medicine*, (September 2012), 207–214. http://doi.org/10.1136/bjsports-2012-090953

Begon, M., Monnet, T., & Lacouture, P. (2007). Effects of movement for estimating the hip joint centre. *Gait and Posture*, *25*(3), 353–359. http://doi.org/10.1016/j.gaitpost.2006.04.010

Bergmark, A. (1989). A study in mechanical engineering, *60*(230).

Blackburn, J. T., Norcross, M. F., & Padua, D. a. (2011). Influences of hamstring stiffness and strength on anterior knee joint stability. *Clinical Biomechanics (Bristol, Avon)*, *26*(3), 278–83. http://doi.org/10.1016/j.clinbiomech.2010.10.002

Blackburn, J. T., & Padua, D. a. (2009). Sagittal-plane trunk position, landing forces, and quadriceps electromyographic activity. *Journal of Athletic Training*, *44*(2), 174–179. http://doi.org/10.4085/1062-6050-44.2.174

Boden, B. P., Torg, J. S., Knowles, S. B., & Hewett, T. E. (2009). Video analysis of anterior cruciate ligament injury: abnormalities in hip and ankle kinematics. *The American Journal of Sports Medicine*, *37*(2), 252–259. http://doi.org/10.1177/0363546508328107

Brereton, L. C., & McGill, S. M. (1998). Frequency response of spine extensors during rapid isometric contractions: effects of muscle length and tension. *Journal of Electromyography and Kinesiology*, *8*(4), 227–232. http://doi.org/10.1016/S1050-6411(98)00009-1

Brown, S. H., Howarth, S. J., McGill, S. M., Marshall, P. W., & Murphy, B. a. (2005). Spine stability and the role of many muscles [1] (multiple letters). *Archives of Physical Medicine and Rehabilitation*, *86*, 1890–1891. http://doi.org/10.1016/j.apmr.2005.07.281

Brown, S. H. M., Haumann, M. L., & Potvin, J. R. (2003). The responses of leg and trunk muscles to sudden unloading of the hands: Implications for balance and spine stability. *Clinical Biomechanics*, *18*(9), 812–820. http://doi.org/10.1016/S0268-0033(03)00167-0

Brown, S. H. M., & McGill, S. M. (2005). Muscle force-stiffness characteristics influence joint stability: a spine example. *Clinical Biomechanics (Bristol, Avon)*, *20*(9), 917–22. http://doi.org/10.1016/j.clinbiomech.2005.06.002

Brown, S. H. M., & McGill, S. M. (2009). The intrinsic stiffness of the in vivo lumbar spine in response to quick releases: implications for reflexive requirements. *Journal of Electromyography and Kinesiology : Official Journal of the International Society of Electrophysiological Kinesiology*, *19*(5), 727–36. http://doi.org/10.1016/j.jelekin.2008.04.009

Brown, S. H. M., & Potvin, J. R. (2007a). Exploring the geometric and mechanical characteristics of the spine musculature to provide rotational stiffness to two spine joints in the neutral posture. *Human Movement Science*, *26*, 113–123. http://doi.org/10.1016/j.humov.2006.09.006

Brown, S. H. M., & Potvin, J. R. (2007b). The effect of reducing the number of EMG channel

inputs on loading and stiffness estimates from an EMG-driven model of the spine. *Ergonomics*, *50*(5), 743–751. http://doi.org/10.1080/00140130701194926

Cashaback, J. G. a, & Potvin, J. R. (2012). Knee muscle contributions to joint rotational stiffness. *Human Movement Science*, *31*(1), 118–128. http://doi.org/10.1016/j.humov.2010.12.005

Chappell, J. D., & Limpisvasti, O. (2008). Effect of a neuromuscular training program on the kinetics and kinematics of jumping tasks. *The American Journal of Sports Medicine*, *36*(6), 1081–6. http://doi.org/10.1177/0363546508314425

Cholewicki, J., & McGill, S. M. (1995). Relationship between muscle force and stiffness in the whole mammalian muscle: a simulation study. *Journal of Biomechanical Engineering*, *117*(August), 339–342. Retrieved from http://biomechanical.asmedigitalcollection.asme.org/article.aspx?articleid=1400191

Cholewicki, J., & McGill, S. M. (1996). Mechanical stability of the in vivo lumbar spine: implications for injury and chronic low back pain. *Clinical Biomechanics*, *11*(1), 1–15.

Cholewicki, J., McGill, S. M., & Norman, R. (1991). Lumbar spine loads during the lifting of extremely heavy weights. *Medicine & Science in Sports & Exercise*, *23*(10).

Cholewicki, J., McGill, S. M., & Norman, R. W. (1995). Muscle Forces and Joint Load From An Optimization and EMG Assisted Lumbar Spine Model.pdf. *Journal of Biomechanics*, *28*(3), 321–331.

Cochrane, J. L., Lloyd, D. G., Besier, T. F., Elliott, B. C., Doyle, T. L. a, & Ackland, T. R. (2010). Training affects knee kinematics and kinetics in cutting maneuvers in sport. *Medicine and Science in Sports and Exercise*, *42*(4), 1535–1544. http://doi.org/10.1249/MSS.0b013e3181d03ba0

Collado, H., & Fredericson, M. (2010). Patellofemoral pain syndrome. *Clinics in Sports Medicine*, *29*, 379–398. http://doi.org/10.1016/j.csm.2010.03.012

Crisco, J. J., & Panjabi, M. M. (1991). The Intersegmental and Multisegmental Muscles of the Lumbar Spine: A Biomechanical Model Comparing Lateral Stabilizing Potential. *Spine*, *16*(7).

Drake, J. D. M., & Callaghan, J. P. (2006). Elimination of electrocardiogram contamination from electromyogram signals: An evaluation of currently used removal techniques. *Journal of Electromyography and Kinesiology : Official Journal of the International Society of Electrophysiological Kinesiology*, *16*(2), 175–87. http://doi.org/10.1016/j.jelekin.2005.07.003

Ford, K. R., Myer, G. D., & Hewett, T. E. (2010). Longitudinal effects of maturation on lower extremity joint stiffness in adolescent athletes. *The American Journal of Sports Medicine*, *38*(9), 1829–1837. http://doi.org/10.1177/0363546510367425

Ford, K. R., Myer, G. D., Smith, R. L., Vianello, R. M., Seiwert, S. L., & Hewett, T. E. (2006). A comparison of dynamic coronal plane excursion between matched male and female athletes when performing single leg landings. *Clinical Biomechanics*, *21*(1), 33–40. http://doi.org/10.1016/j.clinbiomech.2005.08.010

Fukuda, Y., Woo, S. L. Y., Loh, J. C., Tsuda, E., Tang, P., McMahon, P. J., & Debski, R. E. (2003). A quantitative analysis of valgus torque on the ACL: A human cadaveric study. *Journal of Orthopaedic Research*, *21*(6), 1107–1112. http://doi.org/10.1016/S0736-

0266(03)00084-6

Heller, M. O., Bergmann, G., Kassi, J. P., Claes, L., Haas, N. P., & Duda, G. N. (2005). Determination of muscle loading at the hip joint for use in pre-clinical testing. *Journal of Biomechanics*, *38*(5), 1155–1163. http://doi.org/10.1016/j.jbiomech.2004.05.022

Henderson, E. R., Marulanda, G. a, Cheong, D., Temple, H. T., & Letson, G. D. (2011). Hip abductor moment arm - a mathematical analysis for proximal femoral replacement. *Journal of Orthopaedic Surgery and Research*, *6*(1), 6. http://doi.org/10.1186/1749-799X-6-6

Herman, D. C., Oñate, J. a, Weinhold, P. S., Guskiewicz, K. M., Garrett, W. E., Yu, B., & Padua, D. a. (2009). The effects of feedback with and without strength training on lower extremity biomechanics. *The American Journal of Sports Medicine*, *37*(7), 1301–1308. http://doi.org/10.1177/0363546509332253

Herman, D. C., Weinhold, P. S., Guskiewicz, K. M., Garrett, W. E., Yu, B., & Padua, D. a. (2008). The effects of strength training on the lower extremity biomechanics of female recreational athletes during a stop-jump task. *The American Journal of Sports Medicine*, *36*, 733–740. http://doi.org/10.1177/0363546507311602

Hewett, T. E., Ford, K. R., & Hoogenboom, B. J. (2010). UNDERSTANDING AND PREVENTING ACL INJURIES: CURRENT BIOMECHANICAL AND EPIDEMIOLOGIC CONSIDERATIONS - UPDATE 2010. *North American Journal of Sports Physical Therapy*, *5*(4), 234–251.

Hewett, T. E., & Myer, G. D. (2011a). The Mechanistic Connection Between the Trunk, Hip, Knee, and Anterior Cruciate Ligament Injury. *Exercise and Sport Sciences Reviews*, *39*(4), 161–6. Retrieved from http://www.ncbi.nlm.nih.gov/pubmed/21799427

Hewett, T. E., & Myer, G. D. (2011b). The Mechanistic Connection between the Trunk, Knee, and ACL Injury. *Exercise and Sport Sciences Reviews*, 1. http://doi.org/10.1097/JES.0b013e3182297439

Hewett, T. E., Myer, G. D., & Ford, K. R. (2004). Decrease in neuromuscular control about the knee with maturation in female athletes. *The Journal of Bone and Joint Surgery. American Volume*, *86-A*, 1601–1608. http://doi.org/86/8/1601 [pii]

Hewett, T. E., Myer, G. D., & Ford, K. R. (2006). Anterior cruciate ligament injuries in female athletes: Part 1, mechanisms and risk factors. *The American Journal of Sports Medicine*, *34*(2), 299–311. http://doi.org/10.1177/0363546505284183

Hewett, T. E., Myer, G. D., Ford, K. R., Heidt, R. S., Colosimo, A. J., McLean, S. G., … Succop, P. (2005). Biomechanical measures of neuromuscular control and valgus loading of the knee predict anterior cruciate ligament injury risk in female athletes: a prospective study. *The American Journal of Sports Medicine*, *33*, 492–501. http://doi.org/10.1177/0363546504269591

Hewett, T. E., Torg, J. S., & Boden, B. P. (2009). Video analysis of trunk and knee motion during non-contact anterior cruciate ligament injury in female athletes: lateral trunk and knee abduction motion are combined components of the injury mechanism. *British Journal of Sports Medicine*, *43*, 417–422. http://doi.org/10.1136/bjsm.2009.059162

Hewett, T. E., Zazulak, B. T., Myer, G. D., & Ford, K. R. (2005). A review of electromyographic activation levels, timing differences, and increased anterior cruciate ligament injury

incidence in female athletes. *British Journal of Sports Medicine*, *39*(6), 347–350. http://doi.org/10.1136/bjsm.2005.018572

Howarth, S. J. (2006). Locating Instability in the Lumbar Spine: Characterizing the eigenvector. *MSc Thesis*, University of Waterloo.

Howarth, S. J., & Callaghan, J. P. (2009). The rule of 1 s for padding kinematic data prior to digital filtering: Influence of sampling and filter cutoff frequencies. *Journal of Electromyography and Kinesiology*, *19*(5), 875–881. http://doi.org/10.1016/j.jelekin.2008.03.010

Howarth, S. J., & Callaghan, J. P. (2010). Quantitative assessment of the accuracy for three interpolation techniques in kinematic analysis of human movement. *Computer Methods in Biomechanics and Biomedical Engineering*, *13*(6), 847–55. http://doi.org/10.1080/10255841003664701

Ikeda, D.M. (2011). Quantification of Spine Stability: Assessing the role of muscles and their links to eigenvalues and stability. *MSc Thesis*, University of Waterloo.

Jamison, S. T., McNally, M. P., Schmitt, L. C., & Chaudhari, A. M. W. (2013). The effects of core muscle activation on dynamic trunk position and knee abduction moments: Implications for ACL injury. *Journal of Biomechanics*, *46*(13), 2236–2241. http://doi.org/10.1016/j.jbiomech.2013.06.021

Jamison, S. T., McNeilan, R. J., Young, G. S., Givens, D. L., Best, T. M., & Chaudhari, A. M. W. (2012). Randomized controlled trial of the effects of a trunk stabilization program on trunk control and knee loading. *Medicine and Science in Sports and Exercise*, *44*, 1924–1934. http://doi.org/10.1249/MSS.0b013e31825a2f61

Jamison, S. T., Pan, X., & Chaudhari, A. M. W. (2012). Knee moments during run-to-cut maneuvers are associated with lateral trunk positioning. *Journal of Biomechanics*, *45*(11), 1881–1885. http://doi.org/10.1016/j.jbiomech.2012.05.031

Kanamori, A., Woo, S. L. Y., Ma, C. B., Zeminski, J., Rudy, T. W., Li, G., & Livesay, G. A. (2000). The forces in the anterior cruciate ligament and knee kinematics during a simulated pivot shift test: A human cadaveric study using robotic technology. *Arthroscopy*, *16*(6), 633–639. http://doi.org/10.1053/jars.2000.7682

Kibler, W. Ben, Press, J., & Sciascia, A. (2006). The role of core stability in athletic function. *Sports Medicine (Auckland NZ)*, *36*(3), 189–198. http://doi.org/10.2165/00007256-200636030-00001

Klein Horsman, M. D., Koopman, H. F. J. M., van der Helm, F. C. T., Prosé, L. P., & Veeger, H. E. J. (2007). Morphological muscle and joint parameters for musculoskeletal modelling of the lower extremity. *Clinical Biomechanics*, *22*, 239–247. http://doi.org/10.1016/j.clinbiomech.2006.10.003

Kulas, A. S., Hortobágyi, T., & Devita, P. (2012). Trunk position modulates anterior cruciate ligament forces and strains during a single-leg squat. *Clinical Biomechanics*, *27*(1), 16–21. http://doi.org/10.1016/j.clinbiomech.2011.07.009

Laughlin, W. a., Weinhandl, J. T., Kernozek, T. W., Cobb, S. C., Keenan, K. G., & O'connor, K. M. (2011). The effects of single-leg landing technique on ACL loading. *Journal of Biomechanics*, *44*(10), 1845–1851. http://doi.org/10.1016/j.jbiomech.2011.04.010

Lee, S. P., Souza, R. B., & Powers, C. M. (2012). The influence of hip abductor muscle performance on dynamic postural stability in females with patellofemoral pain. *Gait and Posture*, *36*(3), 425–429. http://doi.org/10.1016/j.gaitpost.2012.03.024

Lloyd, D. G., & Buchanan, T. S. (2001). Strategies of the muscular contributions to the support of static varus and valgus loads at the human knee. *Journal of Biomechanics*, *34*, 1257–1267.

Ma, S., & Zahalak, G. I. (1991). A distribution-moment model of energetics in skeletal muscle. *Journal of Biomechanics*, *24*(1), 21–35. http://doi.org/10.1016/0021-9290(91)90323-F

Markolf, K. L., Burchfield, D. M., Shapiro, M. M., Shepard, M. F., Finerman, G. A. M., & Slauterbeck, J. L. (1995). Combined knee loading states that generate high anterior cruciate ligament forces. *Journal of Orthopaedic Research*, *13*(6), 930–935. http://doi.org/10.1002/jor.1100130618

McGill, S. M. (1991). Electromyographic activity of the abdominal and low back musculature during the generation of isometric and dynamic axial trunk torque: Implications for lumbar mechanics. *Journal of Orthopaedic Research*, *9*(1), 91–103. http://doi.org/10.1002/jor.1100090112

McGill, S. M. (2007). *Low Back Disorders: Evidence Based Prevention and Rehabilitation* (Second). Chicago, IL: Human Kinetics.

McGill, S. M. (2014). *Ultimate Back Fitness and Performance* (Fourth). Waterloo: Backfitpro Inc.

McGill, S. M., Juker, D., & Kropf, P. (1996). Technical Note: Appropriately Placed Surface EMG Electrodes Reflect Deep Muscle Activity (Psoas, Quadratus Lumborum,. *Journal of Biomechanics*, *29*(11), 8–1503–1507.

McGill, S. M., & Karpowicz, A. (2009). Exercises for Spine Stabilization: Motion/Motor Patterns, Stability Progressions, and Clinical Technique. *Archives of Physical Medicine and Rehabilitation*, *90*, 118–126. http://doi.org/10.1016/j.apmr.2008.06.026

McGill, S. M., & Norman, R. (1986). Partitioning of the L4/L5 dynamic moment into Disc, Ligamentous, and Muscular Components During Lifting. *Spine*, *11*(7), 666–677.

Mizner, R. L., Kawaguchi, J. K., & Chmielewski, T. L. (2008). Muscle strength in the lower extremity does not predict postinstruction improvements in the landing patterns of female athletes. *The Journal of Orthopaedic and Sports Physical Therapy*, *38*(6), 353–361. http://doi.org/10.2519/jospt.2008.2726

Modenese, L., Phillips, a. T. M., & Bull, a. M. J. (2011). An open source lower limb model: Hip joint validation. *Journal of Biomechanics*, *44*(12), 2185–2193. http://doi.org/10.1016/j.jbiomech.2011.06.019

Myer, G. D., Ford, K. R., Brent, J. L., & Hewett, T. E. (2007). Differential neuromuscular training effects on ACL injury risk factors in"high-risk" versus "low-risk" athletes. *BMC Musculoskeletal Disorders*, *8*, 39. http://doi.org/10.1186/1471-2474-8-39

Myer, G. D., Ford, K. R., Di Stasi, S. L., Foss, K. D. B., Micheli, L. J., & Hewett, T. E. (2015). High knee abduction moments are common risk factors for patellofemoral pain (PFP) and anterior cruciate ligament (ACL) injury in girls: Is PFP itself a predictor for subsequent ACL injury? *British Journal of Sports Medicine*, *49*(2).

http://doi.org/10.1016/j.biotechadv.2011.08.021.Secreted

Myer, G. D., Ford, K. R., & Hewett, T. E. (2011). New method to identify athletes at high risk of ACL injury using clinic-based measurements and freeware computer analysis. *British Journal of Sports Medicine*, *45*(4), 238–44. http://doi.org/10.1136/bjsm.2010.072843

Myer, G. D., Ford, K. R., Khoury, J., Succop, P., & Hewett, T. E. (2010a). Clinical correlates to laboratory measures for use in non-contact anterior cruciate ligament injury risk prediction algorithm. *Clin Biomech (Bristol, Avon)*, *25*(7), 693–699. http://doi.org/10.1016/j.clinbiomech.2010.04.016

Myer, G. D., Ford, K. R., Khoury, J., Succop, P., & Hewett, T. E. (2010b). Development and Validation of a Clinic-Based Prediction Tool to Identify Female Athletes at High Risk for Anterior Cruciate Ligament Injury. *The American Journal of Sports Medicine*, *38*(10), 2025–2033. http://doi.org/10.1177/0363546510370933

Myer, G. D., Ford, K. R., Khoury, J., Succop, P., & Hewett, T. E. (2011). Biomechanics laboratory-based prediction algorithm to identify female athletes with high knee loads that increase risk of ACL injury. *British Journal of Sports Medicine*, *45*, 245–252. http://doi.org/10.1136/bjsm.2009.069351

Myer, G. D., Ford, K. R., Paterno, M. V, Nick, T. G., & Hewett, T. E. (2008). The effects of generalized joint laxity on risk of anterior cruciate ligament injury in young female athletes. *The American Journal of Sports Medicine*, *36*, 1073–1080. http://doi.org/10.1177/0363546507313572

Nakagawa, T. H., Moriya, É. T. U., Maciel, C. D., & Serrão, A. F. V. (2012). Frontal plane biomechanics in males and females with and without patellofemoral pain. *Medicine and Science in Sports and Exercise*, *44*(9), 1747–55. http://doi.org/10.1249/MSS.0b013e318256903a

Owens, S. C., Brismée, J. M., Pennell, P. N., Dedrick, G. S., Sizer, P. S., & James, C. R. (2009). Changes in Spinal Height Following Sustained Lumbar Flexion and Extension Postures: A Clinical Measure of Intervertebral Disc Hydration Using Stadiometry. *Journal of Manipulative and Physiological Therapeutics*, *32*(5), 358–363. http://doi.org/10.1016/j.jmpt.2009.04.006

Panjabi, M. M. (1992). The stabilizing system of the spine. Part 1. Function, dysfunction, adaptation, and enhancement. *Journal of Spinal Disorders*, *5*, 383–389.

Pollard, C. D., Sigward, S. M., & Powers, C. M. (2010). Limited hip and knee flexion during landing is associated with increased frontal plane knee motion and moments. *Clinical Biomechanics*, *25*(2), 142–146. http://doi.org/10.1016/j.clinbiomech.2009.10.005

Potvin, J. R., & Brown, S. H. M. (2005). An equation to calculate individual muscle contributions to joint stability. *Journal of Biomechanics*, *38*(5), 973–80. http://doi.org/10.1016/j.jbiomech.2004.06.004

Powers, C. M. (2003). The influence of altered lower-extremity kinematics on patellofemoral joint dysfunction: a theoretical perspective. *The Journal of Orthopaedic and Sports Physical Therapy*, *33*, 639–646. http://doi.org/10.2519/jospt.2003.33.11.639

Powers, C. M. (2010a). The influence of abnormal hip mechanics on knee injury: a biomechanical perspective. *The Journal of Orthopaedic and Sports Physical Therapy*,

40(2), 42–51. http://doi.org/10.2519/jospt.2010.3337

Powers, C. M. (2010b). The influence of abnormal hip mechanics on knee injury: a biomechanical perspective. *The Journal of Orthopaedic and Sports Physical Therapy*, *40*(2), 42–51. http://doi.org/10.2519/jospt.2010.3337

Powers, C. M. (2012). *Patellofemoral Pain: Proximal, Distal, and Local Factors, 2nd International Research Retreat*. *Journal of Orthopaedic and Sports Physical Therapy* (Vol. 42). http://doi.org/10.2519/jospt.2012.0301

Reeves, N. P., Narendra, K. S., & Cholewicki, J. (2011). Spine stability: Lessons from balancing a stick. *Clinical Biomechanics*, *26*, 325–330. http://doi.org/10.1016/j.clinbiomech.2010.11.010

Reiman, M. P., Bolgla, L. a, & Lorenz, D. (2009). Hip functions influence on knee dysfunction: a proximal link to a distal problem. *Journal of Sport Rehabilitation*, *18*(1), 33–46.

Roewer, B. D., Ford, K. R., Myer, G. D., & Hewett, T. E. (2014). The "impact" of force filtering cut-off frequency on the peak knee abduction moment during landing: artefact or "artifiction"? *British Journal of Sports Medicine*, *48*(6), 464–8. http://doi.org/10.1136/bjsports-2012-091398

Schwartz, M. H., & Rozumalski, A. (2005). A new method for estimating joint parameters from motion data. *Journal of Biomechanics*, *38*(1), 107–16. http://doi.org/10.1016/j.jbiomech.2004.03.009

Segal, R. L. (1992). Neuromuscular compartments in the human biceps brachii muscle. *Neuroscience Letters*, *140*(1), 98–102. http://doi.org/10.1016/0304-3940(92)90691-Y

Shin, C. S., Chaudhari, A. M., & Andriacchi, T. P. (2011). Valgus plus internal rotation moments increase anterior cruciate ligament strain more than either alone. *Medicine and Science in Sports and Exercise*, *43*(8), 1484–1491. http://doi.org/10.1249/MSS.0b013e31820f8395

Shirey, M., Hurlbutt, M., Johansen, N., King, G. W., Wilkinson, S. G., & Hoover, D. L. (2012). The influence of core musculature engagement on hip and knee kinematics in women during a single leg squat. *International Journal of Sports Physical Therapy*, *7*(1), 1–12. Retrieved from http://www.pubmedcentral.nih.gov/articlerender.fcgi?artid=3273878&tool=pmcentrez&rendertype=abstract

Sigward, S. M., Ota, S., & Powers, C. M. (2008). Predictors of frontal plane knee excursion during a drop land in young female soccer players. *The Journal of Orthopaedic and Sports Physical Therapy*, *38*(11), 661–667. http://doi.org/10.2519/jospt.2008.2695

Sigward, S. M., Pollard, C. D., Havens, K. L., & Powers, C. M. (2012). Influence of sex and maturation on knee mechanics during side-step cutting. *Medicine and Science in Sports and Exercise*, *44*, 1497–1503. http://doi.org/10.1249/MSS.0b013e31824e8813

Soma, N. (2015). *INDUCED ANTERIOR CRUCIATE LIGAMENT CREEP INFULENCES GROUND REACTION FORCES AND MUSCLE ACTIVATION IN WALKING*.

Souza, R. B., & Powers, C. M. (2009a). Differences in hip kinematics, muscle strength, and muscle activation between subjects with and without patellofemoral pain. *The Journal of Orthopaedic and Sports Physical Therapy*, *39*(1), 12–19. http://doi.org/10.2519/jospt.2009.2885

Souza, R. B., & Powers, C. M. (2009b). Predictors of hip internal rotation during running: an evaluation of hip strength and femoral structure in women with and without patellofemoral pain. *The American Journal of Sports Medicine*, *37*, 579–587. http://doi.org/10.1177/0363546508326711

Struminger, A. H., Lewek, M. D., Goto, S., Hibberd, E., & Blackburn, J. T. (2013). Comparison of gluteal and hamstring activation during five commonly used plyometric exercises. *Clinical Biomechanics*, *28*(7), 783–789. http://doi.org/10.1016/j.clinbiomech.2013.06.010

Taunton, J., Ryan, M., Clement, D., McKenzie, D., Lloyd-Smith, D., & Zumbo, B. (2002). A retrospective case-control analysis of 2002 running injuries. *Sports Medicine*, *36*, 95–102.

Taylor, K. a., Cutcliffe, H. C., Queen, R. M., Utturkar, G. M., Spritzer, C. E., Garrett, W. E., & DeFrate, L. E. (2013). In vivo measurement of ACL length and relative strain during walking. *Journal of Biomechanics*, *46*(3), 478–483. http://doi.org/10.1016/j.jbiomech.2012.10.031

Taylor, K. a., Terry, M. E., Utturkar, G. M., Spritzer, C. E., Queen, R. M., Irribarra, L. a., … DeFrate, L. E. (2011). Measurement of in vivo anterior cruciate ligament strain during dynamic jump landing. *Journal of Biomechanics*, *44*(3), 365–371. http://doi.org/10.1016/j.jbiomech.2010.10.028

Utturkar, G. M., Irribarra, L. a., Taylor, K. a., Spritzer, C. E., Taylor, D. C., Garrett, W. E., & Defrate, L. E. (2013). The effects of a valgus collapse knee position on in vivo ACL elongation. *Annals of Biomedical Engineering*, *41*(1), 123–130. http://doi.org/10.1007/s10439-012-0629-x

Wu, G., Siegler, S., Allard, P., Kirtley, C., Leardini, A., Rosenbaum, D., … Stokes, I. (2002). ISB recommendation on definitions of joint coordinate system of various joints for the reporting of human joint motion--part I: ankle, hip, and spine. International Society of Biomechanics. *Journal of Biomechanics*, *35*(4), 543–548. http://doi.org/10.1016/S0021-9290(01)00222-6

Zazulak, B. T., Hewett, T. E., Reeves, N. P., Goldberg, B., & Cholewicki, J. (2007a). Deficits in neuromuscular control of the trunk predict knee injury risk: a prospective biomechanical-epidemiologic study. *The American Journal of Sports Medicine*, *35*(7), 1123–30. http://doi.org/10.1177/0363546507301585

Zazulak, B. T., Hewett, T. E., Reeves, N. P., Goldberg, B., & Cholewicki, J. (2007b). The effects of core proprioception on knee injury: a prospective biomechanical-epidemiological study. *The American Journal of Sports Medicine*, *35*, 368–373. http://doi.org/10.1177/0363546506297909

Zazulak, B.T., Ponce, P.L., Straub, S.J, Mendvecky, M.J., Avedisian, L and Hewett, T.E. (2005). Gender comparison of hip muscle activity during single-leg landing. *J Orthop Sports Phys Ther*, *35,* 292-299.

Appendix A

Derivation of the equation to be used in the calculation of hip joint rotational stiffness (JRS).

$$JRS_x = F\left[\frac{A_Y B_Y + A_Z B_Z - r_x^2}{l} + \frac{q r_x^2}{L}\right]$$

Where,

JRS_x = the rotational stiffness contribution of a muscle about the x-axis of the hip joint

F = force of a particular muscle "m" considering muscle activation, stress, PCSA as well as force-length (active and passive) and force-velocity correction factors

l = 3D length of the muscle vector that crosses the hip joint

L = full 3D length of the muscle

r = 3D muscle moment arm

A_X, A_Y, A_Z = origin coordinates with respect to hip joint centre at (0,0,0) m

B_X, B_Y, B_Z = insertion (or initial node) coordinates with respect to hip joint centre at (0,0,0) m

q = muscle stiffness coefficient (proportionality constant) relating muscle force and length to stiffness

Note: for calculations about the z-axis substitute z for x, x for y and y for z. For the y-axis substitute y for x, z for y and x for z.

$$\begin{bmatrix} B2_x \\ B2_y \\ B2_z \end{bmatrix} = \begin{bmatrix} B_x \\ B_y \\ B_z \end{bmatrix} \begin{bmatrix} 1 & 0 & 0 \\ 0 & cos\theta_x & -sin\theta_x \\ 0 & sin\theta_x & cos\theta_x \end{bmatrix} \quad (1)$$

$$B2_X = B_X \quad (2)$$

$$B2_Y = B_Y \cos\theta_X - B_Z \sin\theta_X \quad (3)$$

$$B2_Z = B_Y \sin\theta_X + B_Z \cos\theta_X \quad (4)$$

$$l = \sqrt{(B_X - A_X)^2 + (B_Y - A_Y)^2 + (B_Z - A_Z)^2} \quad (5)$$

$$l_2 = \sqrt{(B2_X - A_X)^2 + (B2_Y - A_Y)^2 + (B2_Z - A_Z)^2} \quad (6)$$

$$l_2 = \sqrt{(B2_X - A_X)^2 + (B_Y \cos\theta_X - B_z \sin\theta_X - A_Y)^2 + (B_Y \sin\theta_X + B_z \cos\theta_x - A_z)^2} \quad (7)$$

$$\Delta l = \sqrt{(B2_X - A_X)^2 + (B_Y \cos\theta_X - B_z \sin\theta_X - A_Y)^2 + (B_Y \sin\theta_X + B_z \cos\theta_x - A_z)^2} - \sqrt{(B2_X - A_X)^2 + (B2_Y - A_Y)^2 + (B2_Z - A_Z)^2} \quad (8)$$

$$U(m) = F\Delta l + \frac{1}{2} k\, \Delta l^2 \quad (9)$$

$$S(m)_X = \frac{d^2 U(m)}{d\theta^2{}_X} \quad (10)$$

$$S_{(m)_X} = F\left[\frac{A_Y B_Y + A_Z B_Z}{l} - \frac{(A_Y B_Z - A_Z B_Y)^2}{l^3}\right] + k\left[\frac{(A_Y B_Z - A_Z B_Y)^2}{l^2}\right] \quad (11)$$

$$r_X = \frac{B_Y A_Z - A_Y B_Z}{l} \quad (12)$$

$$S(m)_X = F\left[\frac{A_Y B_Y + A_Z B_z - r_X^2}{l}\right] + k r_X^2 \quad (13)$$

$$k = \frac{qF}{L} \quad (14)$$

$$S(m)_X = F\left[\frac{A_Y B_Y + A_z B_z - r_z^2}{l}\right] + \frac{q r_X^2}{L} \quad (15)$$

$$W = ph(1 - \cos\theta) \quad (16)$$

$$\frac{d^2 W}{d\theta_X^2} = ph \quad (17)$$

$$V = \sum_{m=1}^{N} U_m - W \quad (18)$$

$$S_X = \frac{d^2 V}{d\theta_X^2} = \sum_{m=1}^{N}\left[\frac{d^2 U}{d\theta_X^2}\right]_m - \frac{d^2 W}{d\theta_X^2} \quad (19)$$

$$S_X = \frac{d^2 V}{d\theta_X^2} = \sum_{m=1}^{N} F_m\left[\frac{A_Y B_Y + A_Z B_Z - r_X^2}{l} + \frac{q r_X^2}{L}\right]_m - ph \quad (20)$$

Appendix B

Muscle Force Calculations for the Hill-Type model to be used in the calculation of hip JRS.

All calculations and equations taken from by McGill & Norman (1986):

$$\mathbf{F_m = G\left[\left(\frac{EMG}{EMG_{max}}\right)(P_0)(\Omega)(\delta) + F_{PEC}\right]}$$

Where,

F_m = Muscle force (N)

G = Error term or gain

$\frac{EMG}{EMG_{max}}$ = Normalised EMG amplitude

P_0 = Maximum isometric force (N)

Ω = Coefficient for force-velocity correction

δ = Coefficient for force-length correction

F_{PEC} = Force due to the passive elastic component

In which,

$P_o = PCSA^* \sigma_{max}$

Where,

PCSA = Physiological Cross Sectional Area

σ_{max} = maximum muscle stress

Force-Length Coefficient Calculation:

$$\delta = \sin\left(\pi\left[\left(\frac{L}{L_0}\right) - 0.05\right]\right)$$

Where,

$\frac{L}{L_0}$ = Muscle length normalised to rest length

Force-Velocity Coefficient Calculation:

For concentric contractions:

$$\Omega = \frac{(P_0 * b - v * a)}{P_0(V + b)}$$

Where,

P_o = Maximum isometric force (N)

a,b = coefficients

V = Muscle velocity in rest lengths per second (L_o/s)

In which,

$$\frac{a}{P_0} = \frac{b}{V_{max}}$$

V_{max} = Maximum velocity at which force can be produced

a = 0.25 * P_0
b = 0.25 * 3.6

For eccentric contractions from V = 0 L_o/s to V = -0.125 L_o/s:

$$\Omega = 1 - 1.6 * V$$

For eccentric contractions < -0.125 L_o/s:

$\Omega = 1.2$

F_{PEC} Calculation:

$$F_{PEC} = e^{\left[-10.671+7.675 * \left(\frac{L}{L_0}\right)\right]P_0}$$

Appendix C

All figures for each variable of every task. Statistical significance is not denoted.

Lumbar JRS pre filtered and filtered using a 12 Hz cut off

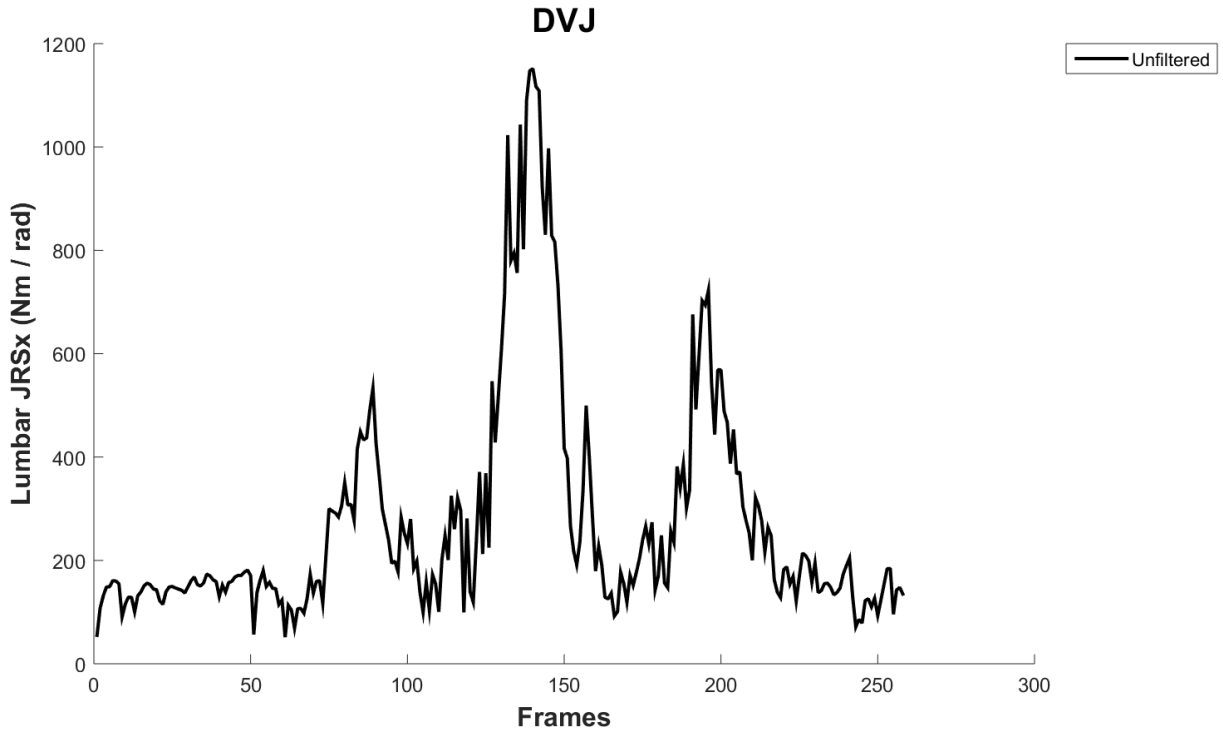

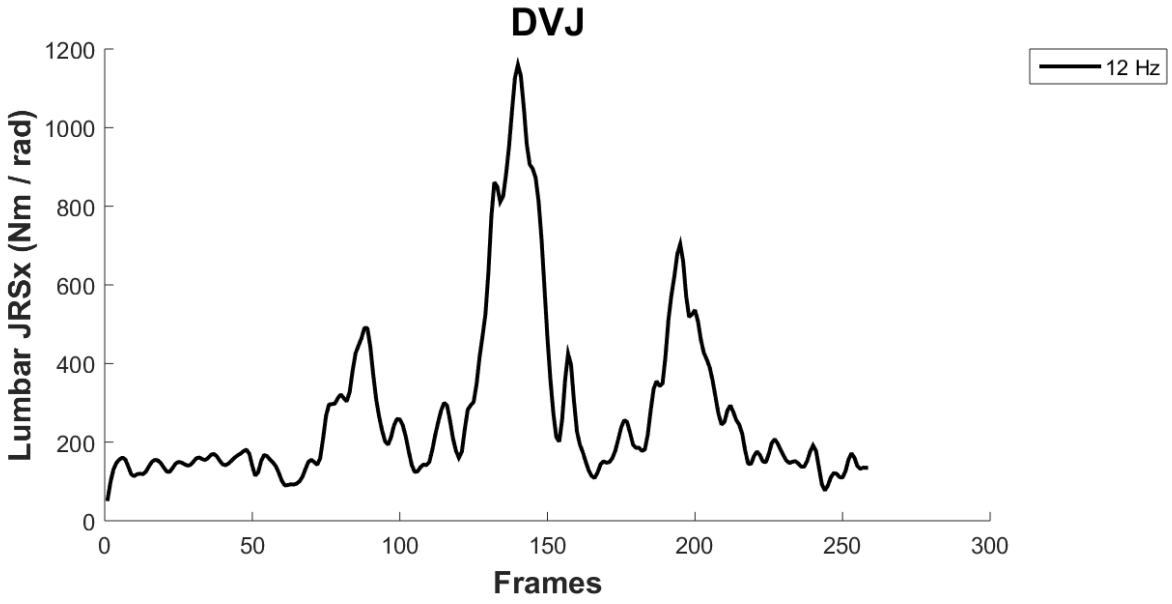

DVJ: Initial Contact to Toe Off

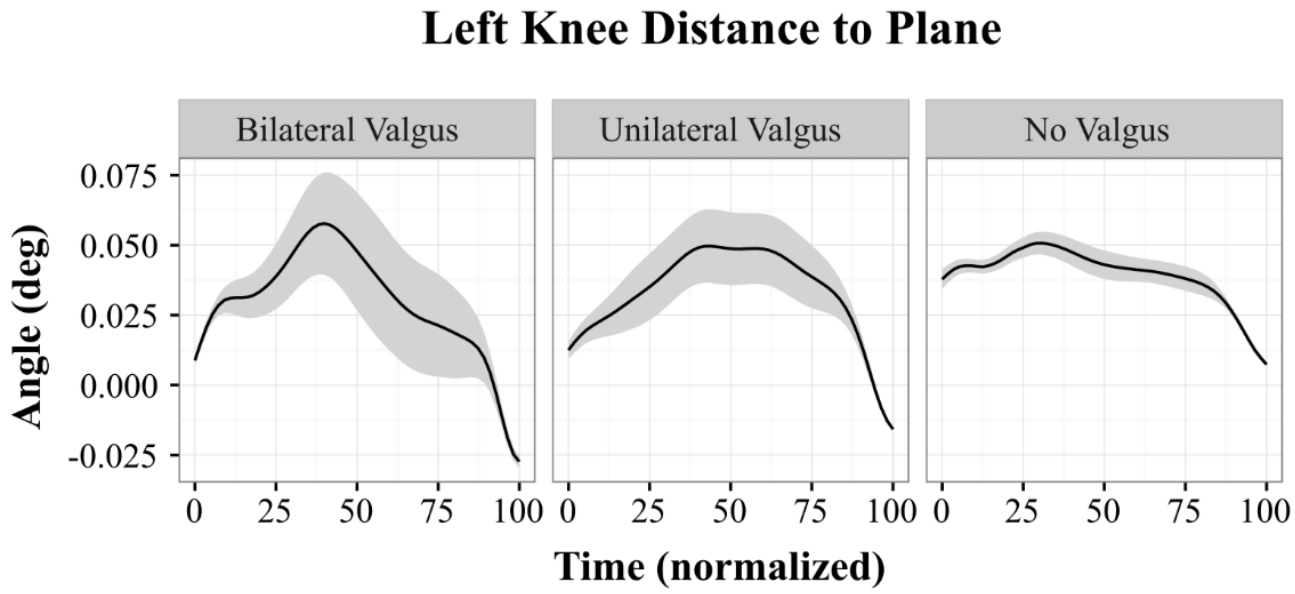

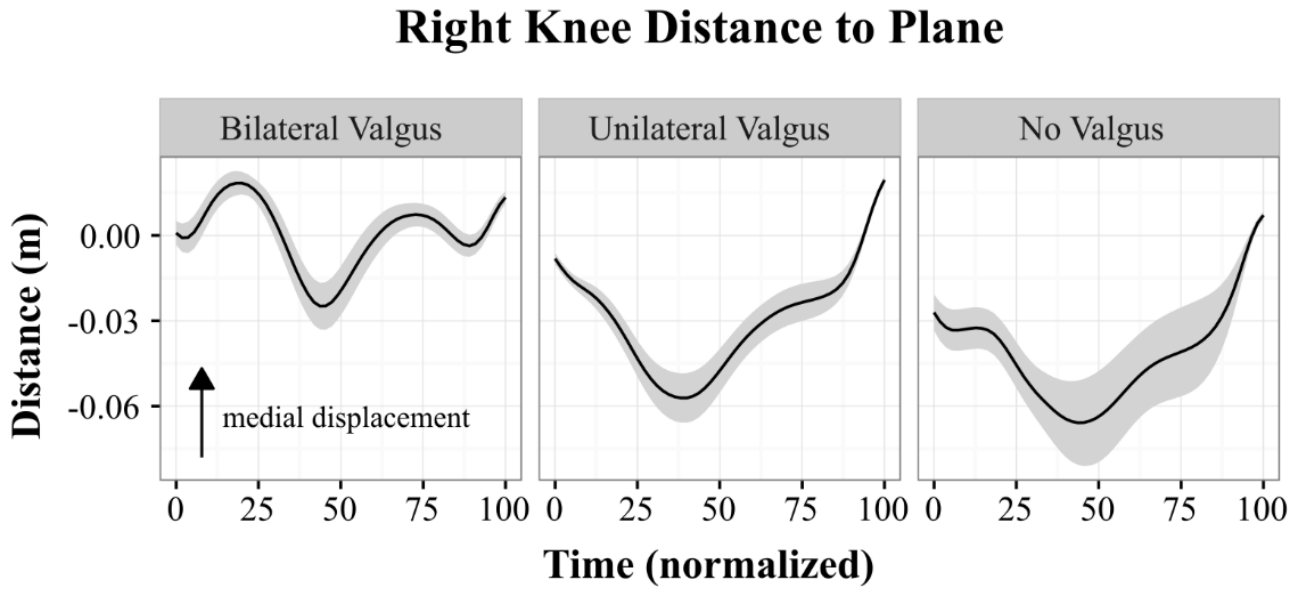

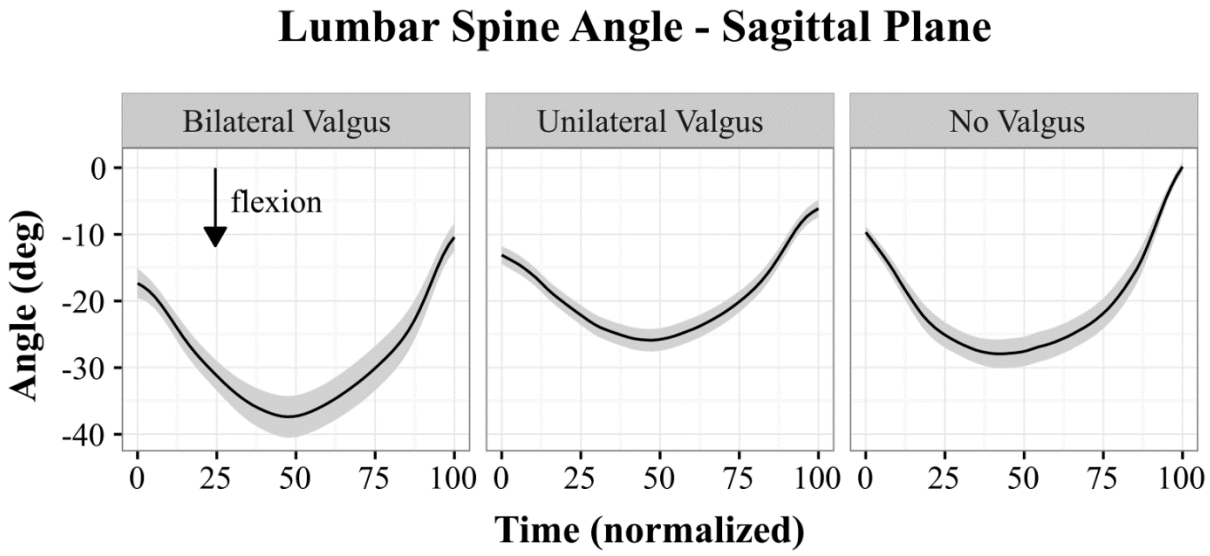
Lumbar Spine Angle - Sagittal Plane
Bilateral Valgus
Unilateral Valgus
No Valgus
flexion
Angle (deg)
0
-10
-20
-30
-40
0
25
50
75
100
Time (normalized)

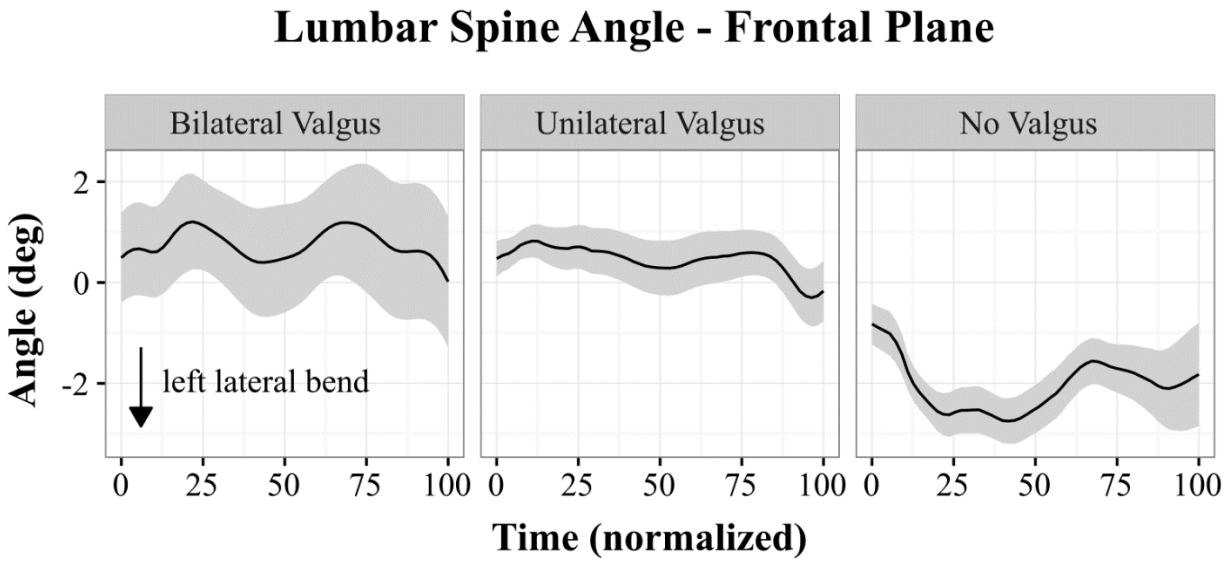
Lumbar Spine Angle - Frontal Plane
Bilateral Valgus
Unilateral Valgus
No Valgus
left lateral bend
Angle (deg)
2
0
-2
0
25
50
75
100
Time (normalized)

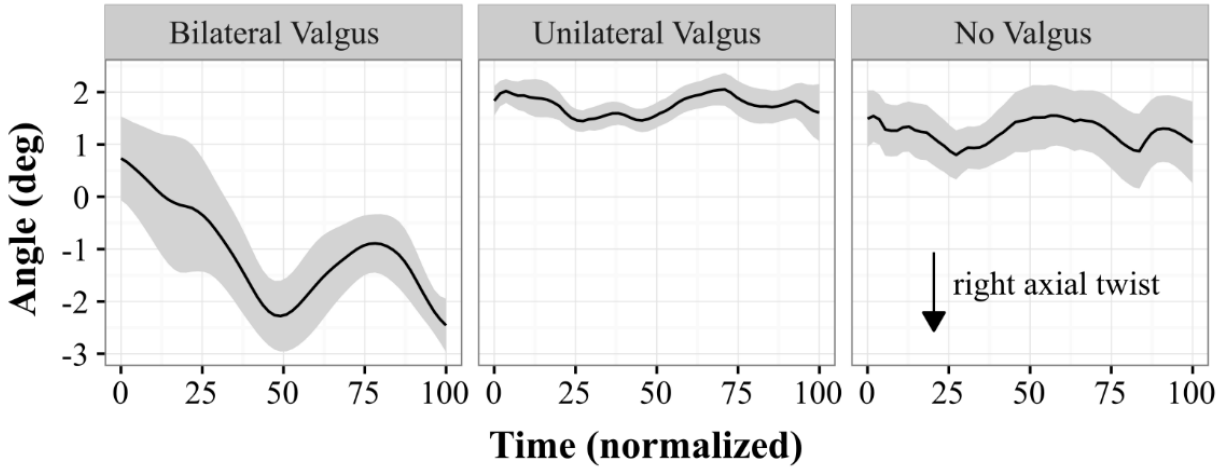
Lumbar Spine Angle - Transverse Plane
Bilateral Valgus
Unilateral Valgus
No Valgus
Angle (deg)
2
1
0
-1
-2
-3
right axial twist
0
25
50
75
100
Time (normalized)

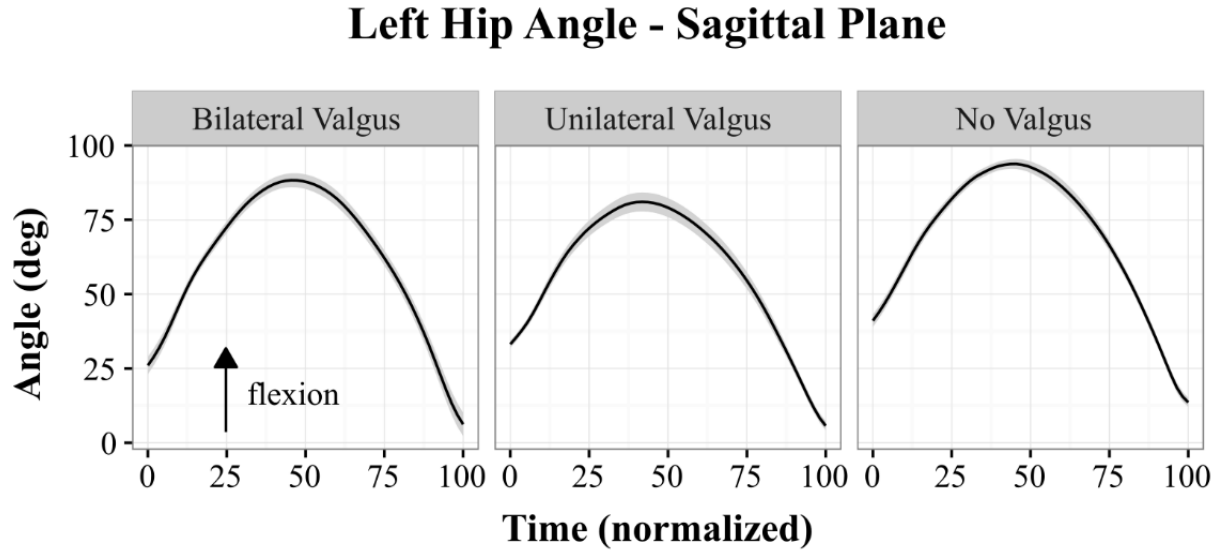
Left Hip Angle - Sagittal Plane
Bilateral Valgus
Unilateral Valgus
No Valgus
Angle (deg)
100
75
50
25
0
flexion
0
25
50
75
100
Time (normalized)

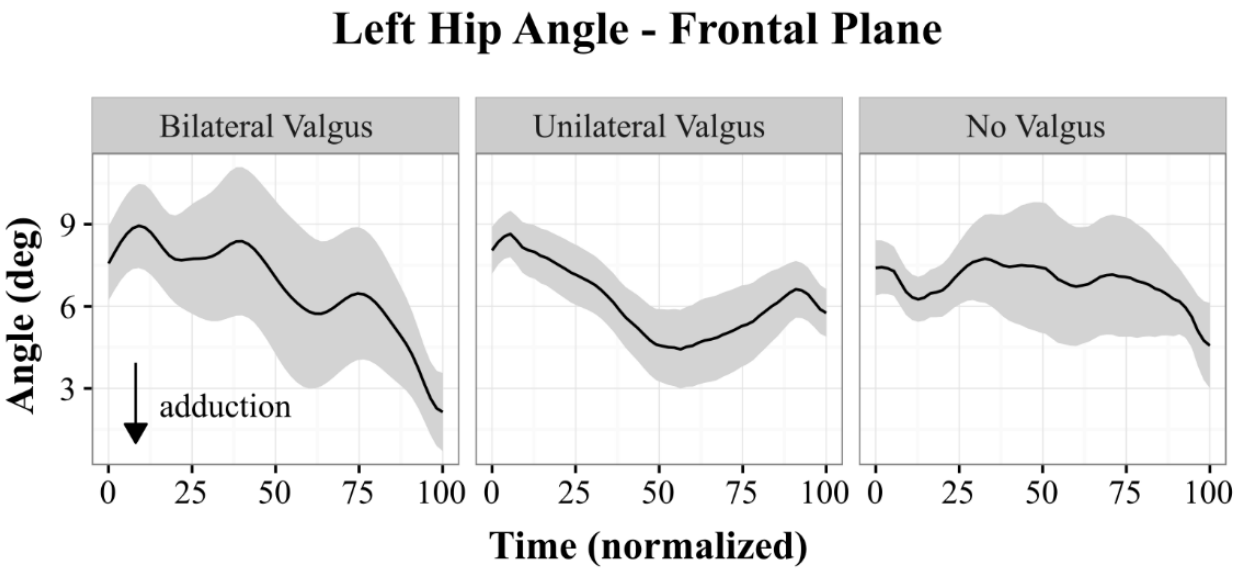
Left Hip Angle - Frontal Plane
Bilateral Valgus
Unilateral Valgus
No Valgus
Angle (deg)
9
6
3
adduction
0
25
50
75
100
Time (normalized)

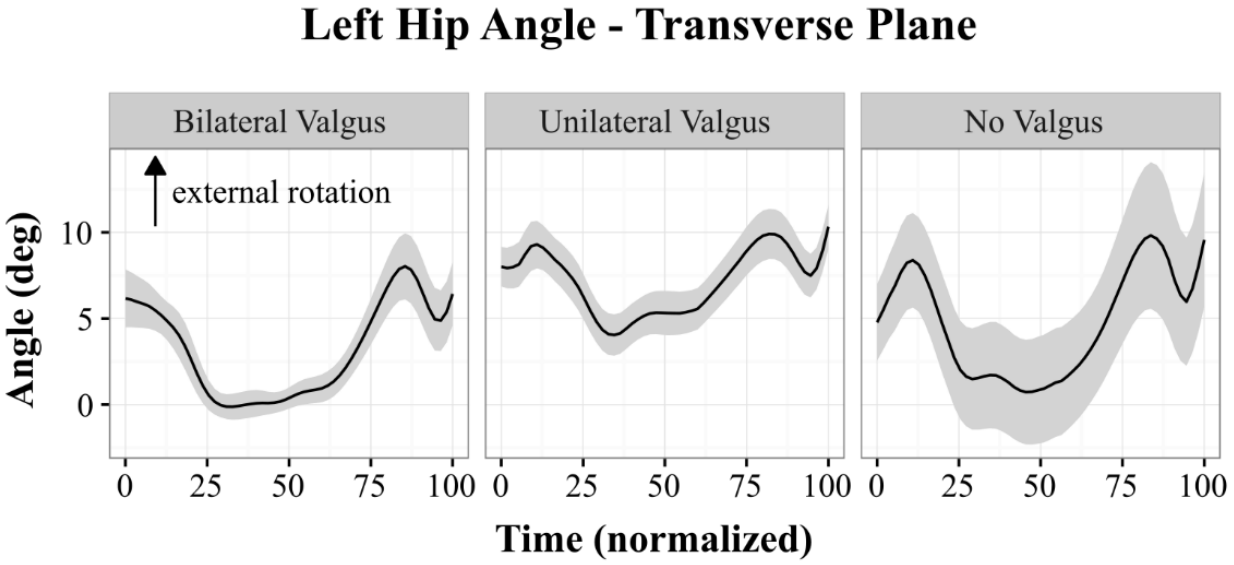
Left Hip Angle - Transverse Plane
Bilateral Valgus
Unilateral Valgus
No Valgus
external rotation
Angle (deg)
10
5
0
0
25
50
75
100
Time (normalized)

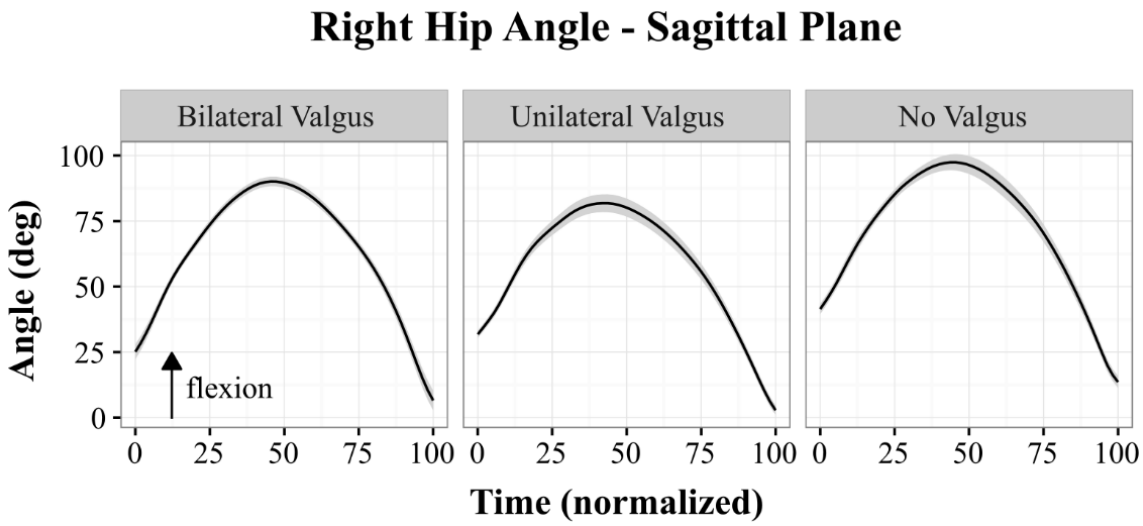
Right Hip Angle - Sagittal Plane
Bilateral Valgus
Unilateral Valgus
No Valgus
Angle (deg)
100
75
50
25
0
flexion
0
25
50
75
100
Time (normalized)

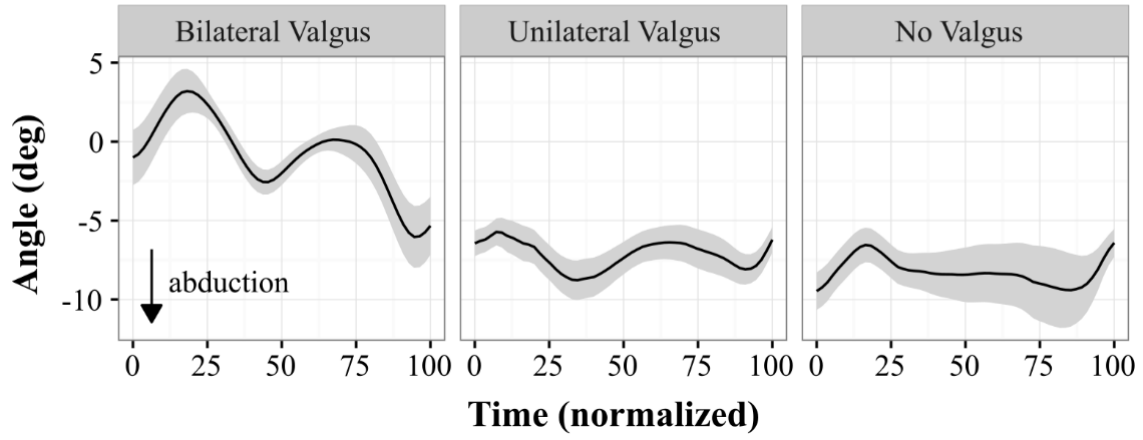
Right Hip Angle - Frontal Plane
Bilateral Valgus
Unilateral Valgus
No Valgus
Angle (deg)
5
0
-5
-10
abduction
0
25
50
75
100
Time (normalized)

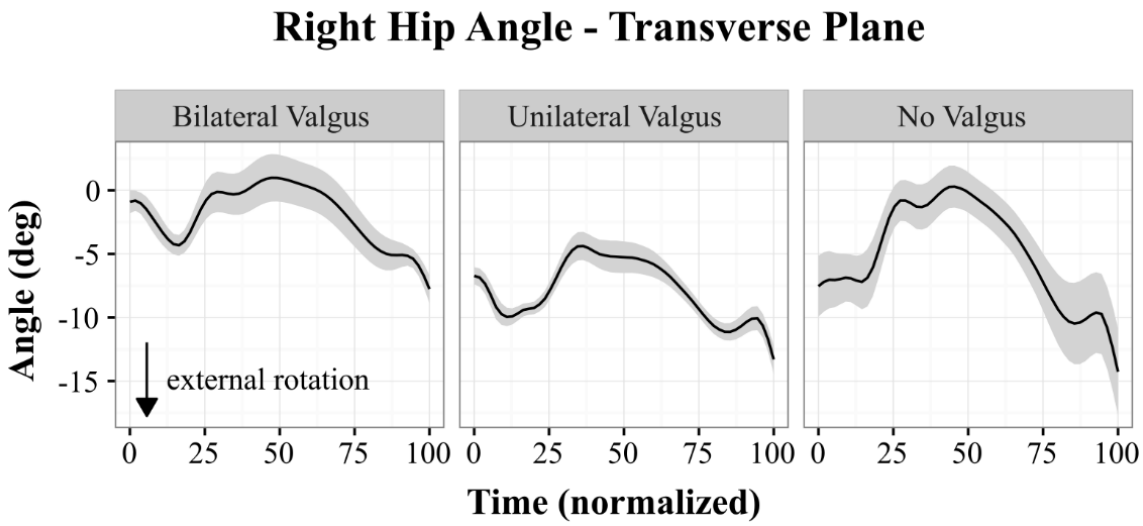
Right Hip Angle - Transverse Plane
Bilateral Valgus
Unilateral Valgus
No Valgus
Angle (deg)
0
-5
-10
-15
external rotation
0
25
50
75
100
Time (normalized)

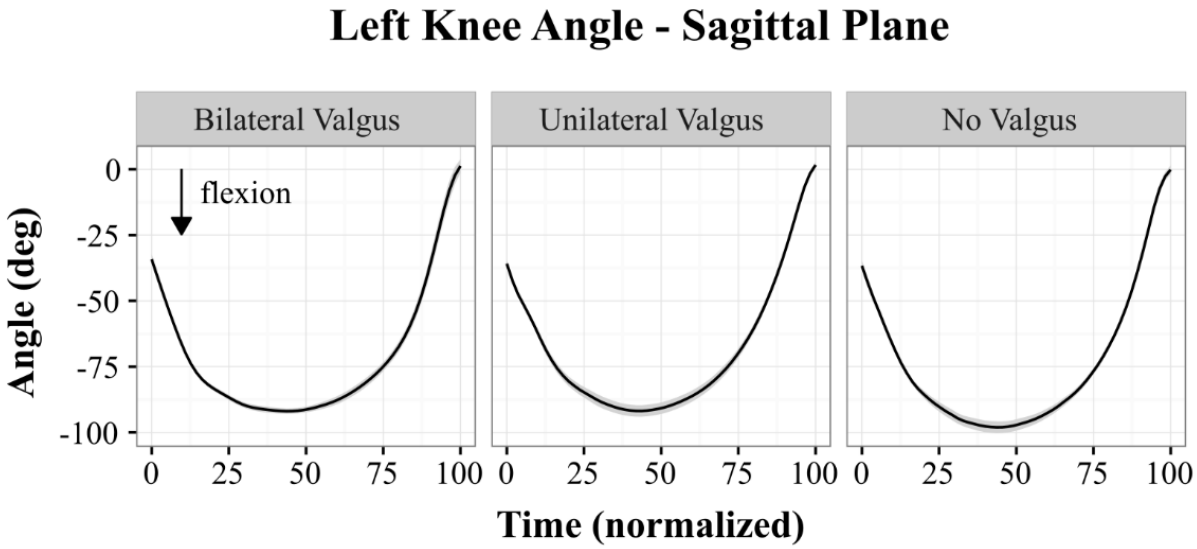
Left Knee Angle - Sagittal Plane
Bilateral Valgus
Unilateral Valgus
No Valgus
Angle (deg)
0
-25
-50
-75
-100
flexion
0
25
50
75
100
Time (normalized)

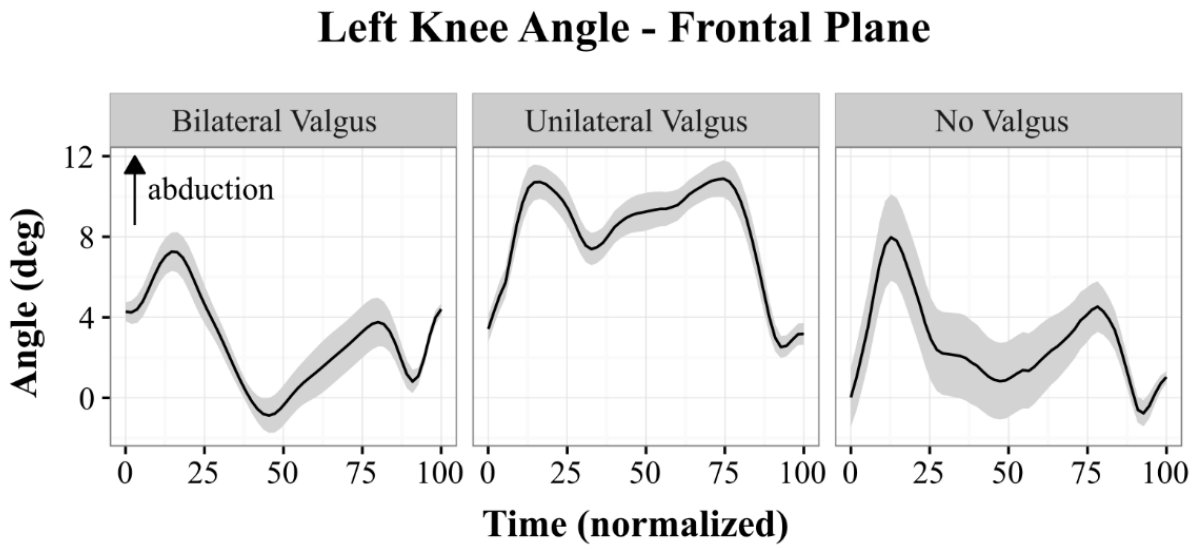
Left Knee Angle - Frontal Plane
Bilateral Valgus
Unilateral Valgus
No Valgus
abduction
Angle (deg)
12
8
4
0
0
25
50
75
100
Time (normalized)

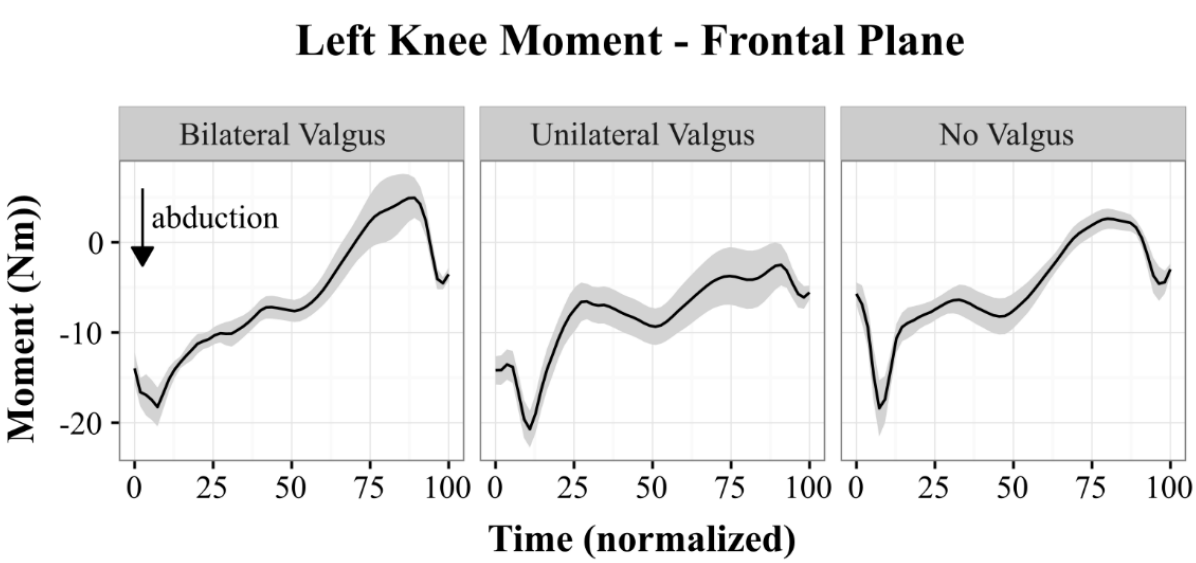
Left Knee Moment - Frontal Plane
Bilateral Valgus
Unilateral Valgus
No Valgus
abduction
Moment (Nm))
0
-10
-20
0
25
50
75
100
Time (normalized)

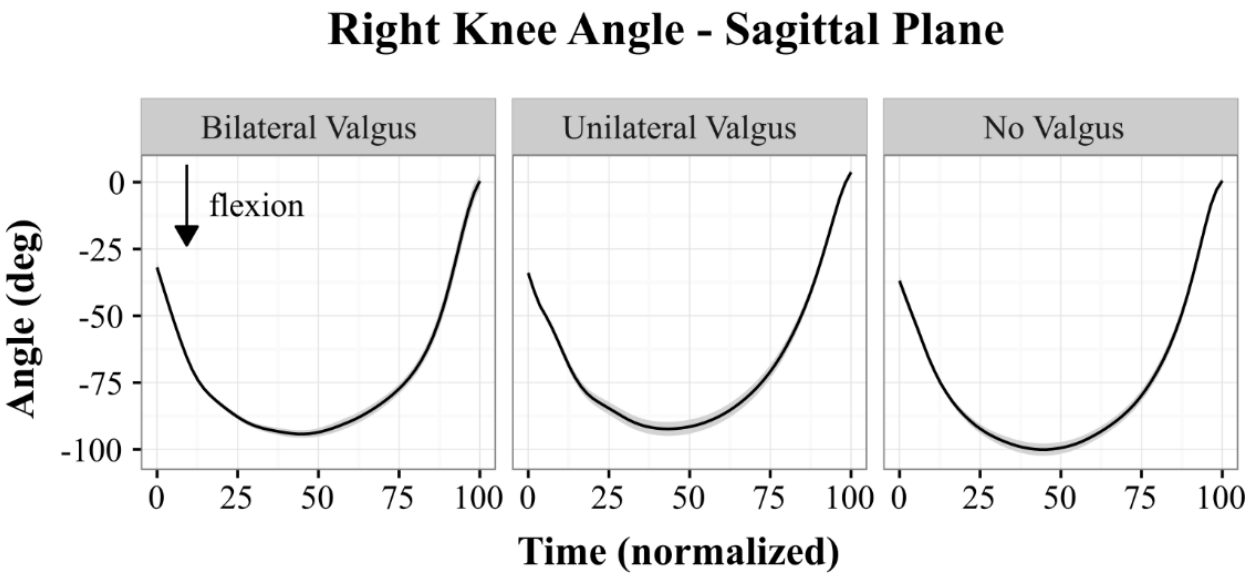
Right Knee Angle - Sagittal Plane
Bilateral Valgus
Unilateral Valgus
No Valgus
flexion
Angle (deg)
0
-25
-50
-75
-100
0
25
50
75
100
Time (normalized)

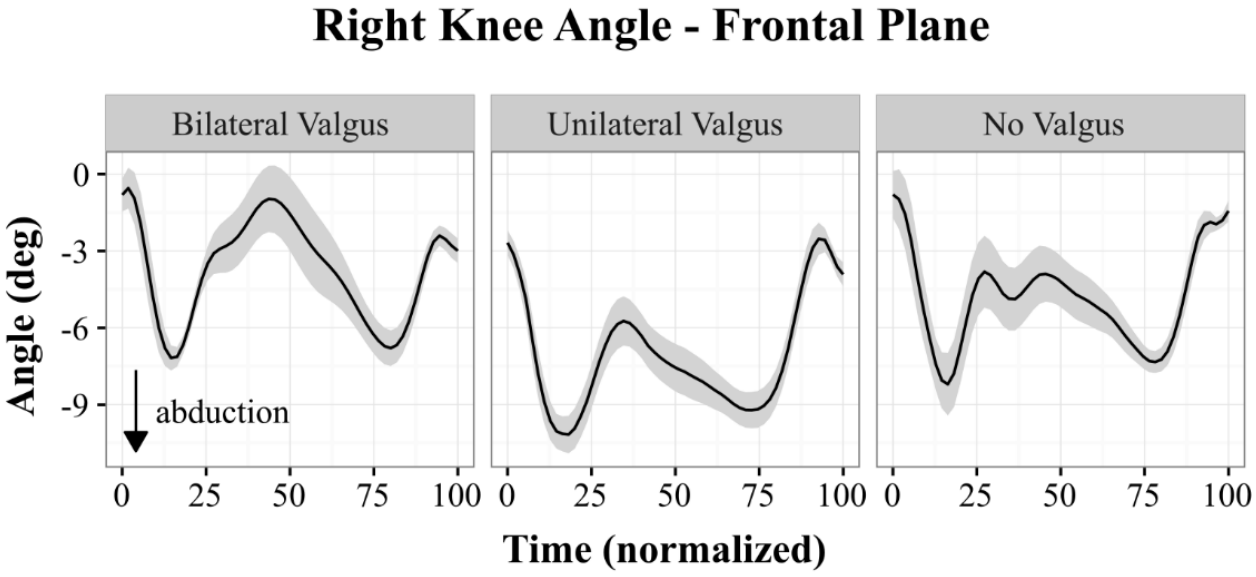
Right Knee Angle - Frontal Plane
Bilateral Valgus
Unilateral Valgus
No Valgus
abduction
Angle (deg)
0
-3
-6
-9
0
25
50
75
100
Time (normalized)

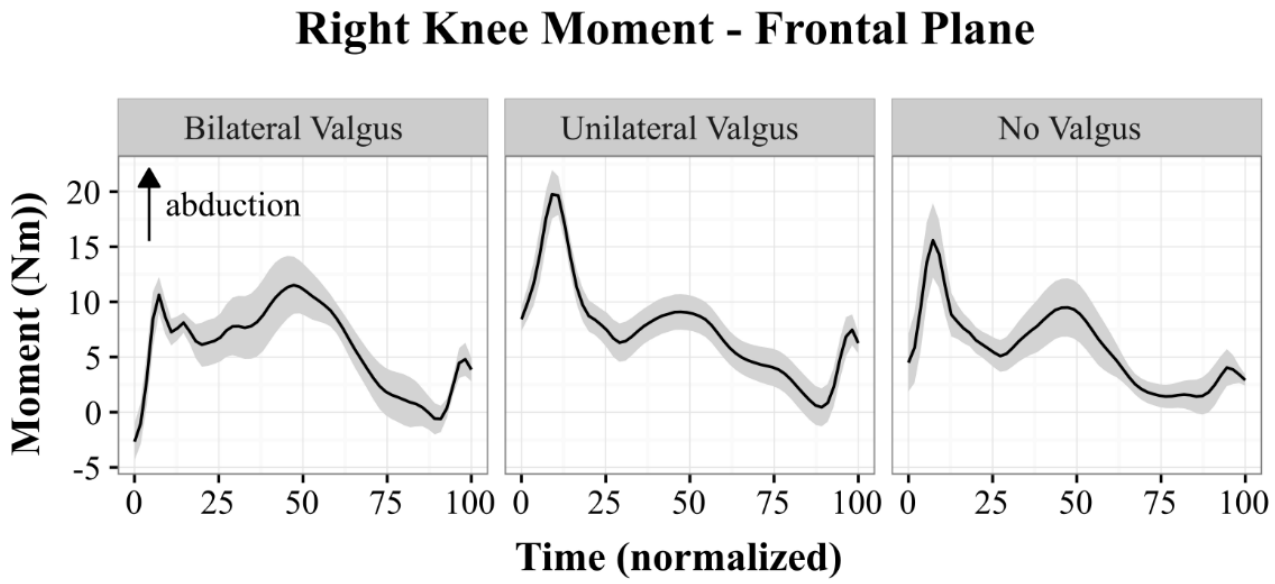
Right Knee Moment - Frontal Plane
Bilateral Valgus
Unilateral Valgus
No Valgus
abduction
Moment (Nm))
20
15
10
5
0
-5
0
25
50
75
100
Time (normalized)

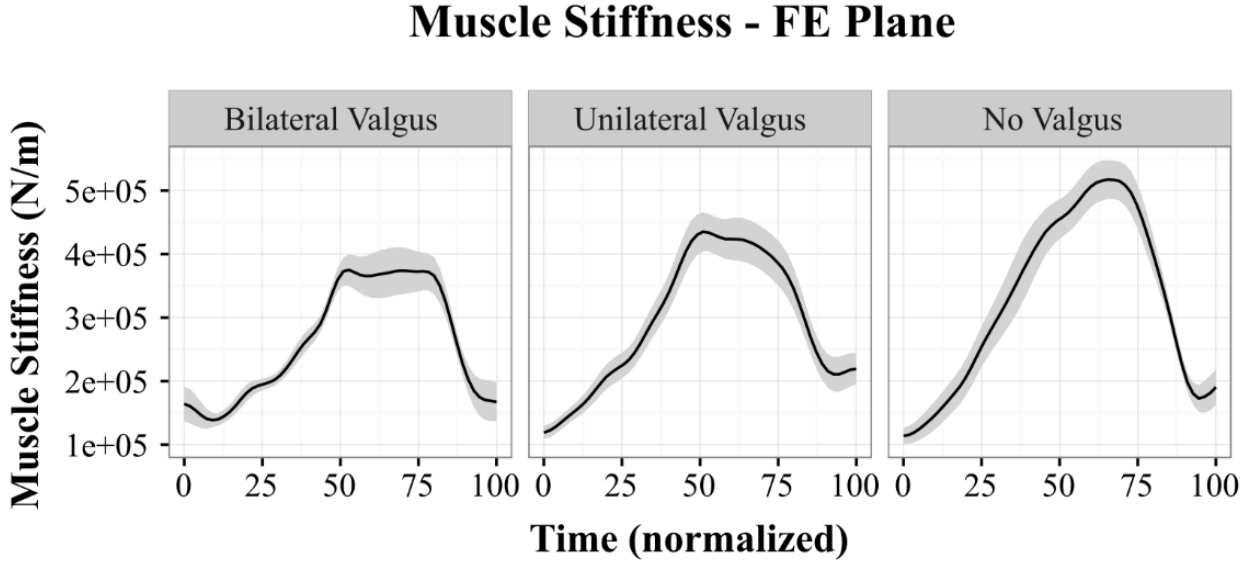
Muscle Stiffness - FE Plane
Bilateral Valgus
Unilateral Valgus
No Valgus
Muscle Stiffness (N/m)
5e+05
4e+05
3e+05
2e+05
1e+05
0
25
50
75
100
Time (normalized)

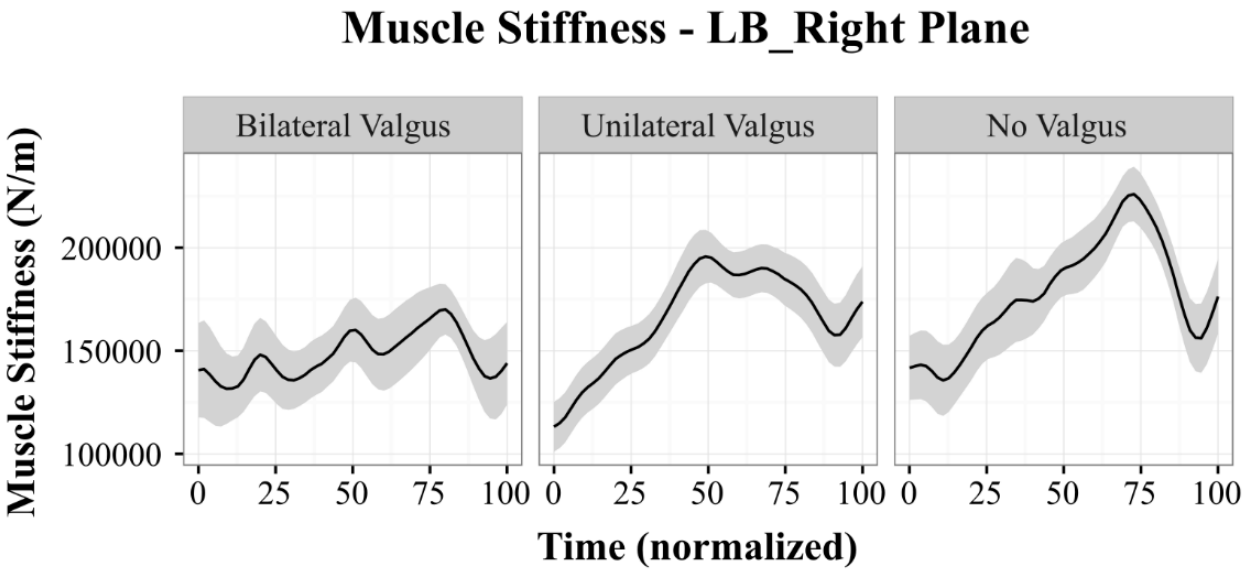
Muscle Stiffness - LB_Right Plane
Bilateral Valgus
Unilateral Valgus
No Valgus
Muscle Stiffness (N/m)
200000
150000
100000
0
25
50
75
100
Time (normalized)

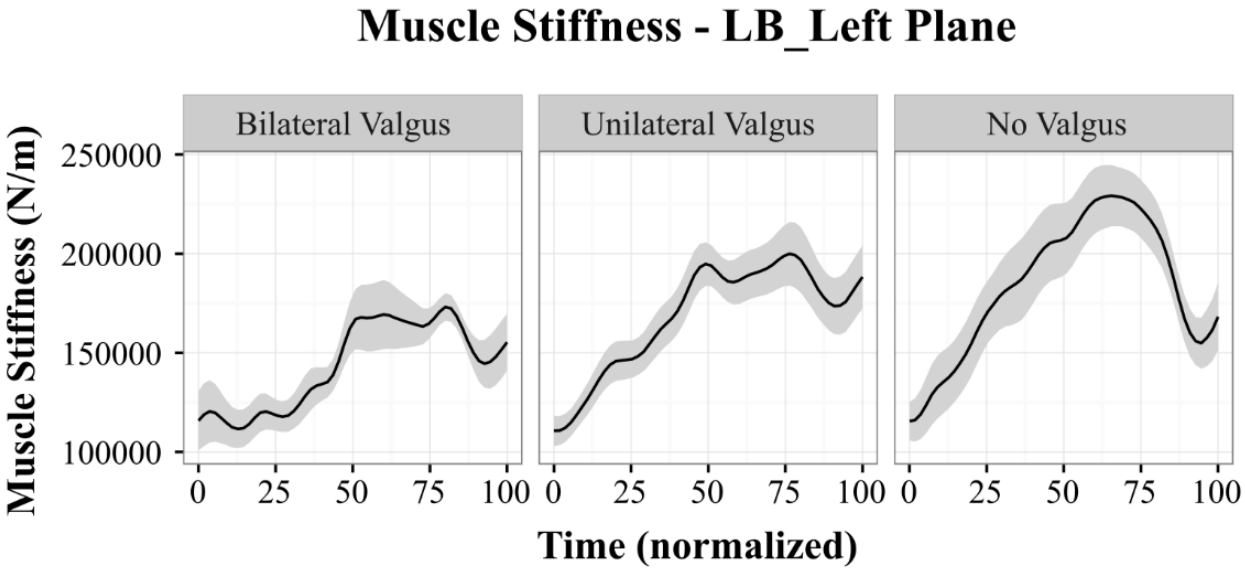
Muscle Stiffness - LB_Left Plane
Bilateral Valgus
Unilateral Valgus
No Valgus
Muscle Stiffness (N/m)
250000
200000
150000
100000
0
25
50
75
100
Time (normalized)

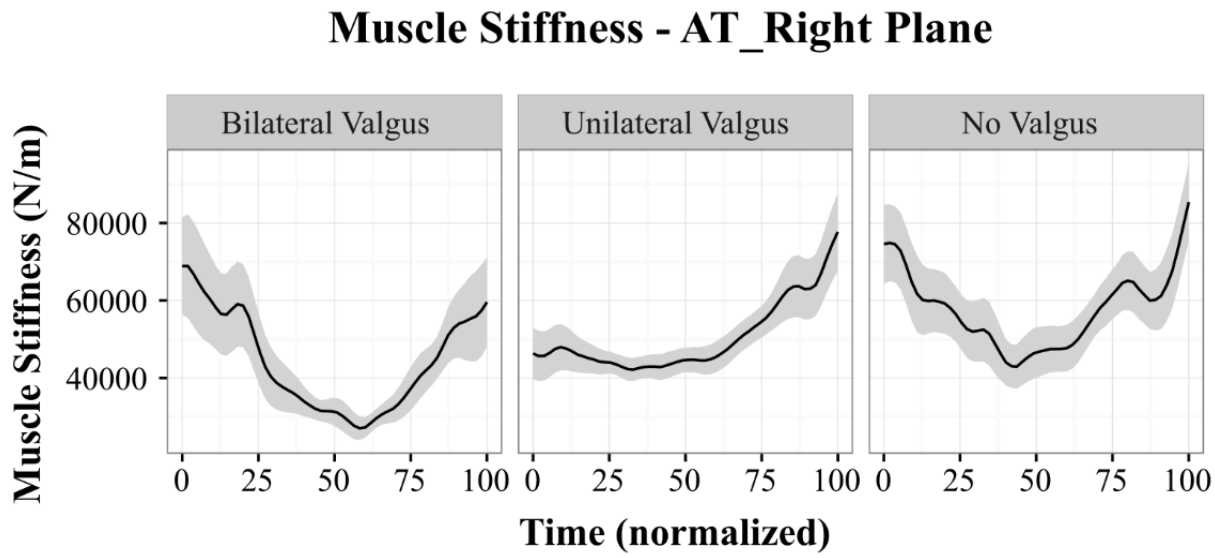
Muscle Stiffness - AT_Right Plane
Bilateral Valgus
Unilateral Valgus
No Valgus
Muscle Stiffness (N/m)
80000
60000
40000
0
25
50
75
100
Time (normalized)

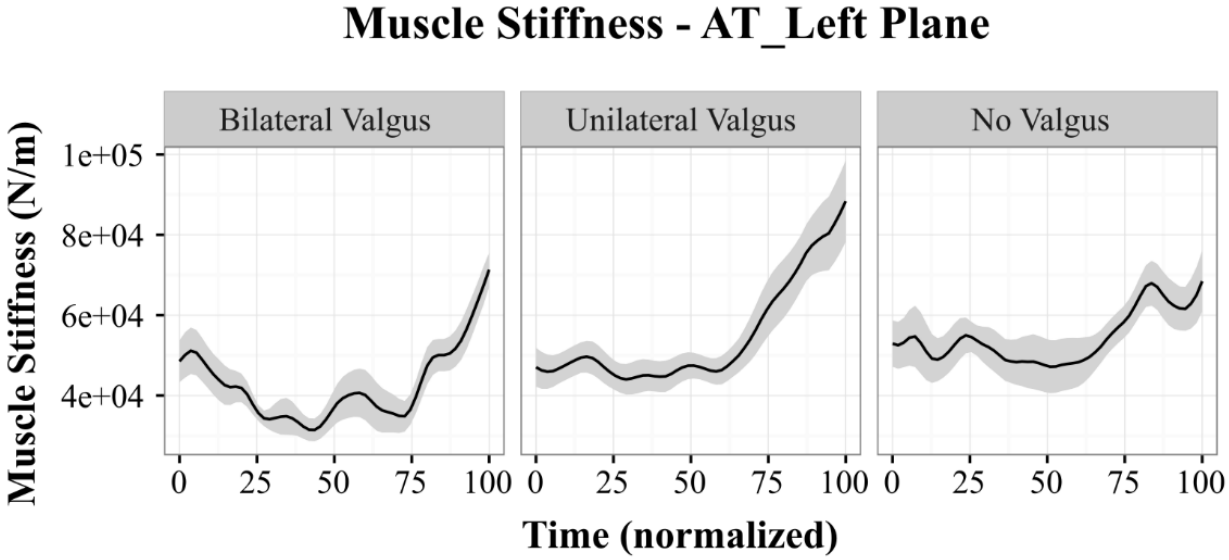
Muscle Stiffness - AT_Left Plane
Bilateral Valgus
Unilateral Valgus
No Valgus
Muscle Stiffness (N/m)
1e+05
8e+04
6e+04
4e+04
0
25
50
75
100
Time (normalized)

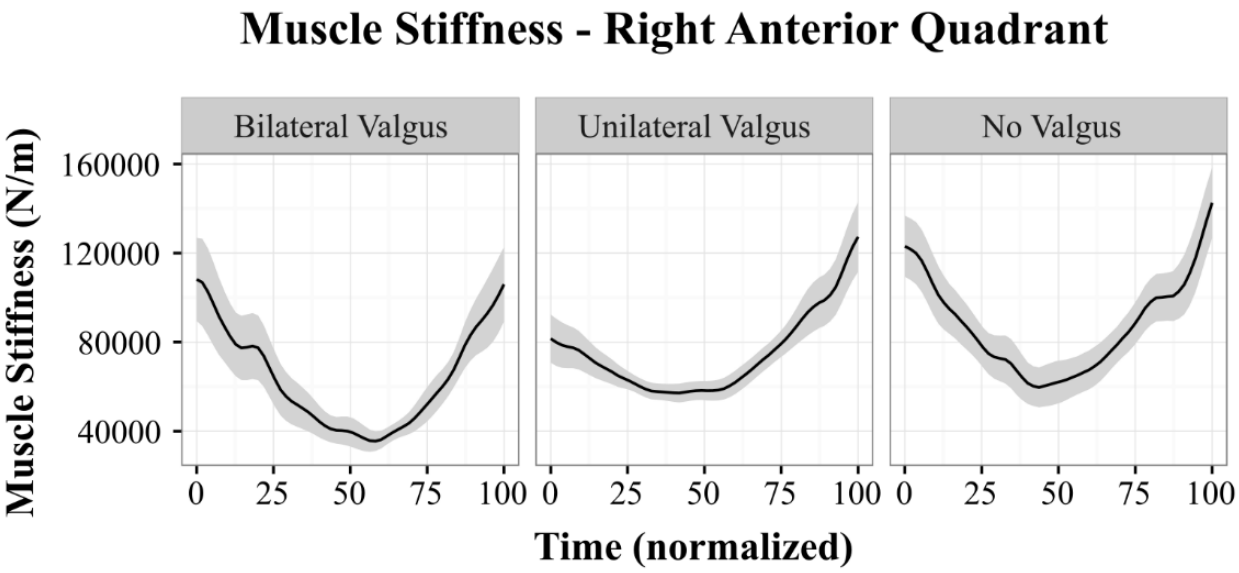
Muscle Stiffness - Right Anterior Quadrant
Bilateral Valgus
Unilateral Valgus
No Valgus
Muscle Stiffness (N/m)
160000
120000
80000
40000
0
25
50
75
100
Time (normalized)

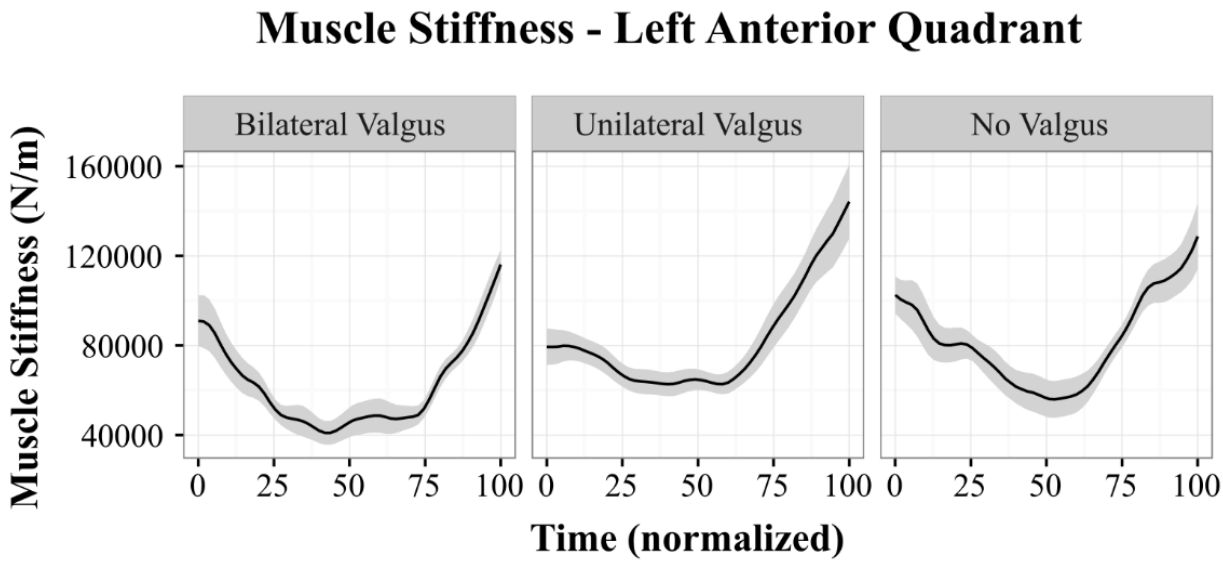
Muscle Stiffness - Left Anterior Quadrant
Bilateral Valgus
Unilateral Valgus
No Valgus
Muscle Stiffness (N/m)
160000
120000
80000
40000
0
25
50
75
100
Time (normalized)

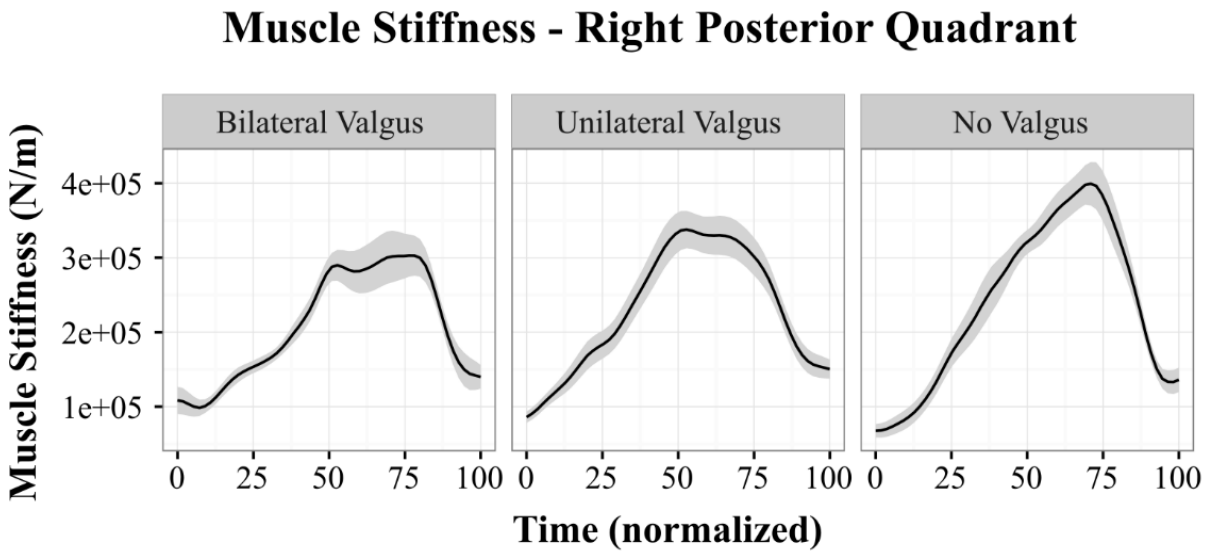
Muscle Stiffness - Right Posterior Quadrant
Bilateral Valgus
Unilateral Valgus
No Valgus
Muscle Stiffness (N/m)
4e+05
3e+05
2e+05
1e+05
0
25
50
75
100
Time (normalized)

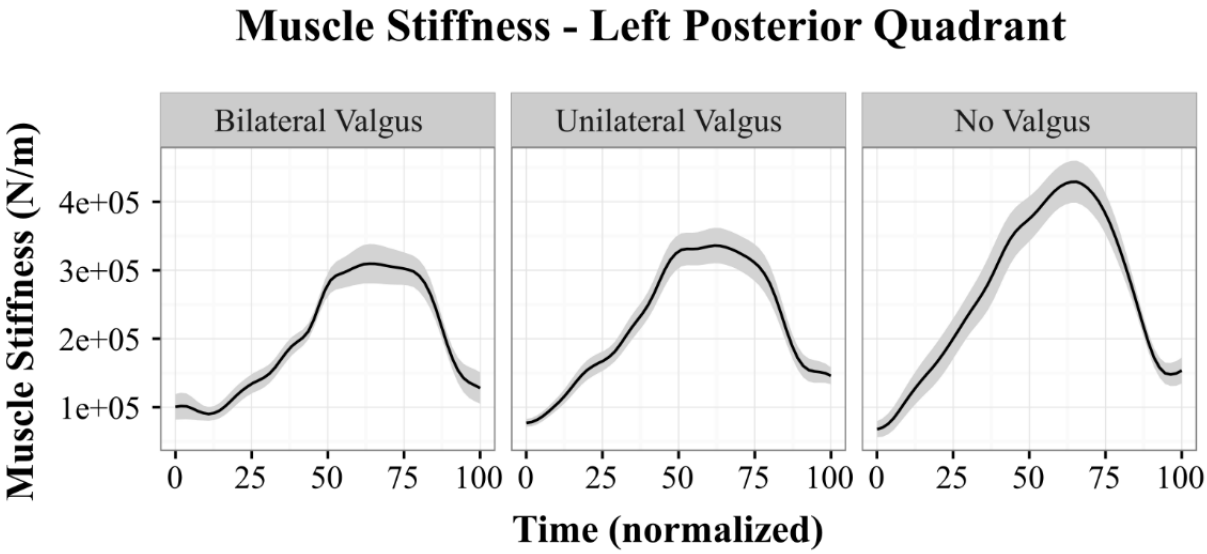
Muscle Stiffness - Left Posterior Quadrant
Bilateral Valgus
Unilateral Valgus
No Valgus
Muscle Stiffness (N/m)
4e+05
3e+05
2e+05
1e+05
0
25
50
75
100
Time (normalized)

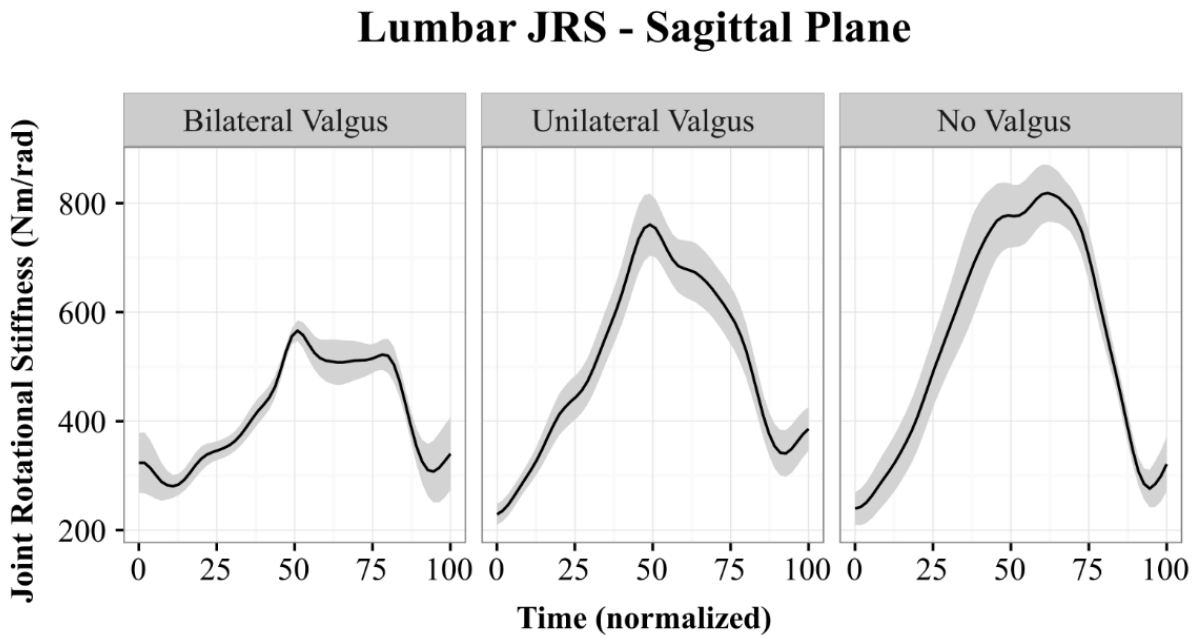
Lumbar JRS - Sagittal Plane
Bilateral Valgus
Unilateral Valgus
No Valgus
Joint Rotational Stiffness (Nm/rad)
800
600
400
200
0
25
50
75
100
Time (normalized)

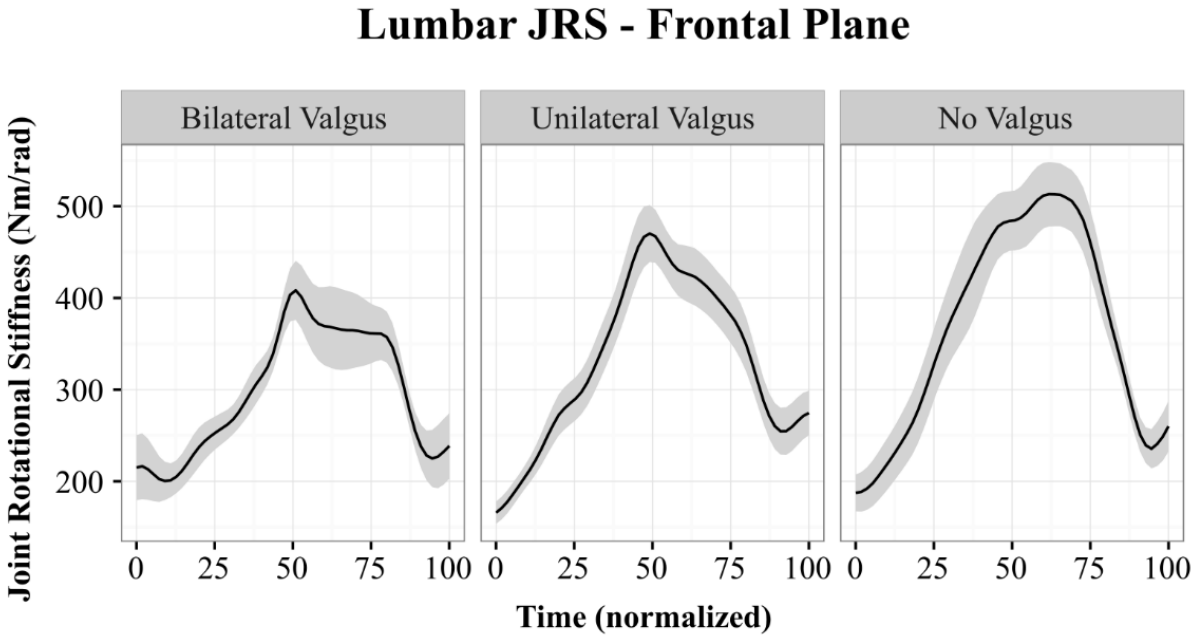
Lumbar JRS - Frontal Plane
Bilateral Valgus
Unilateral Valgus
No Valgus
Joint Rotational Stiffness (Nm/rad)
500
400
300
200
0
25
50
75
100
Time (normalized)

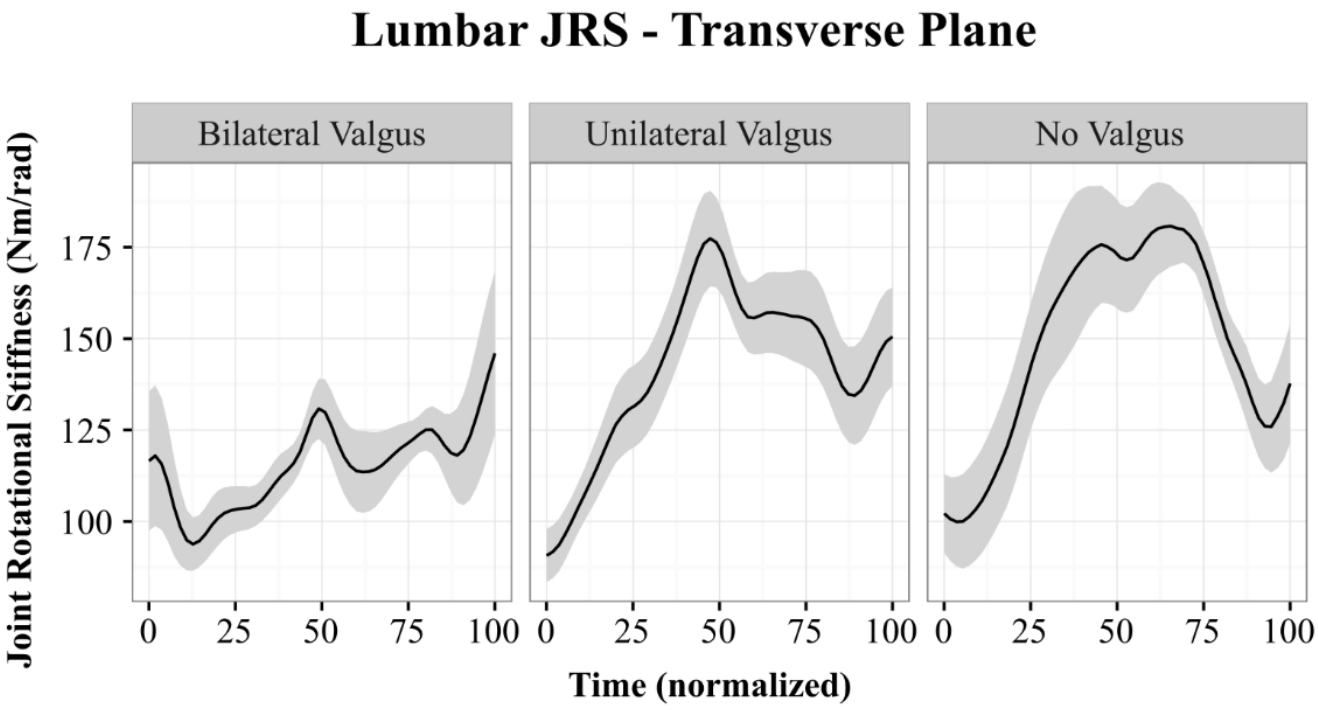
Lumbar JRS - Transverse Plane
Bilateral Valgus
Unilateral Valgus
No Valgus
Joint Rotational Stiffness (Nm/rad)
175
150
125
100
0
25
50
75
100
Time (normalized)

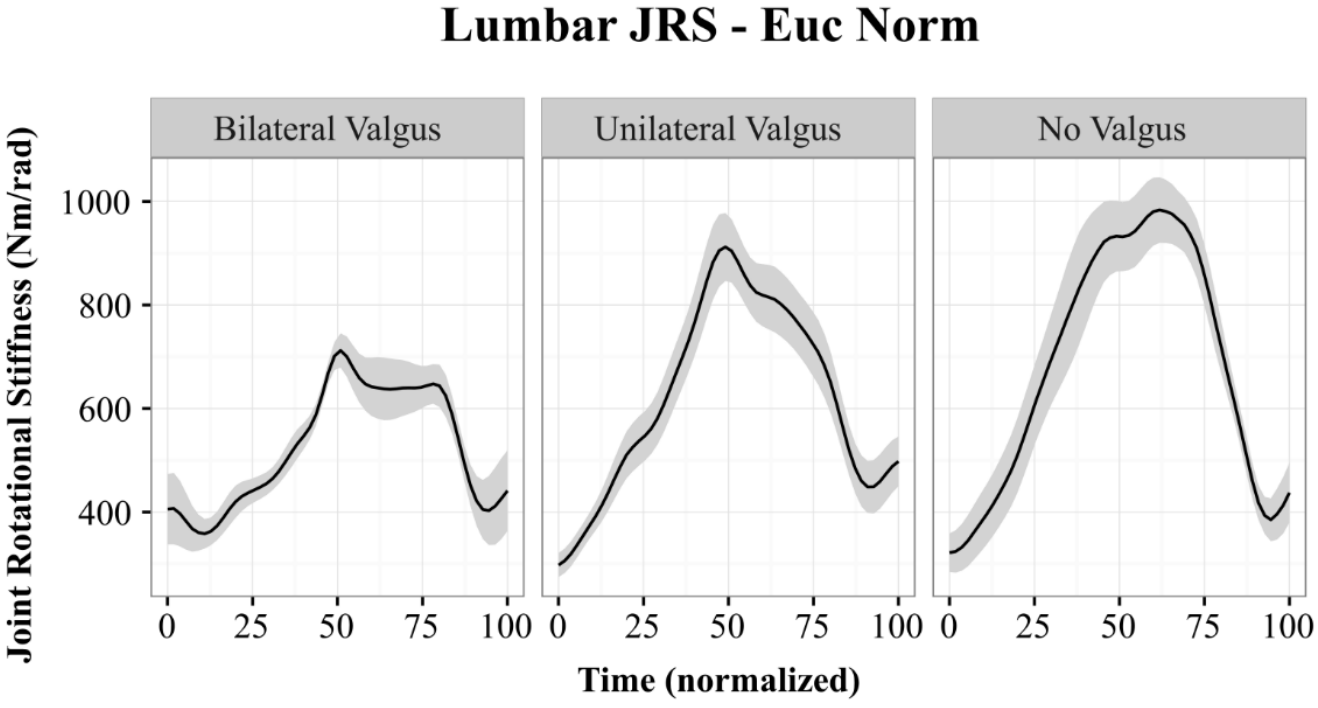
Lumbar JRS - Euc Norm
Bilateral Valgus
Unilateral Valgus
No Valgus
Joint Rotational Stiffness (Nm/rad)
1000
800
600
400
0
25
50
75
100
Time (normalized)

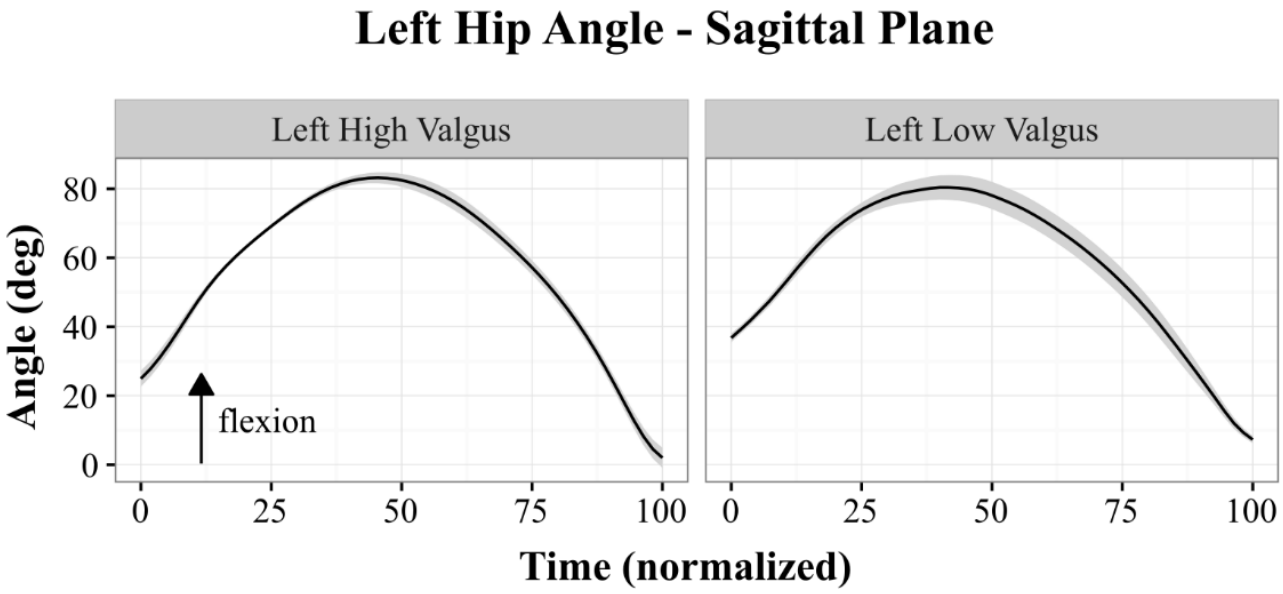
Left Hip Angle - Sagittal Plane
Left High Valgus
Left Low Valgus
Angle (deg)
80
60
40
20
0
flexion
0
25
50
75
100
Time (normalized)

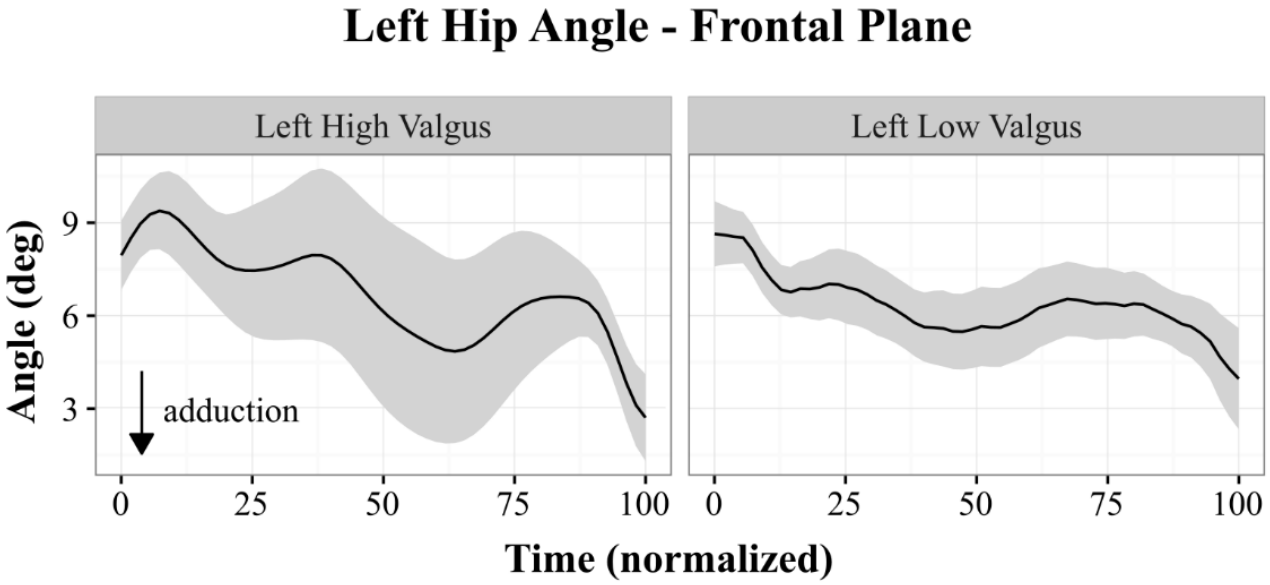
Left Hip Angle - Frontal Plane
Left High Valgus
Left Low Valgus
Angle (deg)
9
6
3
adduction
0
25
50
75
100
Time (normalized)

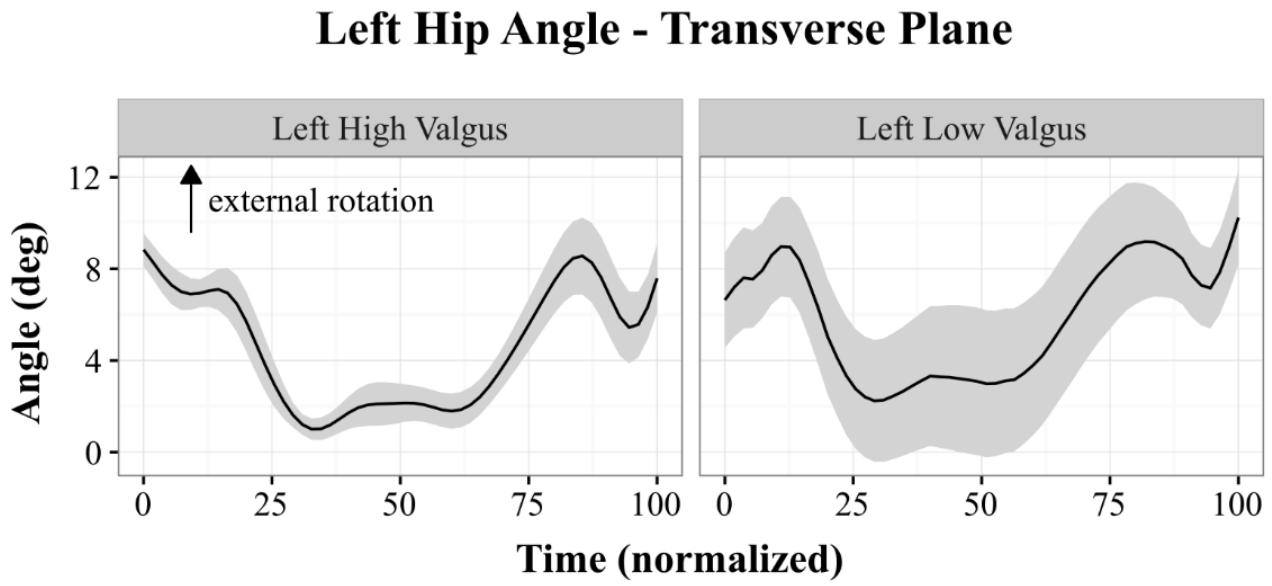
Left Hip Angle - Transverse Plane
Left High Valgus
Left Low Valgus
external rotation
Angle (deg)
12
8
4
0
0
25
50
75
100
Time (normalized)

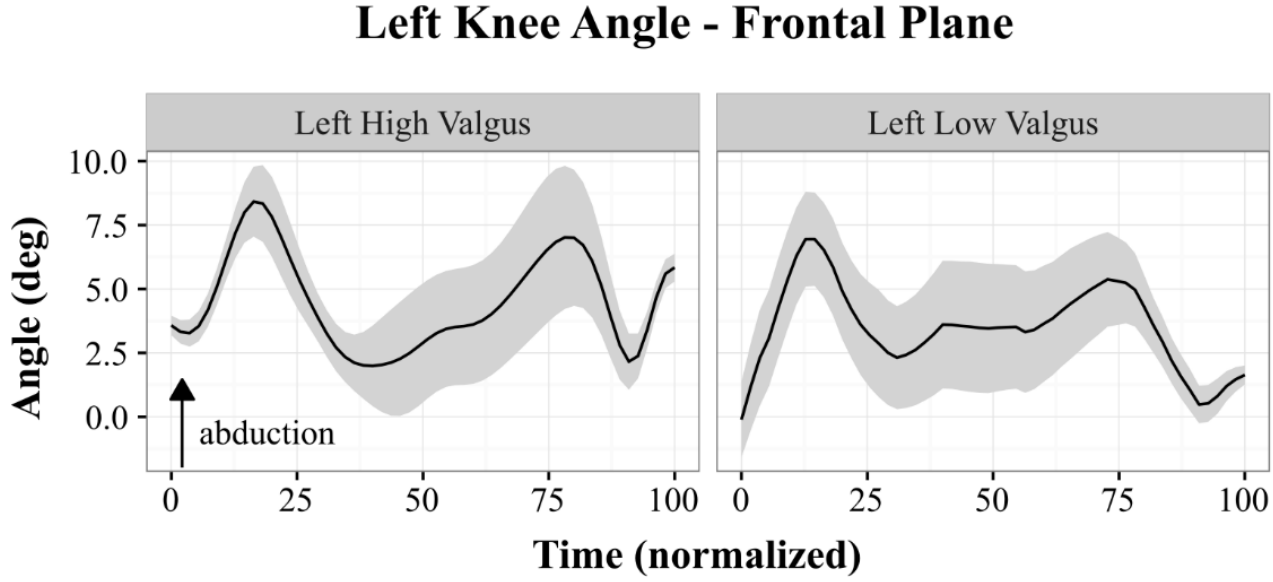
Left Knee Angle - Frontal Plane
Left High Valgus
Left Low Valgus
abduction
Angle (deg)
10.0
7.5
5.0
2.5
0.0
0
25
50
75
100
Time (normalized)

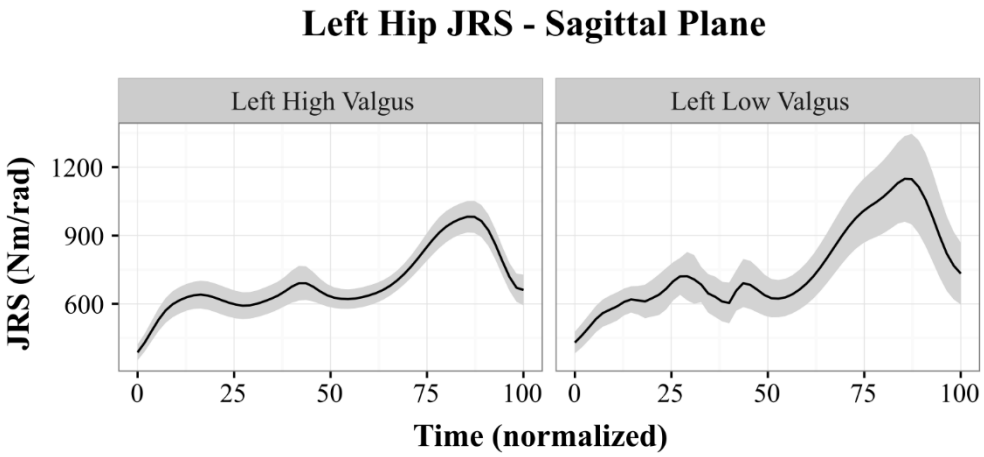
Left Hip JRS - Sagittal Plane
Left High Valgus
Left Low Valgus
JRS (Nm/rad)
1200
900
600
0
25
50
75
100
Time (normalized)

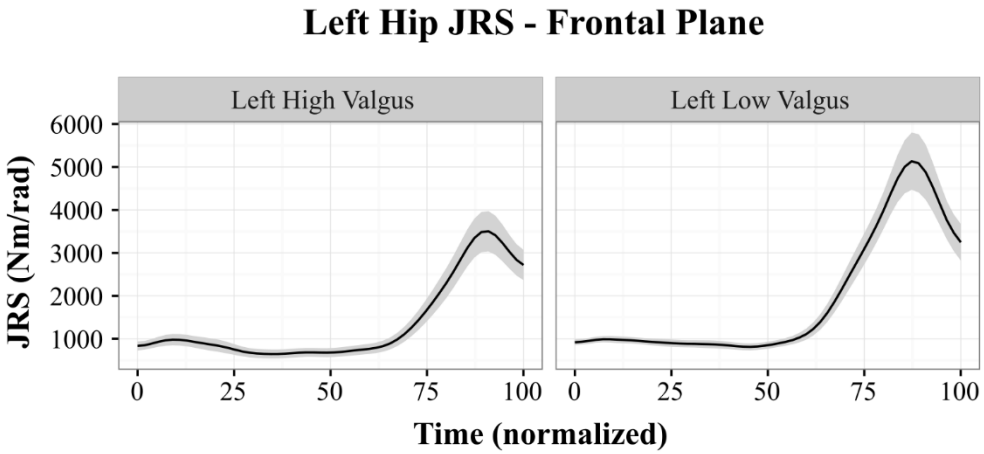
Left Hip JRS - Frontal Plane
Left High Valgus
Left Low Valgus
JRS (Nm/rad)
6000
5000
4000
3000
2000
1000
0
25
50
75
100
Time (normalized)

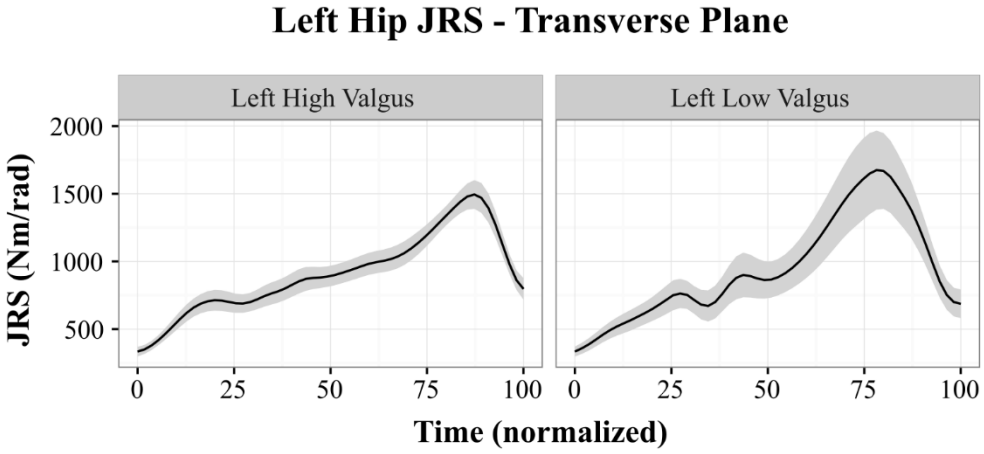
Left Hip JRS - Transverse Plane
Left High Valgus
Left Low Valgus
JRS (Nm/rad)
2000
1500
1000
500
0
25
50
75
100
Time (normalized)

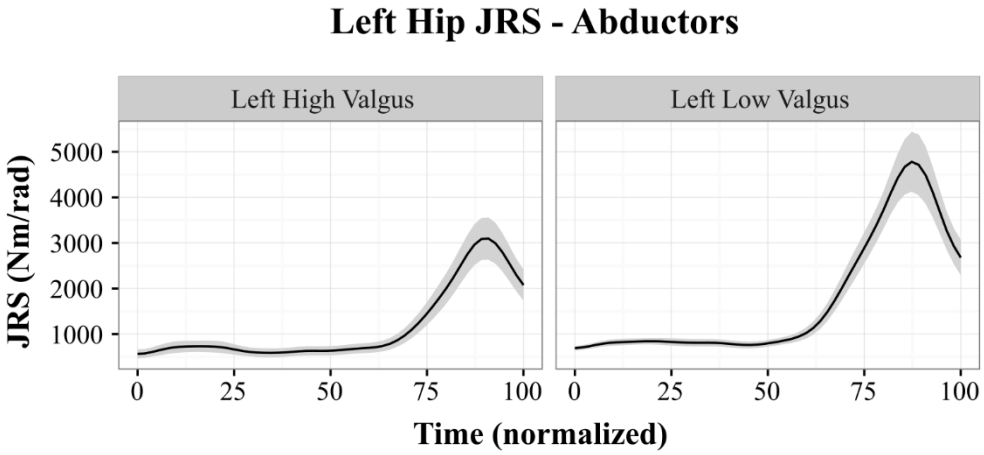
Left Hip JRS - Abductors
Left High Valgus
Left Low Valgus
JRS (Nm/rad)
5000
4000
3000
2000
1000
0
25
50
75
100
Time (normalized)

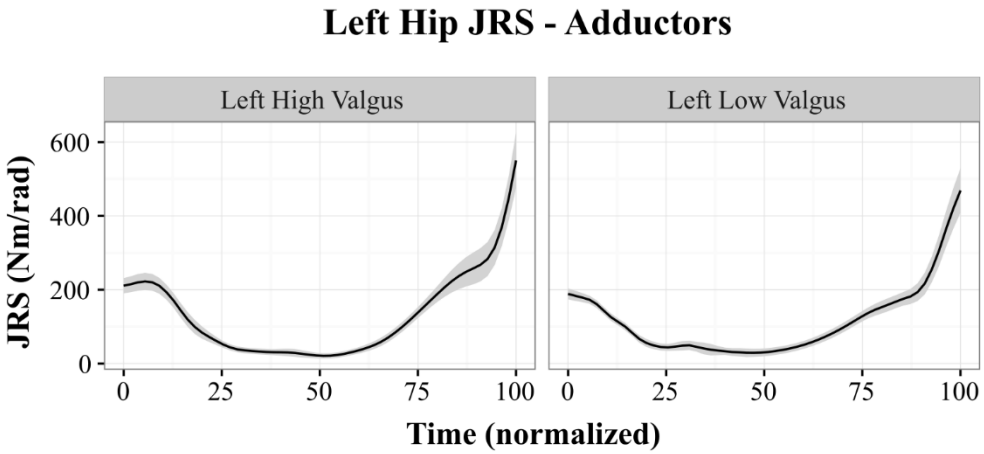
Left Hip JRS - Adductors
Left High Valgus
Left Low Valgus
JRS (Nm/rad)
600
400
200
0
25
50
75
100
Time (normalized)

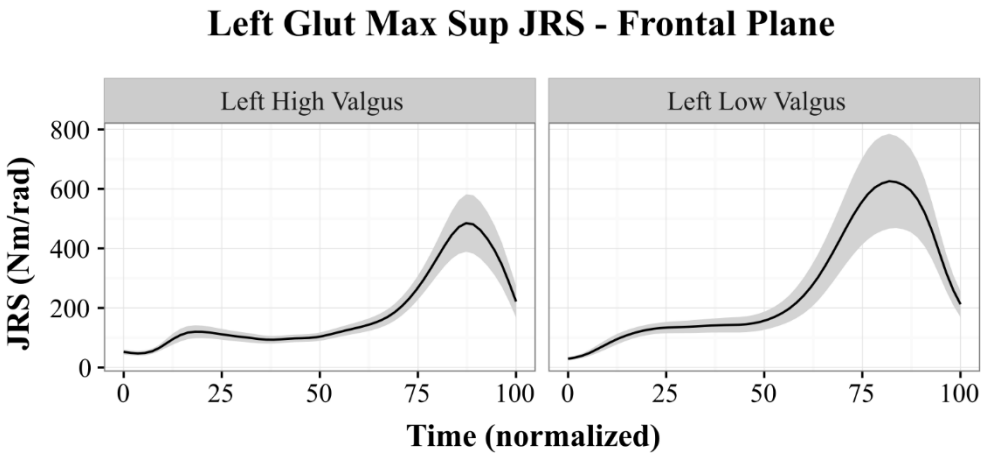
Left Glut Max Sup JRS - Frontal Plane
Left High Valgus
Left Low Valgus
JRS (Nm/rad)
800
600
400
200
0
0
25
50
75
100
Time (normalized)

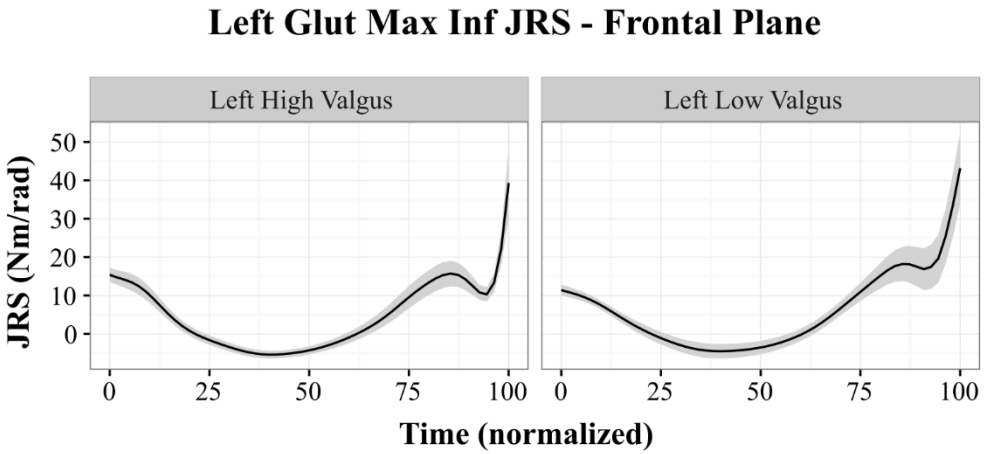
Left Glut Max Inf JRS - Frontal Plane
Left High Valgus
Left Low Valgus
JRS (Nm/rad)
50
40
30
20
10
0
0
25
50
75
100
Time (normalized)

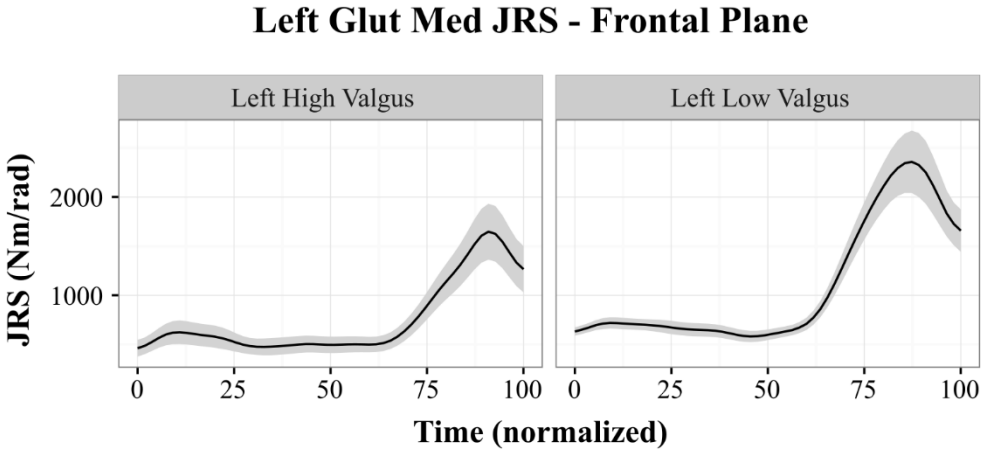
Left Glut Med JRS - Frontal Plane
Left High Valgus
Left Low Valgus
JRS (Nm/rad)
2000
1000
0
25
50
75
100
Time (normalized)

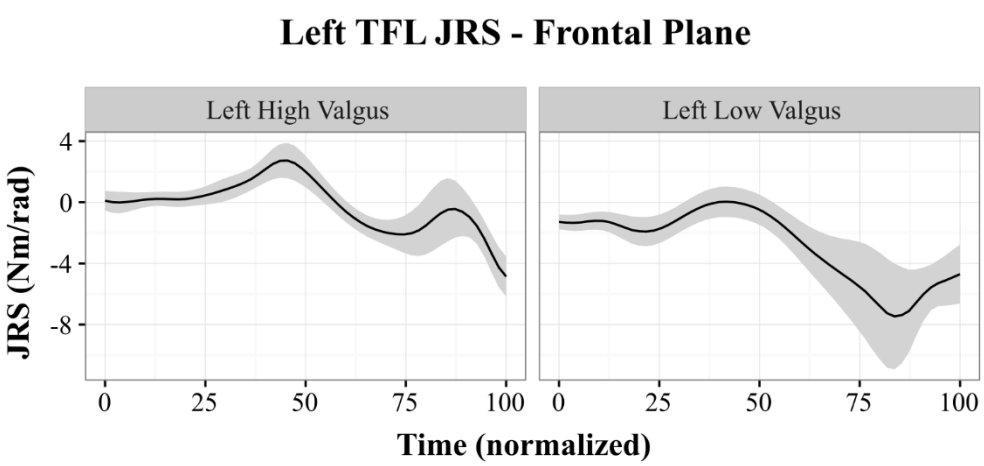
Left TFL JRS - Frontal Plane
Left High Valgus
Left Low Valgus
JRS (Nm/rad)
4
0
-4
-8
0
25
50
75
100
Time (normalized)

Left Glut Max Sup JRS - Transverse Plane

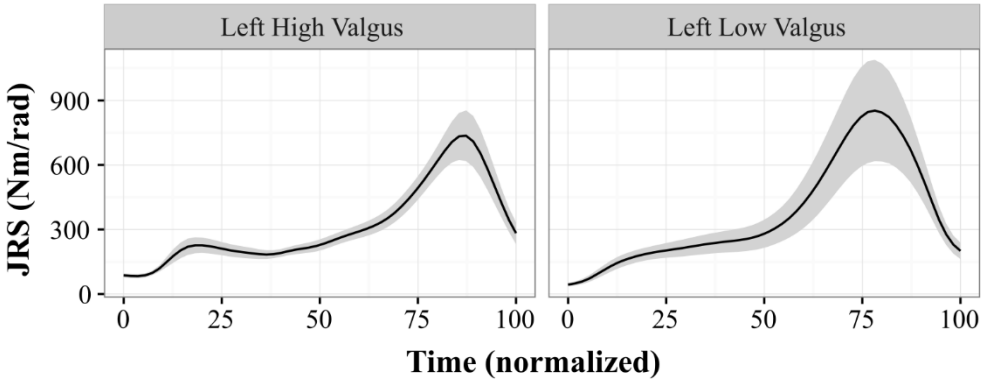

Left Glut Max Inf JRS - Transverse Plane

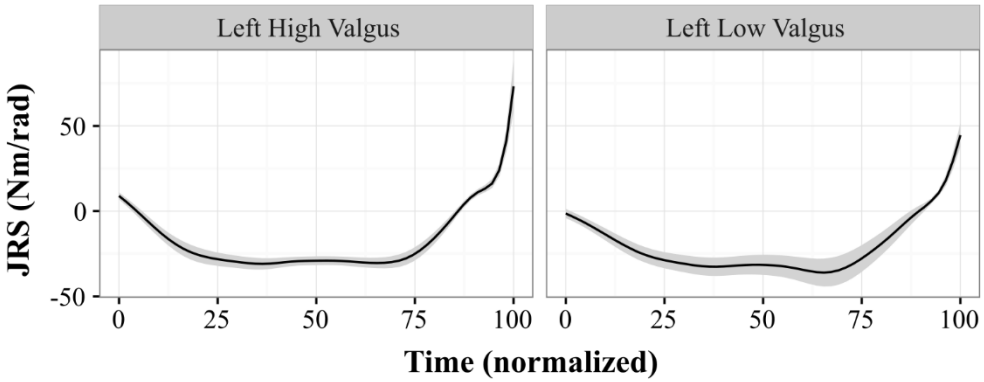

Left Glut Med JRS - Transverse Plane

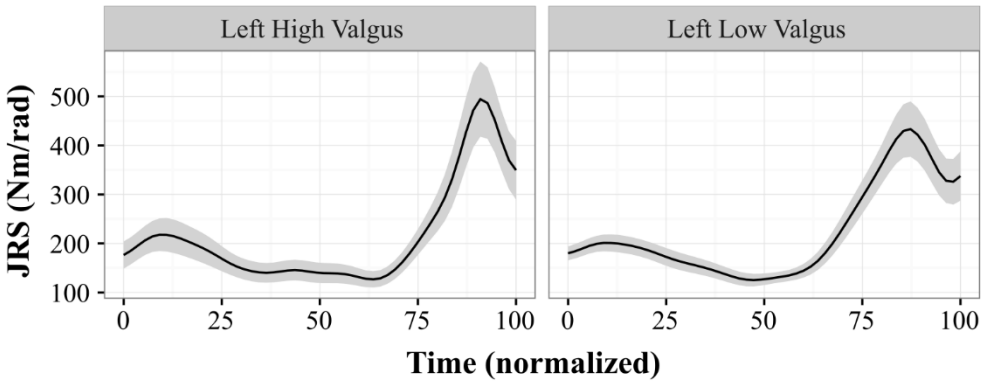

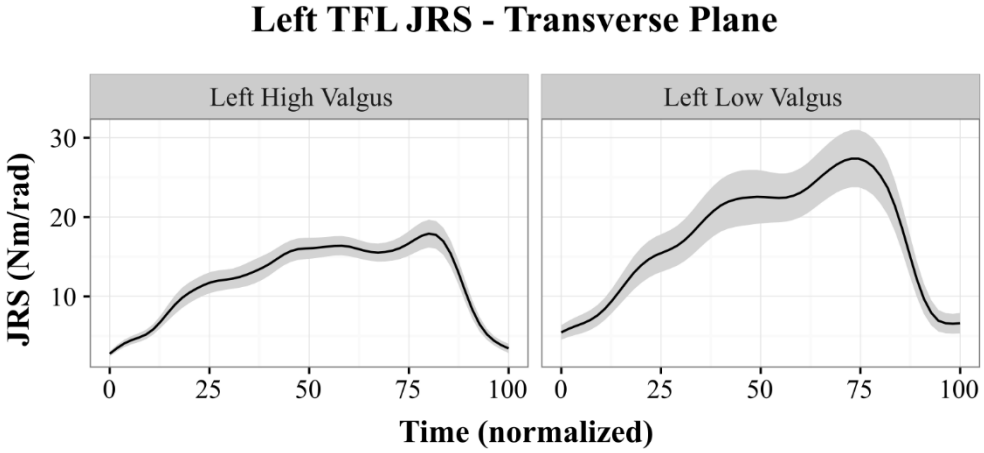
Left TFL JRS - Transverse Plane
Left High Valgus
Left Low Valgus
JRS (Nm/rad)
30
20
10
0
25
50
75
100
Time (normalized)

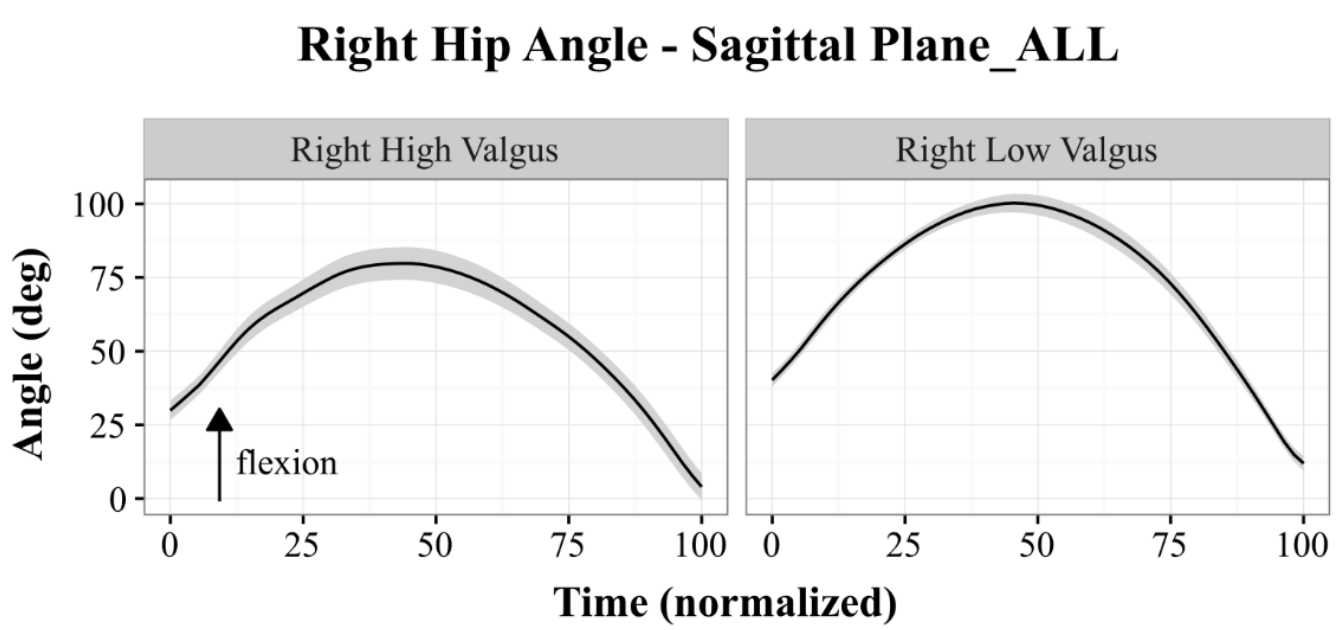
Right Hip Angle - Sagittal Plane_ALL
Right High Valgus
Right Low Valgus
Angle (deg)
100
75
50
25
0
flexion
0
25
50
75
100
Time (normalized)

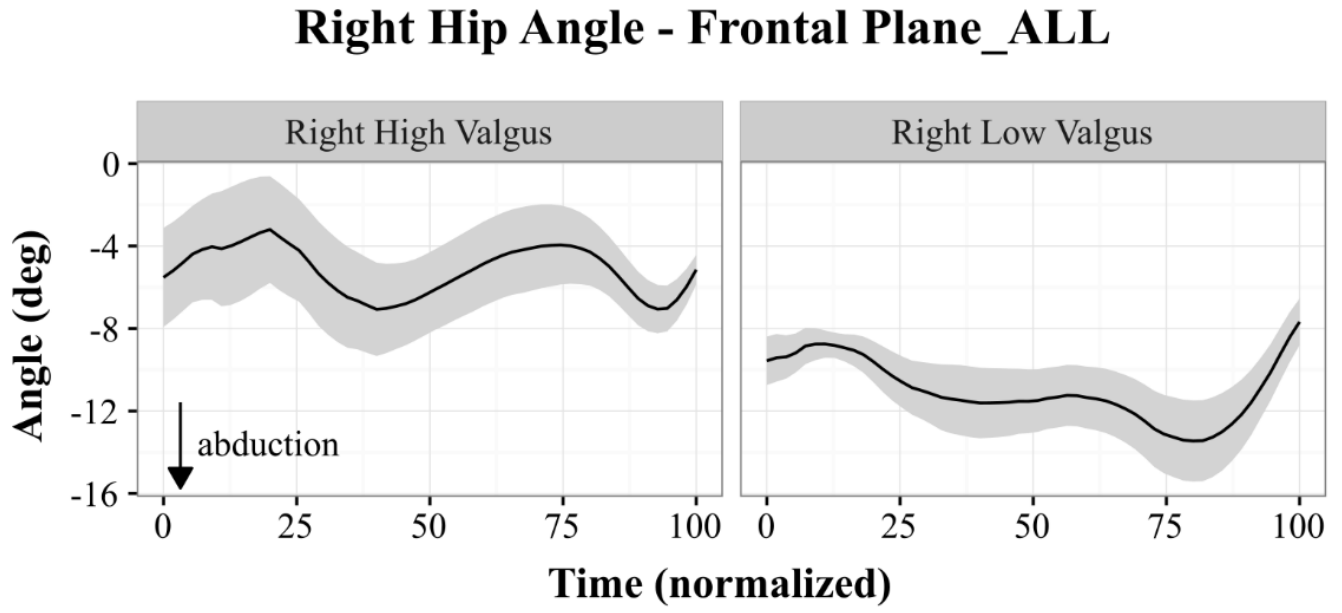
Right Hip Angle - Frontal Plane_ALL
Right High Valgus
Right Low Valgus
Angle (deg)
0
-4
-8
-12
-16
abduction
0
25
50
75
100
Time (normalized)

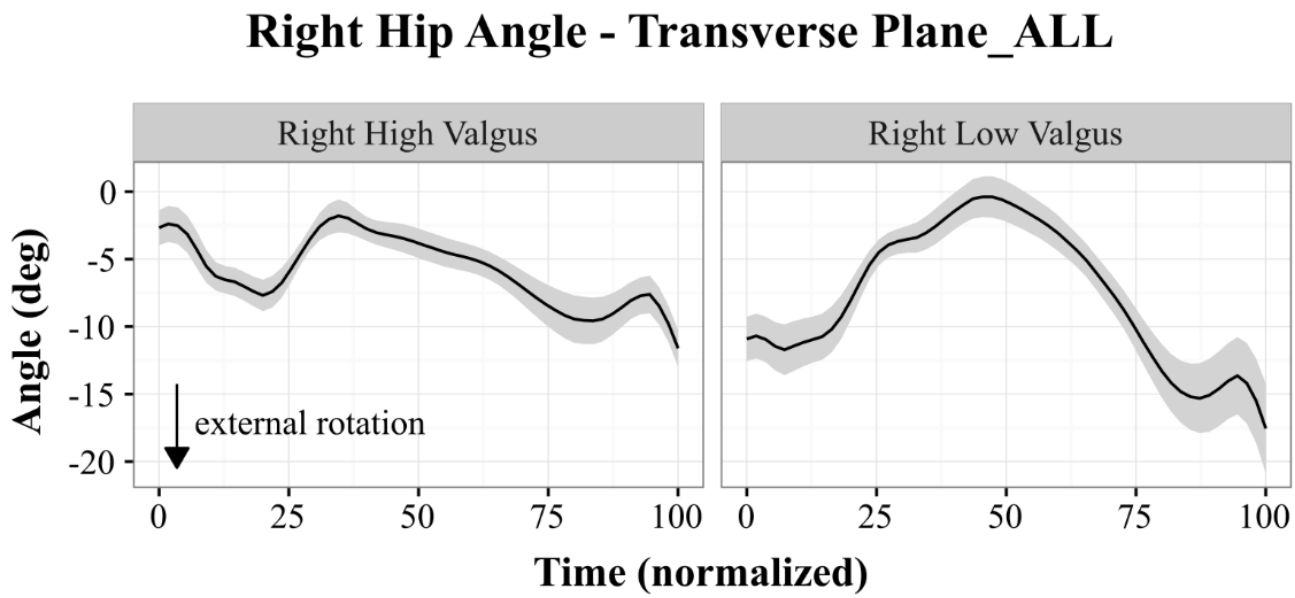
Right Hip Angle - Transverse Plane_ALL
Right High Valgus
Right Low Valgus
Angle (deg)
0
-5
-10
-15
-20
external rotation
0
25
50
75
100
Time (normalized)

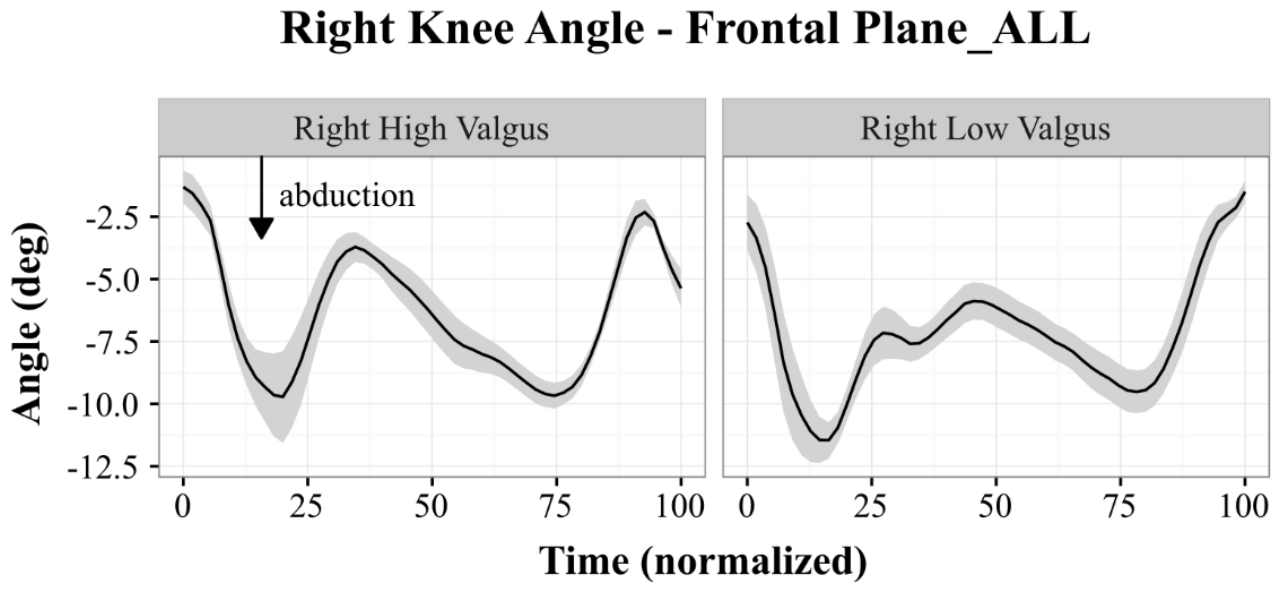
Right Knee Angle - Frontal Plane_ALL
Right High Valgus
Right Low Valgus
Angle (deg)
abduction
-2.5
-5.0
-7.5
-10.0
-12.5
0
25
50
75
100
Time (normalized)

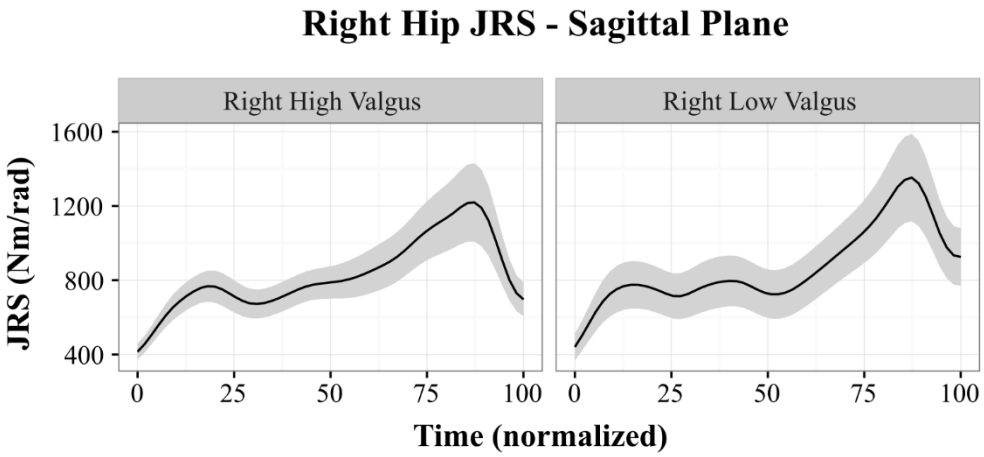
Right Hip JRS - Sagittal Plane
Right High Valgus
Right Low Valgus
JRS (Nm/rad)
1600
1200
800
400
0
25
50
75
100
Time (normalized)

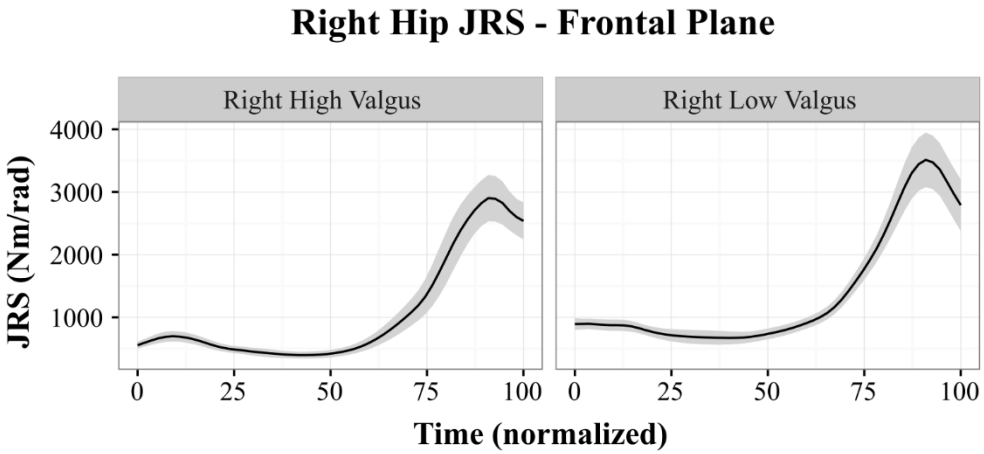
Right Hip JRS - Frontal Plane
Right High Valgus
Right Low Valgus
JRS (Nm/rad)
4000
3000
2000
1000
0
25
50
75
100
Time (normalized)

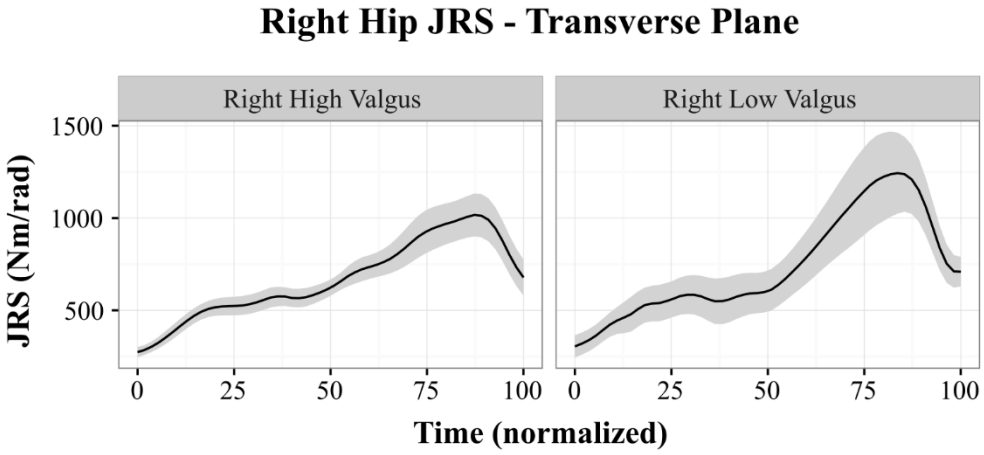
Right Hip JRS - Transverse Plane
Right High Valgus
Right Low Valgus
JRS (Nm/rad)
1500
1000
500
0
25
50
75
100
Time (normalized)

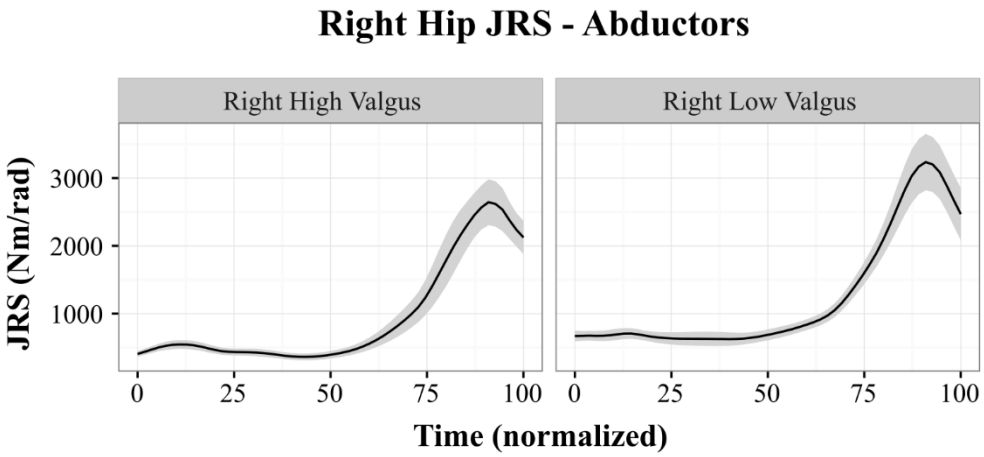
Right Hip JRS - Abductors
Right High Valgus
Right Low Valgus
JRS (Nm/rad)
3000
2000
1000
0
25
50
75
100
Time (normalized)

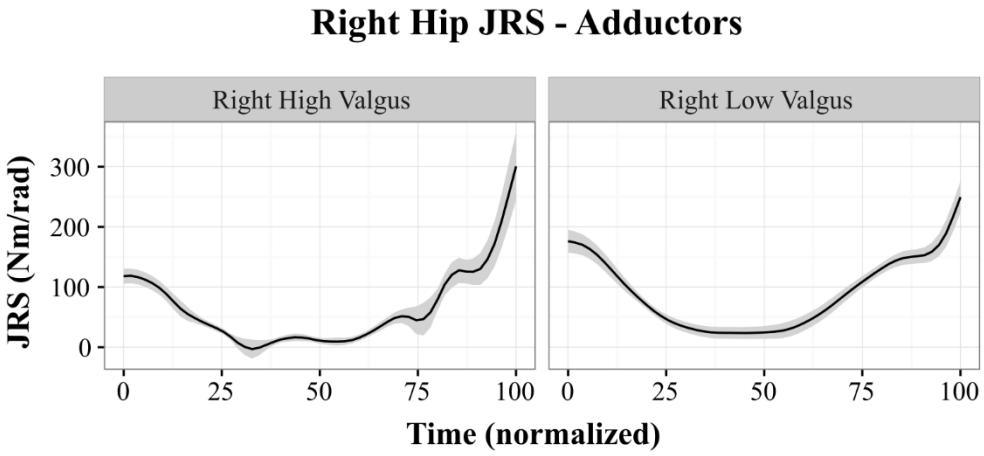
Right Hip JRS - Adductors
Right High Valgus
Right Low Valgus
JRS (Nm/rad)
300
200
100
0
25
50
75
100
Time (normalized)

Right Glut Max Sup JRS - Frontal Plane

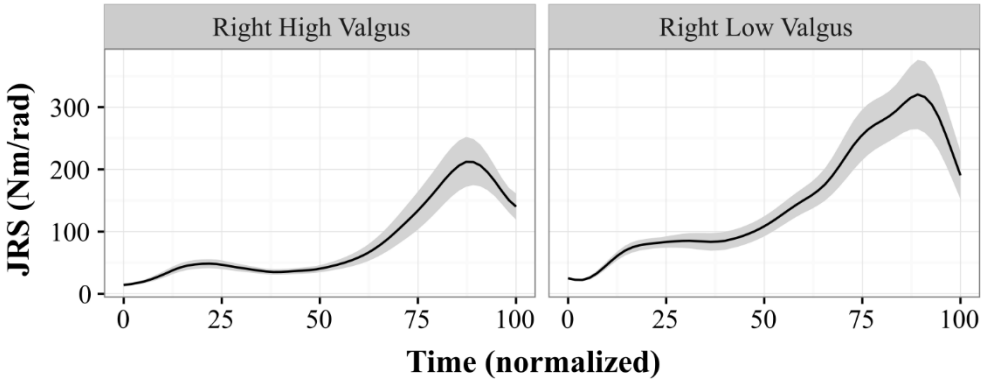

Right Glut Max Inf JRS - Frontal Plane

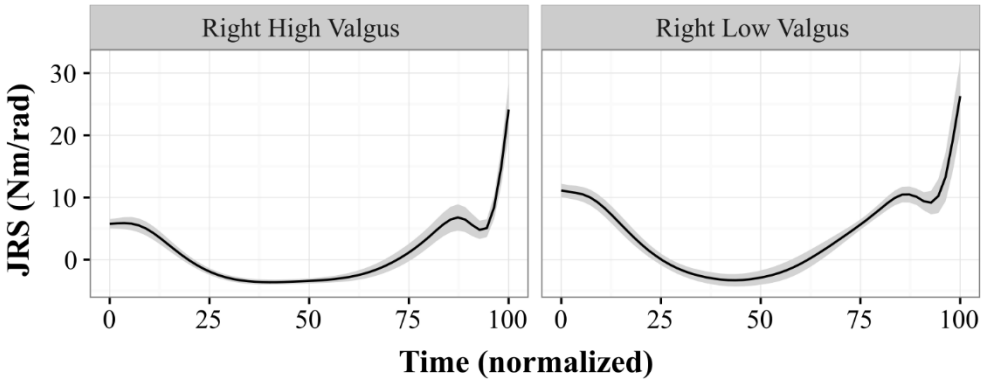

Right Glut Med JRS - Frontal Plane

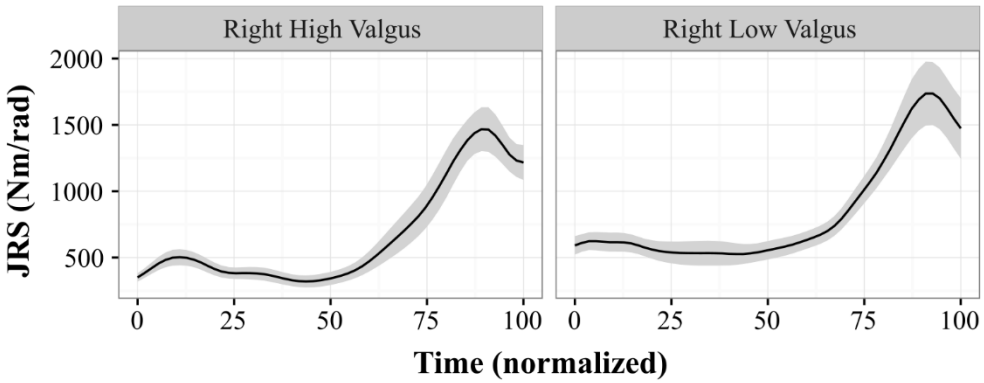

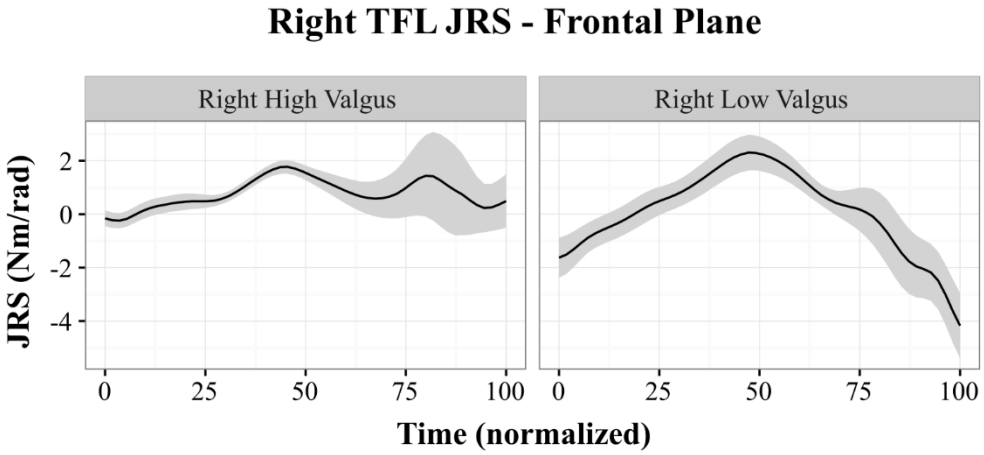
Right TFL JRS - Frontal Plane
Right High Valgus
Right Low Valgus
JRS (Nm/rad)
2
0
-2
-4
0
25
50
75
100
Time (normalized)

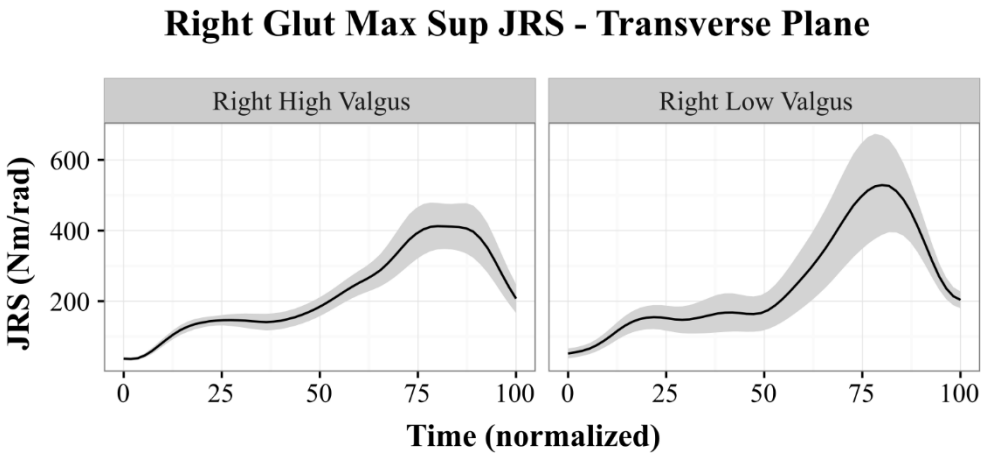
Right Glut Max Sup JRS - Transverse Plane
Right High Valgus
Right Low Valgus
JRS (Nm/rad)
600
400
200
0
25
50
75
100
Time (normalized)

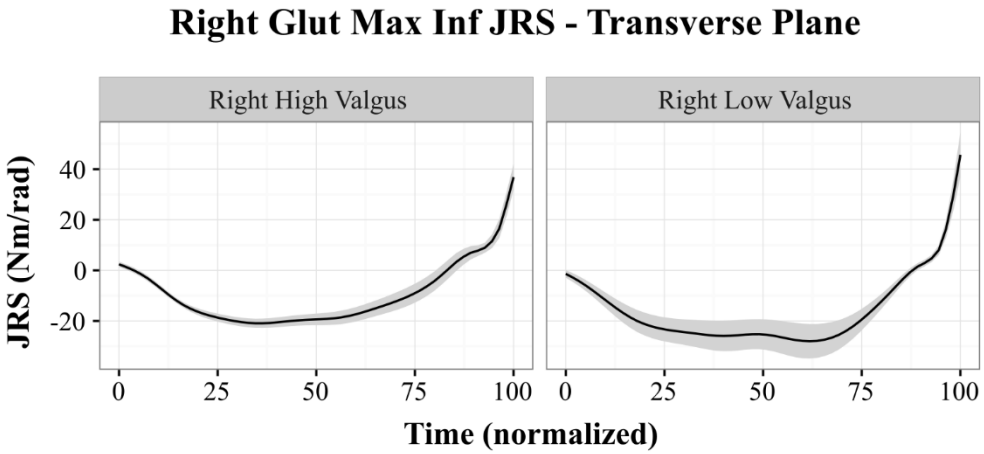
Right Glut Max Inf JRS - Transverse Plane
Right High Valgus
Right Low Valgus
JRS (Nm/rad)
40
20
0
-20
0
25
50
75
100
Time (normalized)

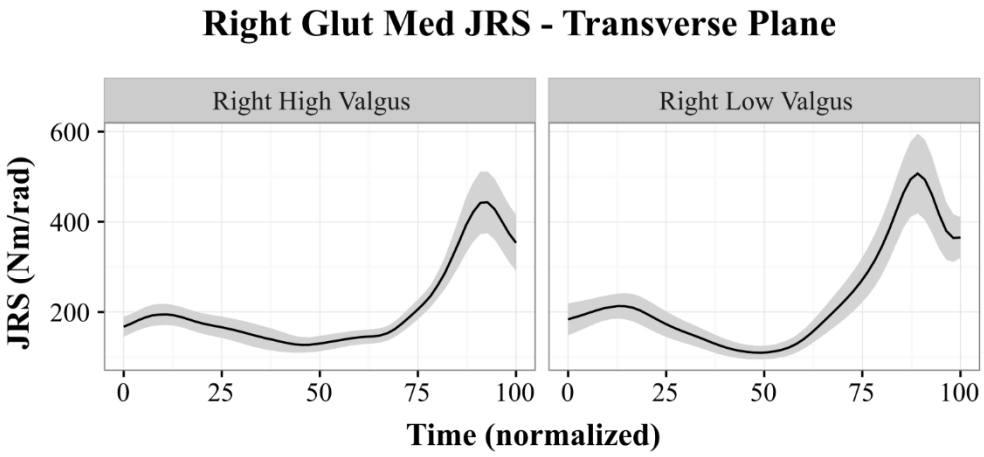
Right Glut Med JRS - Transverse Plane
Right High Valgus
Right Low Valgus
JRS (Nm/rad)
600
400
200
0
25
50
75
100
Time (normalized)

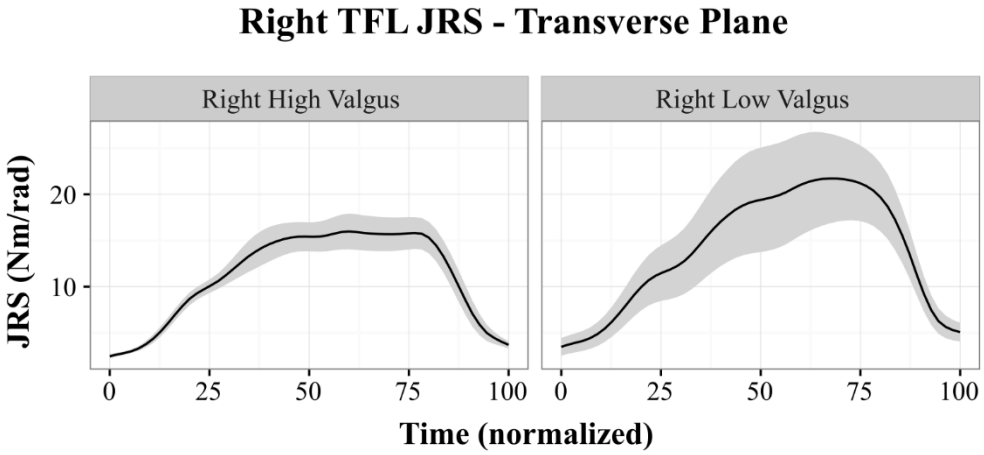
Right TFL JRS - Transverse Plane
Right High Valgus
Right Low Valgus
JRS (Nm/rad)
20
10
0
25
50
75
100
Time (normalized)

Stop Jump: Initial Contact to Toe Off

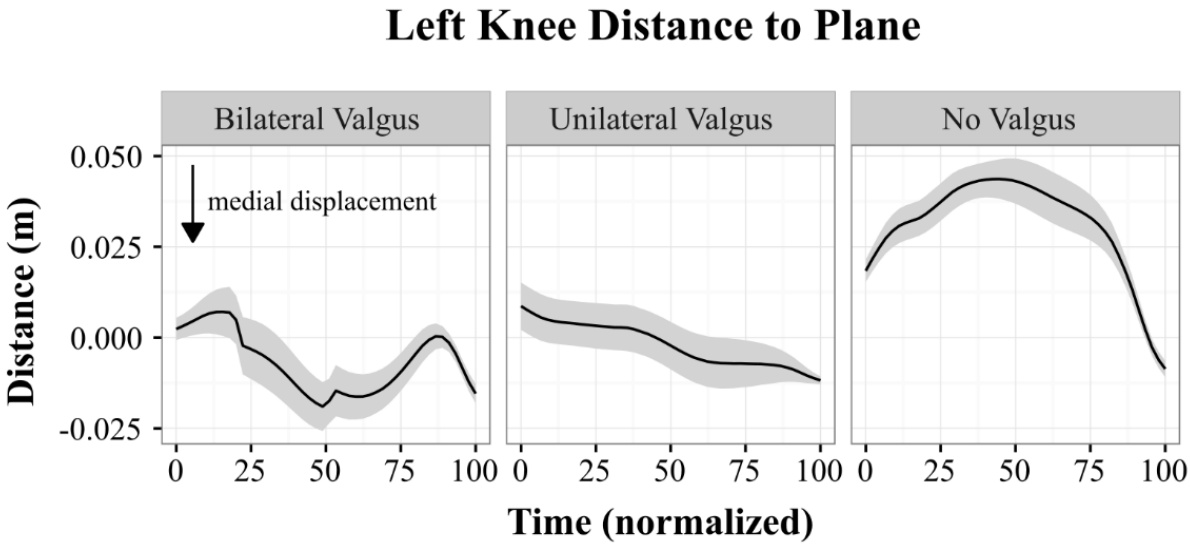

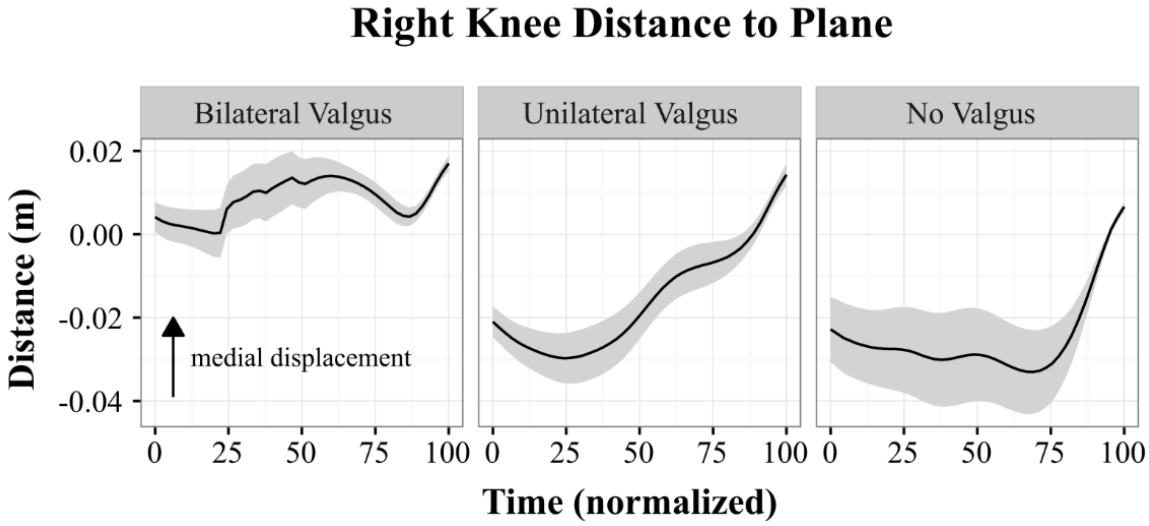

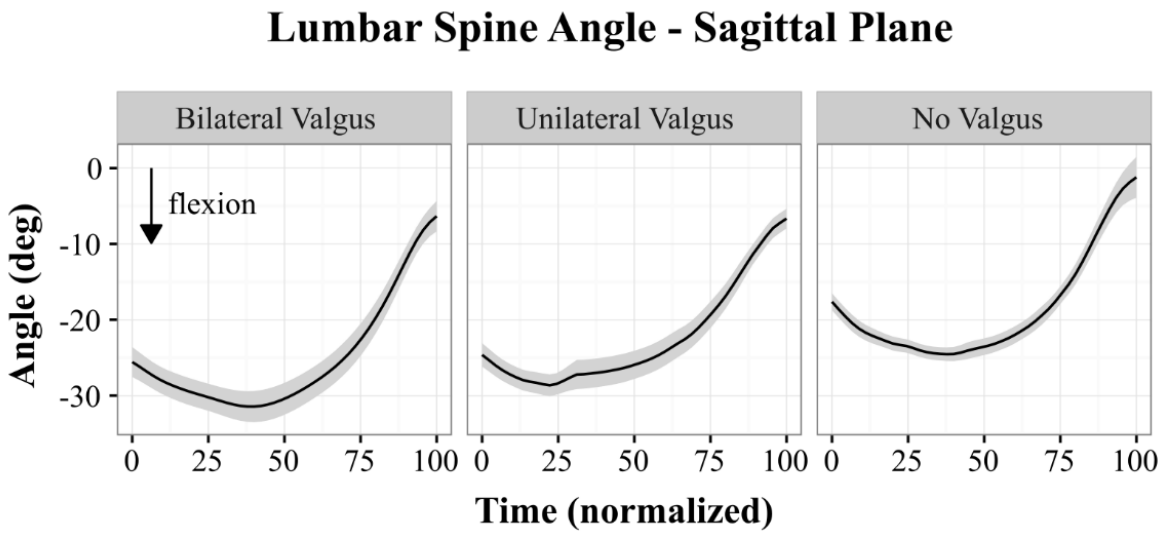
Lumbar Spine Angle - Sagittal Plane
Bilateral Valgus
Unilateral Valgus
No Valgus
flexion
Angle (deg)
0
-10
-20
-30
0
25
50
75
100
Time (normalized)

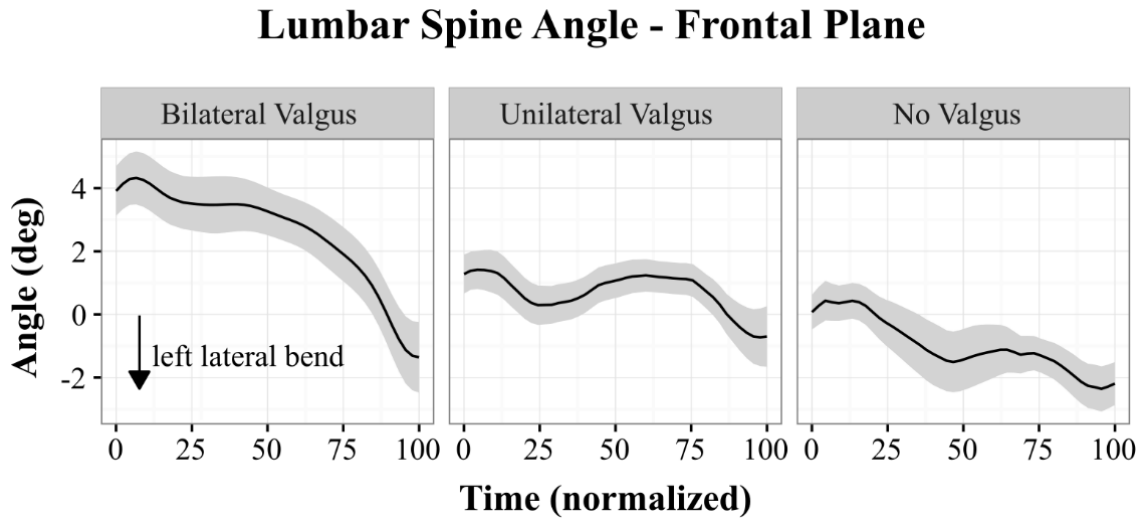
Lumbar Spine Angle - Frontal Plane
Bilateral Valgus
Unilateral Valgus
No Valgus
left lateral bend
Angle (deg)
4
2
0
-2
0
25
50
75
100
Time (normalized)

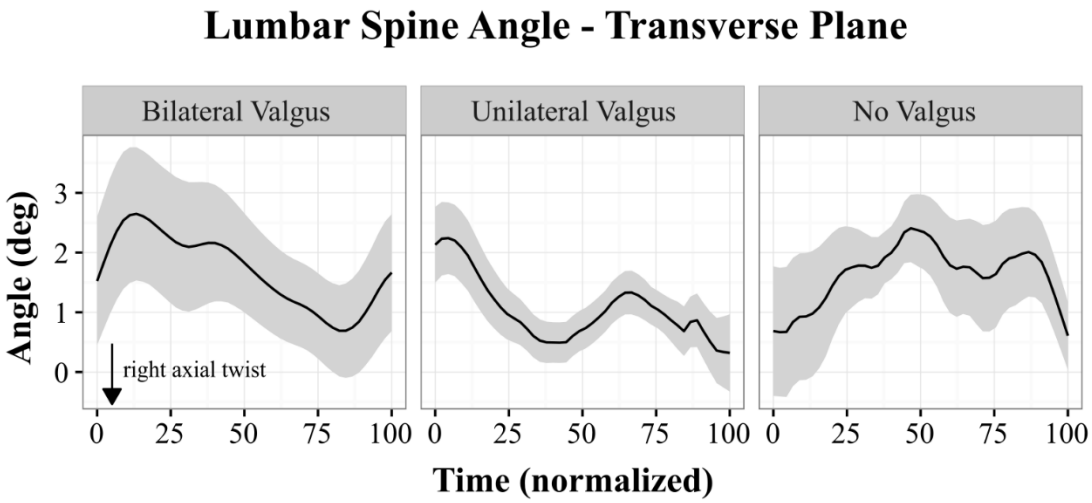
Lumbar Spine Angle - Transverse Plane
Bilateral Valgus
Unilateral Valgus
No Valgus
Angle (deg)
3
2
1
0
right axial twist
0
25
50
75
100
Time (normalized)

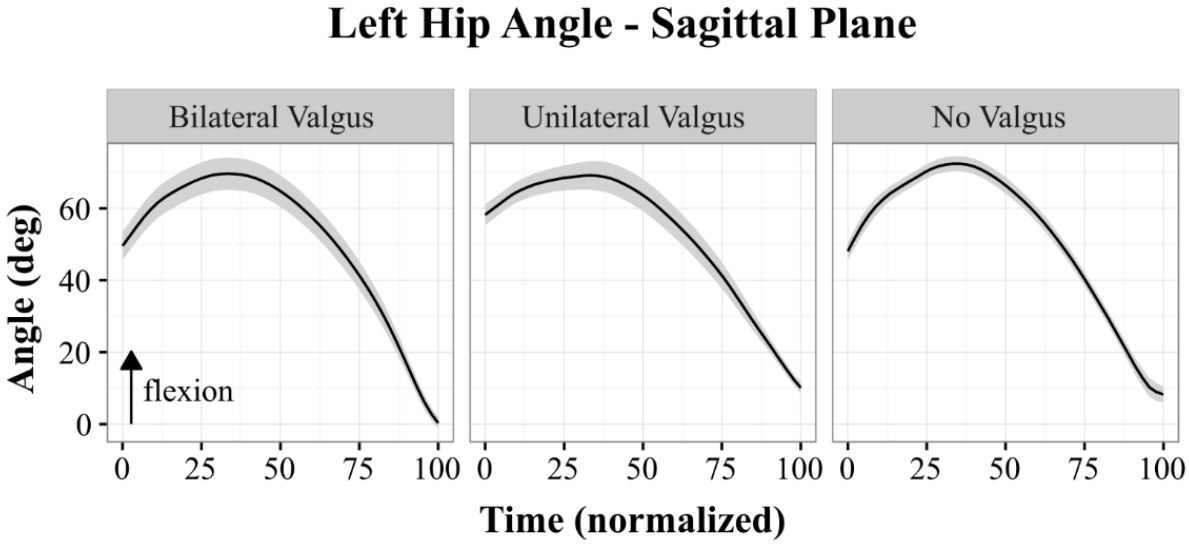
Left Hip Angle - Sagittal Plane
Bilateral Valgus
Unilateral Valgus
No Valgus
Angle (deg)
60
40
20
0
flexion
0
25
50
75
100
Time (normalized)

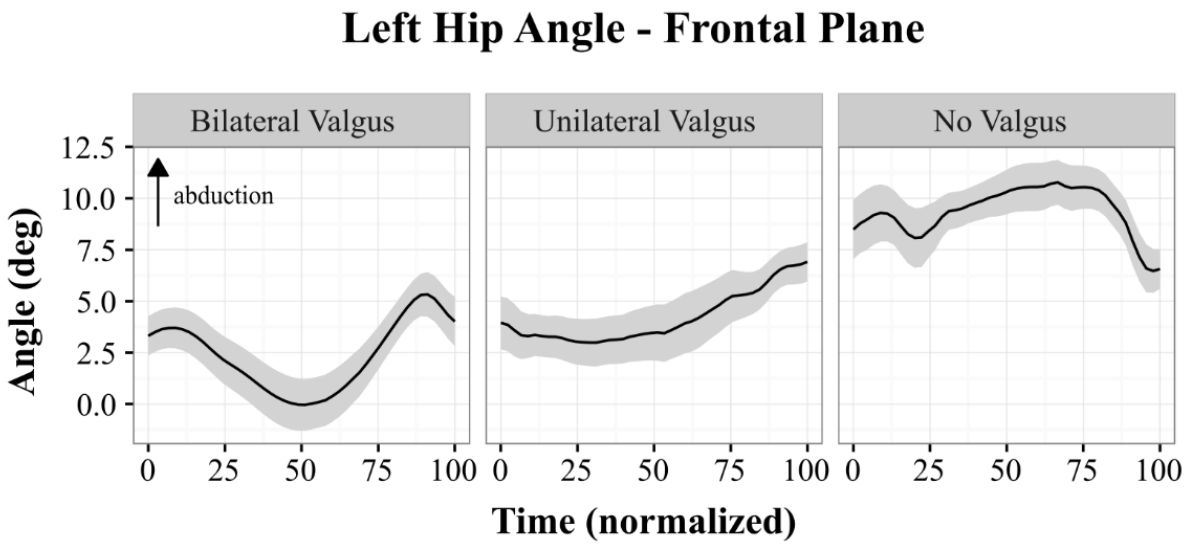
Left Hip Angle - Frontal Plane
Bilateral Valgus
Unilateral Valgus
No Valgus
abduction
Angle (deg)
12.5
10.0
7.5
5.0
2.5
0.0
0
25
50
75
100
Time (normalized)

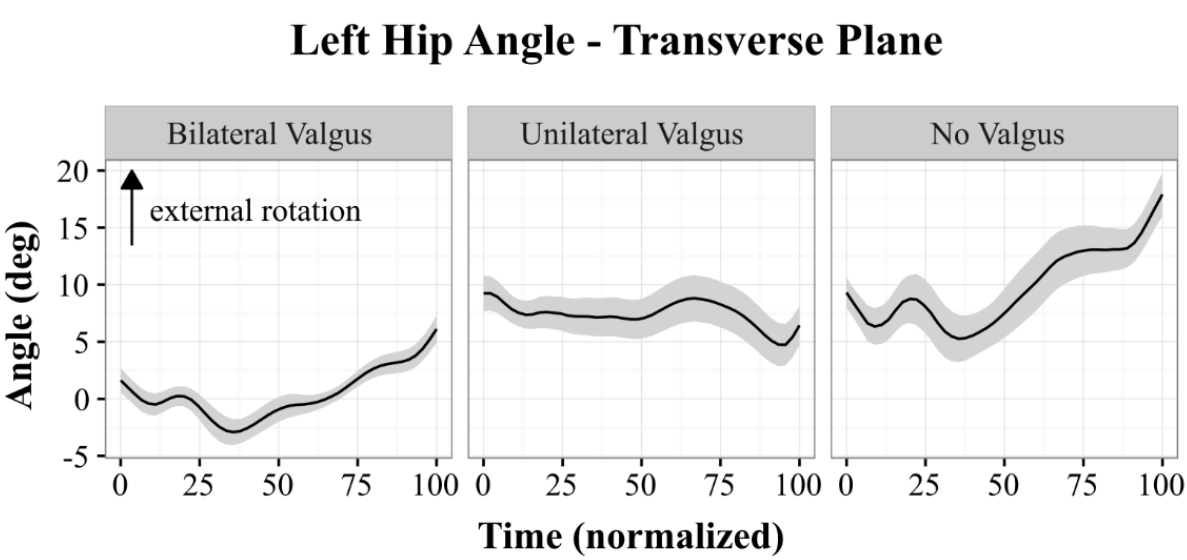
Left Hip Angle - Transverse Plane
Bilateral Valgus
Unilateral Valgus
No Valgus
external rotation
Angle (deg)
20
15
10
5
0
-5
0
25
50
75
100
Time (normalized)

Right Hip Angle - Sagittal Plane

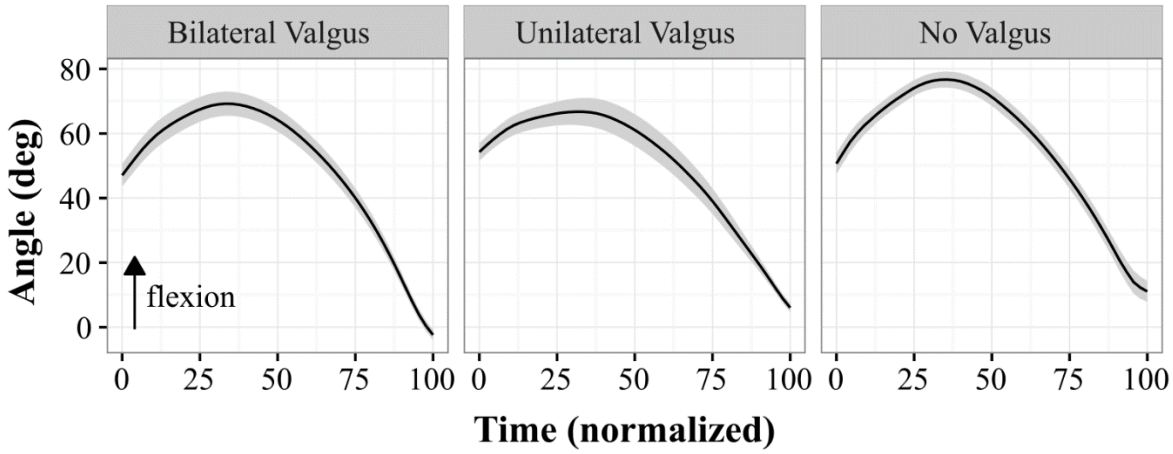

Right Hip Angle - Frontal Plane

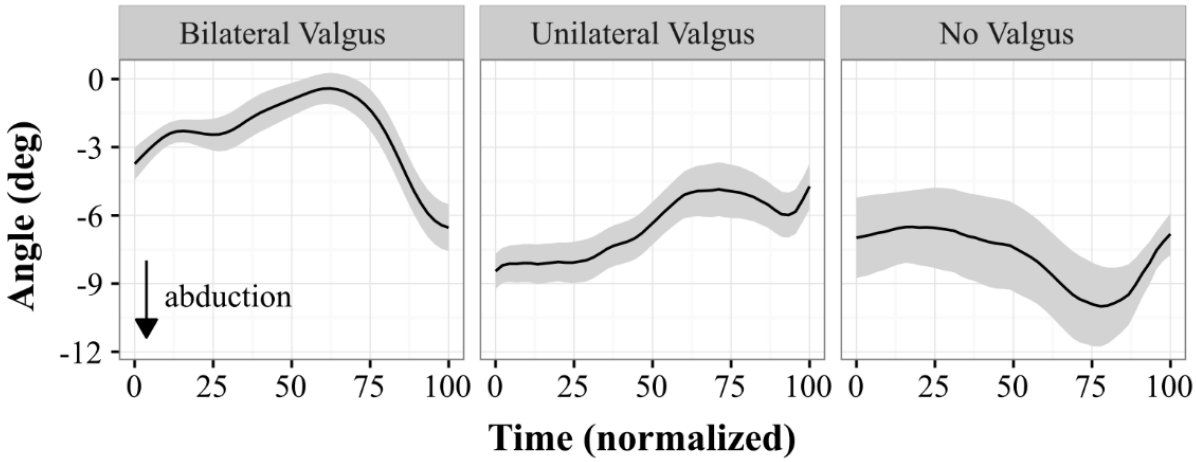

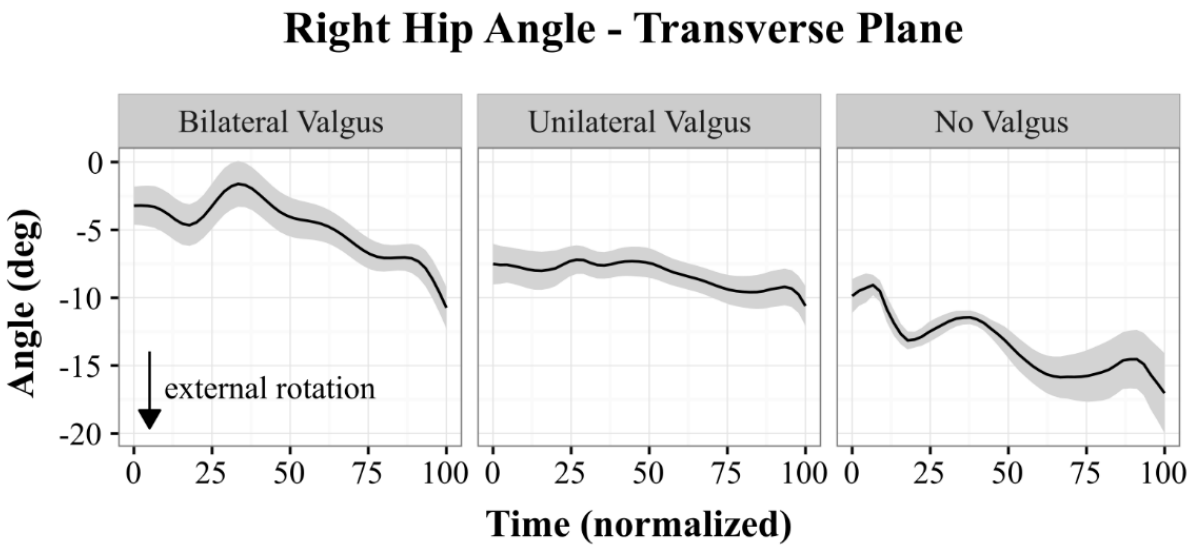
Right Hip Angle - Transverse Plane
Bilateral Valgus
Unilateral Valgus
No Valgus
Angle (deg)
0
-5
-10
-15
-20
external rotation
0
25
50
75
100
Time (normalized)

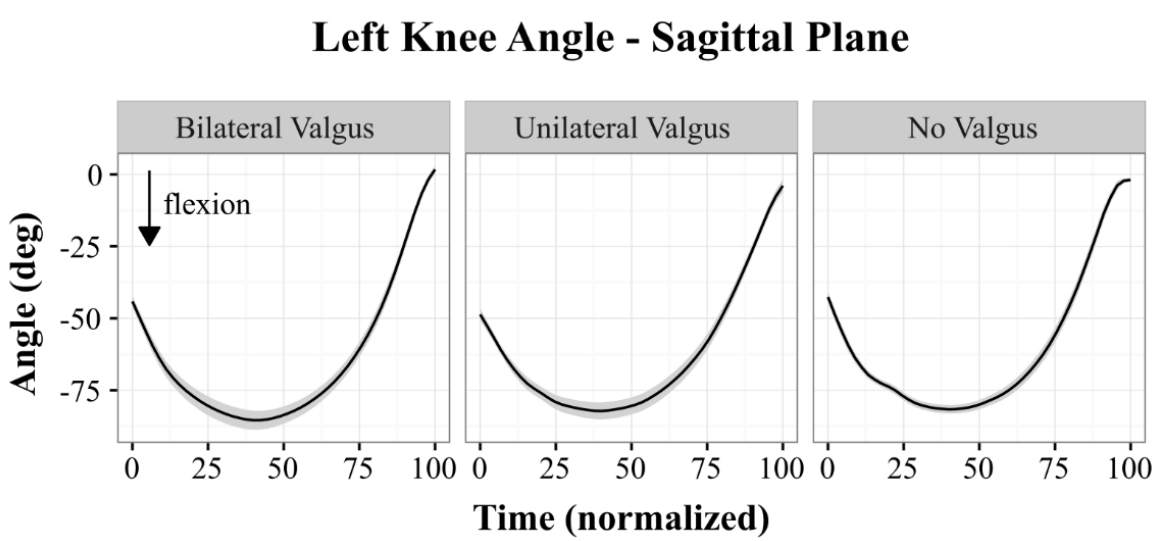
Left Knee Angle - Sagittal Plane
Bilateral Valgus
Unilateral Valgus
No Valgus
Angle (deg)
0
-25
-50
-75
flexion
0
25
50
75
100
Time (normalized)

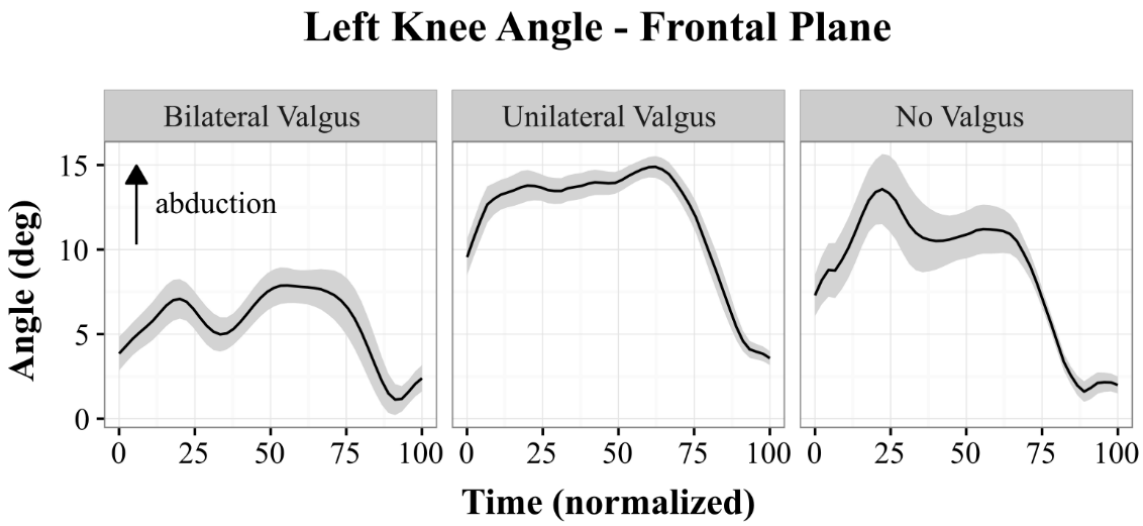
Left Knee Angle - Frontal Plane
Bilateral Valgus
Unilateral Valgus
No Valgus
abduction
Angle (deg)
15
10
5
0
0
25
50
75
100
Time (normalized)

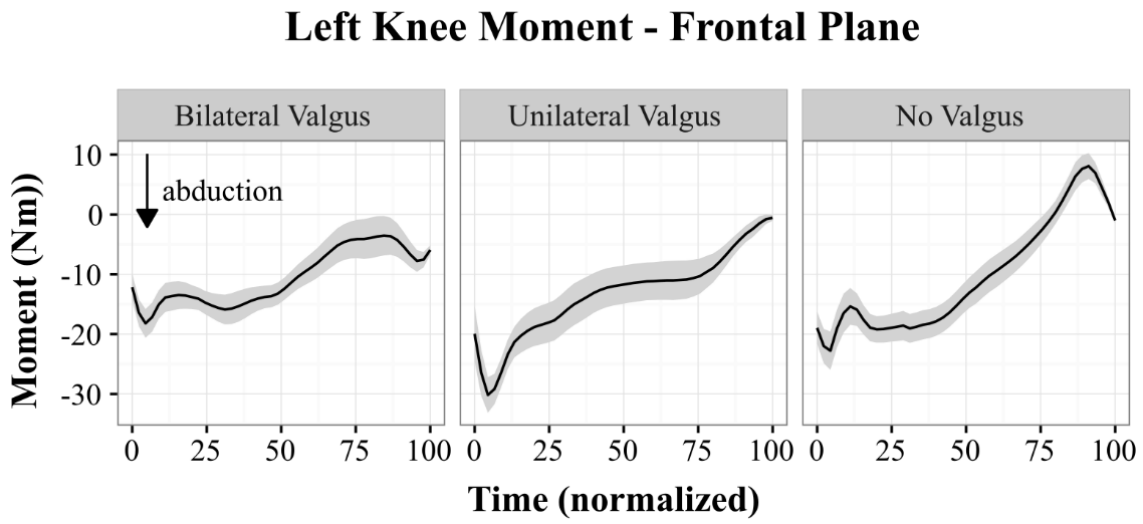
Left Knee Moment - Frontal Plane
Bilateral Valgus
Unilateral Valgus
No Valgus
abduction
Moment (Nm))
10
0
-10
-20
-30
0
25
50
75
100
Time (normalized)

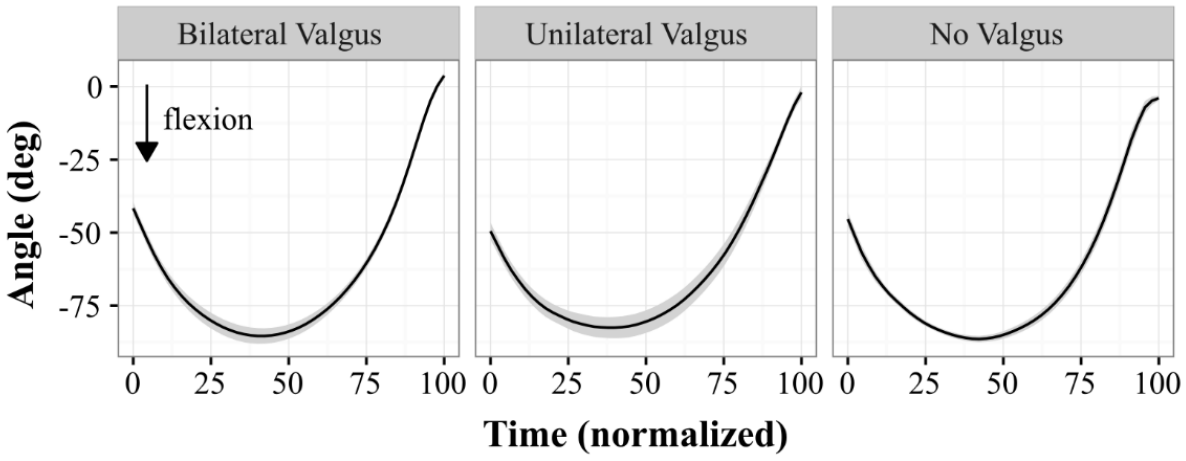
Right Knee Angle - Sagittal Plane
Bilateral Valgus
Unilateral Valgus
No Valgus
Angle (deg)
0
-25
-50
-75
flexion
0
25
50
75
100
Time (normalized)

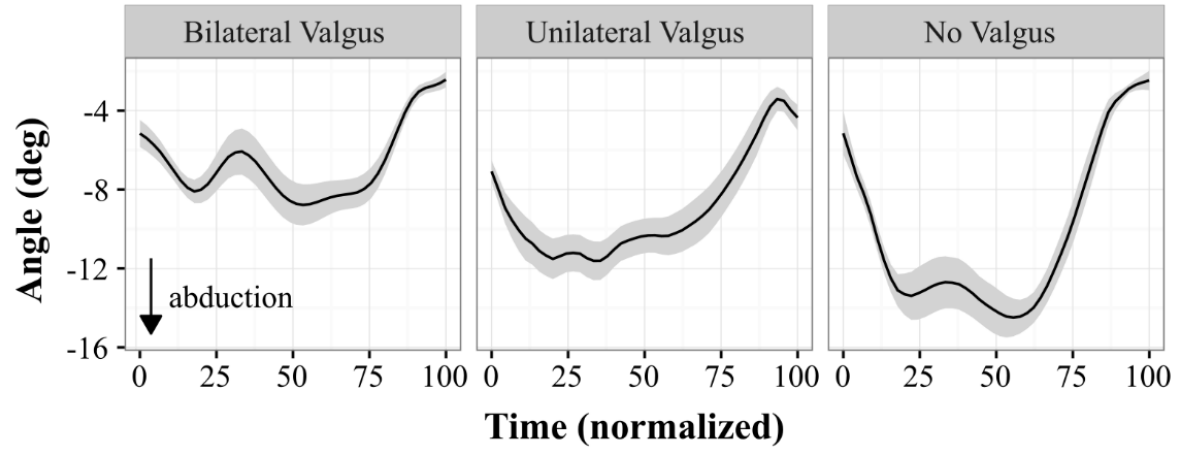
Right Knee Angle - Frontal Plane
Bilateral Valgus
Unilateral Valgus
No Valgus
Angle (deg)
-4
-8
-12
-16
abduction
0
25
50
75
100
Time (normalized)

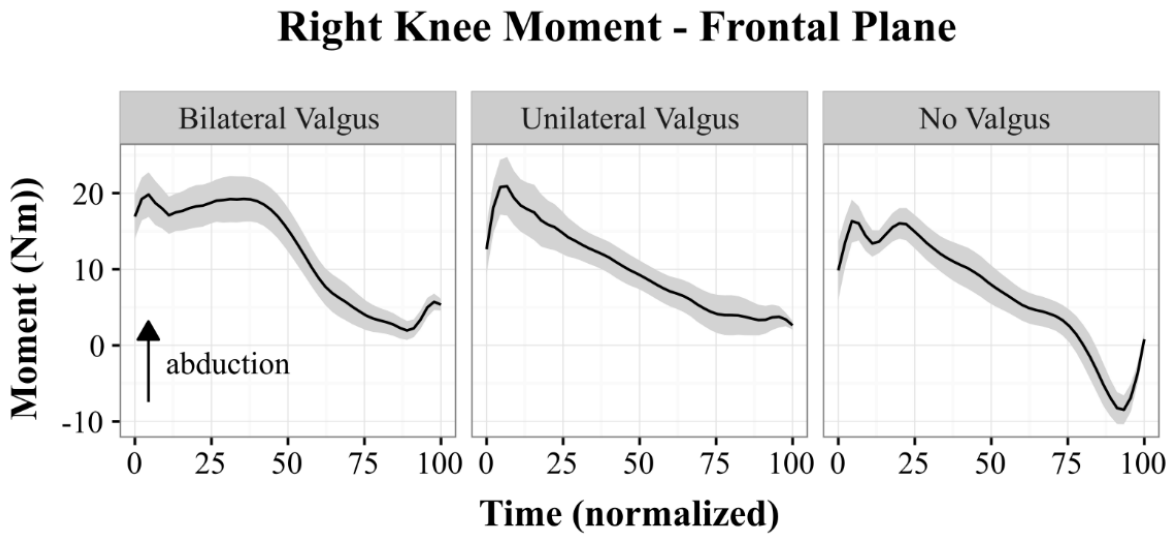
Right Knee Moment - Frontal Plane
Bilateral Valgus
Unilateral Valgus
No Valgus
Moment (Nm))
20
10
0
-10
abduction
0
25
50
75
100
Time (normalized)

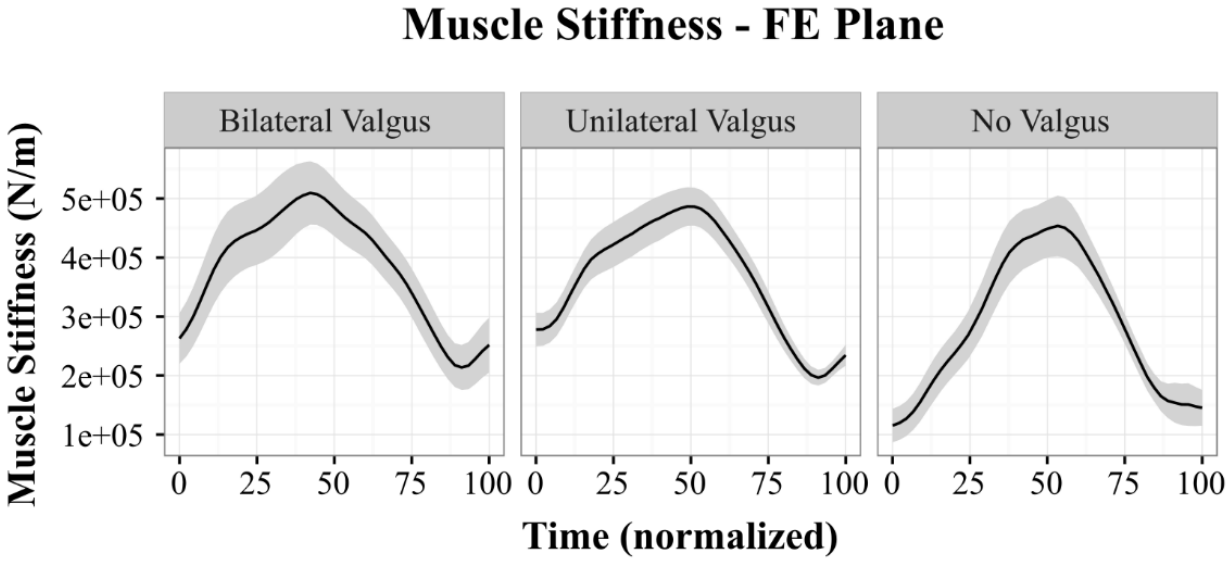
Muscle Stiffness - FE Plane
Bilateral Valgus
Unilateral Valgus
No Valgus
Muscle Stiffness (N/m)
5e+05
4e+05
3e+05
2e+05
1e+05
0
25
50
75
100
Time (normalized)

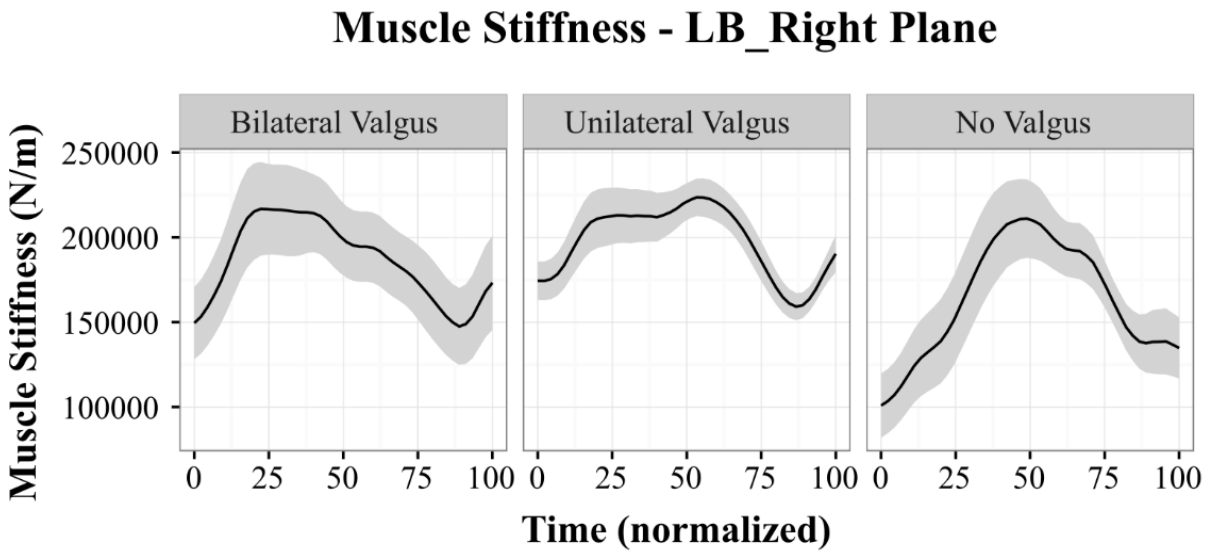
Muscle Stiffness - LB_Right Plane
Bilateral Valgus
Unilateral Valgus
No Valgus
Muscle Stiffness (N/m)
250000
200000
150000
100000
0
25
50
75
100
Time (normalized)

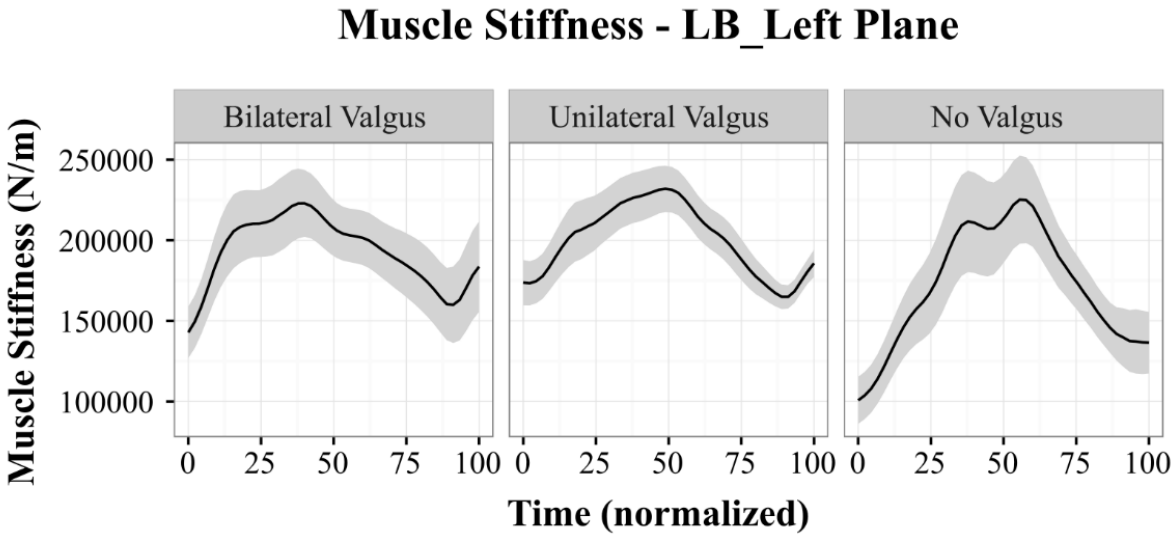
Muscle Stiffness - LB_Left Plane
Bilateral Valgus
Unilateral Valgus
No Valgus
Muscle Stiffness (N/m)
250000
200000
150000
100000
0
25
50
75
100
Time (normalized)

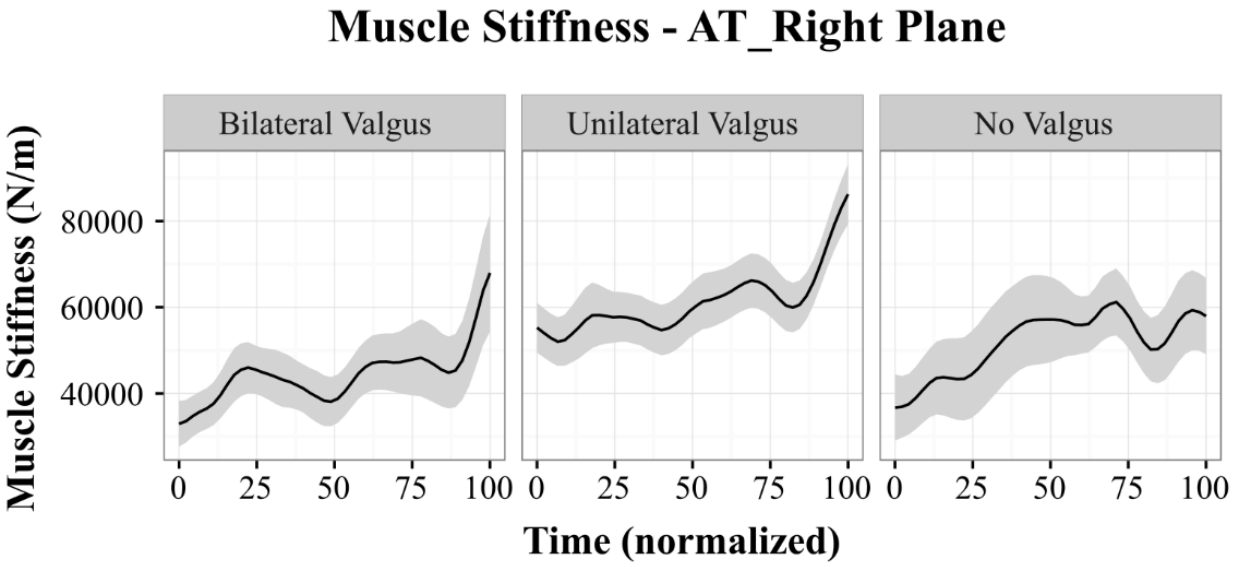
Muscle Stiffness - AT_Right Plane
Bilateral Valgus
Unilateral Valgus
No Valgus
Muscle Stiffness (N/m)
80000
60000
40000
0
25
50
75
100
Time (normalized)

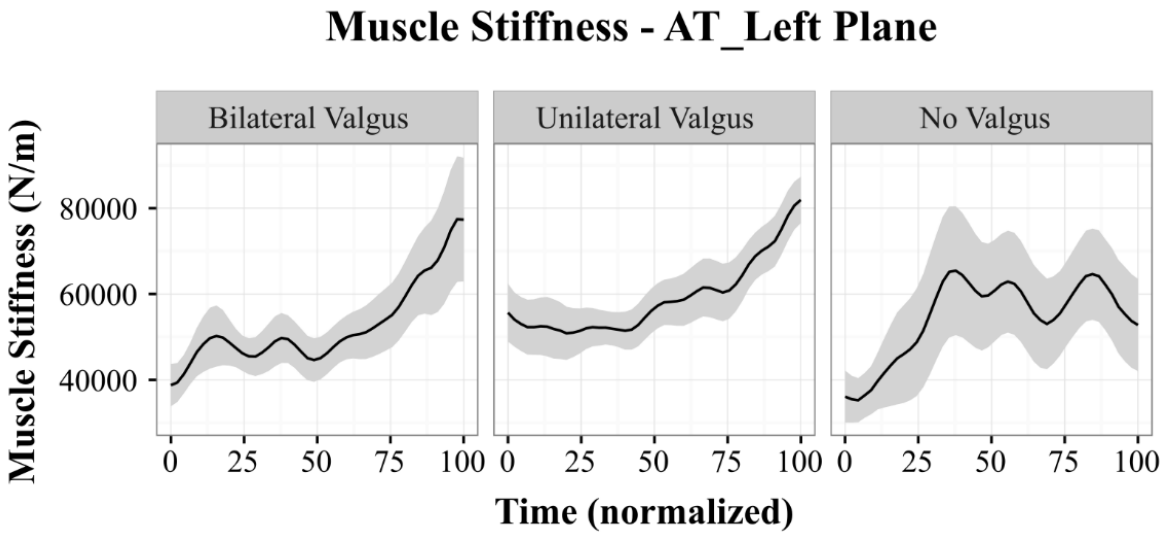
Muscle Stiffness - AT_Left Plane
Bilateral Valgus
Unilateral Valgus
No Valgus
Muscle Stiffness (N/m)
80000
60000
40000
0
25
50
75
100
Time (normalized)

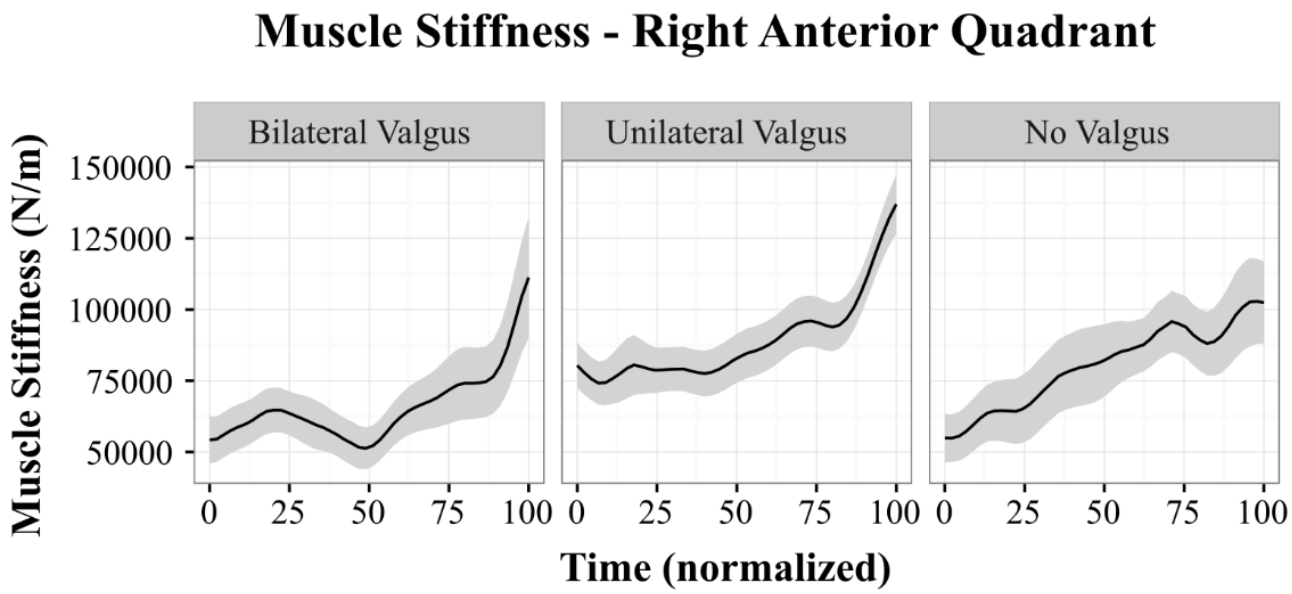
Muscle Stiffness - Right Anterior Quadrant
Bilateral Valgus
Unilateral Valgus
No Valgus
Muscle Stiffness (N/m)
150000
125000
100000
75000
50000
0
25
50
75
100
Time (normalized)

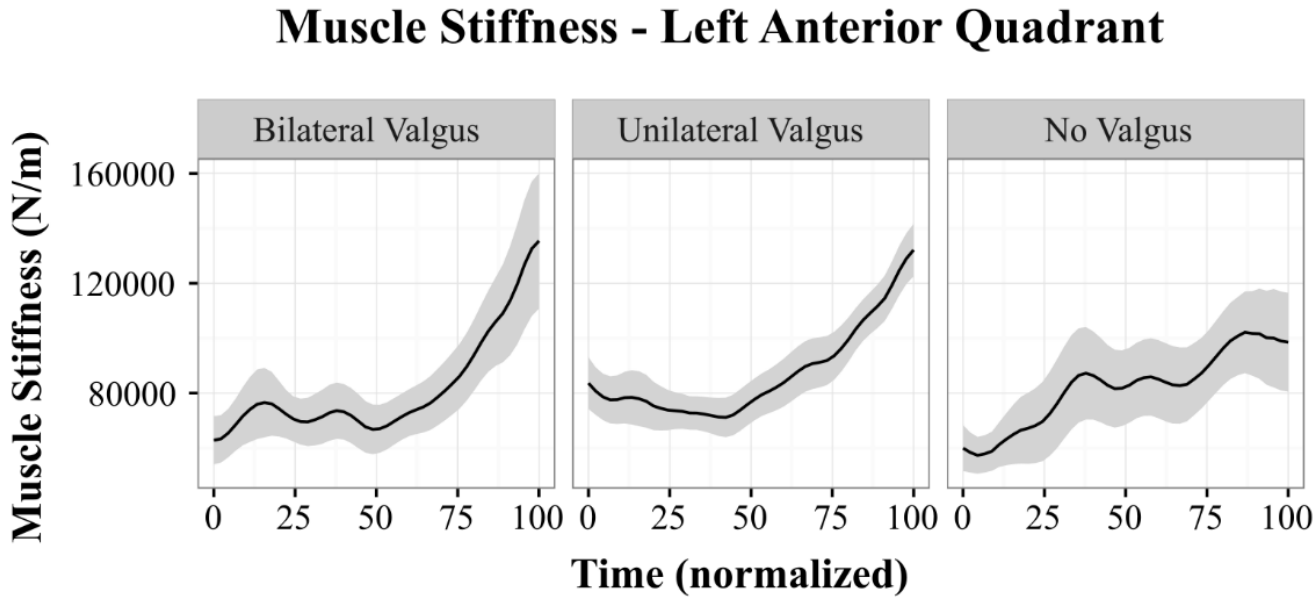
Muscle Stiffness - Left Anterior Quadrant
Bilateral Valgus
Unilateral Valgus
No Valgus
Muscle Stiffness (N/m)
160000
120000
80000
0
25
50
75
100
Time (normalized)

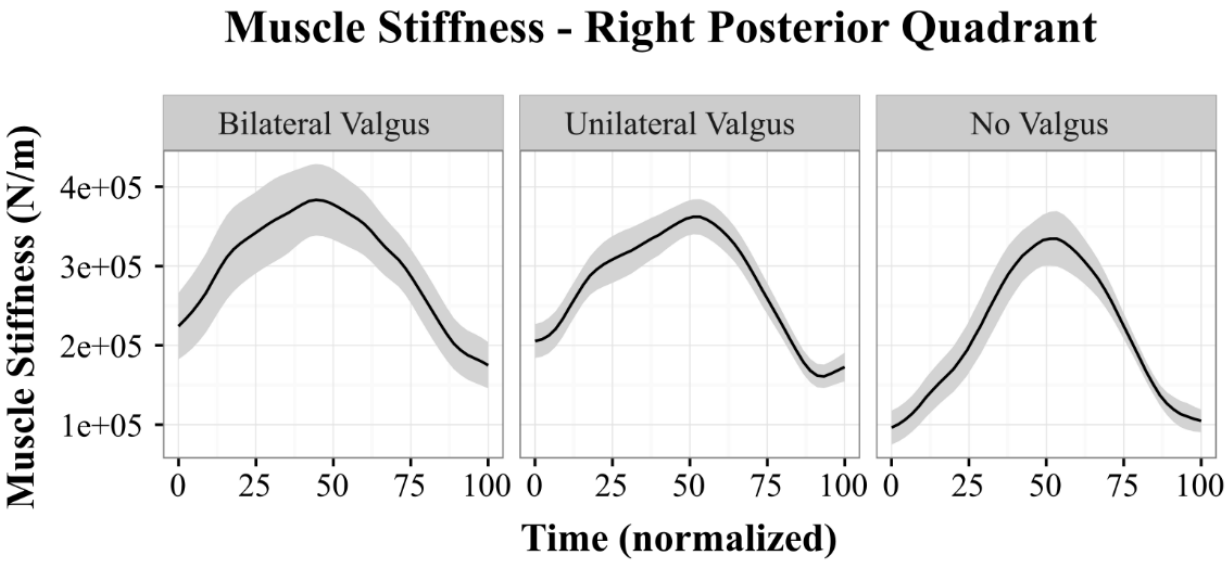
Muscle Stiffness - Right Posterior Quadrant
Bilateral Valgus
Unilateral Valgus
No Valgus
Muscle Stiffness (N/m)
4e+05
3e+05
2e+05
1e+05
0
25
50
75
100
Time (normalized)

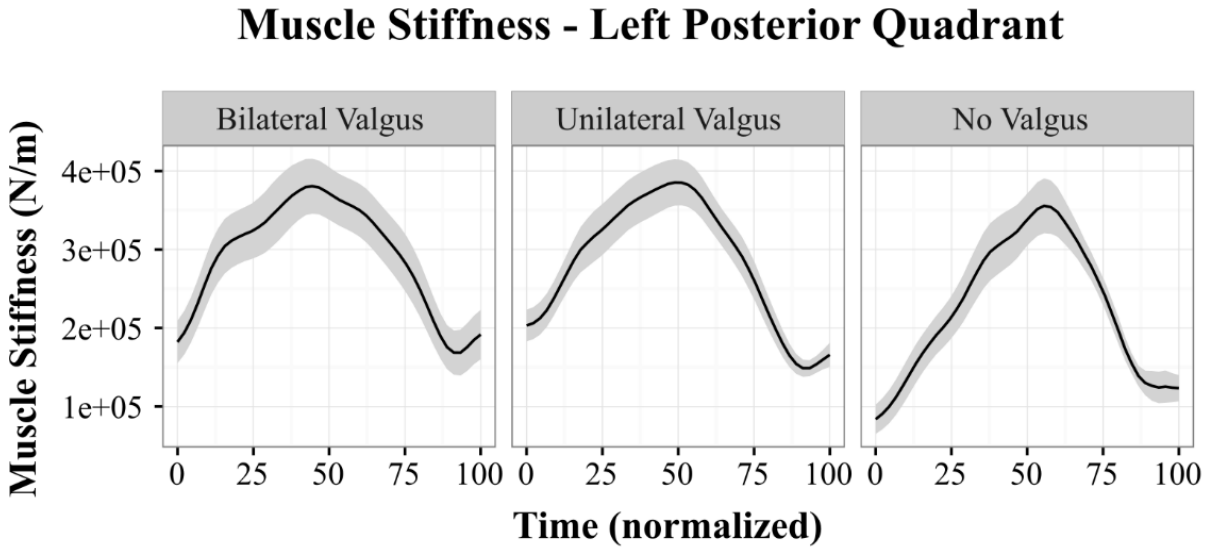
Muscle Stiffness - Left Posterior Quadrant
Bilateral Valgus
Unilateral Valgus
No Valgus
Muscle Stiffness (N/m)
4e+05
3e+05
2e+05
1e+05
0
25
50
75
100
Time (normalized)

Lumbar JRS - Sagittal Plane

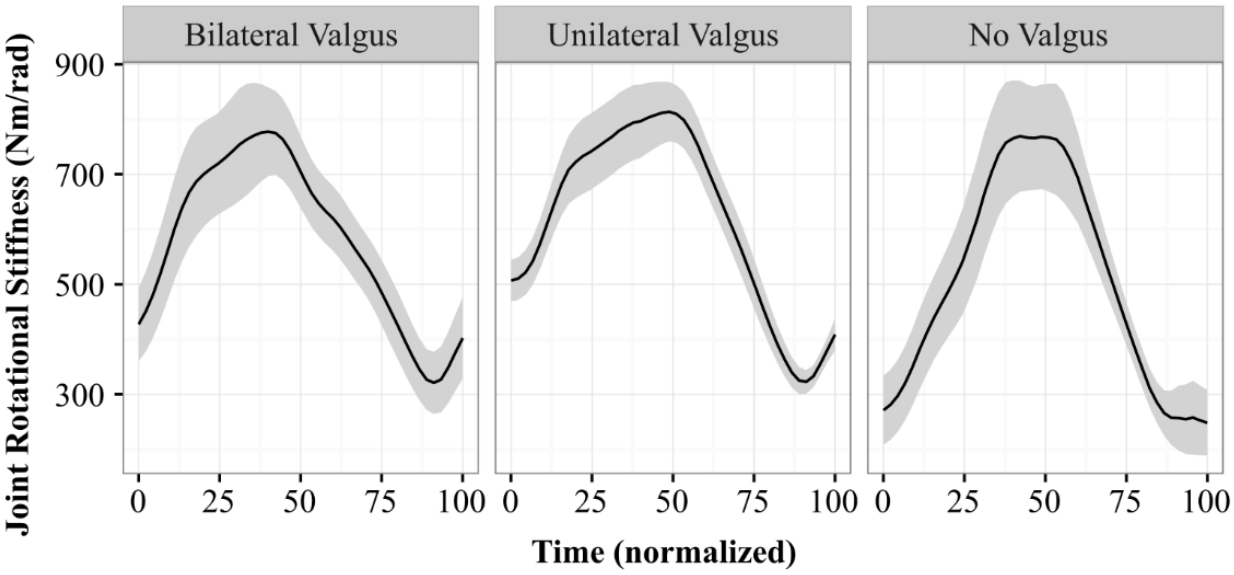

Lumbar JRS - Frontal Plane

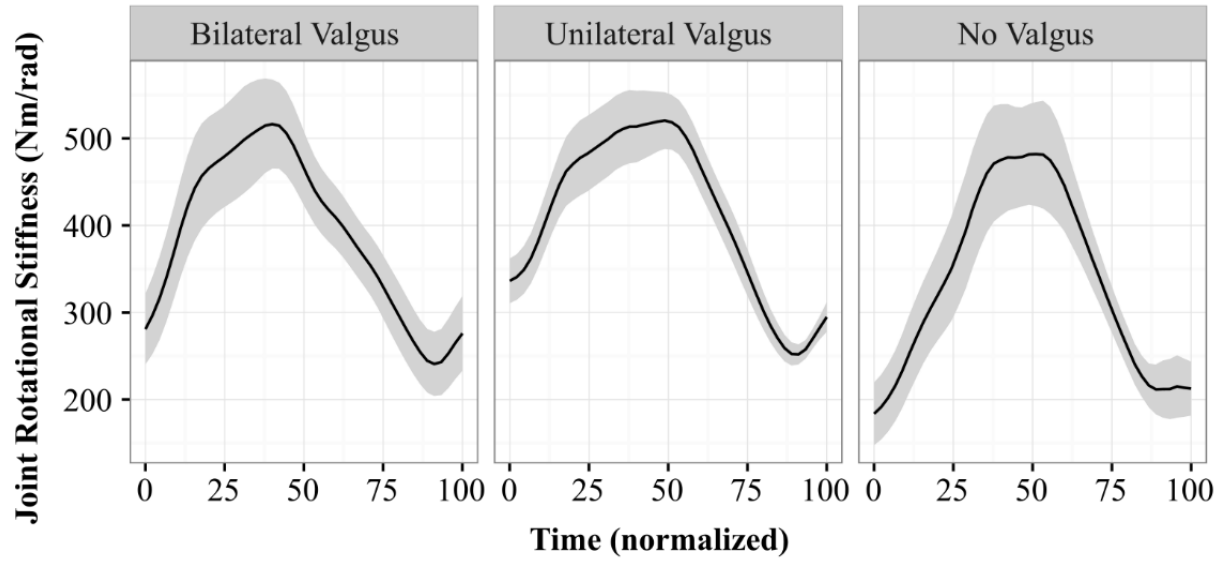

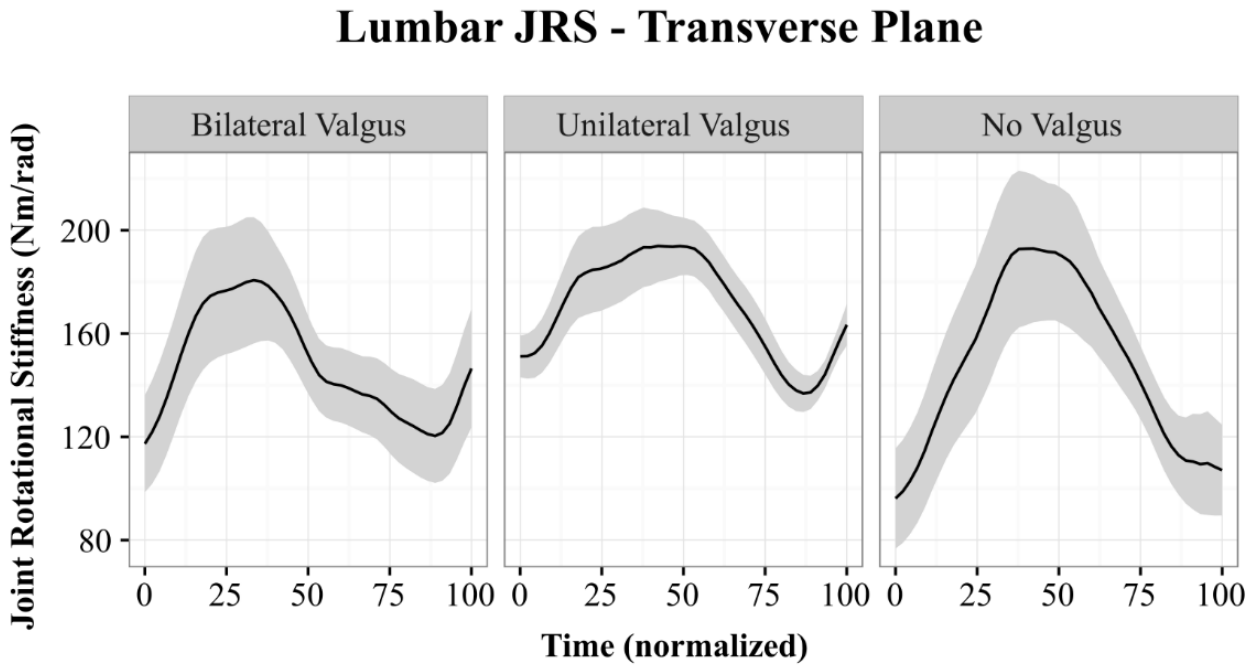
Lumbar JRS - Transverse Plane
Bilateral Valgus
Unilateral Valgus
No Valgus
Joint Rotational Stiffness (Nm/rad)
200
160
120
80
0
25
50
75
100
Time (normalized)

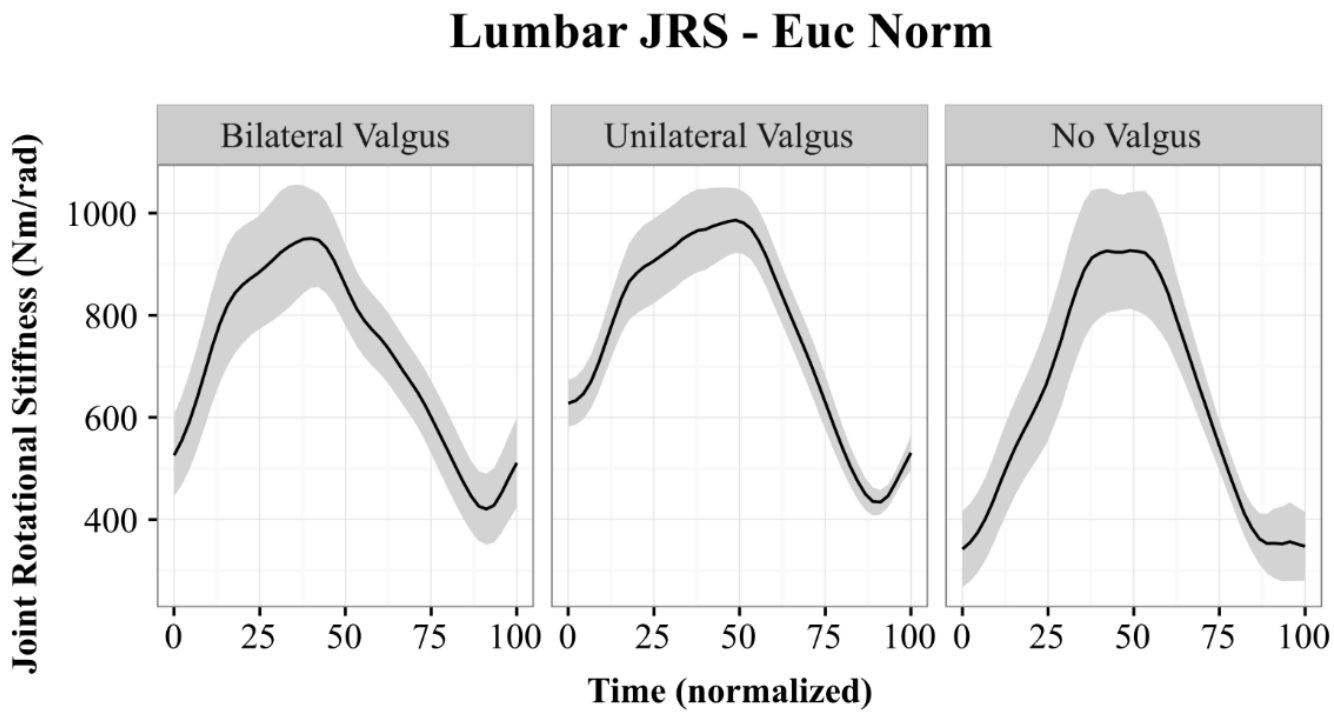
Lumbar JRS - Euc Norm
Bilateral Valgus
Unilateral Valgus
No Valgus
Joint Rotational Stiffness (Nm/rad)
1000
800
600
400
0
25
50
75
100
Time (normalized)

Left Hip Angle - Sagittal Plane

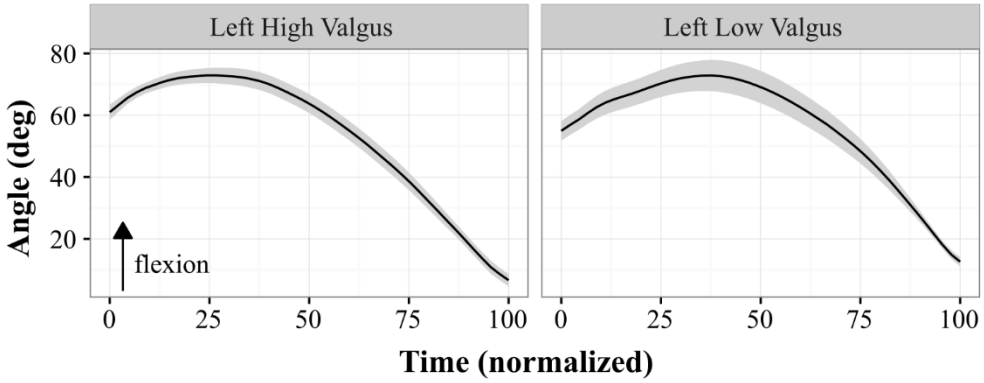

Left Hip Angle - Frontal Plane

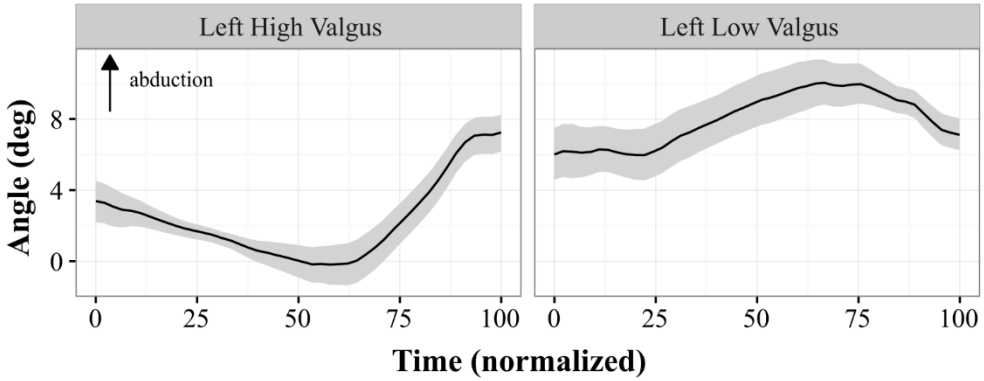

Left Hip Angle - Transverse Plane

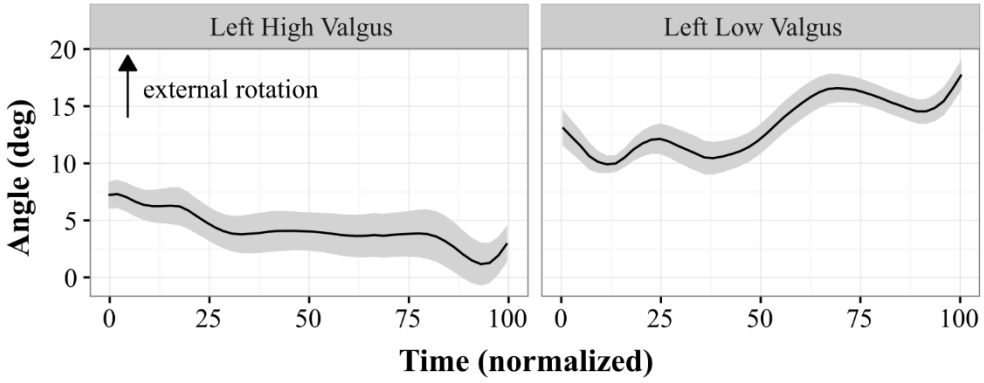

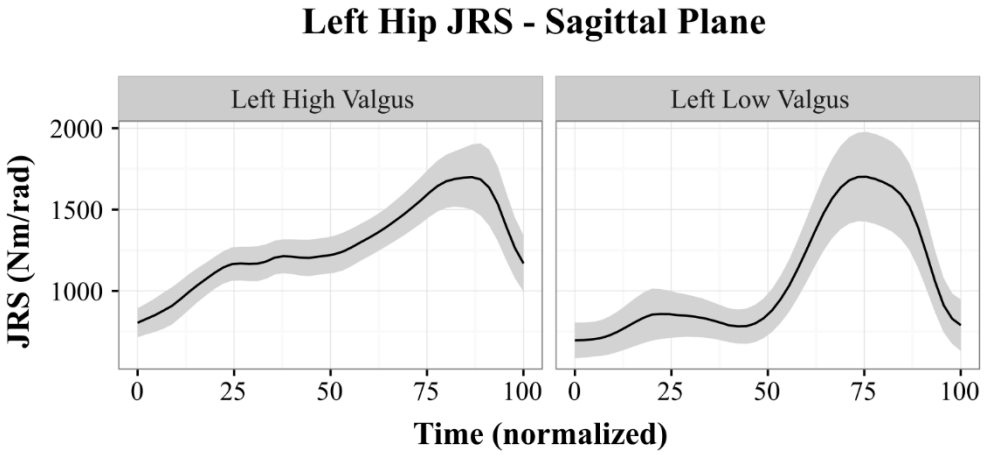
Left Hip JRS - Sagittal Plane
Left High Valgus
Left Low Valgus
JRS (Nm/rad)
2000
1500
1000
0
25
50
75
100
Time (normalized)

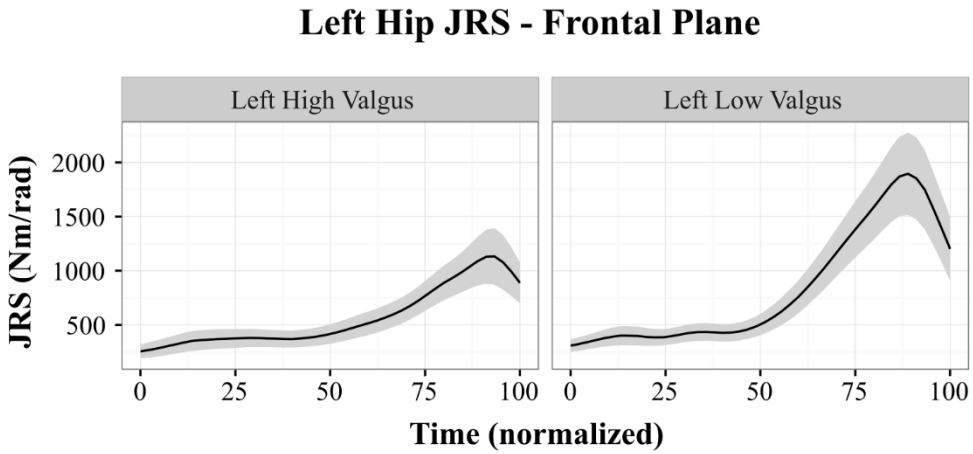
Left Hip JRS - Frontal Plane
Left High Valgus
Left Low Valgus
JRS (Nm/rad)
2000
1500
1000
500
0
25
50
75
100
Time (normalized)

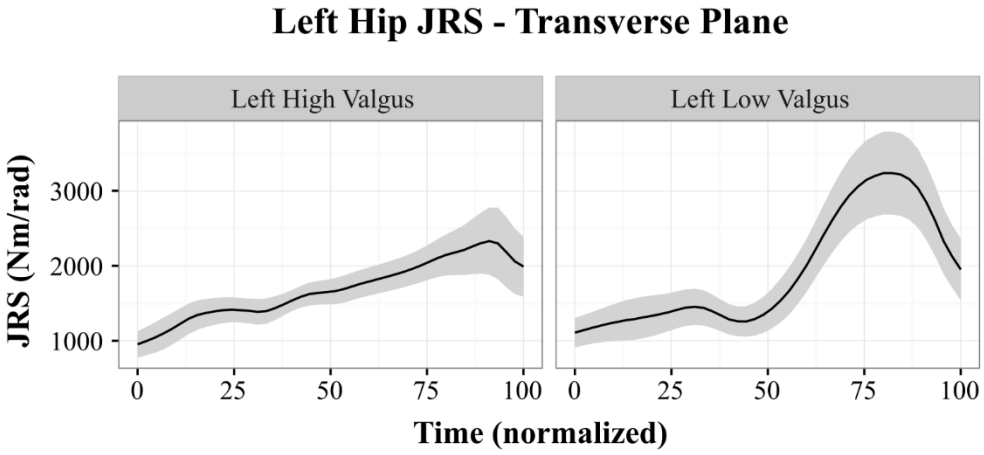
Left Hip JRS - Transverse Plane
Left High Valgus
Left Low Valgus
JRS (Nm/rad)
3000
2000
1000
0
25
50
75
100
Time (normalized)

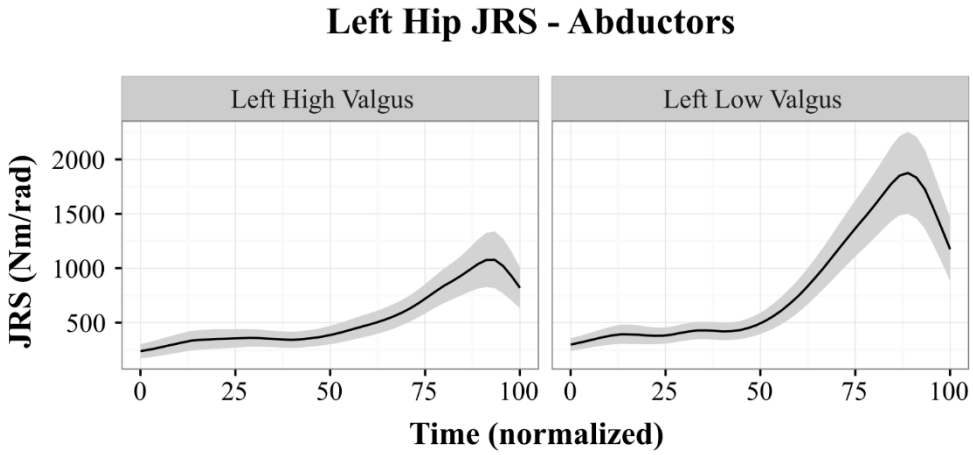
Left Hip JRS - Abductors
Left High Valgus
Left Low Valgus
JRS (Nm/rad)
2000
1500
1000
500
0
25
50
75
100
Time (normalized)

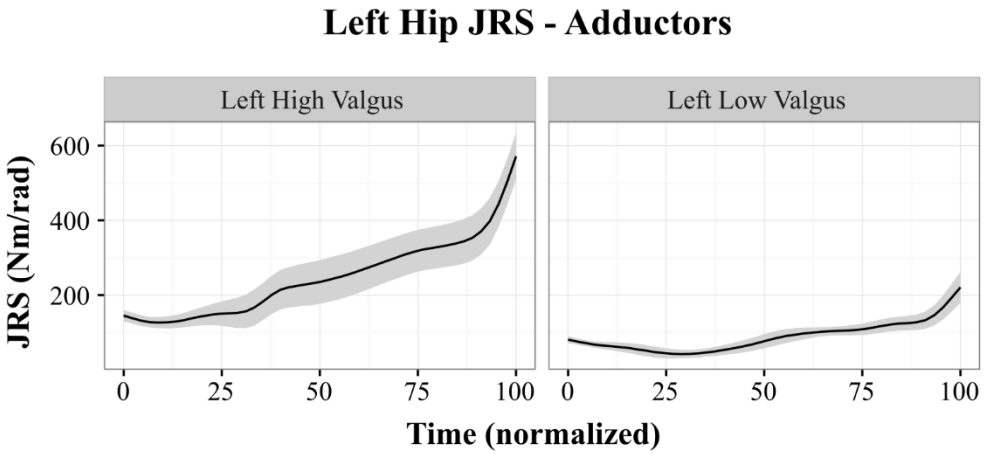
Left Hip JRS - Adductors
Left High Valgus
Left Low Valgus
JRS (Nm/rad)
600
400
200
0
25
50
75
100
Time (normalized)

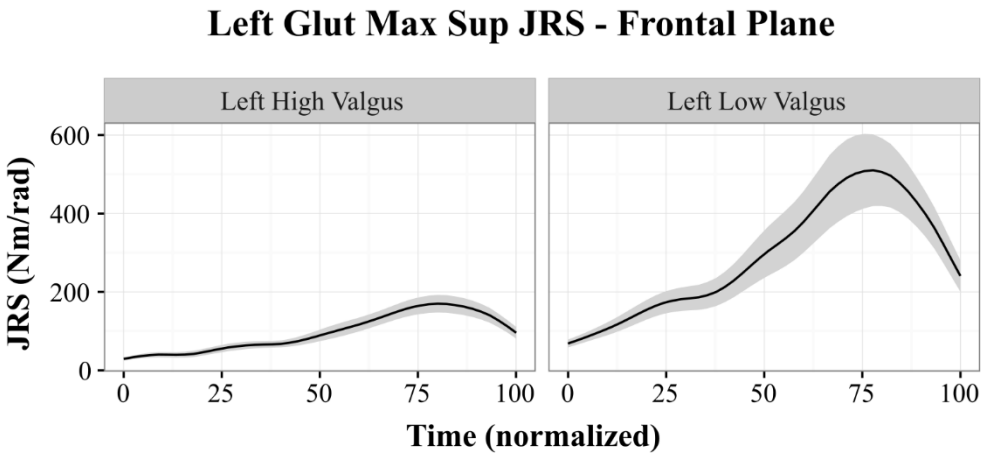
Left Glut Max Sup JRS - Frontal Plane
Left High Valgus
Left Low Valgus
JRS (Nm/rad)
600
400
200
0
0
25
50
75
100
Time (normalized)

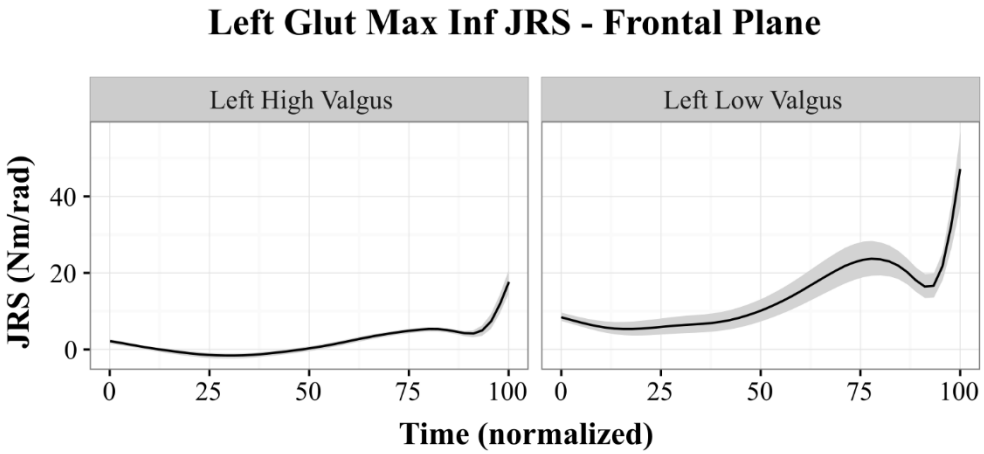
Left Glut Max Inf JRS - Frontal Plane
Left High Valgus
Left Low Valgus
JRS (Nm/rad)
40
20
0
0
25
50
75
100
Time (normalized)

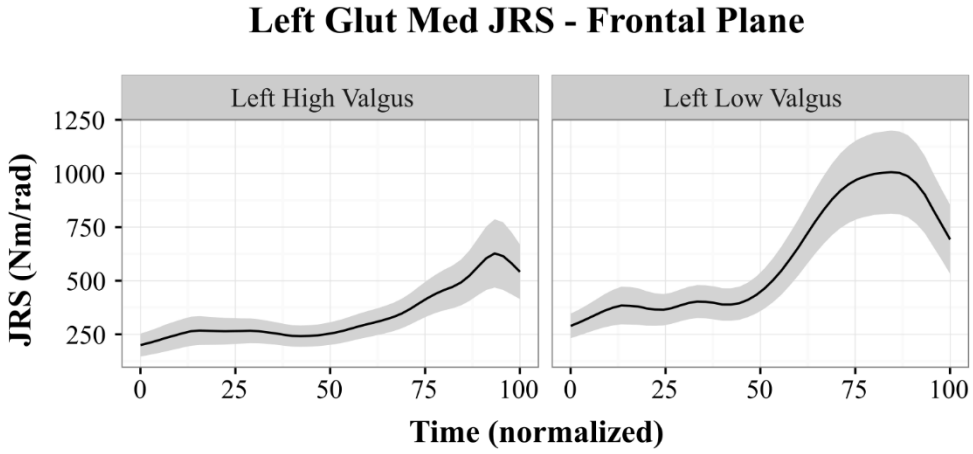
Left Glut Med JRS - Frontal Plane
Left High Valgus
Left Low Valgus
JRS (Nm/rad)
1250
1000
750
500
250
0
25
50
75
100
Time (normalized)

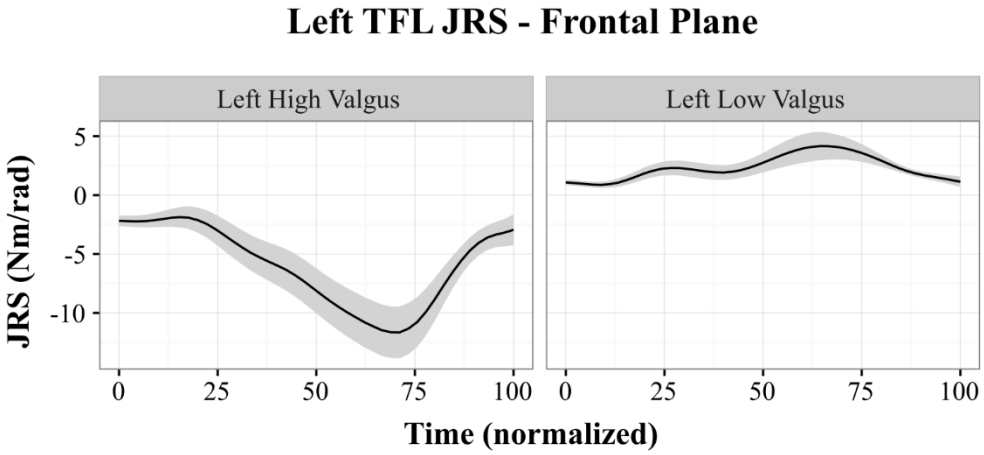
Left TFL JRS - Frontal Plane
Left High Valgus
Left Low Valgus
JRS (Nm/rad)
5
0
-5
-10
0
25
50
75
100
Time (normalized)

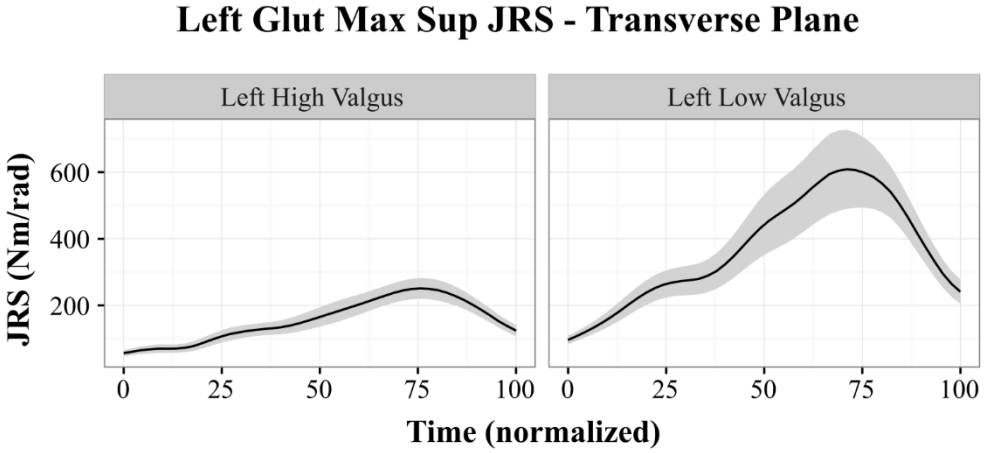
Left Glut Max Sup JRS - Transverse Plane
Left High Valgus
Left Low Valgus
JRS (Nm/rad)
600
400
200
0
25
50
75
100
Time (normalized)

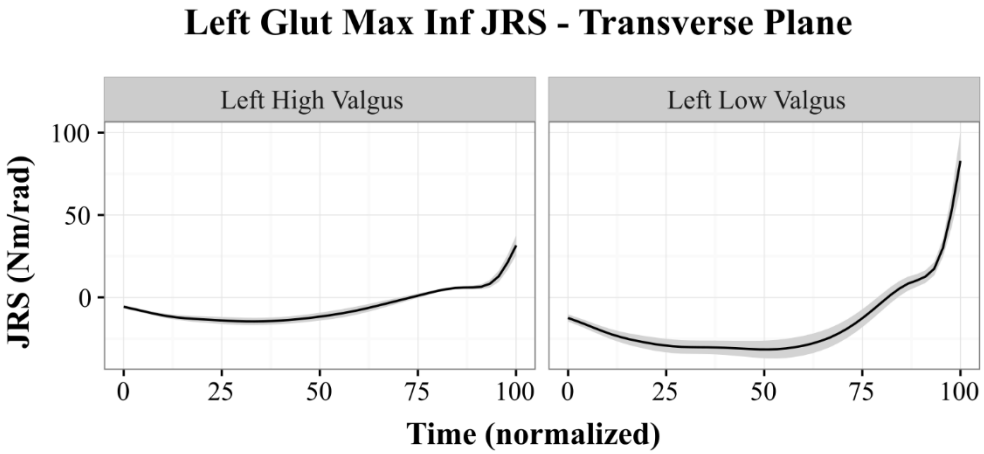
Left Glut Max Inf JRS - Transverse Plane
Left High Valgus
Left Low Valgus
JRS (Nm/rad)
100
50
0
0
25
50
75
100
Time (normalized)

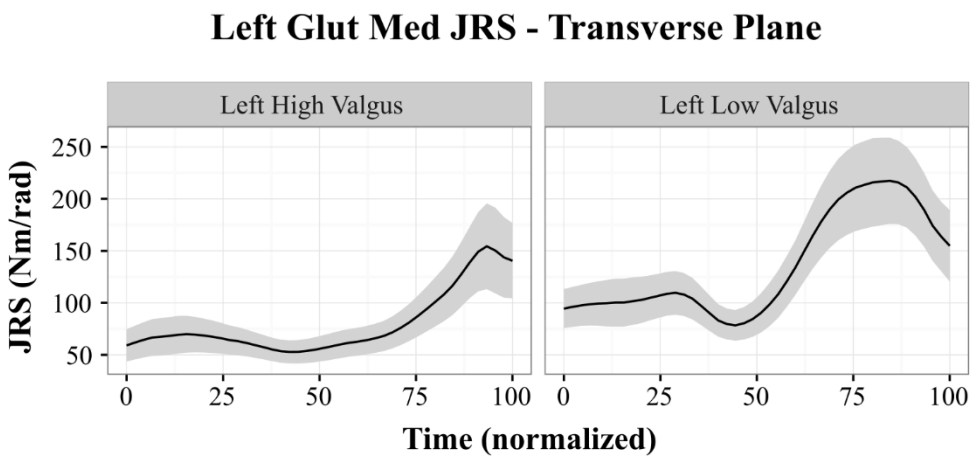
Left Glut Med JRS - Transverse Plane
Left High Valgus
Left Low Valgus
JRS (Nm/rad)
250
200
150
100
50
0
25
50
75
100
Time (normalized)

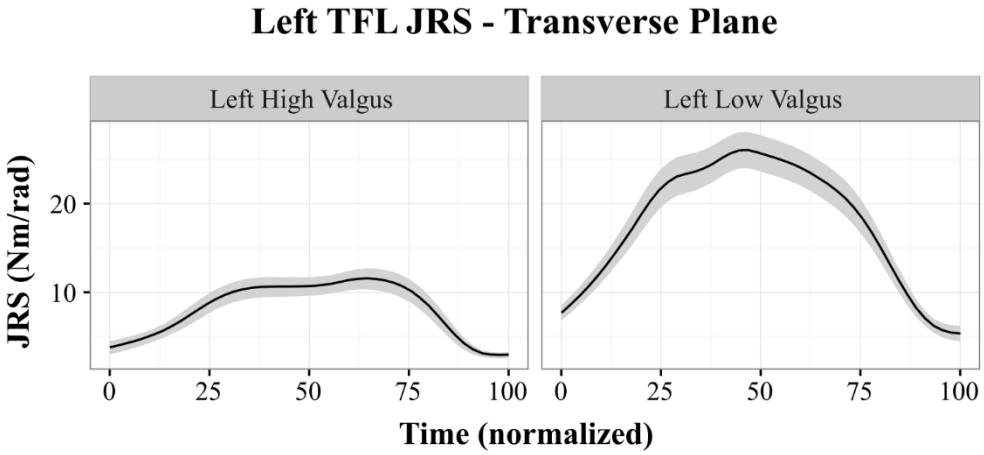
Left TFL JRS - Transverse Plane
Left High Valgus
Left Low Valgus
JRS (Nm/rad)
20
10
0
25
50
75
100
Time (normalized)

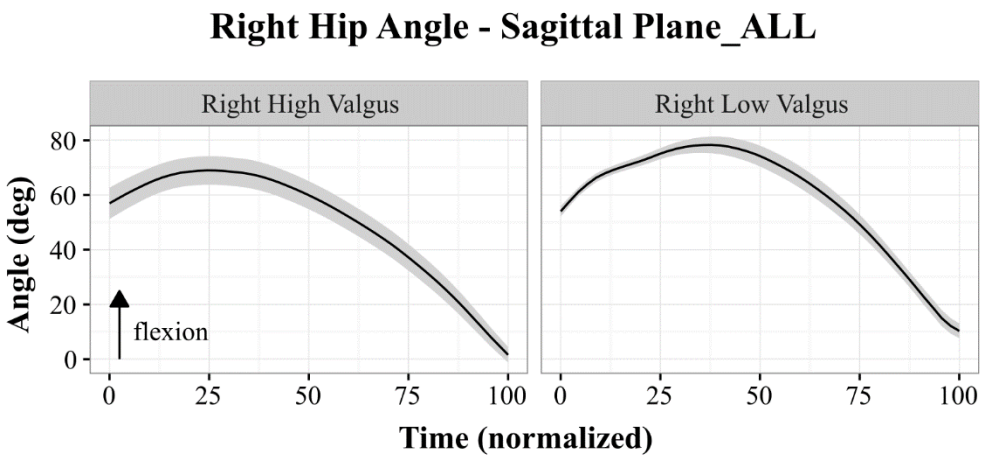
Right Hip Angle - Sagittal Plane_ALL
Right High Valgus
Right Low Valgus
Angle (deg)
80
60
40
20
0
flexion
0
25
50
75
100
Time (normalized)

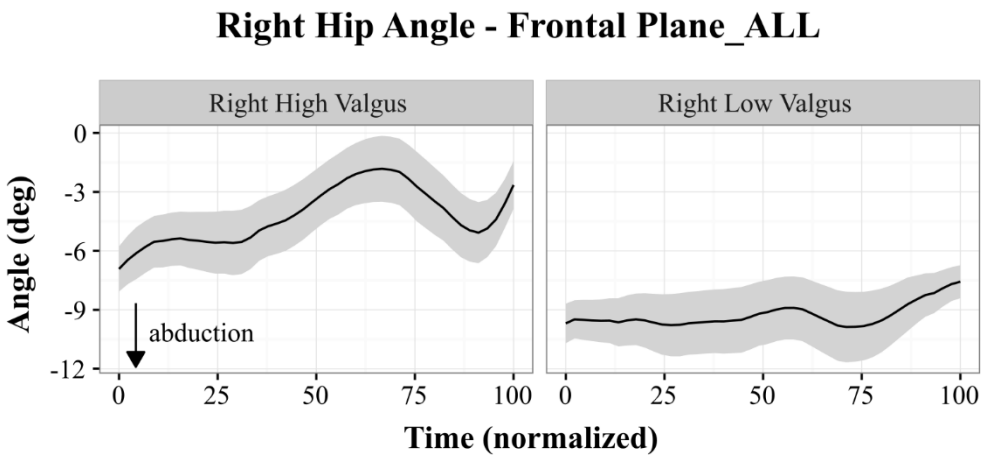
Right Hip Angle - Frontal Plane_ALL
Right High Valgus
Right Low Valgus
Angle (deg)
0
-3
-6
-9
-12
abduction
0
25
50
75
100
Time (normalized)

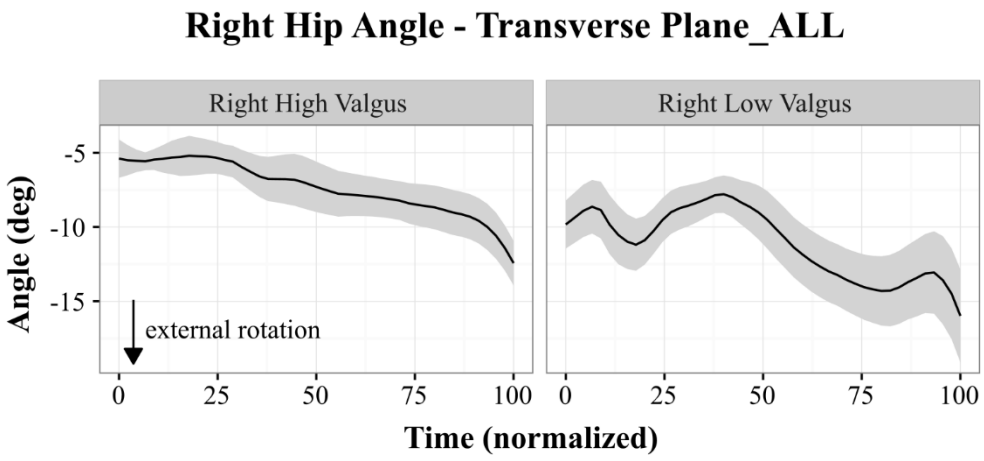
Right Hip Angle - Transverse Plane_ALL
Right High Valgus
Right Low Valgus
Angle (deg)
-5
-10
-15
external rotation
0
25
50
75
100
Time (normalized)

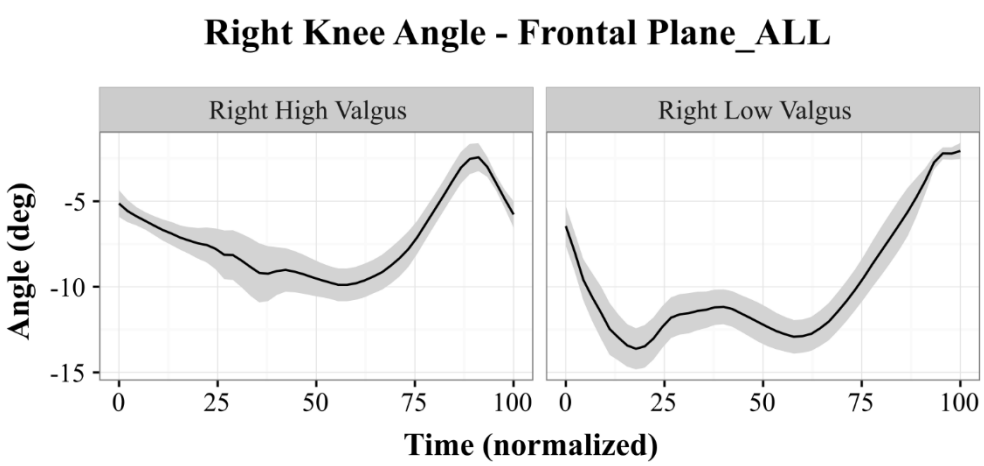
Right Knee Angle - Frontal Plane_ALL
Right High Valgus
Right Low Valgus
Angle (deg)
-5
-10
-15
0
25
50
75
100
Time (normalized)

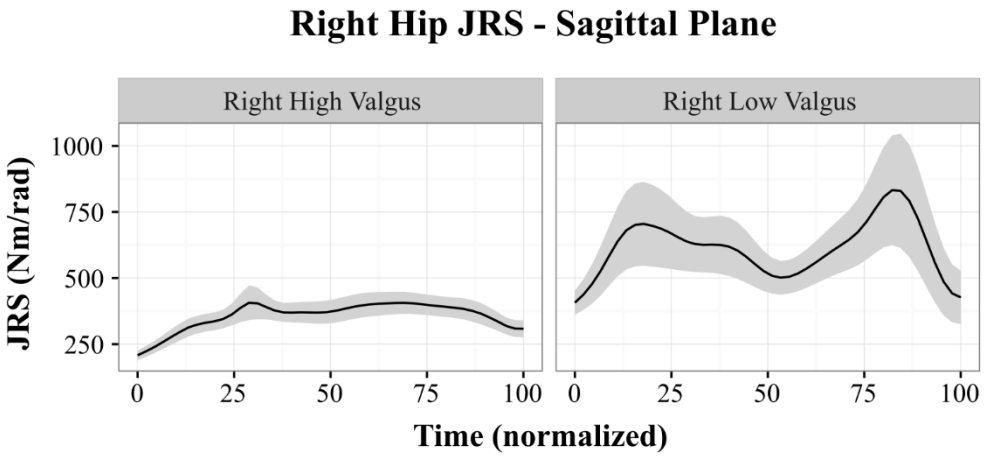
Right Hip JRS - Sagittal Plane
Right High Valgus
Right Low Valgus
JRS (Nm/rad)
1000
750
500
250
0
25
50
75
100
Time (normalized)

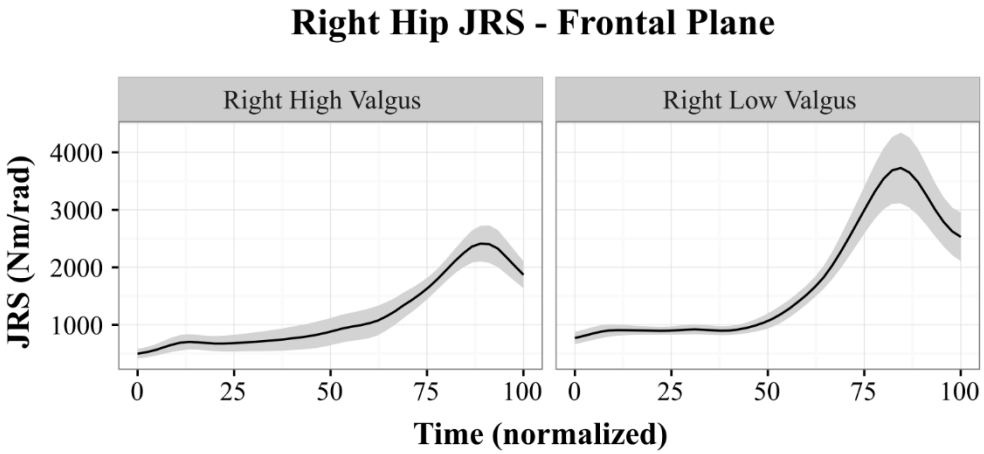
Right Hip JRS - Frontal Plane
Right High Valgus
Right Low Valgus
JRS (Nm/rad)
4000
3000
2000
1000
0
25
50
75
100
Time (normalized)

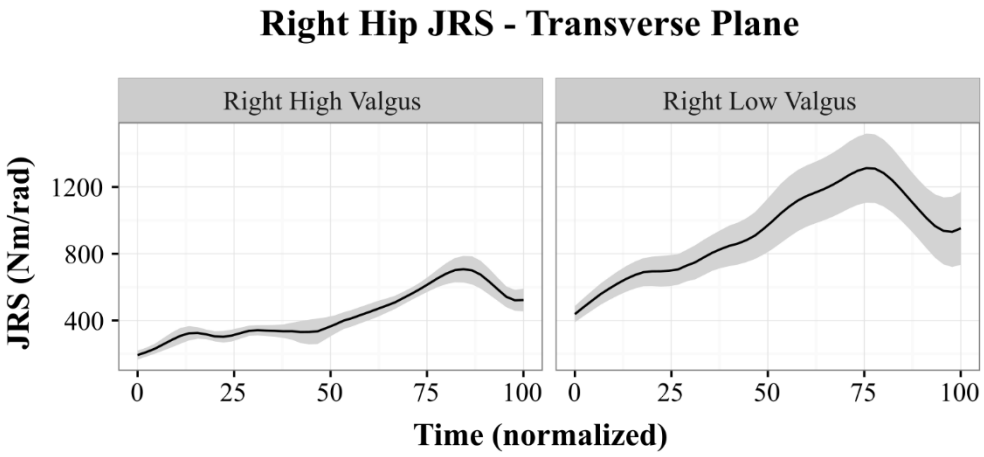
Right Hip JRS - Transverse Plane
Right High Valgus
Right Low Valgus
JRS (Nm/rad)
1200
800
400
0
25
50
75
100
Time (normalized)

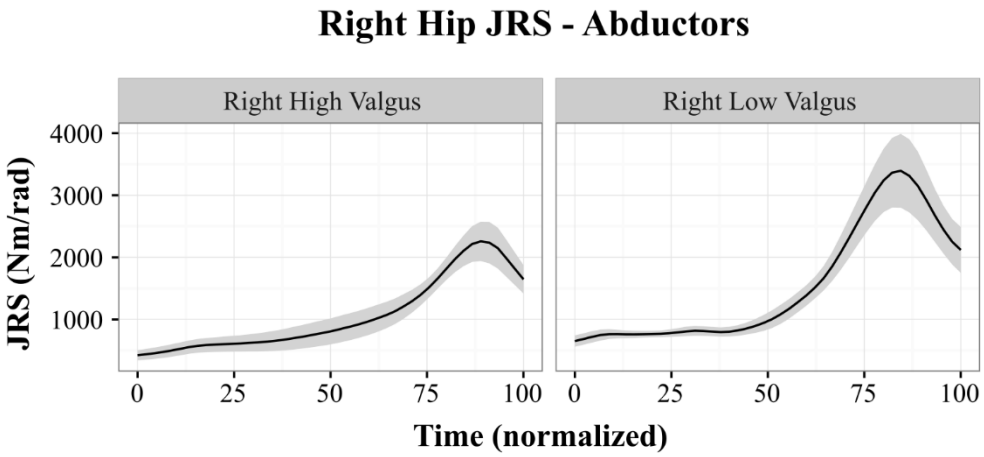
Right Hip JRS - Abductors
Right High Valgus
Right Low Valgus
JRS (Nm/rad)
4000
3000
2000
1000
0
25
50
75
100
Time (normalized)

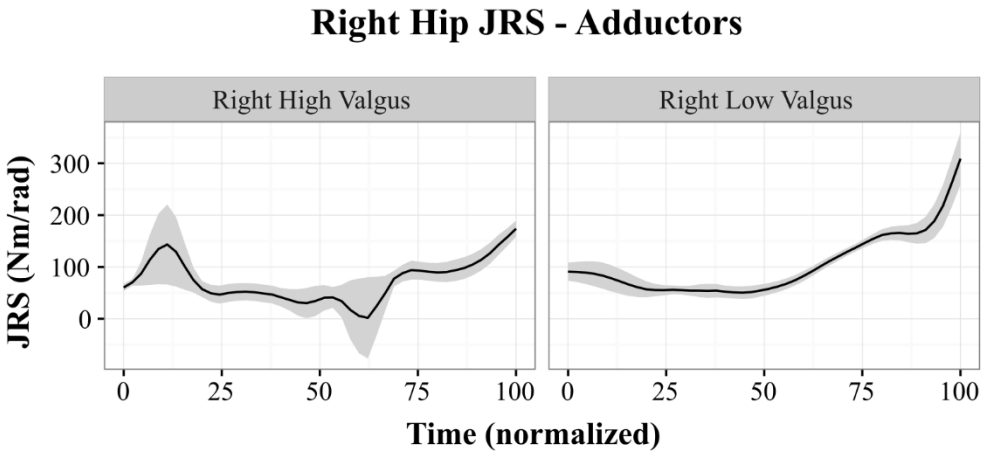
Right Hip JRS - Adductors
Right High Valgus
Right Low Valgus
JRS (Nm/rad)
300
200
100
0
25
50
75
100
Time (normalized)

Right Glut Max Sup JRS - Frontal Plane

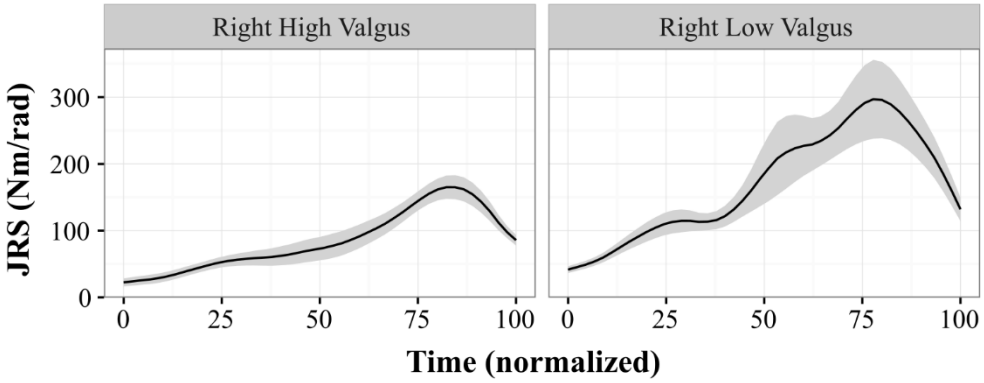

Left Glut Max Inf JRS - Frontal Plane

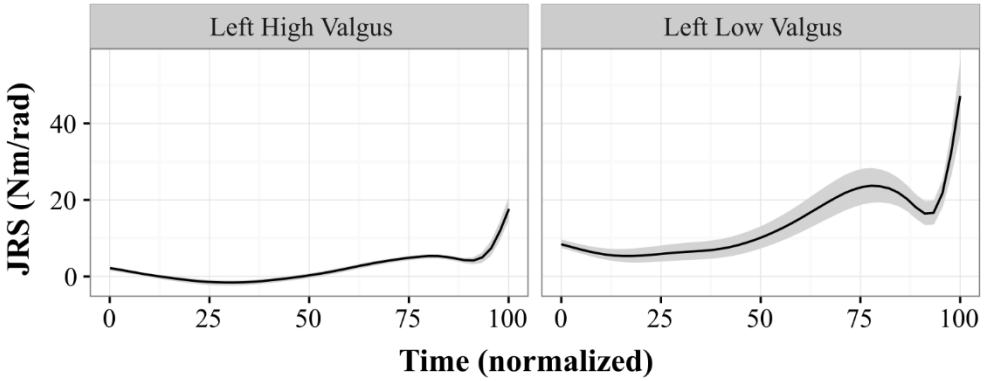

Right Glut Med JRS - Frontal Plane

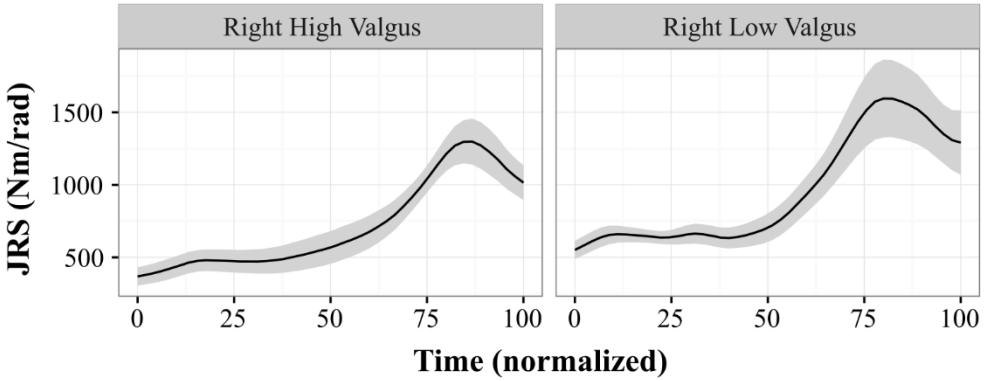

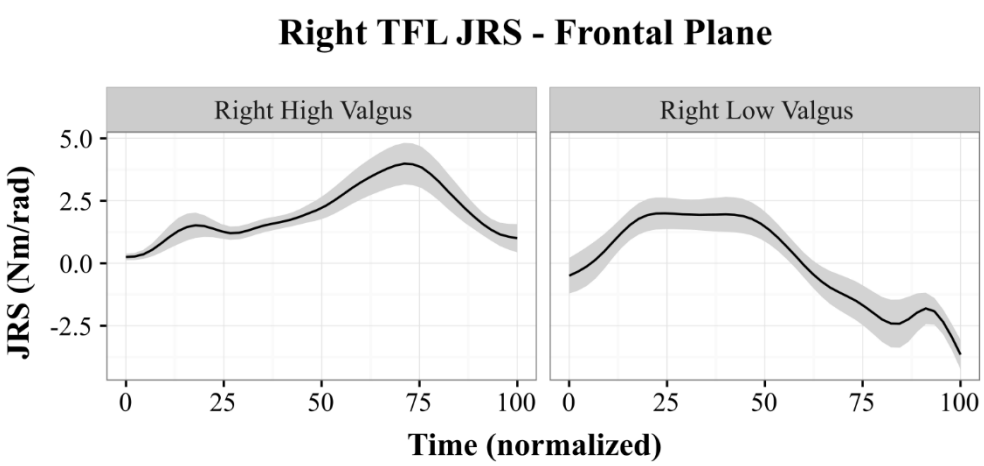
Right TFL JRS - Frontal Plane
Right High Valgus
Right Low Valgus
JRS (Nm/rad)
5.0
2.5
0.0
-2.5
0
25
50
75
100
Time (normalized)

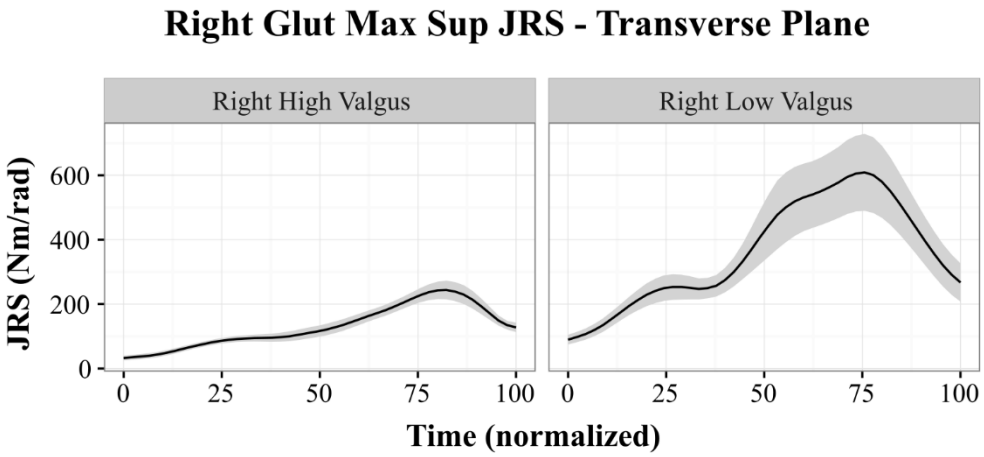
Right Glut Max Sup JRS - Transverse Plane
Right High Valgus
Right Low Valgus
JRS (Nm/rad)
600
400
200
0
0
25
50
75
100
Time (normalized)

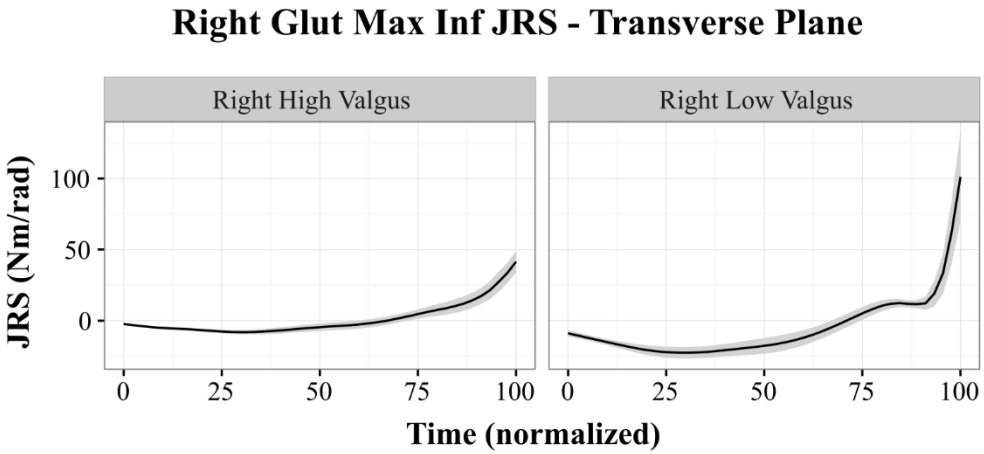
Right Glut Max Inf JRS - Transverse Plane
Right High Valgus
Right Low Valgus
JRS (Nm/rad)
100
50
0
0
25
50
75
100
Time (normalized)

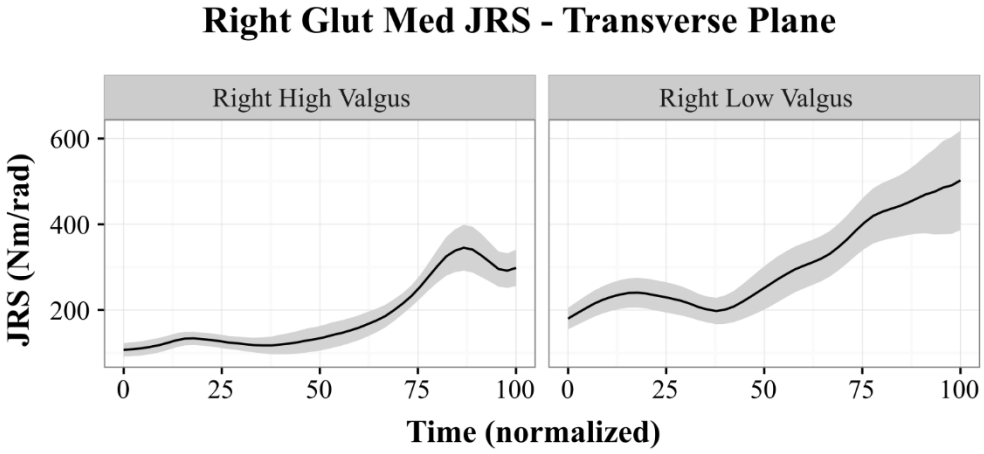
Right Glut Med JRS - Transverse Plane
Right High Valgus
Right Low Valgus
JRS (Nm/rad)
600
400
200
0
25
50
75
100
Time (normalized)

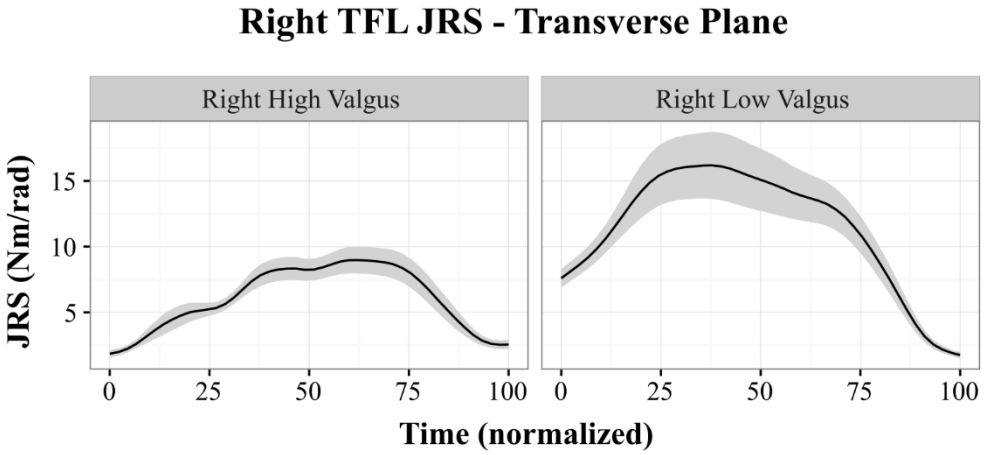
Right TFL JRS - Transverse Plane
Right High Valgus
Right Low Valgus
JRS (Nm/rad)
15
10
5
0
25
50
75
100
Time (normalized)

Single Leg Drop: Land on Left

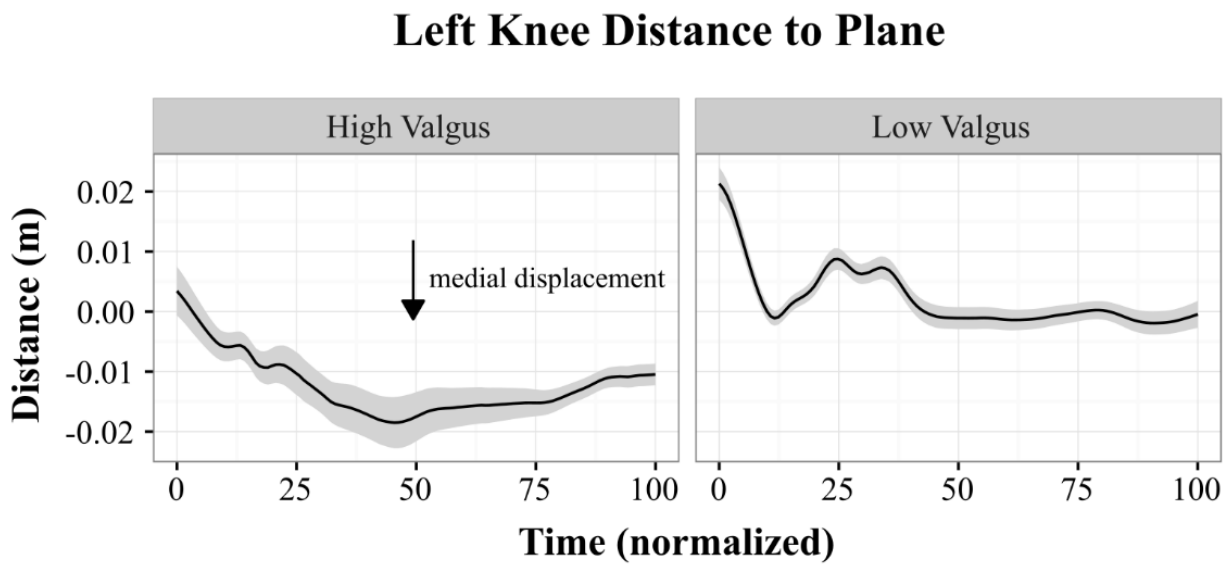

Lumbar Spine Angle - Sagittal Plane

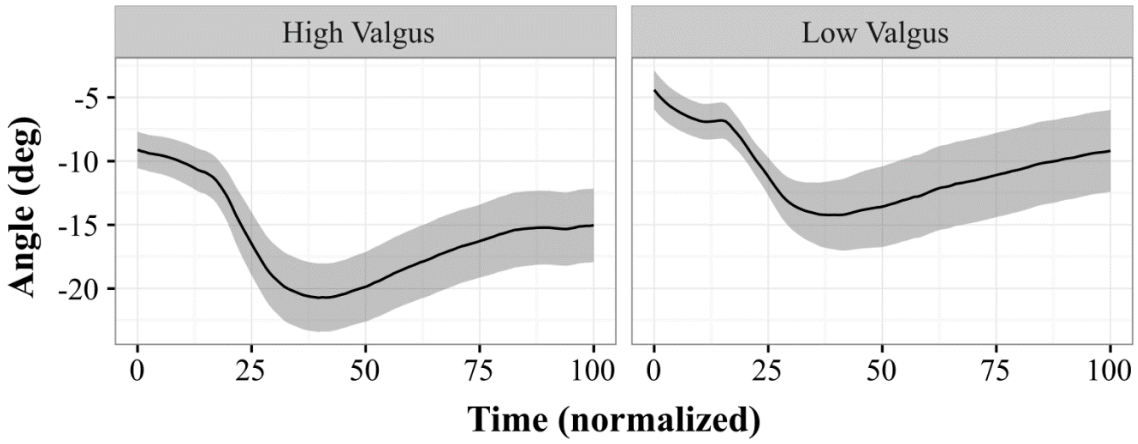

Lumbar Spine Angle - Frontal Plane

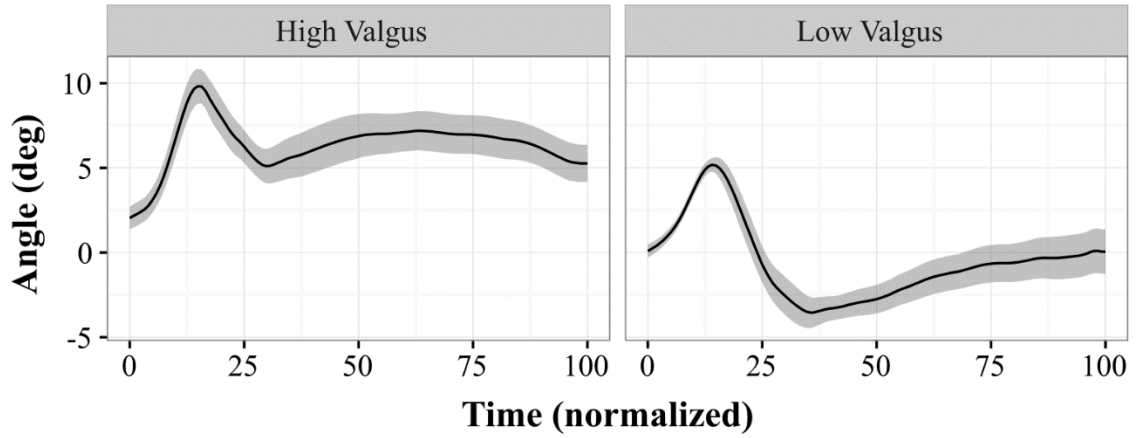

Lumbar Spine Angle - Transverse Plane

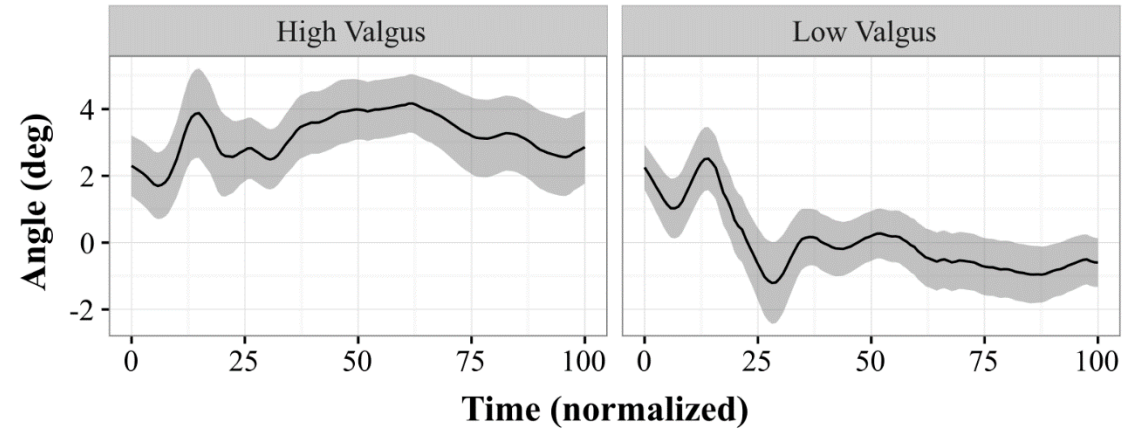

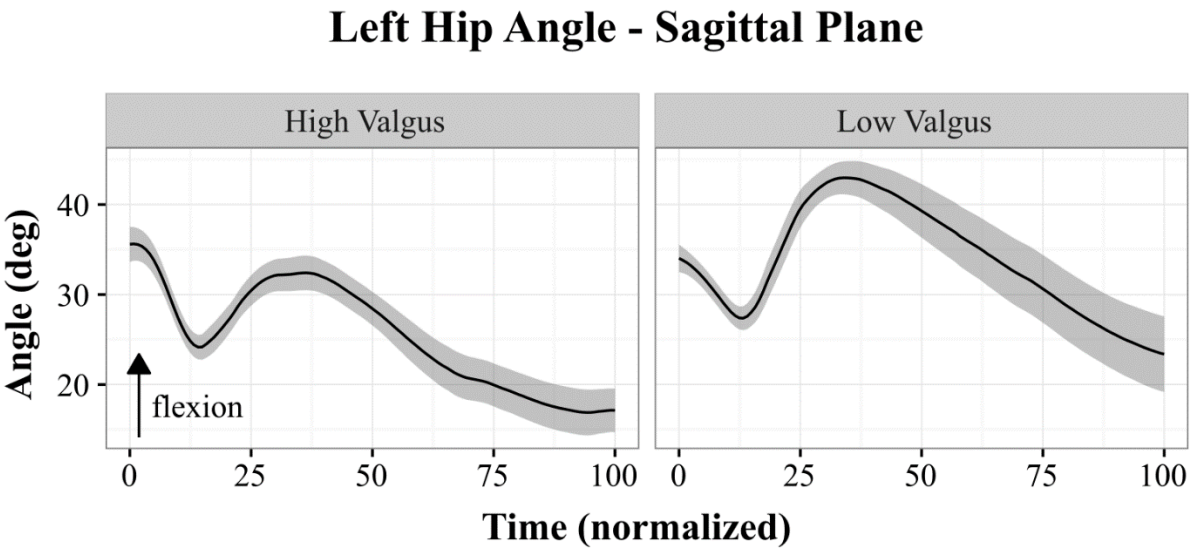
Left Hip Angle - Sagittal Plane
High Valgus
Low Valgus
Angle (deg)
40
30
20
flexion
0
25
50
75
100
Time (normalized)

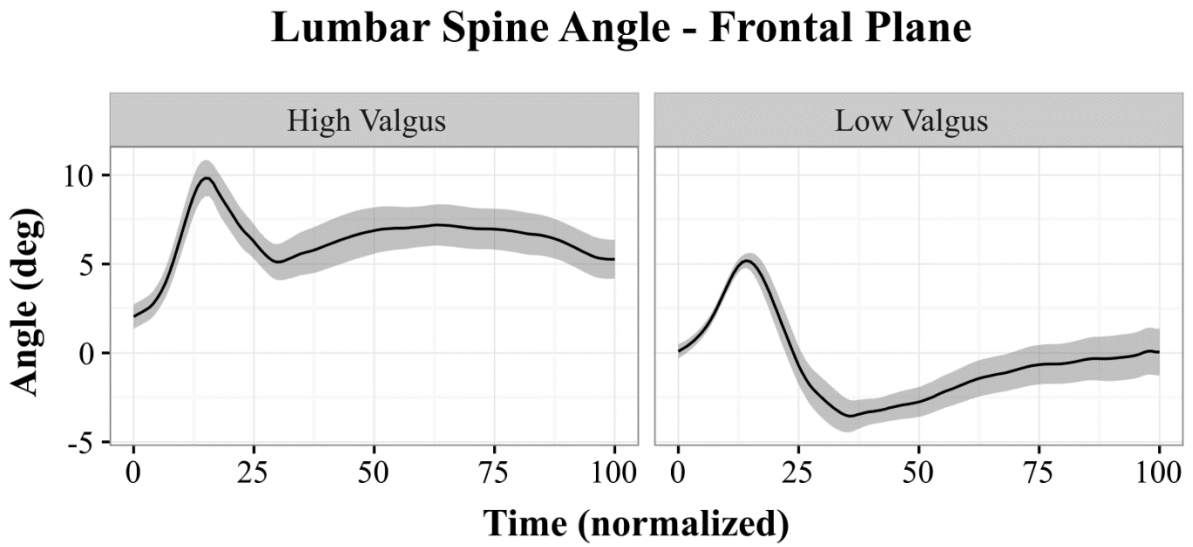
Lumbar Spine Angle - Frontal Plane
High Valgus
Low Valgus
Angle (deg)
10
5
0
-5
0
25
50
75
100
Time (normalized)

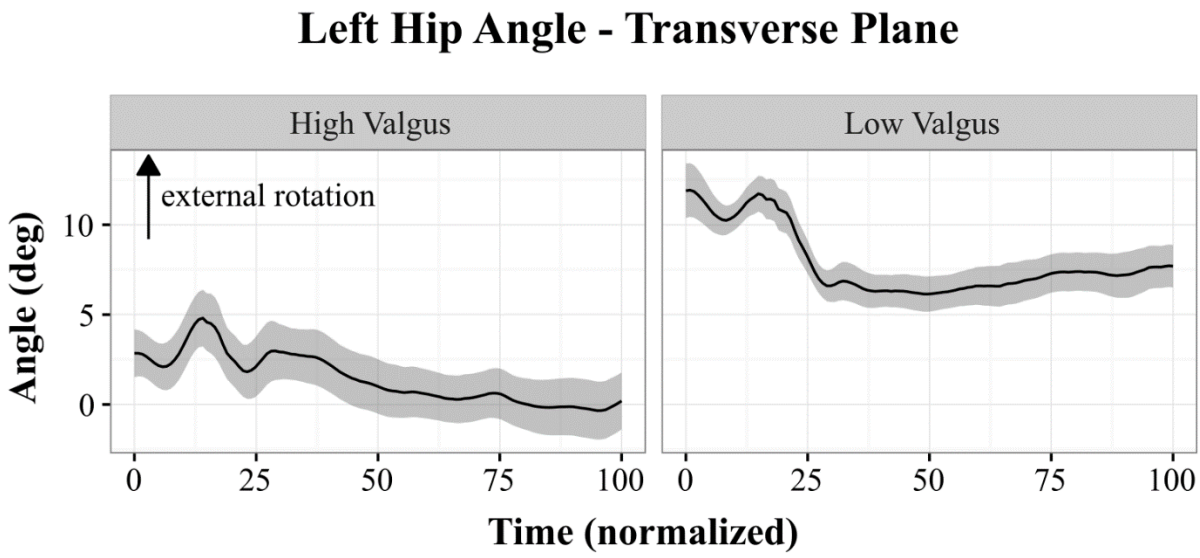
Left Hip Angle - Transverse Plane
High Valgus
Low Valgus
external rotation
Angle (deg)
10
5
0
0
25
50
75
100
Time (normalized)

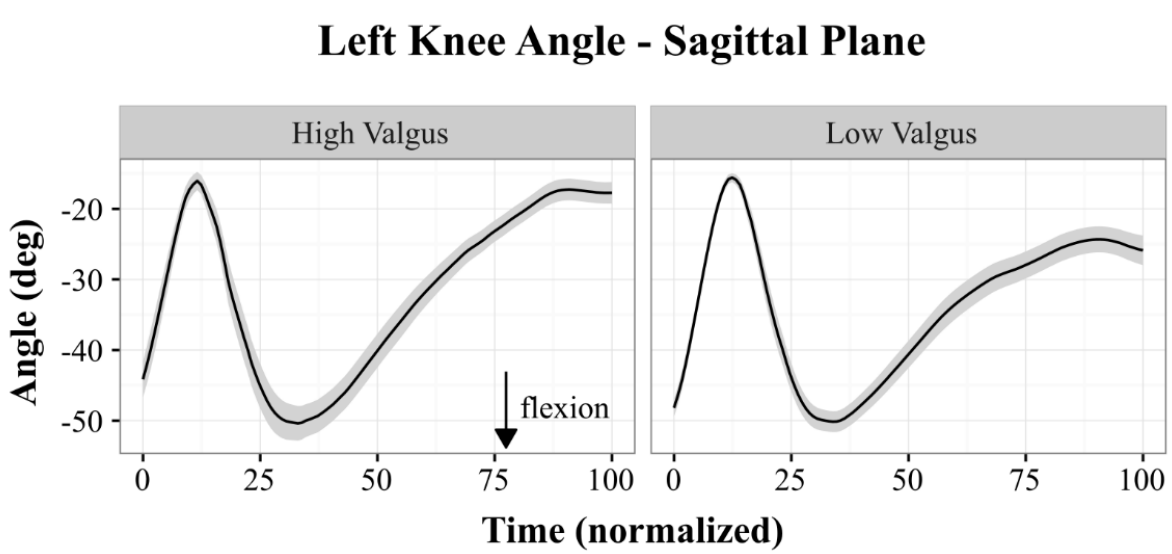
Left Knee Angle - Sagittal Plane
High Valgus
Low Valgus
Angle (deg)
-20
-30
-40
-50
flexion
0
25
50
75
100
Time (normalized)

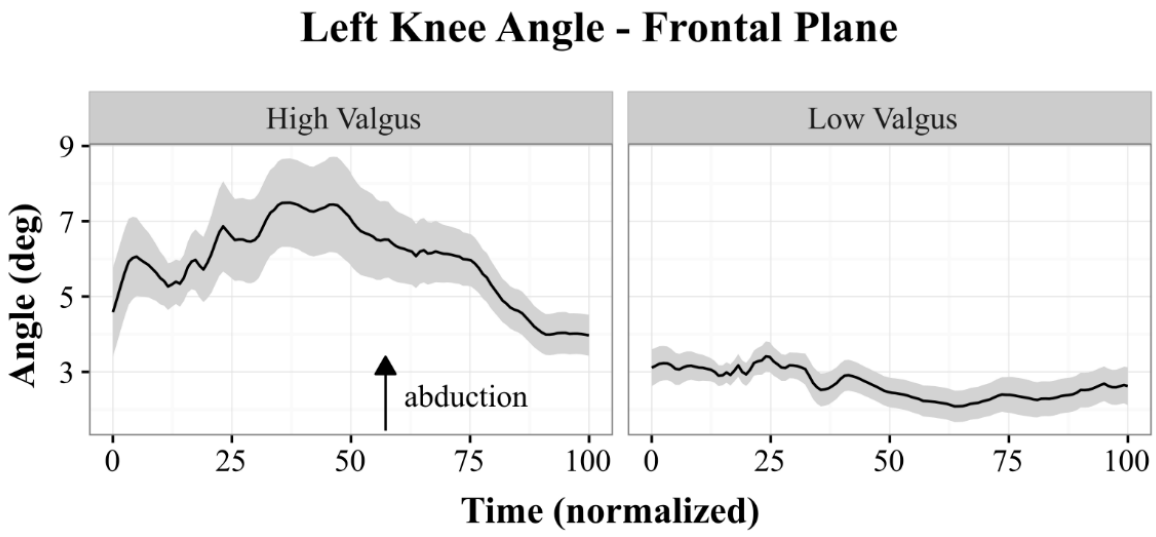
Left Knee Angle - Frontal Plane
High Valgus
Low Valgus
Angle (deg)
9
7
5
3
abduction
0
25
50
75
100
Time (normalized)

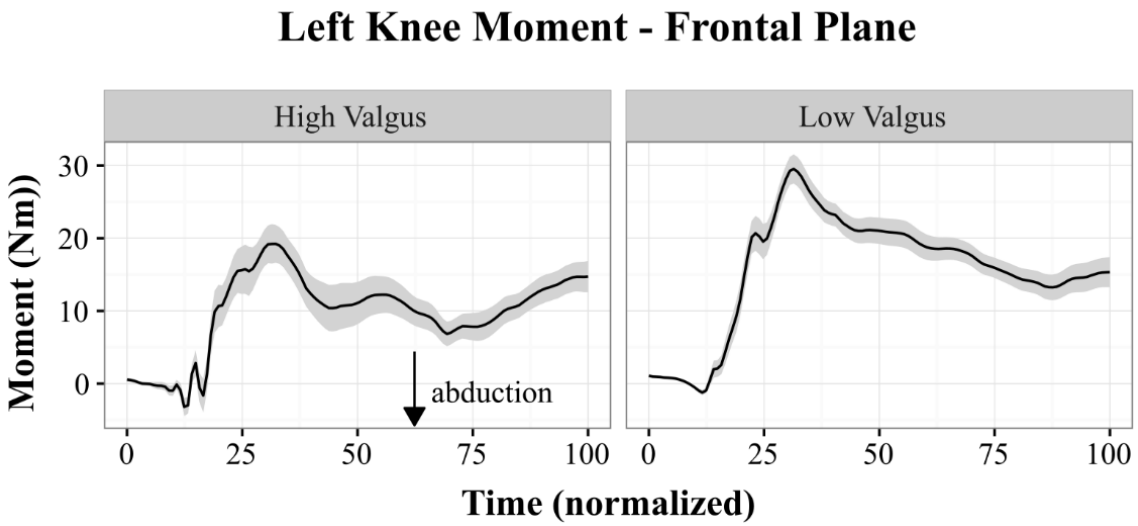
Left Knee Moment - Frontal Plane
High Valgus
Low Valgus
Moment (Nm))
30
20
10
0
abduction
0
25
50
75
100
Time (normalized)

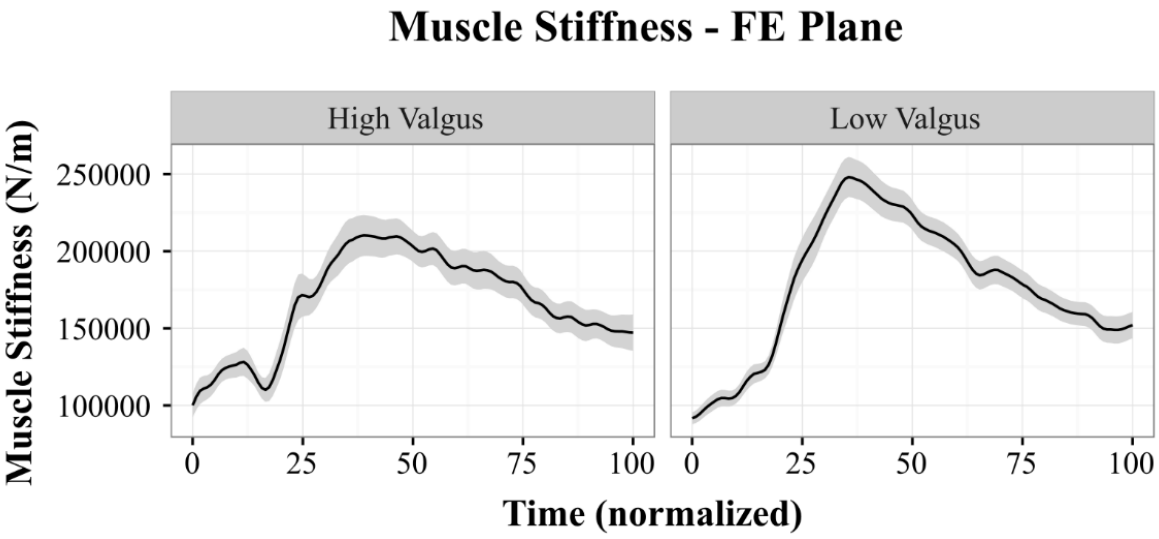
Muscle Stiffness - FE Plane
High Valgus
Low Valgus
Muscle Stiffness (N/m)
250000
200000
150000
100000
0
25
50
75
100
Time (normalized)

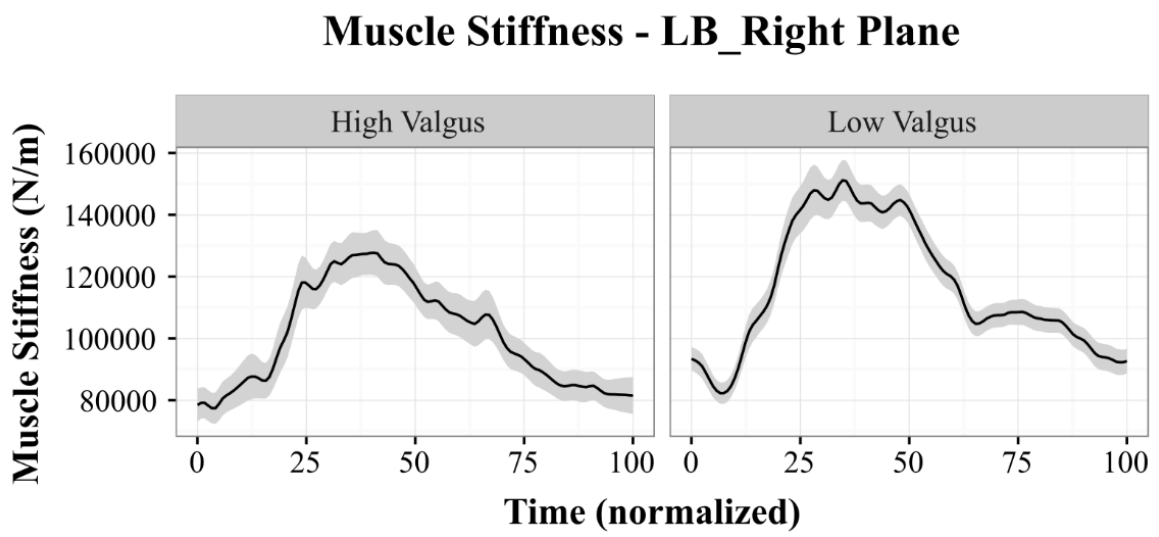
Muscle Stiffness - LB_Right Plane
High Valgus
Low Valgus
Muscle Stiffness (N/m)
160000
140000
120000
100000
80000
0
25
50
75
100
Time (normalized)

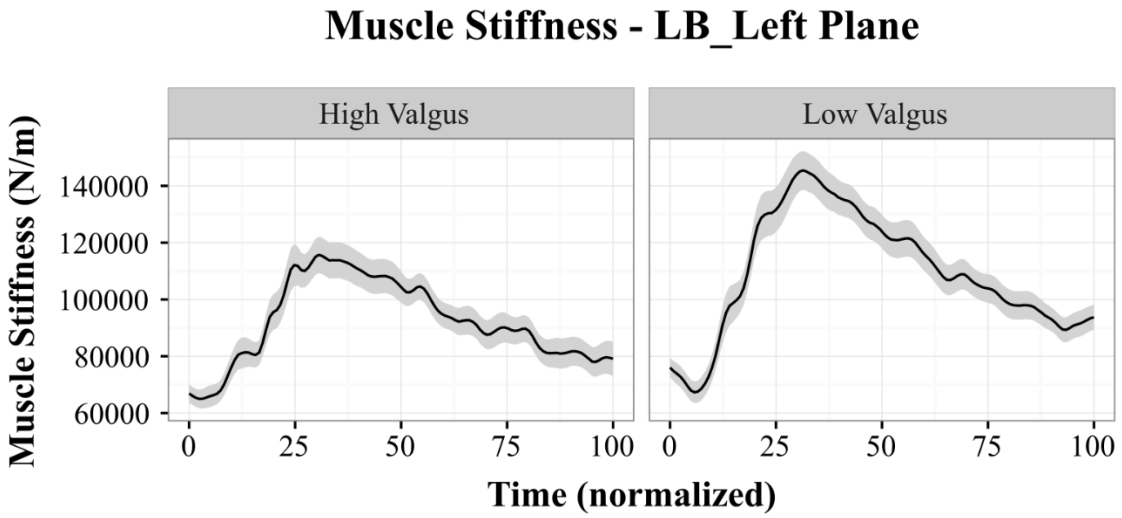
Muscle Stiffness - LB_Left Plane
High Valgus
Low Valgus
Muscle Stiffness (N/m)
140000
120000
100000
80000
60000
0
25
50
75
100
Time (normalized)

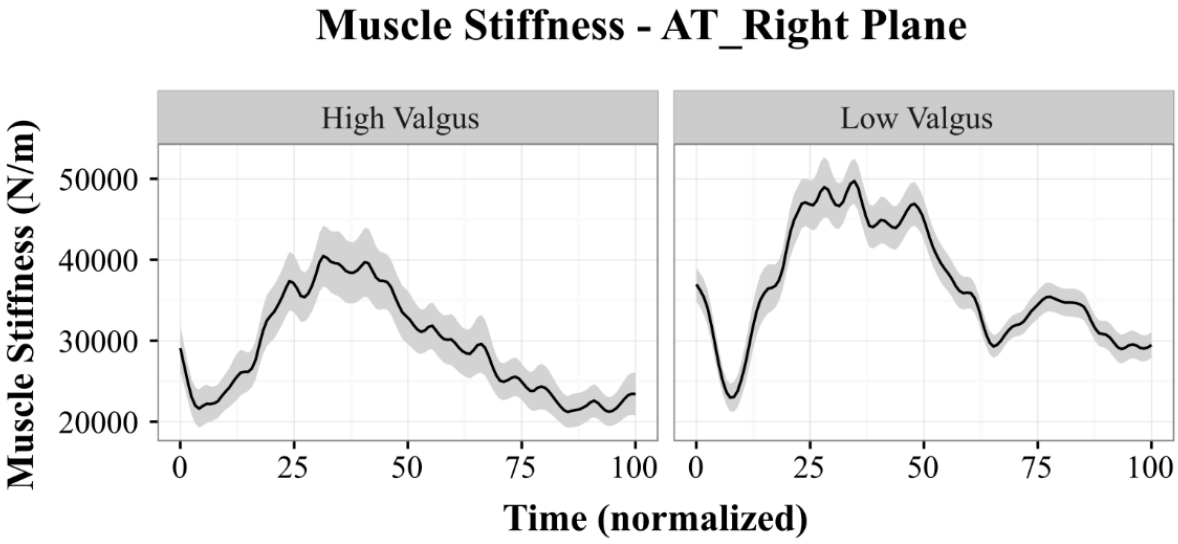
Muscle Stiffness - AT_Right Plane
High Valgus
Low Valgus
Muscle Stiffness (N/m)
50000
40000
30000
20000
0
25
50
75
100
Time (normalized)

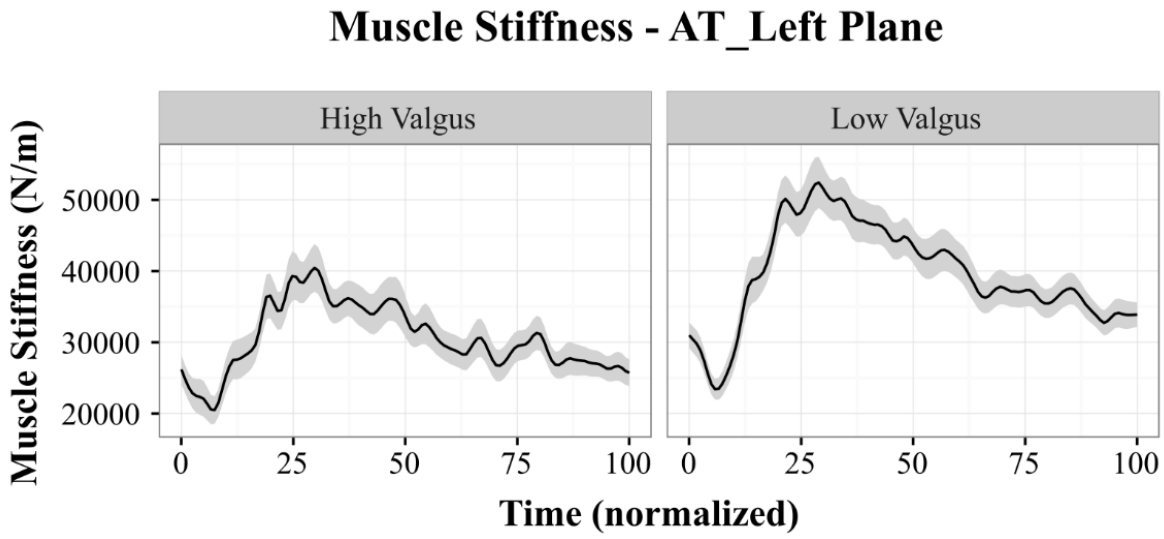
Muscle Stiffness - AT_Left Plane
High Valgus
Low Valgus
Muscle Stiffness (N/m)
50000
40000
30000
20000
0
25
50
75
100
Time (normalized)

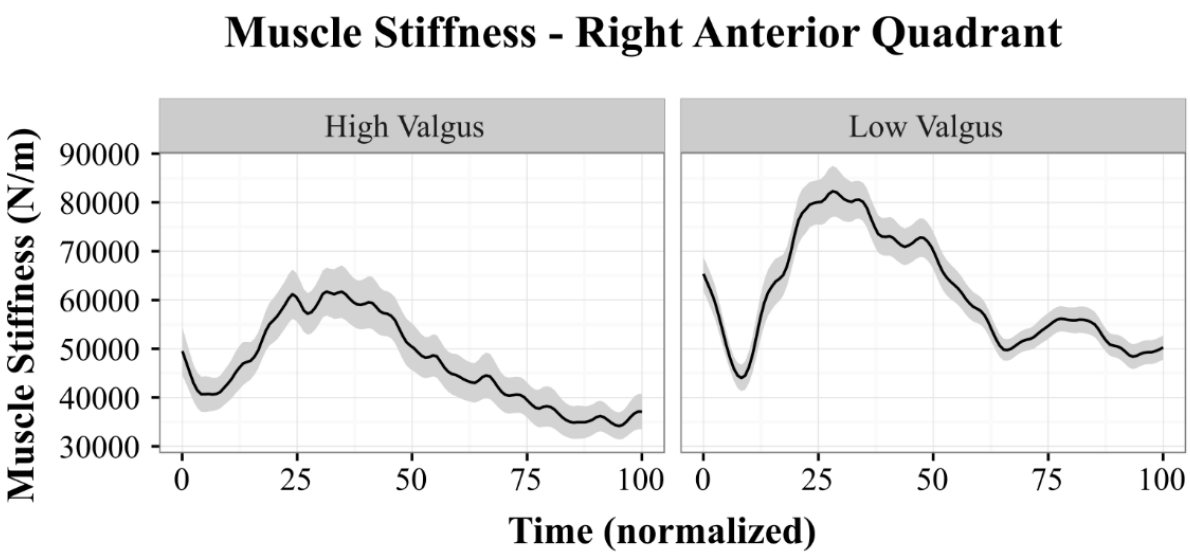
Muscle Stiffness - Right Anterior Quadrant
High Valgus
Low Valgus
Muscle Stiffness (N/m)
90000
80000
70000
60000
50000
40000
30000
0
25
50
75
100
Time (normalized)

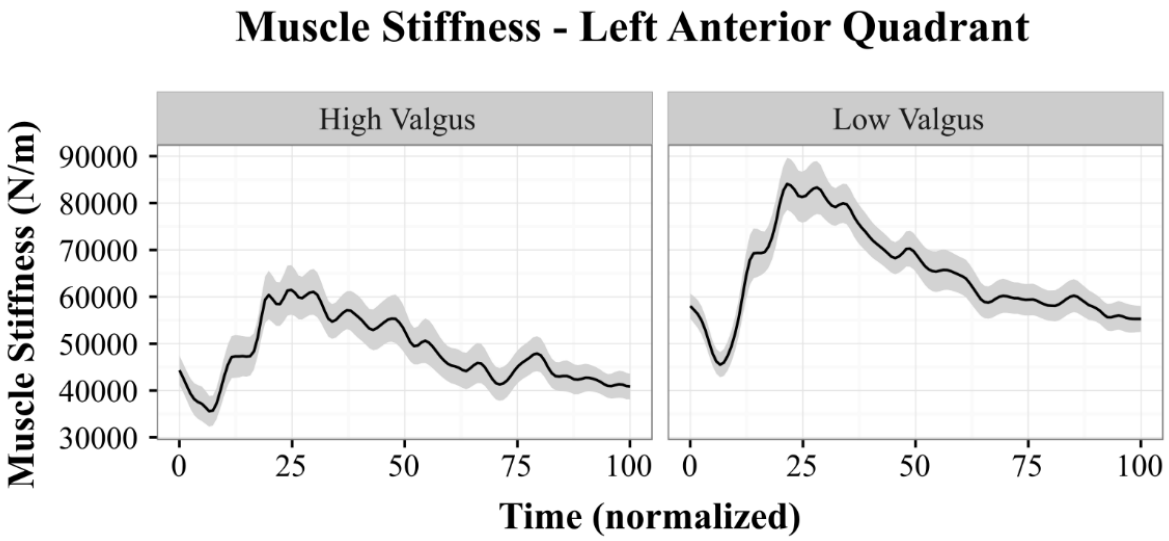
Muscle Stiffness - Left Anterior Quadrant
High Valgus
Low Valgus
Muscle Stiffness (N/m)
90000
80000
70000
60000
50000
40000
30000
0
25
50
75
100
Time (normalized)

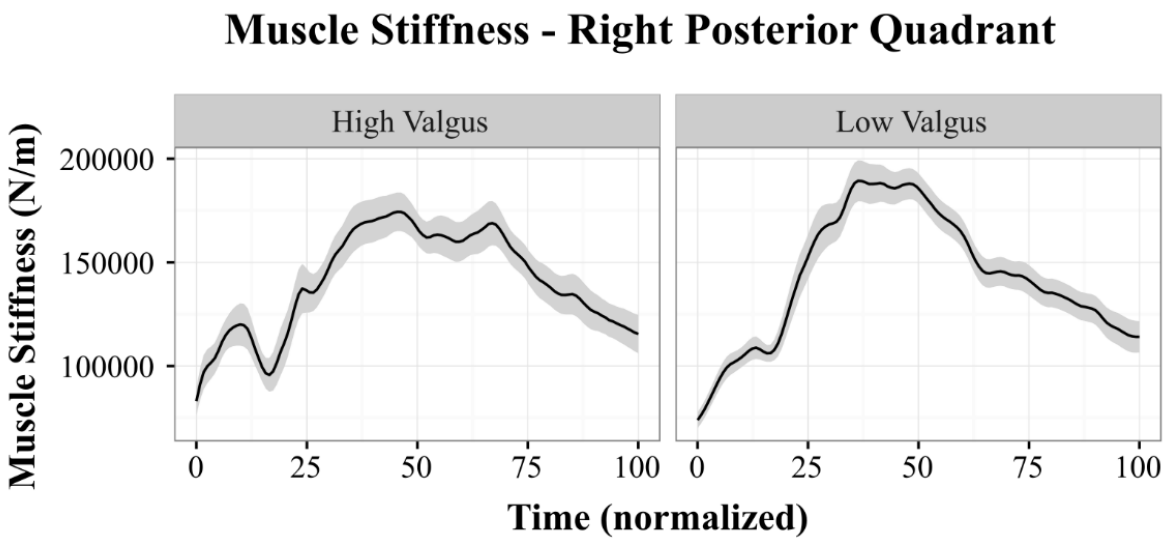
Muscle Stiffness - Right Posterior Quadrant
High Valgus
Low Valgus
Muscle Stiffness (N/m)
200000
150000
100000
0
25
50
75
100
Time (normalized)

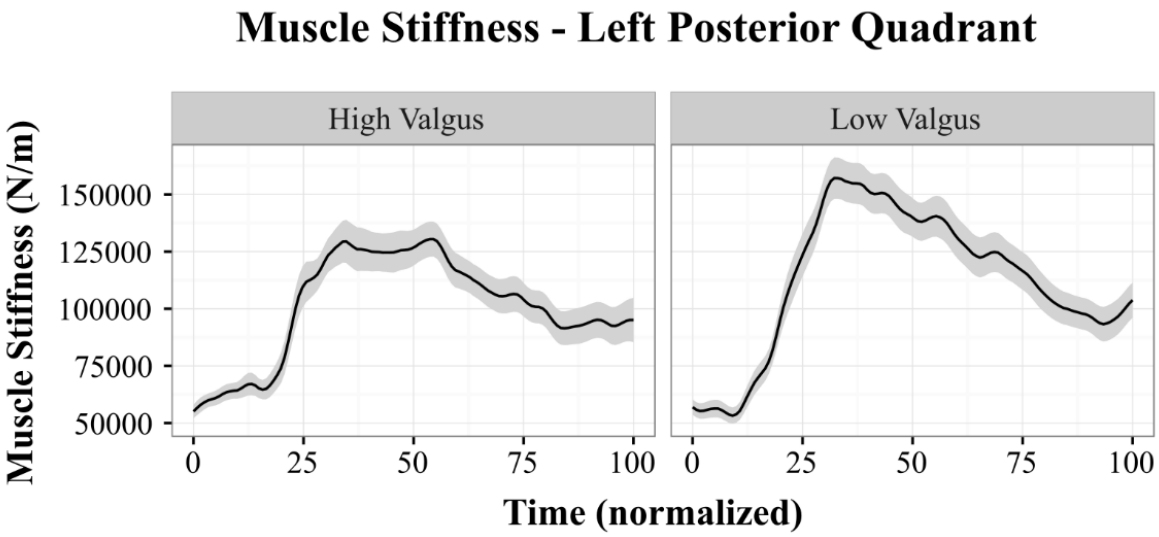
Muscle Stiffness - Left Posterior Quadrant
High Valgus
Low Valgus
Muscle Stiffness (N/m)
150000
125000
100000
75000
50000
0
25
50
75
100
Time (normalized)

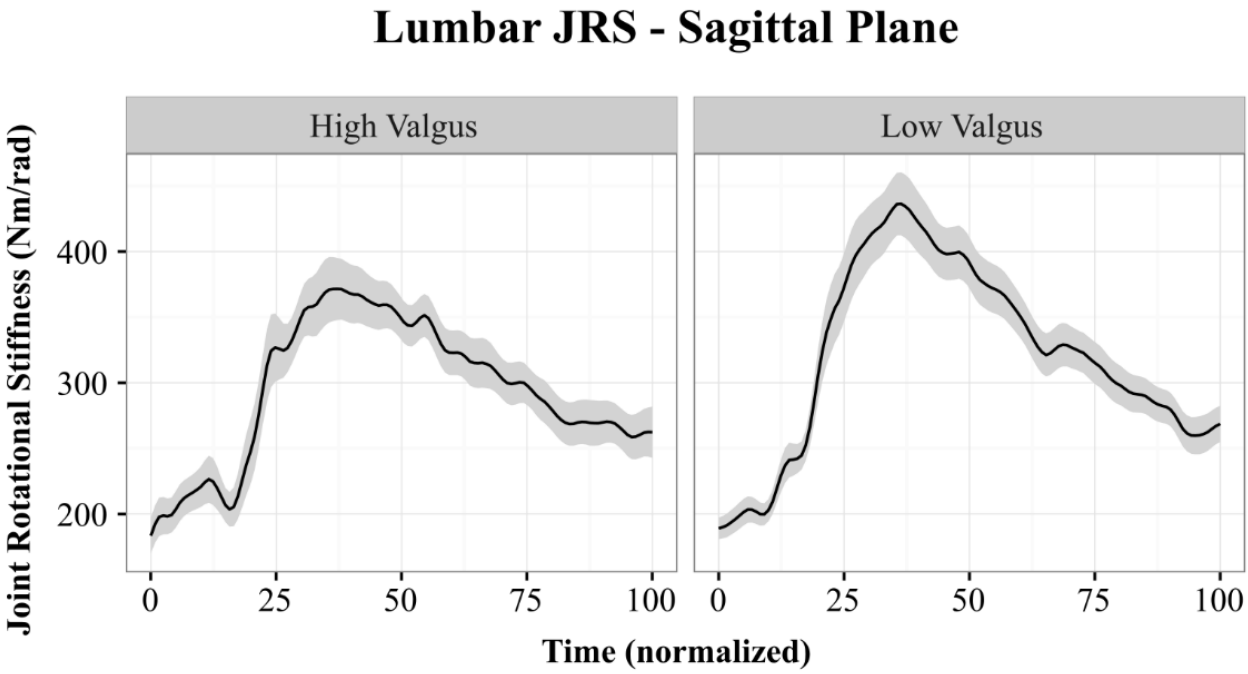
Lumbar JRS - Sagittal Plane
High Valgus
Low Valgus
Joint Rotational Stiffness (Nm/rad)
400
300
200
0
25
50
75
100
Time (normalized)

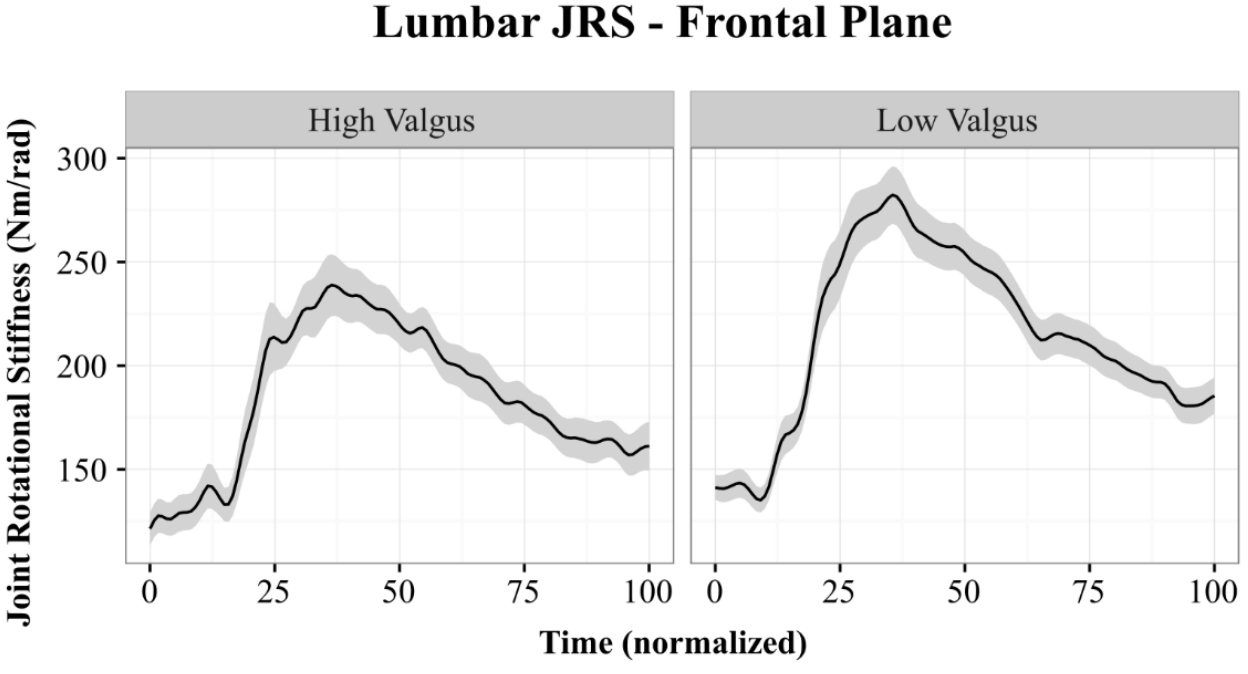
Lumbar JRS - Frontal Plane
High Valgus
Low Valgus
Joint Rotational Stiffness (Nm/rad)
300
250
200
150
0
25
50
75
100
Time (normalized)

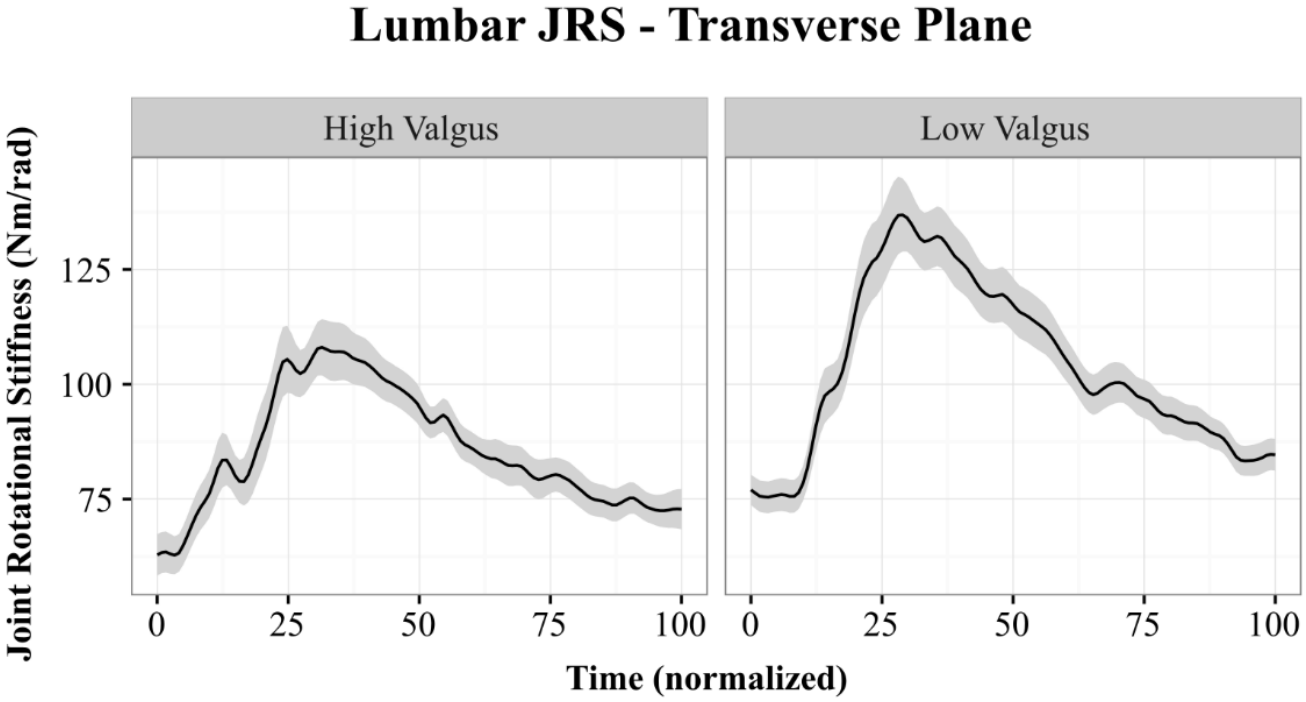
Lumbar JRS - Transverse Plane
High Valgus
Low Valgus
Joint Rotational Stiffness (Nm/rad)
125
100
75
0
25
50
75
100
Time (normalized)

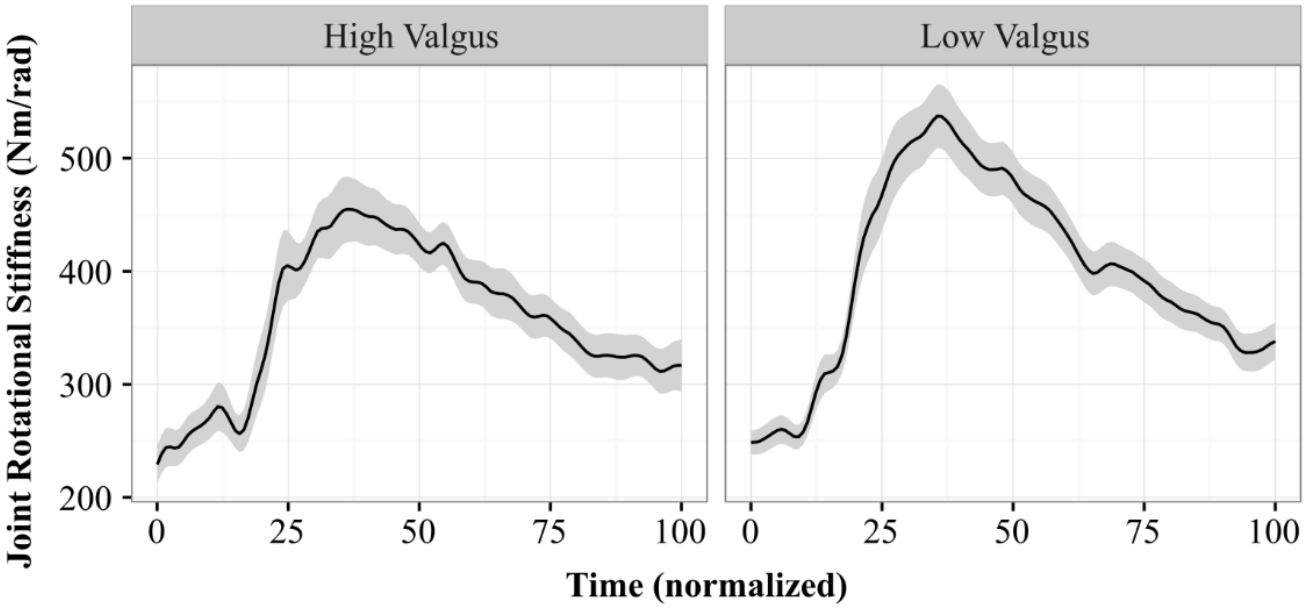
Lumbar JRS - Euc Norm
High Valgus
Low Valgus
Joint Rotational Stiffness (Nm/rad)
500
400
300
200
0
25
50
75
100
Time (normalized)

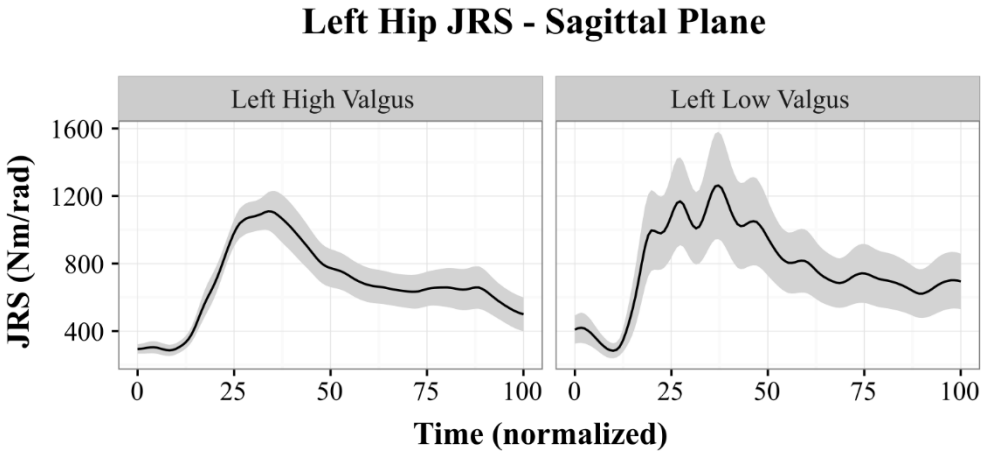
Left Hip JRS - Sagittal Plane
Left High Valgus
Left Low Valgus
JRS (Nm/rad)
1600
1200
800
400
0
25
50
75
100
Time (normalized)

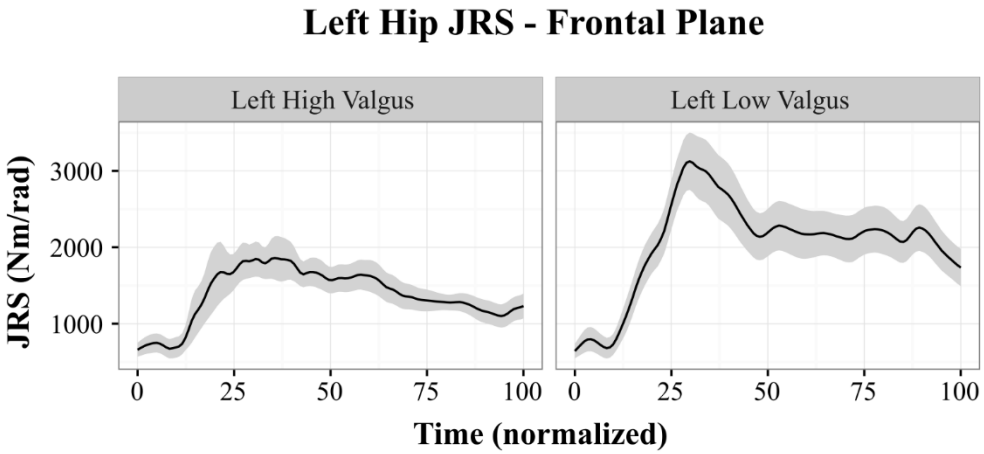
Left Hip JRS - Frontal Plane
Left High Valgus
Left Low Valgus
JRS (Nm/rad)
3000
2000
1000
0
25
50
75
100
Time (normalized)

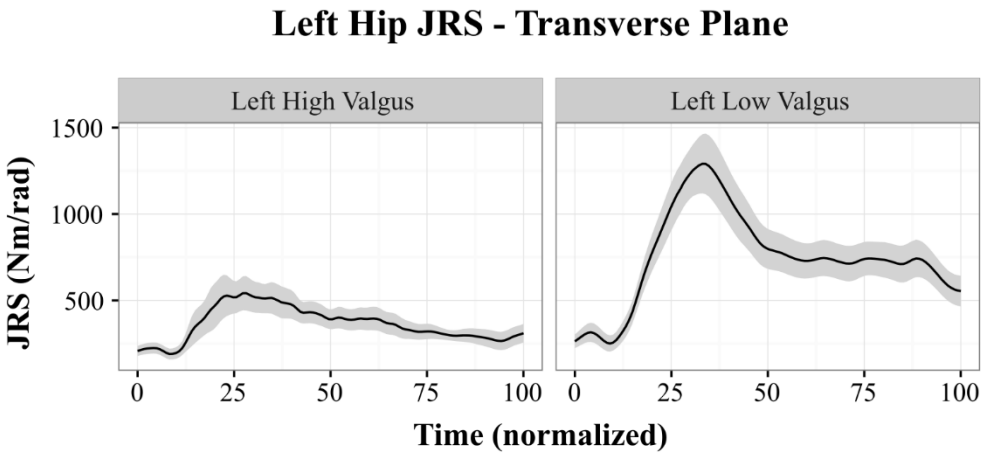
Left Hip JRS - Transverse Plane
Left High Valgus
Left Low Valgus
JRS (Nm/rad)
1500
1000
500
0
25
50
75
100
Time (normalized)

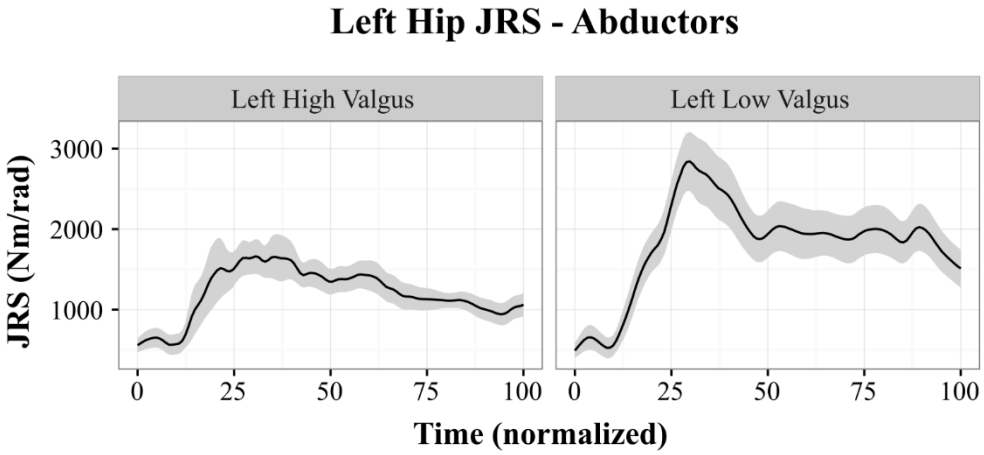
Left Hip JRS - Abductors
Left High Valgus
Left Low Valgus
JRS (Nm/rad)
3000
2000
1000
0
25
50
75
100
Time (normalized)

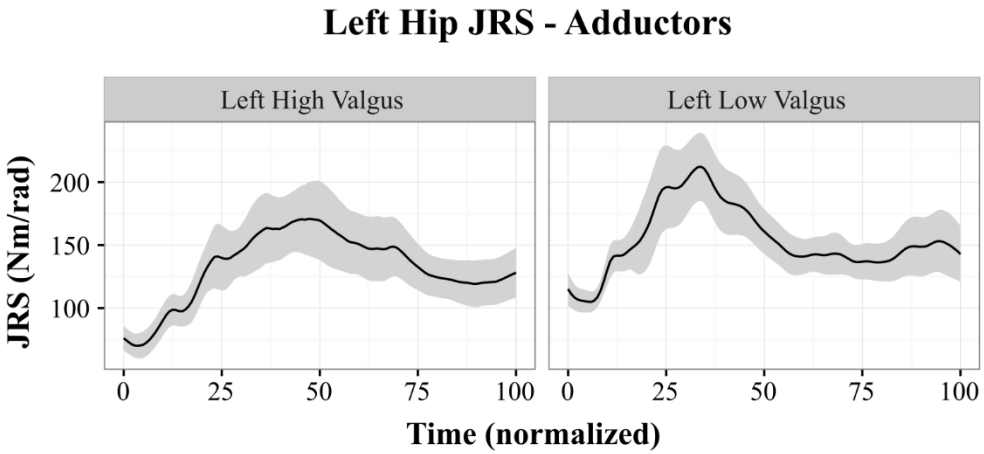
Left Hip JRS - Adductors
Left High Valgus
Left Low Valgus
JRS (Nm/rad)
200
150
100
0
25
50
75
100
Time (normalized)

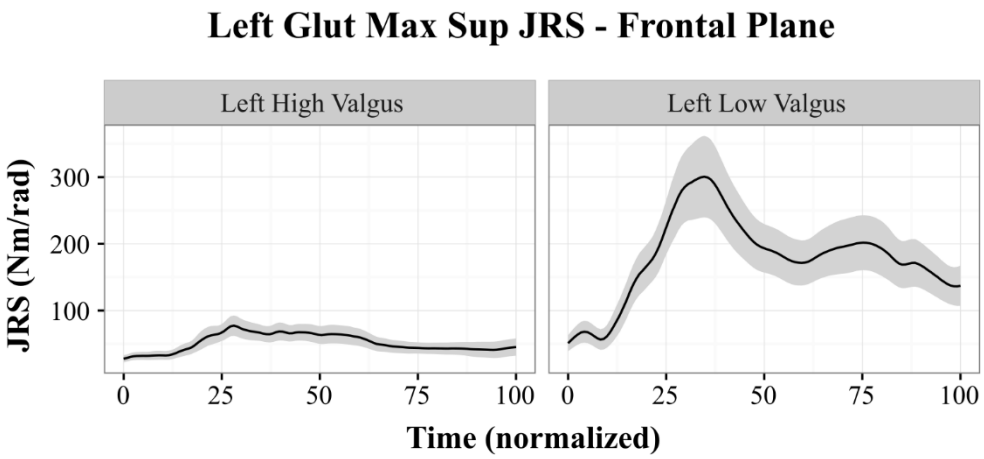
Left Glut Max Sup JRS - Frontal Plane
Left High Valgus
Left Low Valgus
JRS (Nm/rad)
300
200
100
0
25
50
75
100
Time (normalized)

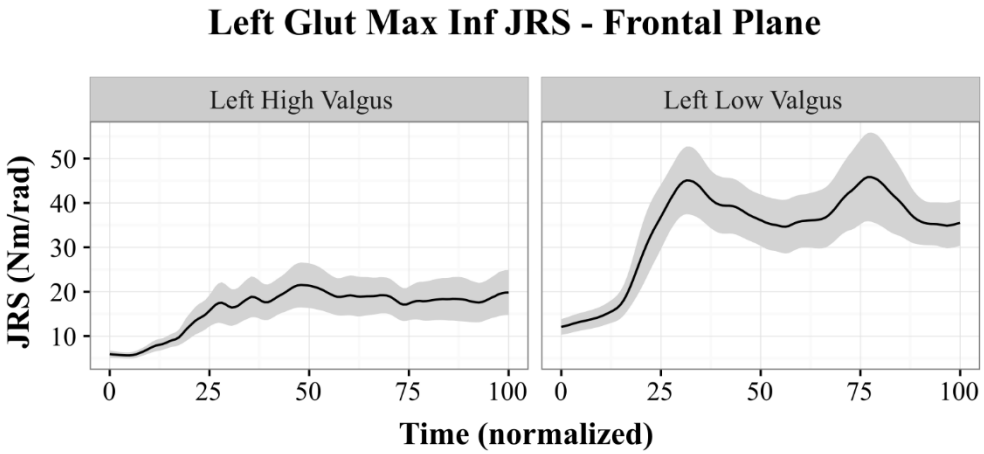
Left Glut Max Inf JRS - Frontal Plane
Left High Valgus
Left Low Valgus
JRS (Nm/rad)
50
40
30
20
10
0
25
50
75
100
Time (normalized)

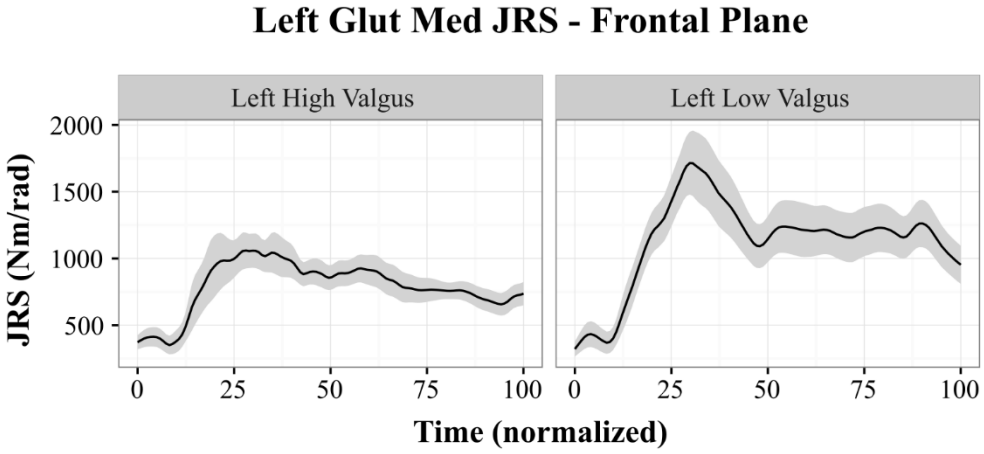
Left Glut Med JRS - Frontal Plane
Left High Valgus
Left Low Valgus
JRS (Nm/rad)
2000
1500
1000
500
0
25
50
75
100
Time (normalized)

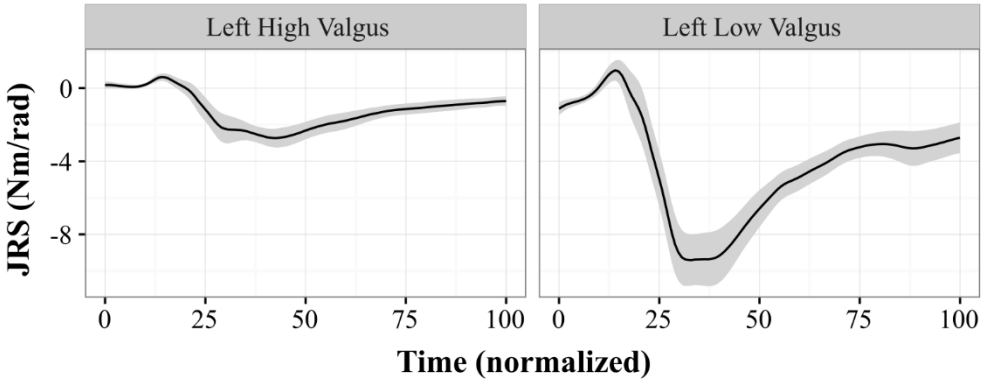
Left TFL JRS - Frontal Plane
Left High Valgus
Left Low Valgus
JRS (Nm/rad)
0
-4
-8
0
25
50
75
100
Time (normalized)

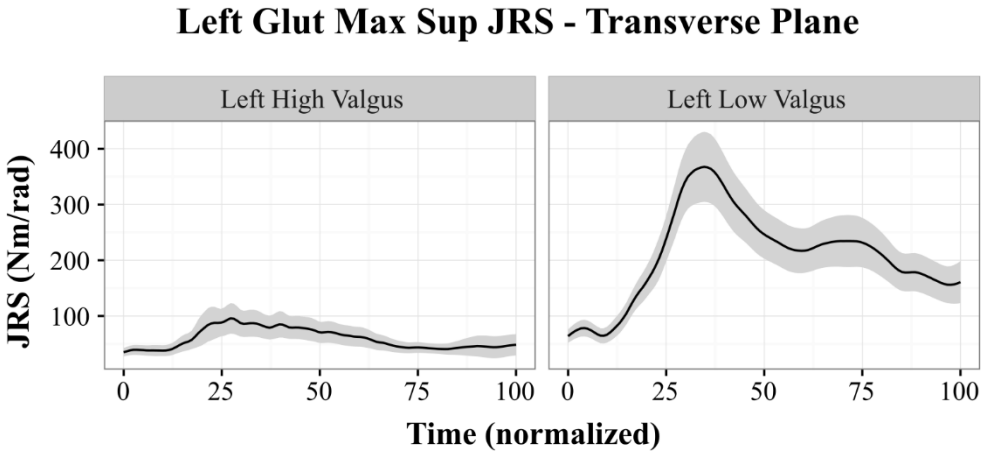
Left Glut Max Sup JRS - Transverse Plane
Left High Valgus
Left Low Valgus
JRS (Nm/rad)
400
300
200
100
0
25
50
75
100
Time (normalized)

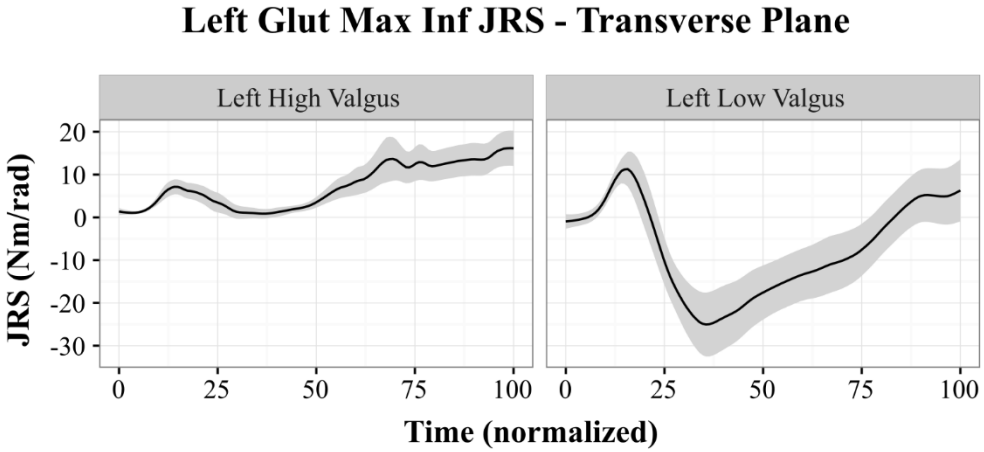
Left Glut Max Inf JRS - Transverse Plane
Left High Valgus
Left Low Valgus
JRS (Nm/rad)
20
10
0
-10
-20
-30
0
25
50
75
100
Time (normalized)

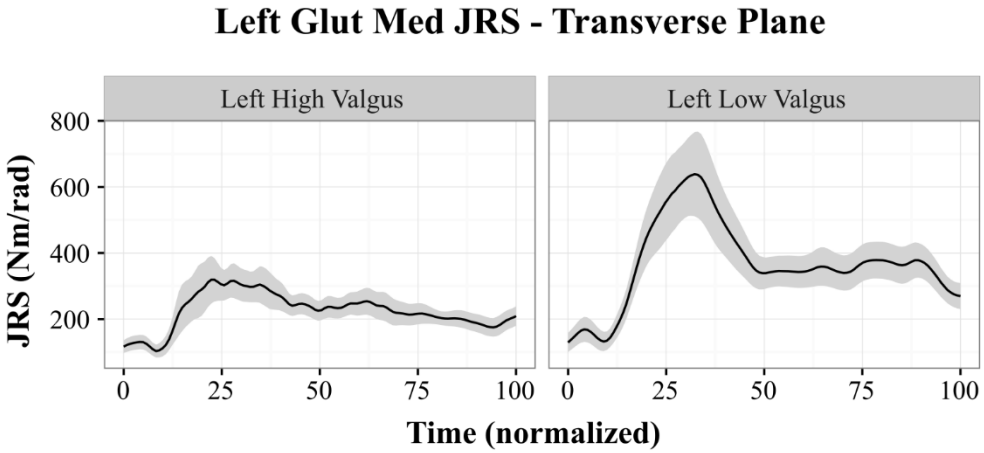
Left Glut Med JRS - Transverse Plane
Left High Valgus
Left Low Valgus
JRS (Nm/rad)
800
600
400
200
0
25
50
75
100
Time (normalized)

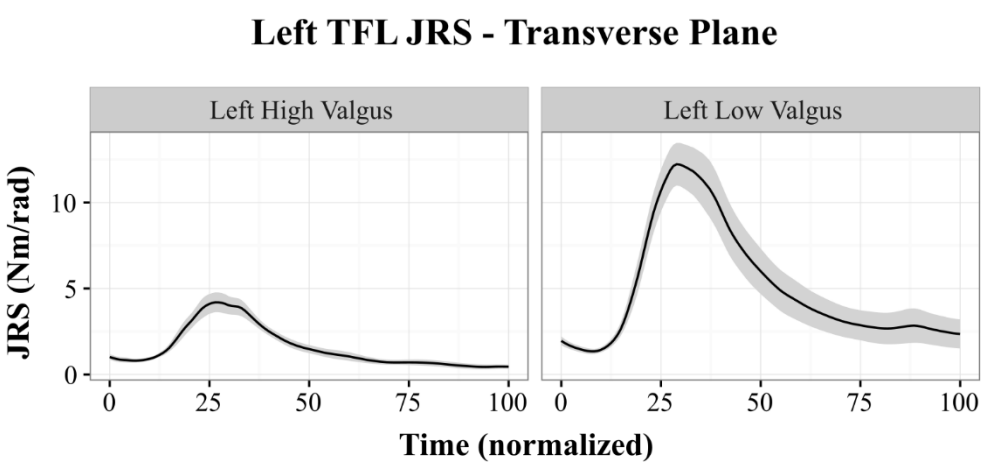
Left TFL JRS - Transverse Plane
Left High Valgus
Left Low Valgus
JRS (Nm/rad)
10
5
0
0
25
50
75
100
Time (normalized)

Single Leg Drop: Land on Right

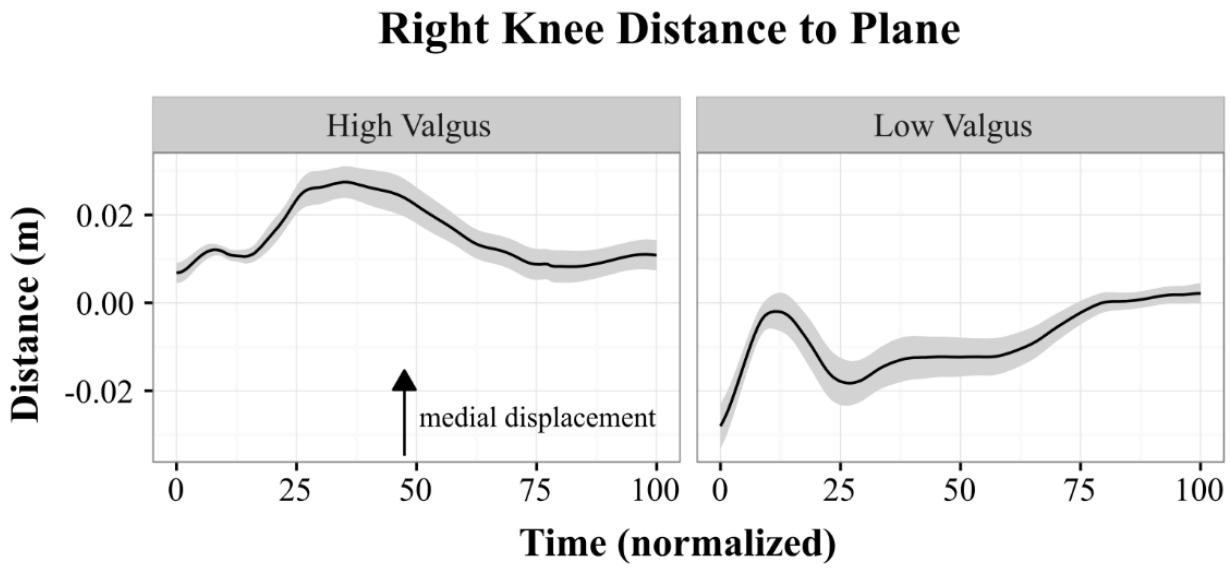

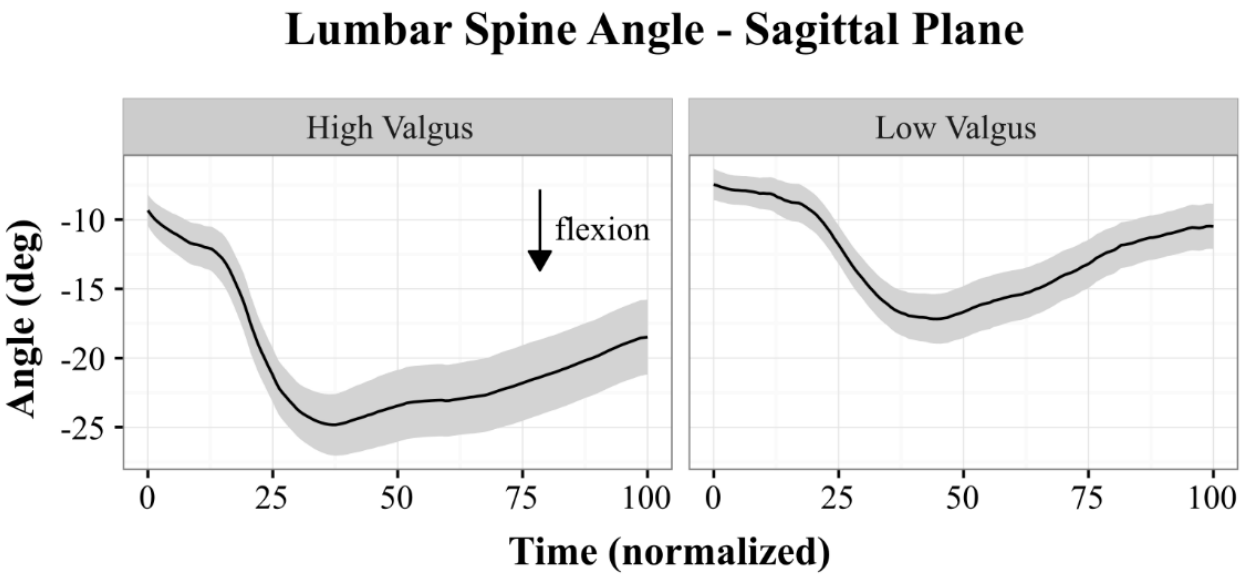
Lumbar Spine Angle - Sagittal Plane
High Valgus
Low Valgus
flexion
Angle (deg)
-10
-15
-20
-25
0
25
50
75
100
Time (normalized)

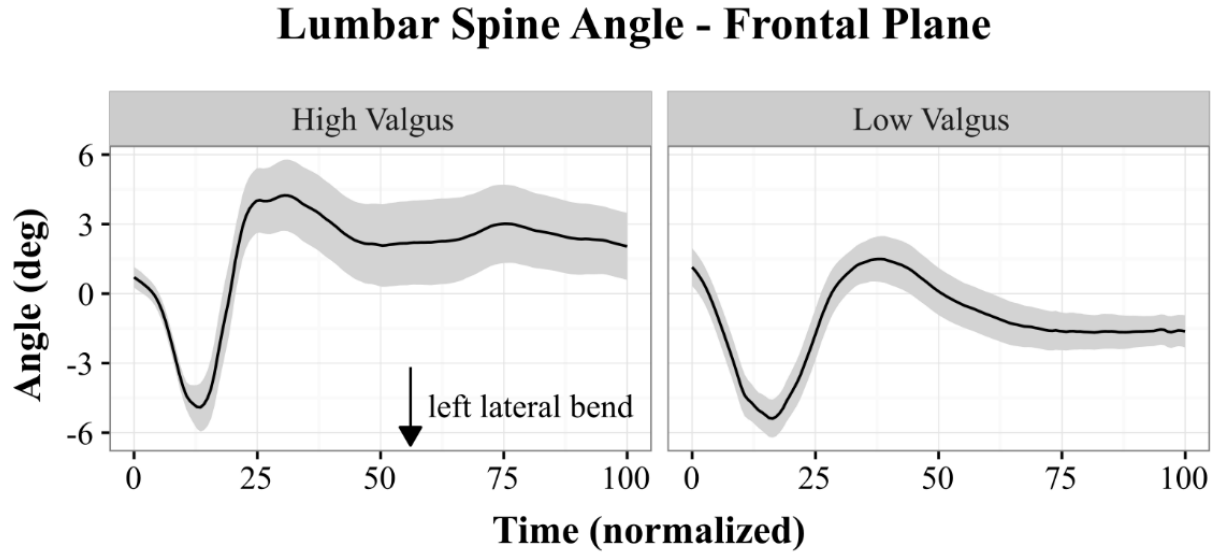
Lumbar Spine Angle - Frontal Plane
High Valgus
Low Valgus
left lateral bend
Angle (deg)
6
3
0
-3
-6
0
25
50
75
100
Time (normalized)

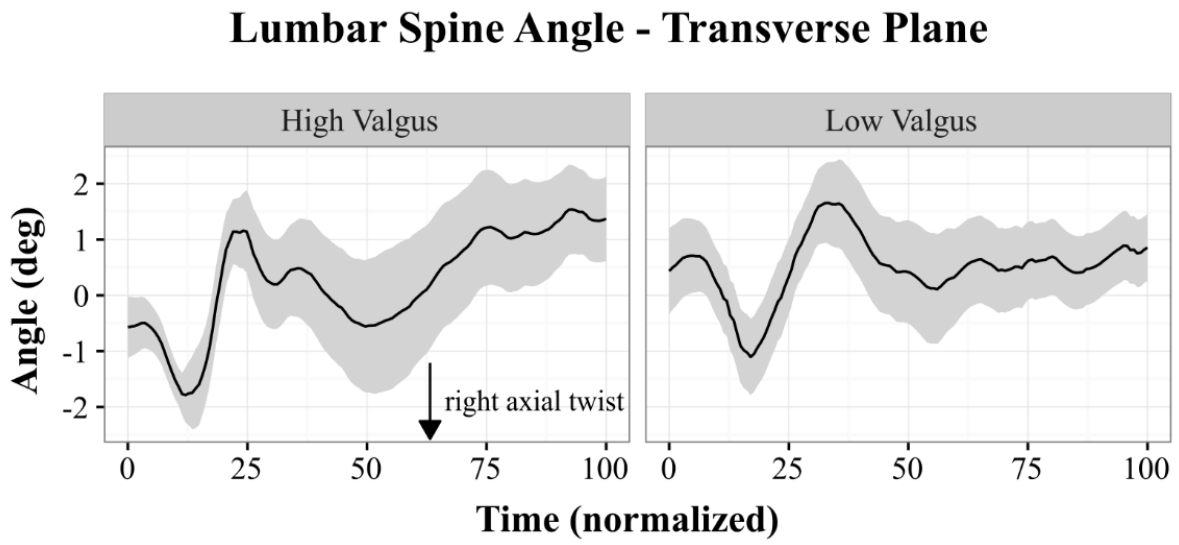
Lumbar Spine Angle - Transverse Plane
High Valgus
Low Valgus
Angle (deg)
2
1
0
-1
-2
right axial twist
0
25
50
75
100
Time (normalized)

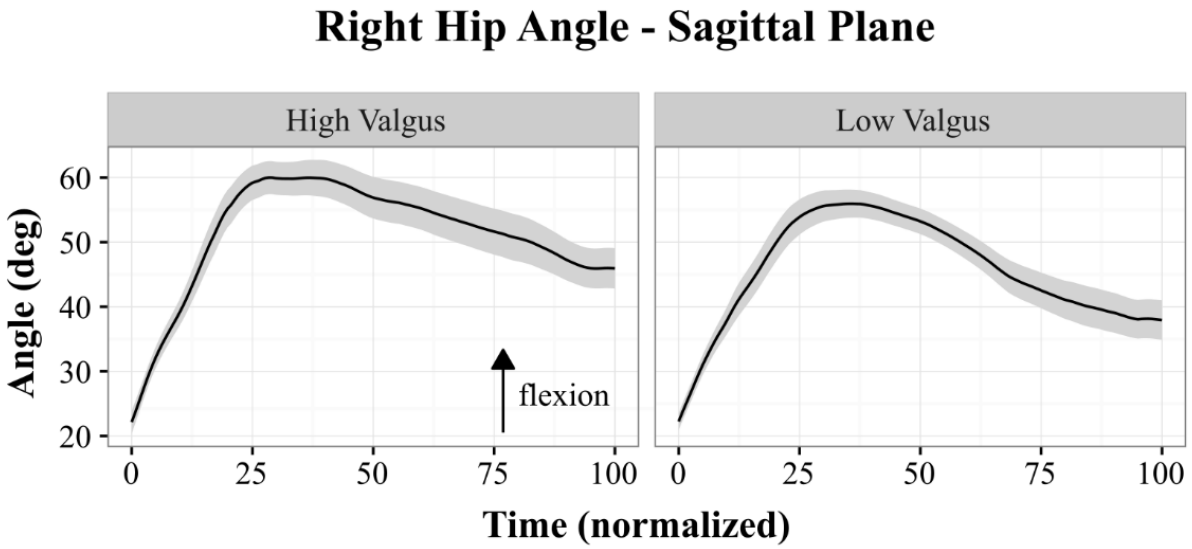
Right Hip Angle - Sagittal Plane
High Valgus
Low Valgus
Angle (deg)
60
50
40
30
20
flexion
0
25
50
75
100
Time (normalized)

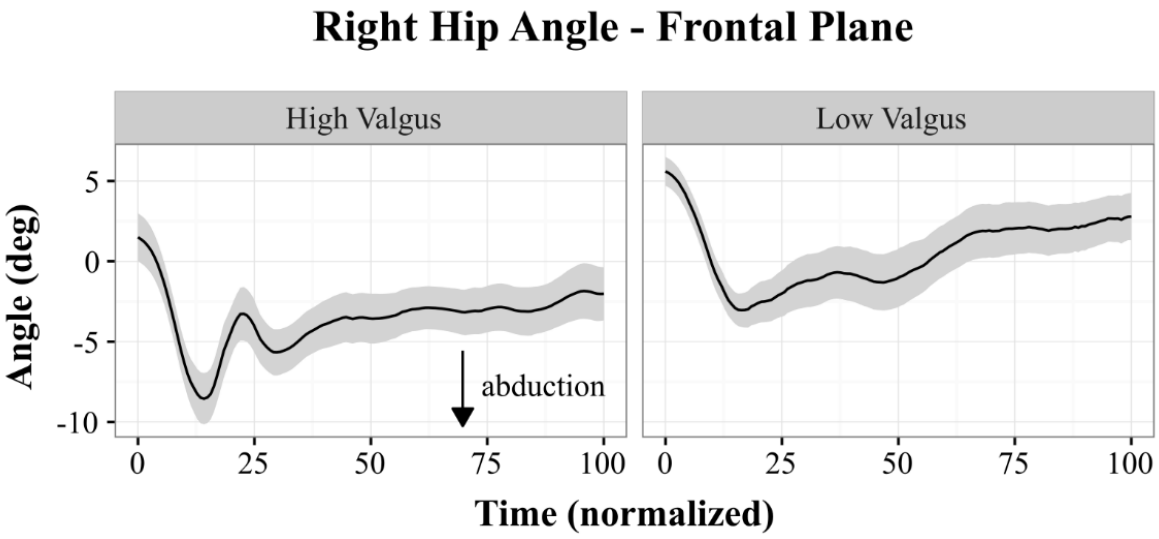
Right Hip Angle - Frontal Plane
High Valgus
Low Valgus
Angle (deg)
5
0
-5
-10
abduction
0
25
50
75
100
Time (normalized)

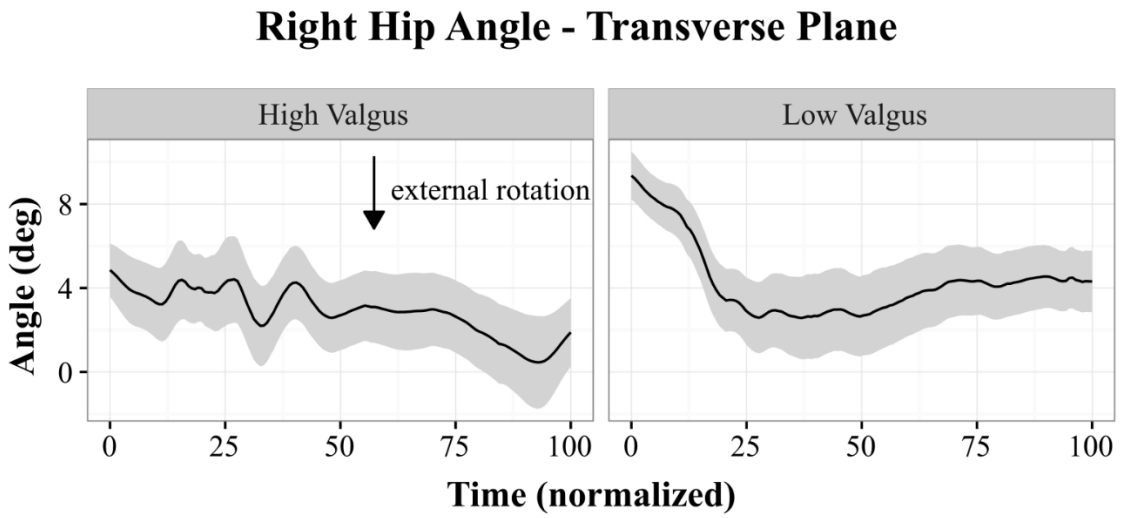
Right Hip Angle - Transverse Plane
High Valgus
Low Valgus
Angle (deg)
8
4
0
external rotation
0
25
50
75
100
Time (normalized)

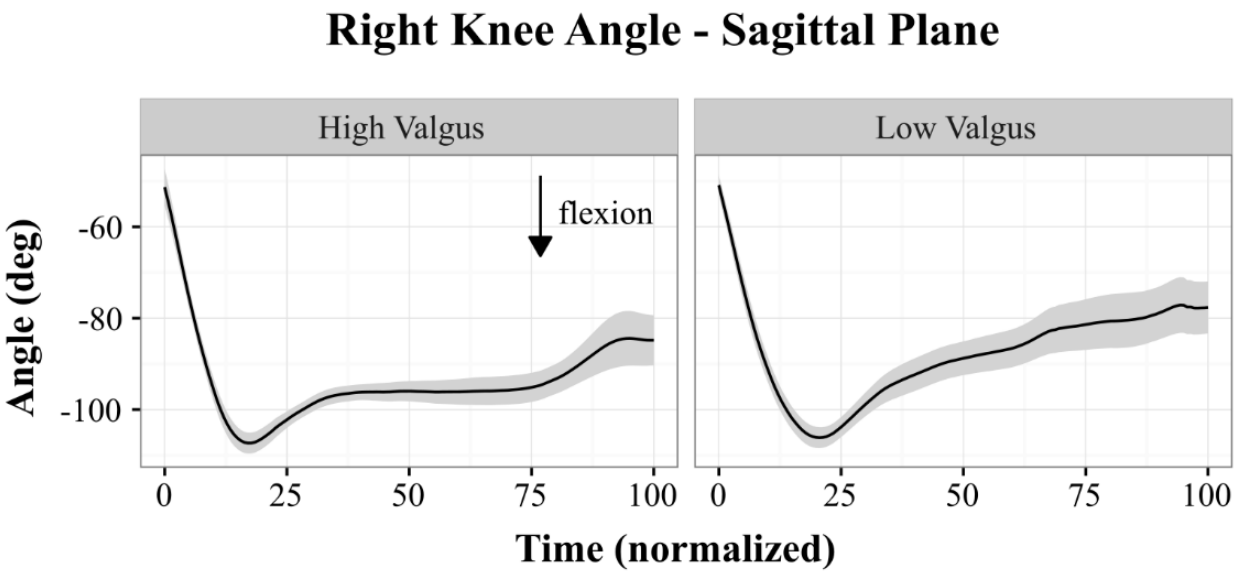
Right Knee Angle - Sagittal Plane
High Valgus
Low Valgus
flexion
Angle (deg)
-60
-80
-100
0
25
50
75
100
Time (normalized)

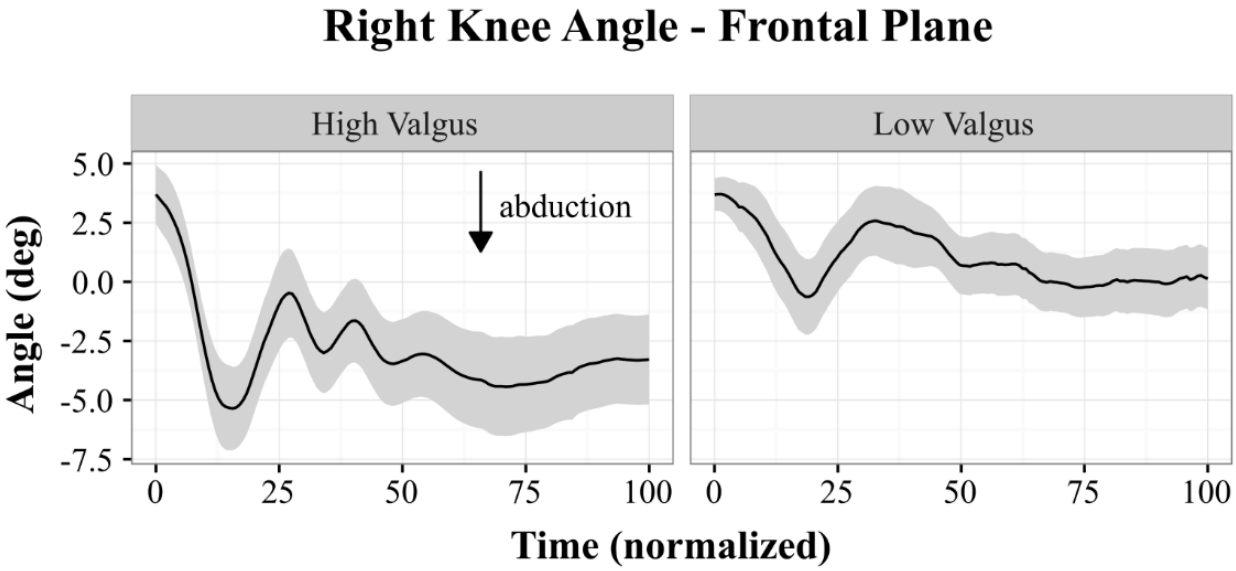
Right Knee Angle - Frontal Plane
High Valgus
Low Valgus
abduction
Angle (deg)
5.0
2.5
0.0
-2.5
-5.0
-7.5
0
25
50
75
100
Time (normalized)

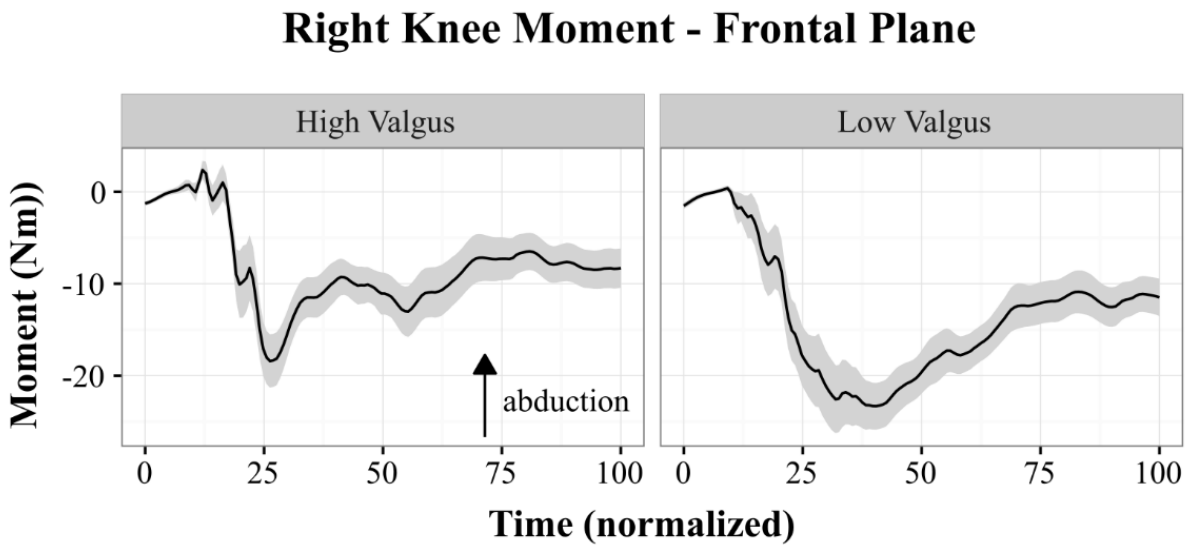
Right Knee Moment - Frontal Plane
High Valgus
Low Valgus
Moment (Nm))
0
-10
-20
abduction
0
25
50
75
100
Time (normalized)

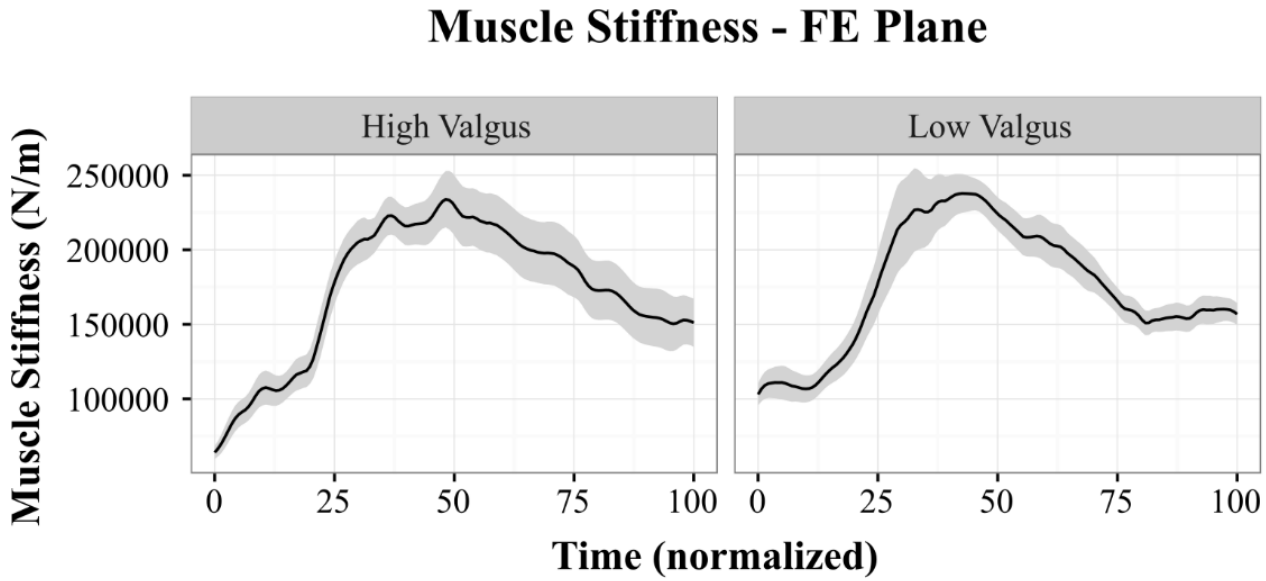
Muscle Stiffness - FE Plane
High Valgus
Low Valgus
Muscle Stiffness (N/m)
250000
200000
150000
100000
0
25
50
75
100
Time (normalized)

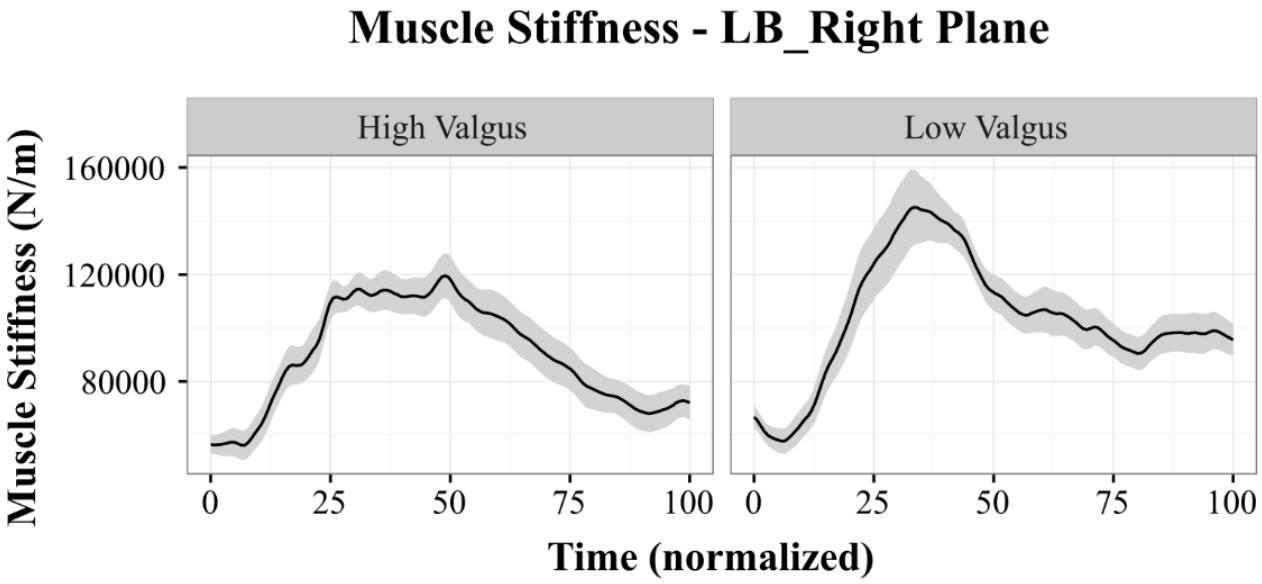
Muscle Stiffness - LB_Right Plane
High Valgus
Low Valgus
Muscle Stiffness (N/m)
160000
120000
80000
0
25
50
75
100
Time (normalized)

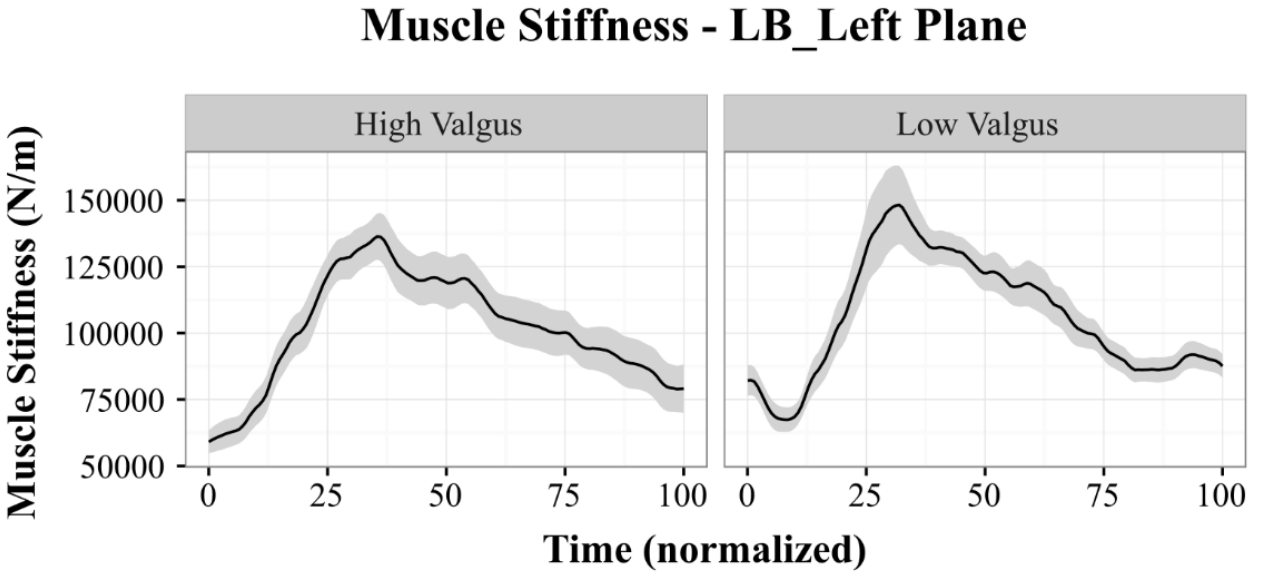
Muscle Stiffness - LB_Left Plane
High Valgus
Low Valgus
Muscle Stiffness (N/m)
150000
125000
100000
75000
50000
0
25
50
75
100
Time (normalized)

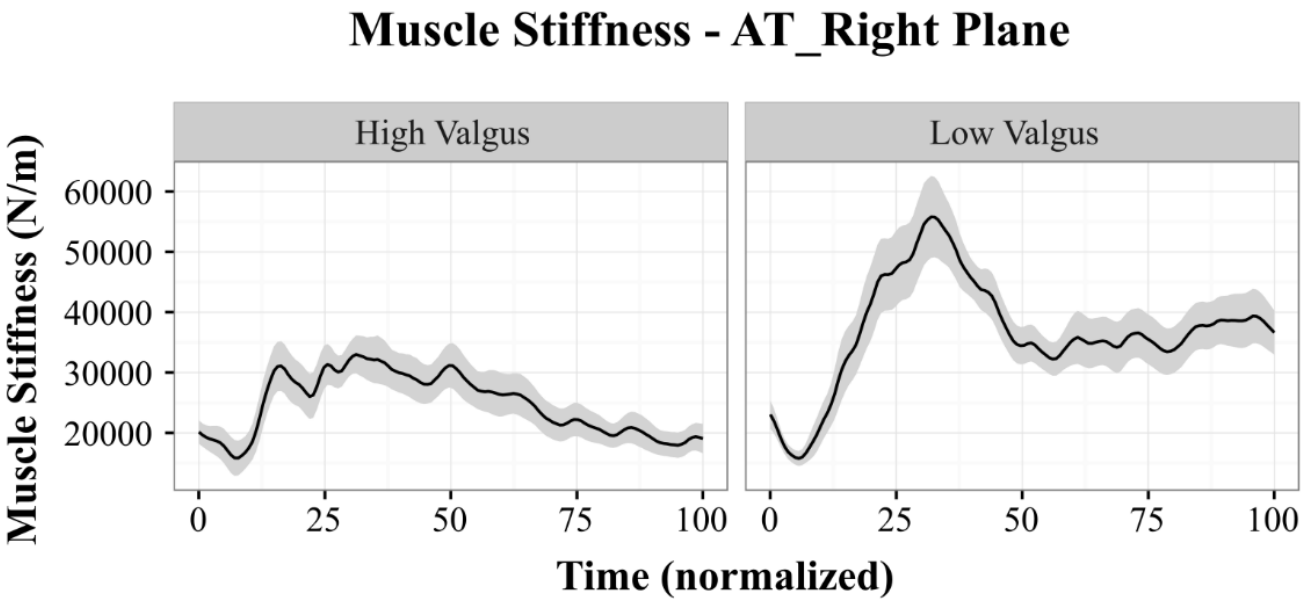
Muscle Stiffness - AT_Right Plane
High Valgus
Low Valgus
Muscle Stiffness (N/m)
60000
50000
40000
30000
20000
0
25
50
75
100
Time (normalized)

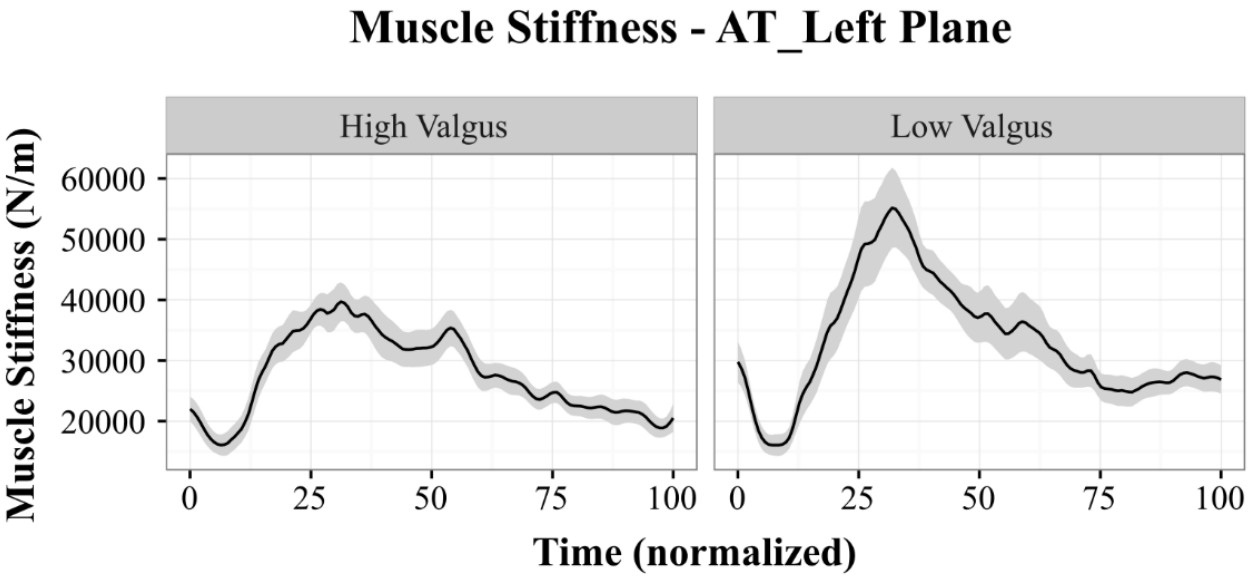
Muscle Stiffness - AT_Left Plane
High Valgus
Low Valgus
Muscle Stiffness (N/m)
60000
50000
40000
30000
20000
0
25
50
75
100
Time (normalized)

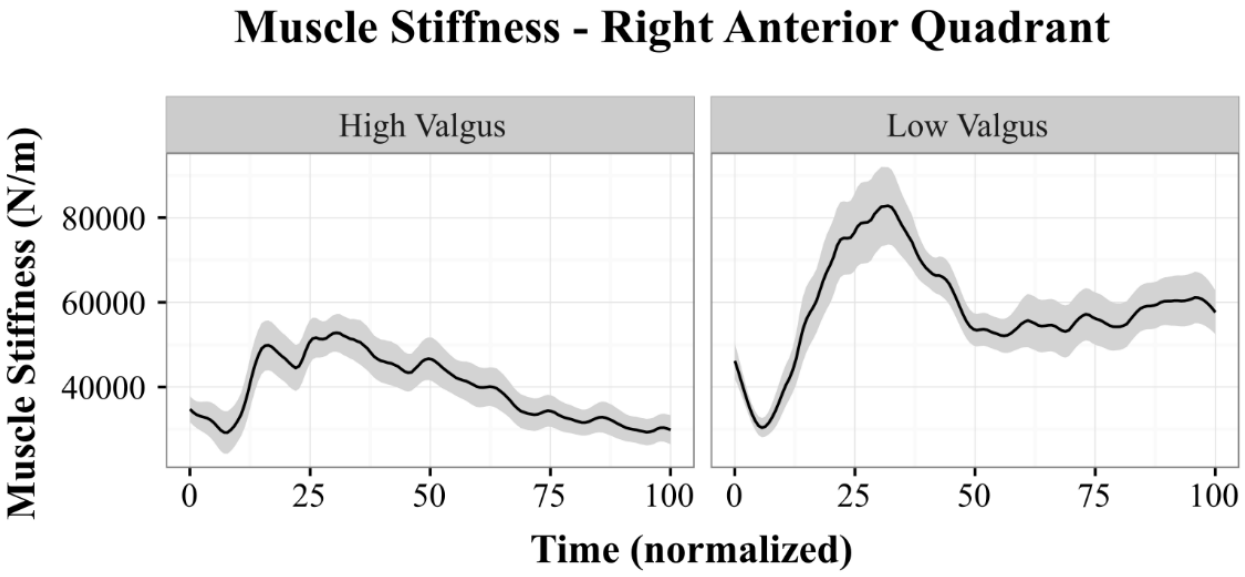
Muscle Stiffness - Right Anterior Quadrant
High Valgus
Low Valgus
Muscle Stiffness (N/m)
80000
60000
40000
0
25
50
75
100
Time (normalized)

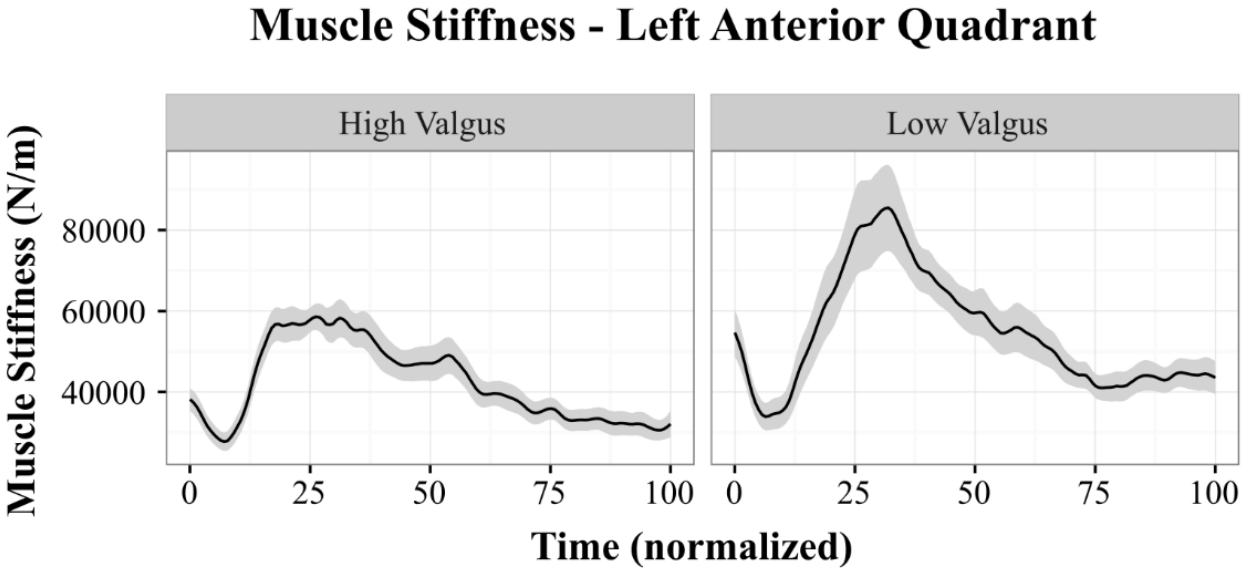
Muscle Stiffness - Left Anterior Quadrant
High Valgus
Low Valgus
Muscle Stiffness (N/m)
80000
60000
40000
0
25
50
75
100
Time (normalized)

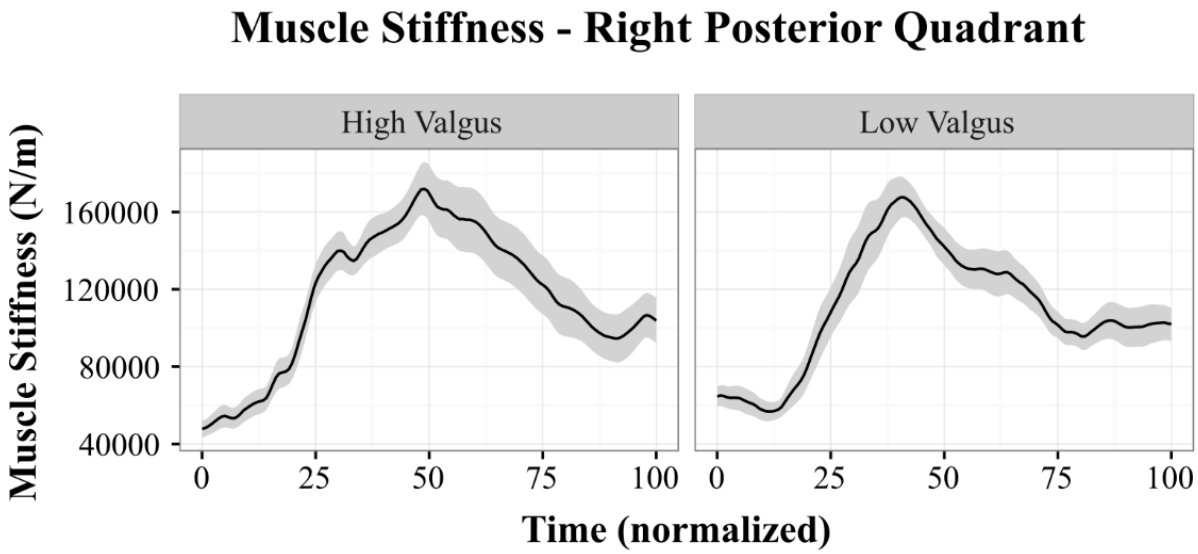
Muscle Stiffness - Right Posterior Quadrant
High Valgus
Low Valgus
Muscle Stiffness (N/m)
160000
120000
80000
40000
0
25
50
75
100
Time (normalized)

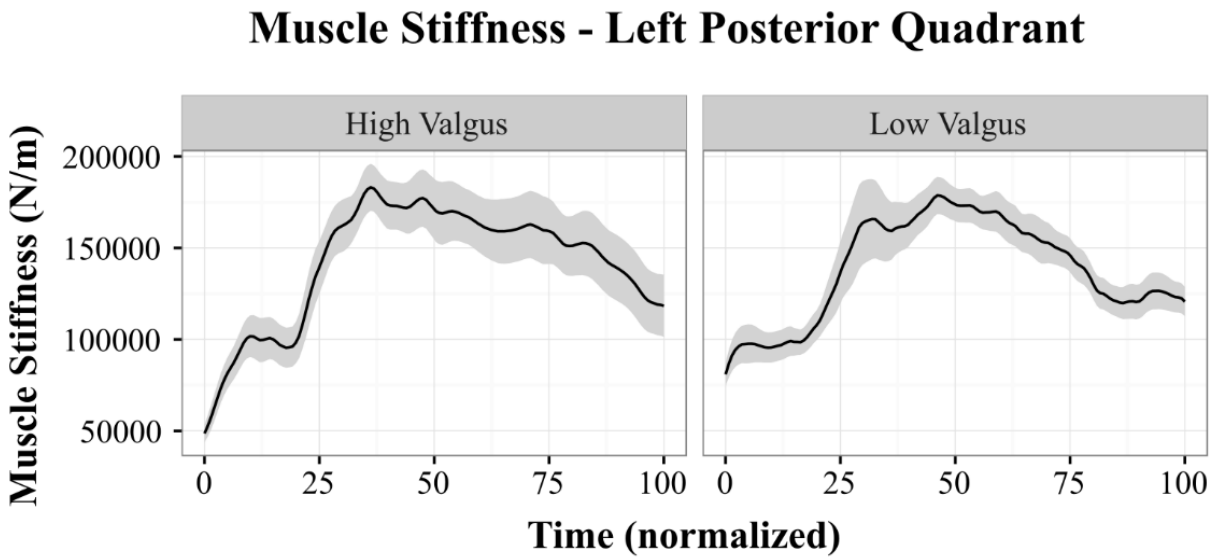
Muscle Stiffness - Left Posterior Quadrant
High Valgus
Low Valgus
Muscle Stiffness (N/m)
200000
150000
100000
50000
0
25
50
75
100
Time (normalized)

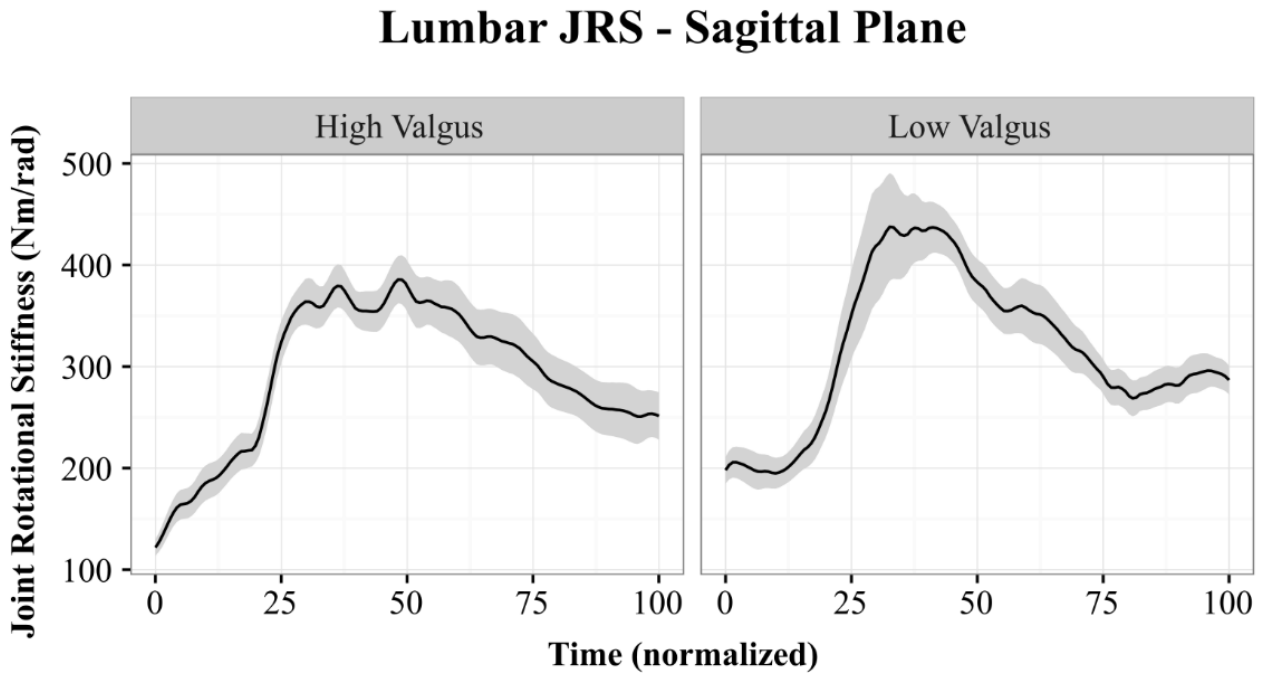
Lumbar JRS - Sagittal Plane
High Valgus
Low Valgus
Joint Rotational Stiffness (Nm/rad)
500
400
300
200
100
0
25
50
75
100
Time (normalized)

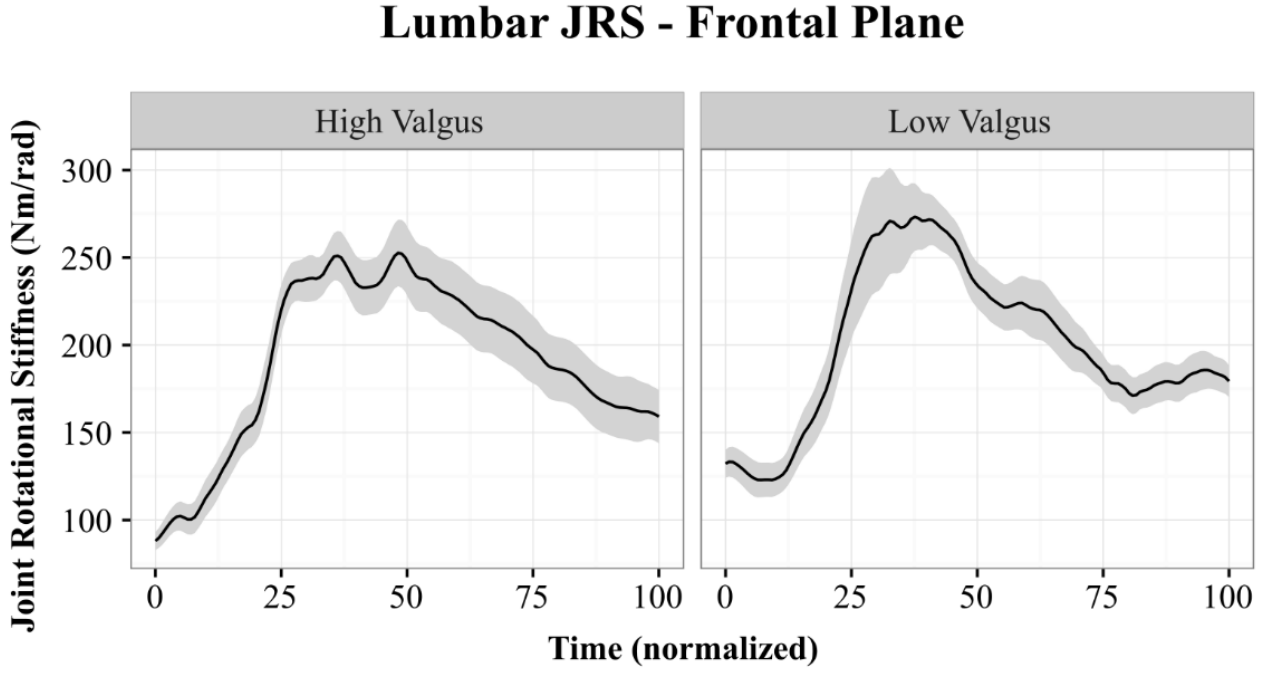
Lumbar JRS - Frontal Plane
High Valgus
Low Valgus
Joint Rotational Stiffness (Nm/rad)
300
250
200
150
100
0
25
50
75
100
Time (normalized)

Lumbar JRS - Transverse Plane

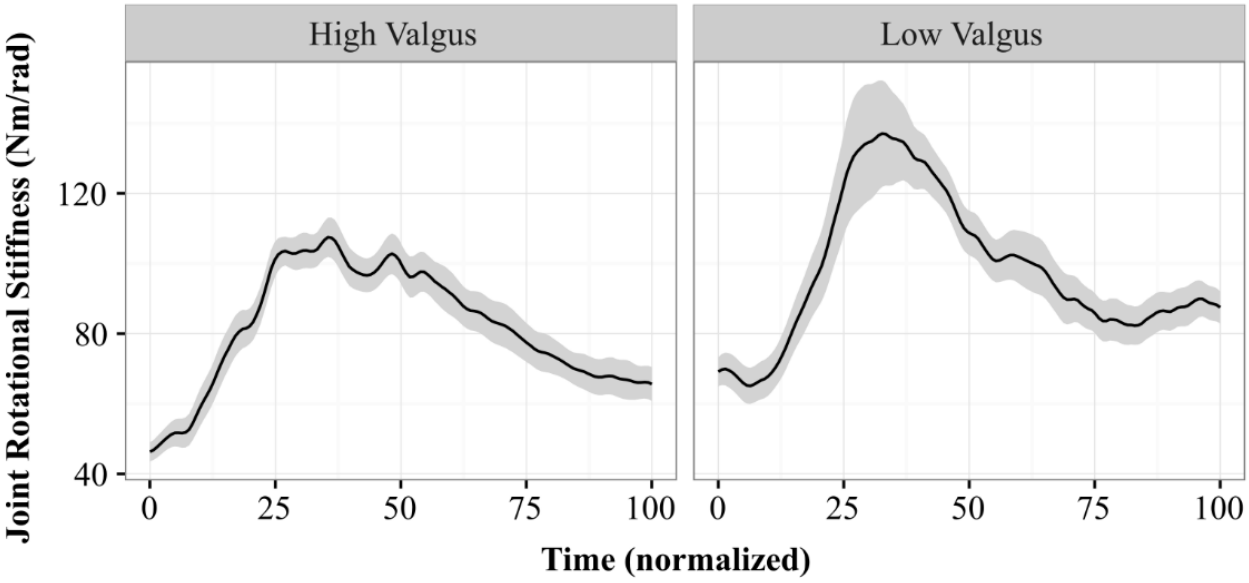

Lumbar JRS - Euc Norm

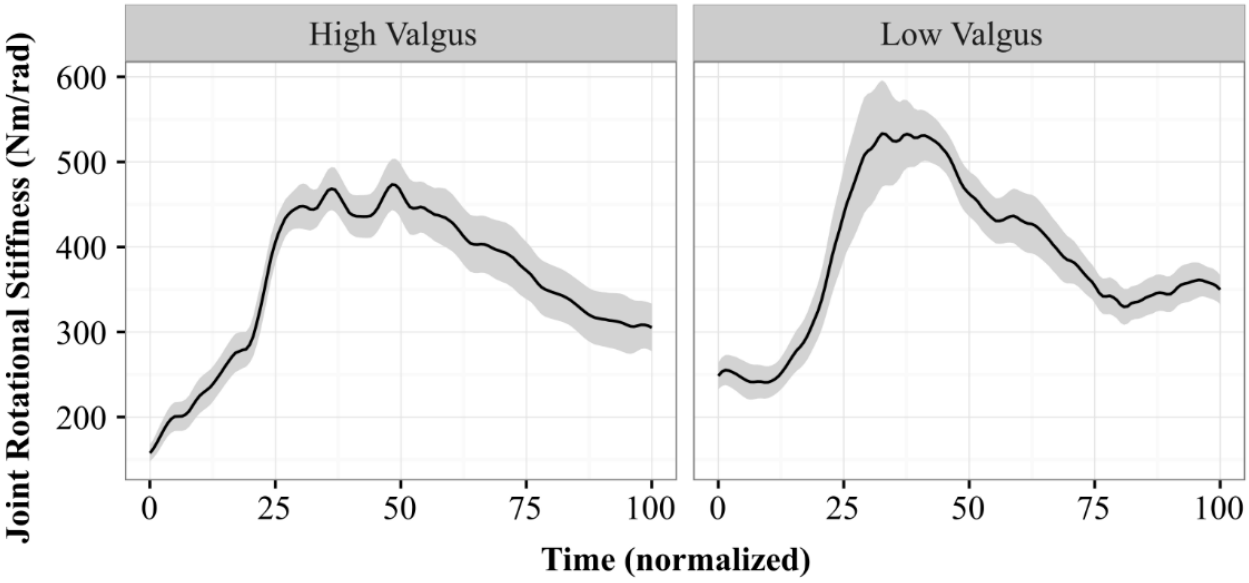

Right Hip JRS - Sagittal Plane

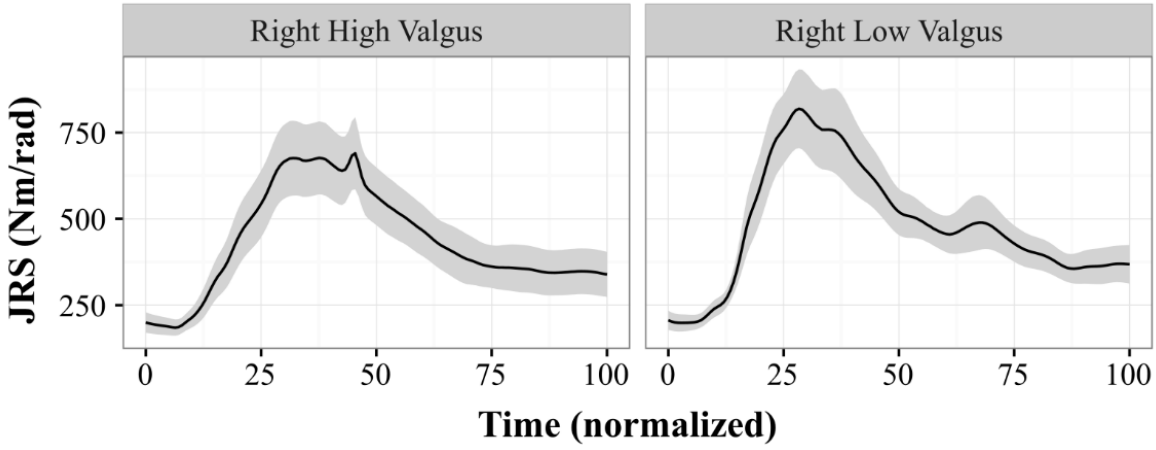

Right Hip JRS - Frontal Plane

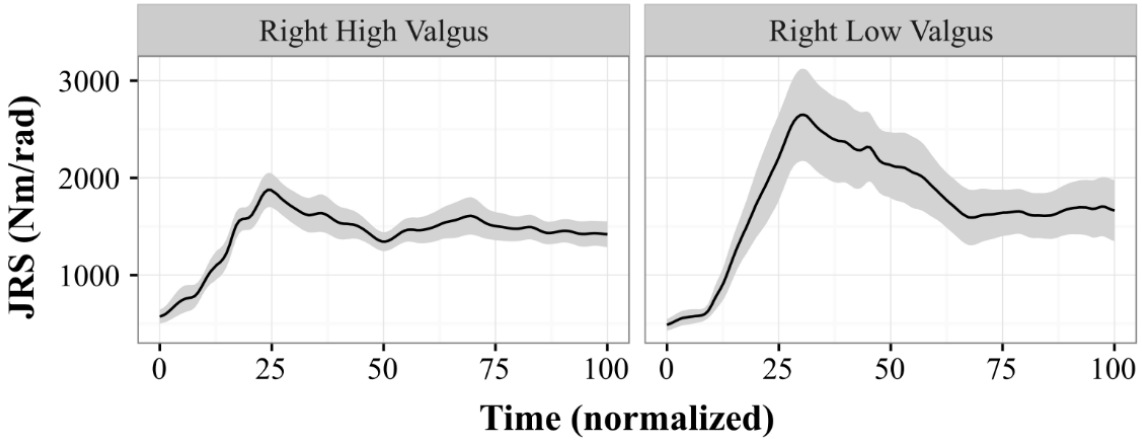

Right Hip JRS - Transverse Plane

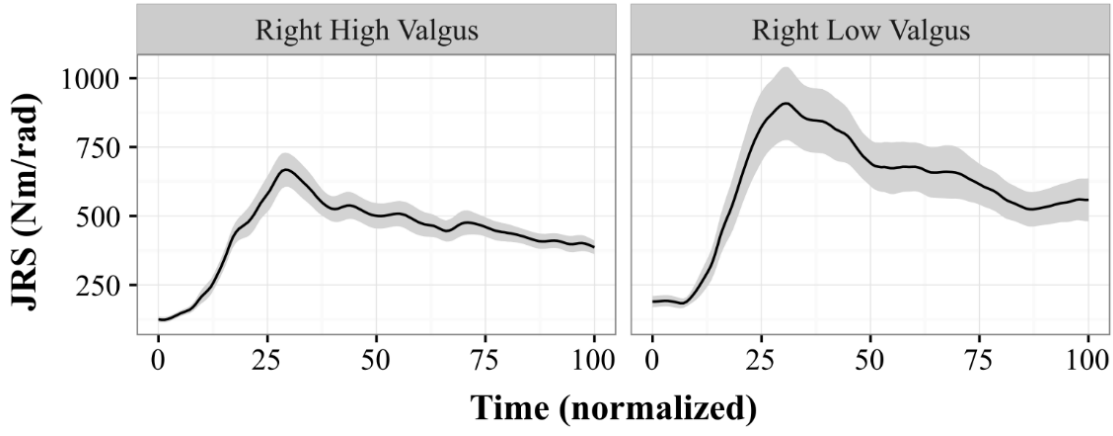

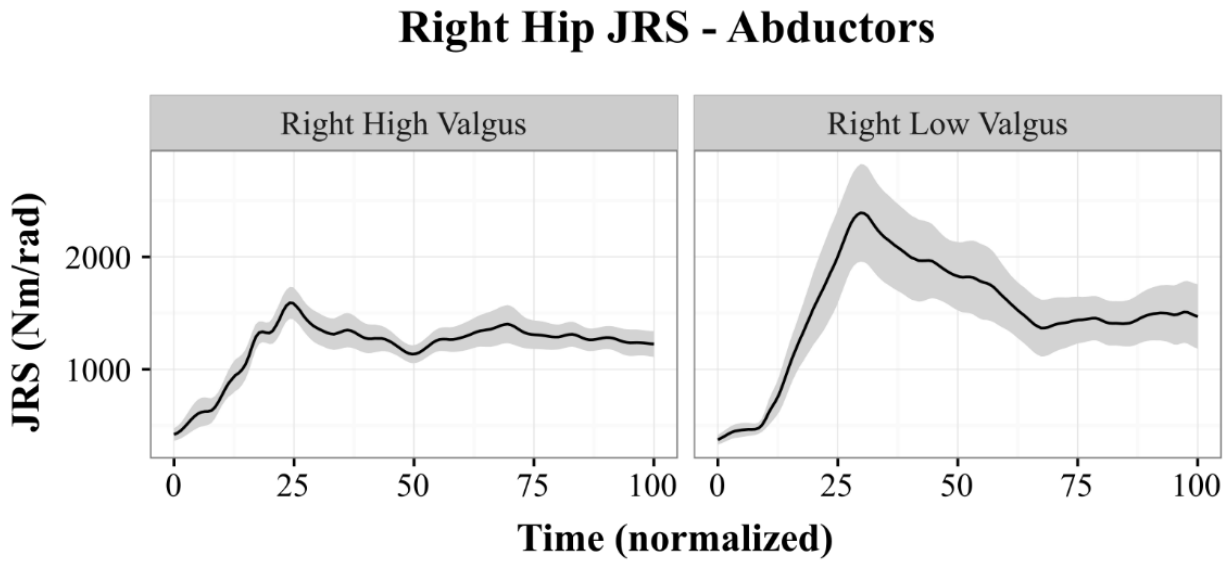
Right Hip JRS - Abductors
Right High Valgus
Right Low Valgus
JRS (Nm/rad)
2000
1000
0
25
50
75
100
Time (normalized)

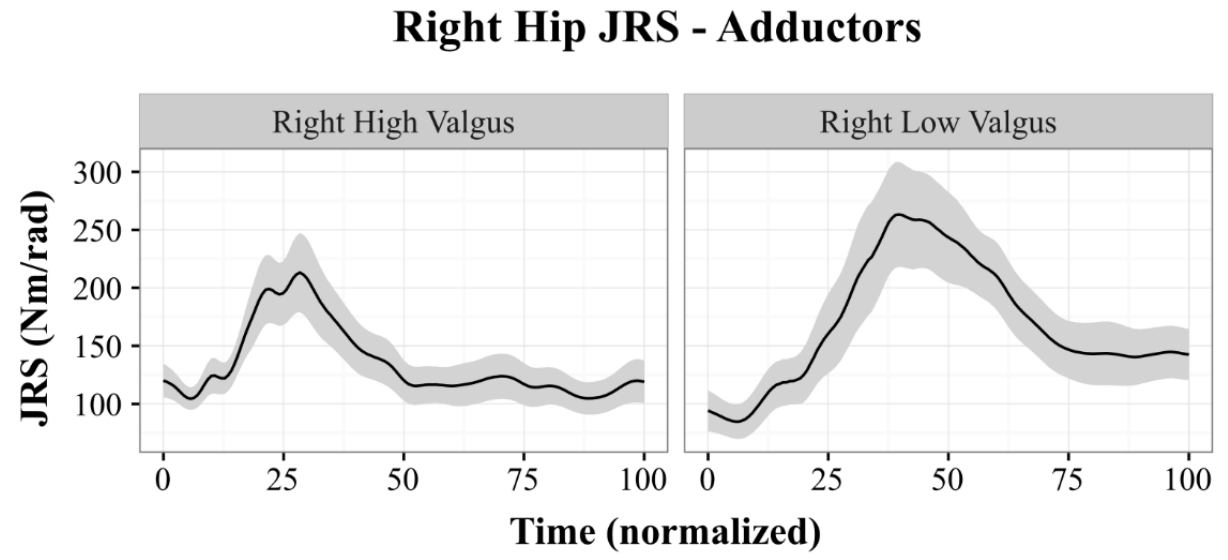
Right Hip JRS - Adductors
Right High Valgus
Right Low Valgus
JRS (Nm/rad)
300
250
200
150
100
0
25
50
75
100
Time (normalized)

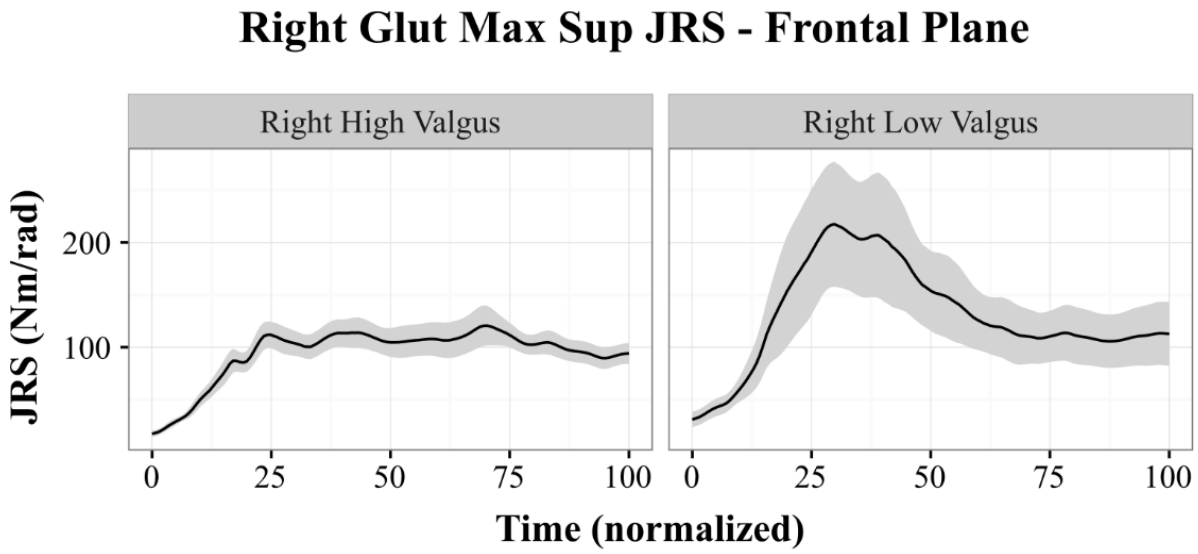
Right Glut Max Sup JRS - Frontal Plane
Right High Valgus
Right Low Valgus
JRS (Nm/rad)
200
100
0
25
50
75
100
Time (normalized)

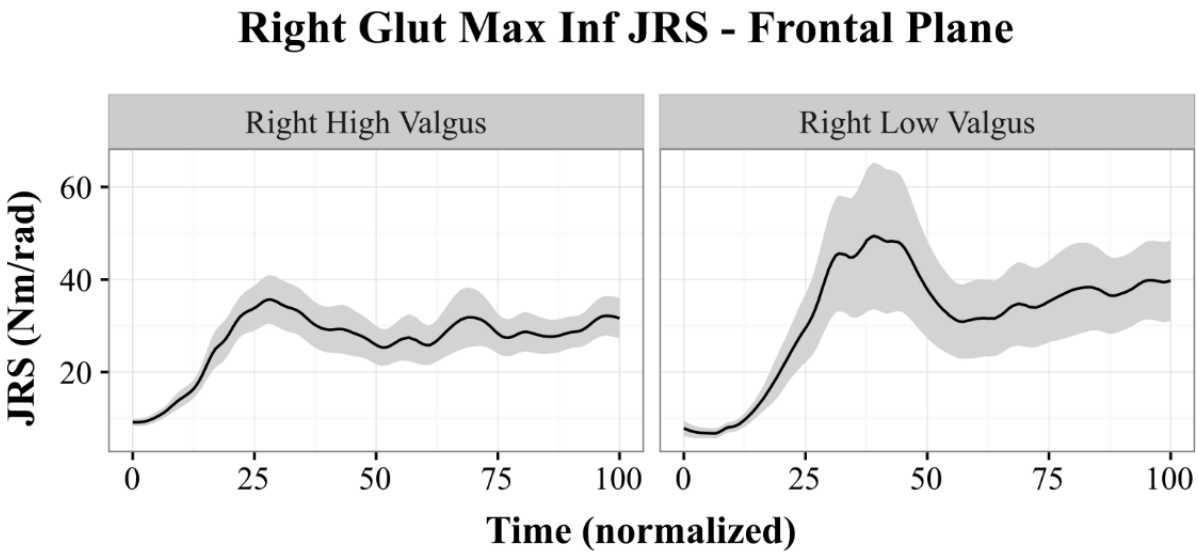
Right Glut Max Inf JRS - Frontal Plane
Right High Valgus
Right Low Valgus
JRS (Nm/rad)
60
40
20
0
25
50
75
100
Time (normalized)

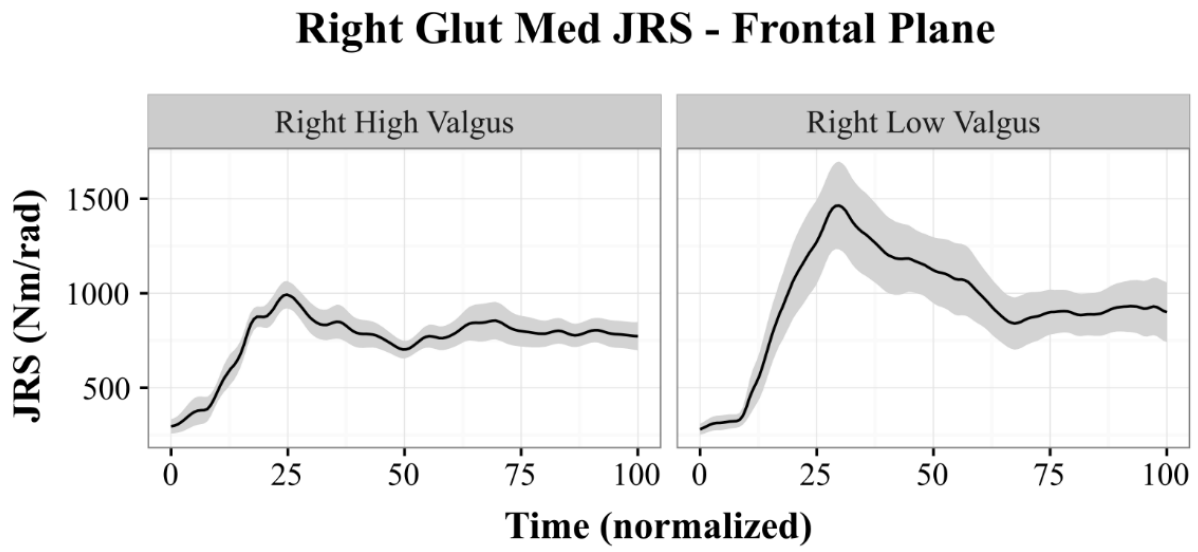
Right Glut Med JRS - Frontal Plane
Right High Valgus
Right Low Valgus
JRS (Nm/rad)
1500
1000
500
0
25
50
75
100
Time (normalized)

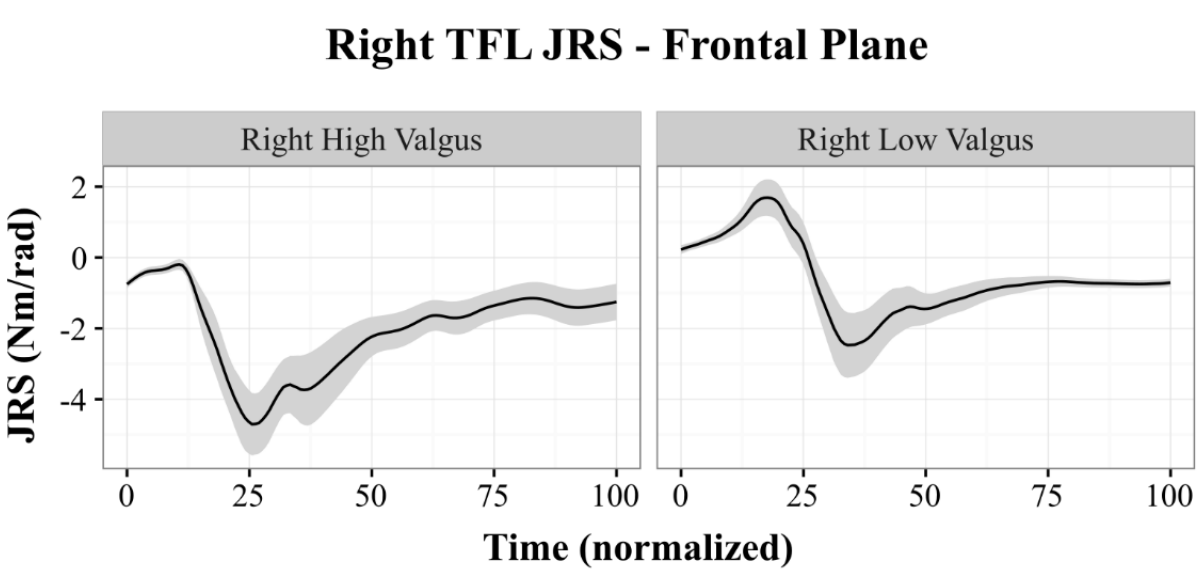
Right TFL JRS - Frontal Plane
Right High Valgus
Right Low Valgus
JRS (Nm/rad)
2
0
-2
-4
0
25
50
75
100
Time (normalized)

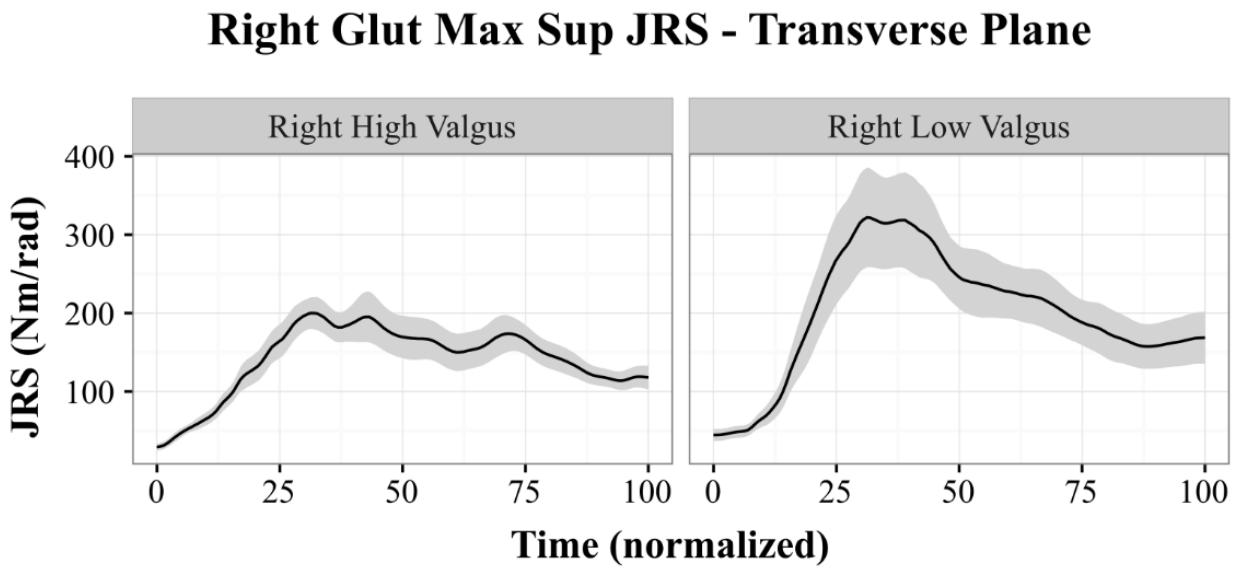
Right Glut Max Sup JRS - Transverse Plane
Right High Valgus
Right Low Valgus
JRS (Nm/rad)
400
300
200
100
0
25
50
75
100
Time (normalized)

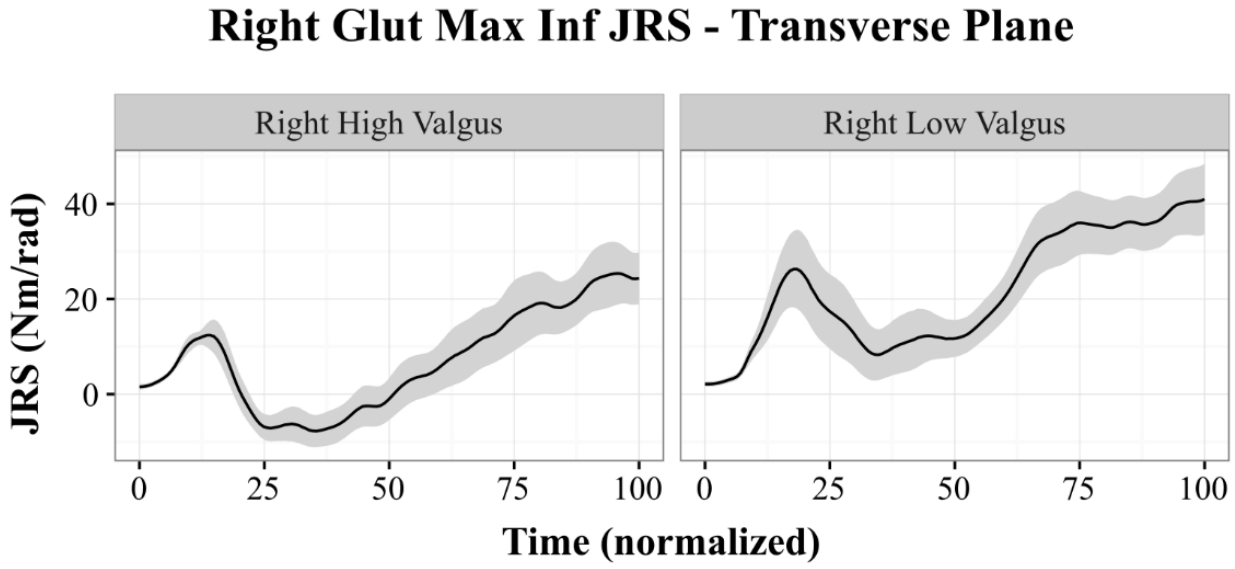
Right Glut Max Inf JRS - Transverse Plane
Right High Valgus
Right Low Valgus
JRS (Nm/rad)
40
20
0
0
25
50
75
100
Time (normalized)

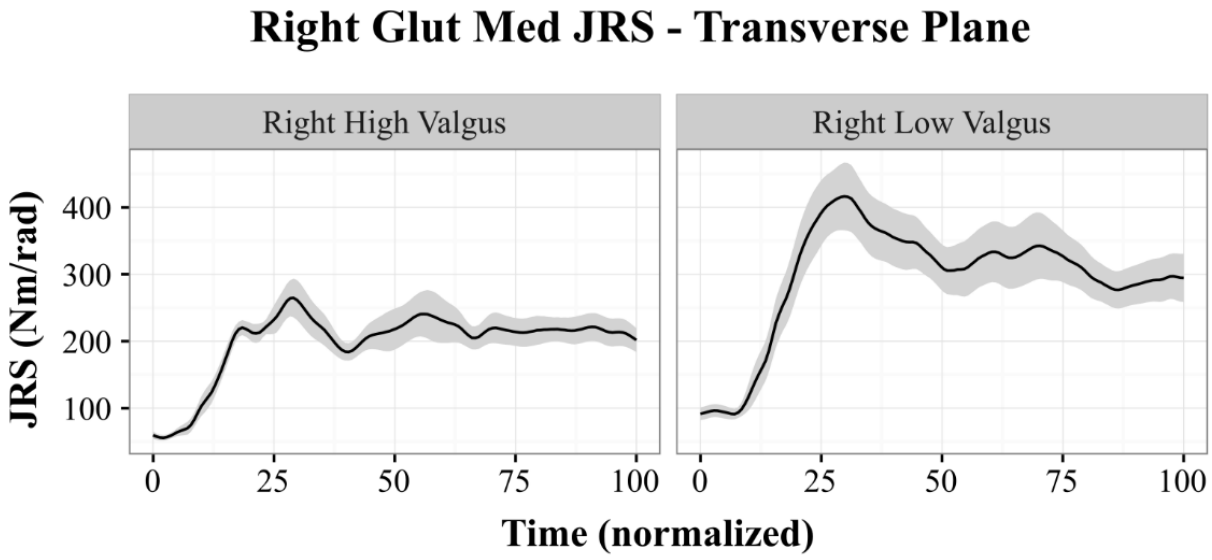
Right Glut Med JRS - Transverse Plane
Right High Valgus
Right Low Valgus
JRS (Nm/rad)
400
300
200
100
0
25
50
75
100
Time (normalized)

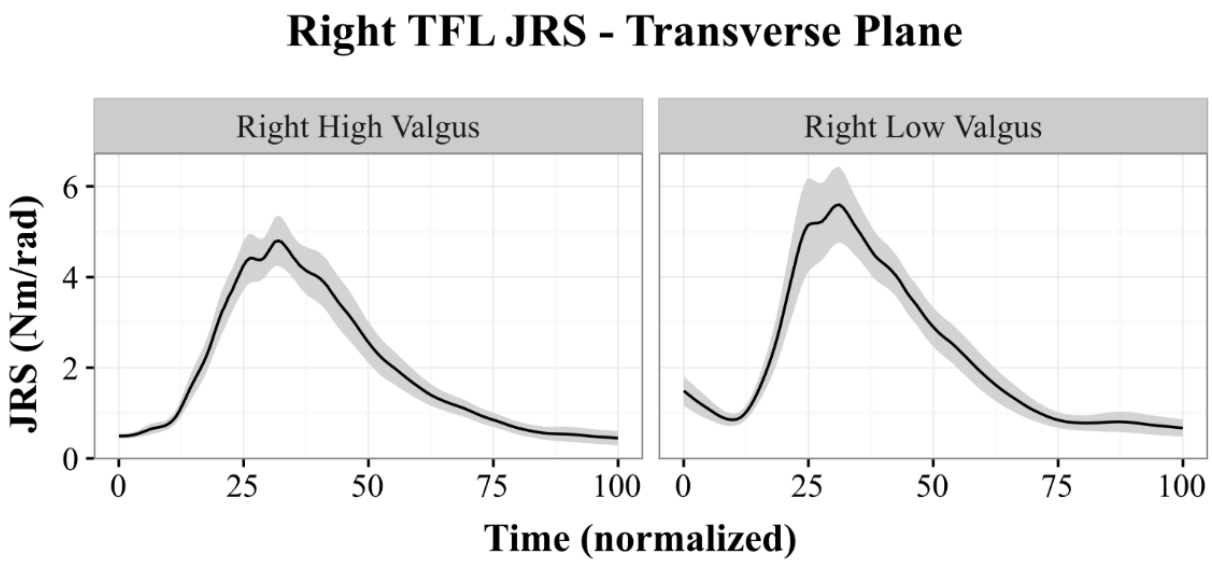
Right TFL JRS - Transverse Plane
Right High Valgus
Right Low Valgus
JRS (Nm/rad)
6
4
2
0
0
25
50
75
100
Time (normalized)

Single Leg Crossover Drop: Land on Left

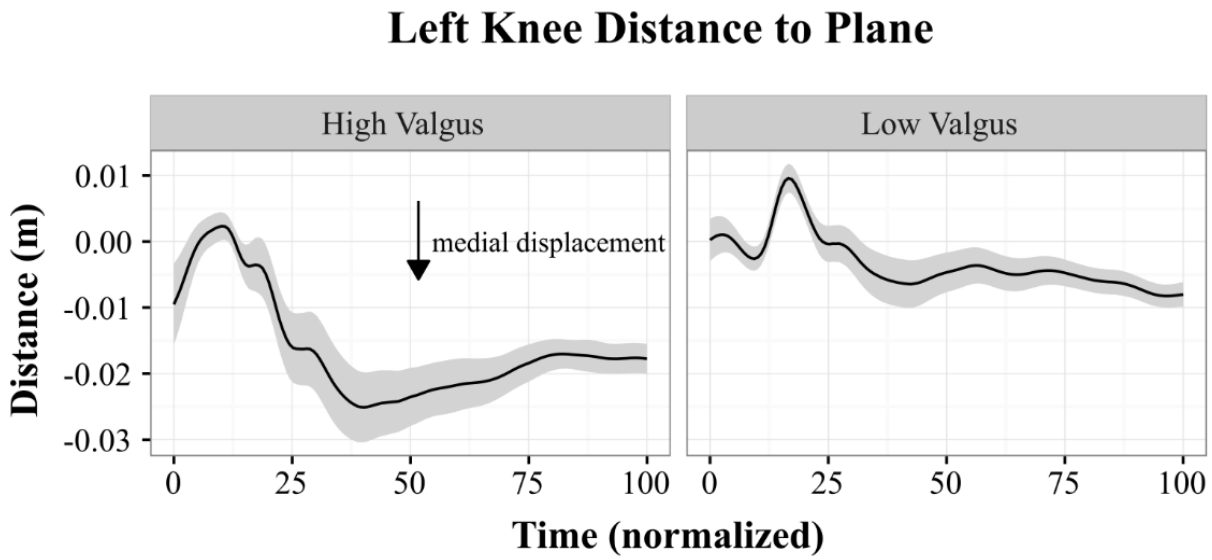

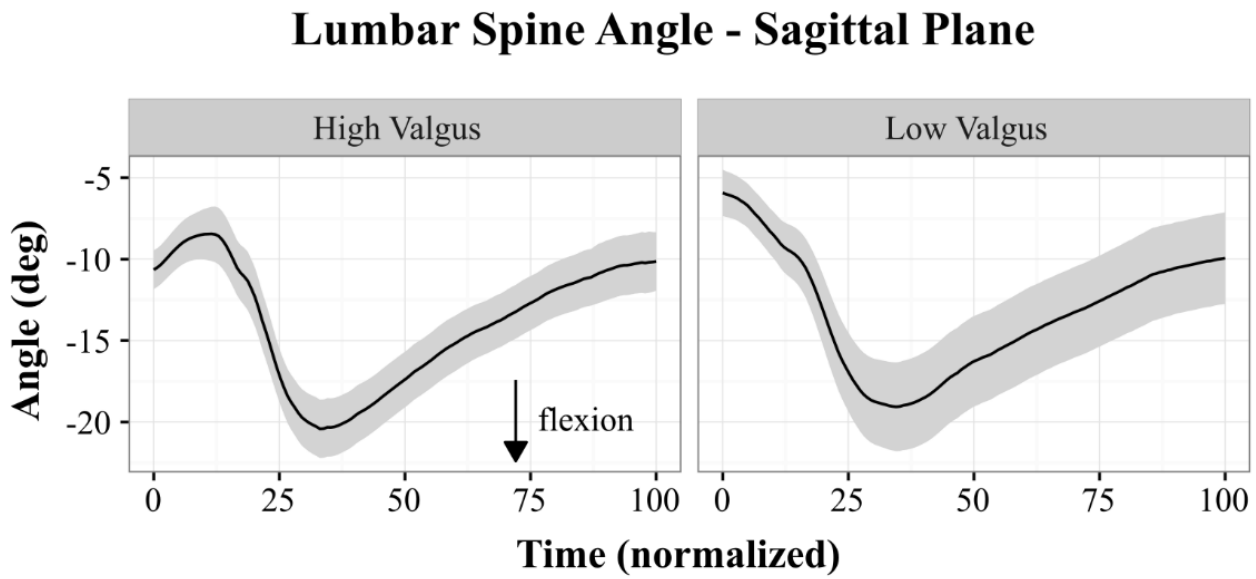
Lumbar Spine Angle - Sagittal Plane
High Valgus
Low Valgus
Angle (deg)
-5
-10
-15
-20
flexion
0
25
50
75
100
Time (normalized)

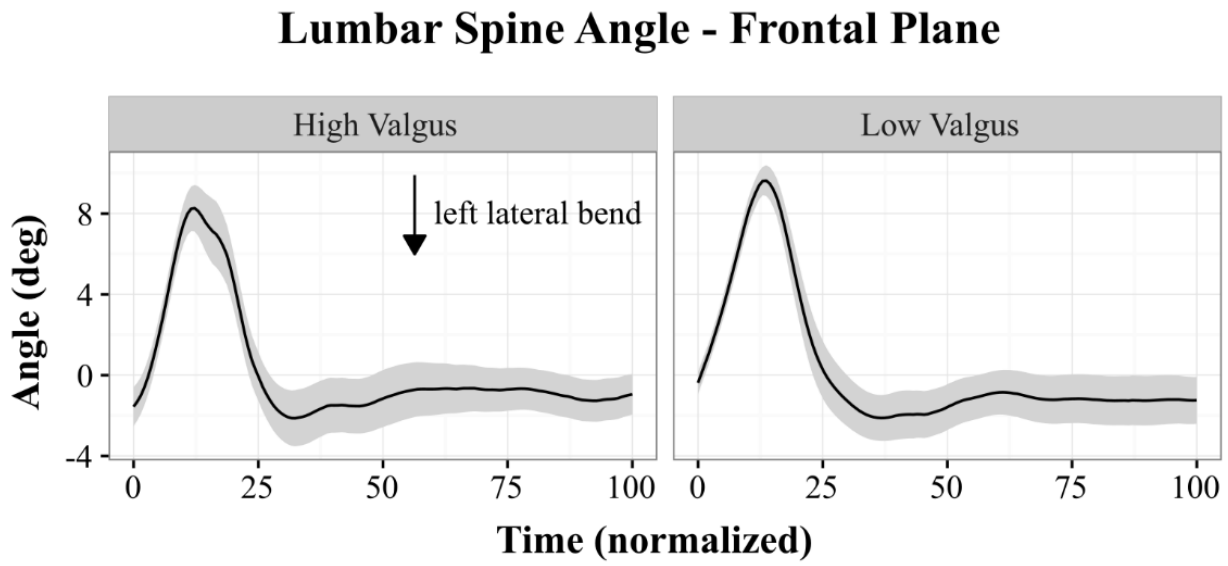
Lumbar Spine Angle - Frontal Plane
High Valgus
Low Valgus
Angle (deg)
8
4
0
-4
left lateral bend
0
25
50
75
100
Time (normalized)

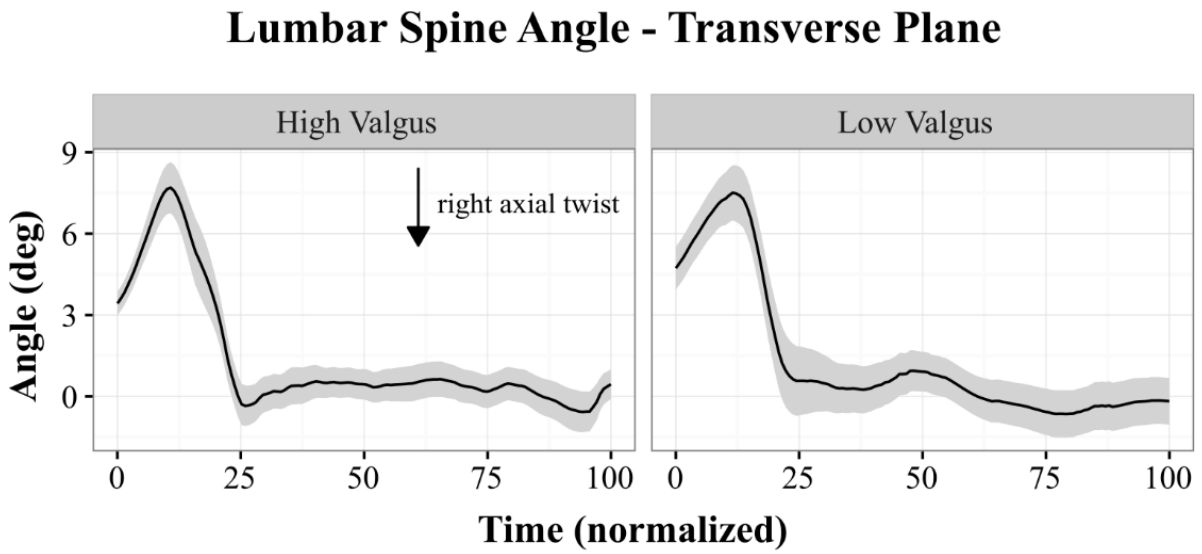
Lumbar Spine Angle - Transverse Plane
High Valgus
Low Valgus
right axial twist
Angle (deg)
9
6
3
0
0
25
50
75
100
Time (normalized)

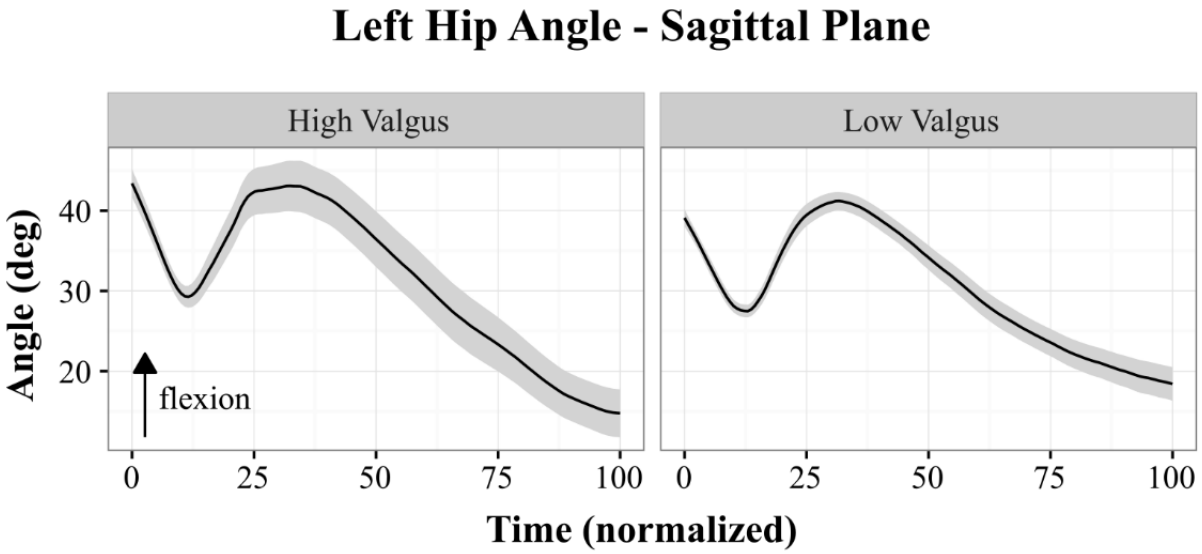
Left Hip Angle - Sagittal Plane
High Valgus
Low Valgus
flexion
Angle (deg)
40
30
20
0
25
50
75
100
Time (normalized)

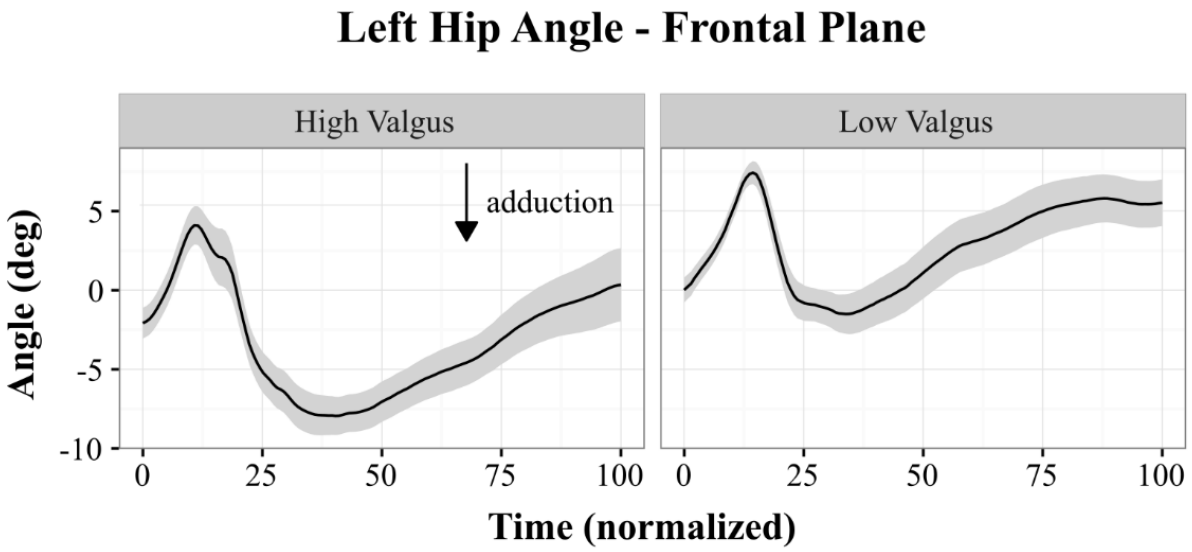
Left Hip Angle - Frontal Plane
High Valgus
Low Valgus
adduction
Angle (deg)
5
0
-5
-10
0
25
50
75
100
Time (normalized)

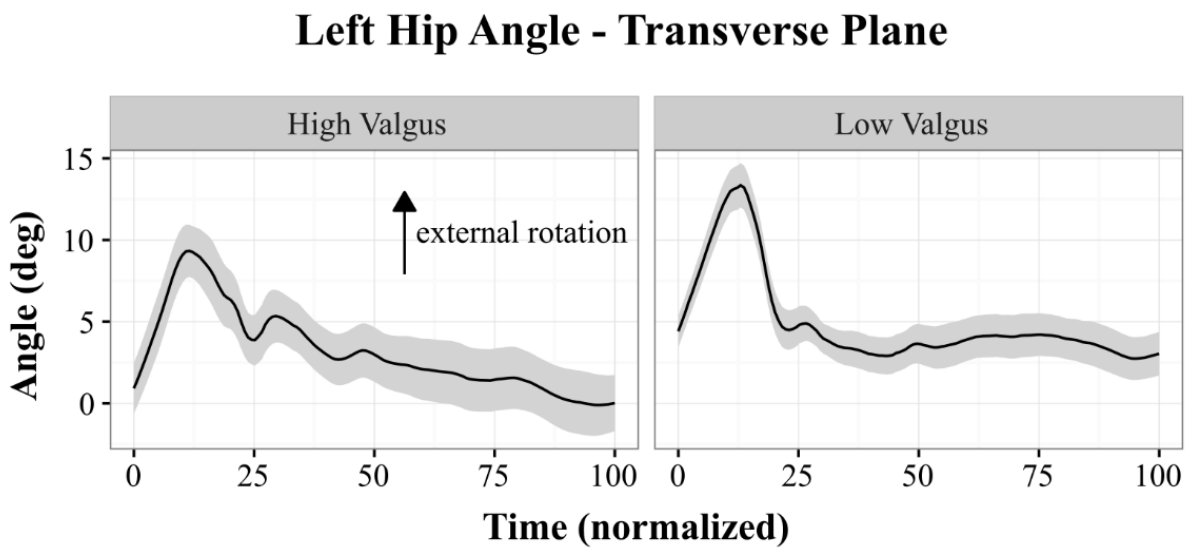
Left Hip Angle - Transverse Plane
High Valgus
Low Valgus
external rotation
Angle (deg)
15
10
5
0
0
25
50
75
100
Time (normalized)

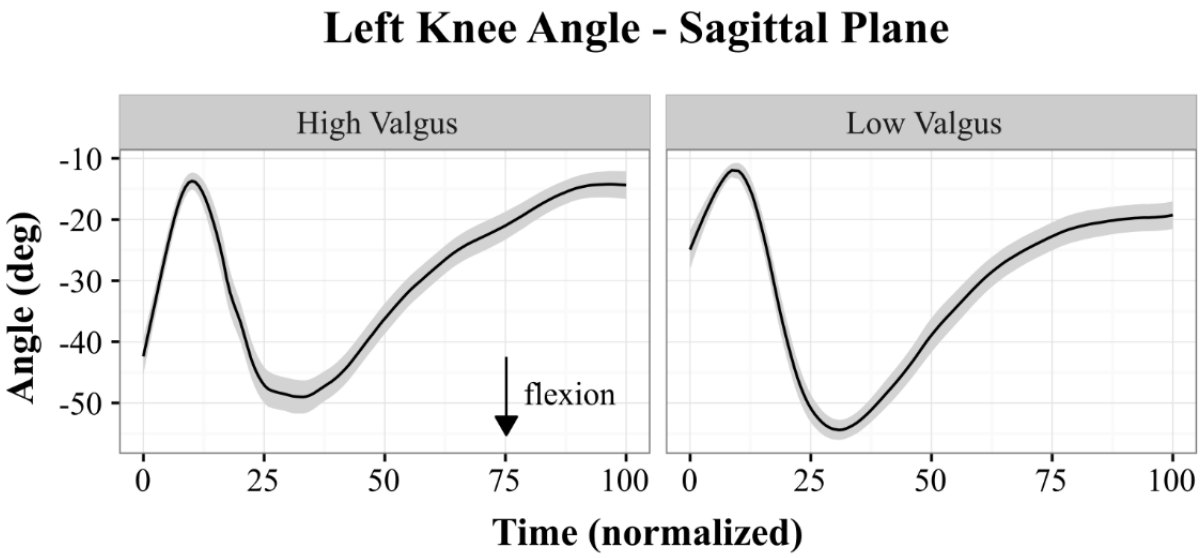
Left Knee Angle - Sagittal Plane
High Valgus
Low Valgus
Angle (deg)
-10
-20
-30
-40
-50
flexion
0
25
50
75
100
Time (normalized)

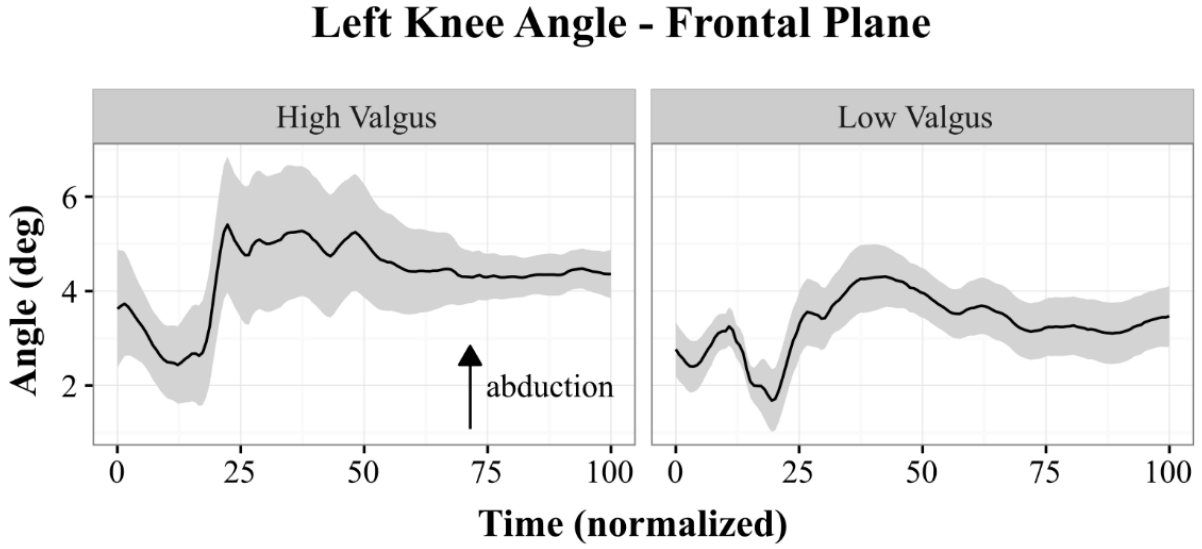
Left Knee Angle - Frontal Plane
High Valgus
Low Valgus
Angle (deg)
6
4
2
abduction
0
25
50
75
100
Time (normalized)

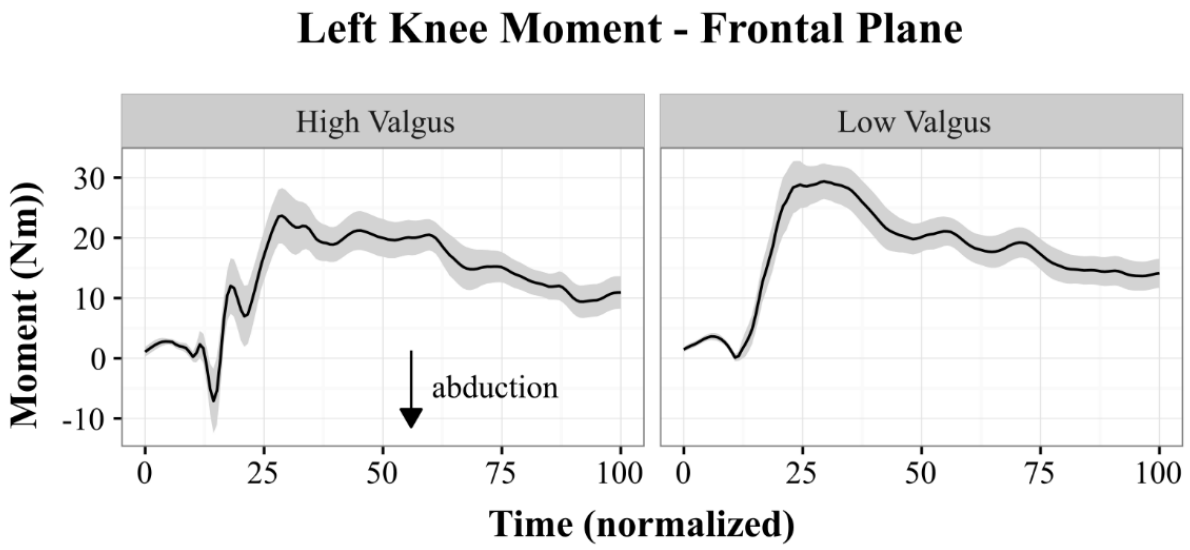
Left Knee Moment - Frontal Plane
High Valgus
Low Valgus
Moment (Nm))
30
20
10
0
-10
abduction
0
25
50
75
100
Time (normalized)

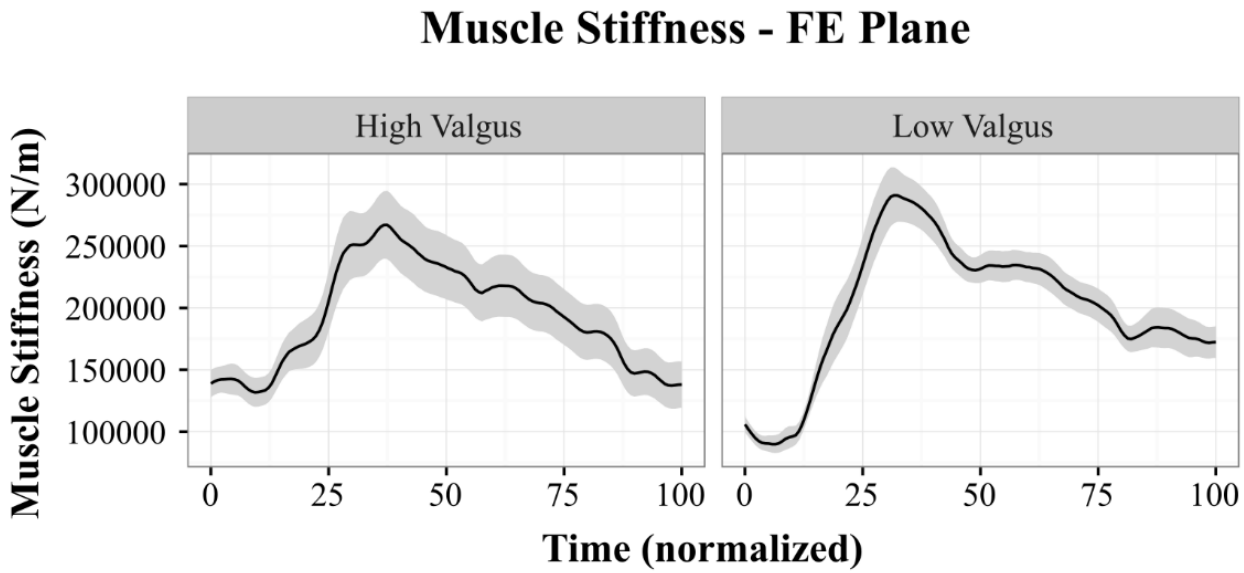
Muscle Stiffness - FE Plane
High Valgus
Low Valgus
Muscle Stiffness (N/m)
300000
250000
200000
150000
100000
0
25
50
75
100
Time (normalized)

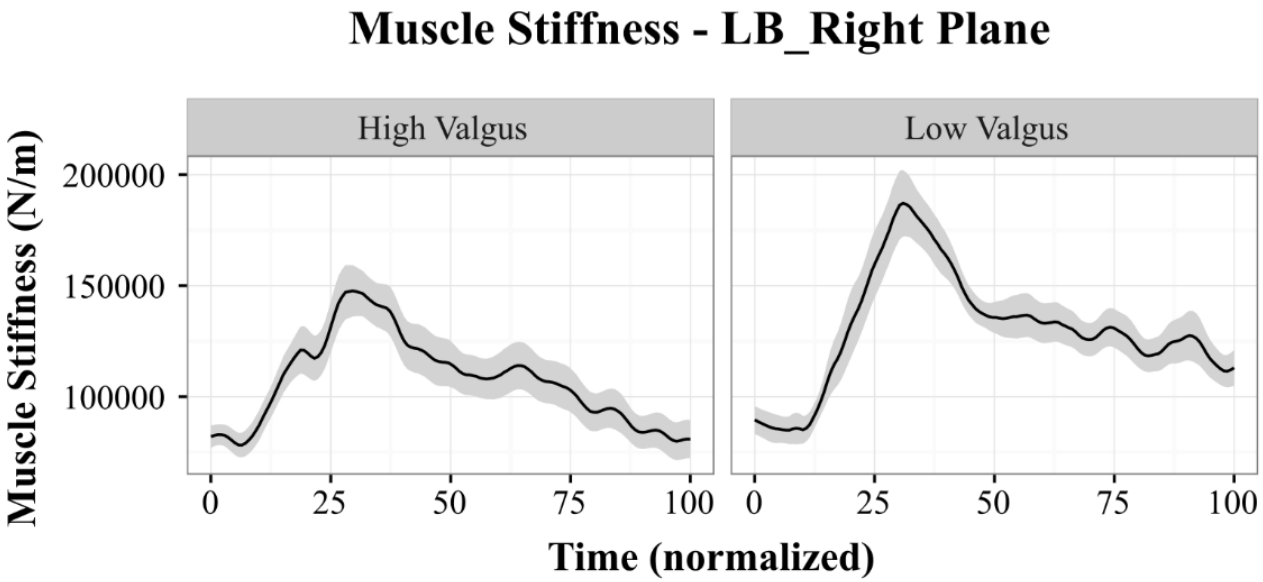
Muscle Stiffness - LB_Right Plane
High Valgus
Low Valgus
Muscle Stiffness (N/m)
200000
150000
100000
0
25
50
75
100
Time (normalized)

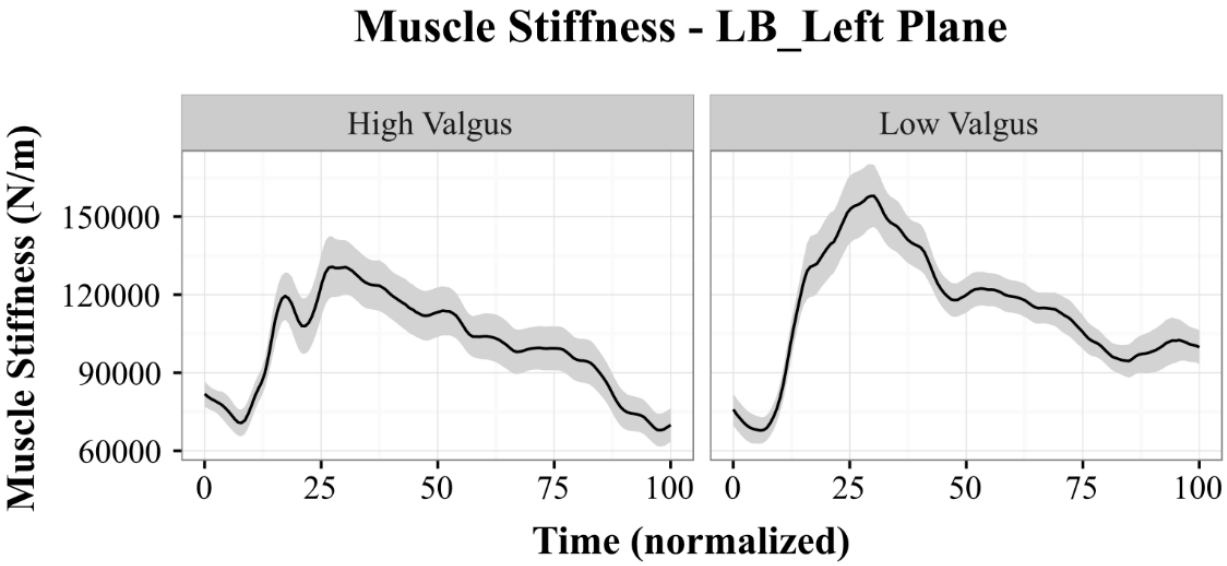
Muscle Stiffness - LB_Left Plane
High Valgus
Low Valgus
Muscle Stiffness (N/m)
150000
120000
90000
60000
0
25
50
75
100
Time (normalized)

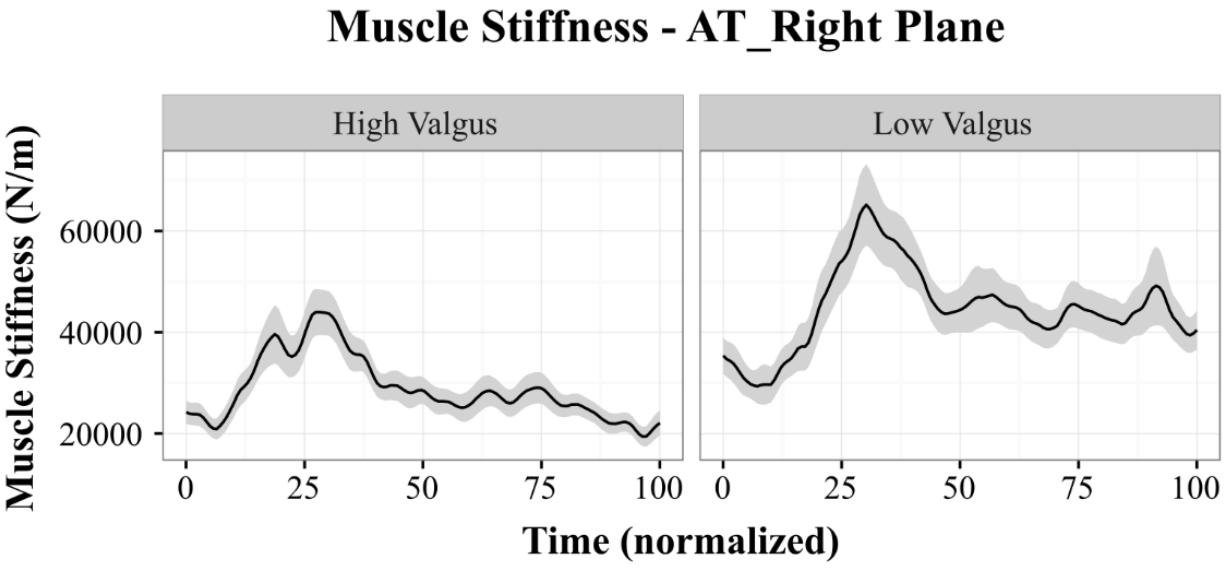
Muscle Stiffness - AT_Right Plane
High Valgus
Low Valgus
Muscle Stiffness (N/m)
60000
40000
20000
0
25
50
75
100
Time (normalized)

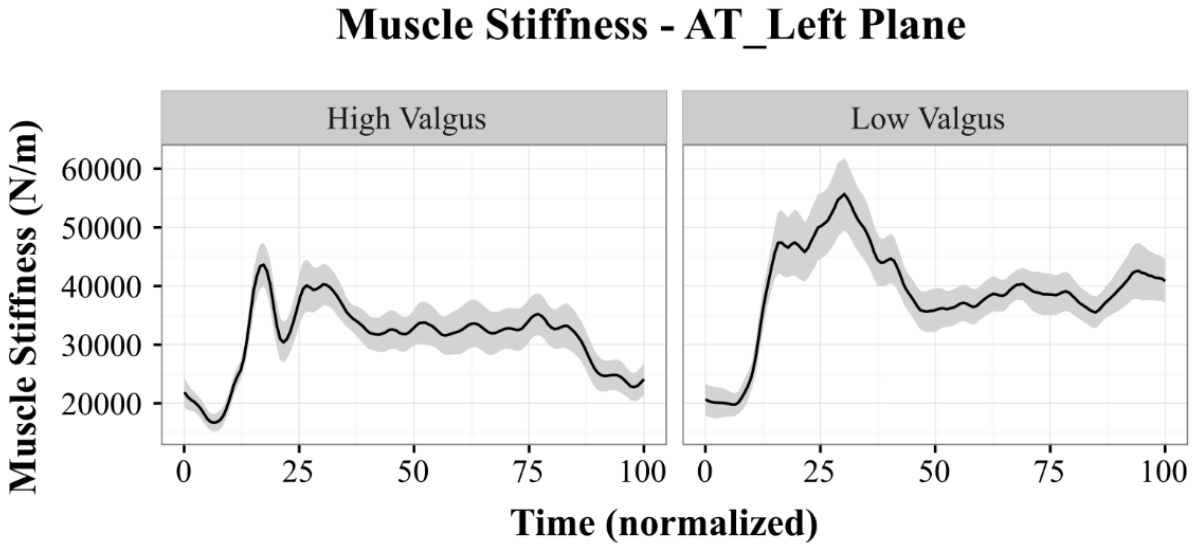
Muscle Stiffness - AT_Left Plane
High Valgus
Low Valgus
Muscle Stiffness (N/m)
60000
50000
40000
30000
20000
0
25
50
75
100
Time (normalized)

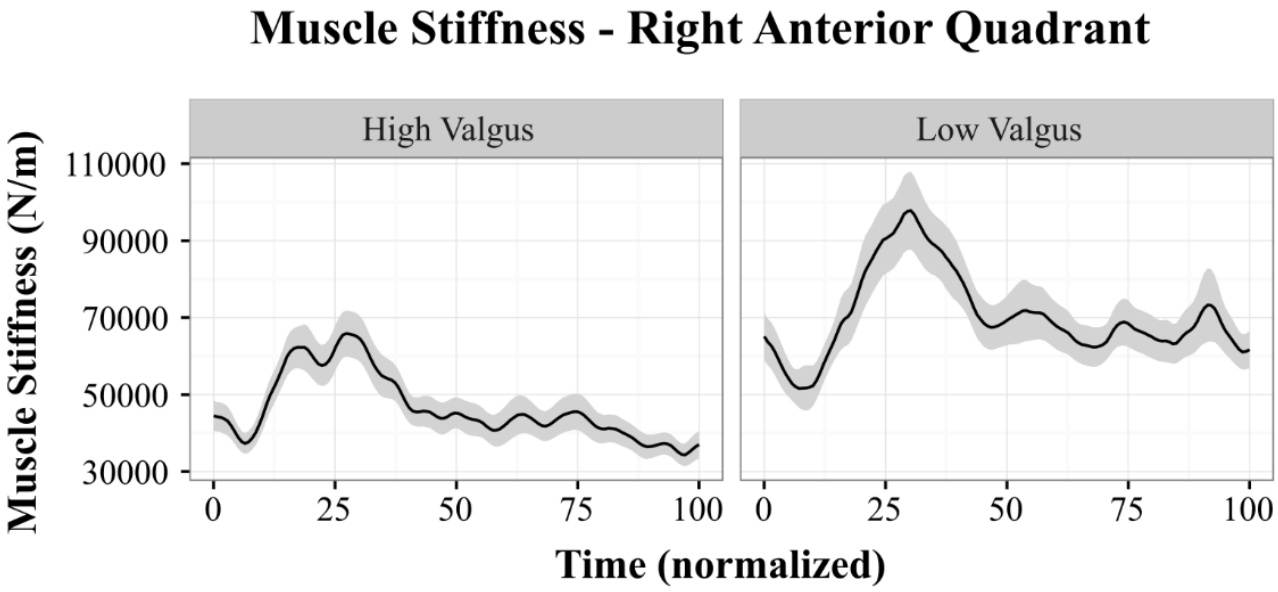
Muscle Stiffness - Right Anterior Quadrant
High Valgus
Low Valgus
Muscle Stiffness (N/m)
110000
90000
70000
50000
30000
0
25
50
75
100
Time (normalized)

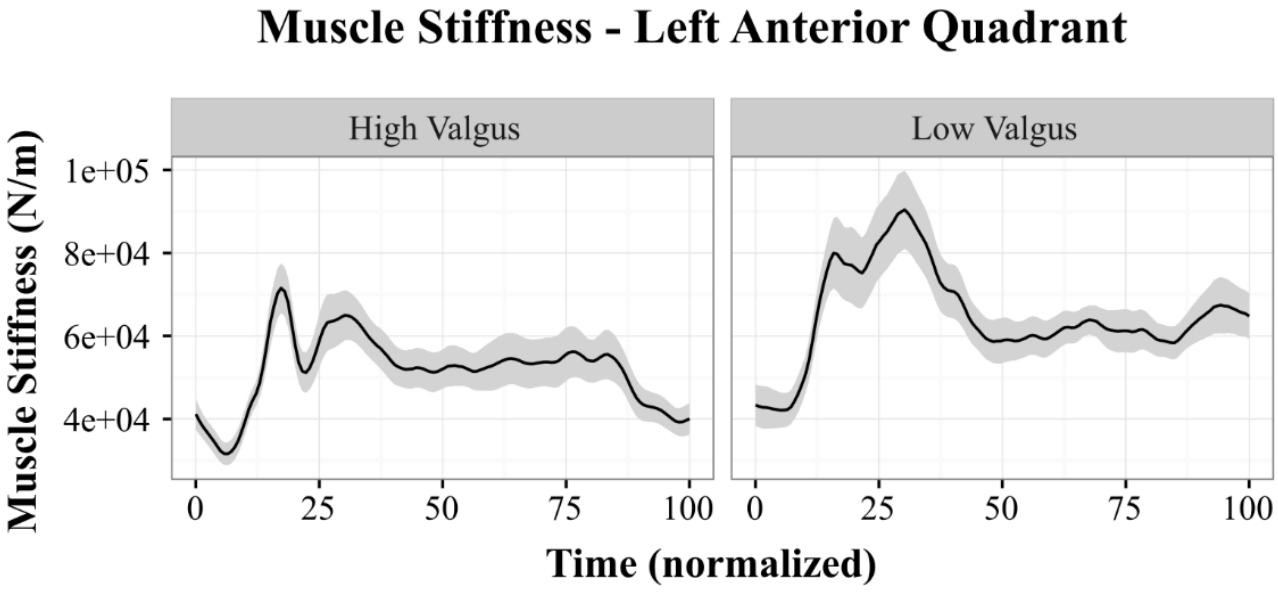
Muscle Stiffness - Left Anterior Quadrant
High Valgus
Low Valgus
Muscle Stiffness (N/m)
1e+05
8e+04
6e+04
4e+04
0
25
50
75
100
Time (normalized)

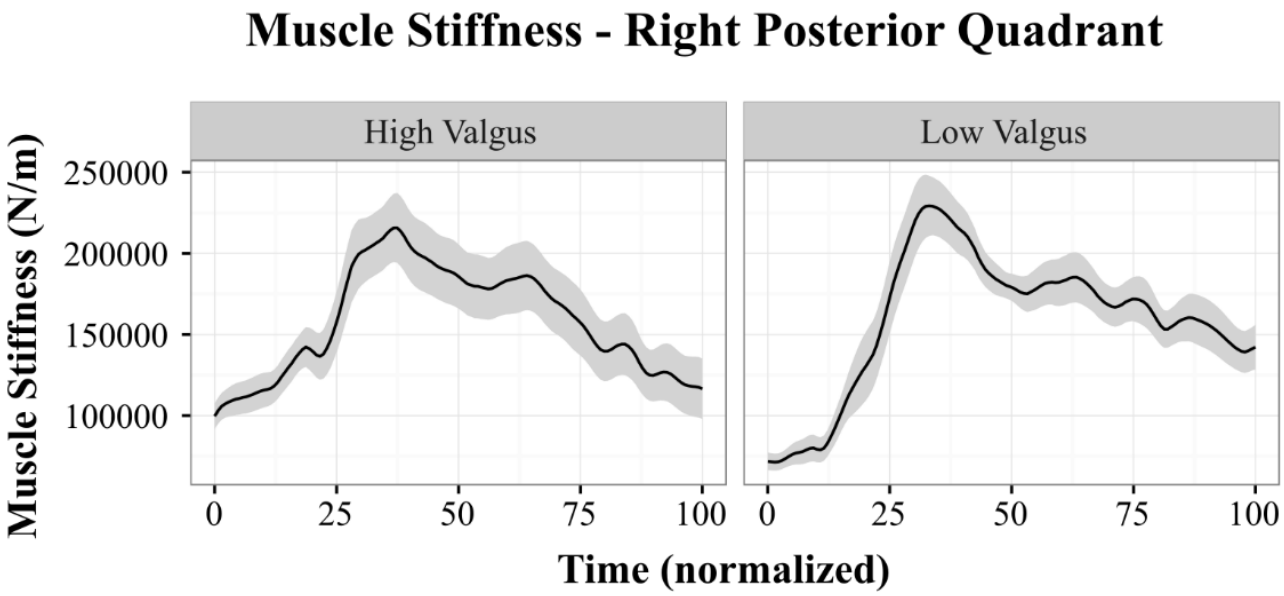
Muscle Stiffness - Right Posterior Quadrant
High Valgus
Low Valgus
Muscle Stiffness (N/m)
250000
200000
150000
100000
0
25
50
75
100
Time (normalized)

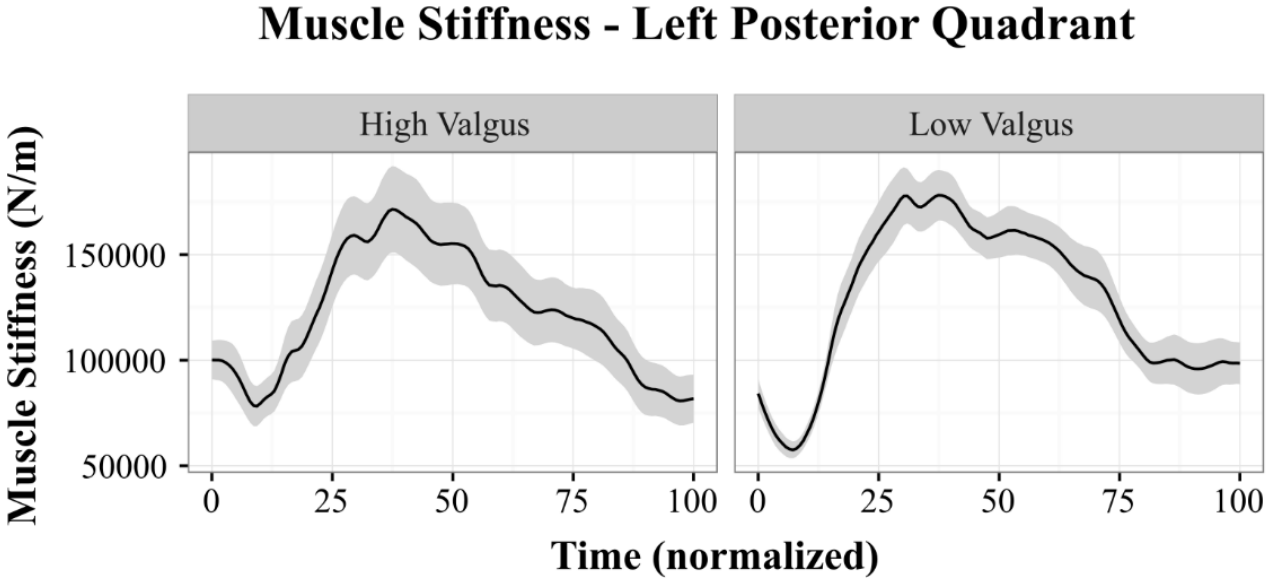
Muscle Stiffness - Left Posterior Quadrant
High Valgus
Low Valgus
Muscle Stiffness (N/m)
150000
100000
50000
0
25
50
75
100
Time (normalized)

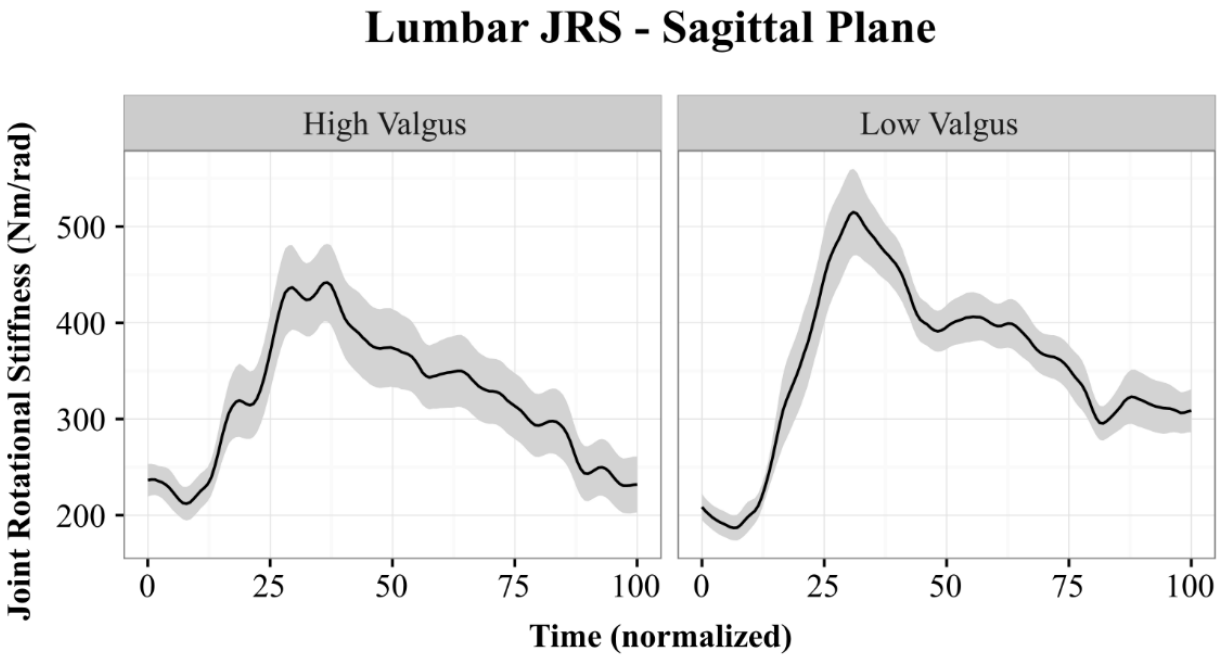
Lumbar JRS - Sagittal Plane
High Valgus
Low Valgus
Joint Rotational Stiffness (Nm/rad)
500
400
300
200
0
25
50
75
100
Time (normalized)

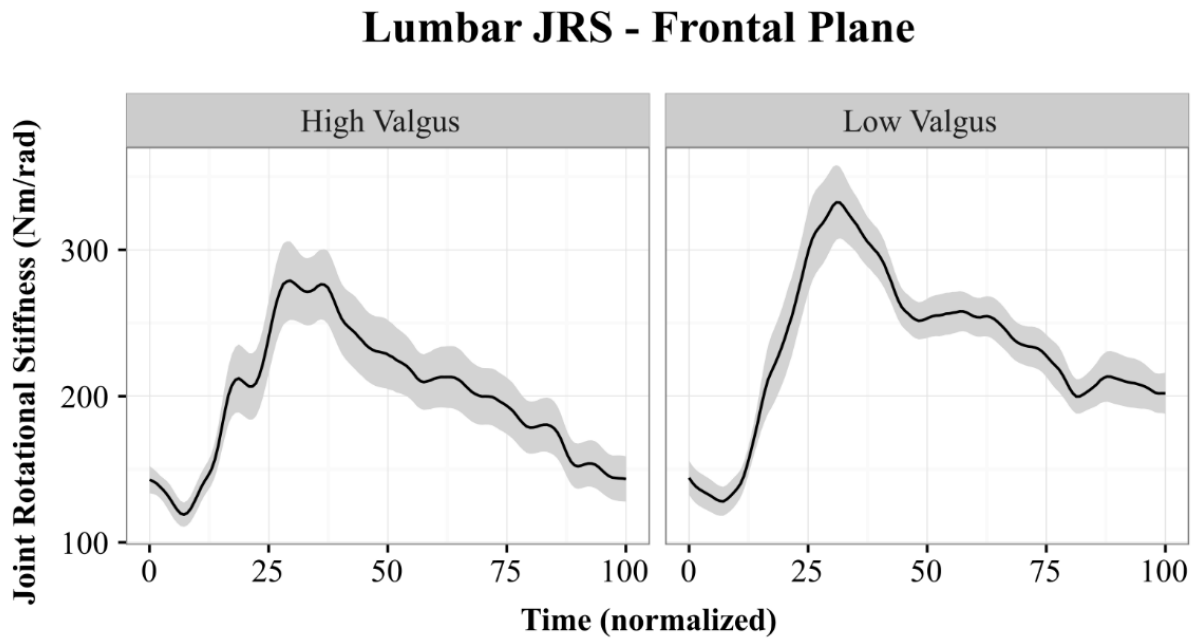
Lumbar JRS - Frontal Plane
High Valgus
Low Valgus
Joint Rotational Stiffness (Nm/rad)
300
200
100
0
25
50
75
100
Time (normalized)

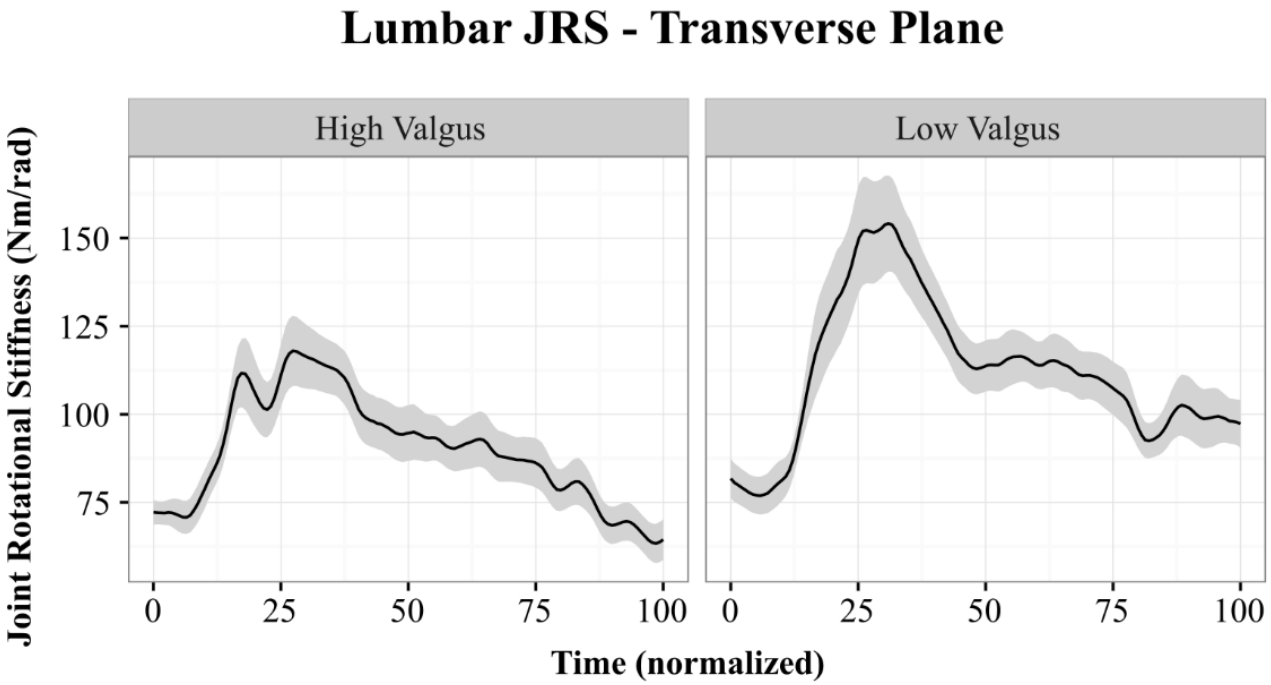
Lumbar JRS - Transverse Plane
High Valgus
Low Valgus
Joint Rotational Stiffness (Nm/rad)
150
125
100
75
0
25
50
75
100
Time (normalized)

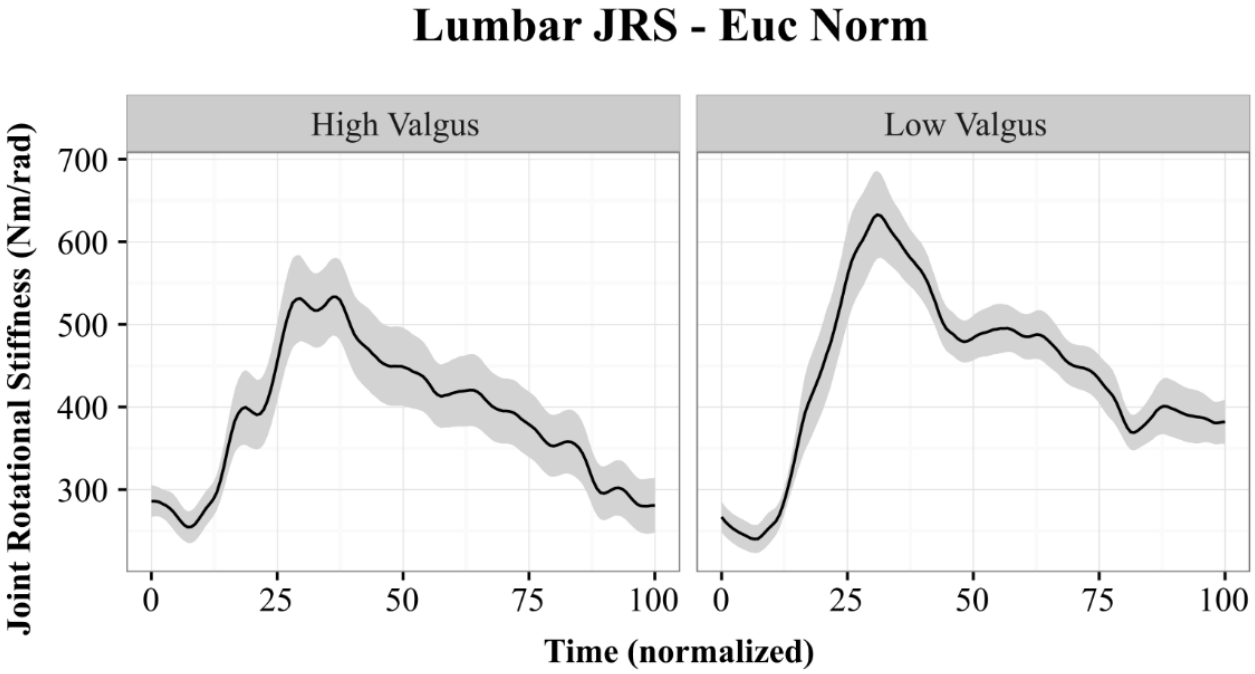
Lumbar JRS - Euc Norm
High Valgus
Low Valgus
Joint Rotational Stiffness (Nm/rad)
700
600
500
400
300
0
25
50
75
100
Time (normalized)

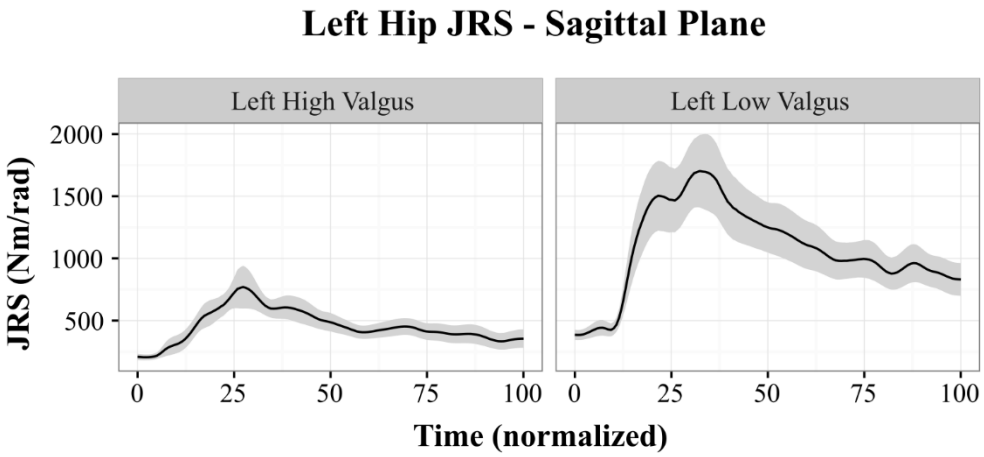
Left Hip JRS - Sagittal Plane
Left High Valgus
Left Low Valgus
JRS (Nm/rad)
2000
1500
1000
500
0
25
50
75
100
Time (normalized)

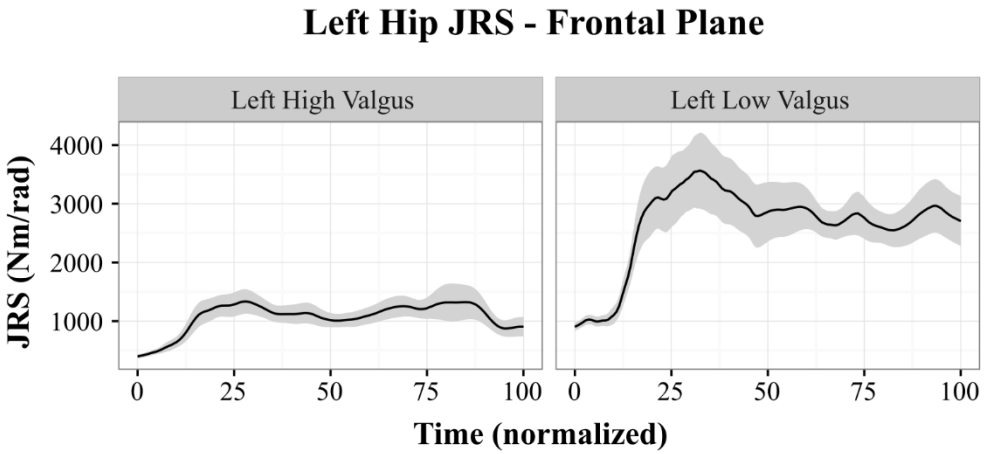
Left Hip JRS - Frontal Plane
Left High Valgus
Left Low Valgus
JRS (Nm/rad)
4000
3000
2000
1000
0
25
50
75
100
Time (normalized)

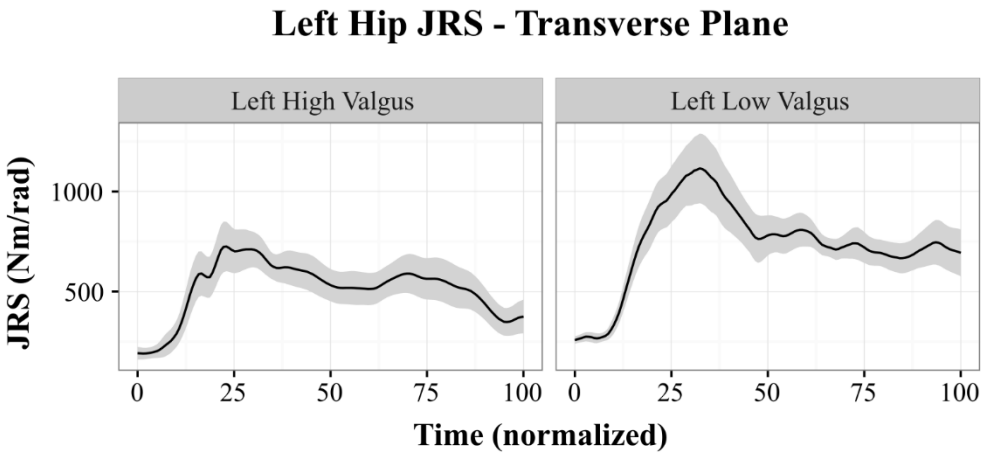
Left Hip JRS - Transverse Plane
Left High Valgus
Left Low Valgus
JRS (Nm/rad)
1000
500
0
25
50
75
100
Time (normalized)

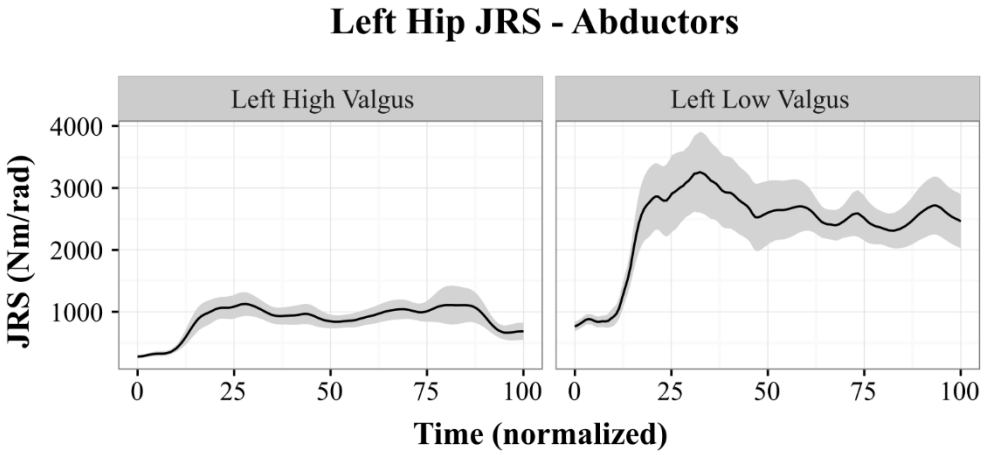
Left Hip JRS - Abductors
Left High Valgus
Left Low Valgus
JRS (Nm/rad)
4000
3000
2000
1000
0
25
50
75
100
Time (normalized)

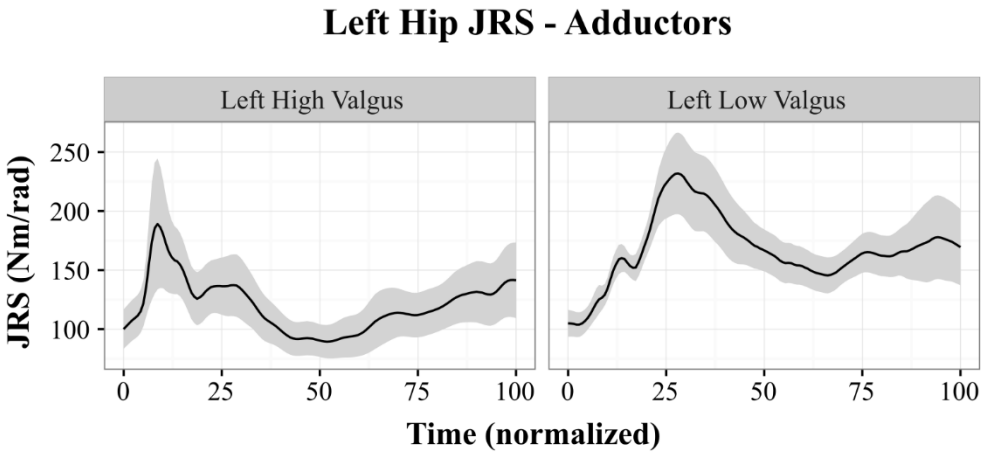
Left Hip JRS - Adductors
Left High Valgus
Left Low Valgus
JRS (Nm/rad)
250
200
150
100
0
25
50
75
100
Time (normalized)

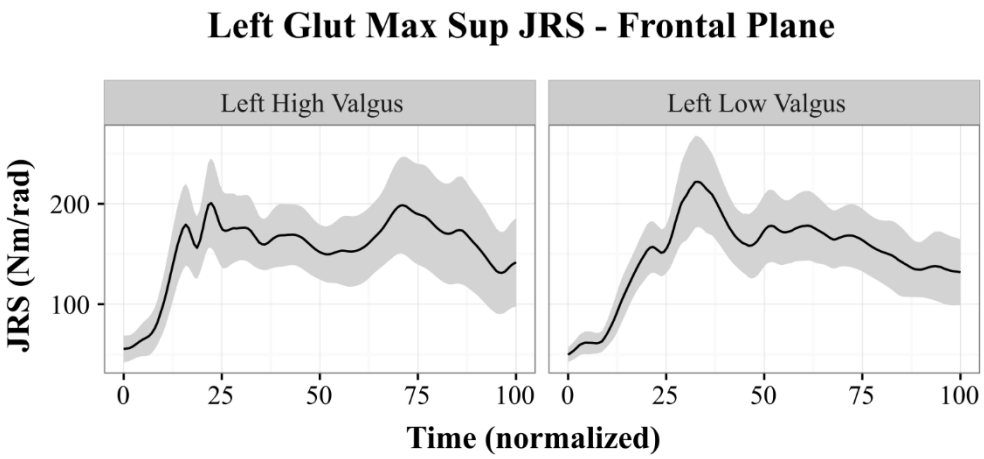
Left Glut Max Sup JRS - Frontal Plane
Left High Valgus
Left Low Valgus
JRS (Nm/rad)
200
100
0
25
50
75
100
Time (normalized)

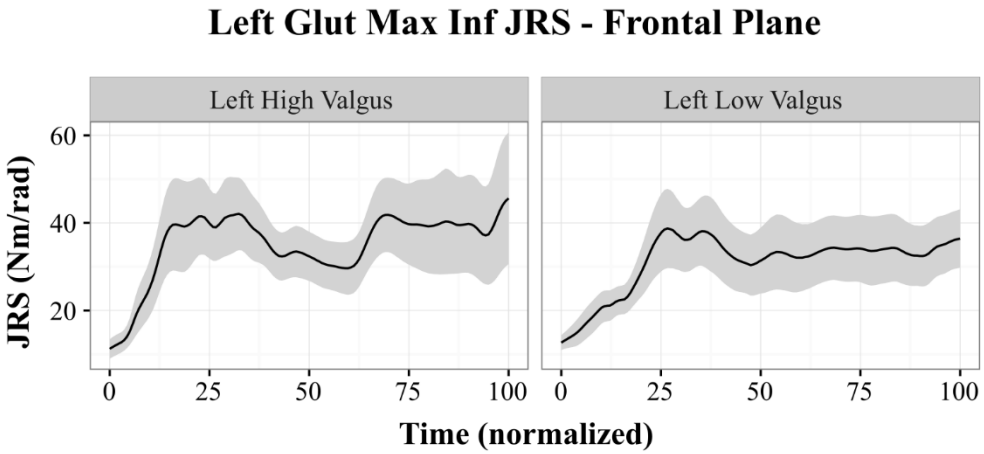
Left Glut Max Inf JRS - Frontal Plane
Left High Valgus
Left Low Valgus
JRS (Nm/rad)
60
40
20
0
25
50
75
100
Time (normalized)

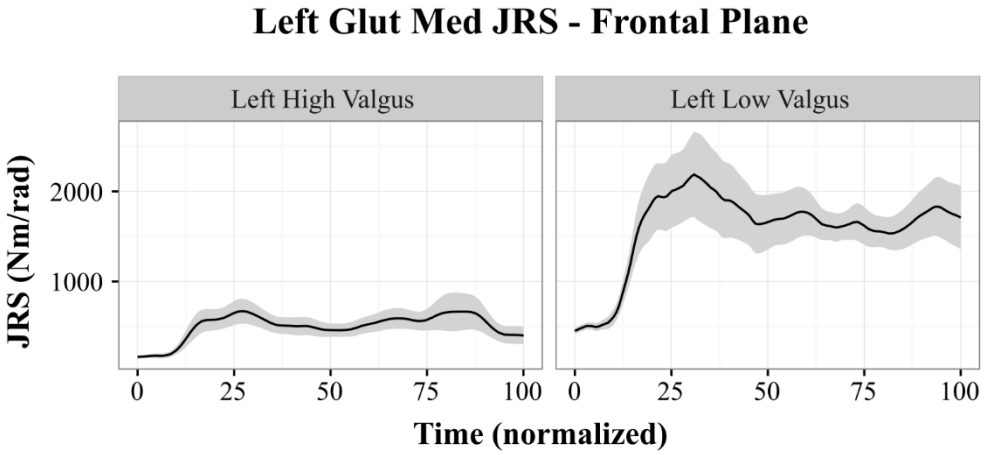
Left Glut Med JRS - Frontal Plane
Left High Valgus
Left Low Valgus
JRS (Nm/rad)
2000
1000
0
25
50
75
100
Time (normalized)

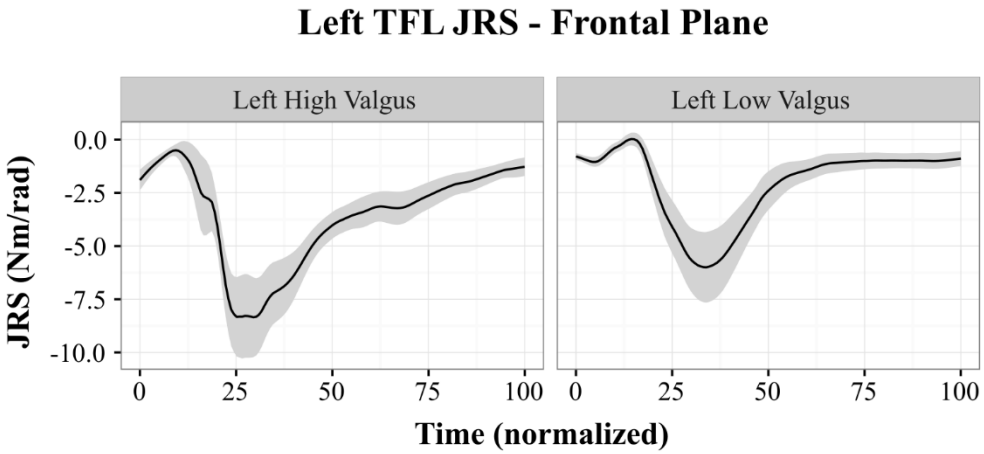
Left TFL JRS - Frontal Plane
Left High Valgus
Left Low Valgus
JRS (Nm/rad)
0.0
-2.5
-5.0
-7.5
-10.0
0
25
50
75
100
Time (normalized)

Left Glut Max Sup JRS - Transverse Plane

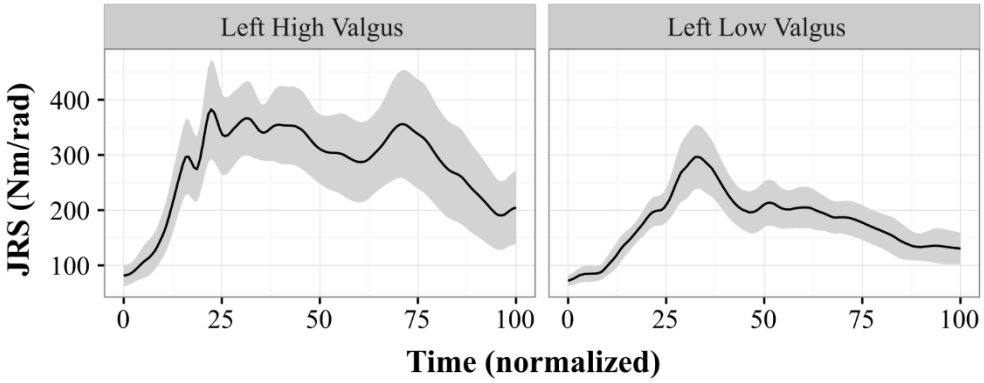

Left Glut Max Inf JRS - Transverse Plane

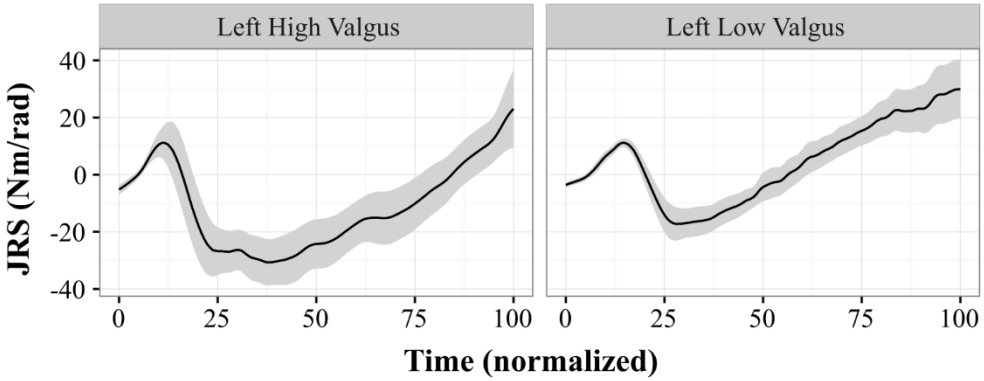

Left Glut Med JRS - Transverse Plane

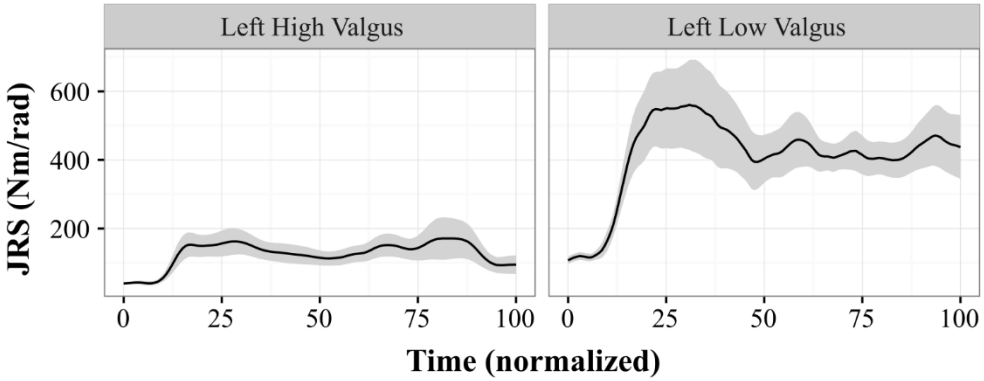

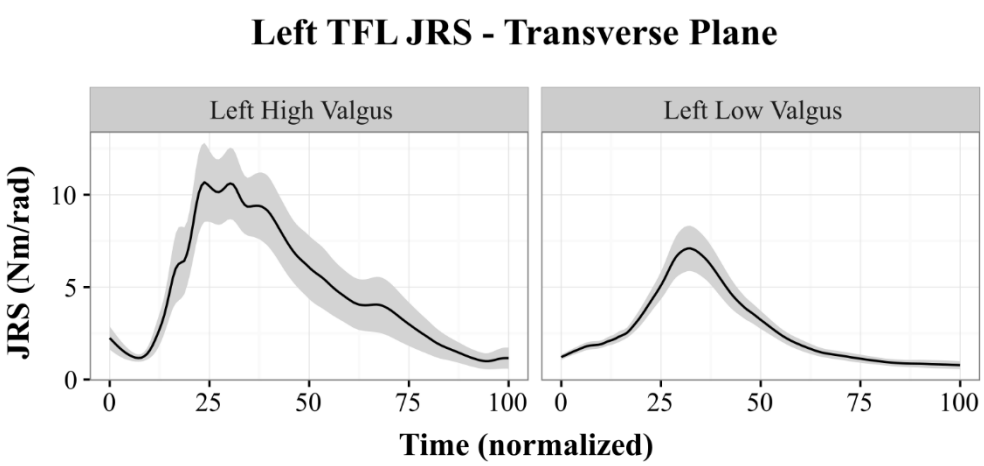
Left TFL JRS - Transverse Plane
Left High Valgus
Left Low Valgus
JRS (Nm/rad)
10
5
0
0
25
50
75
100
Time (normalized)

Single Leg Crossover Drop: Land on Right

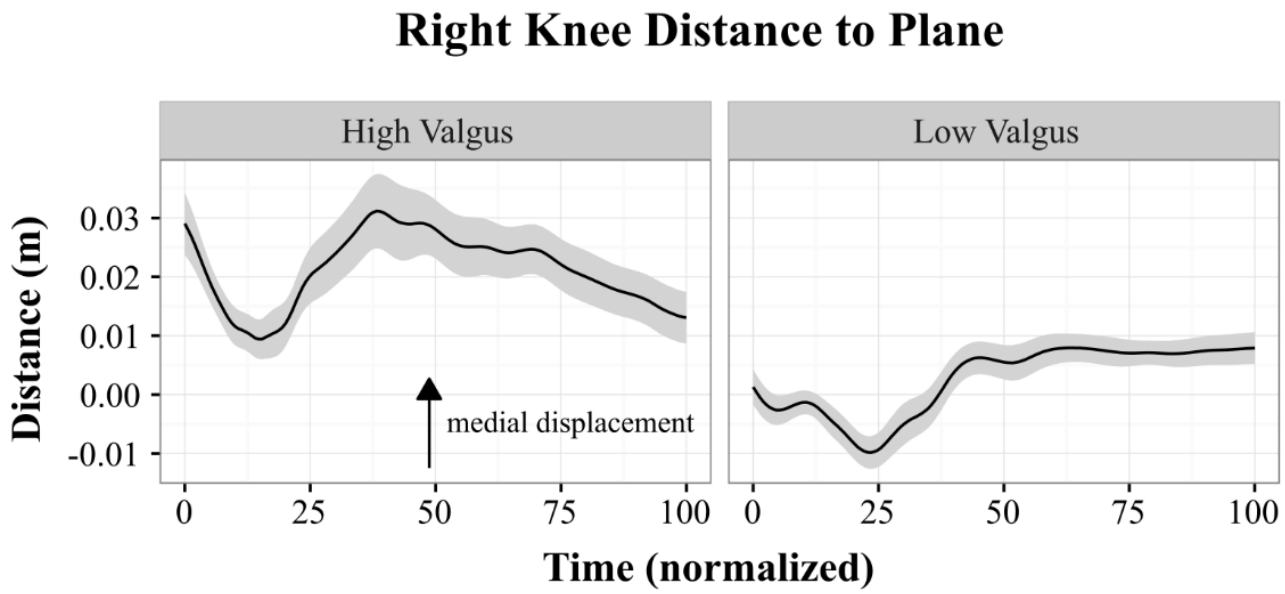

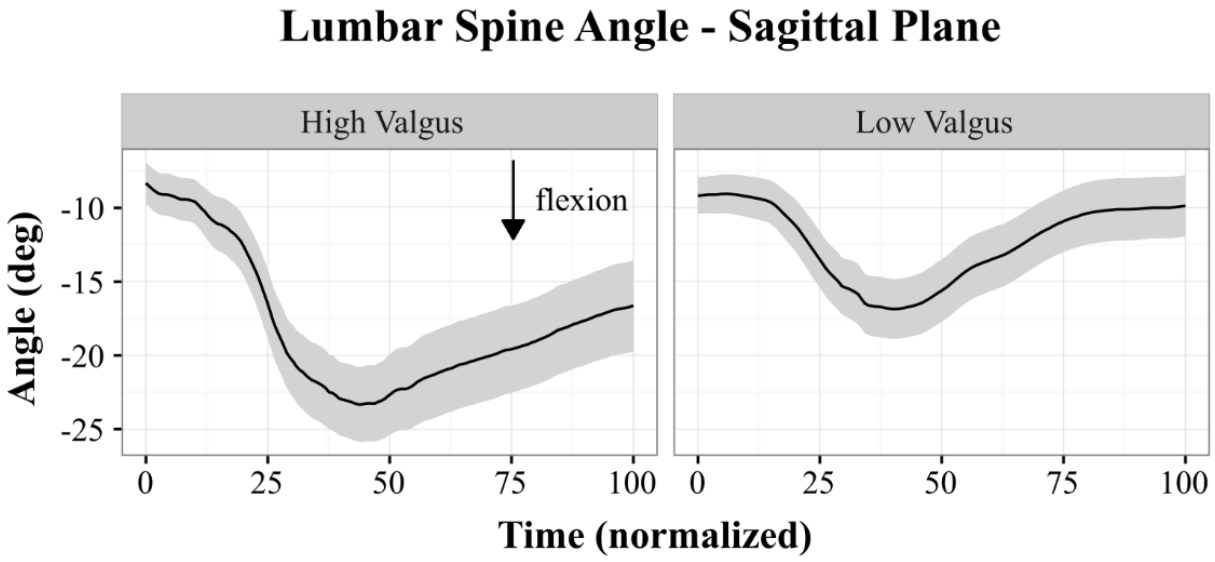
Lumbar Spine Angle - Sagittal Plane
High Valgus
Low Valgus
flexion
Angle (deg)
-10
-15
-20
-25
0
25
50
75
100
Time (normalized)

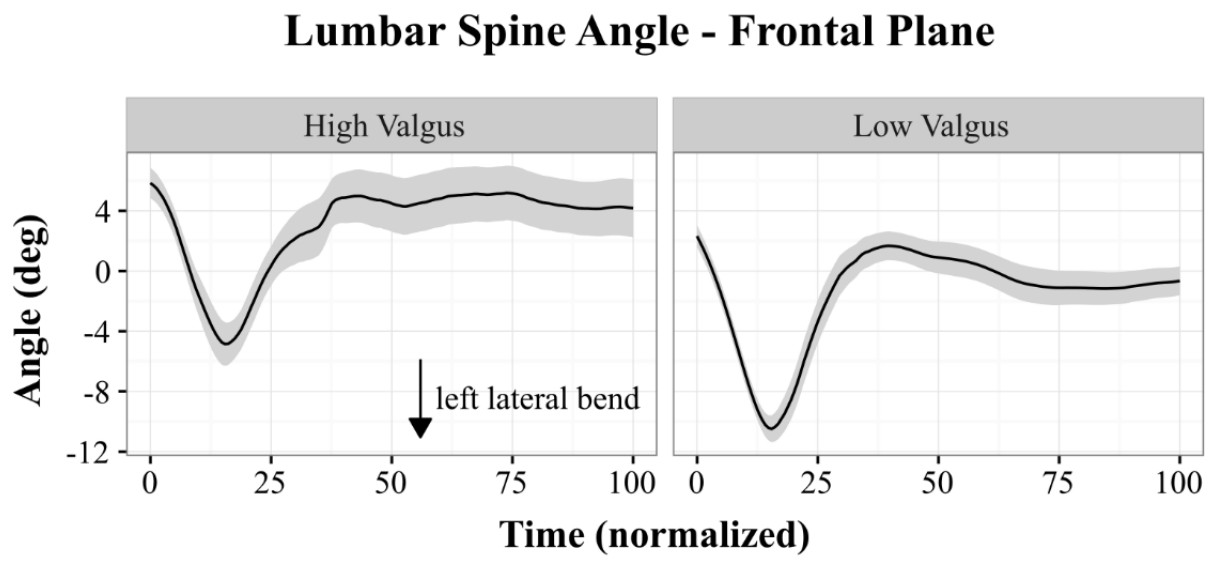
Lumbar Spine Angle - Frontal Plane
High Valgus
Low Valgus
left lateral bend
Angle (deg)
4
0
-4
-8
-12
0
25
50
75
100
Time (normalized)

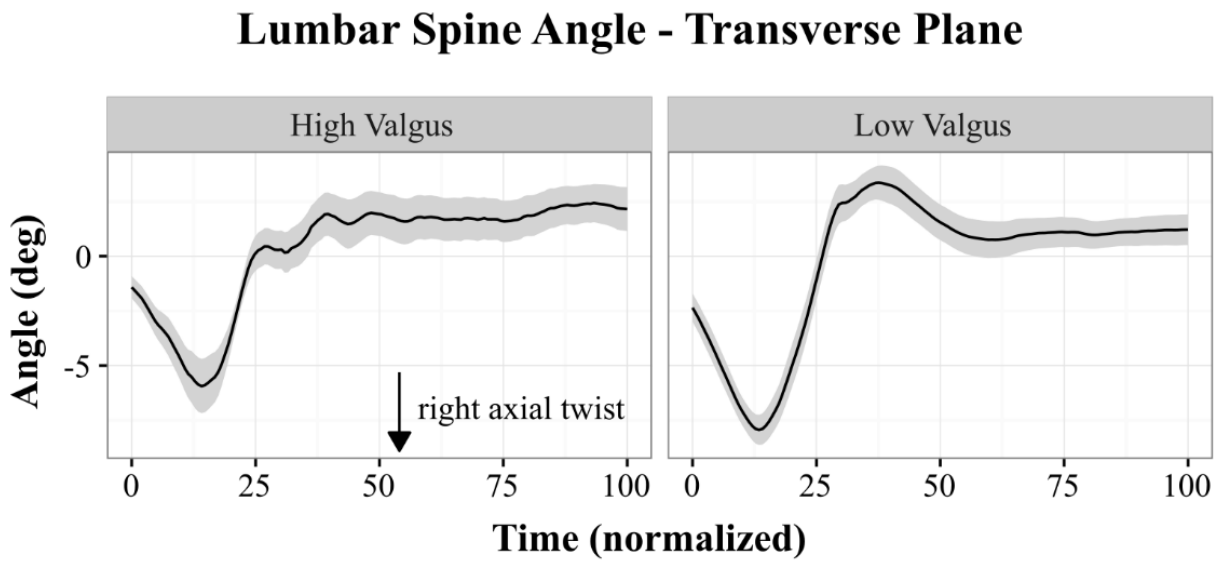
Lumbar Spine Angle - Transverse Plane
High Valgus
Low Valgus
Angle (deg)
0
-5
right axial twist
0
25
50
75
100
Time (normalized)

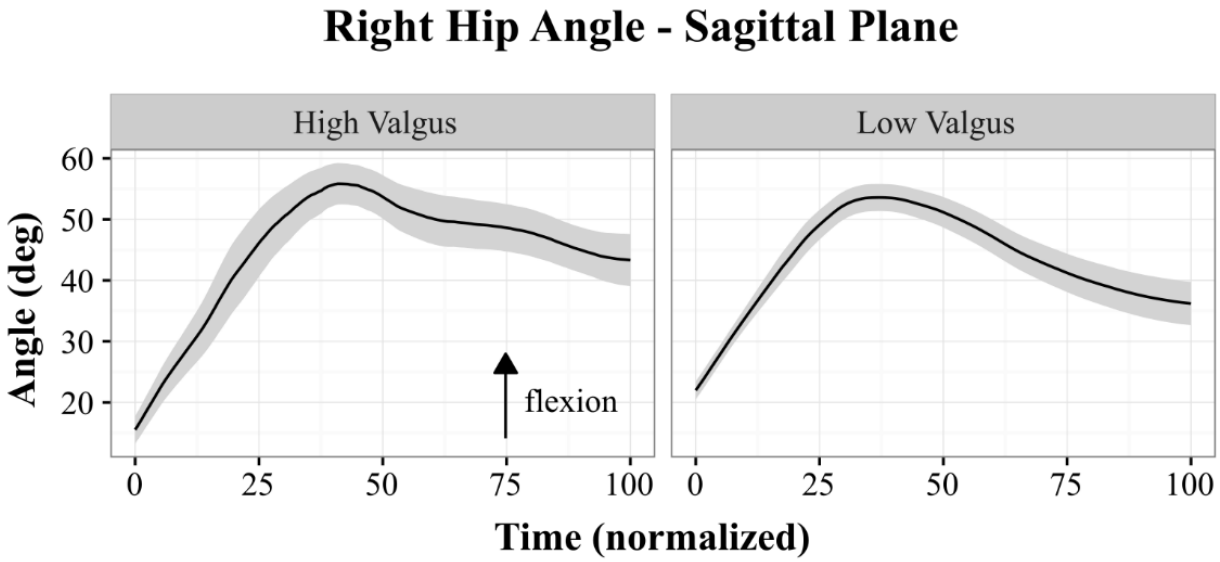
Right Hip Angle - Sagittal Plane
High Valgus
Low Valgus
Angle (deg)
60
50
40
30
20
flexion
0
25
50
75
100
Time (normalized)

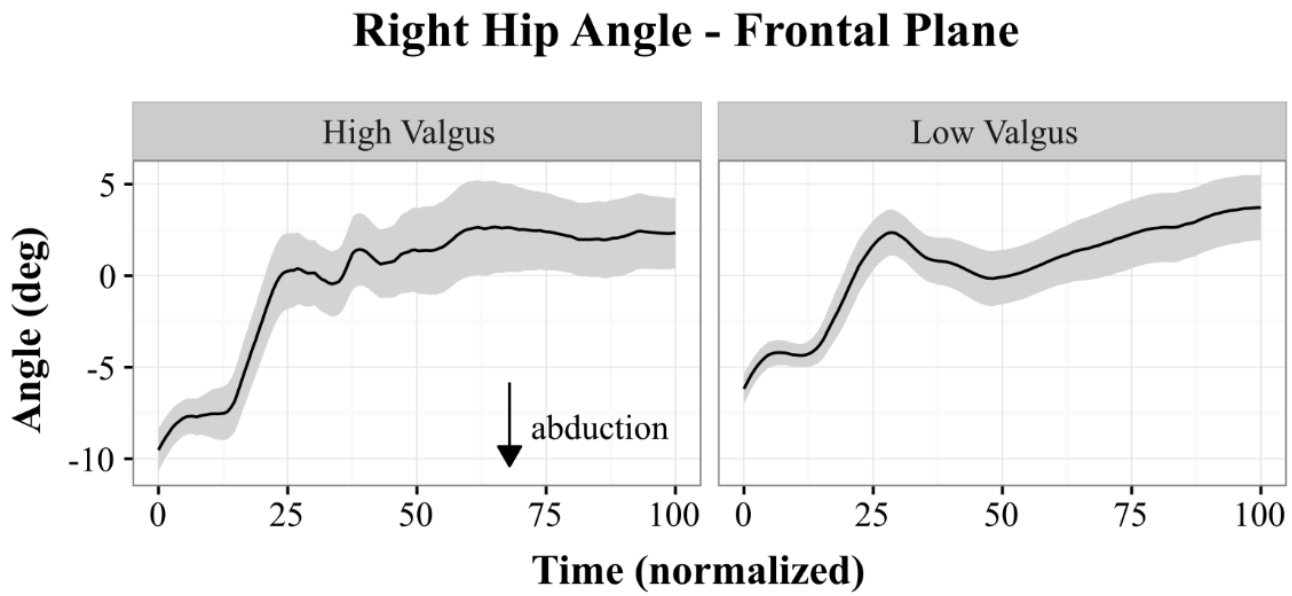
Right Hip Angle - Frontal Plane
High Valgus
Low Valgus
Angle (deg)
5
0
-5
-10
abduction
0
25
50
75
100
Time (normalized)

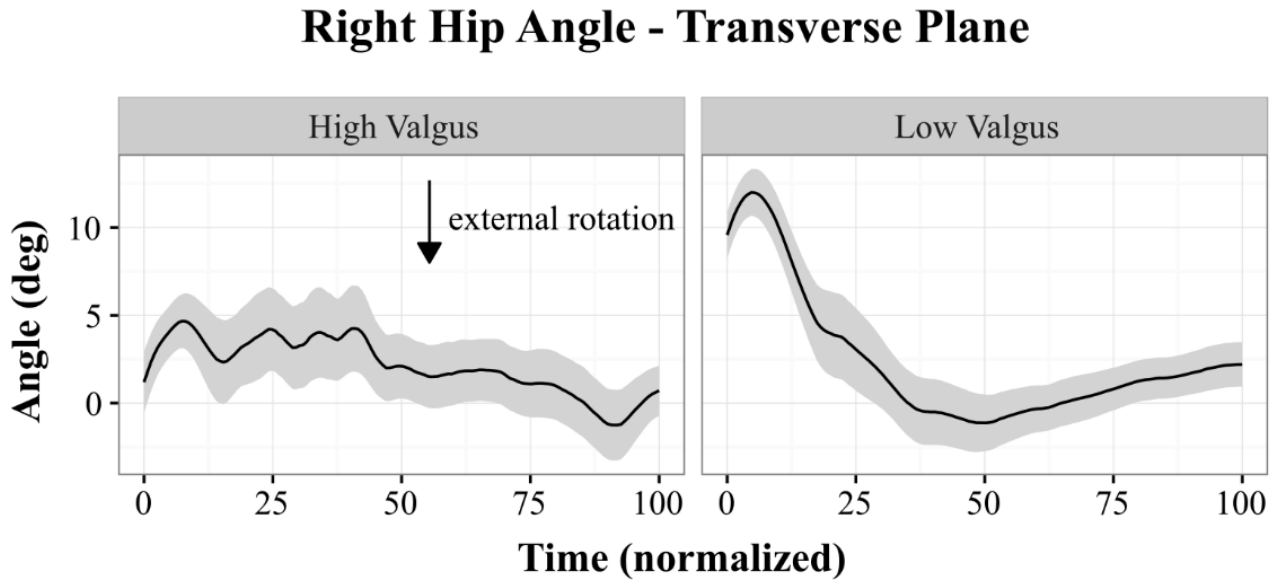
Right Hip Angle - Transverse Plane
High Valgus
Low Valgus
Angle (deg)
10
5
0
external rotation
0
25
50
75
100
Time (normalized)

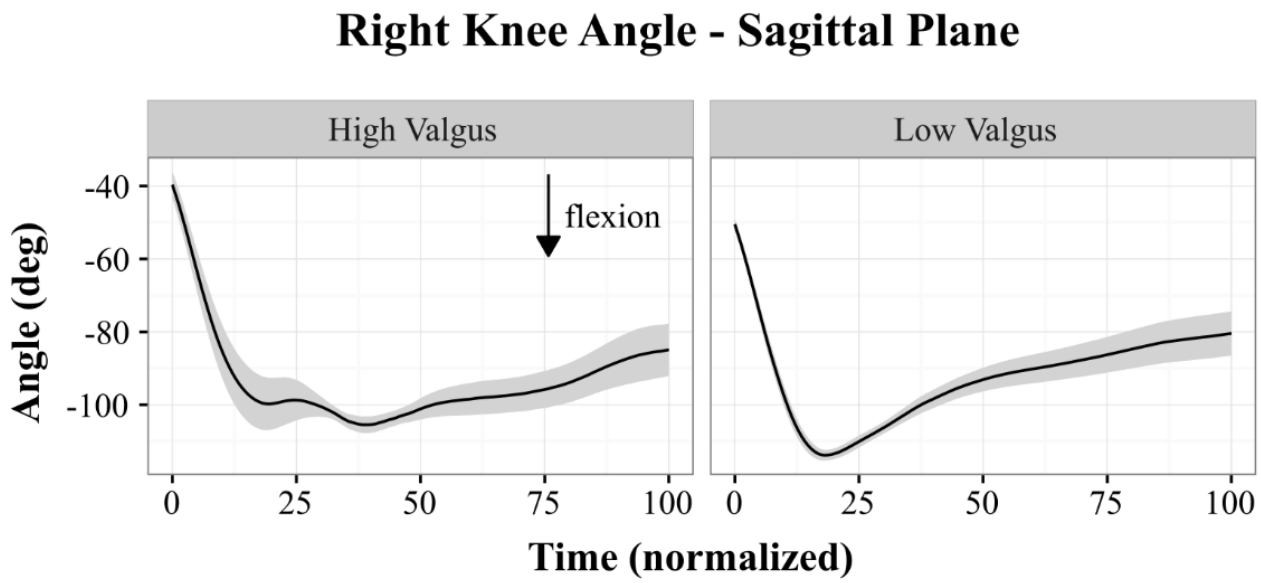
Right Knee Angle - Sagittal Plane
High Valgus
Low Valgus
flexion
Angle (deg)
-40
-60
-80
-100
0
25
50
75
100
Time (normalized)

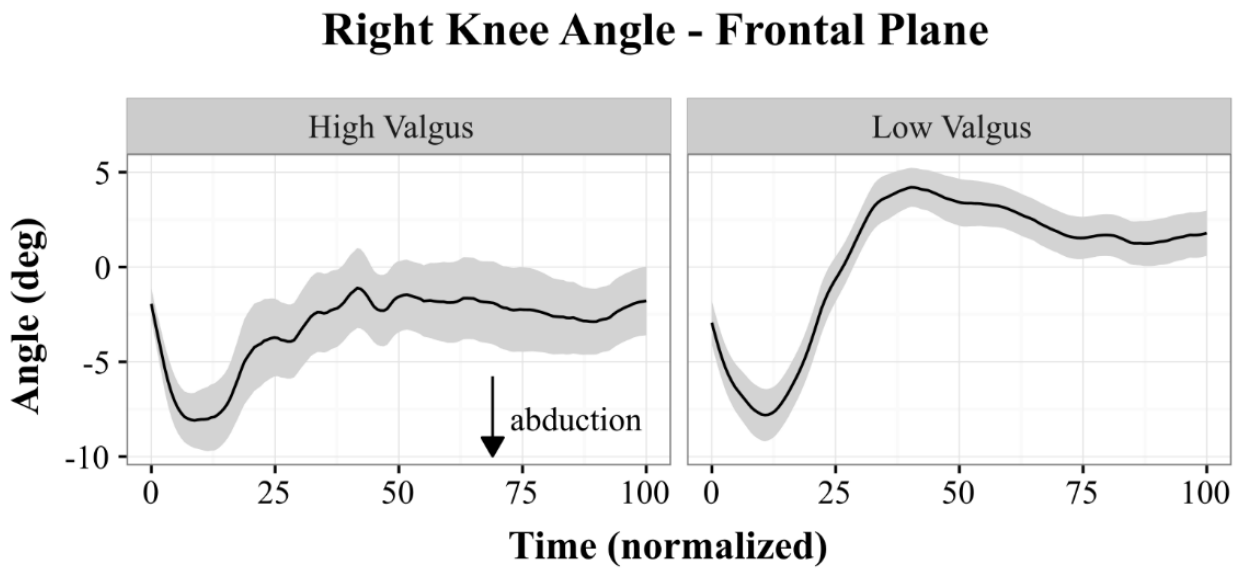
Right Knee Angle - Frontal Plane
High Valgus
Low Valgus
abduction
Angle (deg)
5
0
-5
-10
0
25
50
75
100
Time (normalized)

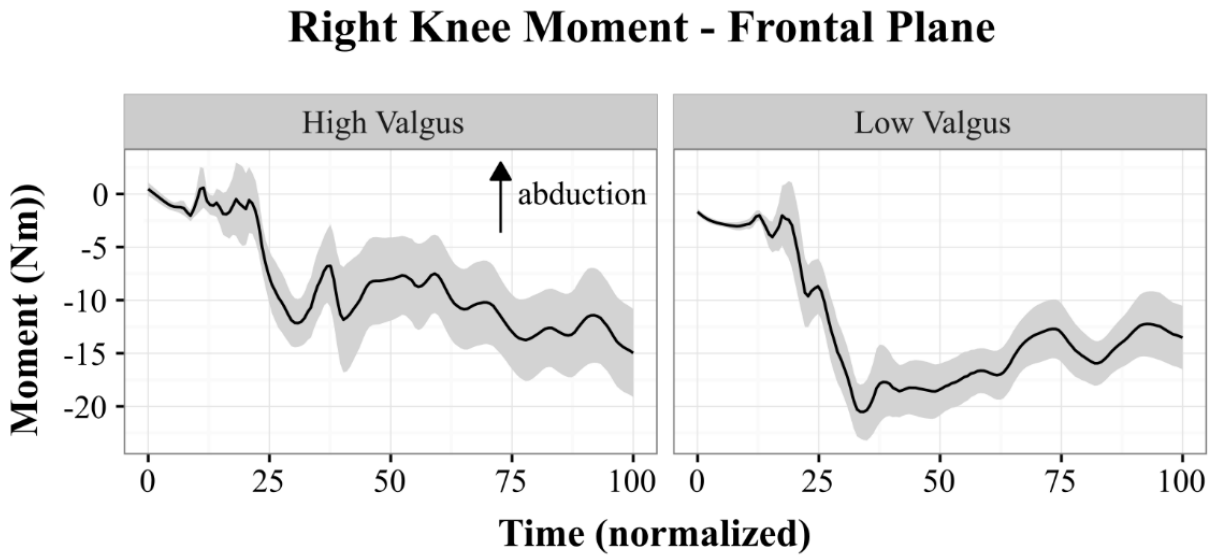
Right Knee Moment - Frontal Plane
High Valgus
Low Valgus
abduction
Moment (Nm))
0
-5
-10
-15
-20
0
25
50
75
100
Time (normalized)

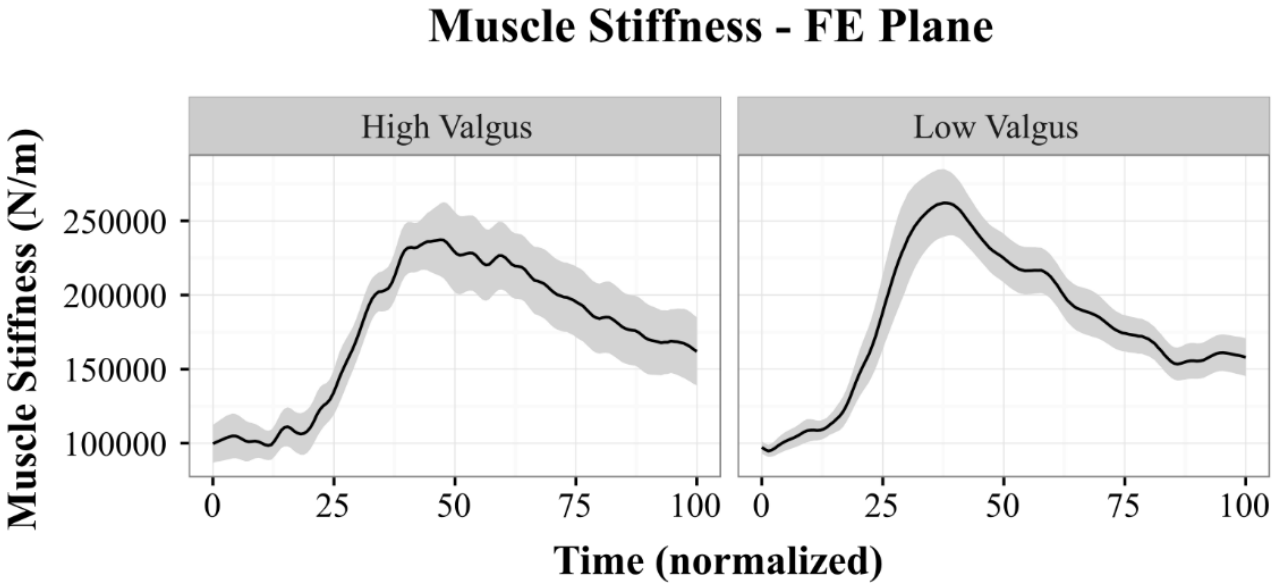
Muscle Stiffness - FE Plane
High Valgus
Low Valgus
Muscle Stiffness (N/m)
250000
200000
150000
100000
0
25
50
75
100
Time (normalized)

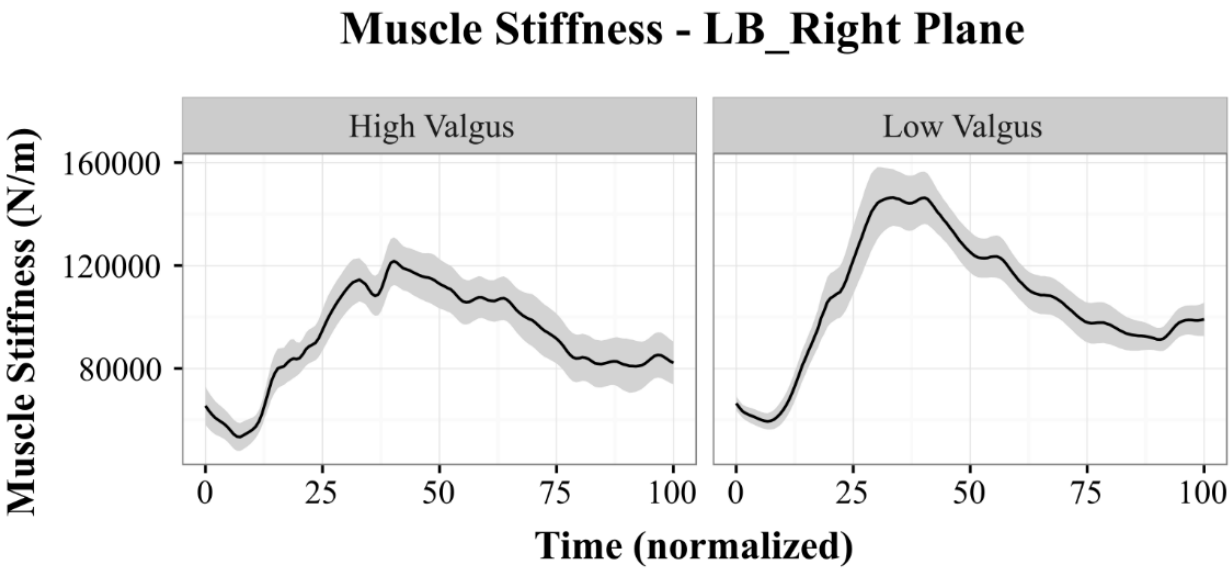
Muscle Stiffness - LB_Right Plane
High Valgus
Low Valgus
Muscle Stiffness (N/m)
160000
120000
80000
0
25
50
75
100
Time (normalized)

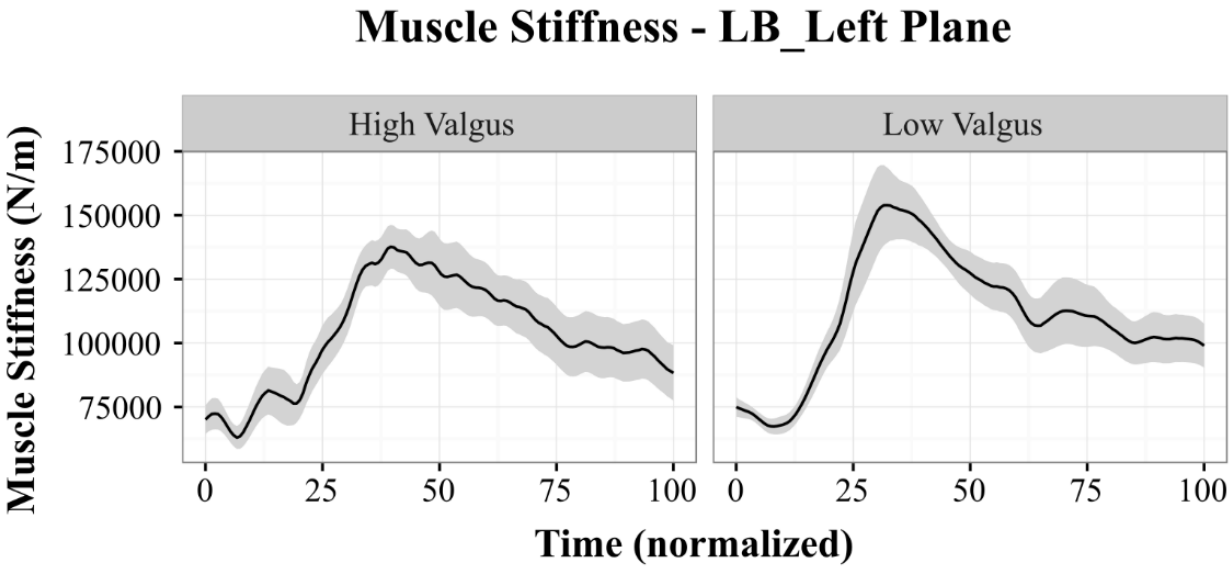
Muscle Stiffness - LB_Left Plane
High Valgus
Low Valgus
Muscle Stiffness (N/m)
175000
150000
125000
100000
75000
0
25
50
75
100
Time (normalized)

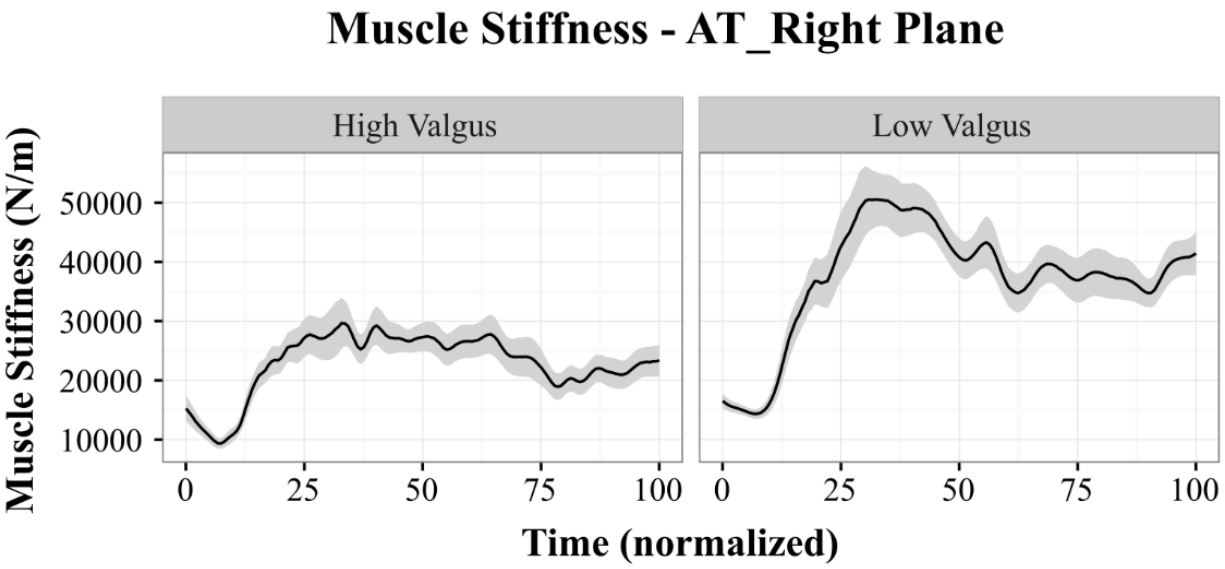
Muscle Stiffness - AT_Right Plane
High Valgus
Low Valgus
Muscle Stiffness (N/m)
50000
40000
30000
20000
10000
0
25
50
75
100
Time (normalized)

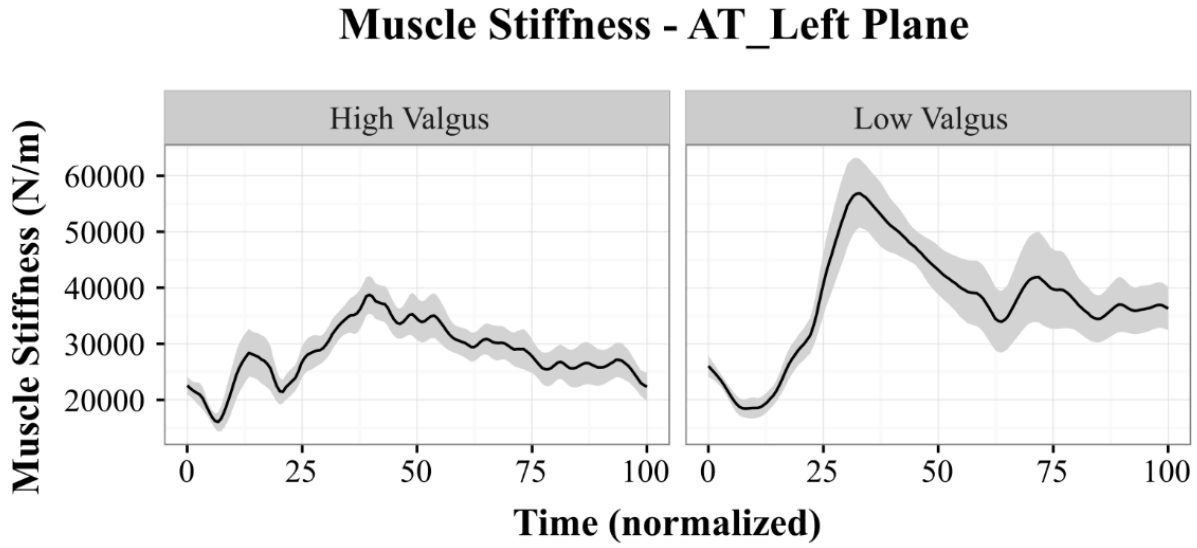
Muscle Stiffness - AT_Left Plane
High Valgus
Low Valgus
Muscle Stiffness (N/m)
60000
50000
40000
30000
20000
0
25
50
75
100
Time (normalized)

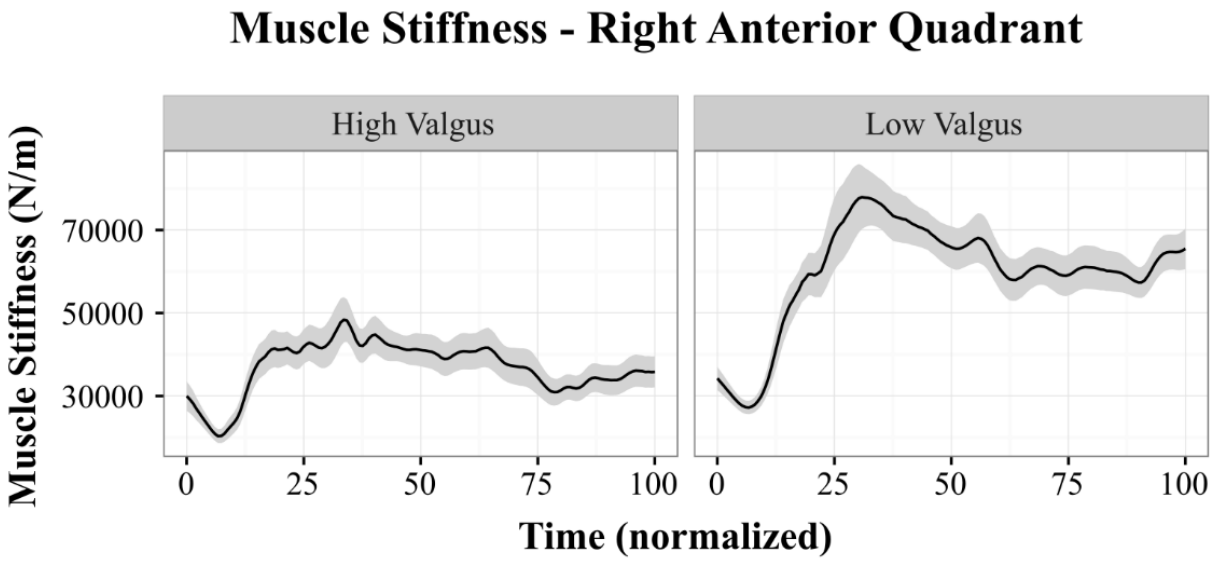
Muscle Stiffness - Right Anterior Quadrant
High Valgus
Low Valgus
Muscle Stiffness (N/m)
70000
50000
30000
0
25
50
75
100
Time (normalized)

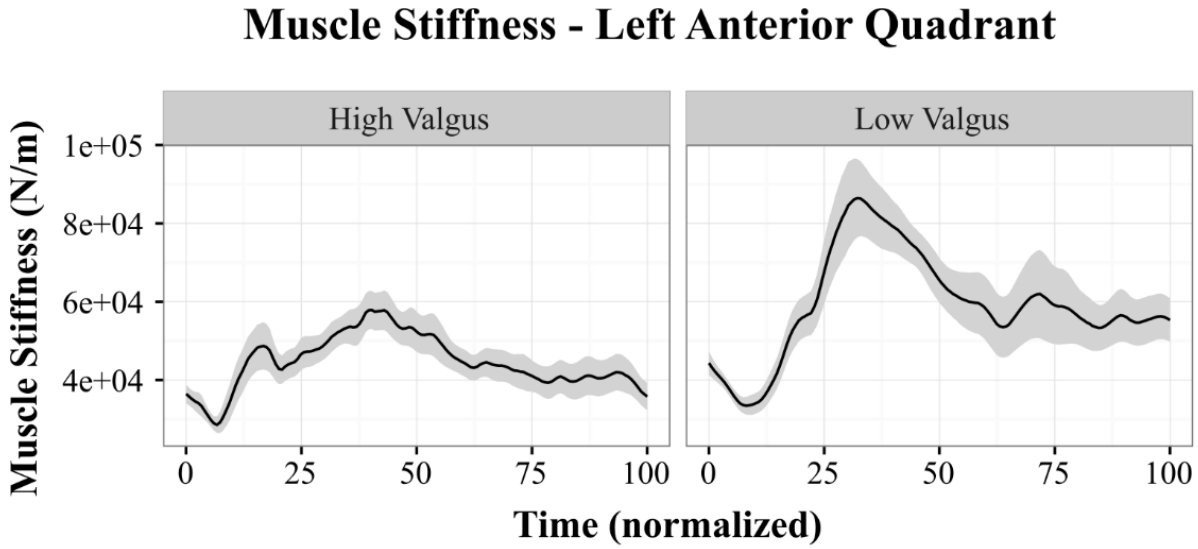
Muscle Stiffness - Left Anterior Quadrant
High Valgus
Low Valgus
Muscle Stiffness (N/m)
1e+05
8e+04
6e+04
4e+04
0
25
50
75
100
Time (normalized)

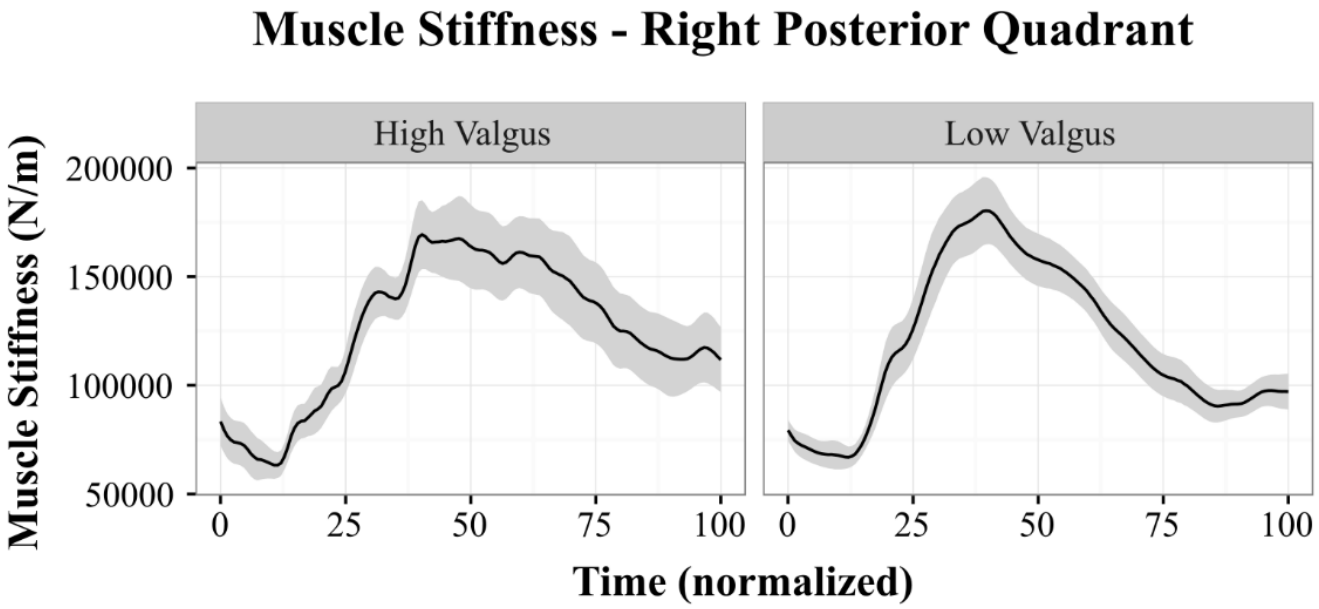
Muscle Stiffness - Right Posterior Quadrant
High Valgus
Low Valgus
Muscle Stiffness (N/m)
200000
150000
100000
50000
0
25
50
75
100
Time (normalized)

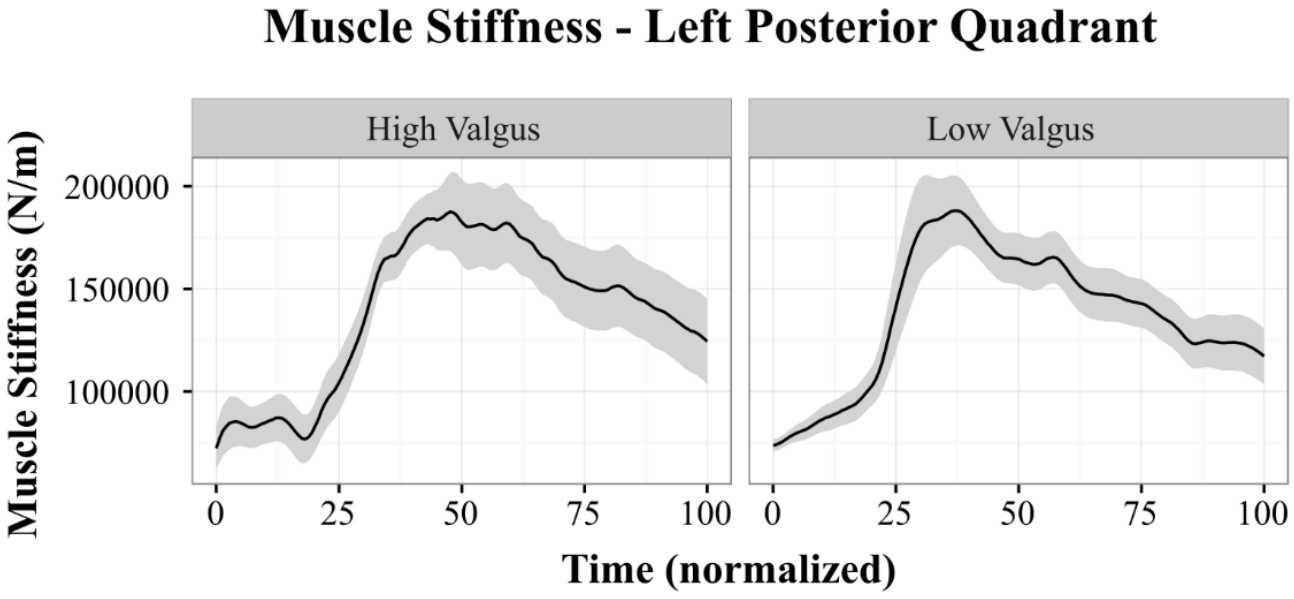
Muscle Stiffness - Left Posterior Quadrant
High Valgus
Low Valgus
Muscle Stiffness (N/m)
200000
150000
100000
0
25
50
75
100
Time (normalized)

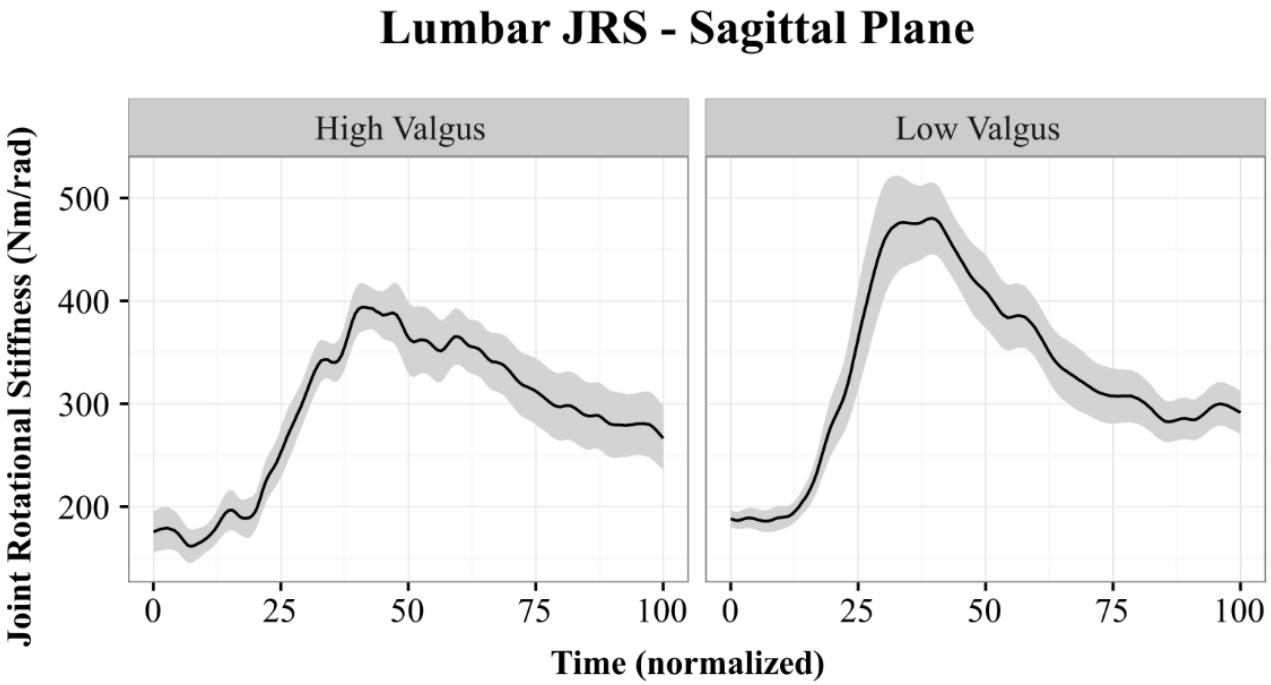
Lumbar JRS - Sagittal Plane
High Valgus
Low Valgus
Joint Rotational Stiffness (Nm/rad)
500
400
300
200
0
25
50
75
100
Time (normalized)

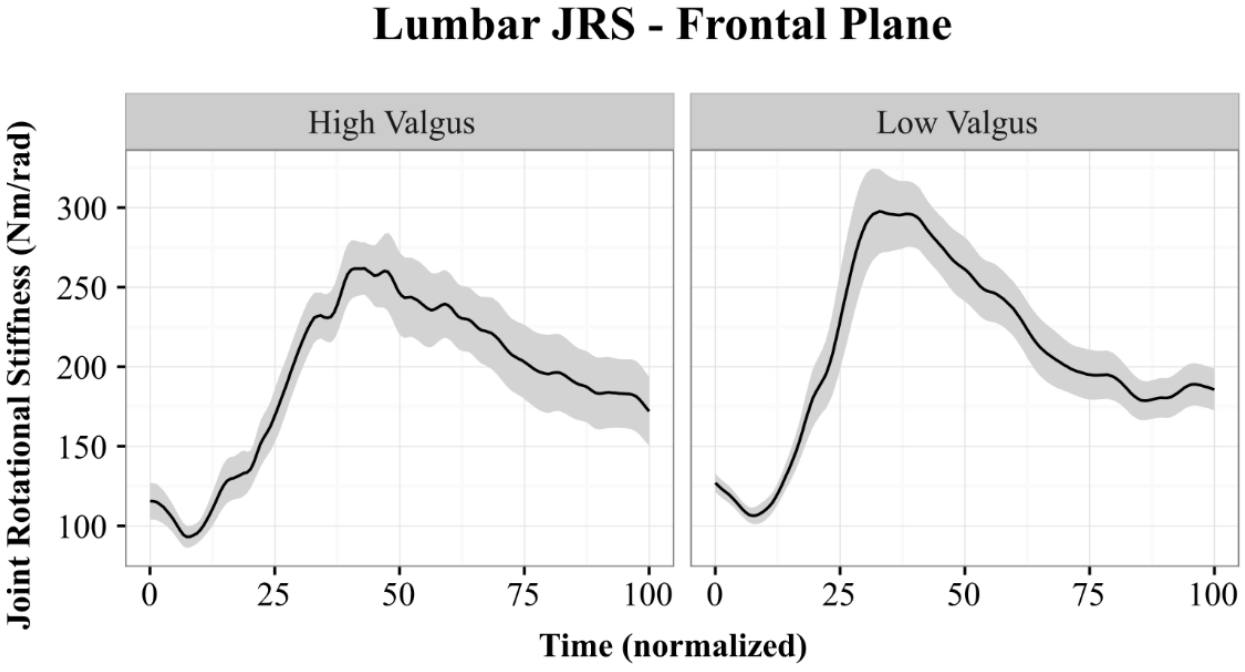
Lumbar JRS - Frontal Plane
High Valgus
Low Valgus
Joint Rotational Stiffness (Nm/rad)
300
250
200
150
100
0
25
50
75
100
Time (normalized)

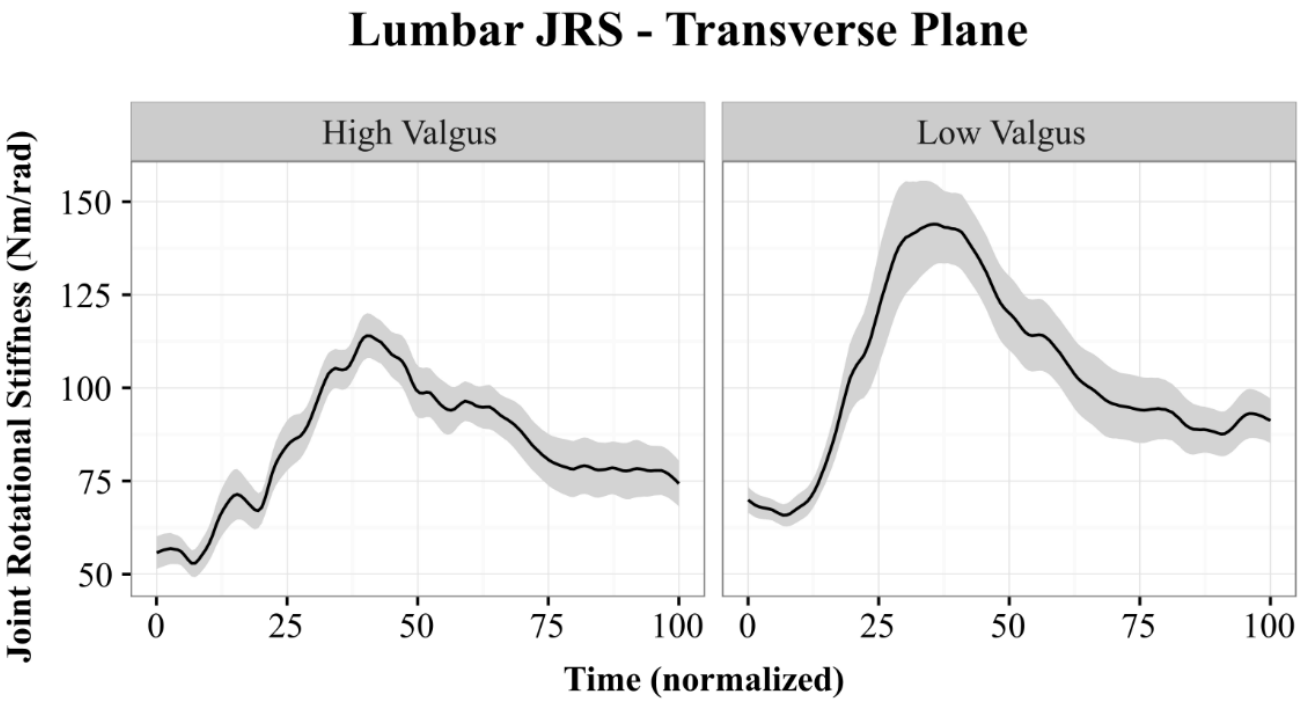
Lumbar JRS - Transverse Plane
High Valgus
Low Valgus
Joint Rotational Stiffness (Nm/rad)
150
125
100
75
50
0
25
50
75
100
Time (normalized)

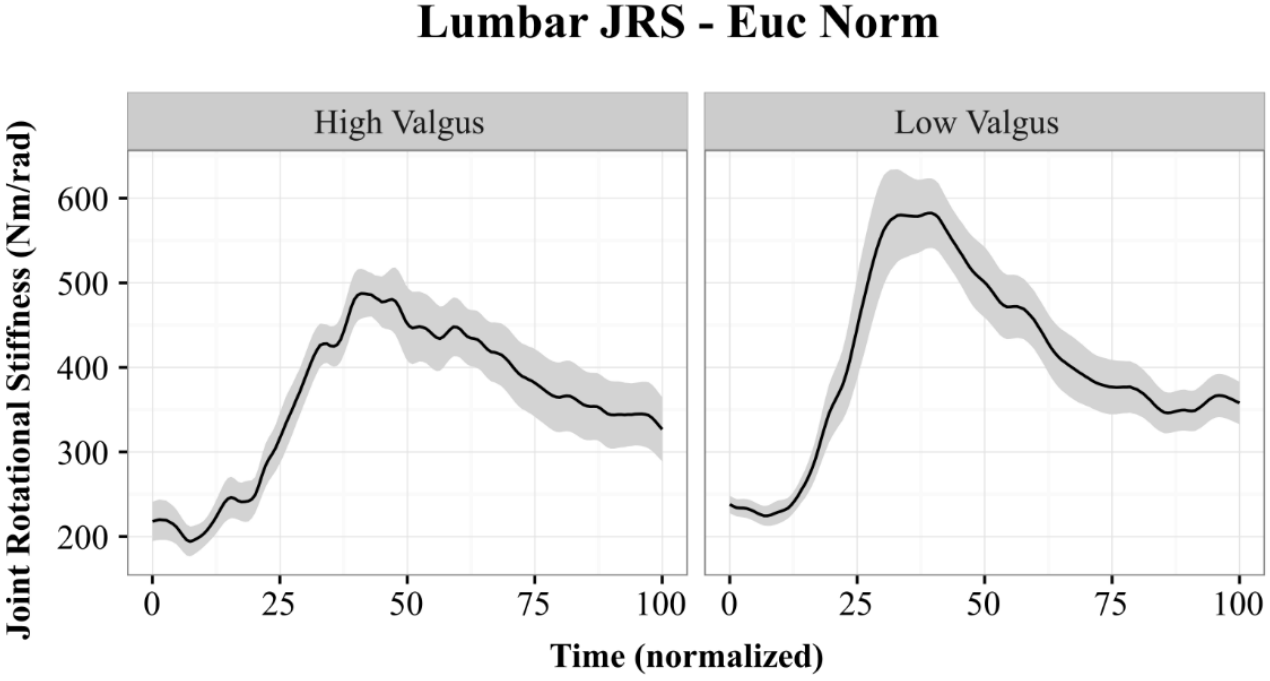
Lumbar JRS - Euc Norm
High Valgus
Low Valgus
Joint Rotational Stiffness (Nm/rad)
600
500
400
300
200
0
25
50
75
100
Time (normalized)

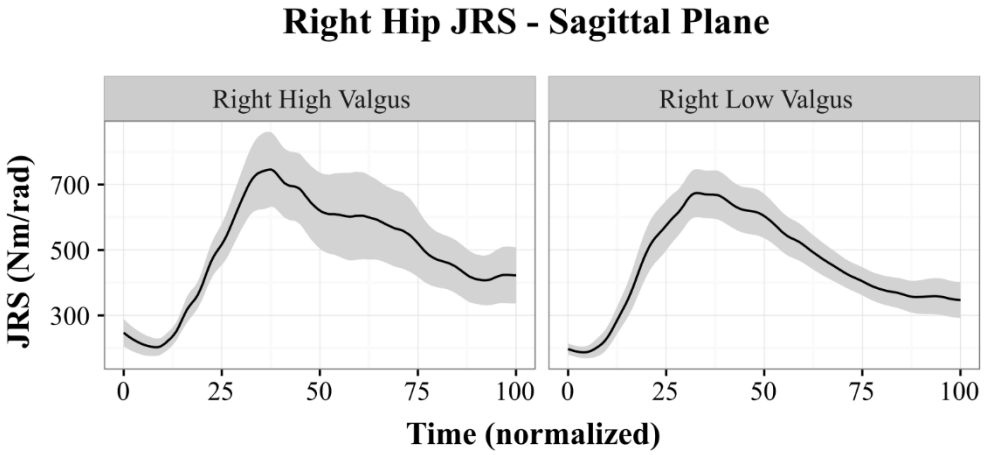
Right Hip JRS - Sagittal Plane
Right High Valgus
Right Low Valgus
JRS (Nm/rad)
700
500
300
0
25
50
75
100
Time (normalized)

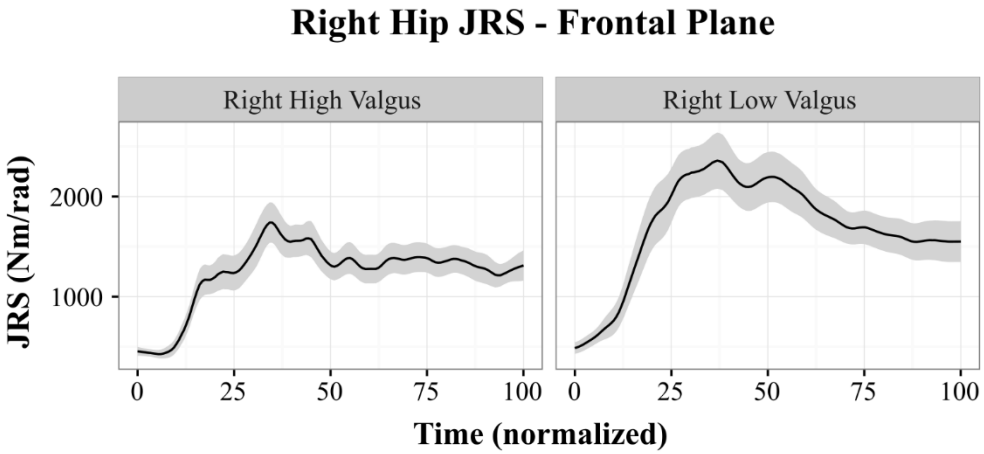
Right Hip JRS - Frontal Plane
Right High Valgus
Right Low Valgus
JRS (Nm/rad)
2000
1000
0
25
50
75
100
Time (normalized)

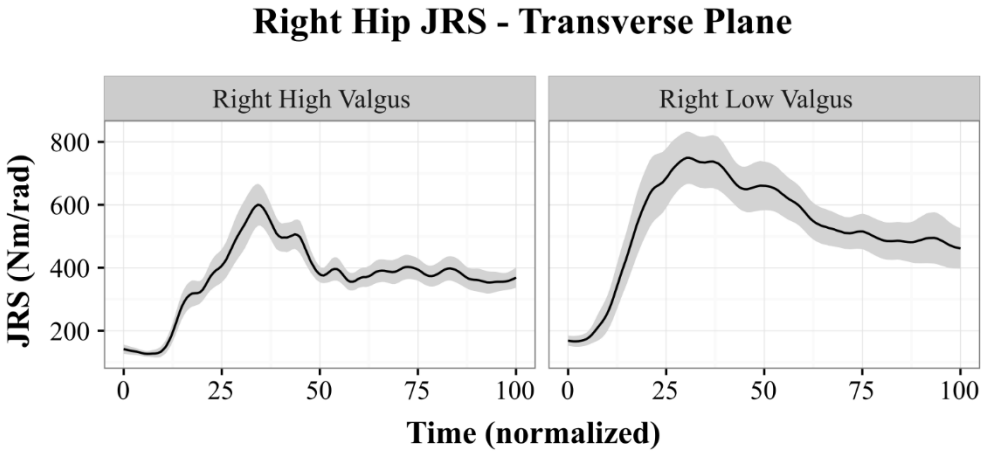
Right Hip JRS - Transverse Plane
Right High Valgus
Right Low Valgus
JRS (Nm/rad)
800
600
400
200
0
25
50
75
100
Time (normalized)

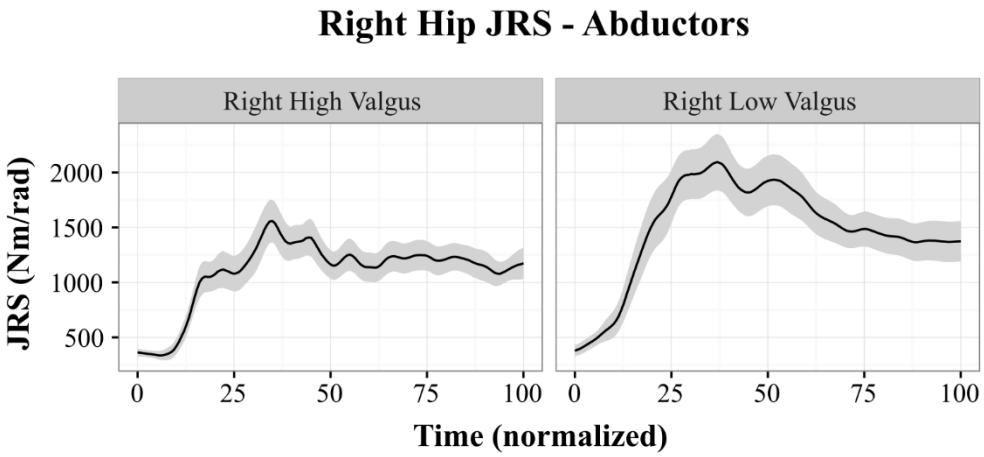
Right Hip JRS - Abductors
Right High Valgus
Right Low Valgus
JRS (Nm/rad)
2000
1500
1000
500
0
25
50
75
100
Time (normalized)

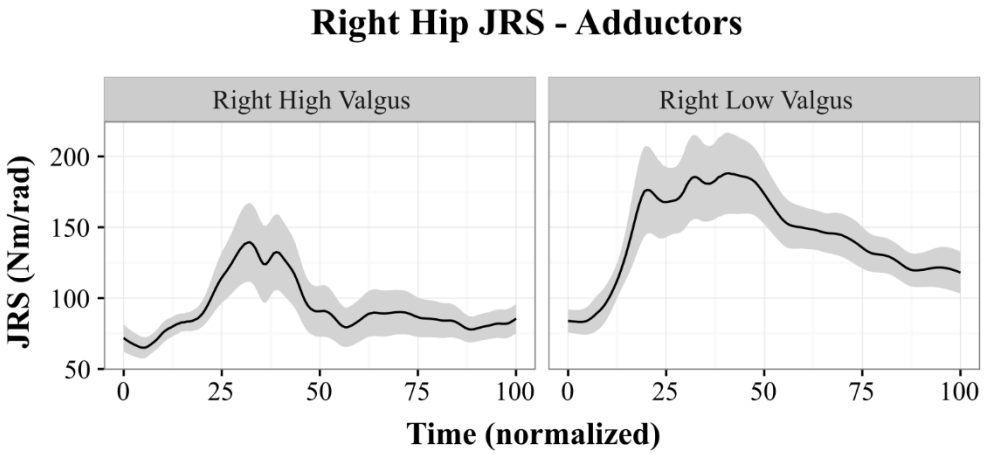
Right Hip JRS - Adductors
Right High Valgus
Right Low Valgus
JRS (Nm/rad)
200
150
100
50
0
25
50
75
100
Time (normalized)

Right Glut Max Sup JRS - Frontal Plane

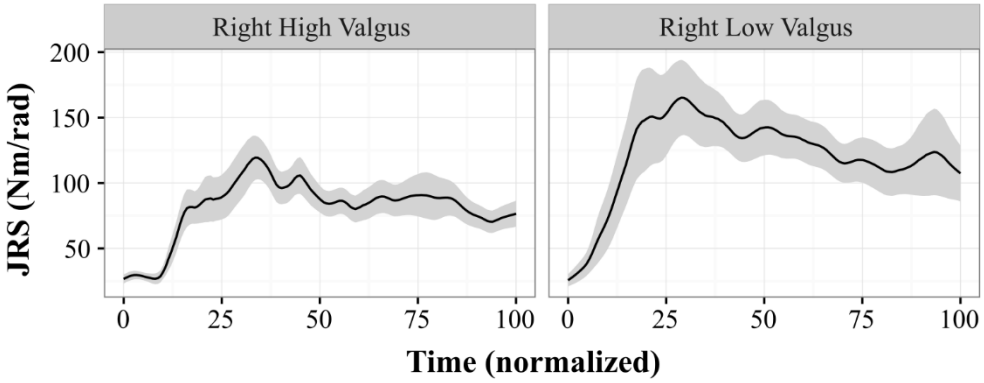

Right Glut Max Inf JRS - Frontal Plane

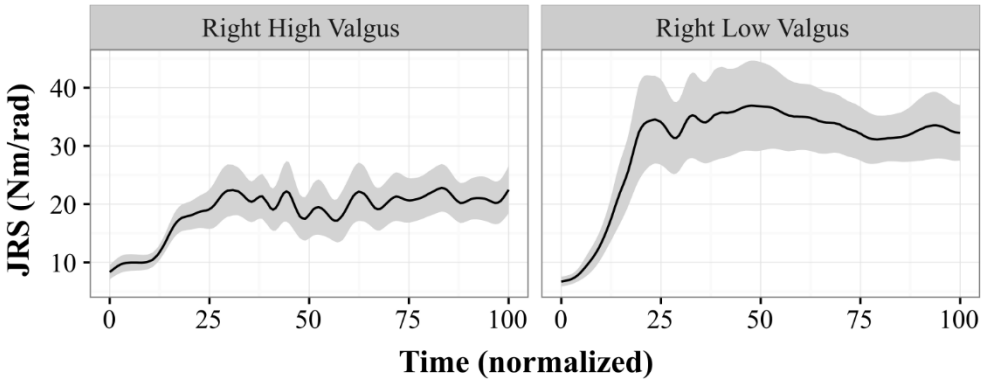

Right Glut Med JRS - Frontal Plane

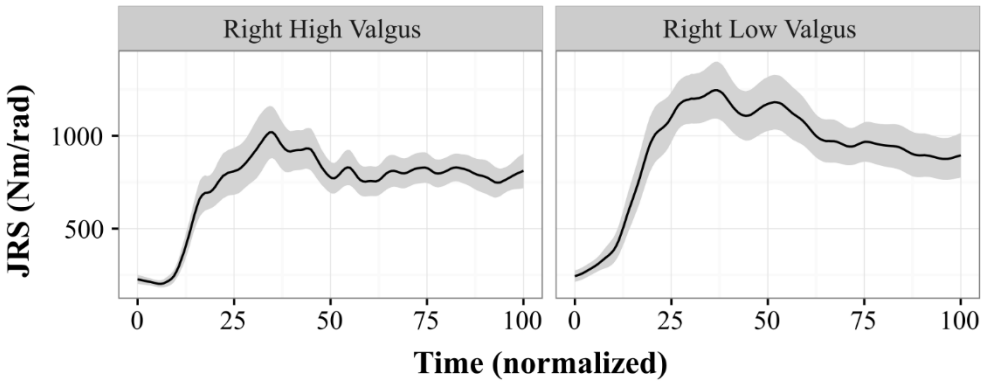

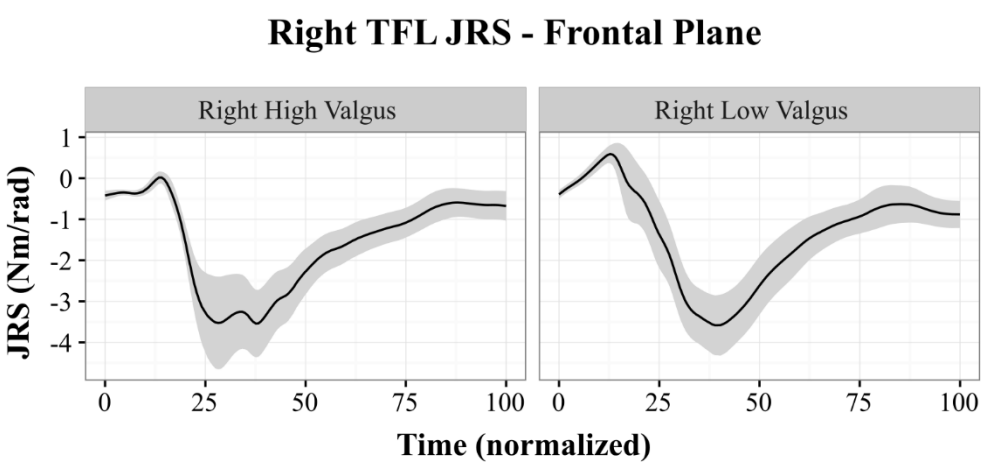
Right TFL JRS - Frontal Plane
Right High Valgus
Right Low Valgus
JRS (Nm/rad)
1
0
-1
-2
-3
-4
0
25
50
75
100
Time (normalized)

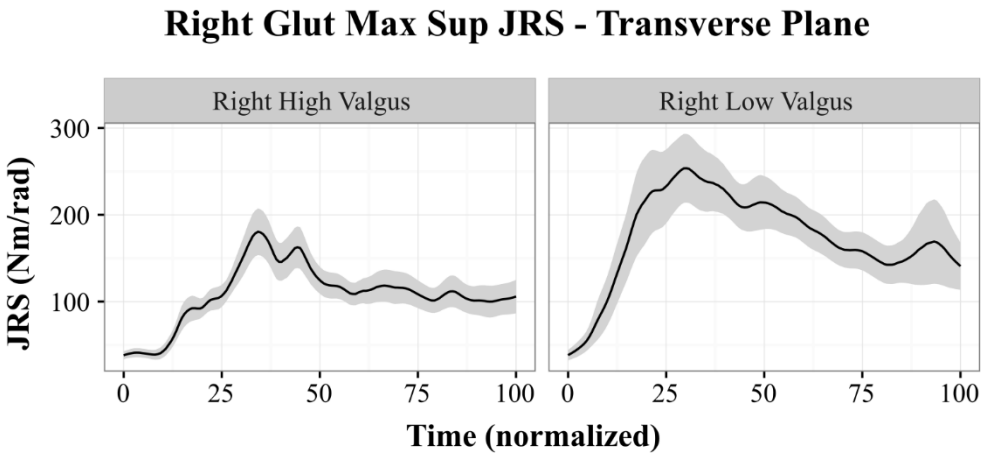
Right Glut Max Sup JRS - Transverse Plane
Right High Valgus
Right Low Valgus
JRS (Nm/rad)
300
200
100
0
25
50
75
100
Time (normalized)

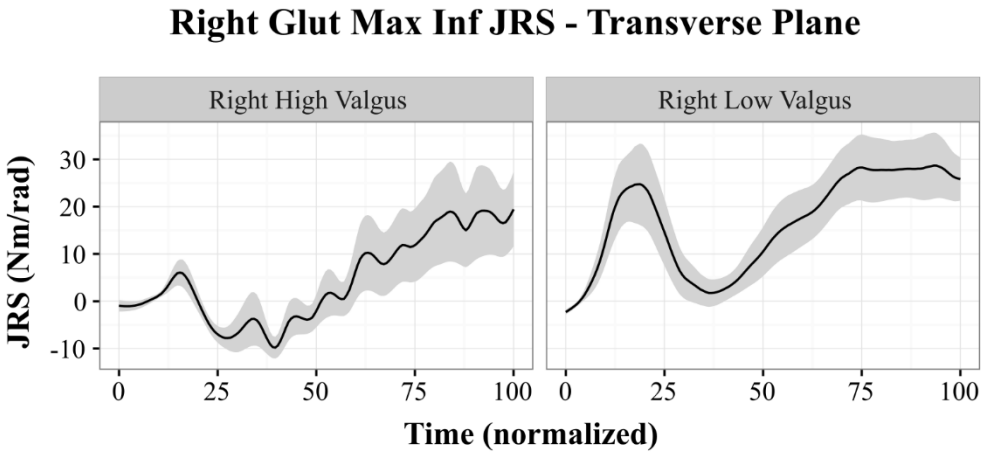
Right Glut Max Inf JRS - Transverse Plane
Right High Valgus
Right Low Valgus
JRS (Nm/rad)
30
20
10
0
-10
0
25
50
75
100
Time (normalized)

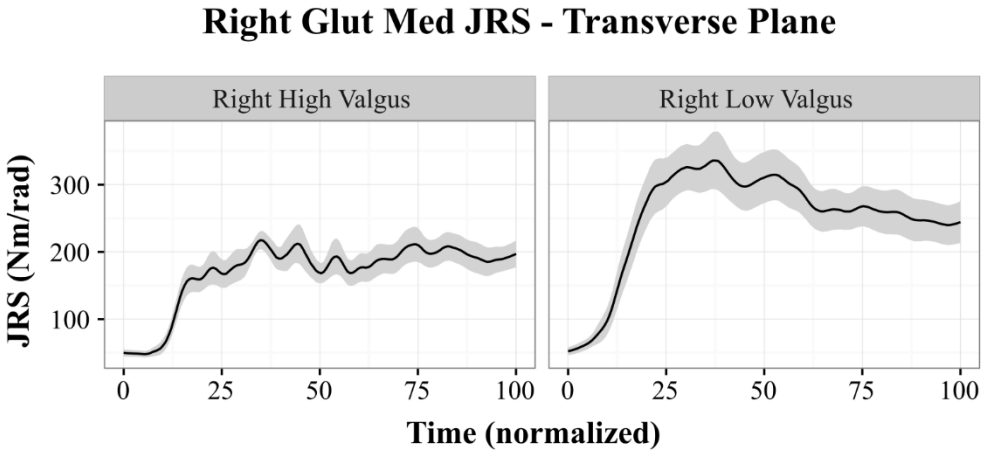
Right Glut Med JRS - Transverse Plane
Right High Valgus
Right Low Valgus
JRS (Nm/rad)
300
200
100
0
25
50
75
100
Time (normalized)

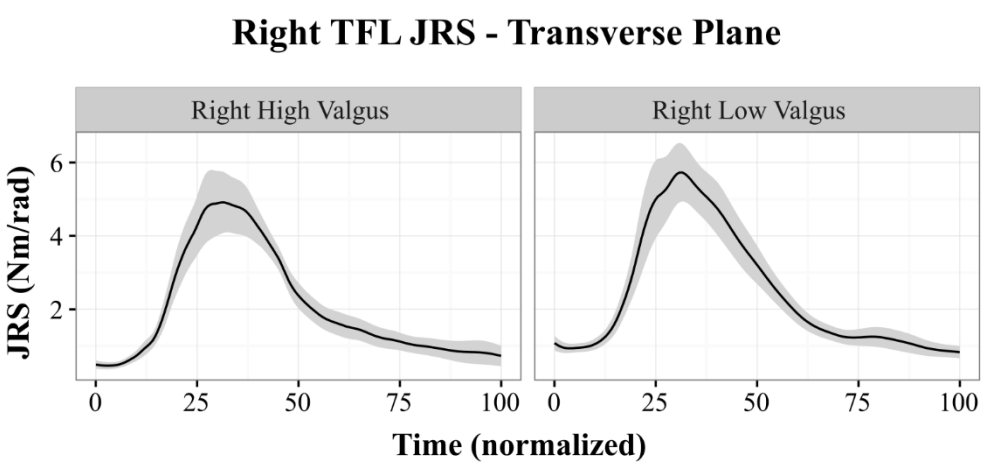
Right TFL JRS - Transverse Plane
Right High Valgus
Right Low Valgus
JRS (Nm/rad)
6
4
2
0
25
50
75
100
Time (normalized)